

# **THE DEVELOPMENT OF A DIRECTIONAL PRIMER CHARGE FOR BLASTING IN MINES**

**JOHN ANTHONY CRUISE**

A thesis submitted to the Faculty of Engineering and the Built Environment, University of the Witwatersrand, in fulfillment of the requirements for the degree of Doctor of Philosophy.

Johannesburg 2005

## DECLARATION

I, John Anthony Cruise, declare that the original idea for, the direction of, the compilation of and the conclusions reached in this thesis are my own. Those persons who have aided me with the undertaking tests at the NASCHEM Detonics Laboratory, the taking of the measurements of the underground tests at Village main gold mine, and with certain calculations are named in the Acknowledgements. Certain aspects of the work which was commissioned by me is given in the Appendix.

This thesis is being submitted for the Degree of Doctor of Philosophy in the University of the Witwatersrand. It has not been submitted before for any degree or examination in any other University.

---

# ABSTRACT

This thesis describes the development of a directional primer charge for use in blasting in mining operations.

The **directional primer charge** is an explosive gun which takes the place of a standard primer charge in a blasthole. It is a shaped charge which directs the explosive energy forwards into the blasthole. Its effectiveness is enhanced by a metal liner which is located at a specified stand-off distance from the toe of the hole.

The explosive energy of the column charge is converted into the kinetic energy of the metal liner which transforms into an ultrasonic slug. This in turn converts into the impact energy of the slug impacting on the rock. This rock is axially compressed to such a degree that a radial fracture is developed. This radial fracture is termed an umbrella crack. Prior to the development of the directional primer charge, the phenomenon of the umbrella crack had only been observed in experimental Perspex blasting models and its formation mechanism had never been satisfactorily explained. If the directional primer charge could cause an umbrella crack in hard rock mining at the end of blastholes, then more rock would be broken out per blast than is currently achieved in practice.

This thesis records the historical development of the explosive shaped charge with particular reference to the development of the explosively-forged projectile. It describes the classical theories and models which apply in determining the theoretical prediction of the physical properties of the designed directional primer charge. It describes the experimental procedures and measurements using flash X-ray radiography and electronic shorting screens to freeze the flight of a metal slug traveling at speeds of over 2000 metres per second. Underground tests were undertaken under full mining production conditions to compare the rock breaking effects of various designs.

The theoretical calculation of the extent of the movement of the rock at the toe of the blasthole indicates that umbrella cracks should be formed. The underground tests confirm their formation.

It is concluded that the use of the directional primer charge in stoping operations can improve the blasting efficiency in South African hard rock mines by up to 15 %.

## **ACKNOWLEDGEMENTS**

I would like to acknowledge the advice and assistance given to me by my colleague Dr. T. Szendrei during the development of the directional primer slug. He facilitated the surface tests at the NASCHEM Detonics Laboratory and supervised Mr. D Ellis in the high velocity slug measurements using flash X-ray radiography and electronic shorting screens. Dr. Szendrei was commissioned by me to undertake certain calculations both theoretical and measured for the velocities of the directional primer slug configurations. These are incorporated in Chapters 7 and 8 of this thesis and acknowledged wherever they appear. Mr J. Whipp assisted me with the underground production blasts by taking the daily measurements before and after each blast.

<b>CONTENTS</b>		<b>Page</b>
DECLARATION		2
ABSTRACT		3
ACKNOWLEDGEMENTS		4
CONTENTS		5
LIST OF FIGURES		13
LIST OF TABLES		15
LIST OF PHOTOGRAPHS (IN MAIN TEXT)		16
LIST OF SYMBOLS		18
<b>CHAPTER 1</b>	<b>INTRODUCTION</b>	<b>20</b>
1.1	Hypothesis	20
1.2	Preview of Contents	21
1.3	Witwatersrand Practice	23
	1.3.1 Stoping	23
	1.3.2 Blasthole Sockets	24
	1.3.3 Development	24
1.4	The Directional Primer Charge	25
<b>CHAPTER 2</b>	<b>HISTORICAL DEVELOPMENT</b>	<b>29</b>
2.1	Development of Explosives	29
	2.1.1 Early recognition	29
	2.1.2 Nobel's contribution	29
	2.1.3 Military explosives	29
	2.1.4 Commercial explosives	30
	2.1.5 Composition B	31
	2.1.6 Super Gelignite	31

	<b>Page</b>
2.2	Development of Shaped Charges 32
2.2.1	Milestone 1 – Earliest Known Reference 32
2.2.2	Milestone 2 – First Recognition of Military Potential 34
2.2.3	Milestone 3 – Munroe Effect 34
2.2.4	Milestone 4 – First Patents for Hollow Charges 34
2.2.5	Milestone 5 – Practical Application for Hollow Charges 35
2.2.6	Milestone 6 – Extent of World War I Interest 35
2.2.7	Milestone 7 – Early Russian Research 35
2.2.8	Milestone 8 – The Case of The Dimpled Blasting Dap 35
2.2.9	Milestone 9 – Early German Military Initiative 36
2.2.10	Milestone 10 – Liner Effect 36
2.2.11	Milestone 11 – Development of the Bazooka 36
2.2.12	Milestone 12 – Jet Formation and Jet Target Interaction 36
2.3	Development of Explosively – Forged Projectiles 38
2.3.1	Ballistic Effect of Blasting Cap 38
2.3.2	Explosive Gun 38
2.3.3	Flat Cone Charges 38
2.4	Shaped Charges in Mining 39
2.4.1	Post-War Attempts 39
2.4.2	Slugshot 41
2.4.3	Other Shaped Charges 41
2.4.4	The Directional Primer Charge 41
<b>CHAPTER 3</b>	<b>FUNDAMENTAL THEORIES CONSIDERED IN THE DEVELOPMENT OF THE DIRECTIONAL PRIMER CHARGE</b> 42
3.1	Hydrodynamic Theory of Detonation 42
3.1.1	Chapman-Jouguet Theory 42
3.1.2	Zeldovich-von Neumann-Doering Model 43
3.1.3	Taylor Wave Analysis 44

	<b>Page</b>	
3.2	Acceleration of Metal Plates	45
	3.2.1 Classical Mechanics Model	46
	3.2.2 Gas Expansion Model	48
	3.2.3 Shock Physics Model	51
3.3	High Velocity Impact	54
	3.3.1 Shock Transmission	54
	3.3.2 Shock Attenuation	55
	3.3.3 Target Reaction	56
	3.3.4 Applicability of Fundamental Theories to The Directional Primer Charge	58
<b>CHAPTER 4</b>	<b>DESIGN OF EXPLOSIVELY - FORGED PROJECTILES</b>	<b>59</b>
4.1	Introduction	59
4.2	Formation of a Jet or Slug from a Shaped Charge	59
	4.2.1 Geometry of Collapsing Shaped Charge Liner	60
	4.2.2 Jet or Slug Formation	62
	4.2.3 Differences Between Conical and Hemispherical Liners	65
	4.2.4 EFP Formation	67
	4.2.5 Tip and Tail Velocity Differences	68
	4.2.6 Types of EFP Slugs	69
4.3	EFP Design Principles	71
	4.3.1 Compact Point-Focus Slug	72
	4.3.2 Compact Forward-Folding Slug	73
	4.3.3 Elongated Forward-Folding Slug	74
	4.3.4 Elongated Backward-Folding Slug	75
	4.3.5 Slugshot Hang-Up Clearance Charge	76
	4.3.6 Directional Primer Charge Slug	77

	<b>Page</b>
<b>CHAPTER 5      DIRECTIONAL PRIMER CHARGE PREMISE</b>	<b>78</b>
5.1      Introduction	78
5.2      Development of Concept of a Directional Mining Charge	80
5.2.1      Dilemma of The Sockets	80
5.2.2      Air Gap Phenomenon	81
5.2.3      Washer-in-Hole Myth	83
5.2.4      Swords-into-Ploughshares	83
5.2.5      Development of Hang-up Clearing Charge	83
5.3      Premise for Directional Primer Charge	84
 <b>CHAPTER 6      DEVELOPMENT OF THE DIRECTIONAL PRIMER CHARGE PROTOTYPE</b>	 <b>86</b>
6.1      Introduction	86
6.2      Disc Parameters	87
6.2.1      Disc Shape	87
6.2.2      Disc Thickness	87
6.2.3      Disc Material	87
6.3      Stand-Off Distance	88
6.3.1      Theoretical Calculation	88
6.3.2      Empirical Determination	88
6.3.3      Flash X-Ray Radiograph Confirmation	89
6.4      Explosive Type	90
6.4.1      Velocity of Detonation	91
6.4.2      Metal / Charge Mass Ratio	92
6.5      Detonation Chain	93
6.5.1      Detonator	93
6.5.2      Booster	93



	<b>Page</b>
6.6 Housing	94
6.6.1 Explosives Container	94
6.6.2 Nose Cone	94
<b>CHAPTER 7      LABORATORY TESTING OF PROTOTYPES</b>	<b>95</b>
7.1 Introduction	95
7.2 Witness Plate Tests	97
7.2.1 Stand-off Distance	97
7.2.2 Explosively-Forged Projectile Confirmation	100
7.2.3 Summary of Witness Plate Tests	101
7.3 Detonics Laboratory Testing	102
7.3.1 The Advanced Detonics Laboratory	102
7.3.2 Basic Design	102
7.3.3 Sets of Tests Undertaken	102
7.4 Experimental Techniques	103
7.4.1 Flash X-Ray Radiographs	103
7.4.2 Electronically – Timed Shorting Screens	105
7.4.3 Typical Set-up Dimensions	108
7.4.4 Time-Distance Data From First Set of Tests	108
7.4.5 Summary of Test Results	110
7.5 Discussion of Test Results	111
7.5.1 Relationship of Slug Velocity of Explosive Mass	111
7.5.2 Limiting Slug Velocity for Single Explosive Type	112
7.5.3 Comparison Between Slug Velocities for Same Cartridge Size	112
7.6 Correlation of Theoretical Models to Experimental Results	114
7.6.1 First Set of Tests Measurements	114
7.6.2 Gurney Model Velocity	114
7.6.3 Modified Gurney Model Velocity	114
7.6.4 Gas Dynamics Model Velocity	115

	<b>Page</b>
7.6.5 Shock Physics Model Velocity	116
7.6.6 Comparison of Calculated Velocities for Composition B	118
7.6.7 Comparison of Calculated Velocities for Different Explosives	118
7.6.8 Applicability of Theoretical Models	119
7.7 Summary of Conclusions Drawn from Surface Tests	121
<b>CHAPTER 8 ANALYSIS OF IMPACT OF HIGH VELOCITY SLUG ON ROCK</b>	<b>122</b>
8.1 Introduction	122
8.2 Air Shock Ahead of High-Velocity Slug	123
8.2.1 Velocity of Air Shock Wave	123
8.2.2 Effect of Air Shock Wave on Rock	124
8.3 Impact Shock of Metal Slug on Rock	124
8.3.1 Shock Phase – Duration and Attenuation	125
8.3.2 Plastic Flow Phase – Mushrooming of Tip	128
8.3.3 Effect of Slug Velocity on Penetration and Duration	130
8.4 Impact Pressure Pulse Profile	131
8.5 The Formation of Umbrella Cracks	133
8.5.1 Initiation of Umbrella Crack	133
8.5.2 Extension of Umbrella Crack	136
<b>CHAPTER 9 UNDERGROUND FIELD TESTING</b>	<b>137</b>
9.1 Introduction	137
9.2 Preliminary Tests	139
9.2.1 President Steyn	139
9.2.2 Randfontein Estates	139

	<b>Page</b>	
9.3	Comparative Tests	142
9.3.1	Village Main Tests Blasting Parameters	144
9.3.2	Village Main – First and Second Series of Tests	145
9.3.3	Village Main – Third Series of Tests	147
9.3.4	Village Main – Fourth Series of Tests	148
9.4	Summary of Results	148
9.5	Analysis of Results	150
9.5.1	Frequency Distribution Curves	151
9.5.2	Zero Socket Ratios	152
9.5.3	Additional Breakout	154
9.6	Economic Implications	155
<b>CHAPTER 10</b>	<b>CONCLUSIONS AND RECOMMENDATIONS</b>	<b>157</b>
10.1	Summary	157
10.2	Conclusions	160
10.3	Recommendations	161
<b>APPENDICES</b>	<b>(Presented in CD format)</b>	<b>162</b>
APPENDIX 1	Explosives	163
	A.1.1 Military Explosives	164
	A.1.2 Commercial Explosives	167
	A.1.3 Super Gelignite	170
	A.1.4 Village Main Field Tests	170
APPENDIX 2	Taylor Wave Equations	171
APPENDIX 3	Gurney Model Equations	186
APPENDIX 4	Gas Dynamics Model Equations	209
APPENDIX 5	Shock Physics Model Equations	227
APPENDIX 6	Advanced Detonation Laboratory Measurements	239
APPENDIX 7	Shock Effects Generated by the Directional Primer Charge	249
APPENDIX 8	Underground Test Measurements and Frequency Distribution Graphs.	270

	<b>Page</b>	
APPENDIX 9	Slugshot Photographs	317
APPENDIX 10	Advanced Detonics Laboratory Photographs	320
APPENDIX 11	Flash X-Ray Photographs	352
APPENDIX 12	Underground Tests Photographs	356
APPENDIX 13	Comparison of Theoretical Model Calculations of Disc Velocities with Measured Velocities for various Masses of Explosives and Discs.	375
A.13.1	A.D.L. Test Series I	376
A.13.1.1	Gurney Model	377
A.13.1.2	Aziz Model	390
A.13.1.3	Fickett Model	399
A.13.2	A.D.L. Test Series II	412
A.13.2.1	Gurney Model	413
A.13.2.2	Aziz Model	435
A.13.2.3	Fickett Model	448
A.13.3	A.D.L. Test Series III(a)	476
A.13.3.1	Gurney Model	477
A.13.3.2	Aziz Model	484
A.13.3.3	Fickett Model	488
A.13.4	A.D.L. Test Series III(b)	495
A.13.4.1	Gurney Model	496
A.13.4.2	Aziz Model	500
A.13.4.3	Fickett Model	503
A.13.5	A.D.L. Test Series IV	507
A.13.5.1	Gurney Model	508
A.13.5.2	Aziz Model	512
A.13.5.3	Fickett Model	515
<b>REFERENCES</b>		<b>519</b>

## LIST OF FIGURES

	<b>Page</b>
<b>Figure 1.1</b> Basic Configuration of Components of a Directional Primer Charge	26
<b>Figure 1.2</b> Practical Design for Directional Primer Charge	27
<b>Figure 1.3</b> Placement of Directional Primer Charge in Blasthole	28
<b>Figure 2.1</b> Title Page of von Baaders' Paper	33
<b>Figure 3.1</b> Initial Configuration for Explosive Projection of Metal Plate	49
<b>Figure 3.2</b> Space-Time Diagram for Metal Plate and Gas Motion	49
<b>Figure 3.3</b> Wave Phenomena During Plate Acceleration	52
<b>Figure 3.4</b> Graph of Interface Velocity versus Distance	53
<b>Figure 3.5</b> Graph of Shock Hugoniots	54
<b>Figure 3.6</b> Schematic Impact of Flyer Plate on Semi-Infinite Target	56
<b>Figure 3.7</b> Wave Model for Initial Phase of High Velocity Rod Impact	57
<b>Figure 4.1</b> Geometry of Collapsing Shaped Charge Liner	60
<b>Figure 4.2</b> Jet Formation by Shaped Charge Liner	61
<b>Figure 4.3</b> Velocity Difference between Jet and Slug from Conical Shaped Charges	62
<b>Figure 4.4</b> Jet Formation from Conical Shaped Charge Liners	63
<b>Figure 4.5</b> Jet Formation from 60 Degree Copper Cone	64
<b>Figure 4.6</b> Radiographs of Jet Formation Process of a Hemispherical Liner	65
<b>Figure 4.7</b> Radiographs of a Fully Developed Jet from a Hemispherical (Top) and Conical (Bottom) Liner	66
<b>Figure 4.8</b> Computer Simulation of EFP Formation	67
<b>Figure 4.9</b> Velocity Differences in Metal During Slug Formation	68
<b>Figure 4.10</b> Various Types of EFP Slugs	70
<b>Figure 4.11</b> Geometry of Acceleration of Liner Mass Element	71

	<b>Page</b>
<b>Figure 4.12</b> Basic Slug Shapes by Explosive Forging	72
<b>Figure 4.13</b> Compact Point-Focus Slug Formation	73
<b>Figure 4.14</b> Compact Forward-Folding Slug Formation	73
<b>Figure 4.15</b> Elongated Forward-Folding Slug Formation	74
<b>Figure 4.16</b> Elongated Backward-Folding Slug Formation	75
<b>Figure 6.1</b> Showing Directional Primer Charge Empty Assembly	86
<b>Figure 7.1</b> Schematics of Flash X-Ray Experiment	104
<b>Figure 7.2</b> Slug Velocity as a Function of Explosive Mass	111
<b>Figure 8.1</b> Wave Structure in High-Velocity Rod Impact	126
<b>Figure 8.2</b> Impact Pressure Pulse Profile for Slug Velocities of 1000 m/s and 2000 m/s.	132
<b>Figure 8.3</b> Formation of Umbrella Crack by Impact of Slug on the Toe of the Hole	134
<b>Figure 8.4</b> Extension of Umbrella Crack by Explosive Gas Expansion	136
<b>Figure 9.1</b> Frequency Distribution of Socket Lengths for Standard Round	151
<b>Figure 9.2</b> Frequency Distribution of Socket Lengths for 85 g Composition B	153
<b>Figure 9.3</b> Frequency Distribution of Socket Lengths for Super Gelignite	153

## LIST OF TABLES

	<b>Page</b>
<b>Table 7.1</b> Summary of Surface Tests	96
<b>Table 7.2</b> A.D.L. Flash X-Ray Set-Up Data	108
<b>Table 7.3</b> Slug Time-Distance Measurements	109
<b>Table 7.4</b> Summary of Test Results	110
<b>Table 7.5</b> Measured and Calculated Velocities	118
<b>Table 7.6</b> Measured and Calculated Velocities for 8 g Disc	119
<b>Table 7.7</b> Ranking of Explosives by Slug Velocity	121
<b>Table 8.1</b> Air Shock Characteristics	123
<b>Table 8.2</b> Impact Shock Characteristics	125
<b>Table 8.3</b> Advance of Interface for Various Slug Velocities	128
<b>Table 8.4</b> Penetration Parameters	130
<b>Table 8.5</b> Impact Pressure and Duration	131
<b>Table 9.1</b> Summary of Underground Test Programme	138
<b>Table 9.2</b> Summary of First and Second Test Series Results	146
<b>Table. 9.3</b> Third Test Series Results	147
<b>Table 9.4</b> Fourth Test Series Results	148
<b>Table 9.5</b> Summary of Results for All Test Series	149
<b>Table 9.6</b> Improvement in Blasting Efficiency	150
<b>Table 9.7</b> Incidence of Zero Sockets	152

## LIST OF PHOTOGRAPHS (IN MAIN TEXT)

		<b>Page</b>
<b>Photograph 2.1</b>	Showing Hang-Up Clearance Charge with its Accessories Underground	40
<b>Photograph 2.2</b>	Showing the Slugshot Set-Up in an Orepass with the Detonator and Fuse Attached	40
<b>Photograph 4.1</b>	Slugshot Hang-Up Clearance Charge Travelling at 2000 m/s Left to Right	76
<b>Photograph 5.1</b>	Showing Socket of Blasthole Remaining in the Stope Face After the Blast	80
<b>Photograph 5.2</b>	Perspex Model Blasting Showing the Formation of Umbrella Cracks at the Toe of the Hole	82
<b>Photograph 6.1</b>	Flash X-Ray Images No. 2 Showing Directional Primer Charge Slug Formation at 15 $\mu$ s and 125 $\mu$ s After Detonation	89
<b>Photograph 7.1</b>	Showing Directional Primer Charge Detonation Chain	97
<b>Photograph 7.2</b>	Showing Directional Primer Charge Positioned on a Witness Plate	98
<b>Photograph 7.3</b>	Showing Penetration of Primer Slug Through the Witness Plate	98
<b>Photograph 7.4</b>	Showing Witness Plate Penetration Results of Various Stand-Off Distances	99
<b>Photograph 7.5</b>	Showing Holes Punched Through Witness Plate	99
<b>Photograph 7.6</b>	Showing Two Slugs Embedded in Witness Plates	100
<b>Photograph 7.7</b>	Showing Flash X-Ray Tests Set-Up	106
<b>Photograph 7.8</b>	Flash X-Ray Images No. 1 Showing Directional Primer Charge Formation After 15 $\mu$ s and 75 $\mu$ s	107
<b>Photograph 9.1</b>	Showing Marked-Off Blasting Round	140



		<b>Page</b>
<b>Photograph 9.2</b>	Showing 32 mm Diameter Directional Primer Charge Cartridge with Plastic Wrapper and Elastic Band Covering of Open End to Prevent Ingress of Drill Chippings	140
<b>Photograph 9.3</b>	Showing 9-Hole Burn Cut	141
<b>Photograph 9.4</b>	Showing Explosives Used Underground at Village Main	144
<b>Photograph 9.5</b>	Showing Rock Broken Beyond the Length of Blasthole	154
<b>Photograph 9.6</b>	Showing Slug Remnants Embedded in the Rock at the Toe of the Hole	155

## LIST OF SYMBOLS

<b>P</b>	=	Pressure of a gas
<b>V</b>	=	Volume of a gas
<b>G</b>	=	Adiabatic exponent
$\mu$	=	Liner half-angle
<b>V<sub>G</sub></b>	=	Gurney limiting velocity
<b>V<sub>GM</sub></b>	=	Modified Gurney velocity
<b>V<sub>p</sub></b>	=	Gas Dynamics velocity
<b>V<sub>s</sub></b>	=	Shock Physics velocity
<b>U<sub>I</sub></b>	=	Interface velocity
<b>E<sub>G</sub></b>	=	Gurney constant
<b>C</b>	=	Charge mass
<b>M</b>	=	Disc mass
<b>z</b>	=	C/M
<b>U<sub>p</sub></b>	=	Particle velocity behind detonation front = $D / (\Gamma + 1)$
<b>D</b>	=	Velocity of detonation
<b>V<sub>GR</sub></b>	=	Velocity using reduced Gurney energy
<b>V<sub>pp</sub></b>	=	$U_p \cdot z / (z + 2)$
<b>E<sub>GR</sub></b>	=	Reduced Gurney energy
<b>a</b>	=	$(1 + 32C / 27M)^{1/2}$

$d_p$	=	Density of disc
$d_e$	=	Density of explosive
$C_p$	=	Acoustic velocity of disc
$S$	=	Shock adiabat
$R$	=	$\delta_p \cdot C_p / \delta_e \cdot D$
$r$	=	$S \cdot \sigma_p / \delta_e$
$P_p$	=	Interface pressure on disc
$P_g$	=	Interface pressure of explosive product gas
$P_o$	=	$\delta_e D^2$

# CHAPTER 1 INTRODUCTION

## 1.1 Hypothesis

This thesis describes the development of a shaped explosive charge, which will enhance the explosive's ability to break out rock in mining operations. Of particular value, is the shaped charge's application in narrow-seam, hard-rock mines. These are typified by the gold and platinum mines of South Africa, where the confinement of the rock in the narrow stopes constricts the break-out of the rock when blasted.

The most confined part of a stoping blasthole during blasting is the toe of the hole. Thus, the function of the shaped charge is to direct the explosive energy towards the toe of the blasthole. This is achieved by shaping the end of the explosive column and leaving a void between the explosive column and the rock at the end of the blasthole, in order to focus the explosive shock waves on the rock at the toe of the hole. These explosive shock waves, or detonation waves, which emanate from the toe of the explosive column can be further enhanced by using a shaped metal liner. This converts the explosive energy of the explosive column to the kinetic energy of a high velocity metal slug. This kinetic energy is then converted to impact energy when the slug strikes the rock at the end of the hole.

This thesis seeks to show that, by using such a specially designed explosive charge, the break-out of rock is sufficiently enhanced to produce a significant improvement in mining blasting efficiency.

As it takes the place of a bottom primer in the explosive column in the blasthole and it directs the explosive energy to the toe of the hole, this specially designed shaped charge is called a directional primer charge.

## 1.2 Preview of Contents

In this thesis the historical development of the explosive shaped charge is documented with particular reference to that of the explosively-forged projectile. The attempts to use shaped charge technology in mining are recorded. The successful modification of a military explosively-forged projectile is also discussed. This projectile has been used for clearing blocked ore passes in South Africa mines over the past decade. The thesis describes the classical theories of explosive detonation, particularly the Hydrodynamic Theory of Detonation showing the development from the Chapman-Jouguet model to the Zeldovich-von Neumann-Doering model and the Taylor Wave analysis (Davis 1987). This thesis also describes the mechanism of acceleration of metal plates driven by explosive detonation according to the classical mechanics model of Gurney, the gas dynamics model of Taylor and the shock physics model of Lambourn and Hartley (Gurney 1943, Taylor 1943, 1950, Lambourn & Hartley 1965 and Fickett 1987).

It will be shown that the shaped charge is enhanced by the presence of a metal liner and that a stand-off distance is required for the metal liner to accelerate to a high velocity before it impacts the toe of the hole. It will be shown that the impact of the high velocity slug is of such a magnitude that the rock at the toe of the hole can be compressed in excess of a millimetre. This is sufficient to cause a perpendicularly-formed umbrella crack at the toe of a blasthole. This is a phenomenon which has never been satisfactorily explained previously. This crack, when it is extended by the expansion of explosive gases which follow the detonation shock wave, assists in the break-out of the rock right up to the toe of the hole. This results in the following advantages for mining: -

- the blasthole sockets are eliminated
- the face advance becomes the length of the drilled hole
- the efficiency of the blasting operation increases proportionately.

Experimental measurements were made using flash X-ray radiograph and electronically-timed shorting screen techniques to determine the shape and velocity of the high velocity metal liner slug. The effects of different types of explosives were compared, as were the effects of different quantities of explosives. Tests were undertaken to demonstrate the forward punching power of the shaped charge and also to ascertain the optimum stand-off distance. The compatibility of various high velocity of detonation explosives with conventional mining explosives was also investigated.

A shaped charge which could act as a directional primer charge in the practical stoping operation has been designed. Underground tests were undertaken under full production mining conditions to compare the rock breaking effects of the designs of the various directional primer charges. These are compared in the thesis to conventional blasting practice and the differences recorded. It will be found that, on average, fewer and shorter sockets remained after the blast using a directional primer charge.

It will be shown that, depending on the mines' previous blasting efficiencies, the use of the directional primer charge can improve the blasting efficiency in South African hard rock mines by up to 15%.

### **1.3 Witwatersrand Practice**

Witwatersrand Practice is the name given to the system of mining employed on the South African gold and platinum underground mines (Watermeyer and Hoffenberg 1932, Biccard Jeppe 1946). These mines are typically deep-level, hard-rock, narrow-seam mines. Witwatersrand Practice has two characteristic mining operational components – stoping and development. (Cruise 1999).

#### **1.3.1 Stoping**

Stoping on South African gold and platinum mines is characterized by the mining of narrow seams of ore called “reef”. The width of the reef is usually less than one metre. The stoping width to mine a single reef horizon is of the order of one metre which is considered to be the minimum mining width to allow men to work in effectively. Traditionally, the blastholes are drilled horizontally in the reef plane with handheld pneumatic jackhammers to a depth of the order of one metre. Each blasthole generates about a ton of broken rock per blast. Thus, many holes are drilled each day to produce the tonnages required. In South Africa alone this is in the order of half a million holes per day, (AEL 2004). When past South African mining literature is studied (Watermeyer et al 1932, Biccard Jeppe 1946), it is apparent that, in reality South African stoping practice has changed little over the past century.

To open up a stoping area requires preparatory excavation. This takes the form of tunnels and rockpasses. This is often not in ore-bearing reef and thus is deemed to be an uneconomic activity. Hence, the quantity of stope face ready to mine is kept at a minimum and utilization of available stope face is at a premium. In order to maintain a constant tonnage rate to the mill to keep it running at maximum capacity, a constant volume of ground must be mined. If the stoping width is greater than the reef width, then the stoping width should be kept to a minimum to avoid unnecessary dilution with waste rock. With limited stope face and the stoping width being kept to a minimum, the only way to ensure maximum tonnage rate is to maximize the face advance. Any loss in face advance affects the total tonnage output of the mine. The old mining adage of “a blast lost is never regained” holds true.

### **1.3.2 Blasthole Sockets**

The pressures on mining production today can therefore be laid at the door of blasting efficiency. An efficient blast is one that maximizes face advance. It is accepted that the maximum that a face can advance per blast is the length of the blasthole drilled. In practice this is hardly ever attained due to inaccurate drilling, which causes too great a burden at the toe of the hole, resulting in the rock not breaking out to the full length of the blasthole, i.e. the leaving behind of blasthole sockets in the face. (see Chapter 5.2.1).

The presence of sockets in the face and their length is a good indicator of the efficiency of a blast. Sockets left behind after a blast are commonly 50 mm to 500 mm in length. Brinkmann (1994) states that a socket length of 300 mm is considered short by general blasting standards. To minimize the socket length or to eliminate the socket altogether is to increase the volume of rock broken per blast, thus increasing the blasting efficiency. In addition, there are many deleterious effects associated with the presence of sockets in stoping. Sockets can produce an uneven face advance. The resultant bulging of the face due to long sockets affects both the drilling and the breaking of the following round. Bulging of the face tends to become exaggerated with each succeeding round making the cleaning of the broken rock away from the face using in-line face scrapers more and more onerous. Although sockets indicate unbroken rock in the face, the rock that lies between sockets has been subjected to explosive energy and tends to be blast-damaged. The drilling of the next round is hampered by stuck drill steel caused by this fractured ground. Also sockets can pose a safety hazard in that they may contain unexploded explosive, which, if drilled into, can cause severe injury or death. Thus, the elimination of sockets is highly desirable in the mining industry for a number of reasons.

### **1.3.3 Development**

The second largest usage of explosives on South African deep level mines is development (or tunnelling). In order to begin stoping an amount of access development is required to be undertaken. This development usually consists of tunnels. These tunnels are called drives or crosscuts if horizontal, raises or winzes if advancing above or below the horizontal respectively. Shafts and rockpasses are special types of raises or winzes. The purpose of development is to open up the ore reserve for economic mining (or stoping) as quickly as possible. Thus, the rate of advance, (either the frequency of the blasts or the length of advance per blasted round) should be maximised.



Again, it is commonly accepted that the maximum length of a blasted round in a tunnel is the length of the drilled hole. This is rarely achieved in practice, resulting in sockets in the face.

#### **1.4 The Directional Primer Charge**

The rock at the toe of the blasthole, being that portion of the hole that is most confined, is the most difficult area to break out. Thus, it was realized that a blasthole requires more explosive energy at its toe than any other part of the hole.

In the old Witwatersrand Practice, this was achieved by placing a more powerful explosive at the toe, namely the placing of an ammon gelignite primer at the bottom of the hole whilst the rest of the column charge consisted of ammon dynamite cartridges.

Some 30 years ago a phenomenon was observed in blasted Perspex models in the blasting laboratory at the University of the Witwatersrand. This was the creation of an umbrella fracture which radiated outwards from the toe of the hole and was perpendicular to the axis of the hole. If this phenomenon could be replicated in rock under mining production conditions, then the rock burden would break out to the full length of the hole, thus eliminating hole sockets. (see Chapter 5.2.2).

In the Perspex models, the umbrella fracture occurred when there was a void between the explosive column and the end of the hole. Thus the creation of umbrella fractures in Perspex models became known as the “air gap phenomenon”.

Preliminary thoughts as to the cause of the air gap phenomenon was that it was the detonation wave of the explosive which travelled on forward down the hole as a shock wave that was responsible for the fracture. It was thought that such a shock wave through air, whilst strong enough to fracture Perspex, would not be strong enough to fracture rock.

Recent attempts to convert the use of military armaments for commercial uses saw the development of an explosively-forged projectile as a converter of explosive energy into impact energy. Thus was born the concept of an explosive gun. By using a metal liner at the end of an explosive column and having a stand-off distance in order to allow the metal liner to fully form into an ultra high speed slug, sufficient shock energy might be developed to fracture rock at the toe of the hole similar to that of the Perspex model namely, an umbrella fracture at the end of the hole.

This explosive gun was described as a directional primer charge and was patented by J.A. Cruise in 1989. (SA Patent No. 89/3235).

Figures 1.1, 1.2 and 1.3 are taken from the patent application.

Figure 1.1 shows the basic configuration of components of the directional primer charge: -

- a base charge of standard commercial explosive.
- a socket in the base charge in which to insert a standard commercial detonator.
- a high velocity of detonation explosive in front of the standard explosive.
- a metal liner in intimate contact with the high velocity of detonation explosive.
- a housing which contains the explosives and the metal liner and protrudes in front of the metal liner to provide a stand-off distance.

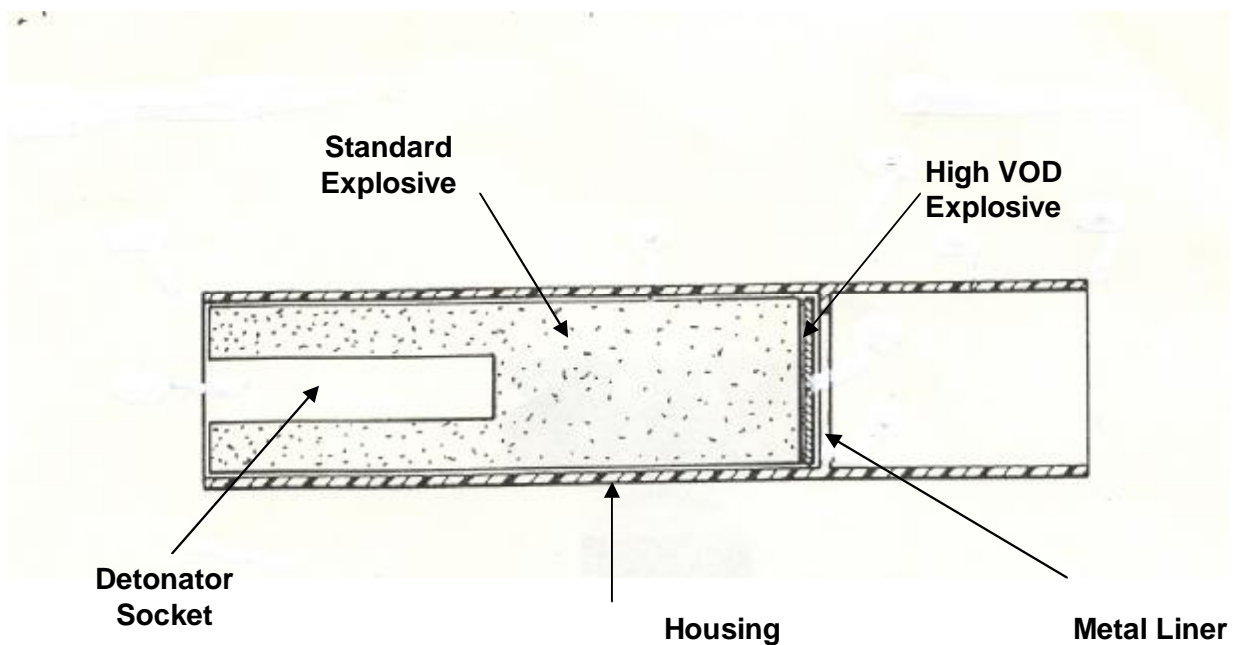


**FIGURE 1.1**

Figure 1.2 shows a more practical design for the directional primer charge: -

- the explosive used is a high velocity of detonation explosive of sufficient length for its characteristic velocity of detonation to be attained.
- the metal liner is formed in the shape of a dished disc of radius  $R$  to optimise the slug formation.

- the distance S is the optimum stand-off distance to allow the slug to fully form and to attain maximum velocity.
- the nose-cone is tapered to allow ease of access of the directional primer slug into the blasthole, allowing it to ride over drill chippings remaining in the hole.
- the degree of tapering is governed by the shape the metal liner disc takes when it is formed into a high velocity slug.
- this directional primer charge can be initiated by the explosive column of standard explosive cartridges placed behind it.

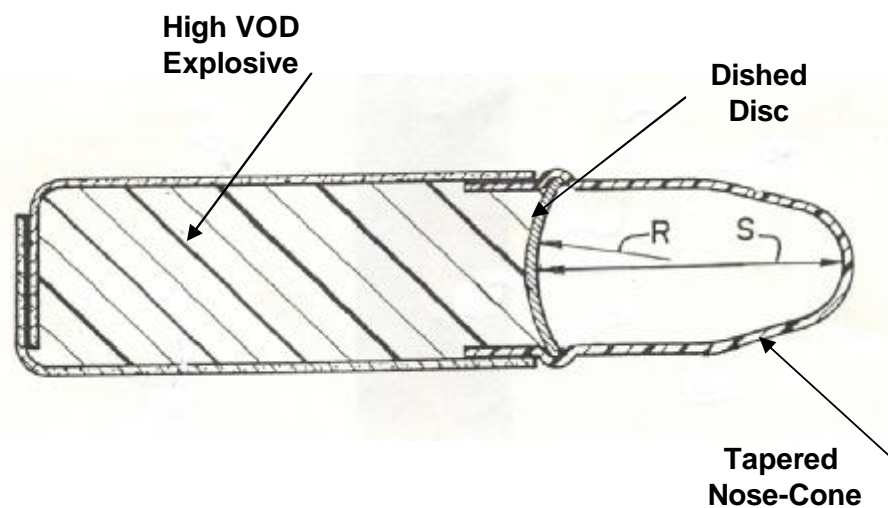


**FIGURE 1.2**

Figure 1.3 shows the placement of the directional primer charge in the blasthole. Note that the directional primer charge is placed at the toe of the blasthole and its function is to increase the breakout of rock at the toe of the hole. An explosive column of standard explosive is then placed behind the directional primer charge.

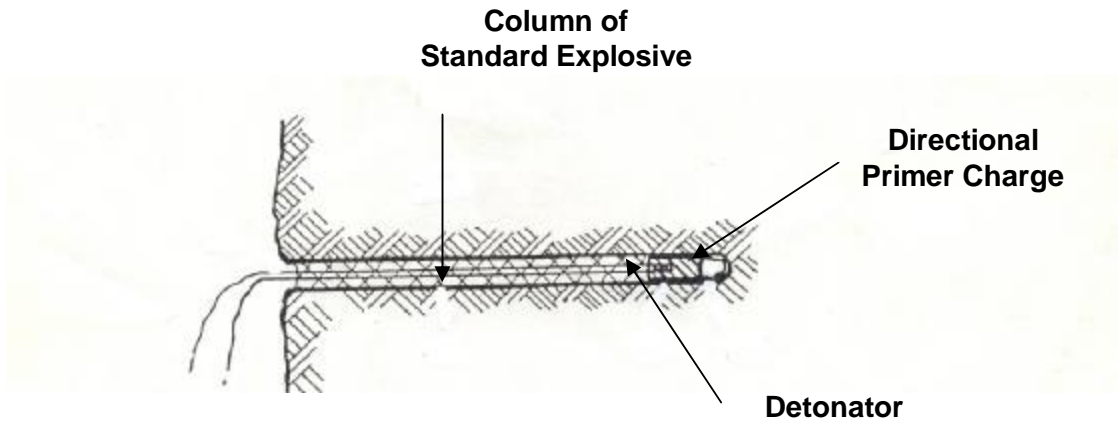


**FIGURE 1.3**

## **CHAPTER 2 HISTORICAL DEVELOPMENT**

### **2.1 Development of Explosives**

#### **2.1.1 Early Recognition**

The du Pont Blaster's Handbook gives the following time-line for the development of explosives and Alfred Nobel's contribution (du Pont Blaster's Handbook 1977). Explosives are traditionally accepted to have had their origin in the use of black powder by the Chinese in the tenth century. It was first mentioned by the Arabian Abd Allah in the thirteenth century. The formula for black powder was written down by the friar Roger Bacon in 1242. Its first use as a firearm propellant was around 1300 recorded by Schwarz. Its first documented use in mines was in 1627 in Hungary. However, the development of the science of explosives is generally accepted as coinciding with the discovery of nitroglycerine by Ascario Sobrero in 1846 and its commercial development by Alfred Nobel, beginning in 1860.

#### **2.1.2 Nobel's Contribution**

The development of the science of explosives is characterized by periods of intense activity and spectacular breakthroughs followed by long periods of dormancy. During the short period from 1860 to 1880, Nobel produced nitroglycerine on a commercial basis (1861), patented black powder – nitroglycerine mixture (1863), developed the first commercial detonator using mercury fulminate (1864-1867), mixed nitroglycerine with diatomaceous earth to produce dynamite (1866), patented the waterproofing of dynamite (1873), discovered blasting gelatin by dissolving nitrocellulose in nitroglycerine (1875) and finally used ammonium nitrate in gelatin dynamites (1879). Thus, most of the basic chemistry of explosives of today was discovered or developed by Nobel in a short, intense period over a century ago.

#### **2.1.3 Military Explosives**

Whereas Nobel was primarily involved in the development of commercial explosives, the military establishment developed explosives for use in warfare. Part of their research was to develop explosives which had greater stability, longer shelf-life and greater destructive ability. This led to the development of the high velocity of detonation explosives:- TNT (first used in World War I), RDX, HMX and their mixtures (first used in World War II and in widespread use today).

The physics of explosives and blasting is also characterized by breakthroughs, sometimes stimulated by increased activity of the military during war years. The Hydrodynamic Theory of Detonation, which in a modified form, still holds sway today, was first proposed independently by both Chapman and Jouguet at the turn of the century (Davis 1987). The ZND (Zeldovich – von Neumann – Doering) model of detonation was again arrived at independently by three researchers in three countries at the same time in the early 1940s. (Davis 1987).

Spurred on by the presence of World War II, Zeldovich of the Soviet Union, von Neumann of the United States of America and Doering of Germany all developed a similar model of detonation. Also during that war, the work of Taylor in describing analytically the motion of product gases behind the detonation front was developed, as were the elegant engineering equations of Gurney to calculate the acceleration of metal plates by explosives. Although there are only a few textbooks on the science of explosives and blasting, there is a large body of literature on it in the form of published papers many of which have only recently been declassified by the military authorities of various countries.

#### **2.1.4 Commercial Explosives**

Commercial explosives are those explosives that are widely used in the civil and mining industries. They are characterised by low cost and rapid turnover – buy it and use it. Therefore, they typically have a short shelf life of only a few months.

As they are a major cost item in production mining, there is a great commercial pressure to keep their cost down and their performance is often judged as the “most bang for the buck” or price per unit mass. The most widely used explosives tend to be those with the cheapest ingredients.

Nitroglycerine explosives as developed by Nobel in the nineteenth century, were the backbone of the mining industry for the next century. The classical nitroglycerine explosives consisted of a mixture of nitroglycerine, a sensitiser and plasticiser such as EGDN, a fuel and an oxidiser such as ammonium nitrate. In South Africa, three types of nitroglycerine explosives were used – ammon dynamite, dynagel and ammon gelignite. The cheapest was ammon dynamite, but it was water-soluble. The most expensive was ammon gelignite, but it was waterproof. Dynagel was manufactured as a compromise, being water-resistant for a period of a few hours and cheaper than ammon gelignite.

During the 1940's, it was realised that ammonium nitrate fertiliser had explosive properties. It was marketed under various acronymic names – ANBA was ammonium nitrate blasting agent, ANFO was ammonium nitrate fuel oil and ANFEX was ammonium nitrate fuel explosive. Due to its far lower cost than nitroglycerine explosives, it was readily accepted and used in the mining industry. However, it was water-soluble and therefore could not be used in wet holes.

To combat the water-solubility of ammonium nitrate, a manufacturing technique was developed to make it waterproof. Ironically, this consisted of dissolving the ammonium nitrate in water and adding binders to keep it in suspension in the form of a gel. These explosives were known as waternit gel explosives. Further refinements produced slurry and emulsion explosives which are used today. (Cruise 1999).

### **2.1.5 Composition B**

In developing the directional primer charge, which appeared to require the use of a high velocity of detonation explosive to drive the metal disc forward at a high velocity, in South Africa both the commercial and the military explosive manufacturers were approached. The manufacturers of military explosives proposed the use of Composition B.

Composition B is a mixture of RDX and TNT in the ratio of 64 % to 36 %. It is castable and stable to handle and is probably the most widely used explosive in high velocity of detonation.

Thus, the majority of trials of the directional primer charge used Composition B as the preferred high velocity of detonation explosive.

### **2.1.6 Super Gelnite**

During the trials of the directional primer charge, a commercial explosives manufacturer let it be known that they could manufacture a special formula ammonium gelnite that had a higher velocity of detonation than standard ammonium gelnite. Although its velocity of detonation was not as high as Composition B, due to its low cost of manufacture it was decided to do comparative tests with Composition B.

Thus, a full set of tests was undertaken using this specially formulated gelnite, which was dubbed "Super Gelnite".

## **2.2 Development of Shaped Charges**

The term shaped charge is a generic term which covers hollow charges and lined cavity charges. A hollow charge is an explosive charge with a hollow cavity at the end of the explosive opposite to the point of detonation. A lined cavity charge is a hollow charge in which the cavity is lined (with a metal or ceramic liner for example) and has a stand-off distance from its target. The two additional features of a lined cavity charge over a hollow charge, namely the liner and the stand-off distance, increases the effect of the hollow charge.

It is generally accepted in English speaking circles that the father of shaped charge technology is Charles Munroe, an American chemist, whose pioneering work was undertaken a century ago. However, knowledge of the hollow charge effects in blasting in mining predate Munroe by a further hundred years, as is evidenced by a publication by Franz von Baader in 1792.

Although shaped and hollow charge effects have been known for two hundred years, it was only in the last century that scientists became aware of its potential. It is in the last seventy years that it has become an integral part of military weaponry (Berkholtz 1985), Berkholtz (1985) and Walters and Zukas (1989) describe the development of shaped charge technology from the earliest Von Baader recorded reference through the various technological breakthroughs to the start of World War II when the military finally recognised the practical potential of the shaped charge.

These developments may best be presented as significant milestones in the following chronological order: -

### **2.2.1 Milestone 1 – Earliest Known Reference**

Shaped charges have been known in mining for over two hundred years. In the earliest known reference to the hollow charge principle, Baader published his paper on the “Investigation of a Theory of Blasting” in the Miner’s Journal of March 1792. (Von Baader 1792). In his paper, Von Baader presents a rebuttal of earlier, but misleading attempts at an explanation of the significance of hollow spaces in mine blasting operations.



# Bergmännisches Journal.

Drittes Stück. März, 1792.

I.

## V e r s u c h einer Theorie der Sprengarbeit, von Franz Baader, Doktor.

I.

Die Wirkungssphäre jeder Masse Pulver, deren Form ein Würfel oder eine Kugel ist, oder diesen nahe kommt, muß man sich gleichfalls als eine vollkommene Kugel denken, vorausgesetzt, daß diese ganze Pulvermenge sich mit einmahl entzündet, und die umgebende Masse von allen Seiten gleichen Widerstand leistet. — Die Größe des Radius dieser Wirkungssphäre ist sodann in geradem Verhältnisse der gleichzeitig entbundenen Kraft, d. i. der Güte und Menge des Pulvers, und dem verkehrten des Widerstandes, den ihr die Festigkeit der umgebenden Masse, oder was hier, besonders wichtig ist, der

Bergm. Journ. B. 1. St. 3. M Mangel

FIGURE 2.1 TITLE PAGE OF von BAADER'S PAPER

## **2.2.2 Milestone 2 – First Recognition Of Military Potential**

In 1883, von Foerster published his book on experiments with compressed guncotton (von Foerster 1883). Von Foerster recognized the application of hollow charges for military purposes.

“The detonation of the primer gives the detonation gases a direction away from itself, a direction towards the side opposite ... In explosive charges of shells, it is best to apply ... both the hollowing of the charge and the placing of the primer at the base of the shell, in order to obtain an increased action towards the head of the shell, in which direction also the object to be destroyed will almost always lie”. (Von Foerster 1883).

## **2.2.3 Milestone 3 – Munroe Effect**

About this time, the American chemist Munroe also experimented with guncotton and discovered the effects of hollow charges (Munroe 1888). His celebrated demonstration of imprinting elm and maple leaves in steel plates “to decorate the fireplace at the Cosmos Club” contributed to his fame and recognition as “the father of shaped charged technology” and firmly established the “Munroe Effect” in the science of explosives.

The Munroe Effect is the apparent concentration of explosive energy by the hollowing out of an explosive charge.

It is the focusing of the detonation wave which passes through the explosive charge and emerges as a converging wave due to the surface geometry of the hollow. Munroe further demonstrated the Hollow Charge Effect by tying sticks of dynamite around an empty tomato can and using it to a hole in a safe door. This was described and published in the *Popular Science* magazine in 1900 (Munroe 1900).

## **2.2.4 Milestone 4 – First Patents For Hollow Charges**

The first patents for hollow charges were applied for in 1910 (granted in 1912) by the Westfaelisch-Anhaltische Sprengstoff A.G. (WASAG). But, as stated by Schardin (Schardin 1954), the publications of von Foerster and Munroe must have been overlooked as the patent contained practically no innovations.

### **2.2.5 Milestone 5 – Practical Applications For Hollow Charges**

Two papers relating to the WASAG patents were published before World War I. The first (M Neumann 1911) concerned the cutting of iron beams and rails. It was found that, contrary to what was expected, namely, that the explosive should be placed in more intimate contact with the target, a “hollow space in the charge, specifically on the side of the item to be blasted, is approximately three to five times as effective”. The second paper (E Neumann 1914) described the influence of the cone angle in the hollow space on the perforation performance on TNT demolition charges. Neumann emphasized the military usefulness of these hollow charges.

### **2.2.6 Milestone 6 – Extent Of World War I Interest**

What the WASAG patent did achieve, however, was to attract the attention of the British Navy and Army. Naval Ordnance records show that in 1913 shaped charges were studied for use as torpedo warheads (Ordnance Board Minute 8220, 1913). The British Army, on the other hand, was more sceptical. It considered that the use of hollow charges in projectiles was impractical because it would be difficult to prevent the forward movement of the charge on impact. In addition a base fuse was not an acceptable feature at that time (Ordnance Board Minute 8847, 1913). Despite the demonstrated advantages of hollow charges, they were not used in World War I.

### **2.2.7 Milestone 7 – Early Russian Research**

The fact that “the principle of the shaped charge was neither introduced in the military explosive technology nor in other practical fields” was incomprehensible to Sukharevskii who conducted extensive practical tests in Russia in the mid-1920s (Sukharevskii 1925, 1926) (IBID). He noted that the dimensions of the perforations achieved with hollow charges were, to a certain degree, proportional to the dimensions of the cavity of the charge. Tragically, his research came to an end when he fell victim to one of Stalin’s purges.

### **2.2.8 Milestone 8 – The Case Of The Dimpled Blasting Cap**

The celebrated case in which Wood attributed the cause of death of a young woman to the dimpled cap of a blasting detonator, demonstrated that a liner of a hollow charge is transformed into a projectile of considerable penetrating power at a substantial stand-off distance (Wood 1936). This is the first instance of the hollow charge being used to produce a directional projectile.

### **2.2.9 Milestone 9 – Early German Military Initiative**

Finally, in the 1930s, the hollow charge principle was taken seriously in military circles. The German Army Ordnance initiated development in three areas of research viz.

- demolition charges with hemispherical and bell-shaped cavities for various charges
- rifle grenade with shallow spherical charge
- shaped charge projectiles for anti-tank guns

### **2.2.10 Milestone 10 – Liner Effect**

During the above research, Thomanek in 1938 accidentally discovered the effect of the liner (Thomanek 1960) on the penetration of the blast.

He established that conical, hemispherical or bell-shaped liners made of brass produced a five-fold improvement on the penetration over unlined charges. He was granted a secret German patent for his performance-enhancing liner in December 1939.

### **2.2.11 Milestone 11 – Development Of The Bazooka**

In January 1939, a Swiss, Mohaupt, approached the British and American military authorities with a new form of munitions, which he claimed to have developed. The Americans acquired the rights of the invention from Mohaupt. The essential features of Mohaupt's invention were similar to that of the American inventor, Hopkins. This was a bomb built with a shaped charge. The Mohaupt design was adopted for the Bazooka anti-tank gun (Green et al 1955). At about the same time the Germans developed a weapon similar to the Bazooka, a high explosive anti-tank rocket known as the Panzerfaust.

### **2.2.12 Milestone 12 – Jet Formation And Jet Target Interaction**

During the years 1941 to 1945, extensive experimental and theoretical research was undertaken in Britain, which led to the considerable increase in the knowledge of the complex mechanisms of jet formation and jet-target interaction.

By the end of 1942, it had been shown that the shaped charge effect was not the result of simply focusing the explosive energy, but was rather a complicated process involving: - the type, shape and size of the explosive charge; the distance between the liner and the target; and the medium through which the jet passed before reaching the target (Taylor 1941, Tuck 1943, Hill et al 1944, Berkholtz 1985, Walters and Zukas 1989).

At the end of the war, the collaboration between the British and American researchers was published in the seminal paper by Birkhoff, McDougal, Pugh and Taylor. (Birkhoff et al 1948).

Thus, by the end of World War II, the basic fundamental theory of shaped charges was understood. Out of this wartime research came the development of a particular type of shaped charge – the explosively-forged projectile or EFP.

## **2.3 Development of Explosively-Forged Projectile or EFP**

### **2.3.1 Ballistic Effect of Blasting Cap**

In a publication in 1936 (Wood 1936), Wood describes the unfortunate death of a young woman who was struck in the chest by a metal fragment as she opened the oven to check on the coal fire. Although the fragment was no bigger than a pin's head, she bled to death in a short time. Wood reasoned that the copper fragment, which was recovered during the autopsy, had come from an unexploded blasting cap which had been delivered in the coal and which had detonated in the fire. By experimenting with blasting caps and interrupting the detonation at various times, he was able to demonstrate the ballistic effect of the dimpled end of the blasting cap. He recreated the shape of the fragment that killed the women. In addition, Wood estimated the velocity of the fragment as approximately 1800 m/s.

### **2.3.2 Explosive gun**

In Germany in 1938, Thomanek discovered the importance of a metallic liner for the terminal ballistic effectiveness of shaped charges. By 1940, the Luftwaffe's Technical Academy's Ballistic Institute at Berlin-Gatow under the direction of Schardin, succeeded in making flash X-ray radiographs of the deformation process of shaped charge liners. These studies focused on hemispherical liners that, as the radiographs show formed an elongated plug that later segmented into a number of fragments.

In 1943, Colonel Misznay of the Hungarian Armed Forces demonstrated to Schardin, Thomer and Trinks from the German Weapons Office that if a suitable metal liner was used, considerable punching power over a long range could be obtained with a shaped charge. This effect held out great promise for the development of an explosive gun for armoured targets. Misznay's flat dish projectile was also studied using flash X-ray radiography., (Schardin 1954).

### **2.3.3 Flat Cone Charges**

After the war, the original German shaped charge work continued under Schardin at Saint Louis in France. The major focus of the research was both the conical liners and the projectile formation from the flat cone charges.

In the 1950s, on the initiative of Trinks, Thomanek began investigating shaped charges. In 1962, they were able to demonstrate a 200 mm calibre off-route mine based on the principle of a flat cone charge. This weapon set a tank on fire at a range of 80 metres. In a review paper by Held in 1977, this work with projectile-forming, flat cone charges produced armour-plate penetration performances of 100 mm depth at close range and 70 mm depth at long range. (Held 1977).

In the 1970s, the possibilities of improving EFP formation by means of disc shaped liners were studied extensively, primarily in the USA. These studies were supported by a number of numerical simulation programmes. In the early 1980s, an EFP was first tried out in mining to bring down hang-ups in sub-level caving (Lindroth 1982).

Towards the end of the Angolan war, the South African military manufacturer, Armscor, developed a remote-controlled off-route mine, an anti-tank EFP known as the “piering” (or flying saucer). Tests showed that this weapon, which consisted of a thick copper liner of mass 2 kg, explosively driven forward at almost 2 000 m/s, could cleanly penetrate 100 mm thick armour-plating. A demonstration on a captured Russian T57 tank showed the piercing could penetrate right through the tank, in one side and out the other (Cruise 1987).

## **2.4 Shaped Charges in Mining**

### **2.4.1 Post-War Attempts**

Although immediately after World War II there were many attempts to apply the newly-found shaped charge technology to mining operations, these were in the main unsuccessful on economic grounds (Lewis and Clark 1946, Huttl 1946, Clark 1947, Draper et al 1948, Davidson & Westwater 1949).

Further attempts were made during the next forty years and apart from the success as perforation charges in the oil industry, the only device that showed some potential, was an explosively-forged projectile as a safe, effective hang-up clearance charge (Austin & Pringle 1964, Austin 1964, Lindroth and Anderson 1982 and 1983).

In 1986, a device similar to that described by Lindroth was successfully developed and marketed on South African mines. This device was called the Slugshot, which was modified for use in the mining industry from the South African military’s P-charge. Its function was to clear hang-ups in rockpasses. (See Photographs 2.1 and 2.2).



**PHOTOGRAPH 2.1 SHOWING THE SLUGSHOT HANG-UP CLEARANCE CHARGE WITH IT'S ACCESSORIES UNDERGROUND**



**PHOTOGRAPH 2.2 SHOWING THE SLUGSHOT SET UP IN AN OREPASS WITH THE DETONATOR AND FUSE ATTACHED**



### **2.4.2 Slugshot**

A hang-up is the bridging or jamming of broken rocks in a rockpass or a draw-point. One method commonly used to bring down the hang-up was for a miner to climb up the rockpass and place a bomb of explosive cartridges against the jammed rock. Due to its extremely hazardous nature, this practice is forbidden by law in South Africa (Minerals Act 1991). Nevertheless, due to pressures for continuity of production, the law was often flouted, resulting in frequent injuries and death.

The advantage of the Slugshot was that it acted as an explosive cannon, which could be aimed at the hang-up from a remote distance. It was accurate to a range of over 100 metres. For a decade, it was used as a standard method for bringing down hung-up rockpasses throughout the mining industry (Cruise and Szendrei 1987). As a result of this success, there has been a renewed interest in shaped charges for use in the mining industry in the past fifteen years. Some applications have been more successful than others.

### **2.4.2 Other Shaped Charges**

Lay-on shaped charges for the breaking up of large rocks are now commercially available although still not in widespread use.

Research by the Chamber of Mines Research Organisation to develop a shaped charge for stoping using the jet formation characteristic of a metal lined shaped charge to simultaneously bore a hole and break-out the burden of rock proved commercially unsuccessful and the research was terminated (Giltner 1992).

As a result of the success of the Slugshot, which was able to transform explosive energy into impact energy sufficient to break large rocks, the concept of a similar directional charge for use in stoping operations was formed, developed and patented in 1989 (S.A. Patent No. 89/3235). This was the "Primerslug" or directional primer charge.

### **2.4.3 The Directional Primer Charge**

This stoping directional charge was much smaller than the Slugshot at a hundredth of its mass and a tenth of its diameter. It was designed to fit into a standard stoping blast-hole and to be located at the toe of the hole. It took the place of the primer charge and thus it is referred to as a directional primer charge, as described in Section 1.4 and shown in Figures 1.1, 1.2 and 1.3.

# **CHAPTER 3      FUNDAMENTAL THEORIES CONSIDERED IN THE DEVELOPMENT OF THE DIRECTIONAL PRIMER CHARGE**

## **3.1      Hydrodynamic Theory of Detonation**

The Hydrodynamic Theory of Detonation, although first proposed a century ago, still holds prominence today as the theory which best describes the act of detonation of an explosive.

Over the years, the original Hydrodynamic Theory of Detonation of Chapman (1899) and Jouguet (1905) has been modified by Zeldovich (1940), von Neumann (1942), Doering (1943) and Taylor (1941). In later years it has been further refined by many researchers.

### **3.1.1      Chapman-Jouguet Theory**

In 1899, the English chemist, Chapman (Chapman 1899), proposed that a detonation wave sweeping through an explosive gas could be considered to be a self-sustaining shock wave (Davis 1987). Chapman maintained that a shock wave travelling through a high explosive precipitates in its wake chemical reactions that supply enough energy to drive the shock wave forward through the explosive.

If this was the case, the equations that describe shock waves could also be used to describe detonation waves – as long as they reflect the state of the exploded rather than the unexploded gas. Some further analysis, however, revealed an important difference between shock and detonation waves. Whilst slowly driven pistons can produce weak, low-velocity shock waves, detonation waves are always strong and always propagate at a high velocity.

Since a detonation wave was observed to travel at a single characteristic velocity, depending only on the explosive through which it propagated, Chapman reasoned that conditions for detonation likewise had to be defined by the singular state. He therefore postulated that the pressure and material velocity for the detonation state of an explosive gas were defined by the unique minimum wave velocity. Chapman calculated detonation velocities according to this postulation and compared them with measured velocities and found that they showed remarkable agreement.

Concurrently in France, Jouguet (Jouguet 1905) had been working on similar lines and had shown that the minimum detonation wave velocity corresponds with the velocity of a sound wave in the hot, compressed, moving detonation products found in the shocked explosive. This meant there was a physical explanation for the fact that a stable detonation wave propagates under the condition described by the minimum detonation velocity.

By initiating a strong shock wave, a rarefaction would eventually travel through the detonated explosive and catch up with the overdriven wave to slow it down. This minimum velocity is called the Chapman-Jouguet velocity. Jouguet's arguments about how a shock wave might speed up to attain this minimum velocity were complicated and not convincing. Nevertheless, investigators could not dispute the experimental data, which seemed to confirm the theory's accuracy of prediction. The theory outlined by Chapman and Jouguet is still the framework on which the most widely accepted theories of detonation are constructed.

The Chapman-Jouguet theory was unsatisfactory in that it lacked a detailed explanation for what takes place physically in a detonation wave. Nevertheless, the fact that it predicted adequately the final state of the gas immediately after it had been detonated satisfied practical-mined explosives engineers.

### **3.1.2 Zeldovich-von Neumann-Doering Model**

The first significant attempt to explain the underlying physics of how chemical reactions are initiated by the shock wave and how they transfer energy to the overall flow of explosion products came from the theoretical work of three men, namely Zeldovich in the Soviet Union, (Zeldovich 1940), von Neumann in the United States of America (von Neumann 1942) and Doering in Germany (Doering 1943). They arrived at their conclusions independently and more or less simultaneously in the early 1940s.

Their key insight was to take the temperature and pressure of a shocked material as given and to concentrate on how chemical reactions in the shocked material proceeded. In other words, a shock wave in an explosive material is simply treated as a discontinuity in the material's properties. The material behind the infinitesimally thin shock wave is at high temperature and pressure, whereas the material in front of it is not.

The explosive's chemical reactions in contrast, are treated as taking place behind the shock wave in a short but finite time and in a steady reaction zone of small but appreciable thickness. They maintained that directly behind the shock wave the explosive is in a state where no chemical reaction has yet taken place. Further back, at the end of the reaction zone, a state is reached in which all energy-releasing chemical reactions have been completed.

Between the shock wave and the far end of the reaction zone must lie other states for partially reacted explosive. Hence, there is a sequence of chemical states in the reaction zone, and each state has its unique pressure and material velocity.

The Zeldovich-von Neumann-Doering (ZND) model for detonation finally enabled scientists to give a fair description of how a detonation proceeds. A shock wave propagating into undisturbed explosive material instantaneously compresses and heats it enough to initiate chemical reactions that, within several nanoseconds, release energy. This energy, in turn, preserves the conditions of high temperature and pressure necessary to drive the shock forward. When the reactions have run to completion at the end of the reaction zone, the gases expand to do work. The reactions are only slightly disturbed by the expansion that occurs behind the zone.

The velocity of the detonation wave should be at least equal to the Chapman-Jouguet velocity. If it is equal, then the final state of the explosive (and the initial state from which the explosive products expand to do work) is identical to the final state specified by the Chapman-Jouguet theory.

However if the velocity is greater, two possibly final states could result, one with higher pressure and material velocity than is stipulated by the Chapman-Jouguet theory and one with lower pressure and material velocity.

### **3.1.3 Taylor Wave Analysis**

In 1941, Taylor published a war-time classified paper that was declassified and republished after World War II (Taylor 1950). Taylor recognized that the Chapman-Jouguet theory avoided the necessity for studying the motion of gases behind the detonation front by making the assumption that small disturbances in the gas immediately behind the detonation front travel at the same speed, as the front itself.

Taylor studied the motion of gases behind the detonation front, recognizing the hydrodynamics of the burnt gas and the distribution of pressure behind the detonation front. He analytically solved the wave equations for polytropic gases and derived explicit solutions for product gas velocity, sound speed, density and pressure.

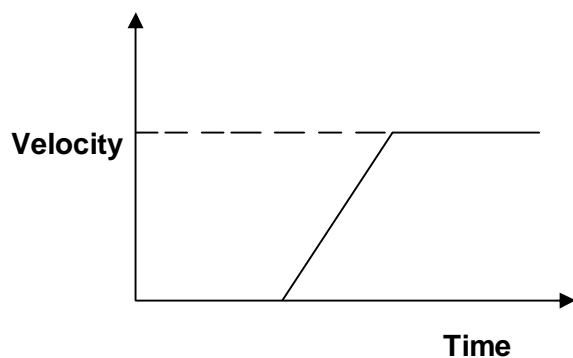
As Taylor appears to be the first person to adopt this approach, the expansion of the detonation product gases is often called the Taylor Wave. The practical importance of Taylor's analysis is that it provides the basis for calculating the parameters and values involved in explosive acceleration of projectiles. (see Appendix 2).

### 3.2 Acceleration of Metal Plates

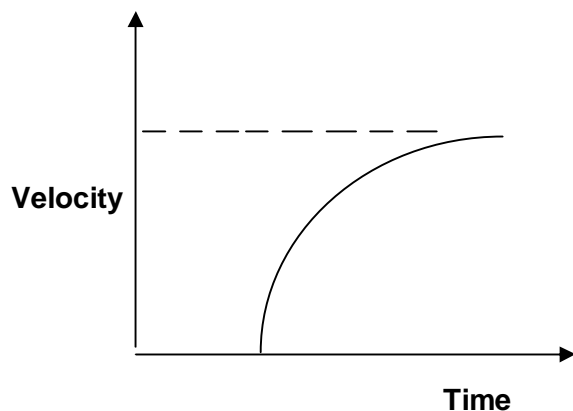
The nature of the acceleration of a metal liner from rest to its maximum velocity as an explosively-forged projectile has been the subject of much speculation and several questions need to be answered, i.e.

How does the metal liner attain its final velocity?

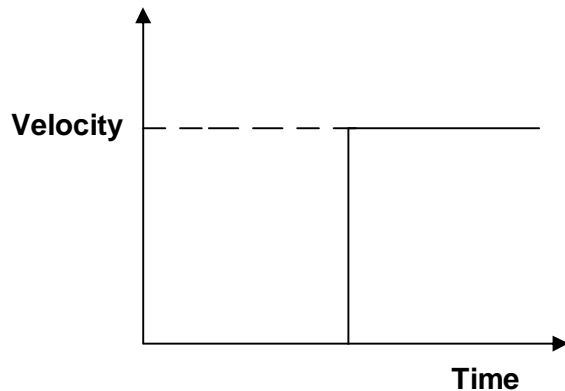
- i) Is it a constant acceleration from rest to final velocity over a short period of time similar to a piston push as shown in the diagram below?



- ii) Or is it more of an exponential acceleration due to the dissipation of expanding gases as shown below?



- iii) Or does it attain its maximum velocity instantaneously as a shock jump condition as a result of the impact of the detonation wave of the explosive as shown below?



All three of the above have been proposed at various times and each has its own merits.

The determination of the acceleration of metal plates by explosives is usually described by one of the three following models: -

- the Classical Mechanics model
- the Gas Expansion model
- the Shock Physics model

The first is an engineering model derived in 1943 by R.W. Gurney for calculating the velocities of shrapnel fragments. Gurney's model is an application of classical mechanics based on energy and momentum balances to consider only the end states i.e. the final velocities at the end of the acceleration phase of the metal fragments. It is commonly referred to as the Classical Mechanics Model or the Gurney Model. (see Appendix 3). The second is a scientific model based on the dynamics of the product gas behaviour of an explosion. It is referred to as the Gas Dynamics Model and is based on the Taylor Solution for the flow of the detonation product gases. This model has subsequently been refined by many researchers, inter alia Aziz et al (1960), Duvall et al (1969) and Yadav and Gupta (1988). (see Appendix 4). The third is an extension of the scientific model but is based on shock physics (Lambourn & Hartley 1965). (see Appendix 5).

### 3.2.1 Classical Mechanics or Gurney Model

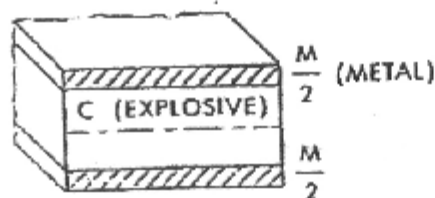
As previously stated, the Gurney model only considers the end states. Gurney make a few simple assumptions, namely: -

- the metal fragments are projected at right angles to the metal surface irrespective of the direction of detonation of the explosive.

- a specific energy (the Gurney Energy) which has a characteristic value for each explosive type, is that portion of the total chemical energy that is available to be converted into kinetic energy.
- the product gases have uniform density at any instant, i.e., the density is only a function of time.
- the product gases possess a spatially linear velocity distribution.

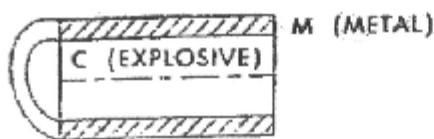
The Gurney method may be applied to any explosive/metal combination with a cross-section admitting one-dimensional transitional motion of the metal normal to its surface regardless of the direction of detonation. Based on the assumption of a known Gurney Energy for the explosive and a linear gas velocity distribution, the total energy balance for any simple geometry can be written out explicitly.

For symmetric configurations, such as a cylinder, a sphere or a flat sandwich, the energy balance equation is sufficient to define the final state (see Appendix 3).



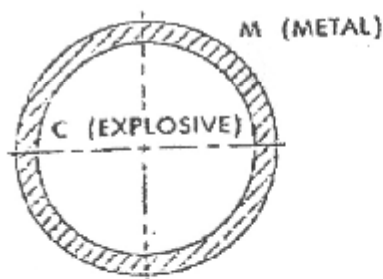
FLAT SANDWICH

$$v = \sqrt{2E} \left[ \frac{M}{C} + \frac{1}{3} \right]^{-\frac{1}{2}}$$



CYLINDER

$$v = \sqrt{2E} \left[ \frac{M}{C} + \frac{1}{2} \right]^{-\frac{1}{2}}$$



SPHERE

$$v = \sqrt{2E} \left[ \frac{M}{C} + \frac{3}{5} \right]^{-\frac{1}{2}}$$

For asymmetric configurations, such as an explosive between two plates of unequal mass or an open sandwich combination of metal and explosive, the momentum balance equation must be solved simultaneously with the energy balance equation. (see Appendix 3).

Over the years, it has been noted that Gurney Model predictions over-estimate measured velocity values. Weickert et al (1995) have suggested a modified Gurney Model to allow for this discrepancy. They suggest that the plate acceleration is a two stage process. In the first stage, the plate acquires momentum from the particle velocity behind the detonation wave. In the second stage, the plate acquires additional momentum by the usual Gurney expansion of gases. The energy available for the second stage is suitably adjusted from the standard Gurney value to account for the initial momentum coupling. The net effect is to predict a significantly lower terminal velocity for the plate. (Szendrei 1996).

This is referred to as the Modified Gurney Model.

### **3.2.2 Gas Expansion Model**

As previously stated, the Gas Dynamics Model is based on the Taylor Solution for the flow of detonation product gases. The essential features of the Gas Dynamics Model are described below using Figures 3.1 and 3.2 as illustrated. (see Appendix 4).

The initial physical configuration is shown in Figure 3.1. The flow after initiation at the surface O, and before the detonation front reaches the plate is given by a simple wave centered at O. This is the Taylor Wave. When the detonation front reaches the piston a shock is reflected. Being a weak shock, this is approximated by a compression wave. The piston is assumed to be rigid, so that it moves as a whole as soon as it is subjected to pressure. Thus its initial velocity increases smoothly from zero as it is accelerated.

The wave diagram that traces the gas/piston motion is given in Figure 3.2. Line OA traces the advance of the detonation front to its arrival at the plate at point A. Region I delineates the simple wave (Taylor Wave) region behind the detonation front. Region II represents the region of interaction between the Taylor Wave and the wave reflected from the piston. The piston itself accelerates smoothly along path AB. Path OC traces the backward flow of gases. Whether this is into vacuum or air is unimportant for the model. Since the reflected wave does not reach the boundary OC, the conditions at the boundary cannot give rise to any signals influencing the behaviour of gases in Region III.



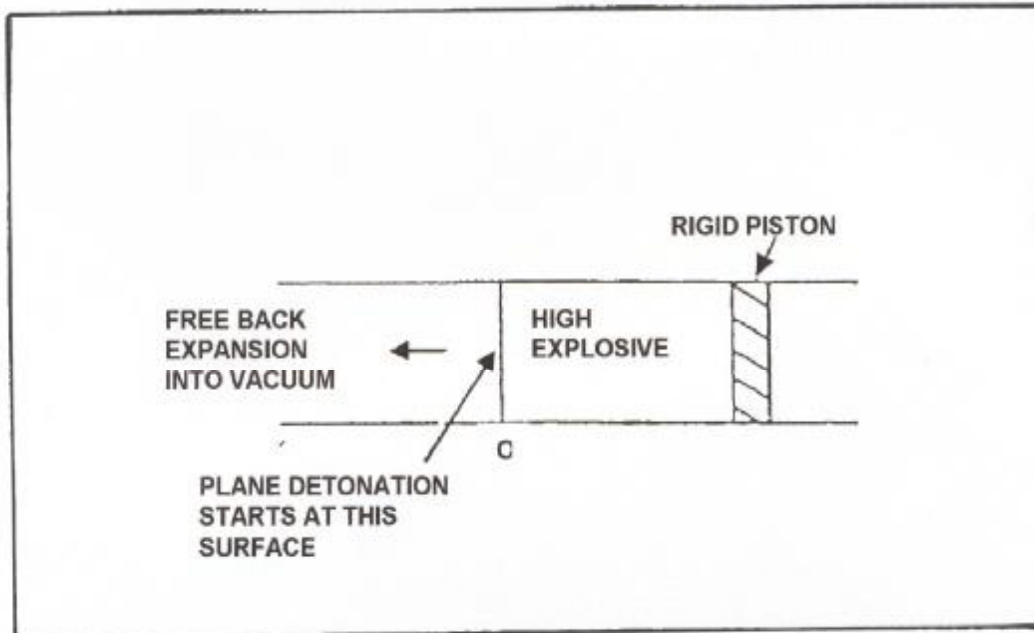


Figure 3.1: Initial Physical Configuration for Explosive Projection of Metal Plate

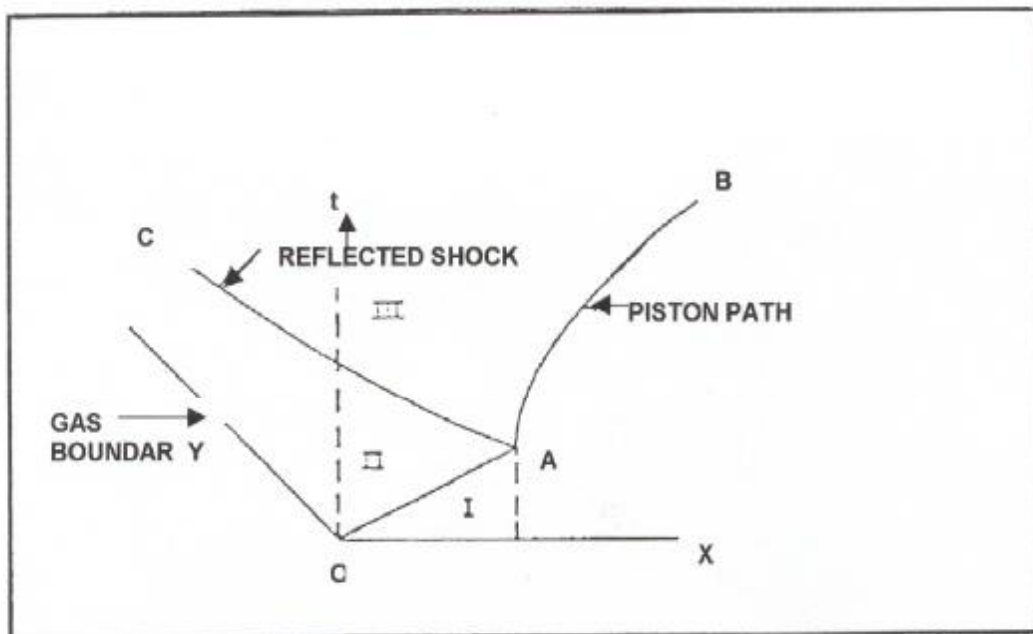


Figure 3.2: Space-Time Diagram for Metal Plate & Gas Motion

Figures 3.1 and 3.2 define the gas dynamic model of piston motion. Although it can be solved exactly and made to yield precise values of all parameters of interest, its basic validity must be assumed *a priori* and judged against accuracy of its predictions. The model assumptions, though simple in concept, lead to certain implications of fundamental importance.

The wave assumption for the reflected shock in Region III gases implied that the linearity of the characteristic equation of Taylor's solution holds good even behind the front of the reflected wave, so that the equation holds along the piston path.

The assumption of a rigid piston obviates the necessity of considering wave phenomena in the piston itself. In an incompressible material acoustic velocity is infinite, and all parts of the piston start moving as whole immediately after the application of pressure on its surface. The subsequent motion of the piston is then governed by Newton's laws of motion.

The refinements made by subsequent researchers may be described as follows: -

Aziz et al (1960), assumed that

1. The gas flow is one-dimensional and implicitly therefore, the lateral extent of the plate and the explosive is infinite.
2. The detonation wave is planar.
3. The piston is rigid and incompressible – therefore no reflective waves occur within the plate.

The Aziz model links the limiting velocity to the characteristics of the explosive i.e., the velocity of detonation and the adiabatic exponent  $\Gamma$  of the detonation product gases, and to the charge-to-metal mass ratio. In the simplest formulation,  $\Gamma = 3$  is assumed. Yadav and Gupta (1988), later derived a solution that admits a general solution of  $\Gamma$ .

**Note:**

Adiabatic means without loss or gain of heat. Adiabatic change is a change in the volume and pressure of the contents of an enclosure without exchange of heat between the enclosure and its surroundings.

The adiabatic equation  $PV^\Gamma = \text{constant}$  expresses the law of variation of pressure (P) with volume (V) of a gas during an adiabatic change,  $\Gamma$  being the ratio of specific heat at constant pressure to that at constant volume.

The value of  $\Gamma$  is approximately 1,4 for air at standard temperature and pressure (stp). (Chambers Dictionary of Science and Technology 2000).

### **3.2.3 Shock Physics Model**

The Shock Physics Model allows for the compressibility of the metal plate and describes the transmitted and reflected waves in the metal plate and the explosion product gases. Appendix 5 describes a simple wave model of explosive-plate interaction.

When a detonation wave strikes a metal plate at the end of an explosive column, a shock wave is transmitted into the plate and a rarefaction wave is reflected into the detonation products. Following the detonation wave is the Taylor wave, a rarefaction centred at the back surface (i.e. plane of initiation) of the explosive. This is transmitted into the plate as a rarefaction wave following the shock wave.

If the shock wave is “weak”, i.e. third order terms in particle velocity, density, and acoustic velocity are negligible, the entropy is unchanged and the flow is isentropic. (Entropy is the quantity which measures the extent to which the energy of a system is available for conversion to do work. Any process in which no change in entropy occurs is said to be isentropic). In this approximation, the locus of the states which can be connected by a shock wave is identical to the states that can be connected by adiabatic compression. In particular, this means that the flow behind a forward-facing shock front moving into a region with constant state is a forward-facing simple wave. Thus, the flow behind both the incident (detonation) shock front in the explosive and the transmitted shock front in the metal is a simple wave.

The state behind the transmitted shock wave is characterised by a particle velocity equivalent to the velocity of the interface between the explosive and the plate. The transmitted shock wave, on reflection from the free surface of the plate, creates a rarefaction wave that moves back towards the interface between the plate and the explosion products. In order to maintain conservation of momentum in which the forward shock wave velocity generates an equal rarefaction wave velocity in the opposite direction, the free surface of the plate is abruptly accelerated to twice the velocity of the particle velocity.

The plate begins to move as a “rigid” whole as soon as the rarefaction wave reaches the interface. Seen in terms of this model, the so-called initial velocity of the plate is twice the velocity at the interface.

Since the detonation products are still at a high pressure, and the pressure in the metal has been released by rarefaction, a second shock wave of lesser amplitude is induced in the moving plate. This second shock wave again reflects off the plate free face and thus increases its velocity. The reverberation of these shock and rarefaction waves within the plate continues until the pressure in the gas reaches a level where further release of pressure by the rarefaction wave does not cause the gas particles to move faster than the metal plate (Yadav & Gupta 1988).

Figure 3.3 shows the wave phenomena during plate acceleration and Figure 3.4 shows the reverberation of the interface on a velocity – distance diagram. Its step function is compared to the smooth velocity increase of the rigid piston gas dynamics method (Lambourn and Hartley 1965).

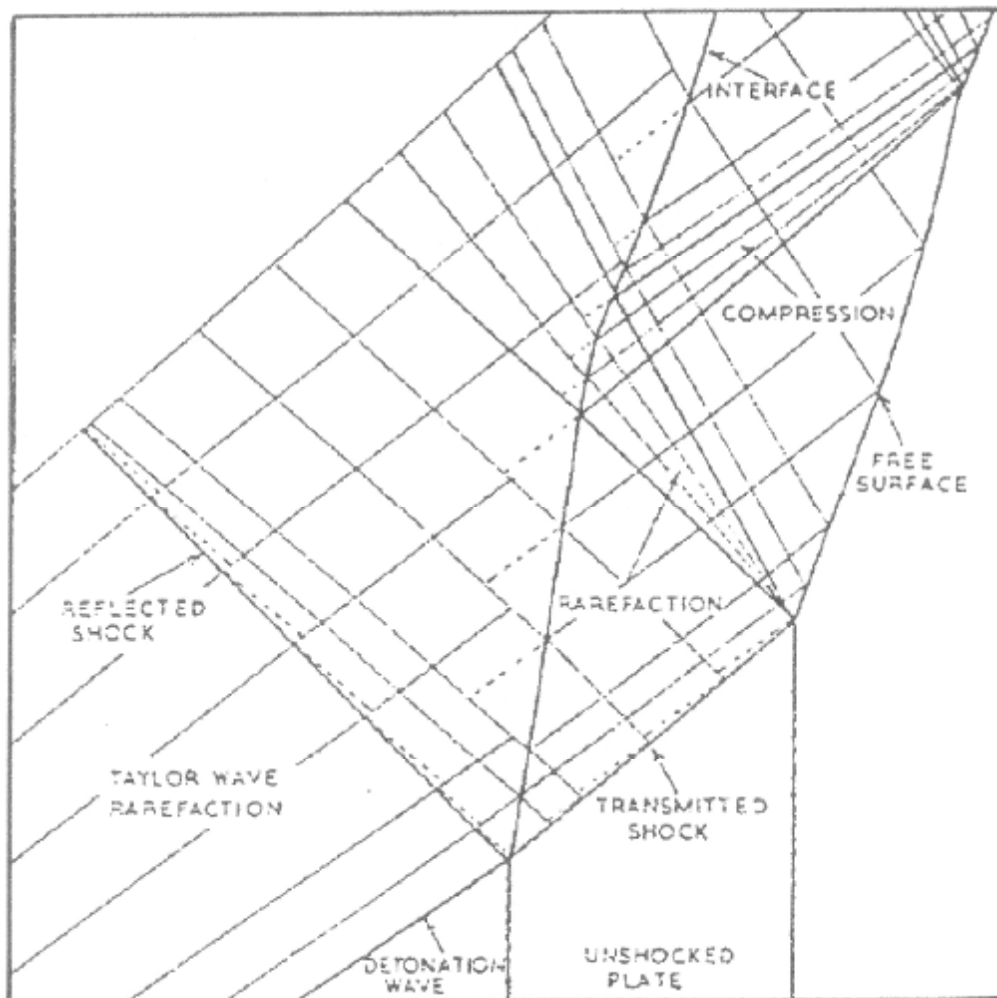


**FIGURE 3.3 WAVE PHENOMENA DURING PLATE ACCELATION**

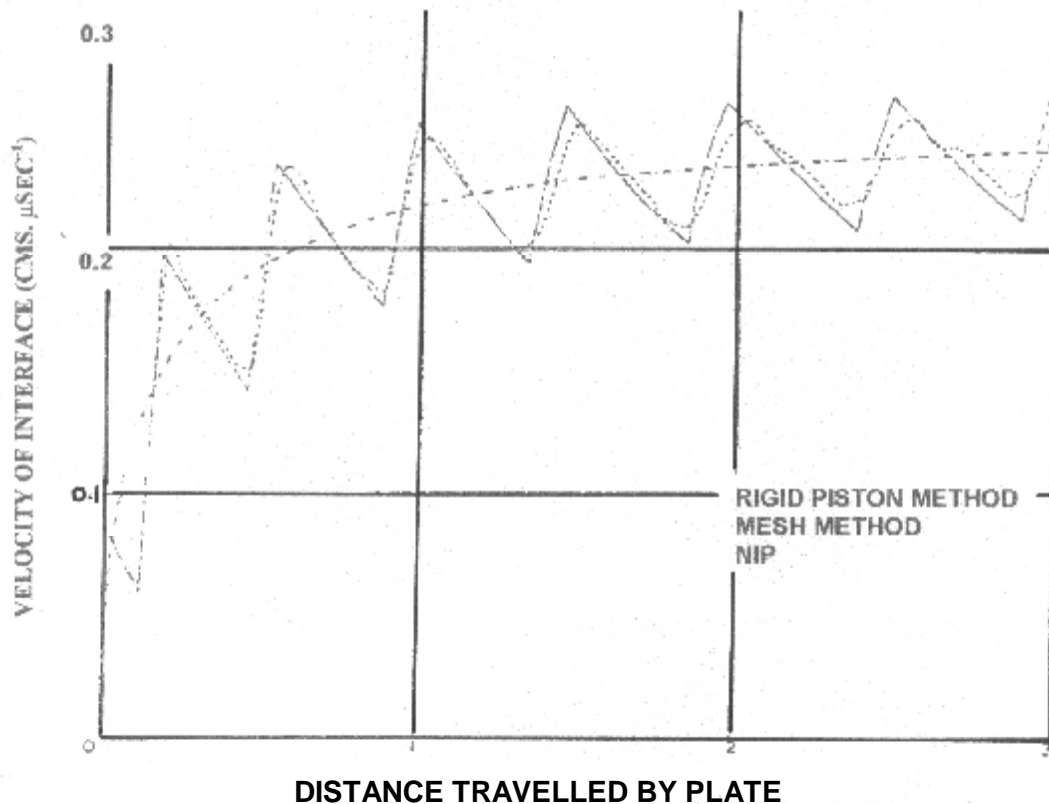


**FIGURE 3.4 VELOCITY-DISTANCE PROFILE**

Lambourn and Hartley (1965) showed that a thin steel plate is accelerated to about 80% of its final velocity after the first reflection of the transmitted wave off the gas-metal interface and that after six reflections, the increase in velocity is negligible.

Fickett (1987) reformulated the Gas Dynamic Model equations to reflect directly the dependence of plate motion on time. From the acceleration time calculated, the number of reverberations can be determined.

The Shock Physics Model essentially describes the acceleration of a metal plate as a jump condition caused by the impact of the detonation shock front.

Implicit in the velocity calculations are the following assumptions: -

- the mass of explosive takes no part in determining the final velocity of the plate. All that is required is that there is a sufficient length of column charge to allow the explosive to run up to its characteristic velocity of detonation.
- the mass of the plate takes no part in determining the final velocity of the plate. The shock is assumed to drive the plate as a rigid whole at a velocity of twice the particle velocity at the interface.

### 3.3 High Velocity Impact

High velocity impact is defined for purposes of this thesis as a stationary target being hit by a projectile travelling in excess of 1000 metres per second. A characteristic of the high velocity impact is that both the projectile and the target materials tend to undergo extensive plastic deformation and flow. A feature of this type of impact is crater formation by compact projectiles and penetration channelling by rod-like projectiles. The impact of the **directional primer charge** slug on the hard brittle rock at the toe of a hole in massive rock is considered.

#### 3.3.1 Shock Transmission

Upon impact shock waves are generated in both the target and the projectile. The response of both the target and the projectile corresponds to uniaxial stress and material flow. Under the influence of material compressibility, a region of compressed material is formed bounded by shock fronts moving away from the interface into the projectile. The interface itself moves into the target at a constant velocity.

Densities, however, may be different in the two shocked regions. This can be demonstrated graphically using the shock Hugoniot for the target and projectile and the method of impedance matching. A Hugoniot is the characteristic curve for a material showing the relationship between pressure and the resultant particle velocity of that material. It is a unique curve for each material.

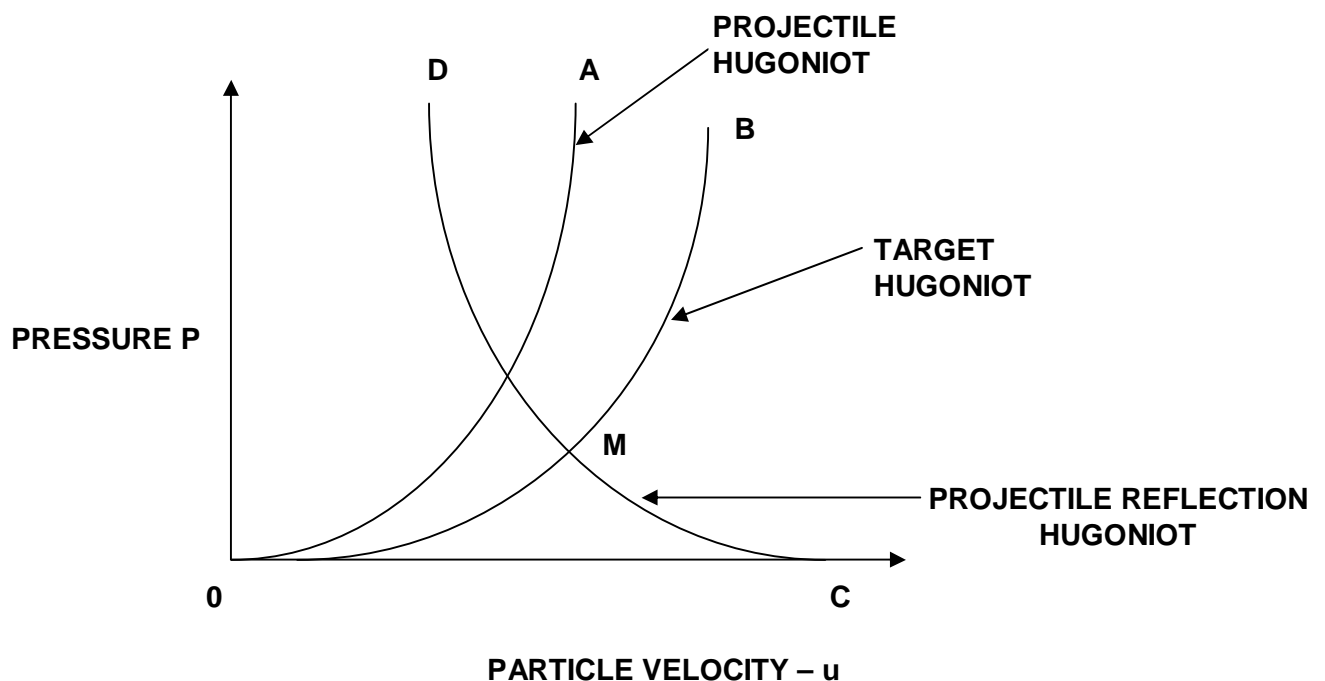


FIGURE 3.5 GRAPH OF SHOCK HUGONIOTS

OA represents the Projectile Hugoniot whose mirror image CD is its reflected Hugoniot, the Projectile Reflection Hugoniot. OB is the Target Hugoniot which is of a similar shape to the Projectile Hugoniot. As there is only one point that satisfies the conditions that both the pressure and the particle velocities of the target and the reflected shock waves be the same, i.e. the intersection of the two Hugoniots, it is this point M that describes the material states at impact.

This graphical solution of shock transmission and reflection is known as the method of impedance matching.

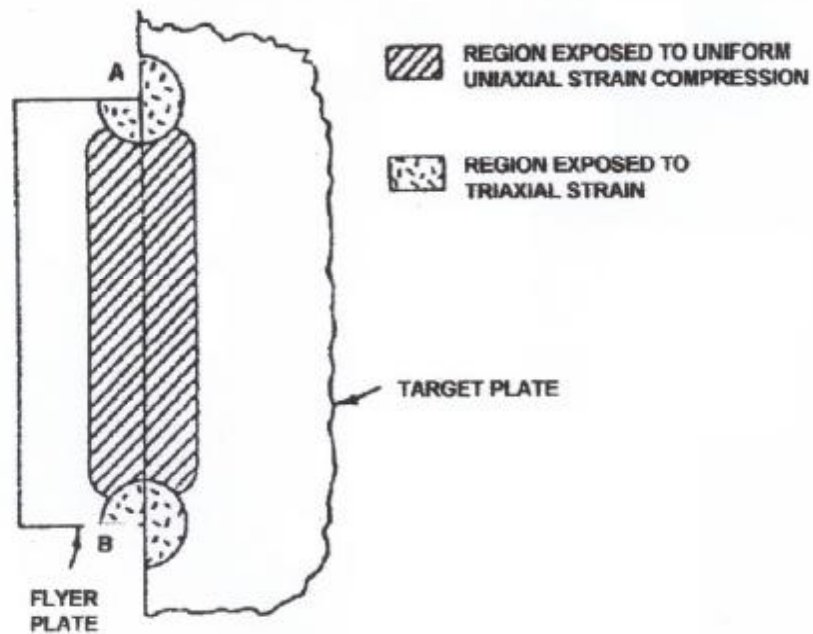
### **3.3.2 Shock Attenuation**

Attenuation of shock waves can be ascribed to many factors such as dissipation of energy by viscosity, heat etc. In the creation of shock waves through impact, it is often the geometry of the projectile which is most important. The projectile is of finite size and consequently there is a presence of free surfaces.

When shock waves encounter free surfaces, they are reflected as rarefaction waves. These in turn reduce the pressure behind the shock wave. It has been shown that rarefaction waves behind a shock wave always travel faster than the shock wave and thus will always overtake it.

The process of attenuation can be illustrated in general terms by considering a flyer-plate impacting normally on a target of large dimensions.

If the flyer-plate impacts a flat surface normally, then a state of pure one-dimensional strain will be produced in both the plate and target. The stress input to the target is essentially a square wave whose amplitude is determined by impact velocity and material Hugoniots. However, the presence of lateral faces will lead to a substantial change of the pressure pulse in time as illustrated schematically in Figure 3.6.



SCHMATIC IMPACT OF A FINITE FLYER PLATE ON A SEMI-INFINITE TARGET AFTER IMPACT EQUAL TO HALF THE SHOCK TRANSIT TIME THROUGH THE PLATE THICKNESS. SOURCE: DeCARLI & MEYER (1981).

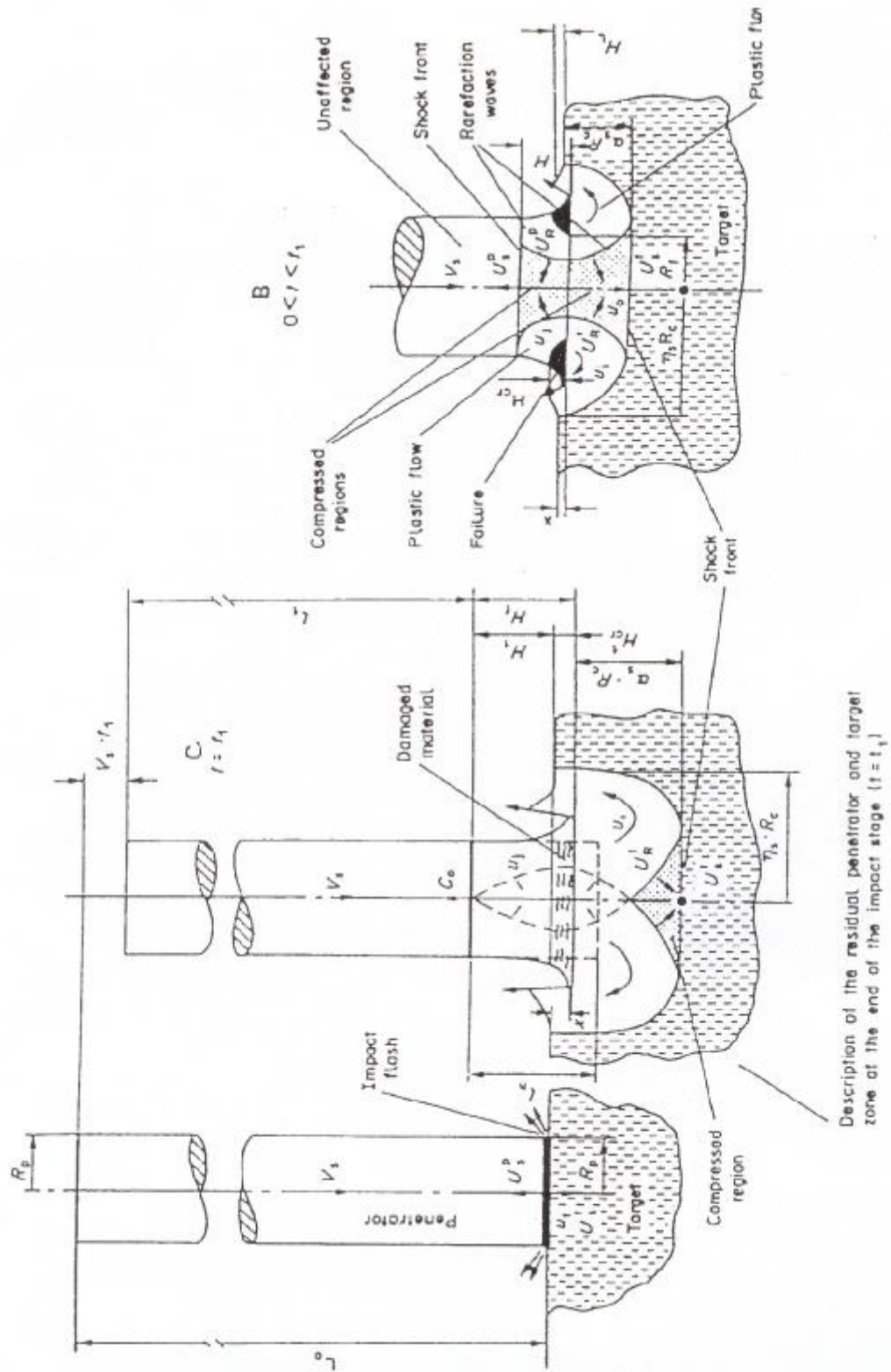
FIGURE 3.6

### 3.3.3 Target Reaction

The impact of a high-velocity rod on a target is shown diagrammatically in Figure 3.7.

On impact, the kinetic energy of the rod is transferred as impact energy to the target. A shock wave is generated in the target and a reflected shock wave is generated in the rod. Both the rod and the target undergo compression in the area of impact. Rarefaction waves are generated at the sides of impact zone. As the material has a free face in which to move, plastic flow can occur and also failure of the material as shown. The central portion of the impact zone undergoes compression. After impact, the characteristic impact crater is formed with its raised rim and its raised conical centre.





WAVE MODEL FOR INITIAL PHASE OF HIGH-VELOCITY ROD IMPACT  
SOURCE: RAVID, BODNER, HOLOMAN (1987)

FIGURE 3.7

### **3.4 Applicability of Fundamental Theories to the Directional Primer Charge**

It is important to understand the physics of the detonation of an explosive and the effect that a detonation wave has on a metal liner. It is also important to understand the nature of the shock waves that are generated within the metal liner and the impact effect of that high-velocity metal slug, formed from the liner, on a target.

The directional primer charge consists of a high explosive with a metal liner, which, on detonation, forms into a high-velocity slug, which then impacts on the rock at the toe of a blast-hole.

In this chapter, the Hydrodynamic Theory of Detonation assists in determining what type of explosive to use. In the Acceleration of Metal Plates, three models are presented which can be tested and measured against laboratory-type experimental results. The High Velocity Impact presents the mechanics of shock transmission and its likely effects on a target.

A thorough understanding of the mechanisms involved assisted in the design of the prototype directional primer charge.

# **CHAPTER 4      DESIGN OF EXPLOSIVELY- FORGED PROJECTILES**

## **4.1      Introduction**

A metal liner can be designed to produce either a jet stream of metal fragments or a high velocity single slug of metal. The thin jet stream can consist of up to fifty individual fragments and is used as a cutting tool. It has been widely used in the demolition of steel structures, where it can cut through steel girders with precision and at a predetermined instant in time. The high velocity slug or explosively-forged projectile (EFP) uses most of the mass of the metal liner to form a single compact slug, and is used for high velocity impact on a target. EFPs have been used successfully as anti-tank weapons and shatterers of large rocks in mines. (see Chapter 2.3 Development of Explosively-Forged Projectiles and Chapter 2.4 Shaped Charges in Mining).

The velocity range of EFPs is generally of the order of 1000 m/s to 3000 m/s and they can have a mass of up to 2 kg.

As previously described in Chapter 2.3 the phenomenon of the EFP was only recognised 70 years ago by Wood in 1936 and subsequently developed during World War II and its aftermath. Its use as an anti-tank weapon was demonstrated 40 years ago and as a mining tool to bring down hung-up rockpasses only 20 years ago.

This chapter will briefly describe how EFPs are formed and the design principles in forming them. A more detailed description can be found in the literature.

## **4.2      Formation of a Jet or a Slug from a Shaped Charge**

Flash X-ray radiographs and ultra-high speed cameras have played an important role in demonstrating the development of ultra high speed jets or slugs from metal liners by capturing their image split-seconds after detonation of the explosive primary source of energy.

The formation of a jet stream of ultra-high-velocity particles or a slower slug of greater mass are often considered to be two mutually exclusive results of metal lined shaped charges (Pugh Et Al (1952) and Chou & Carleone (1977)). The essential difference in the manner of jet or slug formation is related to the geometry of the liner.

#### 4.2.1 Geometry of Collapsing Shaped Charge Liner

The transformation process of the collapse of an at rest metal liner into high velocity metal particles or a slug is illustrated in Figure 4.1.

For rotationally symmetric shapes, the deformation of the liner caused by the detonation pressure wave can be described by the hydrodynamic theory of convergent flow.

The detonation wave velocity has an apparent velocity along the surface of the liner. A given element of the liner is accelerated to a velocity which makes an angle with the normal to the liner section in the direction of the detonation.

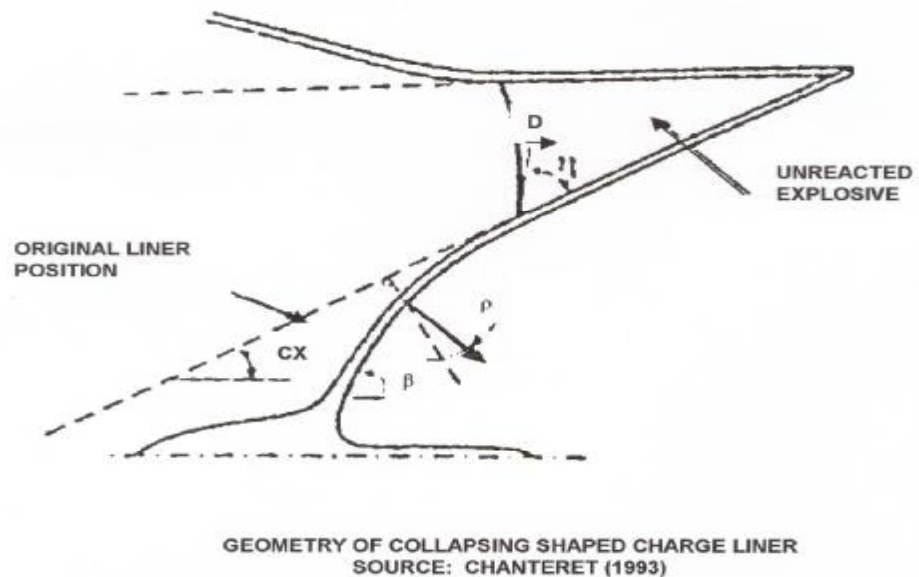
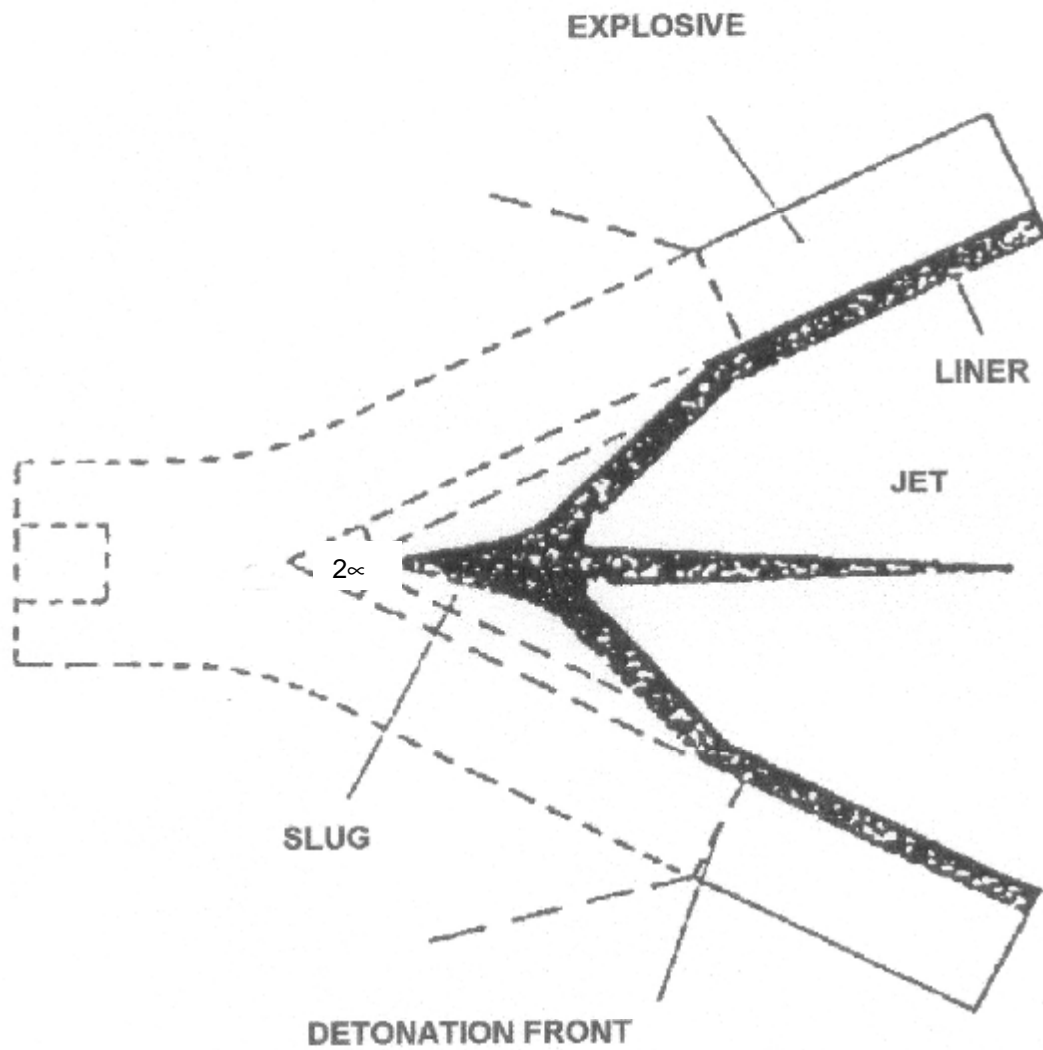


FIGURE 4.1

In the hydrodynamic model of jet formation each ring of material is thus projected both radially and in the direction of the detonation wave as a converging circle.

Conservation of momentum dictates that the flow of the liner material, which reaches the axis of symmetry will split into two flows, oppositely directed. (As shown in Figure 4.2).

The flows form the jet which streams ahead of the collapse point and the slug which follows on behind.



JET FORMATION BY SHAPED CHARGE LINER  
SOURCE: HORNEMANN ET AL 1987

FIGURE 4.2

## 4.2.2 Jet or Slug Formation

Various geometrical factors contribute to the fact that the jet is characterised not by a single velocity but by a velocity gradient. This velocity gradient ranges from the jet tip velocity to the slug velocity.

It should be noted that although the above jetting model represents simplistic idealisation, it only demonstrates the basic principles of jet slug formation.

As the cone angle increases (i.e. the liner becomes flatter), the difference between the jet tip and the slug velocities gradually diminishes until the jet fragments and the cone mass have the same velocity. The jet fragments are then absorbed into the slug mass. Thus, for a flat cone with a cone angle greater than a critical value, which is approximately  $140^\circ$ , there is not jet formation, just a slug.

Figure 4.3 shows the relative velocities for jets and slug for different liner half-angles.

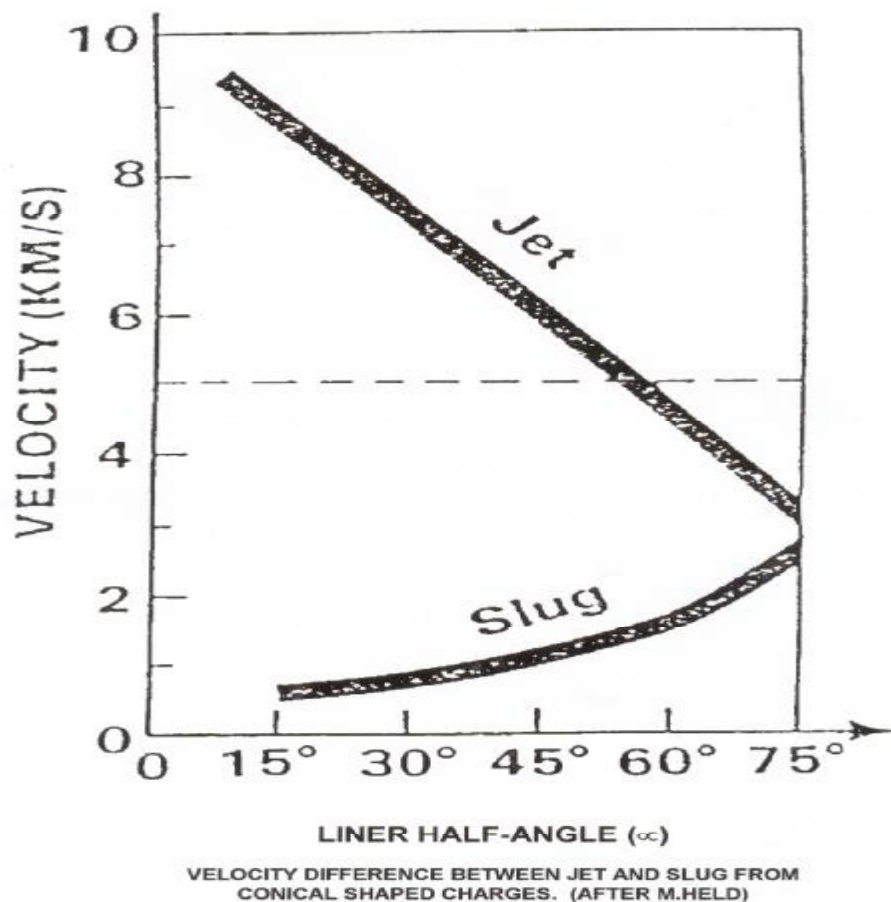
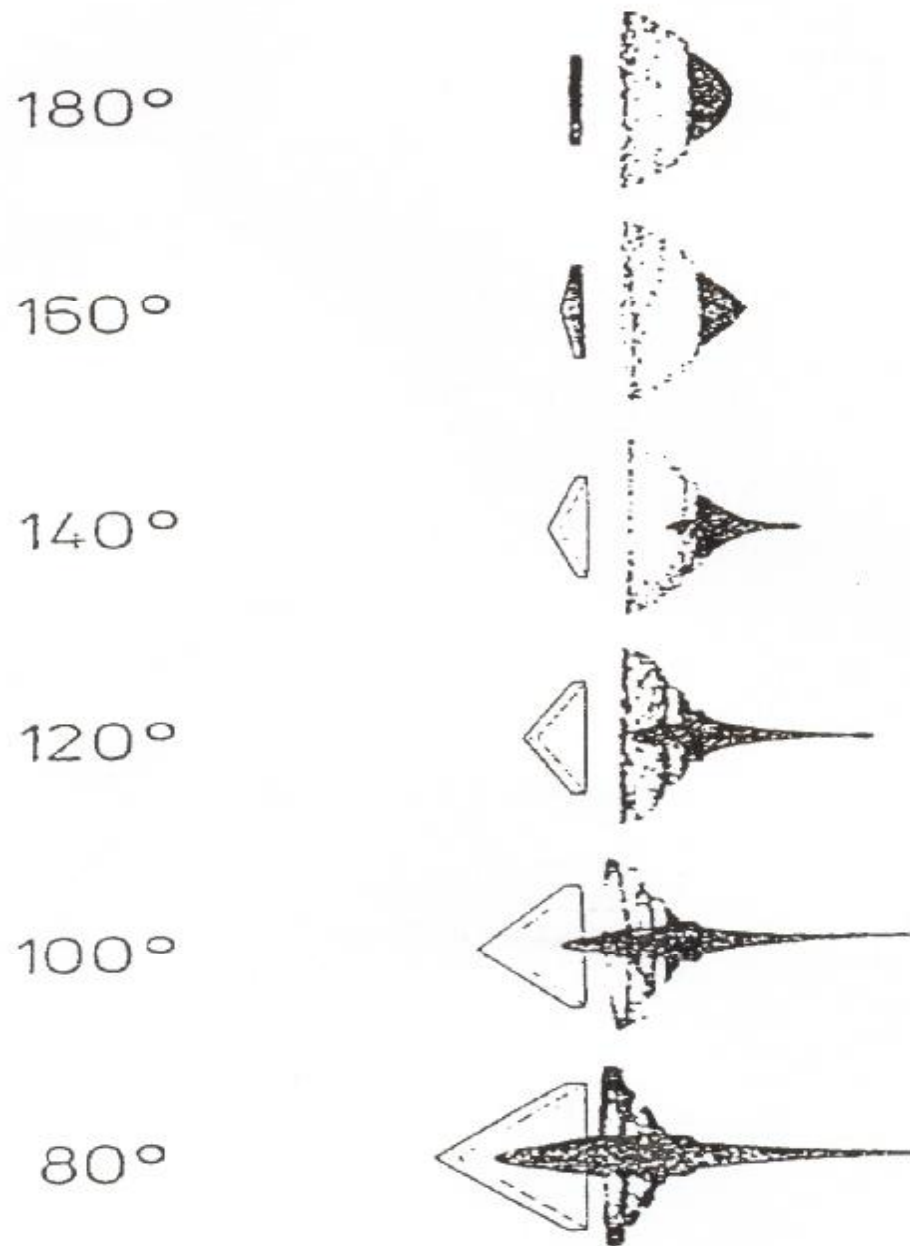


FIGURE 4.3

This is illustrated in the series of radiographs that were taken 35 microseconds after detonation for liners of various cone angles (Figure 4.4).

The jet information can be seen to be commencing at a cone angle of  $140^\circ$  becoming more pronounced with the narrowing of the cone angle.

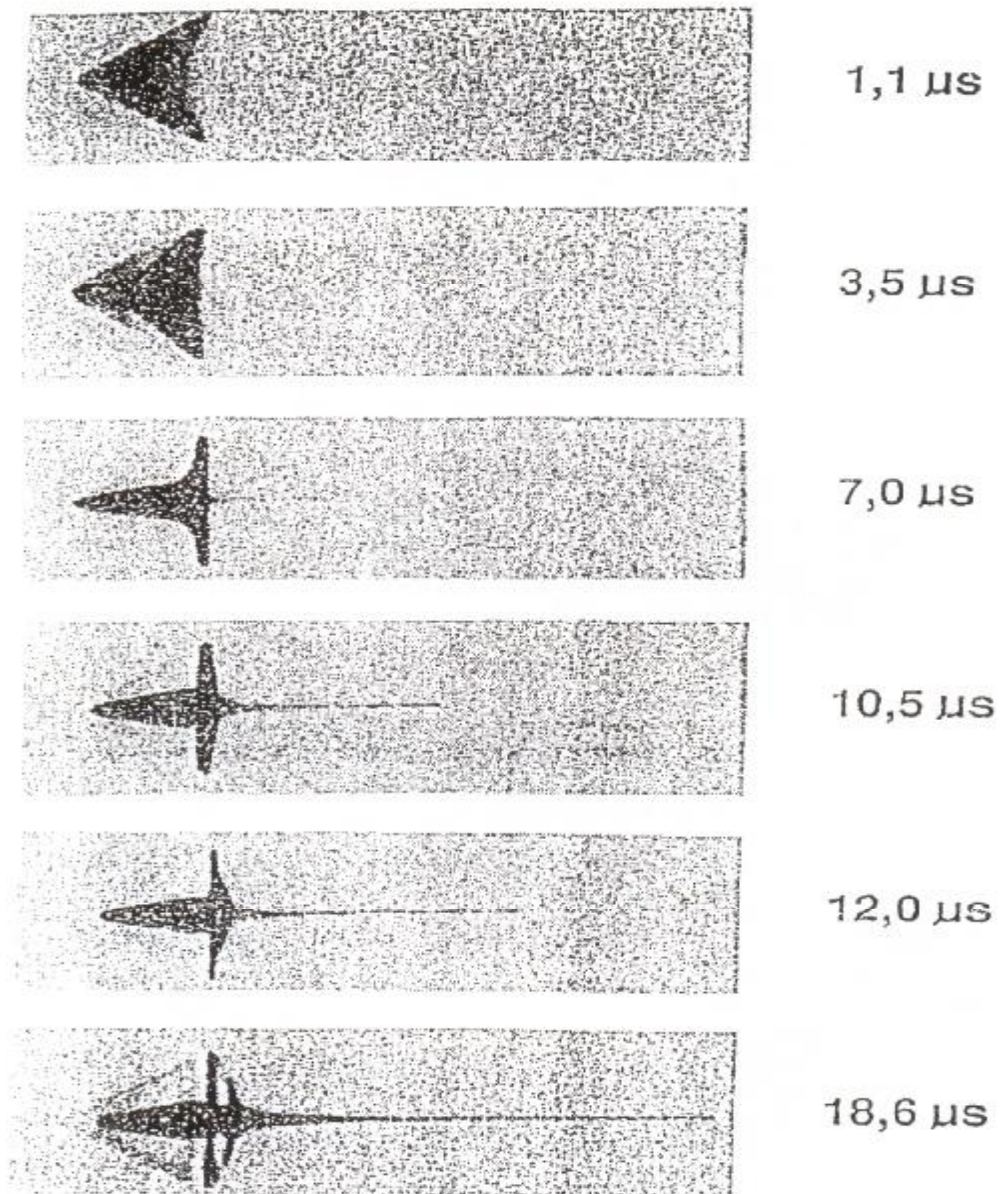


**JET FORMATION FROM CONICAL SHAPED CHARGE LINERS**  
**SOURCE: AFTER HELD FROM WALTERS & ZUKAS (1989)**

**FIGURE 4.4**

To illustrate the development of jet formation, Figure 4.5 shows a series of radiographs of the detonation of a 60° cone angle copper liner shaped charge taken microseconds after detonation.

The development of the jet from the collapsing cone is evident from the third radiograph at 7 microseconds after detonation.



**JET FORMATION FROM 60 DEGREE COPPER CONE  
(SOURCE: M.HELD)**

**FIGURE 4.5**



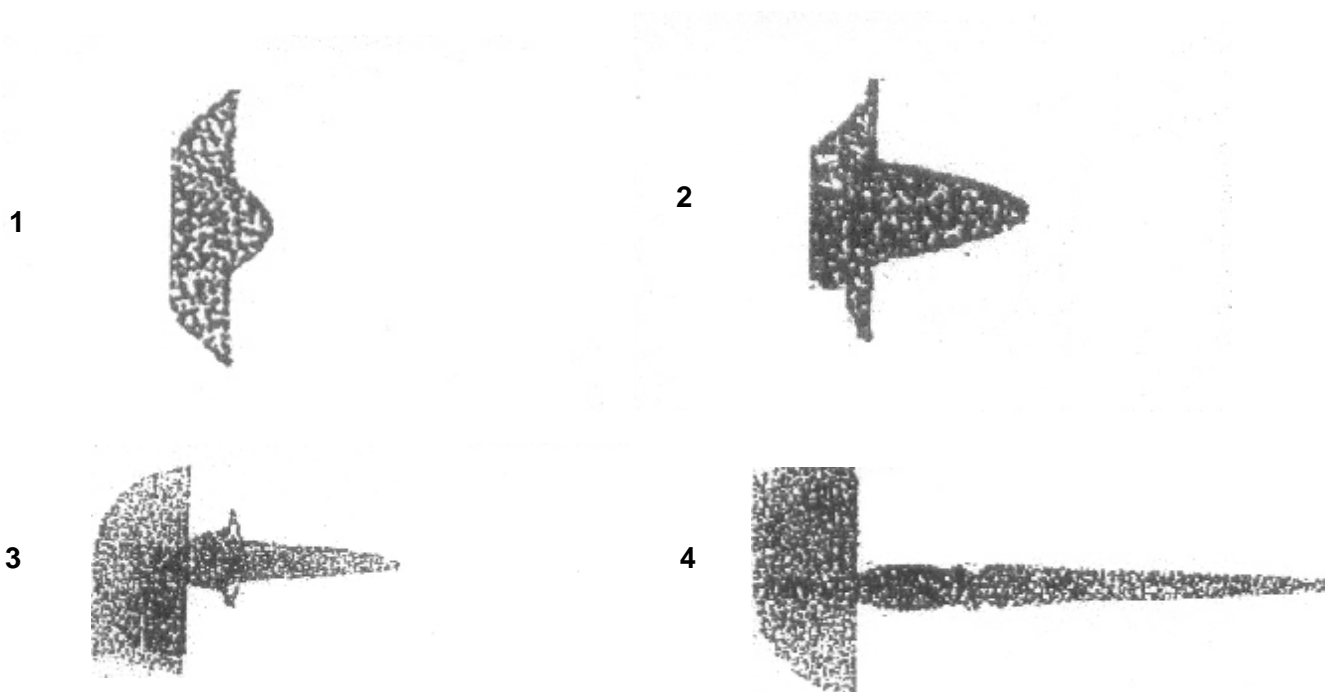
### 4.2.3 Difference between Conical and Hemispherical Liners

These are distinct and fundamental differences in the mechanism of metal flow and jet formation between conical and hemispherical lined charges.

With hemispherical charges, all the liner material is initially compressed into a compact ball which moves forward. A distinct collapse zone and an identifiable division of the mass into jet/slug parts is not evident. Later a certain portion of the compressed mass flows backwards and, in effect, forms a reverse jet. The remaining portion of the mass extrudes forwards as a jet with no identifiable slug. This phenomenon of jet formation is shown in the following radiographs. (Figures 4.6 and 4.7).

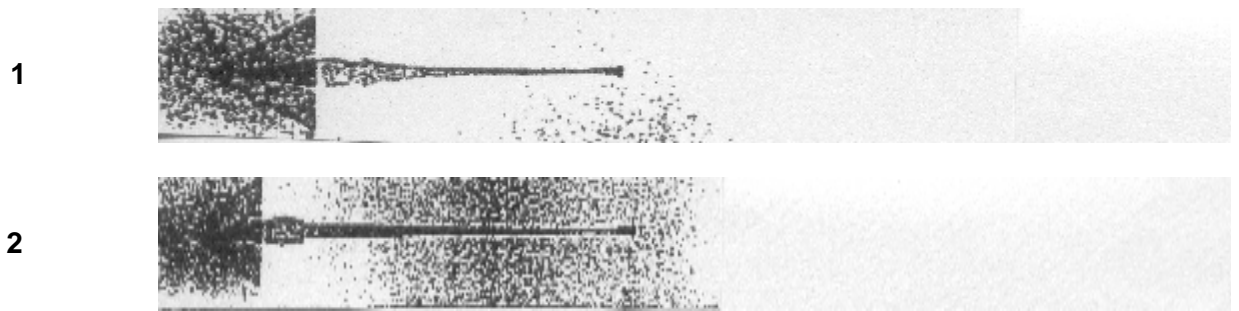
At an even later time, the jet stretches axially and eventually breaks up into fragments. (Figure 4.7).

Jet characteristics are significantly different from those of conical charges. Jet tip velocities for equal thickness liners are slower, typically 4000 m/s for hemispherical to 6000 m/s for conical charges. Jet particle diameters are substantially thicker for hemispherical charges.

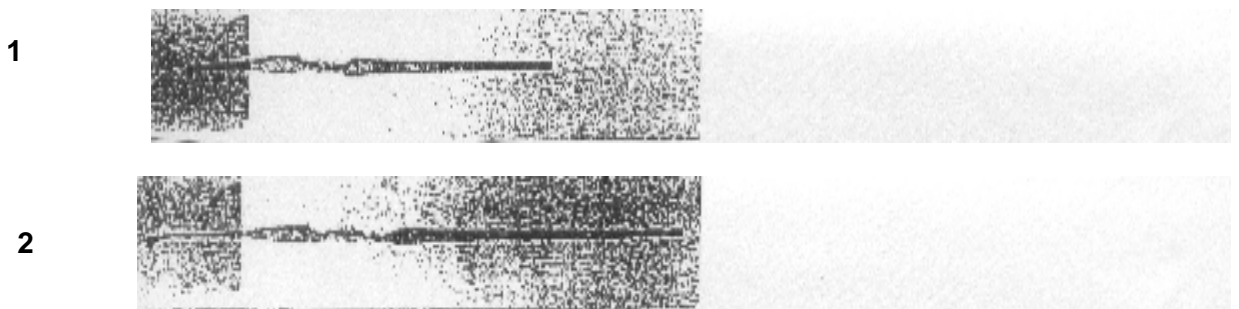


**RADIOGRAPHS OF JET FORMATION PROCESS OF A  
HEMISPHERICAL LINER  
SOURCE: HORNEMANN & HOLZWARTH (1993)**

**FIGURE 4.6**



**HEMISPHERICAL LINER**



**CONICAL LINER**

**RADIOGRAPHS OF A FULLY DEVELOPED JET FROM A HEMISPHERICAL (TOP) AND CONICAL (BOTTOM) LINER  
SOURCE: HORNEMANN & HOLZWARTH (1993)**

**FIGURE 4.7**

These differences from conical shaped charges have been ascribed to the fact that the collapse angle for hemispherical charges is always larger than  $90^\circ$ .

It should be noted that the curvature of the liner and the nature of the resulting mass flow to some stagnation zone can have far-reaching effects on the properties of an axially directed slug. Slug velocity and mass values are influenced by the nature of convergent flow and thus hemispherical charges are not used for EFP charges.

#### 4.2.4 EFP Formation

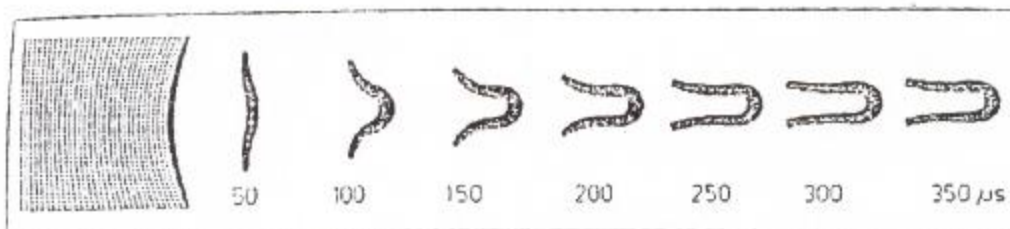
If a projectile is to be formed by the explosive projection of a metal liner, then the geometry of the liner must be such as to avoid the mass division on collapse and compression and to limit the collapse velocity variation that may tend to tear the collapsed material apart by elongation.

As previously shown, these effects can be attained by the use of flat-cone shapes of cone angles greater than  $140^\circ$ . The velocity differences between jet and slug become so small that the compressed mass no longer separates into two parts and the remaining velocity differences are dissipated by internal strains within the compact mass.

With constant thickness liners there tends to be velocity differences between the centre of the liner and the outer rim. This is due to the dissipation of explosive energy around the circumference of an explosive charge. The velocity differences can be minimised with a decrease in the thickness of the liner towards the circumference.

Another solution is to confine the explosive charge in a heavy casing in order to limit the dissipation of explosive energy by radial expansion.

The use of flat-dished liners permits a better use of axial and radial velocity vectors than do flat-cone liners. With dish-shaped liners, the centre portion of the liner is accelerated directly along the longitudinal axis and the collapse of the liner occurs through its inversion from the centre to the rim. This inversion process is well depicted by the computer simulation of EFP formation. (Figure 4.8).



COMPUTER SIMULATION OF EFP FORMATION  
(SOURCE: HERMANN ET AL (1977))

FIGURE 4.8

The formation shows the deforming liner at 50  $\mu$ s intervals. This is an unconfined charge of Composition B Explosive with a mild steel liner. The deformation process was complete after 300  $\mu$ s.

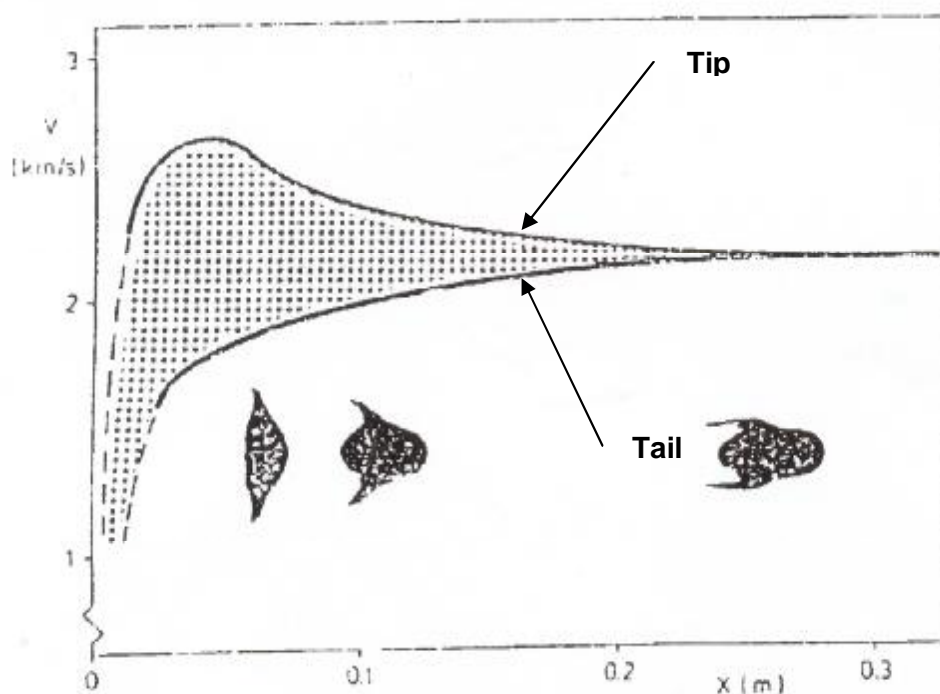
The shape of the slug matches well with the X-ray radiographs of the primer slugs taken during experimentation at the Naschem Boskop facility. (see Appendix 11 – Flash X-Ray Photographs).

#### 4.2.5 Tip and Tail Velocity Differences

EFP slugs have characteristic shapes which are due to differential velocities of the liner at different radii from the central axis. This is due to the fact that the explosive at the axis is confined and therefore forward-directed, whereas the explosive at the edge of the charge also has a tangential component which diminishes the forward – directing effect. Thus the liner at the centre has a higher forward velocity than the liner at the rim.

Depending on the ability of the metal to accommodate the velocity differential, the ability to stretch without breaking up into fragments, the final slug shape can be determined by the liner configuration.

The following diagram demonstrates the velocity differences in the metal liner during the initial slug formation. (Figure 4.9).



VELOCITY DIFFERENCES IN THE METAL DURING SLUG FORMATION. (SOURCE: HORNEMANN ET AL 1987)

FIGURE 4.9

During the initial phase the metal at the centre of the liner accelerates faster than the metal at the rim, thus causing the slug shape to undergo change. The tip initially moves faster than the tail thus causing elongation. However, if the slug does not break up, the tip pulls the tail along increasing the tail velocity and decreasing the tip velocity until they travel at the same speed.

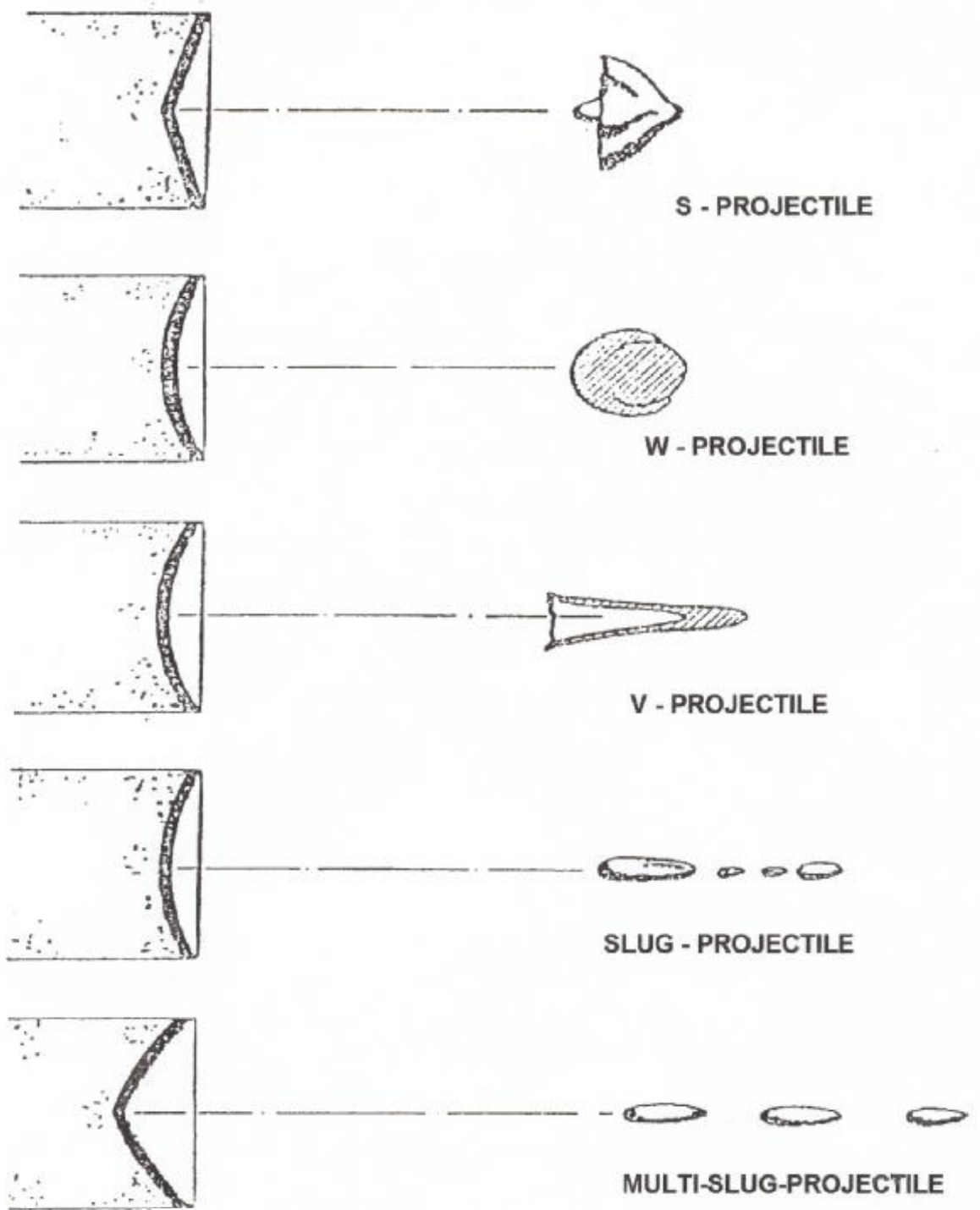
When this occurs, the slug shape becomes fixed and remains constant for the rest of the flight.

The velocity difference between tip and tail usually dissipates within a travel distance of 5 liner diameters.

#### **4.2.6 Types of EFP Slugs**

Liner shapes can be conveniently divided into three categories – conical, hemispherical and EFP.

There are grey areas however, that lie between the distinct categories. It is possible, by design, to collapse an EFP liner in such a way as to create some jetting, which leads to elongation by stretching, and the formation of a number of axially-spaced largish fragments. i.e. the formation of a multi-slug projectile. Some examples of this are illustrated in Figure 4.10.



**VARIOUS MAJOR TYPES OF EFP SLUGS (AFTER HELD)**

**FIGURE 4.10**

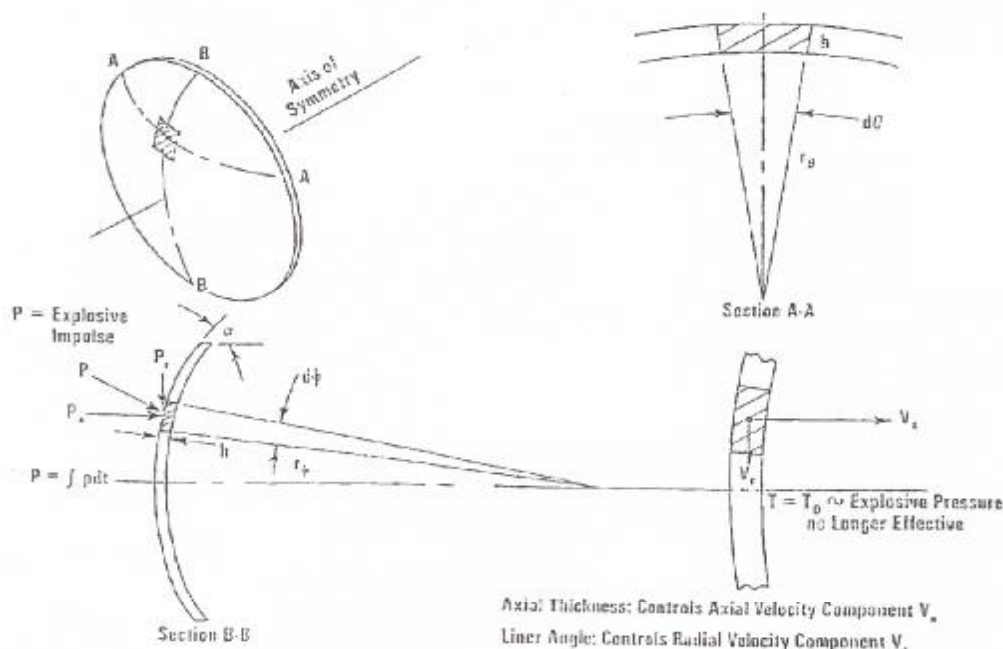
### 4.3 EFP Design Principles

The liner of an EFP is subjected to very high pressures of detonation over a very short period of time. Thus, each element of the liner is impulsively loaded. Material strength of the liner is negligible when compared to the stress loading of the acceleration caused by the high impulse.

Under the influence of the imposed force, material elements tend to move independently of one another and undergo acceleration in two principal directions – axially and radially (Figure 4.11). The resultant velocity vector is determined by the design of the liner in the following manner: -

- axial velocity is determined by liner axial thickness.
- radial velocity is determined by liner tangent angle.

Various projectiles are formed by varying these two liner parameters i.e. thickness and profile.



GEOMETRY OF ACCELERATION OF LINER MASS ELEMENT

FIGURE 4.11

The method of slug formation may also be categorised as follows: -

- Compact Point-Focus
- Compact Forward-Folding
- Elongated Forward-Folding
- Elongated Backward-Folding

Thus, two basic EFP shapes can be formed – compact (ball-like) and elongated (rod-like). Within these two categories many variations are possible. For example, extended shapes can be hollow or solid, and may be formed with a flare at the back for aerodynamic stability. Some of these are illustrated in Figure 4.12.

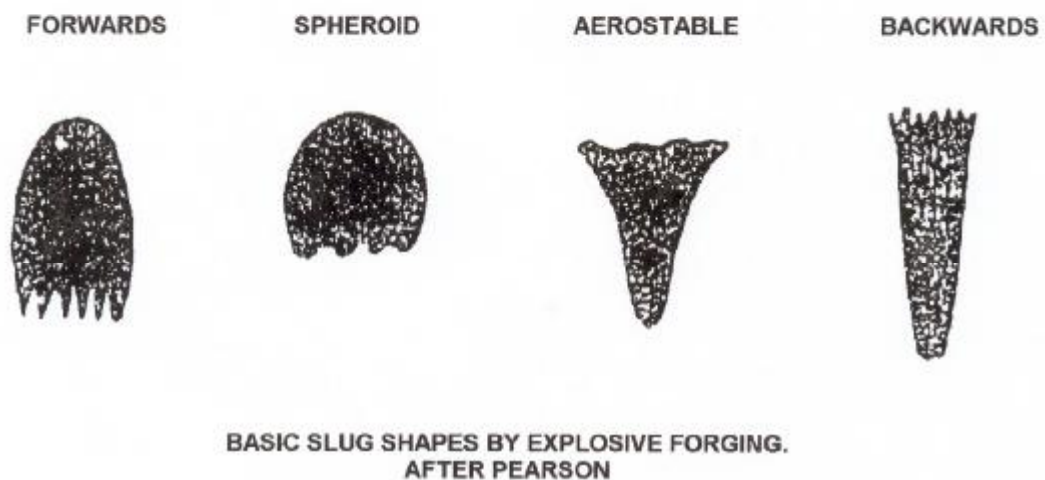
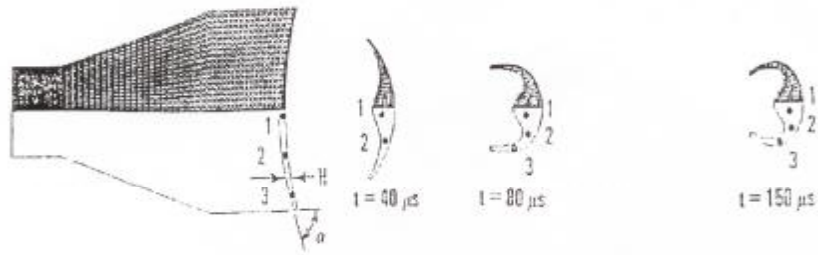


FIGURE 4.12

#### 4.3.1 Compact Point-Focus Slug

With constant liner thickness, the axial velocities are approximately equal. With the liner concave, the radial velocity at the rim is greater than that at the centre and with the movement towards the centre, a compact slug is formed. (Figure 4.13).





- \* AXIAL VELOCITY:  $V_{x1} = V_{x2} = V_{x3}$
- \* AXIAL THICKNESS:  $H_1 = H_2 = H_3$
- \* RADIAL VELOCITY:  $V_{r1} < V_{r2} < V_{r3}$
- \* LINE PROFILE:  $\alpha_1 > \alpha_2 > \alpha_3$

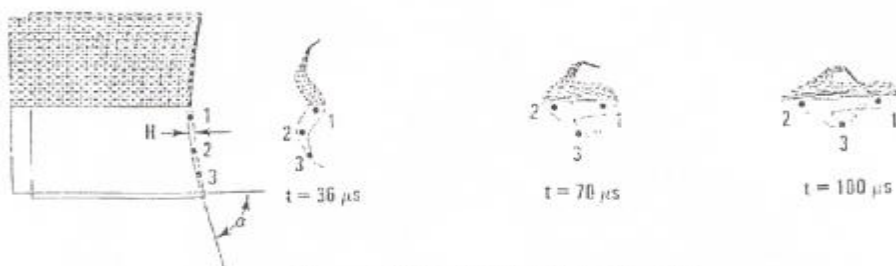
TWO-DIMENSIONAL HYDROCODE SIMULATION

COMPACT POINT-FOCUS SLUG FORMATION

FIGURE 4.13

### 4.3.2 Compact Forward-Folding Slug

With the thickness of the liner varying so that it is thinner at the axis and the rim than the rest of the liner, the velocities vary so that the metal at the axis and the rim move faster than the main body, thus resulting in a forward-folding action (Figure 4.14).



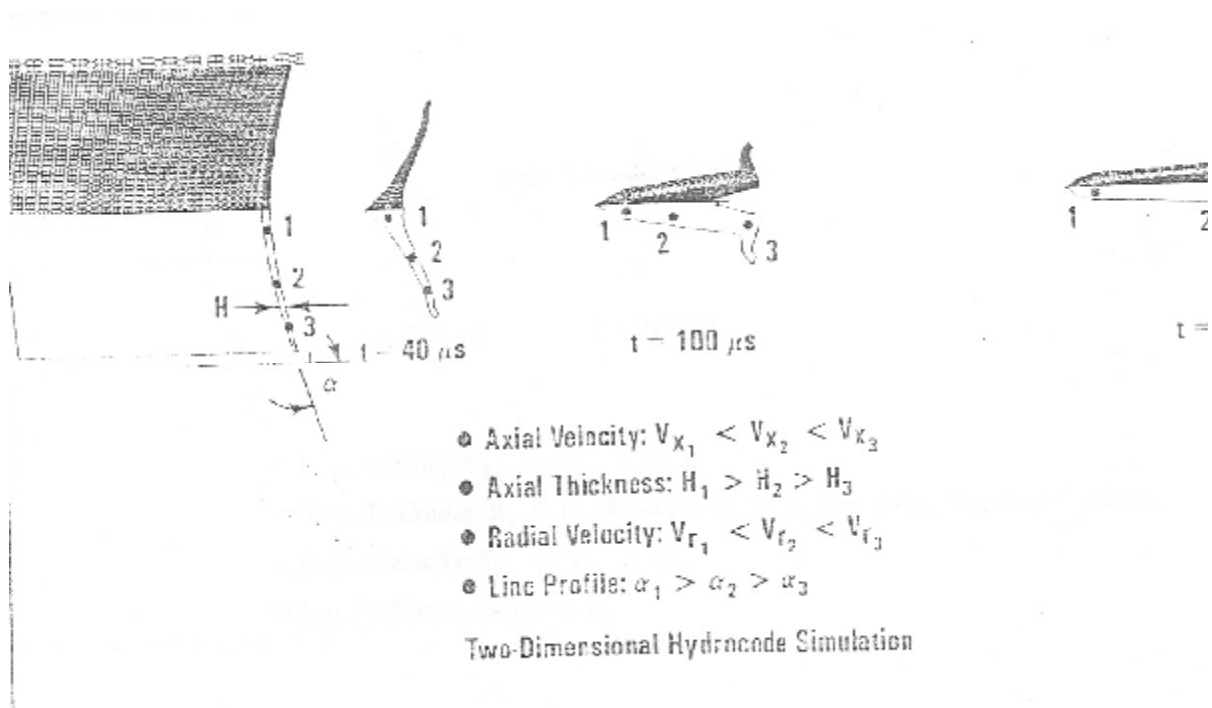
- \* AXIAL VELOCITY:  $V_{x1} > V_{x2} < V_{x3}$
- \* AXIAL THICKNESS:  $H_1 < H_2 > H_3$
- \* RADIAL VELOCITY:  $V_{r1} < V_{r2} < V_{r3}$
- \* LINE PROFILE:  $\alpha_1 > \alpha_2 > \alpha_3$

COMPACT FORWARD-FOLDING SLUG FORMATION

FIGURE 4.14

### 4.3.3 Elongated Forward-Folding Slug

With the thickness of the liner decreasing towards the rim, the axial velocity increases towards the rim. With the liner concave the inward radial velocity also increases towards the rim. This folds the liner forward along its entire length producing the elongated forward folding slug (Figure 4.15).

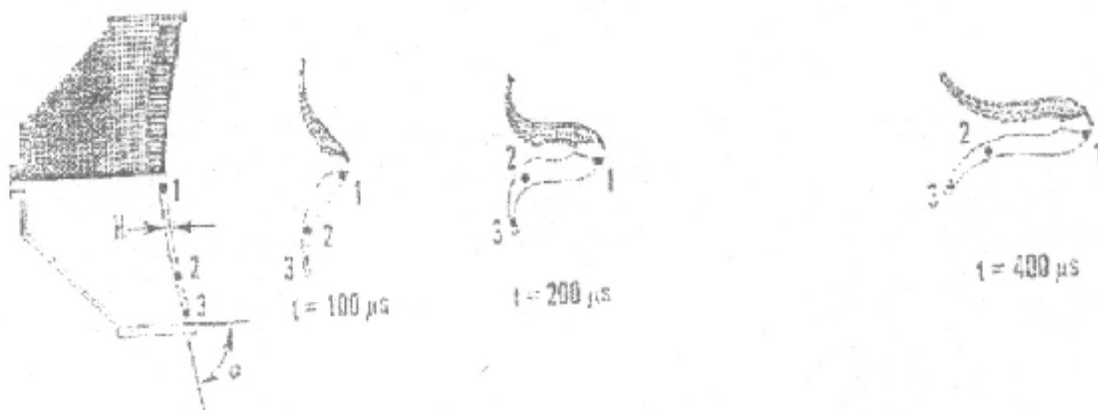


**ELONGATED FORWARD-FOLDING SLUG FORMATION**

**FIGURE 4.15**

### 4.3.4 Elongated Backward-Folding Slug

With the liner thickness thinner at the centre and the rim held back by confinement (of casing, say) the axial velocity is greater along the axis and the radial velocity of the rim is retarded. This produces an elongated backward-folding slug (Figure 4.16).



- \* AXIAL VELOCITY:  $V_{x1} > V_{x2} > V_{x3}$
- \* AXIAL THICKNESS:  $H_1 < H_2$ ; HOWEVER,  $H_3 < H_2$  DUE TO CONFINEMENT CONDITION
- \* RADIAL VELOCITY:  $V_{r1} < V_{r2} > V_{r3}$
- \* LINE PROFILE:  $\alpha_1 > \alpha_2 < \alpha_3$

ELONGATED BACKWARD-FOLDING SLUG FORMATION

FIGURE 4.16

#### **4.3.5 Slugshot Hang-up Clearance Charge**

Photograph 4.1 shows a photograph of a Slugshot Hang-up Clearance Charge in mid-flight. The shape of the copper slug is that of a compact point-focus slug as described in section 4.3.1. It is travelling at approximately 2000 metres per second. Being made of copper, the slug is ductile and has held together as a single slug in flight. The original concave copper dished liner at nest was 200 mm in diameter and it has deformed into a convex slug of approximately 150 mm in diameter. The mass has been maintained, so that the 2 kg copper dished liner has been transformed into a high velocity 2 kg copper slug.



**SLUGSHOT HANG-UP CLEARANCE CHARGE SLUG TRAVELLING AT 2000 m/s  
LEFT TO RIGHT**

**PHOTOGRAPH 4.1**

#### **4.3.6 Directional Primer Charge Slug**

The elongated slugs and the compact forward-folding slugs take more time to form than the compact point-focus slug. As the directional primer charge slug has a limited stand-off distance, it therefore has limited time to form fully before it impacts the rock at the toe of the blast-hole.

Therefore, the chosen configuration of EFP for the directional primer charge is a compact point-focus design.

## CHAPTER 5      DIRECTIONAL PRIMER CHARGE PREMISE

### 5.1      Introduction

Primers have long been used in mining to enhance the performance of column charges of explosives. They have served as an important link in the detonation chain between the detonator and the column charge.

Their function is to run up the velocity of detonation rapidly to that of or above that of the steady-state velocity of detonation of the column charge. In long holes primers are often spaced at intervals down the column charge to ensure that the velocity of detonation of the column charge is maintained and does not die away. This type of primer is called a booster.

Therefore, primers and boosters are characterised by having a higher velocity of detonation than the column charge, and are of a size large enough that their characteristic Chapman-Jouguet velocity of detonation is attained.

The mechanism that drives the velocity of detonation is the detonation pressure. The higher the detonation pressure, the stronger the forward drive of the pressure pulse. This results in higher intermolecular temperature, more rapid and complete chemical combustion and therefore more efficient explosive reaction. The stronger the pulse, the more sustaining the explosive reaction.

In open cast mines, pentalite explosives are commonly used as boosters in the column charge.

In Witwatersrand Practice, primers were traditionally Ammon Gelnite explosives used in conjunction with column charges of lower velocity of detonation explosives such as Dynagel, Ammon Dynamite or Anfex. The gelnite primer was traditionally of shorter length than the standard column charge cartridge being 100 mm long compared to the 200 mm long standard cartridge. This was due to economical reasons, gelnite being the more expensive explosive, so that the shortest length was used provided it was sufficient to attain a steady-state velocity of detonation.

Experiments show that the primer does not influence the velocity of detonation of the primed explosive further away from the primer than ten times the hole diameter.

In summary the following are the characteristics and applications of primers.

- Primers should have higher detonation pressures (hence higher velocity of detonation which are more easily measurable than pressures) than the explosive column detonation pressures.
- Primers should be long enough to allow the run-up to a steady-state velocity of detonation. For this a rule-of-thumb is the length of the primer should be 2 to 4 times its diameter and the primer diameter should not be less than half the hole diameter (decoupling affects the run-up to steady-state velocity of detonation).
- Holes should be bottom-primed for optimum breakage. Gaseous reaction products are confined for a longer period of time allowing greater pressures to act on the walls of the hole towards the toe for longer time. Also there is less fly-rock with bottom-priming than with top-priming.
- In long holes primers or boosters influence the column charge up to a distance of ten times the hole diameter.

Certain other phenomena had been observed empirically over time; such as the incomplete break-out of rock over the entire length of the hole which left behind portions of the blastholes or sockets in the stope face, such as the focussing of explosive energy in the hollow charge phenomenon which appeared to be replicated in an air gap at the end of the column charge of explosive such as the enhancement of the hollow charge phenomenon using a metal liner and the insertion of metal washers in the blasthole prior to charging up and such as the observation of the shattering effects of an EFP on rock. These phenomena gave rise to hopes that a directional primer charge could be designed that would increase current blasting efficiency in stopes in South African mines. These phenomena are described in the following sections.

## 5.2 Development of the Concept of a Directional Mining Charge

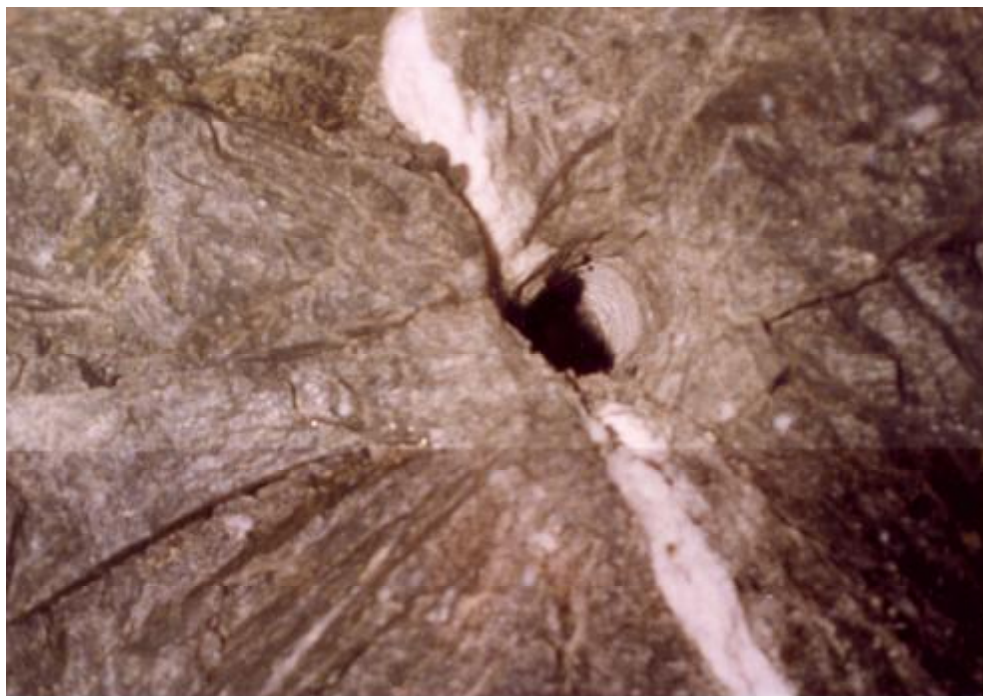
The development of the concept of a directional mining charge, specially for use in stoping and tunnelling, took place over a period of time.

It took the form of

- the acknowledgement of a characteristic of the drilling and blasting method of breaking rock, namely the existence of sockets remaining after the blast,
- the observation of the Air Gap Phenomenon which resulted in a radial “umbrella” fracture at the toe of the blasthole.
- the declassification of military weapons technology and, their possible use in the mining industry.
- the development of a large EFP device, namely the Slugshot hang-up clearance device, which demonstrated directional explosive capabilities.

### 5.2.1 Dilemma of the Sockets

A characteristic of underground drilling and blasting is the presence of sockets, i.e., unbroken portions of the blastholes left on the face after the blast.



**PHOTOGRAPH 5.1 SHOWING SOCKET OF BLASTHOLE REMAINING IN THE STOPE FACE AFTER THE BLAST**



As the length of the drilled hole is taken to be the maximum distance of face advance for a blasted round, the presence of sockets on a face indicates an inefficiency in that less than the maximum distance possible has been advanced.

In the development of tunnels, advance per round is normally the critical parameter by which production is measured. Tunnels are often required to be constructed in the shortest possible time in order to open up ore reserves for mining. Time is of the essence. The longer the round broken per cycle, the quicker will be the total advance of the tunnel and the more efficient the drilling and blasting is viewed. In addition, the presence of sockets which may contain undetonated explosives, holes must be collared in such a manner as to avoid drilling into the sockets. Tunnels in general tend to be over drilled with too many holes in order to reduce the length of the sockets.

In narrow seam stoping, the availability of face is normally at a premium. Thus, in order to improve production with a fixed face length, face advance is required to be increased. The elimination of sockets can be attempted by reducing the burden of the blastholes, i.e., by drilling the holes closer together. This entails the additional cost of drilling and charging of extra holes – an inefficient and unproductive practice.

Thus, it has been recognised in stoping that the optimum in drilling and blasting efficiency lies somewhere between too long sockets and no sockets at all. A rule of thumb has been that the most efficient blast from a technical point of view, i.e., the least quantity of explosive used per volume of rock broken, will produce sockets of the order of 150 mm in length from a drilled length of 1,0 metre.

Thus, if the explosive energy could be directed to the toe of the blasthole such that for the same hole burden no sockets are left after the blast then the advance of an efficient round could be enhanced by some 15% to 20%.

### **5.2.2 Air Gap Phenomenon**

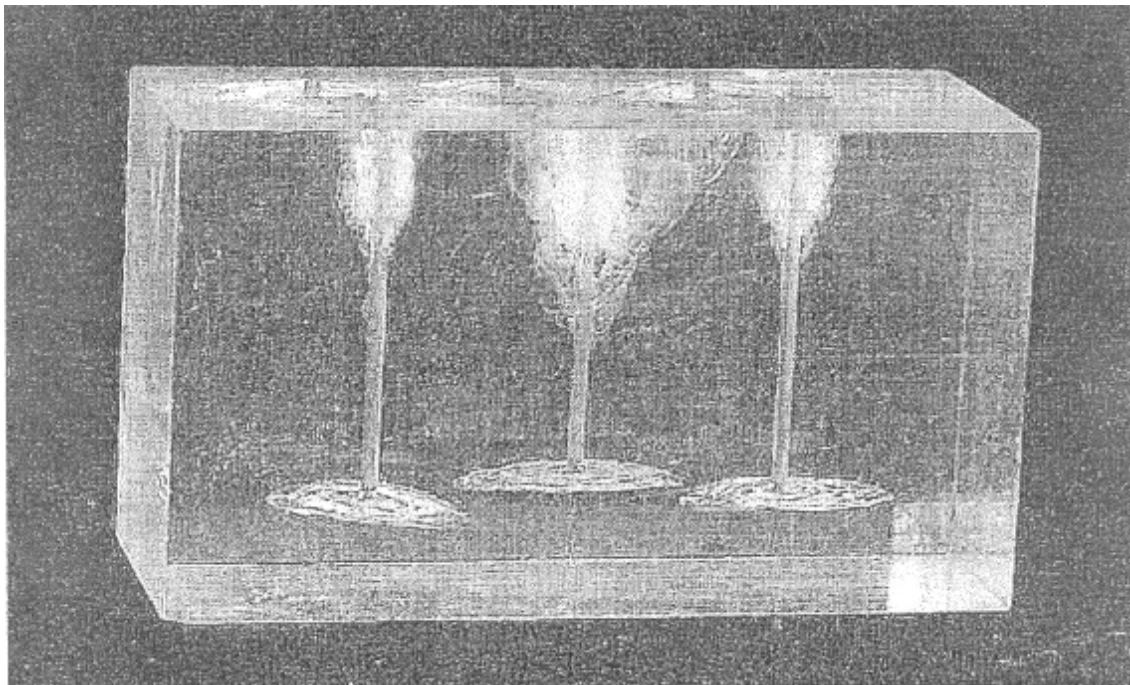
In the 1970's in the Mining Department of the University of the Witwatersrand, a strange phenomenon was observed whilst demonstrating the formation of cracks from blasting using low-energy detonating cord and Perspex models.

Once detected, the phenomenon was found to be repeatable.

The phenomenon was the formation of a circular umbrella crack emanating from the toe of the hole and perpendicular to the axis of the hole. It only occurred when the detonating cord did not extend down the full length of the hole but left a substantial air gap between the end of the explosive and the toe of the hole. (see Photograph 5.2).

At the time this phenomenon created much excitement. If this could be reproduced in the field, then there would be no need to practice sub-drilling in quarrying and opencast mining. The end of the hole would demarcate the level of the floor of the next bench down or the floor of the pit. In addition, it was recognised that its application in underground mining would be the virtual elimination of blasthole sockets.

Unfortunately, this research was never carried further than being an experimental quirk of limited academic value. Prior to this thesis, the mechanism of the formation of the “toe-umbrella-fracture” has never been satisfactorily explained.



**PHOTOGRAPH 5.2 PERSPEX MODEL BLASTING SHOWING THE FORMATION OF UMBRELLA CRACKS AT THE TOE OF EACH HOLE.**

**NOTE THE BLAST DAMAGE CRACKS AT THE COLLAR OF EACH HOLE AND THE LENGTH OF UNDAMAGED HOLE WHERE THERE WAS THE AIR GAP.**

### **5.2.3 Washer-in-Hole Myth**

A practice that was illegal but which was not uncommon on the Witwatersrand gold mines over 40 years ago was to place a metal washer in the blasthole prior to inserting the explosive cartridges. Some of these old miners swore blind that this practice increased the break-out of the rock. No-one knew why this should be so and because the mechanism could not be adequately explained, the practice fell into the realms of mining lore and myth. With the demise of cartridge explosives and the advent of Anflex, the practice of placing washers in the blasthole fell away to the extent that it is unheard of today.

This thesis will provide an explanation of why the metal washer may have enhanced the break-out of the rock in a blast.

### **5.2.4 Swords-Into-Ploughshares**

With the end of the Angolan War and the Iran-Iraq War, the South African armaments manufacturer Armscor, and particularly its explosives manufacturing subsidiary Naschem, sought new markets for their products.

To this end Naschem declassified and opened up its testing and research facility and allowed its current products to be scrutinised for possible commercial use. With the ending of the two major wars mentioned above, there was now a surplus of manufacturing capability of military explosives and explosive devices. Amongst these were shaped charges and explosively-forged projectiles. As the largest user of explosives in South Africa, the mining industry was the obvious target for surplus military explosives and explosive devices.

### **5.2.5 Development of the Hang-Up Clearing Charge**

Of all the products presented by Naschem for scrutiny for potential use in mining one product, the anti-tank weapon known as the P-charge, stood out as the one device which could be used to great effect as a hang-up clearance charge.

The development and modification of the military P-charge into the explosive mining tool of the Slugshot Hang-up Clearance Charge brought the military knowledge of shaped charges to the mining industry.

It demonstrated the transference of energy over relatively long distances. The transformation of explosive energy to kinetic energy and then impact energy using a shaped charge in the form of an explosively-forged projectile, was a useful tool for breaking rock remotely. The accuracy of the device demonstrated the power of focussing the energy as a directional charge.

### **5.3 Premise for the Directional Primer Charge**

From the foregoing, it has become apparent that there existed a need in mining for a device to enhance the break-out of rock at the toe of a blasthole. If this device could increase the break-out to the full length of the drilled hole, then a number of significant advantages would occur namely: -

- there would be no sockets left behind after the blast.
- this would eliminate the chance of drilling into sockets which could contain unexploded explosives thus improving safety.
- this would also ensure a greater advance per blast thus improving blasting efficiency.
- if there was a clean break at the toe of the hole along an umbrella fracture, then the new face would have the characteristics of a smooth blast i.e. there would be less blast damage done beyond the umbrella fracture than with conventional blasting.
- the next drilling cycle would not suffer as much from the problems of sticking drillsteel when drilling through fractured ground.
- stuck drillsteels usually result in drilling of holes with uneven burden and occasional short holes which will exacerbate the problems of poor blasting resulting in successive faces suffering from blast damage and unwanted fracturing.

By using a shaped charge in conjunction with a primer as a single unit, it is considered that explosive energy could be directed to the toe of the hole to enhance the break out and even eliminate sockets altogether. This single unit is called a directional primer charge.

In order for the directional primer charge to be effective it should incorporate the following: -

- it should be placed as a bottom primer.
- the hollow or shaped end should face the toe of the hole.
- the hollow charge effect can be enhanced using a metal liner to line the hollow of the shaped charge.

- a high velocity of detonation explosive should be used to drive the metal liner forward, converting the explosive energy of the charge into kinetic energy of resultant high velocity metal slug, which converts into impact energy as the slug hits the rock at the toe of the hole.
- the length of the high velocity of detonation explosive used to drive the slug should have a long enough run-up to achieve its maximum velocity of detonation, which is its Chapman-Jouguet steady-state velocity.
- the stand-off distance of the metal liner should be sufficient for the metal slug to fully formed and to attain a velocity approaching its maximum velocity for the explosive-type / metal mass configuration.

It is envisaged that upon impact at the toe of the hole, the high velocity metal slug will cause the rock at the toe to fail by crushing and cracking. As the force of the impact is along the axis of the hole, the rock face at the toe is expected to initially move backwards into the rock mass, thus creating tension cracks around its circumference and generating the characteristic “umbrella fracture”.

These umbrella fractures, initiated by the impact of the metal slug and by subsequent shock fronts from the explosive column charge, are expected to be extended further by the build-up in pressure of the reaction product gases which follow. This extension of the umbrella cracks enhances the break-out to the full length of the blasthole.

Thus it would appear that the following conditions are required: -

- a high as possible velocity of detonation explosive to ensure maximum impact at the toe of the hole to initiate the radial umbrella fracture.
- a gaseous explosive to enter the initiated cracks, to extend them and to break out the rock burden by heaving through gaseous expansion.

The former should be attained by the directional primer charge and the latter by the column charge of standard explosive.

## CHAPTER 6 DEVELOPMENT OF A DIRECTIONAL PRIMER CHARGE PROTOTYPE

### 6.1 Introduction

By applying the principles of shaped charge technology, it is apparent that the general configuration for a proposed directional primer charge would be an explosive cartridge of standard dimensions, at the front of which would be a shaped liner at some stand-off distance to the toe of the blasthole.

For the initial tests on surface, a simple directional primer charge was designed. The housing chosen was a 150 mm long section of black plastic pipe, 30 mm in diameter in order to accommodate the standard explosive cartridge used in stoping. Inside the pipe a metal disc was crimped at a short distance from one end to provide the stand-off distance. The disc was curved and acted as the shaped charge liner. (See Figure 6.1 and Photograph 7.1 and 7.2). Various high velocity of detonation explosives were either inserted or cast into the black pipe such that the explosive made good contact with the liner.

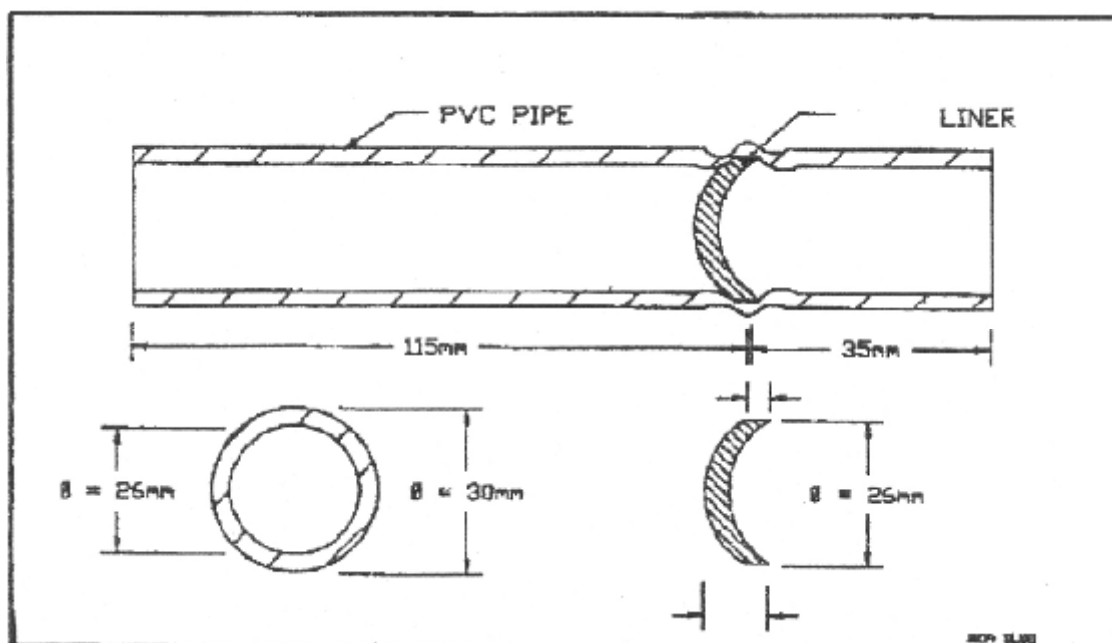


FIGURE 6.1 SHOWING DIRECTIONAL PRIMER CHARGE EMPTY ASSEMBLY

## **6.2 Disc Parameters**

### **6.2.1 Disc Shape**

A shaped charge can act either as a slug or as a jet (see Chapter 4). It is considered that the ability of a shaped charge to cause fracturing perpendicular to the blasthole would be more beneficial to mining than fracturing along the axis of the hole. The perpendicular cracks would extend towards the free face created by the previously detonated blasthole, thus assisting in the break-out of the rock burden. The co-axial fracturing would merely extend the length of the hole.

Therefore, the preferred design of the shaped charge would be a slug-forming EFP and not a jet-forming EFP. Hence the shape of the hollow charge and liner of the directional primer charge took the form of a shallow dished liner (see Chapter 4.2).

As the stand-off distance is limited, the compact point-focus design is chosen for the slug formation (see Chapter 4.3). This design is a concave dish shape of uniform liner thickness.

### **6.2.2 Disc Thickness**

The shallow dished liner was manufactured by punching circular discs out of metal plate. The discs were 25 mm in diameter in order to fit into the black plastic pipe housing.

Two thicknesses of discs were cut – 1,6 mm and 2,0 mm. At 25 mm diameter the respective masses of these two thicknesses were 6 g and 8 g.

As is to be expected from the Gurney Ratios, the 6 g disc has a higher final velocity for the same explosive mass than the 8 g disc. In addition, for each column length, the disc velocity is higher for the 6 g disc than for the 8 g disc (see diagram). However, owing to the heavier mass of the 8 g disc, their kinetic energies are more or less the same. Surface detonics laboratory testing was carried out for both the 1,6 mm and the 2,0 mm thick discs.

### **6.2.3 Disc Material**

Large calibre EFPs, i.e. greater than 100 mm in diameter, commonly use a malleable metal such as copper in order to maintain the integrity of the slug.

A malleable metal is more able to accommodate the difference in tip and tail velocities in the formation of the slug such that the slug will hang together over long stand-off distances of 100 to 1000 calibres and will not disintegrate into a stream of shrapnel pieces.

Small calibre EFPs with a short stand-off distance, e.g. the directional primer charge with a stand-off distance of one calibre, can use more brittle materials such as steel as they are not required to maintain integrity over a long flight distance.

Mild steel was chosen as the metal type for the disc because mild steel is readily available, is relatively inexpensive, and the disc can be formed easily by punching out standard plate.

Flash X-ray radiography (see Appendix 11 – Flash X-Ray Images Nos. 1, 2 & 3) shows that more than 90% of the disc's mass remains in the main slug at a distance of one calibre. There is a slight loss owing to shrapnel effect at the extremities of the disc.

## **6.3 Stand-Off Distance**

### **6.3.1 Theoretical Calculation**

From a modelling approach, using the Gas Dynamics Model, the disc was initially assumed to behave like a rigid piston under loading by high pressure gases. From this modelling approach, velocity versus explosive column length and velocity versus distance travelled can be calculated for various explosive types and disk masses (or equivalent disc thicknesses) – see Appendix 4.

These calculations show that over a distance from 0 to 20 mm, more than 95 % of the final velocity is attained. The build-up of disc velocity is very rapid in the early stages and tapers off to show little increase in velocity over larger distances.

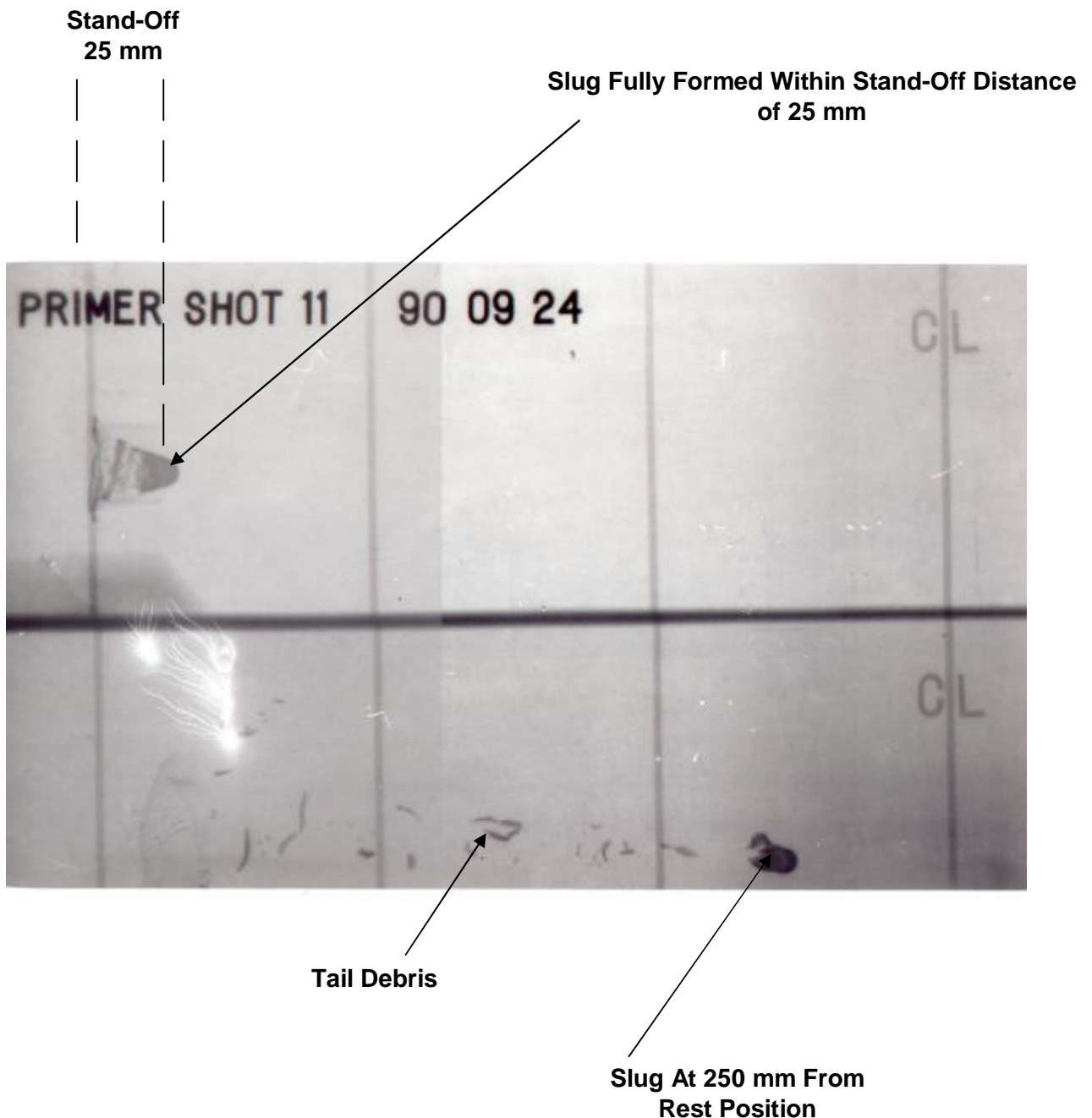
### **6.3.2 Empirical Determination**

From empirical Witness Plate tests using trial and error and subsequent interpolation, the effective stand-off distance was found to correlate closely with the theoretical calculations. An effective stand-off distance was found to be one calibre, i.e., 30mm. This is discussed in detail in Chapter 7.2.1 of this thesis.



### 6.3.3 Flash X-Ray Radiograph Confirmation

Later X-ray Flash Radiography (see Chapter 7.4) showed the disc to have fully transformed itself into the final configuration of the aerodynamic slug within one calibre (25 mm). (see Flash X-Ray Images No's 1,2 and 3 in Appendix 11). Further tests using timing screens along the trajectory of the slug indicated that velocity retardation due to air resistance was negligible over a distance of 1 metre.



**PHOTOGRAPH 6.1 FLASH X-RAY IMAGES NO.2**

**SHOWING DIRECTIONAL PRIMER CHARGE SLUG FORMATION AT 15 ms AND 125 ms AFTER DETONATION**

Thus, a stand-off distance was chosen which would ensure that maximum velocity (and hence maximum momentum and maximum kinetic energy) would be attained without the fear of a drop off in velocity due to air resistance. As less than the optimum stand-off distance would have a marked effect on velocity, and greater than the optimum stand-off had little effect, it was decided, for practical purposes, to err on the side greater than the theoretical optimum distance, i.e., greater than one calibre (or greater than 30 mm for a 30 mm diameter charge).

Conversely, too great a stand-off distance had other deleterious effects on the breaking of the rock, as the stand-off distance would result in a corresponding decrease in explosive column charge and consequently a corresponding decrease in the total available explosive energy in the blasthole.

As a result, of the above considerations, it was decided that, for a primer charge of 30 mm nominal diameter, the designed stand-off distance should be 35 mm.

## **6.4 Explosive Type**

### **6.4.1 Velocity of Detonation**

All the three models for plate acceleration presented in Chapter 3.2, show that the higher the velocity of detonation of an explosive, the greater is the velocity of explosively-forged projectiles.

It is this characteristic that caused the military authorities to develop high velocity of detonation explosives with high shock characteristics. On the other hand commercial manufacturers of explosives for the mining industry have developed lower velocity of detonation explosives with more emphasis on gas production to produce the heave necessary to break out and fragment in situ rock.

In the early stages of development many explosives were randomly used on an ad hoc basis for rough comparison. It soon became apparent that the higher velocity of detonation explosives had greater penetrating power when firing a slug at a metal plate. (see Photographs in Appendix 10).

Three types of ultra high velocity of detonation explosives were chosen for comparative tests. They were: -

- Composition B. A standard military explosive with velocity of detonation of 7600 m/s.
- TNT. A standard military explosive with a velocity of detonation of 6700 m/s.
- Super Gelignite. A specially formulated commercial explosive with a velocity of detonation of 5600 m/s.

Composition B was initially chosen because it is the explosive most commonly used in explosively-forged projectiles. It had a high velocity of detonation. It was easily cast. It had a lower cost than other explosives with similar or higher velocity of detonation such as RDX and HMX.

Super Gelignite was chosen because gelignites were already accepted in the mining industry. It had a relatively high velocity of detonation – higher than other commercial bulk explosives. Its cost was low compared to military explosives.

TNT was chosen as a compromise between Composition B and Super Gelignite. Its cost and velocity of detonation lay between the other two explosives. It could also be made in pellets.

#### **6.4.2 Metal / Charge Mass Ratio**

The other factor that would appear to determine the final velocity of the disk is the mass per unit area of metal to mass per unit area of explosive – i.e. Gurney's M/C ratio. For the directional primer charge with a constant disc configuration and mass, and a cylindrical charge of explosive, the Gurney Ratio value is indirectly proportional to the explosive charge length. Therefore, the longer the length of the explosive charge, the greater will be the final velocity of the disc. (see Chapter 7.6.3 and Appendices 3 and 4).

To illustrate the above, the theoretical calculations show that a 60 mm long column of TNT is equivalent to a 40 mm column of Composition B in generating the final velocity of a metal slug. This fact should be borne in mind when considering equivalent explosive capabilities from an economic viewpoint, i.e., it may be more cost effective to have more of a slightly weaker explosive that is far less expensive, than a smaller amount of stronger explosive which may be far more expensive.

A major factor in the choice of explosive for the directional primer charge prototype was the disc / explosive interface and, hence, the castability of the explosive became important. The interface was critical in that any discontinuity such as entrapped air would be deleterious for the transfer of energy from the explosive to the disc.

## **6.5 Detonation Chain**

### **6.5.1 Detonator**

It was decided to use the most commonly used detonator in the mining industry as the initial detonator in the detonation chain. At the time of the tests, the most common detonators in use were the 6D and 8D type detonators. As the 8D detonator had approximately twice the power of a 6D detonator, any explosive that was 6D sensitive would also be 8D sensitive. The converse does not hold.

To lessen the chance of misfires through initiation under mining conditions caused by an incorrect detonator being used, it was decided that the standard initiating detonator should be the 6D type. Therefore those explosives constituting the primer which were not 6D sensitive e.g., Composition B and TNT would require a booster for initiation.

### **6.5.2 Booster**

For Composition B, it was found that it was sensitive to certain standard commercial explosives used in mining. Thus, the column charge in the primer could be made up of part commercial explosive positioned between the detonator and the Composition B explosive, i.e., the commercial explosive acted as a booster between the detonator and the high velocity of detonation explosive. After a series of initiation tests, Composition B was found to be insensitive to Ammon Dynamite but sensitive to Ammon Gelignite and the emulsion Powergel.

For ease of loading, a half cartridge of Powergel 813 (i.e., 100 mm long) was used as the booster for differing column lengths of Composition B during the underground tests on Village Main mine. For the TNT tests, a Pentalite booster was used. For the Super Gelignite tests, no booster was required.

## **6.6 Housing**

### **6.6.1 Explosive Container**

For the prototype, the housing was designed to be basic and simple, functional enough to locate the disc securely at a fixed stand-off distance, to contain the various masses of high explosive required for the tests and for ease of insertion of the booster explosive. For these purposes the housing was chosen to be a polythene pipe, 150 mm long with a nominal 30 mm outside diameter and 26 mm inside diameter. The polythene material allowed the disc to be located at the given stand-off distance and secured in position by crimping the pipe around the disc.

The internal diameter was chosen to be 26 mm so that a standard explosive cartridge of 25 mm diameter could be inserted as a booster for the Composition B high velocity of detonation explosive. The location of the disc was chosen to be 35 mm from one end with the disc facing concave towards that end. As previously stated in Section 6.4.3, this distance was the chosen optimum stand-off distance. The opposite end of the tube was left open to allow for the insertion of explosive. The primary high velocity of detonation explosive (Composition B) was cast into the housing and the booster inserted later. The detonator was inserted into the booster just prior to the initiation of the charge.

An ad hoc refinement to the directional primer charge was the covering of the leading end of the primer with thin plastic membrane to prevent dirt or other foreign objects from entering the stand-off distance space. This membrane was secured simply by means of a rubber band.

### **6.6.2 Nose Cone**

Drilled holes under production conditions in mining tend to leave drill chippings debris in the hole. Drill holes are rarely flushed out properly to leave the hole clean of drill chippings prior to the insertion of explosives. In South African stoping practice, water is most commonly used as the flushing medium and, as many holes are drilled down slightly below the horizontal, water often accumulates at the toe of the hole.

Thus, a primer with an open end to allow for stand-off distance runs the very real risk that the stand-off space will be filled with extraneous matter such as fine drill chippings, mud and water, which effectively will negate the effect of a stand-off distance. In order to maintain the integrity of the stand-off distance under mining production conditions, a closed nose cone over the front end of the primer is required.

Initially, as described above in Section 9.2.2, a thin plastic membrane was stretched over the front end of the first prototype primer. In subsequent prototype primers designed for mining production, a specific nose cone head was designed. This head consisted of a tapered, closed end plastic nose cone. The nose cone was tapered so that it would ride easily over any debris left in the drillhole after flushing, allowing the primer to be pressed home firmly at the toe of the hole.

The degree of tapering was determined by perusal of the slug formation in the Flash X-ray radiographs. The disc was observed to deform from a 25 mm diameter dished shape to a 15 mm diameter semi-spherically shaped slug within 25 mm of travel. Because of this, the shape of the nose cone was straight (i.e., constant diameter of 25 mm) for the first 10 mm, and then it tapered evenly down to a diameter of 17 mm over the next 25 mm (i.e., to the front end of the cone). The front end of the cone was closed to prevent ingress of deleterious material in the stand-off space (see Figure 1.2 in Chapter 1).

The effect of the above was that the disc could deform fully into the slug within the nose cone without impedance from the sides of the primer housing, and it was able to travel, without resistance, the optimum distance to impact the rock at the end of the hole. The thin plastic constituting the closed end of the primer has a negligible effect on the impact of the ultra-high velocity slug on the rock at the toe of the hole.

For the Surface Tests and Underground Tests described in Chapter 7 and Chapter 9 respectively, the cylindrical prototype without the nose cone was used. In the Surface Tests the prototype was open-ended. (The nose cone was only manufactured as a prototype for production and was used only once later in a production stope at Randfontein Mine. The results were not measured).

As stated earlier, in the Underground Tests the open end was covered with a thin plastic membrane held in place by a rubber band, to prevent drill chippings or other foreign matter entering the stand-off void.

## CHAPTER 7      LABORATORY TESTING OF PROTOTYPES

### 7.1      Introduction

The testing of prototypes for the directional primer charge was carried out on both an empirical basis and an analytical basis.

The empirical basis was used to experimentally determine the optimum stand-off distance and to determine the effect of foreign matter such as drill chippings in the stand-off distance void. These tests used witness plates to determine the efficacy of the prototypes by their demonstrated forward punching power of the impact of the metal slug on a metal plate. They were used as indicative tests only, and therefore showed trends as opposed to absolute values.

The analytical tests, on the other hand, were designed to determine accurate values so that various theoretical models could be assessed for their applicability to describe the action of the directional primer charge and their accuracy in predicting final states such as slug velocity. These tests were undertaken at the Advanced Detonics Laboratory at Naschem's Boskop testing range where various states of the fired directional charge could be captured visually by means of flash X-ray radiographs and the velocity of the slug could be measured at various stages of its flight by means of electronically-timed shorting screens.

Variations in prototype designs involved the type of explosive used and the quantity of explosive per charge. In the empirical tests various commercial explosives were tested being nitroglycerine - based explosives, water gel explosives, emulsion explosives and PETN as well as the military explosive Composition B. As it became apparent that the greater forward punching power was associated with the explosive of highest velocity of detonation, the analytical tests to determine slug velocities for the various design variables of explosive type, charge mass, and disc mass were carried out on the high velocity of detonation explosives of Composition B, Super Gelnite and TNT.

Various prototype designs of the directional primer charge were tested over a three year period. The tests were undertaken to measure experimentally the slug velocities for various design variables which include, explosive type, explosive mass, liner thickness and liner mass.

Using flash X-ray radiography and shorting screens along the trajectory of the slug, the velocity was able to be determined by two independent means.

The experimental work can be summarised in the following table.

**TABLE 7.1 SUMMARY OF SURFACE TESTS**

NAME OF TEST SERIES	PURPOSE OF TESTS	NO. OF TESTS
Witness Plate Tests	To observe the punching power (impact) of directional primer charges to determine the optimum stand-off distance.	±30
Advanced Detonics Laboratory  First Set of Tests  Second Set of Tests  Third Set of Tests	To measure the final slug velocity for a constant mass of Composition B explosive i.e 65 grams.  To measure and determine the change in final slug velocity as a function of the change in explosive cartridge charge length represented by a change in charge mass from 15 grams to 50 grams of Composition B explosive.  To measure the final slug velocity for three different explosives, i.e. Composition B, TNT and Super Gelignite, housed in a constant volume cartridge.	4  9  18
		31



## 7.2 Witness Plate Tests

### 7.2.1 Stand-off Distance

Early tests of the directional primer charge prototype were performed to determine empirically the optimum stand-off distance. These tests were carried out using witness plates. (See photographs in Appendix 10).

Witness plates are metal plates against which the charges are fired and they act as a target for the projected slug.

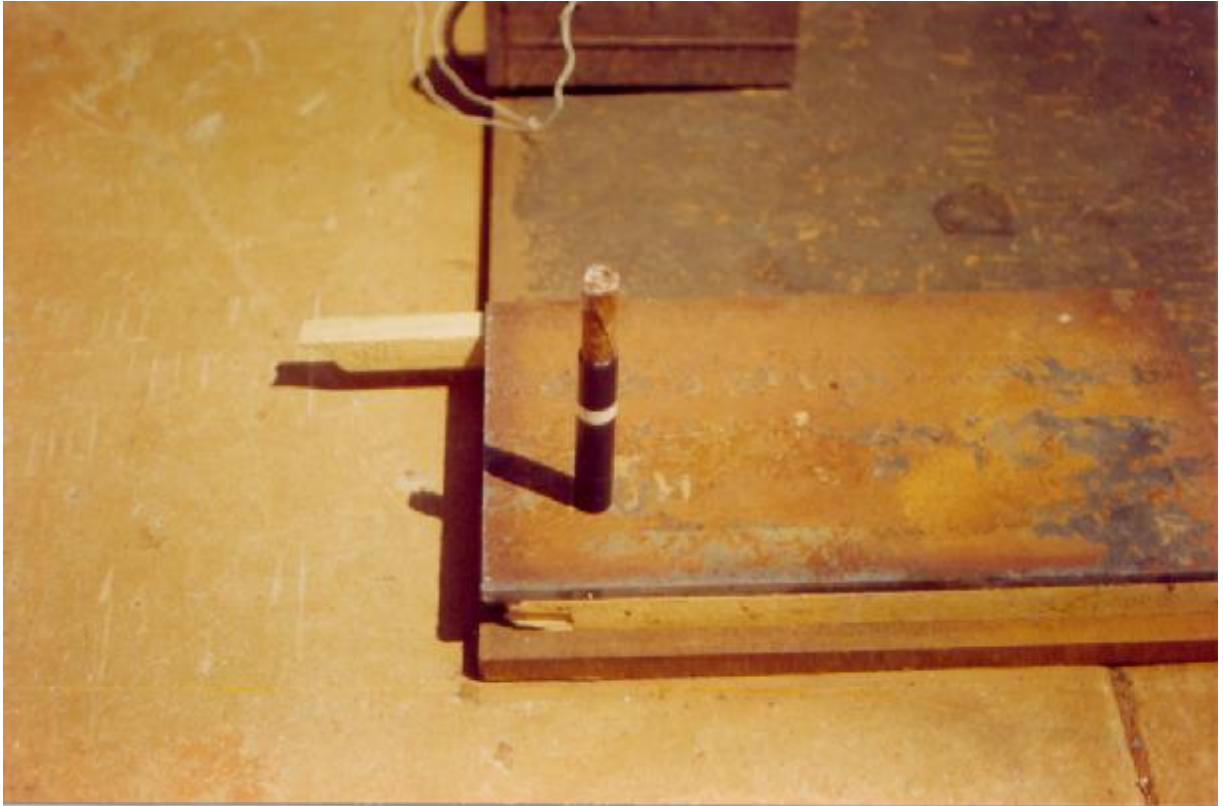
The resultant effect on the plate, its deformation, perforation or rupture, bears “witness” or testimony to the effect of the slug.

When the stand-off distance between the liner and the plate was zero, the effect of the directional primer charge was to “clean” the plate, i.e., all it did was remove particles of rust and any metal burrs from the surface of the plate.

As the stand-off distance increased, the effect of the slug became more pronounced. At a short stand-off distance of 5 to 10 mm, the witness plate bulged out where the slug hit the plate. The bulge grew larger with increasing stand-off.



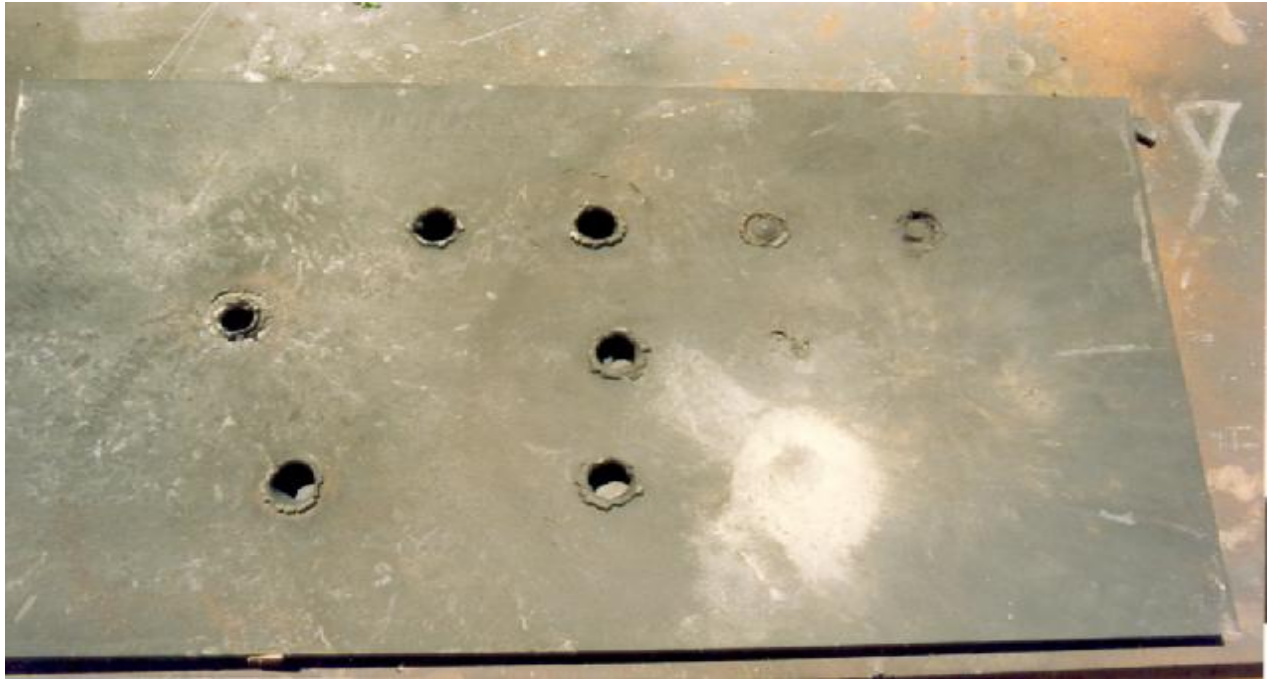
**PHOTOGRAPH 7.1 SHOWING DIRECTIONAL PRIMER CHARGE DETONATION CHAIN**



**PHOTOGRAPH 7.2 SHOWING DIRECTIONAL PRIMER CHARGE POSITIONED ON A WITNESS PLATE**

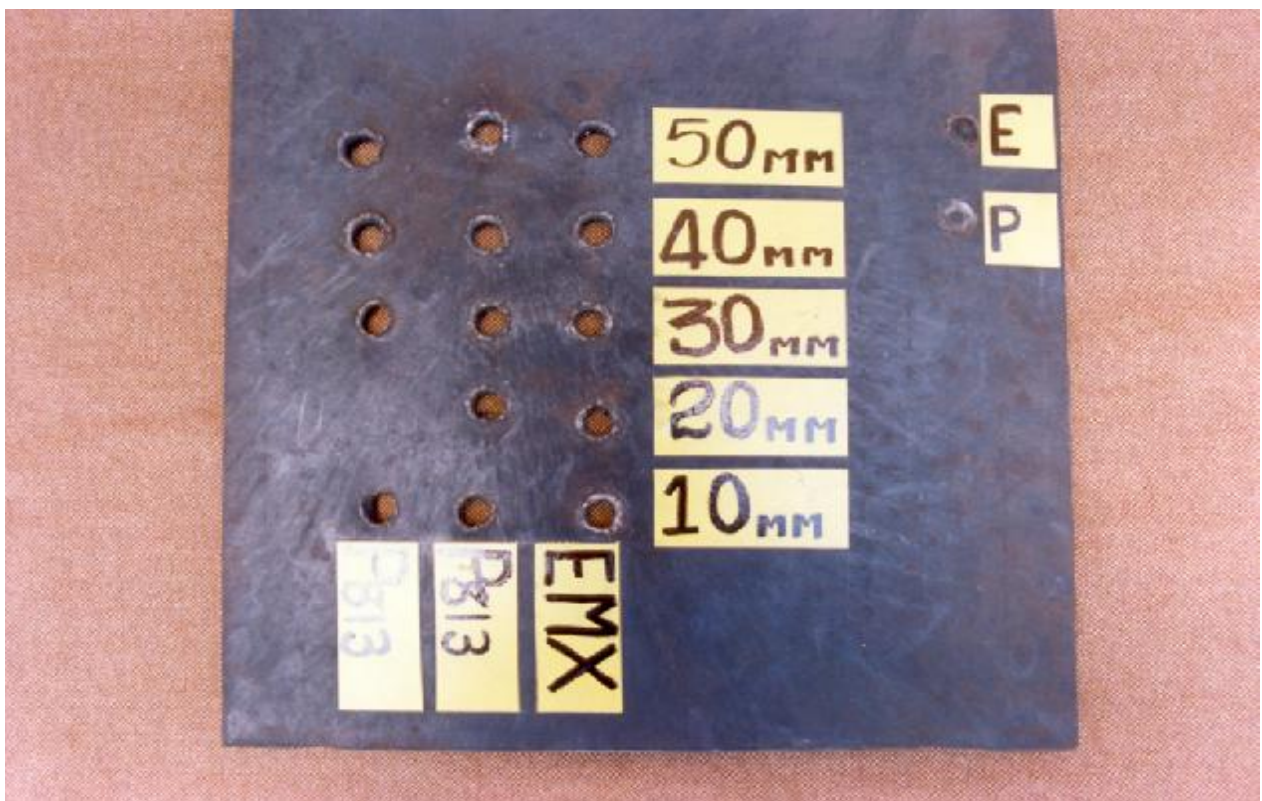


**PHOTOGRAPH 7.3 SHOWING PENETRATION OF PRIMER SLUG THROUGH THE WITNESS PLATE**



**PHOTOGRAPH 7.4 SHOWING WITNESS PLATE PENETRATION RESULTS OF VARIOUS STAND-OFF DISTANCES**

For different types of explosives of different explosive strengths, the punching power of the slug differed. Higher power explosives with higher velocity of detonations had the ability to penetrate thicker witness plates with the same sized disc (metal liner).



**PHOTOGRAPH 7.5 SHOWING HOLES PUNCHED THROUGH WITNESS PLATE**

Simply and empirically, the witness plate test proved the important and fundamentally basic characteristic of the directional primer charge namely that substantial energy from the explosion of the charge is directed forwards. Such was the forward energy that the charge had the power to punch holes through metal plates. The concept had been practically demonstrated and an effective directional primer charge had been developed.

### **7.2.2 Explosively-Forged Projectile Confirmation**

The nature of the slug remnants was such that it appeared that the directional primer charge was an explosively-forged projectile and not a jet; i.e. that the penetration was due to the impact momentum of the slug and not the cutting action of a stream of high velocity small particles.

Whole slugs were recovered from the sand under the perforated witness plate, albeit flattened and deformed. In some instances when the slug did not penetrate fully through a thick plate, it was found embedded in the plate.



**PHOTOGRAPH 7.6 SHOWING TWO SLUGS EMBEDDED IN WITNESS PLATES**

The witness plate test was the first practical test that demonstrated the effect and the extent of the forward-directed hammer-like blow impact energy of the directional primer charge.

A variety of tests with different explosives were undertaken. The importance of a clear stand-off distance, i.e., a clear void in the space between the disc and the plate, was demonstrated. Tests showed that sand or small stones in the stand-off volume had a marked negative effect on the punching power of the directional primer charge. (See photographs in Appendix 10).

Although these were used as indicative-only tests, they contributed significantly to the final design of the directional primer charge as they demonstrated the requirement for a closed nosecone to maintain the integrity of the stand-off void.

### **7.2.3 Summary of Witness Plate Tests**

In summary, the witness plate tests

- provided a practical demonstration of the charge's forward directional power, shown by its ability to punch holes through metal plate of substantial thickness – i.e., 12 mm.
- indicated that the optimum stand-off distance for the test charge prototype was of the order of one calibre, i.e., 30 mm.
- demonstrated that obstructions in the stand-off void, such as sand or small stones, had a deleterious effect on the forward directional power of the charge.

## **7.3 Detonics Laboratory Testing**

### **7.3.1 The Advanced Detonics Laboratory**

For the experimental tests undertaken at the Advanced Detonics Laboratory at Naschem's Boskop testing range, a basic design for the directional primer charge was used. This design comprised the basic components of the charge only, namely the disc, the explosive charge and a cylindrical tube to house the disc and the charge.

### **7.3.2 Basic Design**

The basic design was considered to be sufficient because the purpose of the tests was to determine qualitatively the effect of various parameters, e.g., explosive type, explosive mass and disc mass, on the final velocity of the slug. Therefore, the more elaborate design, which has been conceptualised and would be applicable to practical usage in the mines, and which included such features as an enclosed and tapered nose-cone, perforated rear assembly and compressible housing, was considered to be an over-sophistication for the purpose of surface testing.

### **7.3.3 Sets of Tests Undertaken**

Three sets of tests were carried out at the Advanced Detonics Laboratory at Boskop, as follows.

1. The first set, was the detonation of four similar charges of Composition B of constant explosive mass. The purpose was to determine the final velocity of the disc's slug.
2. The purpose of the second set of tests was to determine the change in slug final velocity as a function of the explosive charge length. Again the explosive tested was Composition B.
3. The third and fourth set of tests was undertaken to compare the slug velocities obtained with Composition B with those obtained using TNT and Super Gelignite. Super Gelignite was purported to be the highest velocity of detonation commercially manufactured nitoglycerine based explosive. At the same time the disc's mass was increased from 6 g to 8 g, as theoretical calculations indicated that a slower velocity might be expected with a greater mass.

## **7.4 Experimental Techniques**

The experimental techniques used to determine the slug velocity were: -

- Flash X-ray Radiography
- Electronically-timed Shorting Screens

### **7.4.1 Flash X-Ray Radiographs**

Flash X-ray radiography is an important diagnostic technique in ballistics as it can capture images of the high velocity projectile in flight. (Held, 1993, Jamet et al, 1976). By using two pulsed X-ray heads, two images of the slug in flight can be captured at two different time intervals. Figure 7.1 depicts schematically the arrangement of the experimental set-up of the tests.

The charge is supported with its axis horizontal and is fixed at right angles to the X-ray heads and towards a steel witness plate. The witness plate acts as a catcher for the slug and is placed just less than a metre from the charge. Behind the charge is positioned the X-ray film cassette. Both the film cassette and the X-ray heads are screened to protect them from blast damage as the charge is fired.

The X-ray heads are triggered sequentially at pre-set delay times after the firing of the charge.

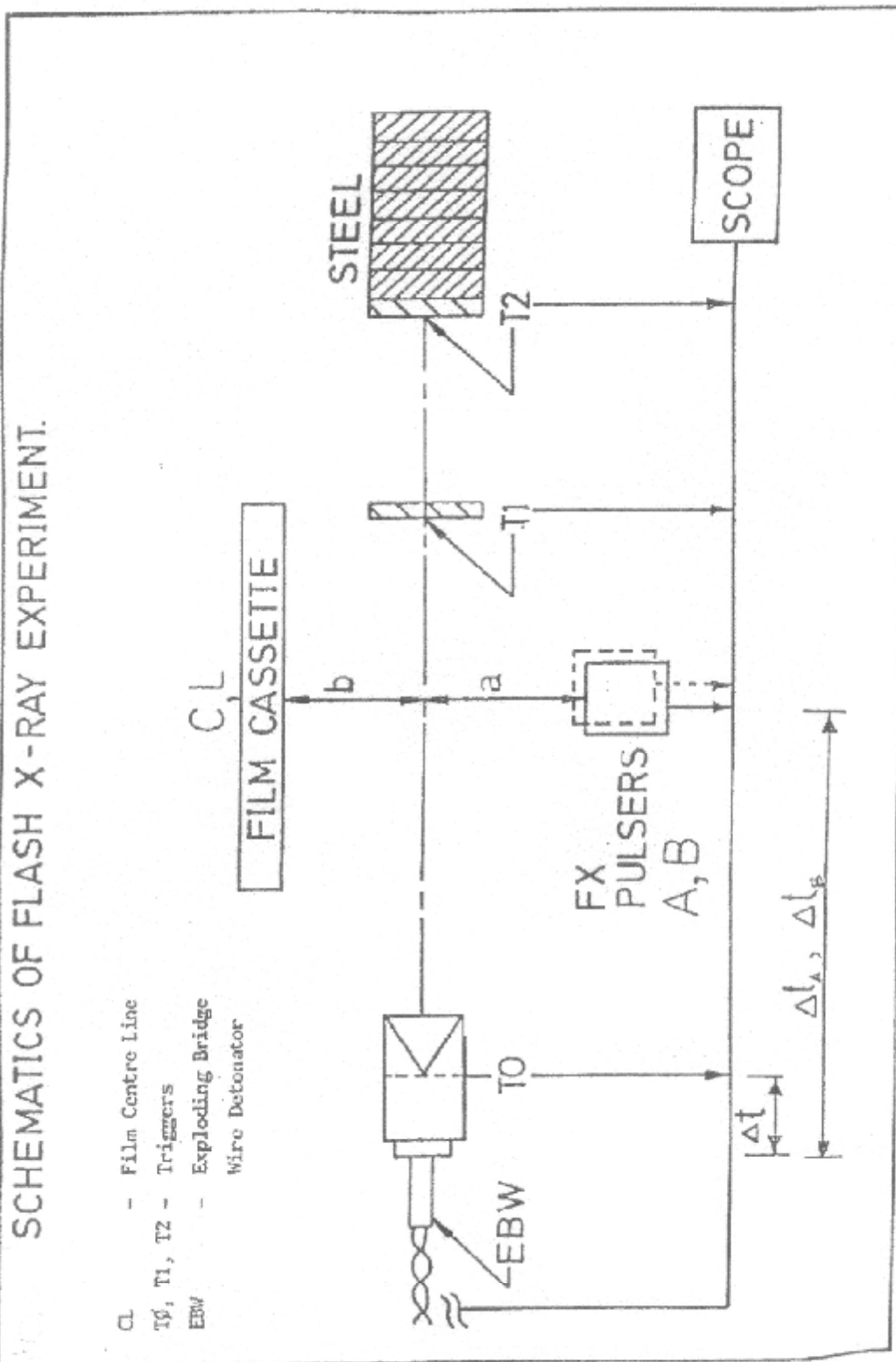


FIGURE 7.1



#### 7.4.2 Electronically-timed Shorting Screens

Although termed “instantaneous” electric detonators, the electric detonators had an initiation time delay variation (or “shudder”) that was too large to guarantee sufficient accuracy to capture the flight of the slug at the prescribed instant. Therefore an ionisation probe was installed on the charge at the position of the disc.

The ionisation probe, in the form of a thin double-stranded wire, is short-circuited by the detonation gases when the detonation front reaches the disc. It activates the delay generator for the X-ray heads. Hence the start signal coincides with the detonation wave front meeting the explosive / disc interface. This represents the start of the movement of the disc.

Shorting screens made up of a grid of thin wires are positioned in the trajectory of the positioned slug, and these are connected to the electronic timing device. The distance from the ionisation probe to the shorting screen can be measured physically prior to the initiation of the charge, and the time intervals from the start of movement of the disc to the breaking (or shorting) of the screens are recorded on the electronic timer.

If the screens are at a relatively large distance (say 300 mm and greater) from the charge compared with the distance the maximum velocity is achieved (say 20 mm), an acceptable approximation of the velocity is obtained.

Obviously, if the screen is close to the charge, errors in accuracy in measuring the small distance will affect the velocity calculation and the acceleration phase from zero to maximum velocity will form a major part of the distance, so the resultant velocity calculation of distance over time will not represent the true maximum velocity.

If there is more than one screen in the trajectory, the distance between the screens can be measured and the time between shortings can be recorded and therefore the mid-flight velocity can be obtained. Also, by taking a number of readings, variations in velocity such as retardation owing to air resistance can be determined.

For the flash X-ray radiography method, the pulsed X-ray heads produce images on the X-ray film. To measure accurately the true distance between images without taking magnification distortion into account, the image of a metal ladder of precisely known distances between the rungs is recorded onto the film prior to the initiation of the charge.

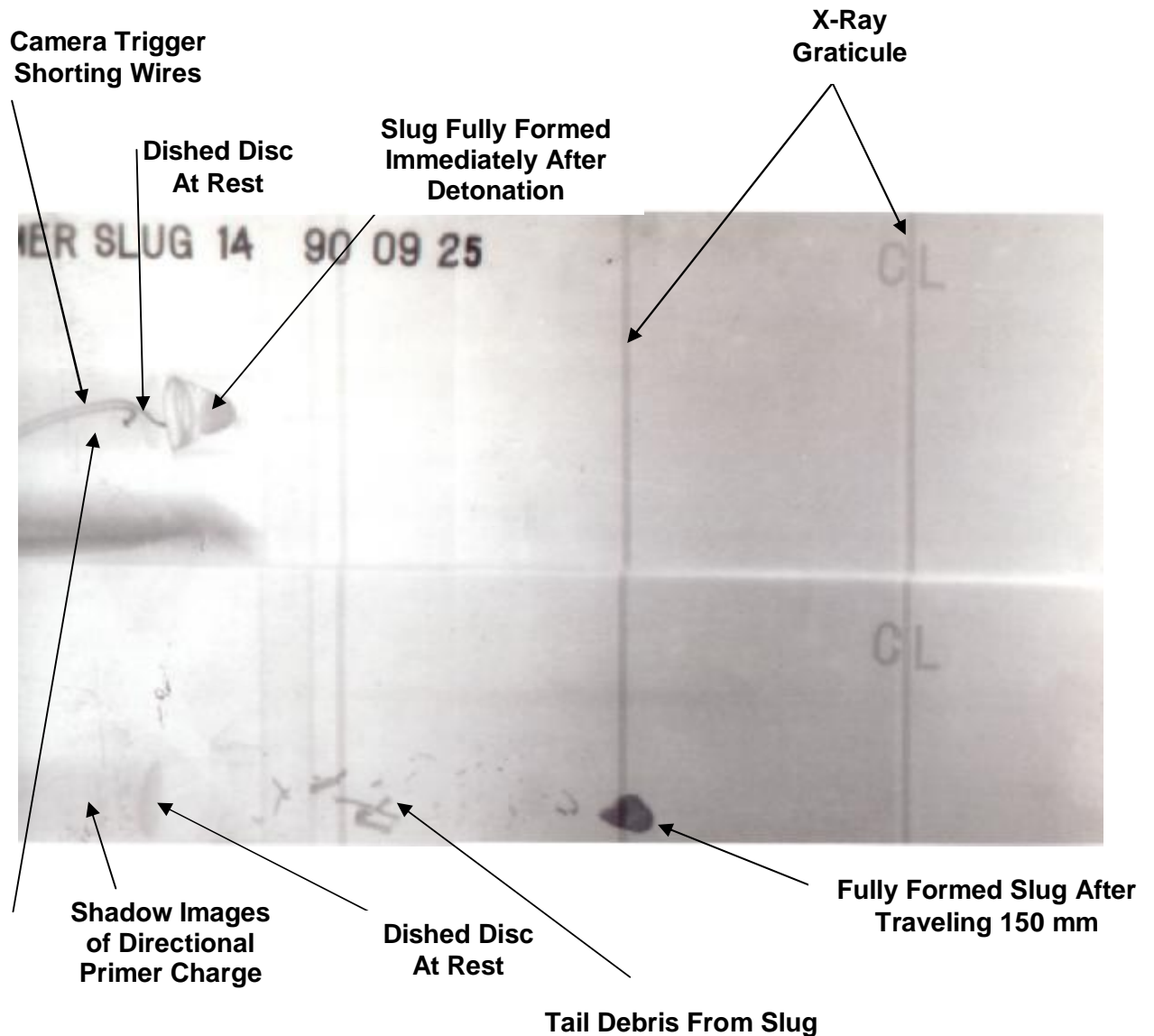


*Photograph 7.7 shows the Flash X-ray Radiography set-up. The board on the left is shielding the large sheet of X-ray film. The directional primer charge is secured in a horizontal position parallel to the X-ray film. As can be seen by the blue-wrapping, the initiating charge is Powergel. Also seen in the foreground are the conducting wires from the ionisation probes which are placed in the directional primer charge in order to trigger the timing mechanisms for the camera. In front of the charge about a metre away is a large cylindrical steel catch plate in front of which is a graticule of wires which serve as a timing screen.*

#### **PHOTOGRAPH 7.7 SHOWING FLASH X-RAY TESTS SET-UP**

This provides a graticule or grid as background on the film to which the distance between the two slug images can be compared and determined precisely. As the time delays,  $t_1$  and  $t_2$  from the trigger time,  $t_0$ , are known, the time between the images can be calculated.

The flash X-ray radiograph also gives a visual image of the disc at rest and the slug in flight and, by suitably adjusting the time delay of the first X-ray head, the transformation of the slug from the disc can be shown. In addition, the second image can show visually any changes in shape or intact mass or rotation in flight of the slug. This provides visual confirmation of the design assumptions and the theoretical design calculations. (see Flash X-Ray Images in Appendix 11).



**PHOTOGRAPH 7.8 FLASH X-RAY IMAGES NO. 1**

**SHOWING DIRECTIONAL PRIMER CHARGE FORMATION AFTER 15 ms AND 75 ms**

### 7.4.3 Typical Set-up Dimensions

Typical set-up dimensions used at the Advanced Detonics Laboratory at Boskop were: -

**TABLE 7.2 A.D.L FLASH X-RAY SET-UP DATA**

Charge to witness plate	600 – 800 mm
Charge to ladder mid-point	300 mm
Ionisation probe	At disc, i.e., 35 mm from front of primer
Film length	900 mm
Magnification	1.3
Shorting screens	One on witness plate in all tests. Second screen in Test 2 only.
Witness plate	100 mm thick x 200 mm diameter metal cylinder.

### 7.4.4 Time-Distance Data From First Set of Tests

The first set of tests comprised the firing of four separate charges each containing 65 grams of Composition B. Time-distance measurements were made using the flash X-ray photographs produced the following results presented in Table 7.3.

**TABLE 7.3 SLUG TIME-DISTANCE MEASUREMENTS**

<b>CHARGE NO.</b>	<b>DISTANCE (mm)</b>	<b>TIME (ms)</b>	<b>CALCULATED VELOCITY (m/s)</b>
1	30 248	15,41 120,9	2070
2	50,4 201	25,41 100,5	2005
3	72,3 288,5	35,49 140,55	2060
4	26,9 175	10,96 80,49	2130
<b>MEAN</b>			2065

Therefore, the first set of tests produced results with a scatter of 5 % i.e. a range from 2005 to 2130 m/s, which gave a mean slug velocity value of 2065 m/s.

Appendix 6 lists all the slug time-distance measurements for the second set of tests i.e. the nine cartridges in the Composition B series of explosive masses ranging from 13,7 g to 48 g, for the third set of tests i.e. the eight cartridges of 65 g Super Gelignite and the two cartridges of 93 g Composition B and for the fourth set of tests i.e. the eight cartridges of 45 g TNT with a 25 g PETN booster. These are summarised Table 7.4.

#### 7.4.5 Summary of Test Results

The results of the four sets of tests undertaken at the Advanced Detonics Laboratory are presented below in Table 7.4.

**TABLE 7.4 SUMMARY OF TEST RESULTS**

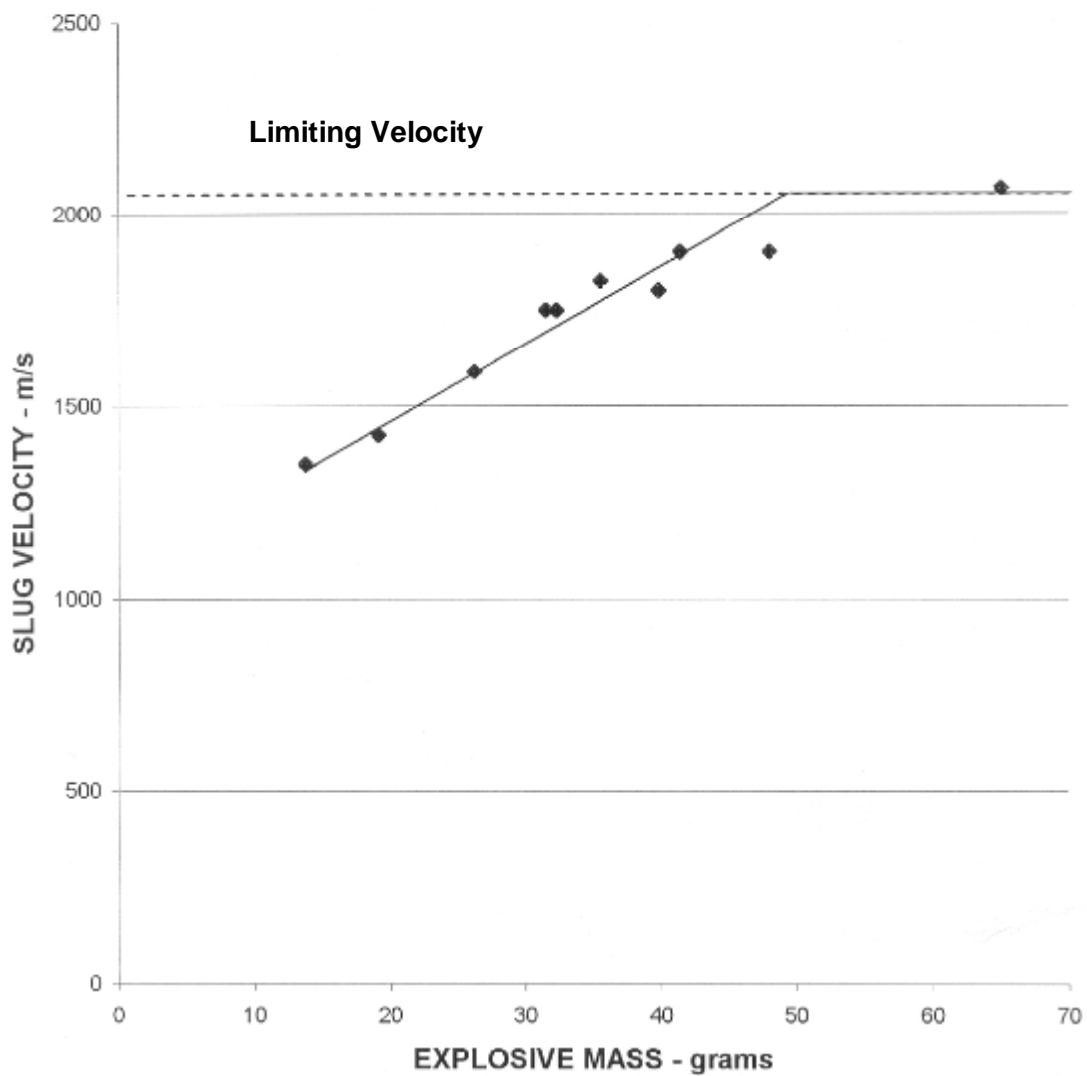
SET OF TESTS	EXPLOSIVE TYPE	DISC MASS (g)	EXPLOSIVE MASS (g)	NO. OF TESTS	MEASURED SLUG VELOCITY (m/s)
First Set	Composition B	6	65	4	2065
Second Set	Composition B	6	13,7	1	1350
		6	19,1	1	1425
		6	26,2	1	1590
		6	31,5	1	1750
		6	32,3	1	1750
		6	35,5	1	1825
		6	39,8	1	1800
		6	41,4	1	1900
		6	48,0	1	1900
Third and Fourth Sets	Composition B	8	93	2	2045
	TNT	8	45 (70)	8	1510
	Super Gelnite	8	65	8	1130
				31	

Note that for the TNT test, the 45 g of TNT explosive was initiated with 25 g of PETN explosive which has a slightly higher velocity of detonation than TNT. Thus, for the purposes of comparison with Composition B and Super Gelnite the equivalent mass for the TNT tests is 70 g of high velocity of detonation explosive.

## 7.5 Discussion of Test Results

### 7.5.1 Relationship of Slug Velocity to Explosive Mass

The following is a graph showing the relationship between the slug velocity and the explosive mass for the first and second sets of tests i.e. for Composition B from 13,7 to 65 grams and a 6 gram disc.



EXPLOSIVE MASS - GRAMS

FIGURE 7.2 SLUG VELOCITY AS A FUNCTION OF EXPLOSIVE MASS

As can be seen from the above the greater the mass of explosive, the greater the final slug velocity.

In the case of the directional primer charge, an increase in the mass of explosives is directly proportional to an increase of explosive charge length as the explosive cartridge has a constant diameter of 25 mm.

### **7.5.2 Limiting Slug Velocity for Single Explosive Type**

It is common knowledge that when an explosive detonation is initiated, there is a run-up in the velocity of detonation to the final velocity of detonation characteristic of that particular explosive. Therefore, the increase in slug velocity can be ascribed to the run-up of the velocity of detonation over the length of the explosive charge. When the characteristic velocity of detonation of the explosive is reached, a maximum velocity of the slug will be attained and any further length in the explosive charge will not produce an increase in the slug velocity. (See graph in Figure 7.2).

For the parameters used for the directional primer slug used in Tests 1 and 2, namely Composition B explosive and a 6 gram disc, it would appear that the run-up in the velocity of detonation is represented by the increase in the slug velocity until a limiting velocity is achieved which is somewhere between 2000 and 2100 m/s.

### **7.5.3 Comparison Between Slug Velocities for Same Cartridge Size**

The third set of tests was to compare cartridges of TNT and Super Gelnite (which have velocity of detonation of 6700 m/s and 5600 m/s respectively) to cartridges of Composition B (which has a velocity of detonation of 7600 m/s).

As theoretical Gurney calculations showed that an increase in the disc mass would show a commensurate decrease in final velocity, it was decided to use an 8 gram disc in place of the previously used 6 gram disc i.e. the disc could be punched out of 2 mm metal plate instead of 1,6 mm metal plate. It was decided to measure the extent of the decrease in slug velocity with the heavier disc to determine what would be the effect of the momentum of the slug and hence the effect of the impact of the slug on the rock at the end of the hole.



However, the theoretical Shock Physics calculation shows that the disc mass is irrelevant, and the slug velocity should be the same for a 8 g disc as for a 6 g disc for the same explosive. Therefore, there would be a greater momentum with the 8 g disc and a greater force on impact on the rock at the end of the hole.

In the third set of tests comparing Super Gelignite to Composition B, the mass of explosive used was determined by the practicality of filling the cartridges for underground usage. Thus, the fact that the mass of explosive per cartridge was less for Super Gelignite than Composition B was due in part to the difference in their relative densities.

Although the tests were not a direct comparison between the two explosives based on mass, the tests provided a practical comparison based on the same production cartridge package. The tests showed that for the same size explosive cartridge, Composition B produces a far higher slug velocity of 2045 m/s than Super Gelignite of 1130 m/s.

When compared with results in the first set, i.e. 65 g of Composition B explosive with a 6 g disc, it should be noted that the 93 g Composition B explosive with the greater 8 g disc produces much the same slug velocity i.e. 2065 m/s and 2045 m/s respectively.

The decision to use TNT was as a compromise between the more expensive Composition B and the cheaper Super Gelignite. As TNT requires a powerful booster to initiate it, a similar sized cartridge as to that which was used in the third set would have a smaller mass of TNT as space would have to be provided for the booster. The TNT explosive cartridge was formed with a 60 mm long pressed pellet of TNT and a PETN explosive as a booster. The respective masses of the two explosives were 45 g of TNT and 25 g of PETN. As both these explosives are high velocity of detonation explosives the total mass of high velocity of detonation explosive in the TNT cartridge is 70 g.

Thus, from a practical production point of view, the TNT explosive cartridge is comparable to the Super Gelignite and the Composition B cartridges of the same size volumetrically. Compared to the Super Gelignite cartridge with its slug velocity of 1130 m/s, the TNT cartridge has a much higher velocity of 1510 m/s but lower than the Composition B cartridge of 2045 m/s. Thus, the more scientific approach of directly comparing three explosives using the same mass of explosive was rejected in this the third and fourth sets of tests, for a more practical approach of comparing cartridges of the same volumetric size, as would be the case under production conditions in the underground mining stopes.

## 7.6 Correlation of Theoretical Models to Experimental Results

How do the measured results correlate to the plate projection models described in Chapter 3.2, namely the Gurney Model, the Gas Dynamics Model and the Shock Wave Model?

The paper presented at the Warheads Seminal by Szendrei in 1996 (Szendrei 1996) specifically refers to the directional primer charge, giving the measurements and calculations which are now presented below.

### 7.6.1 First Set of Tests Measurements

The measured slug velocity as presented in Table 7.3 in Chapter 7.4.4 is 2065 m/s.

### 7.6.2 Gurney Model Velocity

The Gurney limiting velocity ( $V_G$ ) is given by the equation.

$$V_G = E_G \sqrt{\frac{3z^2}{(z+1)(z+4)}}$$

Where $V_G$	=	Gurney limiting velocity
$E_G$	=	Gurney constant = 2700 m/s for Composition B
$z$	=	$\frac{C}{M}$
$C$	=	Charge mass = 65 g
$M$	=	Disc mass = 6 g

Therefore, for the first set of tests, the calculation of the Gurney limiting velocity  $V_G = 3820$  m/s.

### 7.6.3 Modified Gurney Model Velocity

The Modified Gurney Model as suggested by Weickert, Gallager and Backofen (1995) represents plate acceleration as a two stage process. In the first stage, the plate acquires momentum from the particle velocity behind the detonation wave. In the second stage, the plate acquires additional momentum by the usual Gurney expansion of gases. The energy available for the second stage is suitably adjusted from the "standard" Gurney value to account for the initial momentum coupling.

The net effect is to predict a significantly lower terminal velocity for the plate. (Szendrei 1996).

The modified Gurney velocity ( $V_{GM}$ ) is given by the equation

$$V_{GM} = \sqrt{V_{GR}^2 + V_{pp}^2}$$

Where  $V_{pp} = U_p \frac{z}{z+2}$

$U_p =$  Particle velocity behind detonation front  $= \frac{D}{\Gamma + 1}$

$z = \frac{C}{M}$

$D =$  Velocity of detonation = 7600 m/s for Composition B

$\Gamma =$  Polytropic exponent = 3

$C =$  Charge mass = 65 g

$M =$  Disc mass = 6 g

$V_{GR} =$  Velocity using reduced Gurney energy

$= V_G \frac{E_{GR}}{E_G}$

$E_{GR} = E_G \sqrt{\frac{1 - U_p^2}{E_G^2}}$

Therefore, for the first set of tests, the calculation of the modified Gurney velocity  $V_{GM} = 3075$  m/s.

#### 7.6.4 Gas Dynamics Model Velocity

Aziz, Hurwitz and Sternberg (1961) considered plate acceleration to be a piston in one-dimensional gas expansion. On arrival at the disc, the detonation front is reflected and the disc undergoes smooth acceleration under the imposed pressure. The following is assumed.

- the gas flow is one-dimensional along the axis of the charge.
- the disc is incompressible.
- the detonation gases are described by the polytropic equation of state where  $\Gamma = 3$ .

The assumption of rigid disc (infinite sound speed) implies that wave phenomena play no role and plate motion is described by Newton's laws. (Szendrei 1996).

The gas dynamic velocity ( $V_p$ ) is given by the equation

$$V_p = D \frac{a-1}{a+1}$$

where  $a = \sqrt{\frac{1 + 32C}{27M}}$

- D = VOD = 7600 m/s for Composition B
- C = Charge mass = 65 g
- M = Disc mass = 6 g

Therefore, for the first set of tests, the calculation of the gas dynamics velocity  $V_p = 4380$  m/s.

### 7.6.5 Shock Physics Model Velocity

When the detonation shock wave reaches the interface of the explosive and the metal disc, the shock wave splits in two – a shock wave is transmitted across the interface into the disc and a rarefaction wave is reflected back into the explosive product gases. Continuity considerations require that both waves have the same pressure and particle velocity at the interface at this time. The disc material behind the advancing transmitted shock front is accelerated to the interface velocity. On traversing the disc thickness, the transmitted wave is reflected as a rarefaction wave and the disc free surface is accelerated to twice the particle velocity. The rarefaction wave in turn is reflected off the metal / gas interface as a compression wave and the interface is accelerated to approximately the same value as the free surface. At this time the disc as a whole begins to move at more or less the same velocity. (Szendrei 1996). When the compression wave reaches the free surface a second time, a second rarefaction is generated and this is repeated throughout the flight of the disc, although the magnitude rapidly diminishes with each reflection. Calculations by Lambourn and Hartley (1965) show that a thin steel plate is accelerated to 80 % of its final velocity after the first reflection of the transmitted wave off the gas / disc interface and after six reflections there is no real increase in velocity.

The initial plate velocity therefore is twice the interface velocity with the first interaction of the detonation wave with the disc.

The Shock Model interface velocity ( $U_I$ ) is given by the equation

$$U_I = D \frac{\sqrt{\left(1 + \frac{9R}{16}\right)^2 + \frac{4}{3} \left(\frac{9r-1}{16}\right)} - \left(1 + \frac{9R}{16}\right)}{2 \left(\frac{9r-1}{16}\right)}$$

where  $R = \frac{\delta_p \cdot C_p}{\delta_e \cdot D}$

$r = \frac{S \cdot \delta_p}{\delta_e}$

$\delta_p =$  density of disc = 7,8 for mild steel

$\delta_e =$  density of explosive = 1,60 for Composition B

$D =$  velocity of detonation = 7600 m/s for Composition B

$C_p =$  acoustic velocity = 3600 m/s for mild steel

$S =$  shock adiabat constant = 1,68 for mild steel

The Shock Physics Model free face velocity ( $V_s$ ) is twice the interface velocity ( $U_I$ ).

Therefore, for the first set of tests the calculations of the shock velocities are  $U_I = 925$  m/s for the interface velocity and  $V_s = 1850$  m/s for the slug velocity.

As a check the interface pressure on the disc can be calculated from the equation

$$P_p = \delta_p \cdot C_p \cdot U_I + \delta_p \cdot S \cdot U_I^2$$

and the interface pressure on the explosive product gas can be calculated from the equation

$$P_g = \frac{16}{27} \left( \frac{D - U_I}{D} \right)^3 \cdot P_o$$

where  $P_o = \delta_e \cdot D^2$

The interface pressure on the disc should be the same as the interface pressure on the gas. In the above calculation the pressure on either side of the interface is 37,1 GPa, as is calculated using the two different equation given above.

### 7.6.6 Comparison of Calculated Velocities for Composition B

Table 7.5 presents the results of the actual measurement of slug velocity and the theoretical calculations of the slug velocity for each of the proposed models using a 6 gram disc and 65 grams of Composition B explosive.

**TABLE 7.5 MEASURED AND CALCULATED VELOCITIES**

	<b>SLUG VELOCITY</b>
Calculated Gurney Velocity	3820 m/s
Calculated Modified Gurney Velocity	3075 m/s
Calculated Gas Dynamic Velocity	4380 m/s
Calculated Shock Physics Velocity	1850 m/s
<b>Measured Slug Velocity</b>	<b>2065 m/s</b>

From the above, it can be seen that the Gurney Models and the Gas Dynamic Model grossly overestimate the slug velocity by twofold, whereas the Shock Physics Model underestimates the slug velocity by only 10 %.

Therefore, it would appear that the Shock Physics Model is the most applicable of the classical theoretical models for the directional primer charge.

### 7.6.7 Comparison of Calculated Velocities for Different Explosives

The first and second sets of tests dealt with the explosive Composition B only. The third set of tests deals with the comparison between the three explosive types – Composition B, TNT and Super Gelignite.

Table 7.6 presents the results of the calculations of the various theoretical models and the actual measurement of the final slug velocities for an 8 gram disc and Composition B, TNT and Super Gelignite explosives.

**TABLE 7.6 MEASURED AND CALCULATED VELOCITIES FOR 8 GRAM DISC**

	FINAL SLUG VELOCITIES – m/s		
	COMPOSITION B	TNT	SUPER GELIGNITE
Gurney	3870	2930	2675
Modified Gurney	3110	2390	2275
Gas Dynamic	4460	3100	2950
Shock Physics	1850	1520	1120
<b>Measured</b>	<b>2045</b>	<b>1510</b>	<b>1130</b>

Again, it would appear that the Shock Physics Model most closely predicts the actual measured slug velocity. There is a greater degree of predictability with TNT (1520 m/s versus 1510 m/s) and Super Gelignite (1120 m/s versus 1130 m/s) than with the higher velocity explosive Composition B (1850 m/s versus 2045 m/s).

### **7.6.8 Applicability of Theoretical Models**

The Gurney Model, and the Gas Dynamics Model grossly over predict the measured velocity of the slug. Even the Modified Gurney Model, which seeks to reduce the final velocity, is 50% to 100% greater than the measured velocity. Only the Shock Physics Model comes close to accurately predicting the measured velocity.

The reason for the above is probably the nature of the geometry of the directional primer charge. Being a relatively long cylinder, there is probably an inefficient utilization of the available explosive energy, much of which could be dissipated radially into the atmosphere, Only a small portion of the available explosive energy is therefore directed at driving the metal disc forward by explosive product gas expansion.

In addition, the apparent short duration of slug acceleration, as shown by the flash X-ray experiments, does not indicate a gradual increase in acceleration typical of the piston-like push of gas expansion.

The Shock Physics Model assumes that the final velocity of the slug is solely due to the shock wave pulse that the detonation wave of the explosion imposes on the metal disc.

Thus, in the case of the directional primer charge, which is a long cylindrical charge, it would appear that the Shock Physics Model is the more applicable model and appears to predict the final velocity of the slug more accurately than the other classical models.

This is significant in the design of the directional primer charge with particular reference to predicting the effect that various explosives types will have on the final velocity of the slug, i.e. the higher of velocity of detonation, the greater the velocity of the slug. Ideally, Composition B should be used because it has the highest velocity of detonation of the three explosives tested, and therefore will produce the greatest slug velocity. However, from a practical point of view, if all three explosives produce a slug velocity that is sufficient to create the umbrella fracture in rock in the stope face underground, then final slug velocity becomes less important and other factors such as cost start to play a greater role in the choice of which explosive should be used in the final design of the directional primer charge.



## 7.7 Summary of Conclusions Drawn From Surface Tests

The conclusions that may be drawn from the series of surface tests undertaken at the Advanced Detonics Laboratory at Boskop using the directional primer charge prototype are summarised as follows: -

- a) The slug velocity is related to the velocity of detonation of the explosive type – the higher the velocity of detonation, the greater the slug velocity. In order of producing the greatest slug velocity the explosives may be ranked as follows.

**TABLE 7.7 RANKING OF EXPLOSIVES BY SLUG VELOCITY**

<b>RANKING</b>	<b>EXPLOSIVE TYPE</b>	<b>VELOCITY OF DETONATION</b>	<b>8 g SLUG VELOCITY</b>
1	Composition B	7600 m/s	2045 m/s
2	TNT	6700 m/s	1510 m/s
3	Super Gelignite	5600 m/s	1130 m/s

- b) The slug velocity is dependent on charge length. There must be sufficient charge length to allow the detonation velocity to run up to attain the characteristic velocity of detonation of the particular explosive.
- c) For a 25 mm diameter cartridge, a charge length of 50 mm appears to be sufficient to attain the characteristic velocity of detonation and therefore, the limiting slug velocity.
- d) Although Super Gelignite produced the slowest slug velocity of the three explosives tested, the velocity was still high at over 1000 m/s.
- e) From the flash X-ray radiograph images, the slug appeared to be fully formed in the first 20 mm of travel, and did not appear to change in shape or suffer any loss of mass over the next few hundred millimetres.
- f) The results tended to confirm theoretical calculations and predictions of the Shock Physics Model for explosive shock loading of metal plates.

## CHAPTER 8 ANALYSIS OF IMPACT OF HIGH-VELOCITY SLUG ON ROCK

### 8.1 Introduction

For many years, two phenomena were known to exist for which there was no credible explanation, namely the “washer-in-hole” and the “air gap” phenomena. (Both have been discussed in detail in Chapter 5.2). By analysing the shock effects generated by a directional primer charge, an explanation can now be proposed.

Simply stated, the metal liner (read “washer”) of the directional primer charge has sufficient stand-off distance (read “air gap”) to become a high-velocity slug (or explosively-forged projectile). On impact with the rock at the toe of the hole, the slug has sufficient energy to move the surface of the rock at the toe back into the rock mass. Such is the impact that an umbrella crack is created at the toe through tension in the rock on the sides of the hole.

In this Chapter, it will be shown that calculations indicate that the displacement of rock at the toe of hole due to the slug impact ranges from 1,2 mm to 2,1 mm for slugs travelling at 1000 m/s and 2000 m/s respectively. This amount of differential displacement in brittle rock, such as quartzite, may be sufficient to break the rock in tension, thus creating an umbrella fracture at the toe of the hole.

Further calculations will show that the duration of the impact pressure pulse ranges from 48  $\mu$ s to 27  $\mu$ s for a slug velocities of 1000 m/s and 2000 m/s respectively. This is considered to be a sufficient period of time for the expanding explosive product gases to enter the umbrella cracks and extend them further.

Further analysis of the shock regimens indicate that the high-velocity slug generates an air shock wave ahead of the slug and travelling some 25 % faster than the slug. This air shock wave impacts the rock ahead of the metal slug, thus enhancing the effects of the slug impact on the rock.

Thus, it can be expected that the directional primer charge increases the break out of rock at the toe of the hole due to the formation of umbrella fractures caused by slug impact and the further propagation of the umbrella fracture by the subsequent expansion of the explosive gases.

## 8.2 Air Shock Ahead of High-Velocity Slug

The action of an explosively-driven metal slug travelling down a blasthole is akin to a high-velocity piston. Ahead of the slug, the air will be compressed to such an extent and at such a rate that an air shock is formed. This air shock wave will strike the toe of the hole ahead of the oncoming slug. Thus, in effect the toe of the hole is subjected to the onslaught of two impacts – the first an air shock wave and the second a high-velocity metal slug.

### 8.2.1 Velocity of Air Shock Wave

Appendix 7 (Szendrei 1999) gives theoretical calculations for slug velocities between 1000 m/s and 2000 m/s. These show that: -

- the air shock velocity is greater than the slug velocity by some 25 %.
- the air ahead of the slug is compressed to about 5 times its initial value.
- the air shock wave pressure ranges from 16 atmospheres for a 1000 m/s slug to 60 atmospheres for a 2000 m/s slug.

The air shock calculation results are given in the following table.

**TABLE 8.1 AIR SHOCK CHARACTERISTICS**

<b>SLUG VELOCITY m/s</b>	<b>AIR SHOCK VELOCITY m/s</b>	<b>RELATIVE AIR DENSITY</b>	<b>SHOCK PRESSURE ATMOSPHERES</b>
1000	1293	4,42	16,1
1100	1405	4,60	19,1
1200	1519	4,76	22,3
1300	1633	4,90	25,8
1400	1748	5,02	29,6
1500	1864	5,12	33,7
1600	1980	5,21	38,0
1700	2097	5,28	42,7
1800	2213	5,35	47,6
1900	2331	5,41	52,8
2000	2449	5,45	58,2

## **8.2.2 Effect of Air Shock Wave on Rock**

The air pressure ahead of the 1000 m/s velocity slug is 16 atmospheres or 1,6 MPa and the air pressure ahead of the 2000 m/s is 60 atmospheres or 6 MPa.

With the predominate rock in underground Witwatersrand gold mines being quartzite with a uniaxial compressive strength of over 200 MPa, the air shock wave ahead of the slug at a strength of 6 MPa has little or no effect on the blasthole. Even the tensile strength of the rock, which is of the order of 25 MPa say, is still far stronger than even the 6 MPa air shock pressure for the greater velocity 2000 m/s slug of Composition B.

## **8.3 Impact Shock of Metal Slug on Rock**

The enhancing effect of a metal liner on a hollow charge discovered by Thomanek (1960) and reported on in Chapter 2 is ably demonstrated by the directional primer charge. The impact of a high velocity slug on the rock of the toe of the hole subjects the rock to far greater pressures than the impact of the air shock wave ahead of it.

In Appendix 7, theoretical calculations for slug velocities ranging between 1000 m/s and 2000 m/s (i.e. the range of velocities measured in the laboratory tests of Section 7) show that the impact of the slug on the rock

- causes the metal / rock interface to move at a velocity between 700 m/s and 1400 m/s.
- generates a shock wave in the rock ranging between 5200 m/s and 6600 m/s.
- creates an impact pressure on the rock between 10 GPa and 24 GPa.

The results presented in Appendix 7 are summarised in the following table.

**TABLE 8.2 IMPACT SHOCK CHARACTERISTICS**

<b>SLUG VELOCITY m/s</b>	<b>INTERFACE VELOCITY m/s</b>	<b>SHOCK VELOCITY IN ROCK m/s</b>	<b>IMPACT PRESSURE GPa</b>
1000	702	5,22	9,61
1100	769	5,31	10,81
1200	835	5,45	12,06
1300	901	5,59	13,36
1400	967	5,73	14,69
1500	1033	5,87	16,07
1600	1098	6,00	17,49
1700	1164	6,15	18,95
1800	1228	6,28	20,46
1900	1293	6,42	22,01
2000	1358	6,57	23,59

Thus, whereas the air shock wave pressure for an air shock velocity of 2500 m/s (corresponding to a slug velocity of 2000 m/s) generates a shock pressure of 60 atmospheres or 6 MPa, the slug generates an impact shock pressure of 24 GPa.

Taking the compressive strength of rock at 200 MPa and its tensile strength at 20 MPa, then, the air shock pressure at 6 MPa is too weak to break the rock even in tension, whilst the slug impact shock at 24 GPa easily breaks the rock in compression.

### **8.3.1 Shock Phase – Duration and Attenuation**

Given the foregoing calculation of impact pressures, the immediate question of importance is – how long does the pressure last? Although pressure is attenuated due to the dissipative effects of energy losses due to heat, viscosity etc., by far the largest attenuation effect is that of the rarefaction shock waves. Therefore, the size and geometry of the metal slug are of paramount importance in the duration and attenuation of the impact pressure pulse.

Impact, shock waves are created which propagate away from the contact surface in both directions. Because the rod is finite in lateral extent, the shock wave is reflected as a rarefaction wave, reducing the pressure in the shocked regions and allowing material flow to take place. The expansion waves from the sides lead to zones of plastic flow radically in the frontal zones of the rod, the most prominent feature being the formation of the characteristic mushrooming of the tip of the rod. (see Figure 8.1).

Whilst the stress is being relieved at the contact surface by release waves from the side, the shock wave propagates upstream in the rod. However, it does not outrun the release waves.

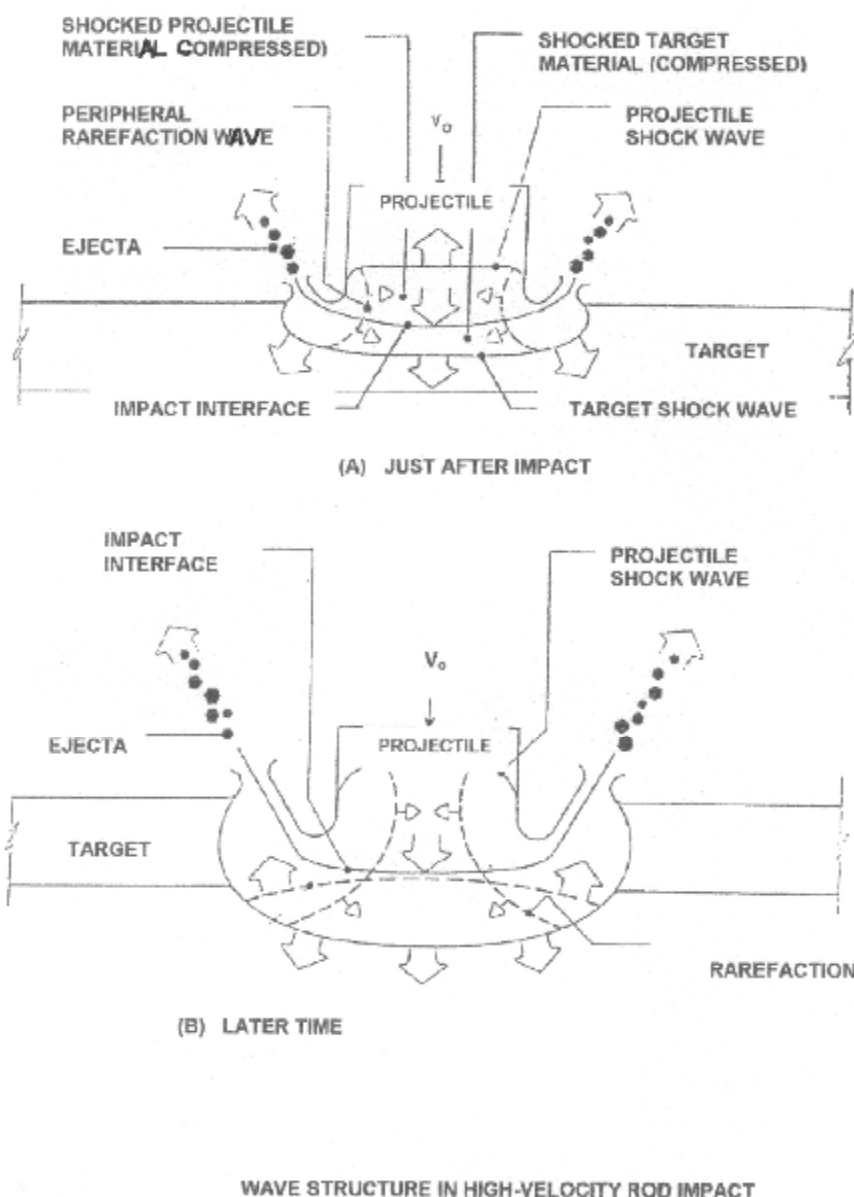


FIGURE 8.1

Fundamentally, it can be shown that any disturbance (i.e. release wave) behind the shock wave will always propagate faster than the shock wave, and thus a rarefaction wave will always overtake the shock front in the rod. When this happens, the high-pressure shock conditions in the rod are destroyed. This attenuation of the impact shock condition is therefore of short but finite duration.

From the above considerations, two approximations can be made for the duration of high-pressure shock conditions, namely: -

- the time required for the release of shock pressure along the contact surface by rarefaction waves from the side, and
- the time required for the release waves to catch up with the shock wave propagated upstream in the rod.

In Appendix 7, Szendrei (1999) gives the MATHCAD calculation for the Ravid model (Ravid et al 1987). Application of the Ravid model in the case of a mild steel rod striking quartzite rock at 1600 m/s yields the following results: -

Interface velocity	=	1098 m/s
Shock velocity (rod)	=	4483 m/s
Shock velocity (rock)	=	6009 m/s
Rarefaction velocity (rod)	=	5020 m/s
Shock duration $t_s$	=	1,61 $\mu$ s
Rod deformation length in $t_s$	=	6,3 mm
Loss length (rod) in $t_s$	=	0,8 mm
Advance of interface	=	1,8 mm

This analysis shows that rarefaction waves destroy the shock wave in the rod in time  $t_s = 1,61$  microseconds and thus reduce the impact pressure to some lower value. In this time, the shock wave has progressed 6,3 mm up the rod and the rod had undergone shortening by 0,8 mm due to the flow of rod material laterally as the rarefaction waves arrived from the sides. The rock / metal interface has advanced 1,8 mm under the influence of the impact shock pressure.

Analysis of transient impact conditions for slug velocities between 1000 m/s and 2000 m/s are given in the following table and explained more fully in Appendix 7.

**TABLE 8.3 ADVANCE OF INTERFACE FOR VARIOUS SLUG VELOCITIES**

SLUG VELOCITY m/s	RAREFACTION VELOCITY m/s	SHOCK $t_s$ ms	ADVANCE OF METAL / ROCK INTERFACE (mm)
1000	4765	1,74	1,22
1100	4806	1,72	1,32
1200	4848	1,70	1,42
1300	4890	1,67	1,52
1400	4933	1,65	1,61
1500	4977	1,63	1,69
1600	5020	1,61	1,77
1700	5064	1,59	1,85
1800	5100	1,57	1,93
1900	5153	1,55	2,00
2000	5198	1,53	2,08

### 8.3.2 Plastic Flow Phase – Mushrooming of Tip

After the rarefaction waves have destroyed the impact shock waves and hence the high shock pressure of finite but short duration, further evolution of contact pressure takes place. This further contact pressure depends on the impact velocity and the relative strengths of rod and target materials.

Tate (1969) has shown that, for a given rod / target combination, there exists a minimum impact velocity below which the rod ceases to deform and proceeds to penetrate as a rigid body. This limit velocity is given as: -

$$V^2 = \frac{2(Y - R)}{P}$$



Where V	=	limit velocity
Y	=	plastic flow strength of rod (= 0,9 GPa for mild steel)
R	=	resistance of target material to penetration (= 0, 3 GPa for quartzite)
P	=	target density (= 2,65 t/m <sup>3</sup> for quartzite)

Therefore, the calculated limit velocity for mild steel impact on quartzite is 670 m/s.

Note that all directional primer slug velocities considered in this thesis are in the range 1000 m/s to 2000 m/s, far in excess of the limit velocity of 670 m/s. This means that, in all cases, the rod will initially deform and not penetrate as a rigid body.

Following the impact shock and its attenuation, it can be expected that the rod will then penetrate the rock in a non-rigid or deforming manner. In fact, the rod will penetrate in the so-called hydrodynamic mode, which is characterised by the erosion of the rod from its tip as it penetrates and the formation of the characteristic mushroom bulb.

The importance of this conclusion is twofold: -

- it defines a transition phase dominated by plastic flow
- it identifies the final pressure obtained by the readjustment of contact surface pressure to the quasi-steady hydrodynamic penetration pressure.

Tate (1987) has argued that the transition phase from shock-dominated impact to the hydrodynamic mode of penetration involves the gross plastic deformation of the rod as its tip forms a mushroom shape. These deformation waves propagate at the shear plastic wave velocity. The details of this phase can be very complex, but as an approximation it may be assumed that the final steady-state penetration pressure is not attained until the plastic waves reach the axis of the rod.

In contrast to impact shock velocities (i.e. interface velocity, shock velocity and rarefaction velocity), plastic waves propagate at much lower velocities (of the order of hundreds of metres per second).

The phase of plastic deformation and pressure reduction is at least as long as the initial transient shock phase and probably significantly longer. In the context of the values given in Table 8.4, this phase is assigned a duration of 5 microseconds.

The Ravid (1993) analysis as given in Appendix 7 shows that rarefaction waves reduce the shock pressure at the contact surface to 20 % of its peak value. This remaining pressure is then reduced further during the phase of plastic flow of the rod to a value corresponding to the steady-state penetration pressure.

For the directional primer charge, the following table gives the calculations for penetration parameters for slug velocities ranging from 1000 m/s to 2000 m/s. This is reproduced from Appendix 7.

**TABLE 8.4 PENETRATION PARAMETERS**

<b>SLUG VELOCITY m/s</b>	<b>PENETRATION VELOCITY m/s</b>	<b>PENETRATION PRESSURE (GPa)</b>	<b>DURATION (ms)</b>
1000	632	0,53	41
1100	696	0,64	37
1200	759	0,76	34
1300	822	0,89	31
1400	885	1,04	29
1500	949	1,19	27
1600	1012	1,35	25
1700	1075	1,53	24
1800	1139	1,72	23
1900	1202	1,91	22
2000	1265	2,12	20

### **8.3.3 Effect of Slug Velocity on Penetration and Duration**

From the above table, it can be seen that penetration on impact increases with slug velocity. This may seem to be obvious but the effect of slug velocity on duration is not so obvious. With an increase in slug velocity, there is a decrease in the duration of impact. This means that the faster the slug, the deeper the penetration into the target on impact, but the duration of the impact is shorter.

## 8.4 Impact Pressure Pulse Profile

Combining three phases of shock, plastic flow and hydrodynamic steady-state penetration, the pressure pulse time history for a 15 mm long metal slug on rock can be described as follows: -

**TABLE 8.5 IMPACT PRESSURE AND DURATION**

IMPACT PHASE	VELOCITY = 1000 m/s		VELOCITY = 2000 m/s	
	PRESSURE (GPa)	DURATION (ms)	PRESSURE (GPa)	DURATION (ms)
Impact Shock	9,6	1,7	23,6	1,5
Plastic Flow	1,9	5	4,7	5
Hydrodynamic Penetration	0,5	41	2,1	20
		48		27

This is shown graphically in Figure 8.2.

What the above shows is that the higher the slug velocity, the greater are the pressures of the various phases but the shorter are the durations. Even at the lower slug velocities the high pressures are attenuated within 50 microseconds, and the ultra-high shock pressures are attenuated within 2 microseconds.

Considering that quartzite rock has a compressive strength of 200 to 250 MPa, in all the above cases for all impact phases, the pressures exceed the compressive strength of the rock.

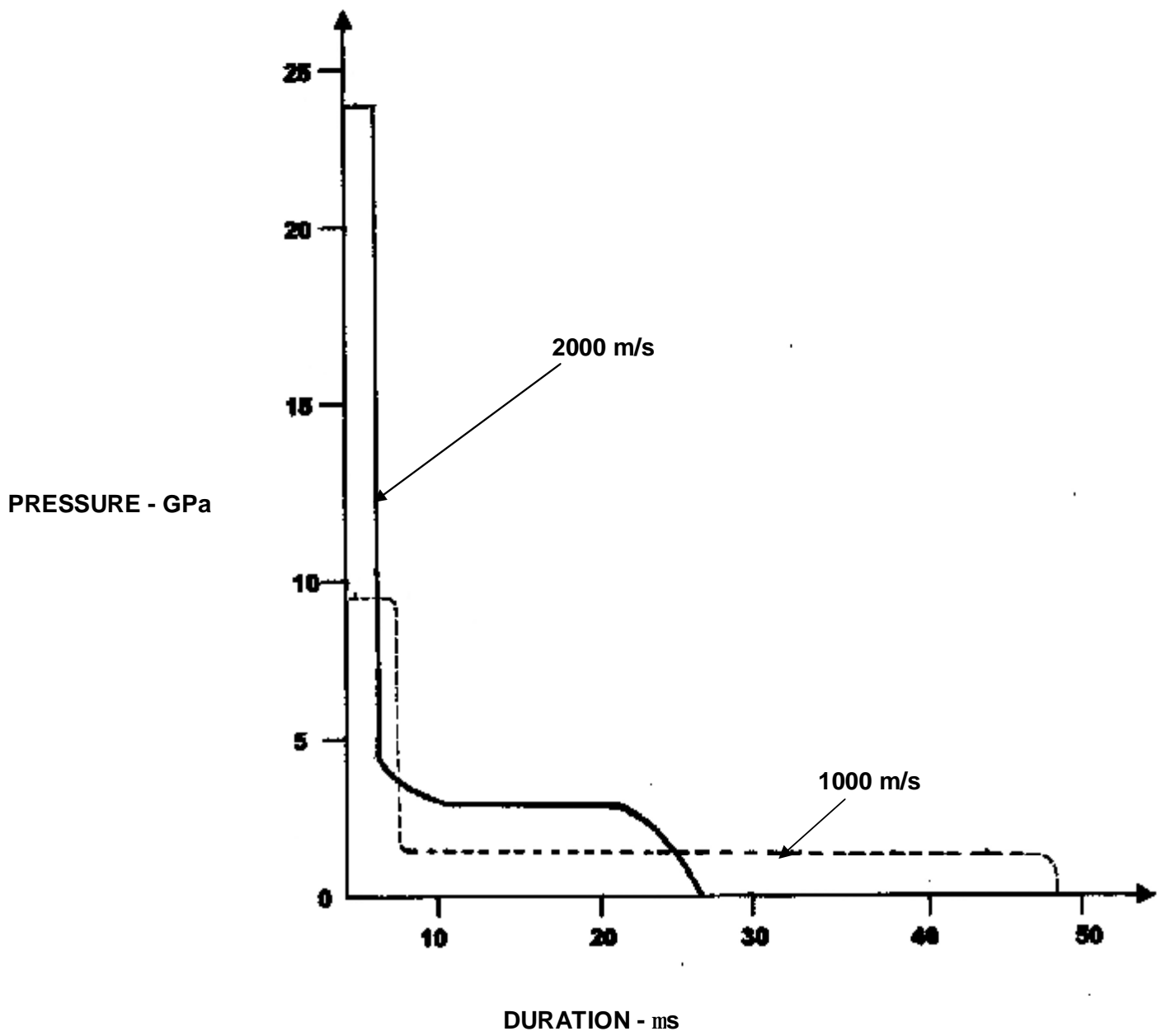


FIGURE 8.2 IMPACT PRESSURE PULSE PROFILE FOR SLUG VELOCITIES OF 1000 m/s AND 2000 m/s

## 8.5 The Formation of Umbrella Cracks

Finally, the formation of umbrella cracks can now be explained. The pressure exerted on the toe of the blasthole, whether shock wave pressure in the case of the Perspex blasting model or impact pressure in the case of the directional primer charge slug in rock, is sufficient to move the interface forward enough for the material to fail in tension. This produces a radial crack at the toe of the blasthole which is perpendicular to the axis of the hole. This is termed an umbrella crack or umbrella fracture.

The complete formation of an umbrella fracture takes place in two distinct phases - the first phase is the initiation of the crack due to the impact of the slug on the toe of the hole and the second phase is the extension of that crack by the action of the pressure of the product gases.

### 8.5.1 Initiation of Umbrella Crack

Figure 8.3 shows diagrammatically the initiation of an umbrella crack through the action of the directional primer charge slug impacting on the rock at the toe of the hole.

Figure 8.3 (a) shows the directional primer charge at rest after placement in the blasthole. Note that the dished metal disc is at a stand-off distance of 35 mm from the rock face at the toe of the blasthole. Figure 8.3 (b) shows the slug fully formed and moving forward at its maximum velocity. At 2000 m/s, it would have taken 15  $\mu\text{s}$  to travel 30 mm i.e. just prior to impact. Figure 8.3 (c) shows the slug just after impact on the rock at the toe and its deformation as the slug tail catches up to the slug tip to flatten out against the rock. This would be the situation at about 30  $\mu\text{s}$  after the detonation shock wave had struck the metal disc. Figure 8.3 (d) shows the situation at the end of the impact pressure pulse, which for a slug at 2000 m/s would have a duration of 25  $\mu\text{s}$ , i.e. 40  $\mu\text{s}$  after the explosive shock wave meets the stationary disc. This is the point at which the maximum forward movement of the rock at the toe of the blasthole is achieved. In the case of the 2000 m/s slug, this forward displacement is 2 mm and it has taken place over a duration of 25  $\mu\text{s}$ . In the case of the 1000 m/s slug, this forward displacement is 1,2 mm and it takes place over 50  $\mu\text{s}$ . The result of this forward displacement is the failure of the rock in tension at the corners of the toe of the hole.

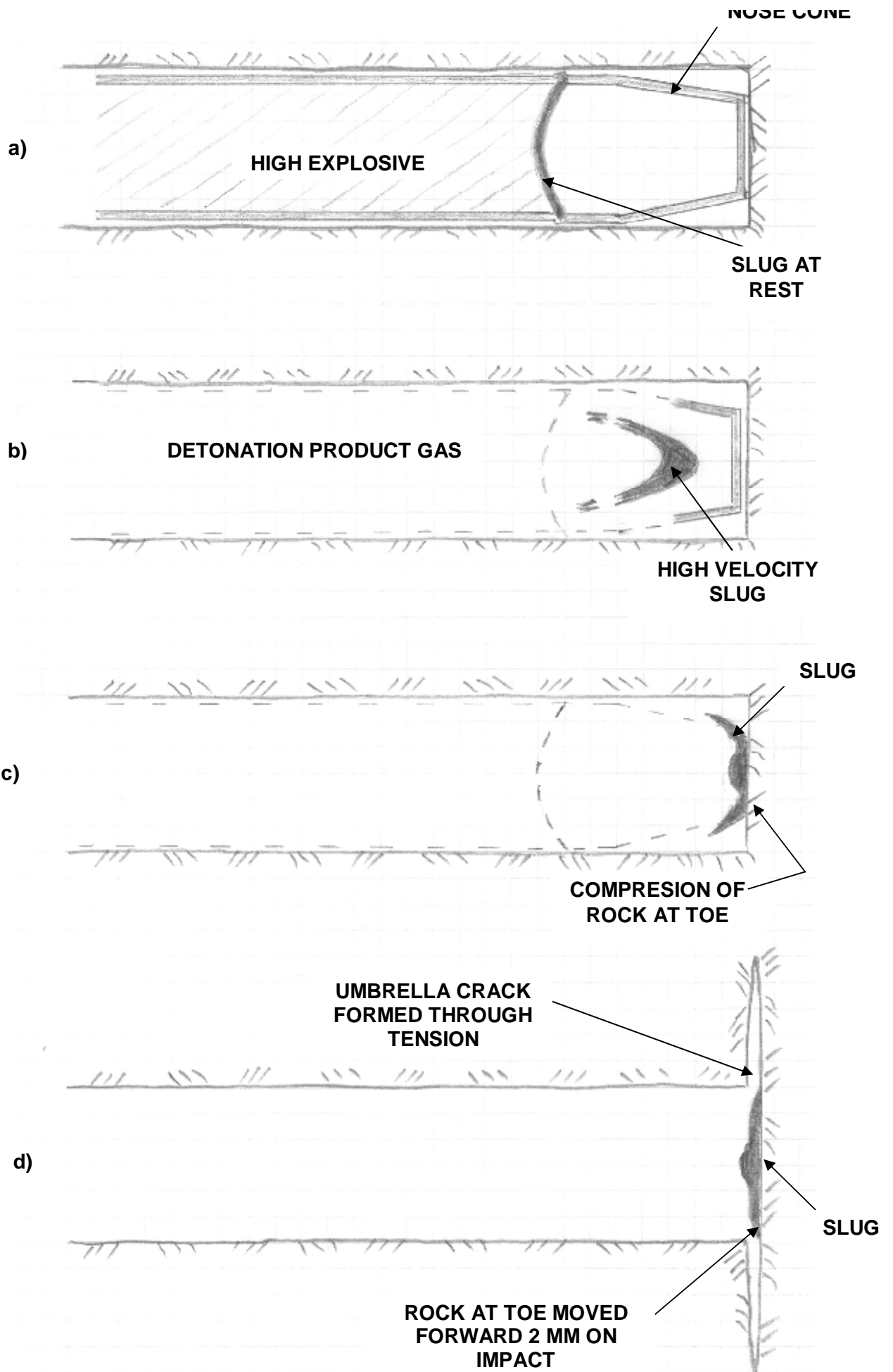


**FIGURE 8.3 FORMATION OF UMBRELLA CRACK BY IMPACT OF SLUG ON THE TOE OF THE HOLE**

This failure is characterised by a radial crack perpendicular to the axis of the blasthole i.e. an umbrella crack. As the pressure diminishes after impact, so the tension relaxes and the rock can revert to its original position if the deformation was purely elastic, or some intermediate position if it was partially plastic. The impact of the slug on the rock has initiated the umbrella crack. In the second phase of the detonation of a blasthole, the explosive product gases expand thus exerting pressure on the walls of the blasthole. This gas pressure tends to open up and extend any existing cracks or fractures. Thus, the explosive product gases from the column charge of standard explosive in the blasthole will extend the umbrella cracks and provide the breakout heave of the blasted burden of rock. This extension of the umbrella crack is shown in Figure 8.4.

In an attempt to estimate the extent of the umbrella crack due to the impact of the slug on the toe of the hole, the force on the area of the toe should diminish as the area of the umbrella fracture increases. Assume that the pressure for the 2000 m/s slug, i.e. the Composition B cartridge, is 2 GPa during the time period that the crack forms. Assume also that the tensile strength of the rock is 20 MPa. Then the force will have to diminish a hundredfold before it can no longer break the rock in tension. For this to happen the area of the umbrella fracture will have to increase 100 times that of impact area of the blasthole i.e. the diameter will have to increase tenfold.

In this simplistic calculation, the umbrella crack would extend from an impact area of 25 mm diameter to final area of 250 mm diameter as a result of the slug impact on the toe of the hole. For the 1000 m/s slug of the Super Gelignite cartridge, the impact pressure of 500 MPa would have to decrease to 20 MPa i.e. a twenty-five-fold increase in area and a corresponding fivefold increase in diameter to produce an umbrella fracture 125 mm in diameter as a result of the impact of the slug on the toe of the hole. Note the above two simplistic calculations are for the size of the umbrella fracture caused by impact only.

Thus, many years after it was first recognised as a phenomenon which could only be repeated in Perspex blasting models, the umbrella fracture can now be explained and its formation mechanism can be described in engineering terms. With this understanding of the conversion of explosive energy to the kinetic energy of the explosively-forged metal slug to the impact energy of the metal slug on the rock at the toe of the blasthole, not only can the parameters be calculated theoretically, but also they have been measured and have been applied to quartzitic rock fracturing. It has been demonstrated that the use of a lined shaped charge of high velocity of detonation explosive, produces the directional energy sufficient to create the umbrella fracture at the toe of the blasthole under production stoping conditions.

### 8.5.2 Extension of Umbrella Crack

The second phase of the formation of the umbrella crack is its extension due to explosive product gases from the main column charge shown in Figure 8.4.

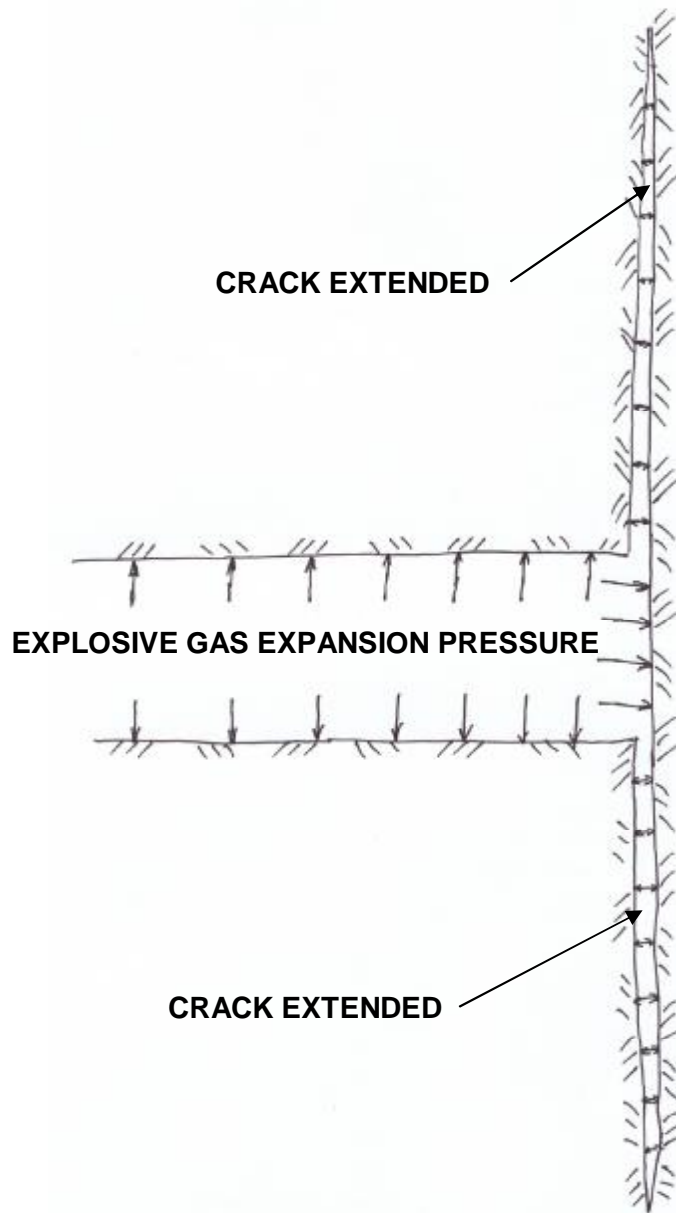


**FIGURE 8.4 EXTENSION OF UMBRELLA CRACK BY EXPLOSIVE GAS EXPANSION**



## CHAPTER 9 UNDERGROUND FIELD TESTING

### 9.1 Introduction

The surface testing described in Chapter 7 indicated the forward directional power of the directional primer charge and the effect various high velocity explosives had on the velocity of the slug. They also demonstrated the shape of the slug in flight and its development over a relatively short distance. Although the punching power through metal plate was demonstrated, the purpose for which directional primer charge had been designed had not been tested, i.e., its effect on rock at the toe of a blasthole under confined conditions and in an underground environment.

The first underground test was undertaken in a stope on the then President Steyn gold mine in Welkom, Free State. The purpose of the test was to determine whether the directional primer charge premise was feasible in stoping under production conditions. The second underground test that was undertaken was in a development on Randfontein Estates gold mine. The purpose of this test was to determine whether the directional primer charge premise could be applied to a tunnelling blasting round. These two tests, namely the President Steyn test and the Randfontein Estates test, were preliminary tests prior to full scale major tests being undertaken under rigorously controlled production condition.

The full production underground tests were undertaken on Village Main gold mine and consisted of series of tests undertaken at four different time periods. The tests have therefore been separated into four distinct series of tests as each of the directional primer charge blasts were to be compared with standard blasts under similar conditions. It was recognised that to ensure similar conditions the same drilling and blasting personnel should be used, the same stope face should be blasted thus ensuring a similar rock type and similar ground conditions occur.

The second series of tests on Village Main was an extension of the first series i.e. the first series of tests was to compare the effect of different masses of Composition B explosive namely 20 gram, 35 gram and 55 gram with each other and the standard round, the second series was to extend the first by using 75 gram and 95 gram **directional primer charges**. Due to the delay in the start of the second series, the drilling and blasting personnel could have changed as could the geology and ground conditions. Therefore, new standard rounds were recorded. In practice however, these standard rounds did not differ significantly from the previous standard rounds and the results have been combined as well as shown separately.

The same philosophy for testing applied to the third series of tests which was a large test with a constant mass (85 grams of Composition B explosive) directional primer charge, and also for the fourth series of tests which compared the effect of Super Gelignite as the explosive in the directional primer charge to the standard round.

The underground tests can be summarised in the following table.

**TABLE 9.1 SUMMARY OF UNDERGROUND TEST PROGRAMME**

<b>NAME OF TEST SERIES</b>	<b>PURPOSE OF TEST</b>	<b>SIZE OF TEST</b>
<b>PRELIMINARY TESTS</b>		
1. President Steyn	To determine whether the directional primer charge premise was feasible for stoping.	20 holes
2. Randfontein Estates	To determine whether the directional primer charge premise was feasible for development.	60 holes
	<b>TOTAL:</b>	<b>80 holes</b>
<b>MAJOR TESTS</b>		
1. Village Main Series I	To compare the effect of different masses of Composition B, namely 20 g, 35 g and 55 g, directional primer charge in stoping under production conditions.	351 holes
2. Village Main Series II	Extension of Series I with 75 g and 95 g mass of Composition B.	141 holes
3. Village Main Series III	Large scale test comparing standard blasting round with rounds containing directional primer charge with 85 g Composition B	536 holes
4. Village Main Series IV	To compare the effect of standard blasting round with directional primer charges containing 80 g Super Gelignite.	215 holes
	<b>TOTAL:</b>	<b>1243 holes</b>

## **9.2 Preliminary Tests**

Two sets of preliminary underground tests were undertaken. The first set was under stoping conditions on President Steyn gold mine. The second set was the testing of larger diameter cartridges in development ends on Randfontein Estates gold mine.

### **9.2.1 President Steyn**

The first set of tests at President Steyn mine utilised the nominal 30 mm outside diameter and 26 mm inside diameter polythene pipe housing. Two explosives were tested – Dynagel and Pentalite. The Dynagel was tested by placing a standard 25 mm diameter cartridge inside the housing and ramming it manually up against the disc which was located at a stand-off distance of 25 mm. Dynagel was used because at that time it was the preferred cartridge explosive in use in stoping in South African gold mines.

Pentalite was used as the other explosive because it was the highest velocity of detonation commercially manufactured explosive in use in mining at that time.

The tests were undertaken as coarse comparative tests with standard charges in blastholes. In an experimental stope, the mining face was divided up into mini-panels of some five metres in length, each with its own breaking face. Each mini-panel was charged with a different explosive type.

The results of this single test indicated that the directional primer charge appeared to have a beneficial extra breaking effect over the standard charge round. However, with the limited number of holes, some 20 holes of each explosive type, and other parameters such as accuracy of drilling playing a role, the results were not conclusive.

In certain holes charged with the Pentalite directional primer charge, where the burden between the holes was too great, the charge made a comparatively large cavity at the base of the hole. It appeared to have crushed the rock around the blasthole, the broken material being easily pumped out on desludging the hole.

### **9.2.2 Randfontein Estates**

At Randfontein Estates, the tests were conducted in a development end. A larger diameter directional primer charge of 32 mm was used due to the larger diameter holes that are drilled in development ends – 45 mm diameter compared to 38 mm for stoping. The development end at Randfontein Estates was a heading 3,5 metres high by 6,5 metres wide.

The drilling pattern was a “square” pattern with hole burdens of 700 mm horizontal and 800 mm vertical. The round consisted of 73 holes – 9 hole burn cut, 4 easer holes and 60 production holes. (see the following photographs.)



**PHOTOGRAPH 9.1 SHOWING MARKED-OFF BLASTING ROUND**



**PHOTOGRAPH 9.2 SHOWING 32 MM DIAMETER DIRECTIONAL PRIMER CHARGE CARTRIDGE WITH PLASTIC WRAPPER AND ELASTIC BAND COVERING OF OPEN END TO PREVENT INGRESS OF DRILL CHIPPINGS**



**PHOTOGRAPH 9.3 SHOWING 9 – HOLE BURN CUT**

The result of the blast was only five sockets ranging from 50 mm to 500 mm deep, four of which were on the right hand side which had water-logged holes.

The disc diameter used in the directional primer charge was changed to 32 mm compared to 25 mm diameter for the stoping directional primer charge. Again, the tests were merely preliminary tests to assess practicality in the underground working environment. In the President Steyn test, it was observed that the drillholes were not pumped entirely clean prior to the charges being inserted. Drill chipping's accumulated in the stand-off distance section of the directional primer charge as it was inserted and pushed to the toe of the hole. For the Randfontein test therefore, the open end at the front of the directional primer charge was enclosed using a plastic wrapper held in place with a rubber band. The test results at Randfontein, as at President Steyn, were inconclusive but indicated that the directional primer charge had potential to enhance rock breakage.

What the tests did show was that, although they were inconclusive in quantifying any advantage, they did indicate that the use of the directional primer charge did not have a deleterious effect on standard blasting practice. It did appear however, that the holes, when they broke cleanly, appeared to exhibit the umbrella fracture and the round appeared to break out more. The visual results were sufficient evidence to give encouragement to proceed with further more detailed and controlled underground trials. A suitable site was identified in an underground stope on Village Main gold mine and large scale trials were planned and subsequently implemented.

### **9.3 Comparative Tests**

As a result of the preliminary tests at President Steyn gold mine and Randfontein Estates gold mine, and the results from the surface testing of prototypes at the Advanced Detonics Laboratory at Boskop, it was decided to undertake extensive testing underground under working conditions.

The design of the tests was to fire a large number of blastholes to obtain a sample size large enough to determine trends. It was recognised that there are a number of factors at work in the practical underground environment, which affect the blasting of rock and therefore, which could affect the result of an individual hole. These are, inter alia, the geology of the rock, its strength, its joints, its parting planes, the stoping width, the drilling accuracy of the holes, the collar burden, the toe burden, the placing of the explosives in the hole, the quantity of explosives placed in each hole, etc.

The site chosen for the underground testing of the prototype was Village Main gold mine. This was a small gold mine in Johannesburg at the end of its life of over 100 years. It had one operating shaft and was mining a few isolated stopes to obtain ore to supplement surface dump reclamation operations and at the same time provide a grinding medium for the crushing circuit. It operated on a single underground shift per day and also blasting only once per day. It also had an advantage for this research that after the blast at the end of the shift each afternoon, the stopes were left undisturbed until the start of the shift the following morning.

Thus, the site could be visited first thing each day and the results of the previous day's blast could be inspected and measurements taken and recorded prior to the stope cleaning operations being commenced i.e. undisturbed blast results could be easily obtained.

The tests at Village Main comprised four series of tests over a twelve-month period.

The first series of tests compared the results of directional primer charges containing various masses of Composition B explosive, namely 20 g, 35 g and 55 g. These were compared against the standards of a conventionally charged blasthole.

The second series of tests was essentially an extension of the first series. Directional primer charges containing 75 g and 95 g of Composition B explosive were compared. Again these were measured against a standard of conventionally charged holes in the same stope. The standards of both tests were also compared with each other to ensure that comparisons between both series of tests were valid.

The third series of tests comprised directional primer charges containing 85 g of Composition B explosive. Again, these were compared to the standard charge. Whereas the first two series of tests were designed to obtain indicative-only results, the third series was designed to evaluate the difference between what appeared to be the optimum mass of directional primer charge and the standard charge. Thus, the number of tests undertaken (450 holes) in the third series was designed to provide a large enough sample to statistically analyse the results to identify a significant trend should one exist and to quantify it. At the time, this third series was intended to be the final series.

The fourth series of tests was undertaken after it became known that there existed a cheaper high velocity of detonation commercial explosive than the expensive military explosive Composition B. This explosive, Super Gelignite, was a special formulation of gelignite and had a far higher velocity of detonation than standard Ammon Gelignite. These tests were undertaken to provide a direct comparison to the 85 g Composition B tests.

The standard stoping blasting round at Village Main used Tovex 220 watergel explosive as the main column charge and Stopecord 9 (i.e. medium speed) igniter cord with 0,9 m long capped safety fuse for initiation. (See photograph below). The directional primer charge was inserted first at the bottom of the blasthole ahead of the main column charge.



**PHOTOGRAPH 9.4 SHOWING STANDARD EXPLOSIVES USED UNDERGROUND AT VILLAGE MAIN**

### **9.3.1 Village Main Tests Blasting Parameters**

The blasting parameters in the stope on Village Main is typical Witwatersrand Practice. The stoping width is nominally of the order of one metre but ranges from about 850 mm to 1400 mm in practice. Holes are drilled on a square pattern with bottom holes collars drilled about 200 mm from the footwall and the top holes collars are drilled about 200 mm from the hanging wall. Where the stoping width is wide a third row of middle holes may be drilled in between the top and bottom rows.

From the above it can be seen that the hole spacing, i.e. the distance between rows, ranges between 500 mm and 900 mm. The burden, i.e. the horizontal distance between holes, is nominally 600 mm with a range of 500 mm to 700 mm in practice.

The length of holes drilled varied between two standard lengths for each blasting round namely, either 900 mm or 1200 mm.

Appendix 8 lists the raw data measured underground. For each blasting round, pre-blast and post-blast measurements were recorded.



Pre-blast each hole was individually numbered indicating positional sequence and whether it was a top row, middle row (where drilled) or a bottom row hole and is designated by a T, M or B respectively.

The length (or depth) of the drilled hole was measured to ascertain if it corresponded with the drill steel length or whether it had been short-drilled. The stopping width was measured at each hole position and the collar burden and spacing measured for each drilled hole.

Post-blast measurements were taken for of each hole. The length of the socket left after the blast was measured. The burden and spacing at the toe of the holes were measured using the position of the sockets and where there were no sockets the apparent position deduced from blasting fracturing was used. These measurements i.e. the burden and spacing at the toe of the blasthole, were made so that they could be compared with the collar burden and spacing and so the parallelity of the drilled holes could be ascertained.

### **9.3.2 Village Main – First and Second Series of Tests**

A more detailed description of these tests is given in Appendix 8. As mentioned previously, the second series of tests was an extension of the first series and therefore the two series of tests will be treated as one.

The purpose of the tests was to compare the rock breaking efficiency of the various masses of Composition B explosive in the directional primer charge. From the theoretical calculations, which were confirmed by the surface laboratory tests, it was known that the greater the mass of Composition B explosive, the greater was the velocity of the slug and therefore the greater was the kinetic energy and the greater was the impact on the target. Extrapolating on this line of reasoning, it was assumed that the greater the impact at the toe of the blasthole, the greater the damage to the rock in the form of fracturing and the more likely that the blasthole would breakout to the full length of the hole. Therefore, from theory and surface test results, it was assumed that a larger mass of Composition B in the directional primer charges would produce a greater break-out of the rock.

The method used to determine the degree of rock break-out was one of negative deduction. Instead of measuring the quantity of rock that had broken out, a method was devised which, in effect, measured the quantity of rock that had not broken out. This was to measure the length of the blasthole remaining after the blast i.e. the length of the blasthole socket.

The socket lengths were measured after the blasts before broken rock removal operations (“stope cleaning”) commenced.

In order to ascertain whether the directional primer charge improved the breakout of rock from the blast, certain blasts called “standard blasts” were taken in which no directional primer charges were inserted in the blastholes. These were then compared to those blasts in which directional primer charges were inserted into the blastholes.

This comparison was undertaken by measuring the length of the sockets and calculating the mean socket length for each blast.

The first and second series of tests were to compare the effect of different amounts of Composition B explosive in the directional primer charges. These were 20 grams, 35 grams, 55 grams , 75 grams and 95 grams respectively.

Appendix 8 gives tables of the sample size of each blast and the mean socket length per blast. This data has been summarised in Table 9.2.

**TABLE 9.2 SUMMARY OF FIRST AND SECOND TEST SERIES RESULTS**

<b>ROUNDS</b>	<b>NO. OF ROUNDS</b>	<b>NO. OF BLASTHOLES</b>	<b>MEAN SOCKET LENGTH</b>
Standard (0,9 m)	4	77	120 mm
Standard (1,2 m)	4	93	176 mm
20 g Composition B	3	53	104 mm
35 g Composition B	4	104	62 mm
55 g Composition B	1	24	120 mm
75 g Composition B	3	53	86 mm
95 g Composition B	4	88	71 mm

Four standard rounds had hole lengths of 0,9 metres and four standard rounds had hole lengths of 1,2 metres. As most of the directional primer charge rounds had hole lengths of 1,2 metres, the latter four standard rounds have been used for purposes of comparison. The former four standard rounds have been recorded and included for completeness.

From the first two series of tests, it was apparent that due to the shorter mean socket length after the blast, a greater amount of rock was breaking out from each blast when a directional primer charge was used.

Apart from an apparent aberration for the 55 grams Composition B directional primer charge, which could be explained by the small sample size of blastholes and only one blast, blasting results appeared to improve with increased mass of Composition B explosive. However, for 35 g and above there was no significant improvement.

### 9.3.3 Village Main – Third Series of Tests

The purpose of the third series of underground testing at Village Main was to evaluate a large number of blastholes containing the same quantity of Composition B explosive in the directional primer charge namely 85 grams. This quantity is equivalent to a charge length of 75 mm and is three times the cartridge diameter of the directional primer charge. From the literature (Persson et al (1994)), this length of charge should be adequate for the detonation front to run up to the explosive's characteristic velocity of detonation. In the case of Composition B this was shown to be so from the disc velocities for varying quantities of explosive measured during the trials undertaken at the Advanced Detonics Laboratory. The graph of slug velocity versus explosive mass shown in Figure 7.2 indicates that the limiting slug velocity occurs at a mass of Composition B explosive of over 50 grams.

Further measurements of blasts with standard configurations of explosives were taken to ensure that fewer parameters changed e.g. the same drillers are used to drill the holes which assumes the same degree of inaccuracy of drilling occurs each time, the same stopes are used which assumes similar rock type, geological and mining conditions etc.

All in all seven standard blasts were measured during the same time that seven 85 gram of Composition B explosive directional primer charge blasts were undertaken.

In summary, from the seven standard blasting rounds and the seven rounds with 85 grams of Composition B directional primer charge, the following comparison appears to confirm the improvement of rock breakout with the directional primer charge.

**TABLE 9.3 THIRD TEST SERIES RESULTS**

<b>ROUNDS</b>	<b>NO. OF ROUNDS</b>	<b>NO. OF BLASTHOLES</b>	<b>MEAN SOCKET LENGTH</b>
Standard	7	168	121 mm
85 g Composition B	7	368	94 mm

Again the study of individual blasts shows that drilling accuracy plays a role in the creation of long sockets. However, both the standard rounds and the directional primer charge rounds had statistical distribution of similar shape, ranging from 50 mm to 252 mm average socket lengths for the standard round, to 37 mm to 212 mm average socket length for directional primer charge round. (see Appendix 8).

### 9.3.4 Village Main – Fourth Series of Tests

The fourth series of tests at Village Main which were undertaken almost as an afterthought were to determine the effect of a high velocity of detonation commercial explosive which had just become available. The explosive was a specially formulated ammon gelignite, which is referred to as Super Gelignite.

Again measurements of blasts of standard explosives configurations were measured during the period of the trials of the Super Gelignite. Four standard rounds and three Super Gelignite rounds were measured.

In summary, from four standard blasting rounds and three rounds containing Super Gelignite directional primer charges, the following comparison once again appears to confirm the improvement of rock breakout with the directional primer charge.

**TABLE 9.4 FOURTH SERIES TESTS RESULTS**

<b>ROUNDS</b>	<b>NO. OF ROUNDS</b>	<b>NO. OF BLASTHOLES</b>	<b>MEAN SOCKET LENGTH</b>
Standard	4	188	175 mm
Super Gelignite	3	93	67 mm

It is interesting to note that this series of tests showed the most improvement of the directional primer charge round over the standard round.

## 9.4 Summary of Results

Due to the many factors which can affect the length of sockets e.g. accuracy of drilling, out-of-sequence initiation, misfires etc., the results of the underground field testing are presented as coarse results purely to indicate whether there is a trend that the use of directional primer

charges produce a greater break out of rock per round. (This being measured by the average length of sockets remaining after the blast).

A summary of the blasting rounds gives the following results.

**TABLE 9.5 SUMMARY OF RESULTS FOR ALL TEST SERIES**

ROUNDS		SAMPLE SIZE	MEAN SOCKET LENGTHS	
TYPE ROUNDS	NO	NO. OF HOLES	PER ROUND	RANGE OF ROUND MEANS
Standard (0,9 m)	4	77	120 mm	73 to 208 mm
Standard (1,2 m)	4	93	176 mm	113 to 326 mm
20 g Composition B	3	53	104 mm	66 to 125 mm
35 g Composition B	4	104	62 mm	44 to 136 mm
55 g Composition B	1	24	120 mm	120 mm
75 g Composition B	3	53	86 mm	65 to 97 mm
95 g Composition B	4	88	71 mm	53 to 85 mm
Standard	7	168	121 mm	50 to 252 mm
85 g Composition B	7	368	94 mm	37 to 212 mm
Standard	4	188	175 mm	147 to 229 mm
Super Gelnite	3	93	67 mm	32 to 101 mm

The blasting rounds are divided into three groups on a time basis i.e. the standard rounds were blasted in the same period that the respective directional primer charge rounds were blasted. This was done to obviate changes in drilling parameters when using different drilling crews.

Note that the final column in the table is the **range of round means** i.e. for the 55 g Composition B blast, there was only one round blasted and therefore only one value can be given, whereas all other round types consisted of a number of blasted rounds and therefore a range of mean socket lengths per round can be presented.

**TABLE 9.6 IMPROVEMENT IN BLASTING EFFICIENCY**

		<b>MEAN SOCKET LENGTH</b>	<b>BREAK-OUT LENGTH</b>	<b>IMPROVEMENT IN BREAK-OUT</b>
Series I	Standard Round	176 mm	1024 mm	-
	20 g Composition B	104 mm	1096mm	7%
	35 g Composition B	62 mm	1138mm	11%
	55 g Composition B	120 mm	1080 mm	5%
Series II	75 g Composition B	86 mm	1114 mm	9%
	95 g Composition B	71 mm	1129 mm	10%
Series III	Standard Round	121 mm	1079 mm	-
	85 g Composition B	94 mm	1106mm	3%
Series IV	Standard Round	175 mm	1025 mm	-
	Super Gelnite	67 mm	1133 mm	11%

In all cases, the directional primer charge rounds showed improvements over their respective standard rounds.

In the case of Super Gelnite an improvement of breakout of 108 mm over a 1,2 metre long blasthole, represents an increase in efficiency of 11 % (i.e.  $1133 \text{ mm} \div 1025 \text{ mm} = 1,11$ ).

## **9.5 Analysis of Results**

Although the field testing produced coarse results whose values should be accepted with reservations, the quantity of observations allowed trends to be identified.

It would appear that an increase in the quantity of high velocity of detonation explosives resulted in better breaking of the rock at the toe of the hole as represented by the decrease in socket length.

Surprisingly the Super Gelignite appears to perform the best with an improvement of 11% although it has a lower velocity of detonation than Composition B.

### 9.5.1 Frequency Distribution Curves

In Appendix 8, the distribution curves of socket lengths for each explosive type shows a distribution which is skewed to the left. At first it appears to be log-normal but on closer examination this is due to the fact that there is a high preponderance of zero sockets and also at the other end of the scale there is a maximum length that a socket can attain namely the length of the drill hole.

The frequency distribution of socket lengths for The Standard Rounds is presented in Figure 9.1 as a typical example.

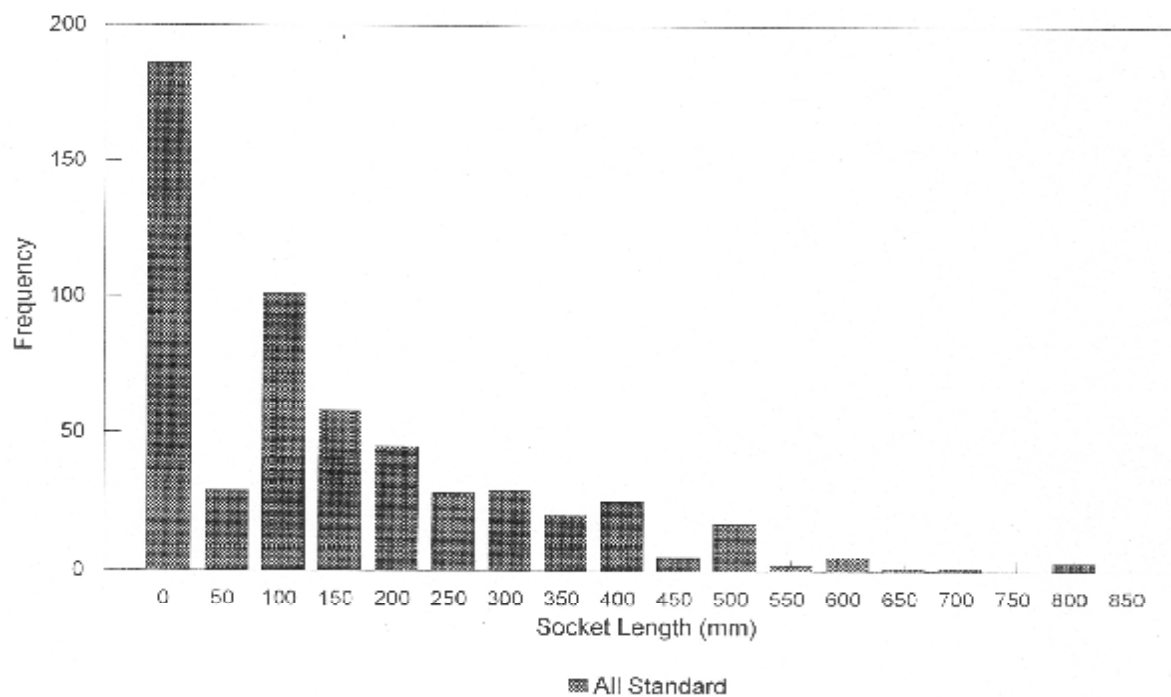


**FIGURE 9.1 FREQUENCY DISTRIBUTION OF SOCKET LENGTHS FOR STANDARD ROUNDS**

### 9.5.2 Zero Socket Ratios

The difficulty of using sockets as the measurement of breaking efficiency is that it assumes that a zero socket cannot be improved upon. If the standard round had produced no sockets, then the directional primer charge would not be able to show improvement.

Ideally the standard round should give constant socket lengths for each hole. It is often said that 150 mm long sockets are an indication of the most efficient blasting from a powder factor point of view. The difference in powder factor for a directional primer charge to give the same constant 150 mm socket per hole, would demonstrate the difference in the efficiency of the new technique.

However, due to the variability of the parameters in underground production blasting, even poorly drilled rounds produce some holes with sockets of zero length.

Another indication of blasting efficiency is the number of zero sockets produced per blast and observe the change in their proportion of the total.

For example the incidence of zero sockets was recorded for the standard round, the 85 g Composition B round and the Super Gelignite Rounds and are tabulated in Table 9.7.

**TABLE 9.7 INCIDENCE OF ZERO SOCKETS**

<b>ROUND TYPE</b>	<b>NO. OF HOLES</b>	<b>NO. OF ZERO SOCKETS</b>	<b>RATIO</b>
Standard (all rounds)	537	186	35%
85 g Composition B	368	214	58%
Super Gelignite	93	59	63%

It is interesting to note that a third (35%) of the holes in the standard rounds broke out cleanly and left no socket, whereas for both the 85 g Composition B rounds (58%) and the Super Gelignite rounds (63%) the number of zero sockets was almost double that for the standard rounds. (see Frequency Distribution Graphs in Figures 9.1, 9.2 and 9.3).



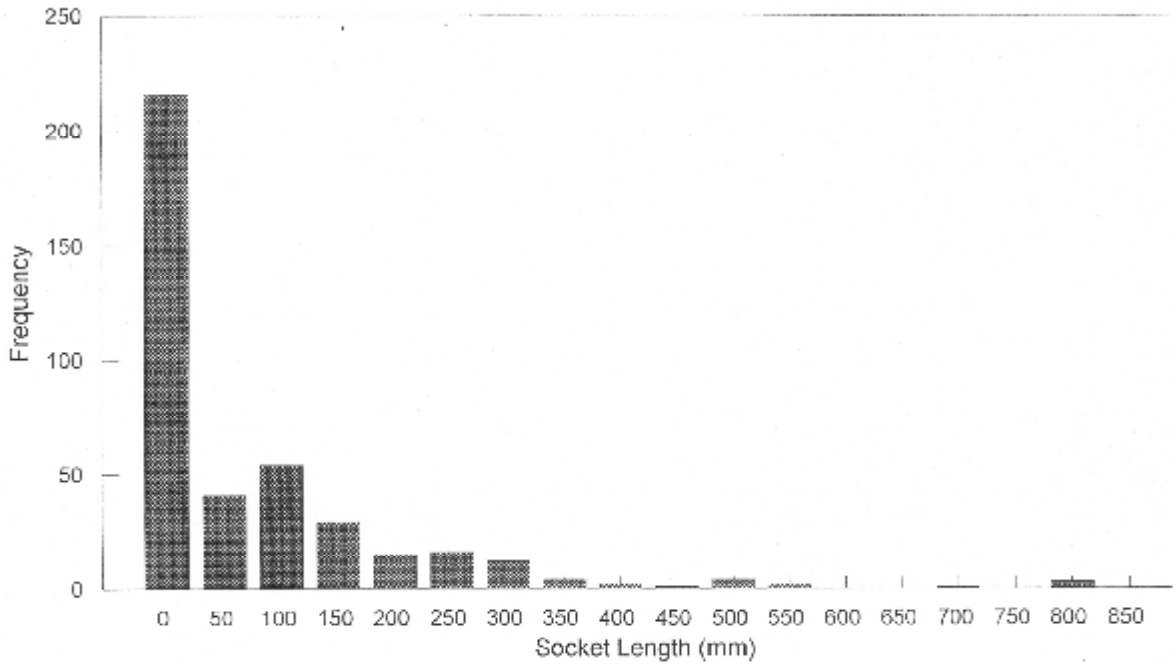


**FIGURE 9.2 FREQUENCY DISTRIBUTION OF SOCKET LENGTHS FOR 85 g COMPOSITION B**

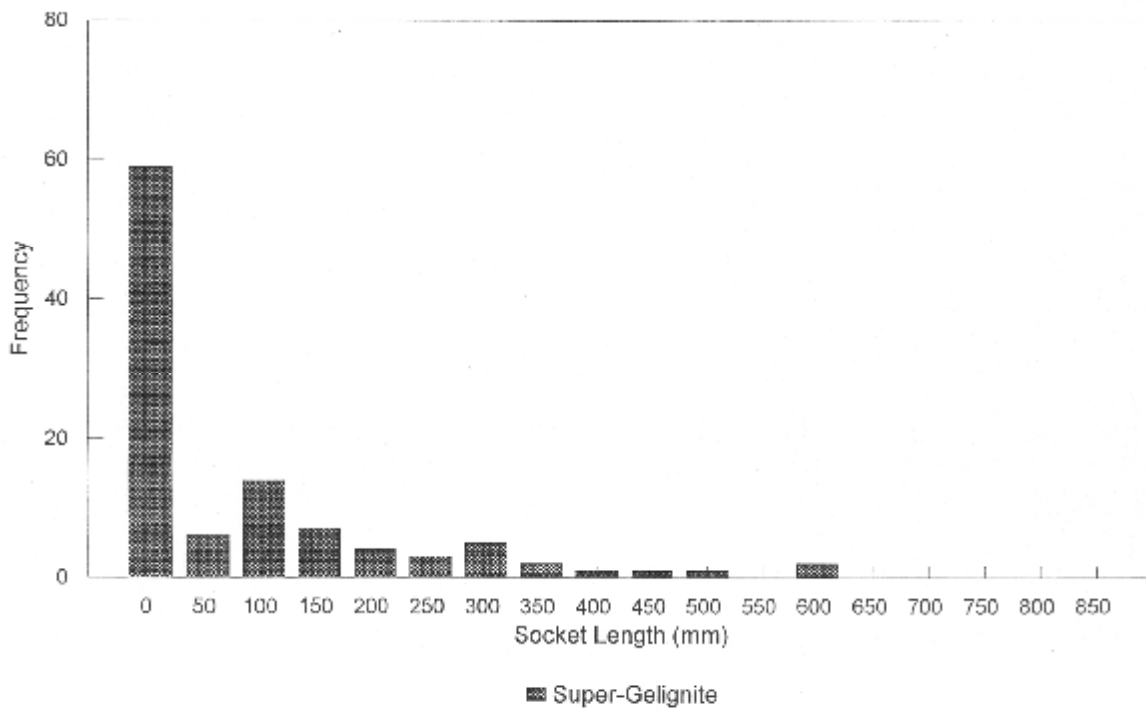


**FIGURE 9.3 FREQUENCY DISTRIBUTION OF SOCKET LENGTHS FOR SUPER GELIGNITE**

This is indicative of the umbrella fracturing due to the directional primer charge. What is of interest is that there is no significant difference between Composition B and Super Gelignite charges. This is indicative of the fact that lower velocity of detonation charge is sufficient to cause a significant umbrella fracture.

### **9.5.3 Additional Breakout**

Although only zero length sockets were recorded, there were drill holes observed which actually broke out more than the full hole length (see Photographs 9.5 and Photographs 12.13 to 12.18 in Appendix 12).

Photograph 9.6 not only shows a hole that is broken out beyond the end of the blasthole, but also shows the remnants of a slug embedded in the rock at the toe of the hole.

This additional breakout of rock beyond the drilled length was not measured and is therefore not quantified. However, it does exist and would contribute to a greater efficiency value being ascribed to the use of a directional primer charge in stoping.



**PHOTOGRAPH 9.5    SHOWING ROCK BROKEN BEYOND THE LENGTH OF BLASTHOLE**

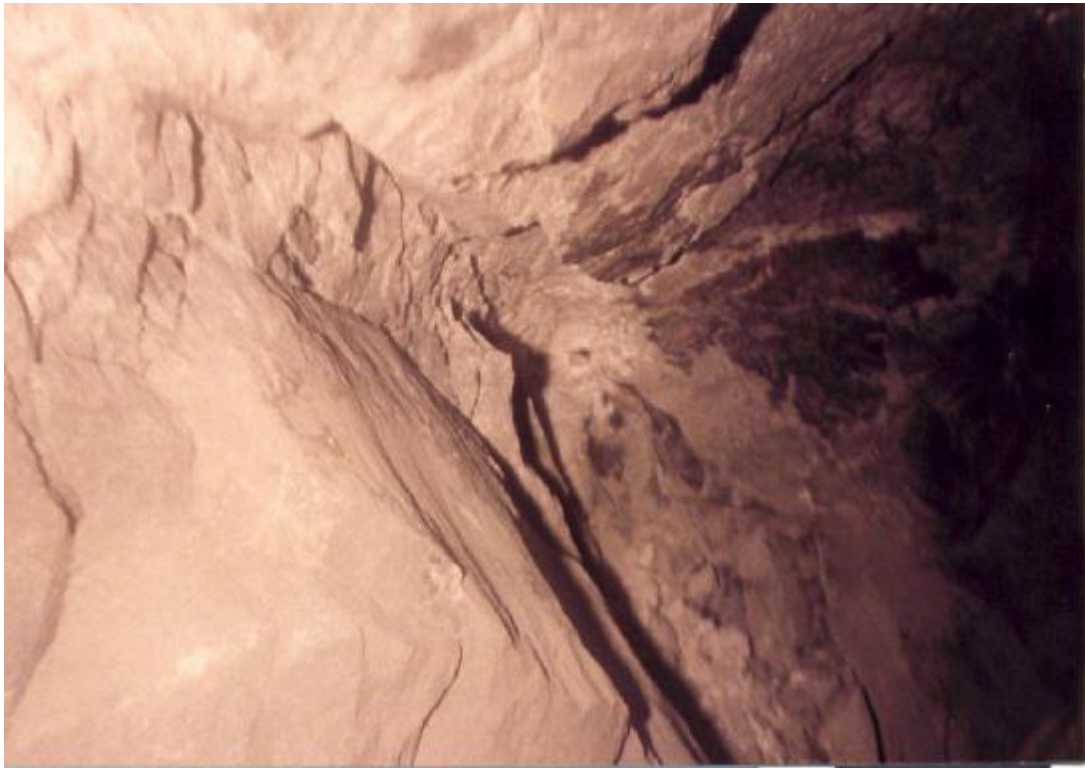


**FIGURE 9.6 SHOWING SLUG REMNANTS EMBEDDED IN THE ROCK AT THE TOE OF THE HOLE**

## 9.6 Economic Implications

The economic implications of the enhancement of the breakout of rock during blasting in underground stopes which can be ascribed to the use of directional primer charges are considerable.

Consider an average South African gold mine with the following parameters for tonnage and grade and current market conditions: -

Production rate	=	200 000 tons per month
Recoverable grade	=	5 grams of gold per ton
Gold price	=	R80 000 per kilogram

Therefore,

Revenue per ton	=	5g/t x R80 000/kg	=	R400/t
Monthly revenue	=	200 000t/month x R400/t	=	R80 million / month.

If there is additional breakout beyond the length of the blasthole of an average of only 50 mm say, then over the length of a 1,2 metre long blasthole this represents an additional increase in the breakout of rock of 4%. If a Super Gelignite directional primer charge is used in each stoping blasthole of 1,2 metre length, then the total increase in breakout of rock over the conventional standard stoping round will be 15%, being the 11% for Super Gelignite in Table 9.6 plus the 4% for additional breakout.

An increase of 15% breakout represents an increase in revenue of R60 per ton ( $0,15 \times R400/t$ ), R12 million per month ( $0,15 \times R80 \text{ million / month}$ ) or R150 million per annum for an average South African gold mine.

In South Africa, there are currently 550 000 holes drilled every day on the gold and platinum mines. (AEL 2004).

Assuming that the platinum mines produce the same revenue as the gold mines (a conservative assumption), i.e. a recoverable grade of 2,5 g/t and a platinum price of R160 000/kg, and assuming that one blasthole produces one ton of broken rock, then the additional revenue which could accrue to the gold and platinum mining industry in South Africa would be R33 million per day ( $550 \text{ 000 holes} \times R60 \text{ per hole}$ ) or R10 billion per annum.

## CHAPTER 10 CONCLUSIONS AND RECOMMENDATIONS

### 10.1 Summary

The objective of this thesis was to design and develop a shaped charge explosive which would enhance the explosives' ability to break out rock in mining operations. This was to be achieved by focussing the explosive energy towards the toe of the blasthole using a hollow charge with a shaped metal liner positioned at a given stand-off distance from the toe – in essence, an explosive gun directed at the toe of the blasthole.

For its use in the narrow-reef, hard-rock underground stoping operations of the South African gold and platinum mines, this explosive gun was termed a directional primer charge, as it took the position of the bottom primer charge in a column charge of explosives and it directed the explosive energy forward towards the toe of the blasthole.

The directional primer charge was designed and developed on surface under laboratory conditions using the sophisticated measuring devices of flash X-ray radiography and electronically-timed shorting screens. It was then tested underground under production conditions in a gold mine. The results of over 1300 production blastholes were recorded and analysed.

The mechanism of directing explosives energy forwards is the use of a hollow or shaped charge to focus the explosive energy and the use of a metal liner to enhance the effect. The shock wave generated when the explosive is detonated, is focussed using a concave hollow at the end of the explosive. This effect is further enhanced by the use of a thin concave metal disc which lines the hollow of the explosive and which itself then deforms by turning itself inside out transforming the disc into a high velocity metal slug. In order to complete this transformation, a certain distance is required. The disc is therefore placed at a distance from its target. This distance is termed the stand-off distance. The distance between the disc at rest and that over which the slug becomes fully formed is termed the minimum effective stand-off distance. Flash X-ray radiography showed that this distance was of the order of one to two calibres and in the particular case of the directional primer charge was 30 mm.

The mechanics of the action of the directional primer charge on the breaking of rock in a blasthole is one of energy conversion. Explosive energy from the column charge of explosives is partially converted into kinetic energy of a high velocity metal slug using the shaped liner or metal disc.

This concave disc attains a high velocity over a very short space of time and hence over a very short distance. The shock impact of the detonation wave causes a jump condition in the velocity of the disc from zero at rest to its final velocity as an explosively-forged projectile i.e. a high velocity metal slug. From electronic timing and flash X-ray radiography, the disc is shown to attain this high velocity also within one calibre i.e. for the directional primer charge also within a distance of 30 mm.

The kinetic energy of the high velocity metal slug is then converted into impact energy as it impacts on the rock at the toe of the blasthole. This impact energy is dissipated by compacting the rock at the toe of the blasthole. This compaction results in movement of the rock interface back into the rock mass and resultant crushing and cracking of the rock. Theoretical calculations show that for the explosive types of directional primer charge tested and for the rock type in the underground environment, the rock interface could be expected to move 1 to 2 mm into the rock mass. This movement places the rock at the perimeter of the toe of the blasthole in tension which could initiate a radial fracture at the toe at right angles to the long axis of the blasthole. Such a radial crack would be typical of an “umbrella crack”. Such cracks were observed in the directional primer charge blastholes in the underground tests.

The surface experiments in the Advanced Detonics Laboratory indicated that the transference of explosive energy to the kinetic energy of the metal disc was a shock impulse which produced slug velocities in practice which were close to the theoretical calculations for slug velocity using the Shock Physics Model. This meant that the actual velocities could be predicted with a degree of accuracy, given the directional primer charge parameters, such as explosive type. Experiments with different explosives types showed that explosives with a higher velocity of detonation produced slugs with greater velocities. Composition B, TNT and Super Gelignite explosives with nominal velocities of detonation of 7600 m/s, 6700 m/s and 5600 m/s respectively were tested and produced measured slug velocities of 2045 m/s, 1510 m/s and 1130 m/s respectively.

The impact of the slug on the toe of the hole, is characterised by a shock impact phase followed by a plastic flow phase and then a hydrodynamic phase. The shock impacts of the directional primer charges in the range of explosives tested (i.e. those explosives which produced slug velocities from 1000 m/s to 2000 m/s) are calculated to produce shock impact pressures between 10 GPa and 25 GPa over time durations of 1,75  $\mu$ s to 1,5  $\mu$ s respectively.

The impact of the slug is calculated to move the rock face at the toe into the in situ rock mass a distance of 1,2 mm and 2,1 mm for slug velocities of 1000 m/s and 2000 m/s respectively. During the shock impact phase, the slug impacts against the rock. During the plastic flow phase, the slug flattens itself against the rock face and the rock face starts to move into the rock mass. It is suggested that the duration of this phase is of the order of 5  $\mu$ s and pressure drops to 20 % of the original impact shock pressure. During the third phase of impact, the hydrodynamic phase, the reflected rarefaction waves destroy the original shock wave as the slug penetrates the rock further. The penetration pressure for this phase is calculated to range from 0,5 GPa to 2,1 GPa for slug velocities of 1000 m/s to 2000 m/s respectively. This phase lasts for a duration within the range 48  $\mu$ s to 27  $\mu$ s. Thus, the effects of the slug on the rock at the toe of the hole lasts for a duration of under 50  $\mu$ s. In this time, the slug has caused the rock at the toe of the hole to move forward between 1 mm and 2 mm thus initiating the formation of an umbrella crack at the toe which propagates radially outwards at right angles to the axis of the hole. It is calculated that the extent of the propagation of the umbrella crack caused by the shock impact is five times the slug diameter for a slug travelling at 1000 m/s and ten times the slug diameter for one travelling at 2000 m/s.

On the arrival of the expanding explosive product gases at the toe of the hole following the impact of the slug, these gases enter the cracks made by the impact of the slug and extend them further, thus enhancing the break out of the rock at the toe. This enables the burden rock to break out to the full length of the blasthole, and in some of the observed cases, beyond the full length.

The underground tests were undertaken to determine the effectiveness of the directional primer charge on standard blasting practice in stopes. Thus, as a control, "standard" rounds were blasted in which no directional primer charges were inserted. These control rounds were used as a base against which any improvement or otherwise could be measured. As each series of tests took place at different times, a new set of "standard" rounds were recorded to obviate the effect of changes in ground conditions, drilling crews etc.

The first two series of tests, used different masses of Composition B explosive ranging from 20 g to 95 g. Compared to the standard round, each directional primer charge round showed an improvement, although above 35 g of Composition B the improvement remained constant at about 10%. The third series of tests used 85 g of Composition B and again the directional primer charge showed an improvement in break-out over the standard round.

The fourth series of tests used Super Gelignite which surprisingly enough, given its lower velocity of detonation, produced the same improvement over the standard round of the order of 10%.

The hole length frequency distribution curves showed interesting results particularly with the incidence of zero socket lengths. It showed that rounds with the directional primer charge had almost twice the percentage frequency of the standard rounds. Examination of the stoping face after blasting, showed a number of holes that had been recorded as zero socket length actually broke out the rock beyond the length of the hole. If this were to average 50 mm it would represent an additional break-out of 4% above the full length of 1200 mm.

Thus, it can be said that the use of a directional primer charge can increase the break-out of a blast from 10% to 15%. Should the standard conventional blasting in a mine be less efficient than the experienced at Village Main, as is indicated to be so by Brinkmann (1994), then the increase in the break-out of rock from a blast could be in excess of 15%.

An additional break-out of 15% represents a potential additional revenue of R150 million per annum for the average South African gold mine or R10 billion per annum for the South African gold and platinum mining industry.

## **10.2 Conclusion**

This thesis has demonstrated through theoretical calculation and practical application that the breakout of rock in underground stoping operations can be enhanced by up to 15% by the use of a directional primer charge which has been designed and developed during this research and is recommended for commercial use in mines.

This thesis describes the mechanisms involved in the process and in doing so has provided a credible explanation for the hitherto unexplained "air gap phenomenon" which produced the umbrella fracture in Perspex model blasting. The directional primer charge appears to produce a similar umbrella fracture in rock at the toe of the blasthole in underground stoping operations.

The economic implications of this improvement in blasting efficiency due to the increased break-out volume of rock per blast is significant.



### 10.3 Recommendations

There is a large amount of further work that could be undertaken; namely to ascertain the effectiveness of the directional primer charge on

- the platinum mines
- development ends
- open pits

The platinum mines would be of interest because, although their stoping methods are similar to Witwatersrand gold mines, their Merensby Reef and UG2 Reef are known to have different breaking characteristics from both quartzite and each other.

The use of directional primer charges in development ends or tunnels would be of interest in that, whereas stoping has two free faces from which the rock has to break, development ends have only one free face. However, the development blastholes tend to be drilled closer to one another and if a parallel round is drilled, all holes should be of the same lengths and therefore the umbrella cracks could interact with one another enhancing break-out effect.

In open pit mining, sub-drilling could be eliminated, as the blasthole need only to be drilled to the bench floor level. This would result in a commensurate saving of drilling and explosives costs. In addition, the umbrella fracture should result in less fractured rock on the bench floor resulting in easier drilling conditions and more controlled blasting in subsequent production cycles.

**APPENDICES**  
**(SEE ENCLOSED CD)**

		<b>Page</b>
<b>APPENDIX 1</b>	Explosives	163
<b>APPENDIX 2</b>	Taylor Wave Equations	171
<b>APPENDIX 3</b>	Gurney Model Equations	186
<b>APPENDIX 4</b>	Gas Dynamics Model Equations	209
<b>APPENDIX 5</b>	Shock Physics Model Equations	227
<b>APPENDIX 6</b>	Advanced Detonation Laboratory Measurements	239
<b>APPENDIX 7</b>	Shock Effects Generated by the Directional Primer Charge	249
<b>APPENDIX 8</b>	Underground Test Measurements and Frequency Distribution Graphs	270
<b>APPENDIX 9</b>	Slugshot Photographs	317
<b>APPENDIX 10</b>	Advanced Detonics Laboratory Photographs	320
<b>APPENDIX 11</b>	Flash X-Ray Photographs	352
<b>APPENDIX 12</b>	Underground Tests Photographs	356
<b>APPENDIX 13</b>	Comparison of Theoretical Model Calculations of Disc Velocities with Measured Velocities for Various Masses of Explosives and Discs	375

# APPENDIX 1      EXPLOSIVES

## A.1.1 Military Explosives

A.1.1.1      TNT, RDX, HMX

A.1.1.2      Composition A, Composition B, Composition C

A.1.1.3      Cyclotol, Octol

## A.1.2 Commercial Explosives

A.1.2.1      Nitroglycerines

A.1.2.2      Ammonium Nitrates

A.1.2.3      Watergels, Slurries, Emulsions

A.1.2.4      Initiating Systems

## A.1.3 Super Gelignite

## A.1.4 Village Main Field Tests

## References

### **A.1.1 MILITARY EXPLOSIVES**

Military explosives are characterized by their ability to be stored in magazines for long period of time and then be used at short notice with no apparent deleterious effects in their performance. To achieve this they require to be chemically stable for a period of years until they are required to be handled and detonated.

As they are also required to pack as much energy into a small a package as possible, they tend to have as high a density as practicable. In addition, as they are often required to drive shrapnel as far and as wide as possible, they tend to have a high velocity of detonation.

Therefore, military explosives tend to differ from commercial explosives, i.e. those that are widely used in civil and mining operations, in that they have

1. a longer shelf life
2. a greater density
3. a higher velocity of detonation (VOD).

As a consequence of the above, military explosives tend to be more expensive than commercial explosives.

#### **A.1.1.1 TNT, RDX, HMX**

The three most common single compound military explosives are trinitrotoluene (TNT), cyclotrimethylenetrinitramine (RDX) and cyclotetramethylenetetranitramine (HMX).

TNT was developed in the First World War and is the acronym for trinitrotoluene. It has the chemical formula, given in explosive nomenclature,  $C_7H_5N_3O_6$ .

RDX was developed in the Second World War and is the acronym for Research Department Explosive, which was the code name given to it for security reasons. Its explosive chemical formula is  $C_3H_6N_6O_6$ . It is also known in some countries as Hexogen due to its chemical structure.

HMX was produced after the Second World War as a by-product of RDX and has a higher melting point than RDX. HMX is the acronym for High Melting Explosive again a code name and has the explosive chemical formula  $C_4H_8N_8O_8$ . It is also known as Octogen.

It is believed in some quarters that HMX was the acronym for His Majesty's Explosive, but as it merely is a code name, it is of interest sake for trivia only and is of little consequence.

ACRONYM	COMPOSITION	DENSITY	V.O.D.
TNT	$C_7H_5N_3O_6$	1,55 g/cm <sup>3</sup>	6700 m/s
RDX	$C_3H_6N_6O_6$	1,80 g/cm <sup>3</sup>	8750 m/s
HMX	$C_4H_8N_8O_8$	1,90 g/cm <sup>3</sup>	9100 m/s

#### A.1.1.2 COMPOSITION A, COMPOSITION B, COMPOSITION C

The first practical military explosive based on RDX was a mixture of RDX with beeswax in the ratio 91:9 by weight. This explosive mixture was known as Composition A.

Composition B was developed as a castable mixture of RDX with TNT and a small amount of desensitizing beeswax in the ratio 60:39:1. It became the most frequently used high-energy military explosive and even today is the most common projectile fill in military projectiles. Its ability to be precision cast has made it the ideal filling for shaped charges.

Composition C was developed as a hand-mouldable “plastic” explosive of RDX with polyisobutylene and beeswax in the ratio 90:9:1. Composition C1, C2, C3 and C4 were later modifications of Composition C with different binders. Composition C4 is most often used in demolition.

#### A.1.1.3 CYCLOTOL, OCTOL

Further mixtures of RDX and HMX with TNT are known as Cyclotol (RDX:TNT=75:25) and Octol (HMX:TNT=76:24).

The properties of these most common military explosives are given below (Persson et al 1994).

<b>NAME</b>	<b>COMPOSITION</b>	<b>DENSITY g/cm<sup>3</sup></b>	<b>VOD m/s</b>	<b>DETONATION PRESSURE GPa</b>	<b>EXPLOSIVE ENERGY MJ/kg</b>
TNT	100 % TNT	1,55	6700	22,2	4,4
Comp B	60:40 RDX:TNT	1,60	7600	24,4	5,0
Comp C-4	90:10 RDX:Polysisobutylene	1,72	8040	25,7	5,9
Cyclotol	75:25 RDX:TNT	1,74	8250	24,6	5,1
Octol	76:24 HMX:TNT	1,81	8480	34,3	4,5

## **A.1.2 COMMERCIAL EXPLOSIVES**

Commercial explosives are typically those that are widely used in the civil and mining industries. They are characterized by rapid turnover – buy it and use it – and thus they can have a short shelf-life, typically six months.

As they are a cost item in production, there is great commercial pressure to keep the cost down and their performance is often judged as the “most bang for the buck” or price per kilogram. Thus, typically the most widely used commercial explosives are those with the cheapest ingredients.

### **A.1.2.1 NITROGLYCERINES**

Nitroglycerine explosives were first manufactured commercially by Nobel in the 1860's (Blasters Handbook 1977).

The classical nitroglycerine explosives consist of a mixture of nitroglycerine and a similar liquid explosive nitroglycol-ethylene glycol dinitrate or EDGN ( $C_3H_4(ND_3)_2$ ) as sensitiser and plasticiser, mixed with a blend of fuel and oxidizer such as ammonium nitrate or sodium nitrate.

Basically there were three types of nitroglycerine explosives manufactured in South Africa. They were Ammon Dynamite, Dynagel and Ammon Gelnite and were for many years the backbone of the South African gold mining industry.

The cheapest, Ammon Dynamite, was water soluble. The most expensive, Ammon Gelnite, was waterproof. As a result of the foregoing, Dynagel was manufactured as a compromise. Its price lay between the former two and it was partially waterproof, effective for a shift of 12 hours only.

### **A.1.2.2 AMMONIUM NITRATES**

During the 1940's it was realized that ammonium nitrate fertilizer had explosive properties. Ammonium nitrate was marketed under various names, ANBA – ammonium nitrate blasting agents, ANFO – ammonium nitrate fuel oil, ANFEX – ammonium nitrate fuel explosive.

Due to its low cost, ammonium nitrate explosives were readily accepted and used. However, it was water-soluble so that it could not easily be used in wet holes.

### **A.1.2.3 WATERGELS, SLURRIES, EMULSIONS**

To combat the water-solubility of ammonium nitrate, it was made waterproof, ironically by dissolving it in water and adding binders to produce a watergel explosive. Further refinements produced slurry and emulsion explosives.

In the watergel explosives, a gelled water solution, which contained ammonium nitrate or sodium nitrate together with water-soluble fuels and explosive ingredients such as monomethylamine nitrate (MMAN) replace NG and EDGN as sensitiser and plasticiser.

The rest of the mixture, suspended in the gel to form a thick grainy fluid, consists of granular TNT or finely powdered aluminum as a sensitiser; undissolved AN or SN oxidizers; and added fuel components, of which granular aluminum is most commonly used to compensate for the low energy due to the cooling capacity of the water.

Slurry explosives are basically watergel explosives used in bulk for large diameter blastholes and can be mixed on site immediately prior to loading the holes. The ability to bring the constituents to site in bulk as non-explosive transport. The mixing on site at each individual hole allowed for custom-designed explosives for each blast, thus allowing for an increase in blasting efficiency, which again resulted in a reduction of explosive cost.

Emulsion explosives are a further development and refinement of watergel explosives. By using suitable emulsifiers, a concentrated hot solution of ammonium nitrate in water can be dispersed to form micron-sized droplets in a fuel oil. This produces an explosive mixture which has the texture similar to that of margarine or Vaseline. As each ammonium nitrate solution droplet is enclosed by a thin film of oil, the emulsion explosive is waterproof and can be used in wet holes. The small size of the droplet and the submicron thickness of oil film gives a large contact area of oxidizer and fuel which allows for more complete combustion and minimizes deleterious blasting fumes such as nitrous oxides, carbon monoxide and dioxide. However, the emulsion matrix is essentially nondetonable as it has a low temperature increase when compressed by a shock wave. To overcome this, artificial hotspots are created by the addition of glass micro balloons or fine gas bubbles.

### **A.1.2.4 INITIATING SYSTEMS**

In Witwatersrand practice for many years the initiation of stoping blasts have been capped fuse and igniter cord.



With cartridge nitroglycerine explosives the detonators have been 6D cap – sensitive. However, with the advent of the less sensitive Anflex into the mines in the 1960s, a stronger detonator was required to initiate the stoping and development blastholes. The 8D detonator which has twice the mass of initiating explosive, and hence twice the power, of the 6D detonator was found to adequately initiate Anflex.

As the mining is narrow reef stoping with a stoping width of the order of one metre, the blast is a confined blast, not dissimilar to a narrow trench on its side, and therefore it is important that the blastholes are fired in sequence. As each hole is blasted a new free face is created for the following hole. If the burden is correct, then each hole as it is blasted breaks out the rock between it and the free face. If holes are blasted out of sequence, the resulting burden between the hole and the free breaking face becomes too large and the intervening rock will not break out. Thus, sequential firing of holes is of paramount importance in narrow reef stoping.

To achieve sequential firing igniter cord has traditionally been used to remotely light up the capped fuses in sequence. Igniter cords with different burning speeds have been used for different applications. In general, the longer the capped fuse the slower the igniter cord burning speed must be to ensure sequential firing. However, too slow a burning speed may result in cut-offs caused by blasting fly-rock severing the igniter cord.

Traditionally, igniter cord came in fast, medium or slow speeds being less than 6 s/m, 8 to 16 s/m and 30 to 45 s/m respectively. Medium igniter cord was used in stoping for 0,9 long capped fuses. With the advent of longer holes in stoping and longer fuses an intermediate speed igniter cord 1C57 with a burning speed of 13 to 26 s/m was developed for 1,2 m long fuses.

Electric detonators were not used on South African narrow reef hard rock mines for two main reasons. Firstly, the number of delay detonators was for less than the average number of holes per stoping panel (15 delay numbers as apposed to 100 holes and more per panel), and so the holes would not be able to be fired in sequence. Secondly, it was considered hazardous to use electric detonators due to the presence of stray electric currents in the working places underground.

Finally PETN (pentaerythritol tetranitrate –  $C_5H_8N_4O_{12}$ ) is an explosive which is often used commercially as a booster. It has a high velocity of detonation of 8000 m/s and a higher density than most commercial explosives of 1,67.

Its use in commercial applications is not restricted to boosters but is an integral constituent of detonating cord which is commonly used in long holes to ensure initiation of the entire length of the column charge.

### **A.1.3 SUPER GELIGNITE**

Super Gelignite was a special formulation of ammonium gelignite manufactured to produce a high velocity of detonation explosive and it was seen as the most practical and cost effective explosive for the directional primer slug. It is more dense than the more common nitroglycerine explosives at  $1,49 \text{ g/cm}^3$  and has a higher velocity of detonation at 5600 m/s.

### **A.1.4 VILLAGE MAIN FIELD TESTS**

The testing of the directional primer charge underground at Village Main mine was undertaken using Tovex 220 watergel explosive as the secondary explosive and Stopecord 9 (i.e. medium speed) igniter cord with 0,9 m long capped safety fuse.

## **REFERENCES**

1. COURSE NOTES (1978)
2. ROCK BLASTING & EXPLOSIVES ENGINEERING (1994)
3. BLASTERS HANDBOOK (1977)
4. EXPLOSIVES TODAY SERIES (1966 to 1976)
5. EXPLOSIVES TODAY SERIES 2 (1976 to 1988)
6. EXPLOSIVES TODAY SERIES 3 (1988 to 1990)

## **APPENDIX 2**

### **THE TAYLOR WAVE EQUATIONS**

# DYNAMICS OF GAS FLOW BEHIND PLANE DETONATION FRONTS

## I. The Taylor Wave

### Synopsis

*Taylor employed Riemann's equations to construct the nonsteady flow of detonation product gases behind the Chapman-Jouguet discontinuity. The flow is described as a simple wave region centred on the backface of the explosive where detonation is initiated. The wave equations are solved analytically for the case of polytropic gases and explicit solutions are derived for gas velocity, sound speed, density and pressure. The solution is interpreted in terms of space distributions of these parameters behind the detonation wavefront.*

Prepared by  
*Dynamic Physics Consultants CC*  
for  
Mr J.A. Cruise  
EXPLODE (Pty) Ltd

May 1993

# DYNAMICS OF GAS FLOW BEHIND PLANE DETONATION FRONTS

## I. The Taylor Wave

### TABLE OF CONTENTS

	<i>Page</i>
1. Gaseous Products of Detonation	1
2. Dynamics of Gas Flow Behind Plane Detonations	2
2.1 Taylor Model & Characteristic Equations	2
2.2 Taylor Solution for Polytropic Gases	4
2.3 Physical Interpretations of Taylor Wave	6
3. Derivation of Taylor Wave Equations	9
3.1 Particle Velocity	9
3.2 Sound Velocity	10
3.3 Pressure	10
3.4 Density	11

*Figures 1-3*

## Symbols

$c$	gas acoustic velocity
$D$	velocity of detonation
$P$	gas pressure
$t$	time
$U$	gas (particle) speed
$X$	general axial coordinate
$z$	dimensionless axial coordinate
$\rho$	density
$\Gamma$	adiabatic exponent
$\sigma$	Riemann invariant
CJ	Chapman-Jouguet state

Subscript 1 denotes initial values at the CJ state

## Gaseous Products of Detonation

A detonation in a solid HE is a shock wave with rapid exothermic chemical reaction immediately behind the shock front. The chemical reaction provides the energy needed to sustain the propagation of the shock wave as it traverses the HE. For lateral dimensions larger than some minimum size corresponding to each HE, and if the reaction rates are effectively infinite and chemical equilibrium is attained, one has a steady-state detonation whose properties are governed solely by thermodynamics and hydrodynamics. When this state is attained, the detonation front has a constant velocity and advances through the HE at a constant peak pressure behind the shock front. This is referred to as an ideal detonation.

The various states of an ideal detonation can best be described with the pressure-volume Hugoniot curves shown in *Figure 1*.

A shock wave enters a block of solid explosive at state 1, usually at standard atmosphere. The end states of the material behind the shock, if the material is inert, fall onto the locus of the Hugoniot. In the case of a condensed explosive, the Hugoniot represents the unreacted material. The straight line connecting the initial and final states on the P-V Hugoniot in *Fig. 1* is referred to as the Rayleigh line. If energy is released from the HE, the possible end states form a Hugoniot of reaction products. For a plane detonation, Chapman-Jouguet hypothesized that the Rayleigh line is tangent to the Hugoniot of the products. This point of tangency is referred to as the C-J point. An important property of this point is that the propagation velocity of pressure disturbances (i.e. the sound velocity) in the products represented by the C-J point is equal to the difference between the shock front velocity and the local particle velocity, thus:

$$c_{CJ} = D - U_{CJ} \quad \text{or} \quad D = c_{CJ} + U_{CJ} \quad [1]$$

Taylor (1948) pointed out that this hypothesis avoids the necessity for studying the motion of gases behind the detonation front. The hypothesis, represented by eq. [1], in combination with the usual hydrodynamic equations of ideal plane detonations suffices to yield a full description of the gases at the CJ point. Of course, in many practical applications of detonation theory the motion of gases away from the CJ state is important.

In ideal detonations the reaction is complete at the CJ plane which also represents the boundary between steady and nonsteady flow regions in the reaction product gases. As the gases expand away from the CJ state, the sound velocity is less than given by eq. [1] and the flow is no longer steady. Riemann's equations for one-dimensional isentropic (constant entropy) fluid flow can be used to construct the nonsteady flow behind the Chapman-Jouguet discontinuity. Taylor appears to have been the first to adopt this approach and for this reason, the expansion of detonation product gases is often referred to as the Taylor wave. As an example of wave propagation in unsteady flows, a paper by Duval et al on explosive acceleration of projectiles may be consulted.

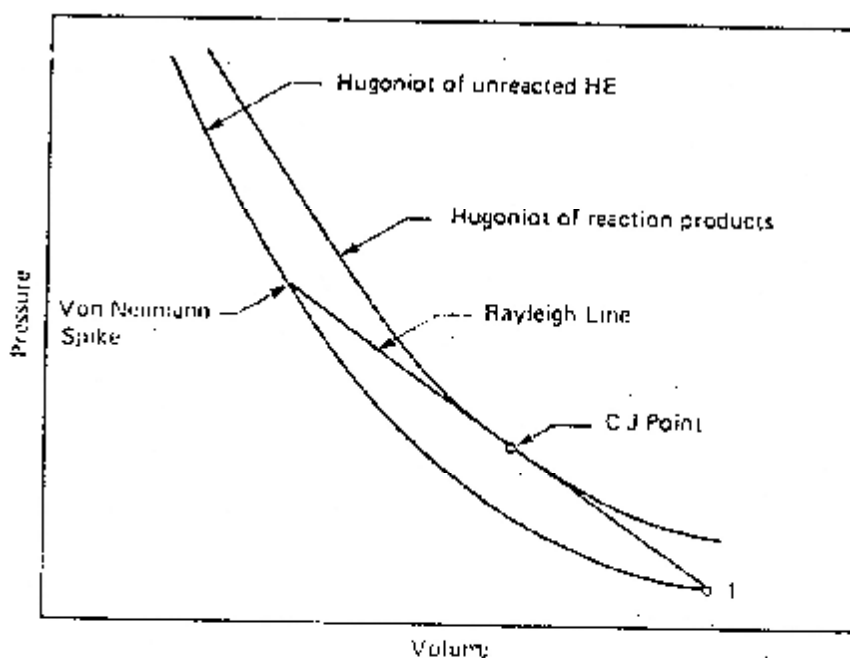


FIGURE 1 -Hugoniot Curves Representing Detonation of Condensed Explosives

## 2 Dynamics of Gas Flow Behind Plane Detonations

### 2.1 The Taylor Model & Characteristic Equations

At the Chapman-Jouguet discontinuity, located at  $x=Dt$ , the explosion products are characterized by the quantities  $U_1$ ,  $\rho_1$ , and  $c_1$ , which are determined by the Chapman-Jouguet condition, the Hugoniot equation, and the equation of state. The basic assumptions of the Taylor model are:



- the flow is one-dimensional
- the whole flow can be determined as a simple wave (an unsteady rarefaction wave)
- density  $\rho$  is a function of pressure  $P$  only .

The significance of the model assumptions lies in the fact that when only one wave is present, the particle velocity  $U$  is found to be a function of density only. Furthermore, if  $U$  and  $P$  are known at all points at one instant they are known at all other times.

For definiteness, we suppose that the steady detonation begins at a piston face located at  $x=0$  at  $t=0$ . (If the point  $x=0$  represents an interface between explosive and air, then there will result a backward flow of explosion products in the  $-x$  direction. This flow is the same as though the piston of the model is conceived to move at a constant velocity sufficient to reduce the pressure on the piston to the ambient air pressure.) The Chapman-Jouguet particle velocity  $U_1$  is accommodated to the piston velocity, assumed to be less than  $U_1$ , by a centred simple wave, i.e. by an unsteady rarefaction wave. This wave is described by

$$x := (U + c) t \quad [2]$$

Furthermore, the so-called Riemann invariant  $\sigma$  is constant throughout this simple wave.  $\sigma$  is defined as

$$\sigma = \int_0^P \frac{1}{\rho \cdot c} dp \quad [3]$$

and at all points in the flow the following equality holds

$$U - \sigma(P) = U_1 - \sigma(P_1) \quad [4]$$

Hence

$$\begin{aligned} U - U_1 &= \int_{P_1}^P \frac{1}{\rho \cdot c} dP \\ &= \int_{\rho_1}^{\rho} \frac{c}{\rho} d\rho \quad [5] \end{aligned}$$

since

$$\delta P := c^2 \delta \rho \quad \square$$

Eq.[2-5] represent standard equations from Riemann's analysis of nonsteady flows and describe the propagation of pressure disturbances (waves). For the purposes of this study, it is best to assume the validity of these equations and merely to examine their consequences when applied to the gas expansion model. Taylor's analysis (1948) starts with eq.[5]. If deemed necessary, a large number of textbooks in fluid dynamics may be consulted on the treatment of unsteady gas flows, particularly those discussing wave phenomena and their analysis by the method of characteristics.

## 2.2 Taylor Solution for Polytropic Gases

Taylor derived a solution to eq.[5] in the case of polytropic gases. These gases are characterized by a constant adiabatic exponent  $\Gamma$  as they expand and their properties are described by:

$$P \rho^{-\Gamma} := \text{constant} \quad \square$$

It can be shown that for polytropic gases the sound speed is related to the density as

$$c = c_1 \left[ \frac{\rho}{\rho_1} \right]^{\frac{\Gamma-1}{2}} \quad \square \quad [6]$$

Substituting (6) in (5) and integrating yields

$$U = U_1 - \frac{2c_1}{\Gamma-1} \left[ 1 - \left[ \frac{\rho}{\rho_1} \right]^{\frac{\Gamma-1}{2}} \right] \quad \square \quad [7]$$

Using eq.[6] again in [7] and rearranging yields one of the fundamental equations of the Taylor wave, namely:

$$U + c = U_1 + c_1 - \frac{\Gamma-1}{2} \left[ \frac{U - U_1}{c_1} \right] \quad \square \quad [8]$$

This relates the particle velocity to its initial value and describes its distribution since  $U$  is an implicit function of  $x$ . This equation in combination with eq. [2] provides a complete description of the Taylor expansion wave. If the explosion products obey a polytropic law, eqs. [2 & 8] can be solved explicitly. Given the adiabatic exponent  $\Gamma$ , the results can be written in terms of the reduced distance along the wave  $z=x/Dt$  in the following form:

$$\frac{U}{U_1} = 1 + \frac{2}{\Gamma + 1} \frac{D(z - 1)}{U_1} \quad [9.1]$$

$$\frac{C}{C_1} = \frac{2}{\Gamma + 1} + \frac{\Gamma - 1}{\Gamma + 1} \left[ \frac{D(z - U_1)}{D - U_1} \right]^{\frac{2}{\Gamma - 1}} \quad [9.2]$$

$$\frac{P}{P_1} = \left[ \frac{2}{\Gamma + 1} + \frac{\Gamma - 1}{\Gamma + 1} \left[ \frac{D(z - U_1)}{D - U_1} \right]^{\frac{2}{\Gamma - 1}} \right]^{\frac{2}{\Gamma - 1}} \quad [9.3]$$

$$\frac{\rho}{\rho_1} = \left[ \frac{2}{\Gamma + 1} + \frac{\Gamma - 1}{\Gamma + 1} \left[ \frac{D(z - U_1)}{D - U_1} \right]^{\frac{2}{\Gamma - 1}} \right]^{\frac{2}{\Gamma - 1}} \quad [9.4]$$

The method of derivation of the above equations for particle velocity (gas flow velocity), acoustic speed, gas density and pressure is outlined in Section 3. It will be noted that the particle velocity and acoustic velocity are linear functions of the reduced distance  $z$ . This solution for the unsteady flow of a polytropic gas behind the Chapman-Jouguet detonation is called the Taylor wave. The eqs. [9] assume a particularly simple form when  $\Gamma=3$ . Then

$$\frac{U}{U_1} = 1 + \frac{1}{2} \left[ \frac{Dz - U}{D - U} \right] \quad [10.1]$$

$$\frac{c}{c_1} = \frac{1}{2} \left[ \frac{Dz - U}{D - U} + 1 \right] \quad [10.2]$$

$$\frac{P}{P_1} = \frac{1}{8} \left[ \frac{Dz - U}{D - U} + 1 \right]^3 \quad [10.3]$$

$$\frac{\rho}{\rho_1} = \frac{1}{2} \left[ \frac{Dz - U}{D - U} + 1 \right] \quad [10.4]$$

In this case, the density is also a linear function of the reduced distance  $z$ . This particular solution is of particular interest because the explosion products of condensed explosives obey, approximately, a polytropic law with an adiabatic exponent in the neighbourhood of 3. It can, therefore, be expected to display the features of the flow associated with such explosives, particularly in the case of high brisance explosives.

### 2.3 Physical Interpretation of Taylor Wave

In the above equations  $U$  is the gas velocity at a given instant  $t$  at the axial location defined by  $z$ . At this location and at this time  $c, \rho$  and  $P$  have the values defined by eqs. [9]. By considering certain boundary conditions specific to given physical situations (eg. explosive column unconfined or initiated at a rigid wall), one can derive a general picture of the nature of gas flow from detonations.

The flow behind the reaction zone consists of a column of forward moving explosion products, the length of which increases linearly with time. For solid explosives, the length of this column is approximately one-half the distance travelled by the detonation front from its point of initiation. When the rear surface of the explosive is unconfined and the point  $x=0$  represents the interface between explosive and air, then there will also result a backward flow of explosion products in the negative  $x$ -direction. The forward- and backward-moving columns of gases are smoothly joined by a stationary column of zero gas velocity and constant pressure. The length of the backward-flowing column also increases in time and its length (for solid explosives) is of the order of twice the length of the forward-moving products. The velocity of the air/products interface is about twice the initial value of particle velocity in the Chapman-Jouguet state.

Fig.2 illustrates the variation of pressure and particle velocity through the Taylor wave for a detonation originating at a rigid surface (eg. the bottom of a hole). In the reduced coordinates employed, the detonation front is located at 1.0. In this case there is no backward movement of gases. The particle velocity decreases linearly along the length of the forward-moving column of gases which is followed by a column of quiescent gases.

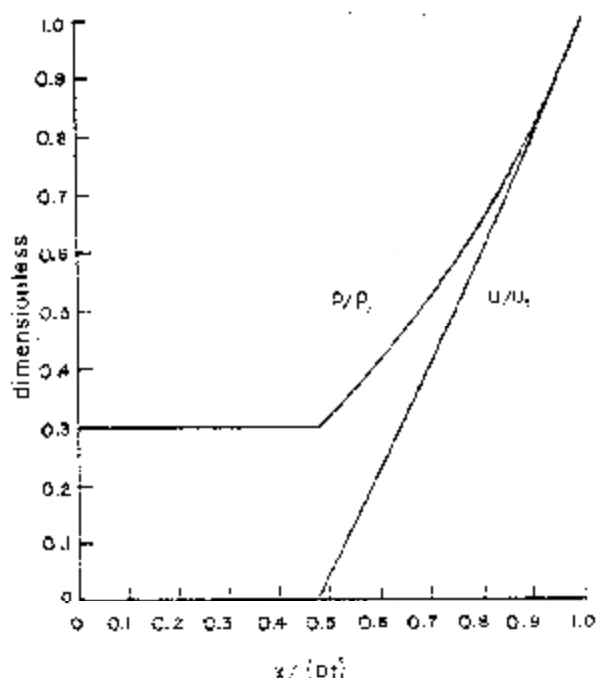


FIGURE 2: Pressure and Particle Velocity Variation Behind a Chapman-Jouguet Detonation  
Source: R. E. Shear (1961)

A qualitative representation of Chapman-Jouguet detonation and the resultant gas flow is given in Fig.3. Here specific physical terms and the sequence of gasdynamic regions are identified. Taylor's solution is applicable over the axial distance starting at the Chapman-Jouguet plane and ending at the gas-air interface.

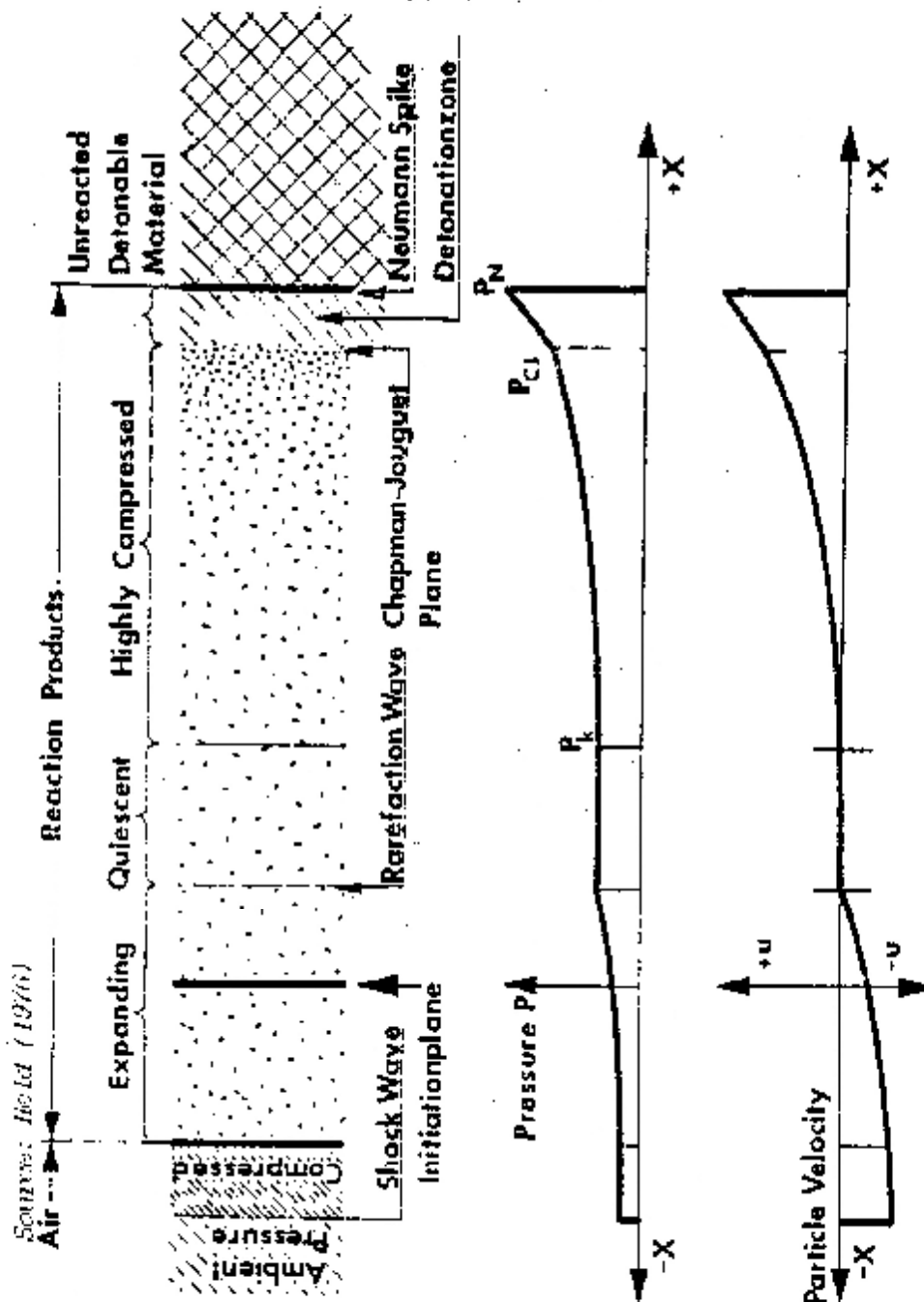


FIGURE 3 - Qualitative Illustration of Gas Flow Regions Behind the Detonation Wave.

### 3 Derivation of Taylor Wave Equations

#### 3.1 Particle Velocity

The two fundamental equations are:

$$D + c = \frac{x}{t} \quad (1)$$

$$D + c = U_1 + c_1 - \frac{\Gamma + 1}{2} \left[ \frac{U}{U_1} - 1 \right] \quad (1)$$

where the subscript 1 denotes the values at the C-J state. A further supplementary identity from the theory of detonation is that

$$D = U_1 + c_1 \quad (1b)$$

Hence, by substitution in [1]

$$\frac{x}{t} = D - \frac{\Gamma + 1}{2} \left[ \frac{U}{U_1} - 1 \right] \quad (2)$$

By solving [2] for  $U$ , and normalizing to its C-J value, [2] yields

$$\frac{U}{U_1} = 1 + \frac{\frac{x}{t} - D}{\frac{\Gamma + 1}{2} \frac{U_1}{U_1}} \quad (3)$$

Introducing the dimensionless distance parameter  $z = x/Dt$  eq[3] may be written in the form:

$$\frac{U}{U_1} = 1 + \frac{2}{\Gamma + 1} \frac{z - 1}{D \frac{U_1}{U_1}} \quad (4)$$

which is the solution, eq.[9.1].

### 3.2. Sound Velocity

Eq.[1] is rearranged to solve for  $c$  in terms of  $U$ :

$$c = U \frac{1 - \Gamma}{2} + c_1 + \frac{\Gamma - 1}{2} U \quad (9)$$

Then by substituting for  $U$  from eq.[4], and collecting terms, we obtain

$$\frac{c}{c_1} = \frac{U}{c_1} \left[ \left[ 1 - \frac{\Gamma}{2} \right] + \frac{\Gamma - 1}{2} \right] + 1 + \frac{\Gamma - 1 D (z - 1)}{\Gamma + 1 c_1} \quad (10)$$

Further substitution for  $D$  in terms of eq.[1b] and some tedious algebra, leads to the simplification of the above equation:

$$\begin{aligned} \frac{c}{c_1} &= 1 - \frac{\Gamma - 1}{\Gamma + 1} + \frac{\Gamma - 1}{\Gamma + 1} \left[ \frac{D z - u}{D - U} \right] \quad (11) \\ &= \frac{2}{\Gamma + 1} + \frac{\Gamma - 1}{\Gamma + 1} \left[ \frac{D z - U}{D - U} \right] \quad (11) \end{aligned}$$

Eq.[11] is the desired solution eq.[9.2] of Section 2.

### 3.3 Pressure

Pressure and acoustic velocity are related by the following relations describing the isentropic expansion of polytropic gases:

$$\frac{c}{c_1} = \left[ \frac{\rho}{\rho_1} \right]^{\frac{\Gamma - 1}{2}} \quad \text{and} \quad \frac{P}{P_1} = \left[ \frac{\rho}{\rho_1} \right]^{\Gamma} \quad (12)$$



Combining these relations gives the following relationship between  $P$  and  $c$ :

$$\frac{P}{P_1} = \left[ \frac{c}{c_1} \right]^{\frac{2}{\Gamma-1}} \quad [13]$$

Substitution of eq.[11] in eq.[13] yields the desired Taylor solution, eq.[9.3].

#### 3.4 Density

Density is related to sound velocity as may be seen from the first of eqs.[12]:

$$\frac{\rho}{\rho_1} = \left[ \frac{c}{c_1} \right]^{\frac{2}{\Gamma-1}}$$

Again, by substitution using eq. [11] for the sound velocity, we obtain the Taylor solution for density, namely eq. [9.4]. ■

## **APPENDIX 3**

### **THE GURNEY MODEL EQUATIONS**

# ACCELERATION OF METAL PLATES BY EXPLOSIVES

## II. The Gurney Method

### Synopsis

*The Gurney method for calculating the terminal velocity of metal driven by explosives is reviewed and applied to the analysis of a plate projected from the end of a column of explosives. It is shown that the method is based on the conversion of a particular fraction of the chemical energy of the explosive to mechanical work. This fraction -- often called the Gurney energy -- is directly related to the change of internal energy of detonation product gases as they undergo isentropic expansion. Gasdynamic calculations show that the terminal state of gases is quite similar to those assumed in the Gurney model. The domain of applicability of the model is defined, its limitations identified and some examples of its use are described.*

Prepared by  
*Dynamic Physics Consultants CC*  
for  
Mr J.A. Cruise  
EXPLODE (Pty) Ltd

May 1993

ACCELERATION OF METAL PLATES BY EXPLOSIVES  
II. The Gurney Method

TABLE OF CONTENTS

1	<i>The Gurney Method: An Overview</i>	1
1.1	<i>Gurney Model for Explosive-Driven Plates</i>	1
1.2	<i>Gurney Equations</i>	3
2	<i>Explosive Projection of Plates</i>	8
2.1	<i>Flat-Plate Gurney Equations</i>	8
2.2	<i>Derivation of Gurney Equation</i>	10
3	<i>Physical Interpretations of Gurney Model</i>	12
3.1	<i>Gasdynamic Analysis of Gurney Gas Model</i>	12
3.2	<i>Thermochemical Analysis of Gurney Energy</i>	15
3.3	<i>Limitations of the Gurney Method</i>	17
4	<i>Applications</i>	19
	<i>Figures 1-6</i>	
	<i>Tables 1</i>	

### Notation

$C$	=	charge mass
$D$	=	detonation velocity
$E$	=	Gurney energy
$E_G$	=	Gurney energy
$\sqrt{2E}$	=	Gurney characteristic velocity
$E_o$	=	chemical energy (explosive)
$E_v$	=	internal energy (gas) at volume $V$
$M$	=	metal mass
$V$	=	volume
$V_g$	=	gas velocity
$V_G$	=	Gurney velocity of plate
$V_o$	=	outflow velocity (gas)
$V_P$	=	plate velocity
$H_d$	=	heat of detonation
$\rho$	=	density

## 1 The Gurney Method: An Overview

### 1.1 Gurney Model for Explosive-Driven Metal.

In many practical applications of explosives, the primary interest lies in imparting some particular impulse, acceleration or velocity to metal which is in contact with the explosive. Engineering variables which may be tailored to achieve the desired end effects include the shape and size of the system, the choice of the explosive material (including its density) and of the inert (metal) cladding, and the geometrical disposition of the explosive/metal combination.

The motion of metal driven by detonating explosives can be very accurately calculated by computer codes provided an accurate equation of state for the detonation products is available (eg. MADER and KORY). Gasdynamic models are also available for modelling the acceleration of plates by planar, normally-incident detonation waves (eg. AZIZ). Gasdynamic calculations are however limited in their usefulness for engineering calculations. A change in the geometry or of the boundary conditions necessitates the formulation of a new mathematical problem which needs to be solved independently. Very few problems lead to results which can be expressed algebraically, and it is difficult to compensate for deviations from the strict idealizations that arise in practical systems.

In the event that the principal parameter of interest is the final metal velocity after acceleration is accomplished, overall energy and momentum balance considerations can be made to yield reliable estimates of the velocity. This is the basis of the so-called Gurney model. It is sufficiently accurate for many engineering applications (normally 10% uncertain).

In 1943, Gurney correlated fragment velocity data from artillery shells and grenades of a wide variety of sizes by assuming that a given explosive material will deliver a characteristic value of specific energy, different for each explosive, in the form of kinetic energy of the reaction products and the driven metal. The partitioning of the final energy delivered can be evaluated on the basis of two assumptions made by Gurney. These are that at any instant during the expansion of the detonation product gases they possess a spatially linear velocity distribution and their density is uniform. Figure 1 illustrates these assumptions for a cylindrical charge in a metal tube.

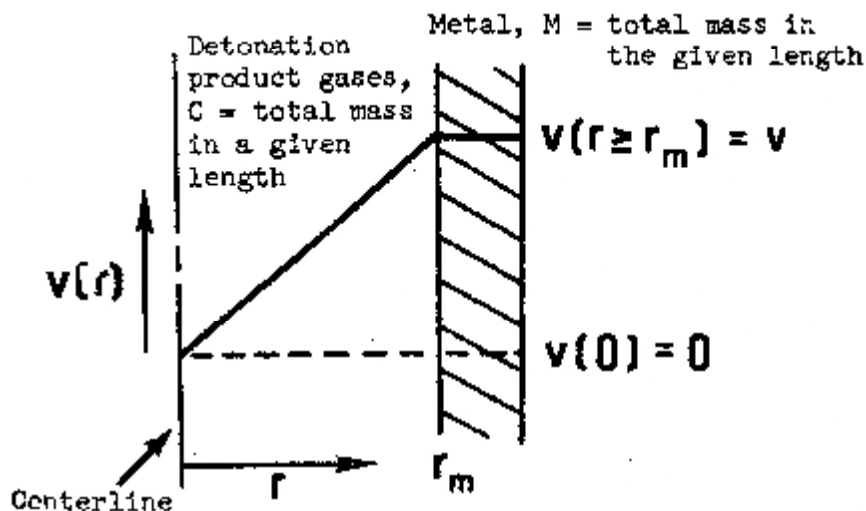


FIGURE 1: Linear Gas Velocity Profile

Gas velocity varies linearly from that of the plate at the right hand boundary to zero on the axis of symmetry. Gas density in the total volume behind the metal is uniform (but changes in time).

The two assumptions of uniform density and spatially linear velocity profile may be restated as a single requirement -- that of a linear velocity profile in Lagrangian or material coordinates. (In the Lagrangian scheme coordinate positions are identified with moving particles rather than fixed spatial locations: see KENNEDY and HARDESTY & KAMLET). Although originally introduced for reasons of simplicity and mathematical tractability, Gurney's assumptions have been shown to represent the physical situation quite accurately under a wide range of conditions (see Section 2).

The Gurney method may be applied to any explosive/metal combination with a cross-section admitting one-directional translational motion of the metal normal to its surface, regardless of the direction of detonation. Based on the assumption of a known Gurney energy for the explosive and a linear gas velocity distribution, the total energy balance for any simple geometry can be explicitly written out. For symmetric configurations such as a cylinder or sphere or flat sandwich, the energy balance equation is sufficient to define the final state. For asymmetric configurations such as explosive between two plates of unequal mass or an *open sandwich* combination of metal and explosive, the momentum balance equation must be solved simultaneously with the energy balance equation.

The resulting equations represent the final state of metal acceleration, that is, when final metal velocity is attained. For each geometry, the result is an analytical expression representing the final metal velocity as a function of the Gurney energy and the charge-to-metal ratio, M/C. This ratio is generally evaluated for a representative portion of the configuration under consideration. Thus it could pertain to the volume normal to a unit area in flat configurations, and to a unit length or solid sector in cylindrical configurations.

The Gurney method affords a simple but rational approach to explosive system performance calculations where the velocity imparted to metal elements is the primary concern. The power of the model derives from its ability to handle a large variety of engineering problems in a realistic way. Extensions and new applications continue to emerge because the physical formulation is intuitively satisfying and mathematically tractable at various levels of sophistication (JONES et al 1980). Two broad areas of its applications are in flyer plate studies of the constitutive properties of materials and in explosive characterization.

### 1.2 Gurney Equations

Gurney equations for some common symmetric and asymmetric metal/explosive combinations are discussed in STERNE and KENNEDY and are presented in Fig.2.

In Fig. 2A symmetric configurations are presented -- charges of cylindrical, spherical and planar symmetry. Considering cylinders, the kinetic energy balance per unit area of the expanded cylinder can be written as

$$E = \frac{1}{2} \frac{M V^2}{p} + \frac{1}{4} \frac{C V^2}{p}$$

where

- E = Gurney energy of explosive (per unit mass)
- M = mass of metal per unit area
- C = mass of charge per unit area
- V<sub>p</sub> = velocity of metal shell

The factor 1/4 derives from the assumption of a linear velocity profile (as in Fig.1) Solving the above equation for V<sub>p</sub>



$$V_P = \sqrt{2 \cdot E} \cdot \frac{\frac{C}{M}}{\sqrt{1 + \frac{C}{M}}} \quad [1]$$

Plate and sphere velocities may easily be derived in a similar fashion. The equation for the so-called *open-sandwich* configuration which is of direct interest to this study -- since it is also the basic model for the projection of a metal plate from the end of a column of explosive -- is handled in Section 2.2. A derivation of the asymmetric sandwich equation is given by STERNE.

Considering *Fig. 2*, a basic similarity of all Gurney-type equations is evident: the quantity  $\sqrt{2E}$  occurs in each expression, and the ratio of final plate velocity to this quantity is in all cases an explicit function of the metal-to-charge mass ratio. In asymmetric configurations where a distinction can be made between the metal plate and confinement or *tamper*  $N$ , the metal velocity is a function also of the *tamper-to-charge* mass ratio,  $N/C$ . In cases where cavities are present in the charge, with or without metal sleeves, the Gurney equations will include the initial radii of inner and outer metal/explosive interfaces.

The quantity  $\sqrt{2E}$  has units of velocity, and it is known as the Gurney constant or Gurney characteristic velocity.  $E$  is the maximum amount of chemical energy (per unit mass of explosive) in the initial state that can be converted to energy of motion in the final state. This energy is always less than the energy of detonation. The relationship between this quantity and more conventional measures of the strength of explosives is discussed in Section 3.2. In summary it can be stated that whereas the quantity  $\sqrt{2E}$  was originally an empirically measured parameter, it can now be accurately predicted by code calculations of the energy of expansion of detonation product gases.

Table 1 lists the values of Gurney velocity for some common explosives.



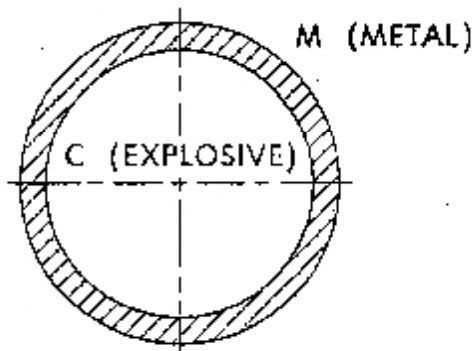
FLAT SANDWICH

$$V = \sqrt{2E} \left[ \frac{M}{C} + \frac{1}{3} \right]^{-\frac{1}{2}}$$



CYLINDER

$$V = \sqrt{2E} \left[ \frac{M}{C} + \frac{1}{2} \right]^{-\frac{1}{2}}$$



SPHERE

$$V = \sqrt{2E} \left[ \frac{M}{C} + \frac{3}{5} \right]^{-\frac{1}{2}}$$

FIGURE 2 (A): Gurney Equations for Symmetrical Explosive/Metal Combinations

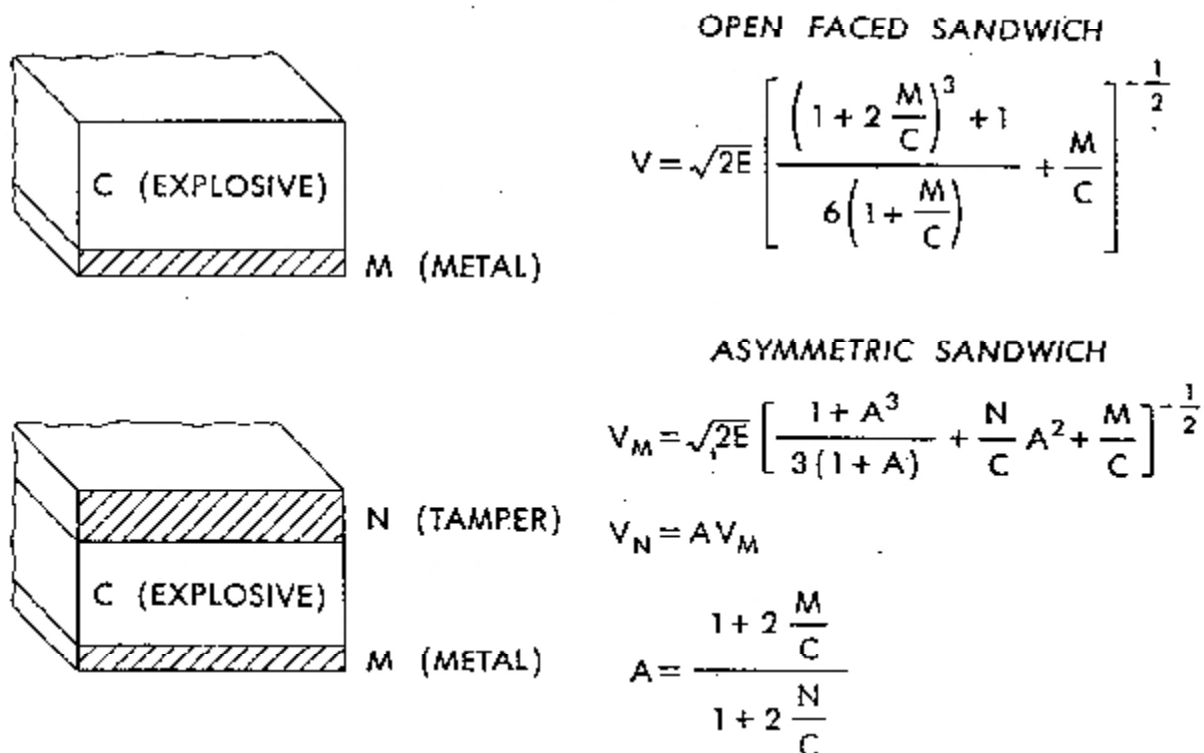


FIGURE 2(B): Gurney Equations for Asymmetrical Explosive/Metal Combinations.

Occurrence of end losses, the presence of parasitic mass, or the early fracturing of metal (as in cylinder expansion) may decrease the effective value of  $\sqrt{2E}$  by as much as 20%. For a given explosive composition,  $\sqrt{2E}$  is also sensitive to the value of its density and whether it is powdered, pressed or cast.

Limits on the applicability of the Gurney model are discussed in Section 3.3.

*Table 1*  
Gurney Constants

Source:  
*Kinney & Graham (1985); Kennedy (1972); Dohrutz & Crawford (1985)*

<i>Explosive</i>	<i>Density kg/litre</i>	<i>Gurney Constant m/s</i>
Ammonium Nitrate	1.73	1761
Nitromethane	1.13	2978
Nitroguanadine	1.72	2308
Nitroglycerine	1.59	3575
Nitrocellulose	1.67	2473
ANFO	1.60	2769
Amatol	1.60	2908
Composition B	1.71	2870
Pentolite	1.65	2970
Octol	1.81	2965
RDX/Wax 93/7	1.65	2727
TACOT	1.61	2120
TNT	1.63	2370
Tritonal (TNT/Al 80/20)	1.72	2320
Explosive D	1.72	2137
Detasheet	1.43	2200

References:

1. Gilbert Kinney & Kenneth J. Graham  
EXPLOSIVE SHOCKS IN AIR Springer-Verlag (1985)
2. B.M. Dohrutz & P.C. Crawford  
PROPERTIES OF CHEMICAL EXPLOSIVES AND EXPLOSIVE SIMULANTS  
Lawrence Livermore National Laboratory (LRL-52997 (1985))

## 2 Explosive Projection of Plates

### 2.1 Flat Plate Equations

The flat-plate explosive/metal combination is also referred to as the open-faced sandwich, flyer plate, Missnay-Schardin charge or ballistic disk. Similarly, a number of seemingly different analytical formulations have been presented for the Gurney velocity of such plates. In view of its importance for the present (*PrimerSlug*) study, the Gurney analysis of this asymmetrical explosive/metal combination is presented in some detail here.

The original STERNE flat-plate formula is

$$\frac{V}{G} = \sqrt{\frac{\frac{3 \cdot C}{5 \cdot M}}{1 + \frac{C}{5 \cdot M} + \frac{4 \cdot M}{5 \cdot C}}} \quad [2]$$

where the plate velocity has been normalized to the Gurney characteristic velocity.

KENNEDY has presented an alternate derivation which yields

$$\frac{V}{G} = \sqrt{\frac{1 + 2 \frac{M^3}{C^3} + 1}{6 \left( 1 + \frac{M}{C} \right)} + \frac{M}{C}} \quad [3]$$

By expanding the power, doing the addition and collecting terms, it can be shown that eq. [3] may be written in the form

$$\frac{V}{G} = \sqrt{\frac{3 z^3 + 18 z^2 + 12 z + 2}{6 (1 + z)}}$$

where  $z = \frac{C}{M}$

After further simplifications the above equation reduces to the form

$$\frac{V}{G} = \sqrt{\frac{3}{1 + 5 \frac{M}{C} + 4 \frac{M^2}{C^2}}} \quad [4]$$

Through algebraic manipulations it can be shown that eqs.[2] and [4], or the STERNK and KENNEDY flat-plate formulae, are equivalent. Eq.[4] may also be rewritten in a form that has been specifically applied to Missnay --Schardin charges: using the same abbreviation  $z$  as before, and multiplying both numerator and denominator by its square

$$\frac{V}{G} = \sqrt{\frac{3z^2}{z^2 + 5z + 4}} \quad [5]$$

$$1 = \sqrt{\frac{3z^2}{(z+1)(z+4)}} \quad [6]$$

A further substitution can be made, namely

$$z = \frac{\rho_e t_e}{\rho_p t_p} \quad \text{where } z = \frac{M}{C}$$

where  $\rho$  = density  
 $t$  = thickness  
 $e$  = explosive  
 $p$  = plate

Eq.[6] written in terms of material thicknesses and densities seems to be the best suited to an engineering analysis of the projection of metal plates from the end of a column of explosive.

### 2.2 Derivation of Gurney Flat-Plate Equation

The Gurney model that may be used to derive the KENNEDY equation, eq.[3], is shown in Fig.3.

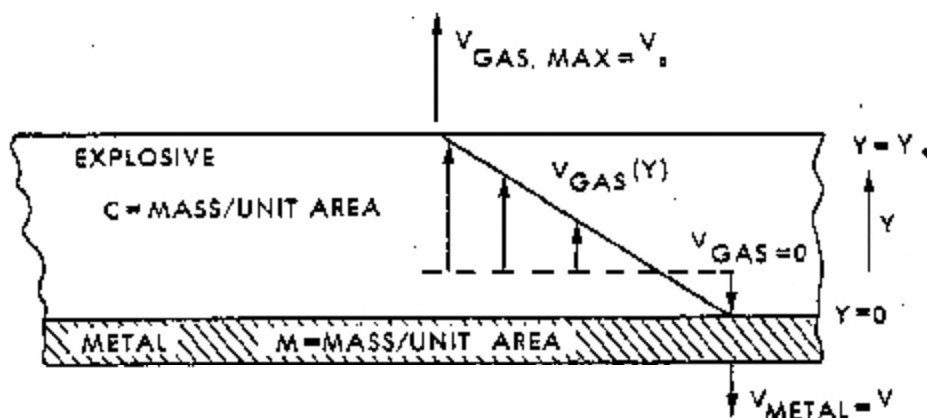


FIGURE 3: Gurney Gas Model for Open-Faced Sandwich Explosive/Metal Combination

A slab of explosive is confined on one side by metal; its initial thickness and density are  $Y_0$  and  $\rho_e$  respectively. Gas expansion velocity at the boundary defined by the metal plate is equal to that of the plate, namely,  $V_p$ . In the opposite direction, the outflow velocity of gases is  $V_0$ . Between these limits the velocity distribution is a linear function of the Lagrangian coordinate  $Y$ , so that at a general position  $Y$

$$v_g(Y) = V_0 + V_p \frac{Y}{Y_0} - V_p$$

The Gurney energy balance may be written as

$$E = \frac{1}{2} M V_p^2 + \frac{1}{2} \rho_e \int_0^{Y_0} \left( V_0 + V_p \frac{Y}{Y_0} - V_p \right)^2 dY$$

The momentum balance equation is

$$M \frac{V_p}{\rho} = \rho_e \int_0^Y \left[ \left( V_o + V_p \right) \frac{Y}{Y_o} - V_p \right] dy$$

Integration of these equations between the given limits and substitution of C/M for the equivalent ratio

$$\frac{\rho_e Y_o}{M} = \frac{C}{M}$$

yields by rearrangement eq. [3].



### 3 Physical Interpretations of the Gurney Model

#### 3.1 Gasdynamic Analysis of Gurney Gas Model

A gasdynamic model presented in a previous study described the acceleration of an inert plate by a normally-incident, planar detonation wave. Though this treatment is somewhat oversimplified, it does provide insight into the process of plate acceleration. KENNEDY presents a comparison of one-dimensional gasdynamic models and Gurney equations for the open-faced sandwich configuration. He shows that as the expansion of gases proceeds, their state approaches the Gurney assumptions, that is, a linear velocity profile is established and the gas density is almost uniform. Paradoxically it is precisely the physical phenomena that the Gurney model ignores -- namely, transient wave propagation -- that lead to the creation of these conditions soon after the detonation front is reflected from the plate.

The correspondence between gasdynamic and Gurney model predictions is shown in *Fig. 4*. Here the final plate velocity is plotted as function of  $M/C$ . Significant and systematic deviations occur only at  $M/C < 0.1$ .

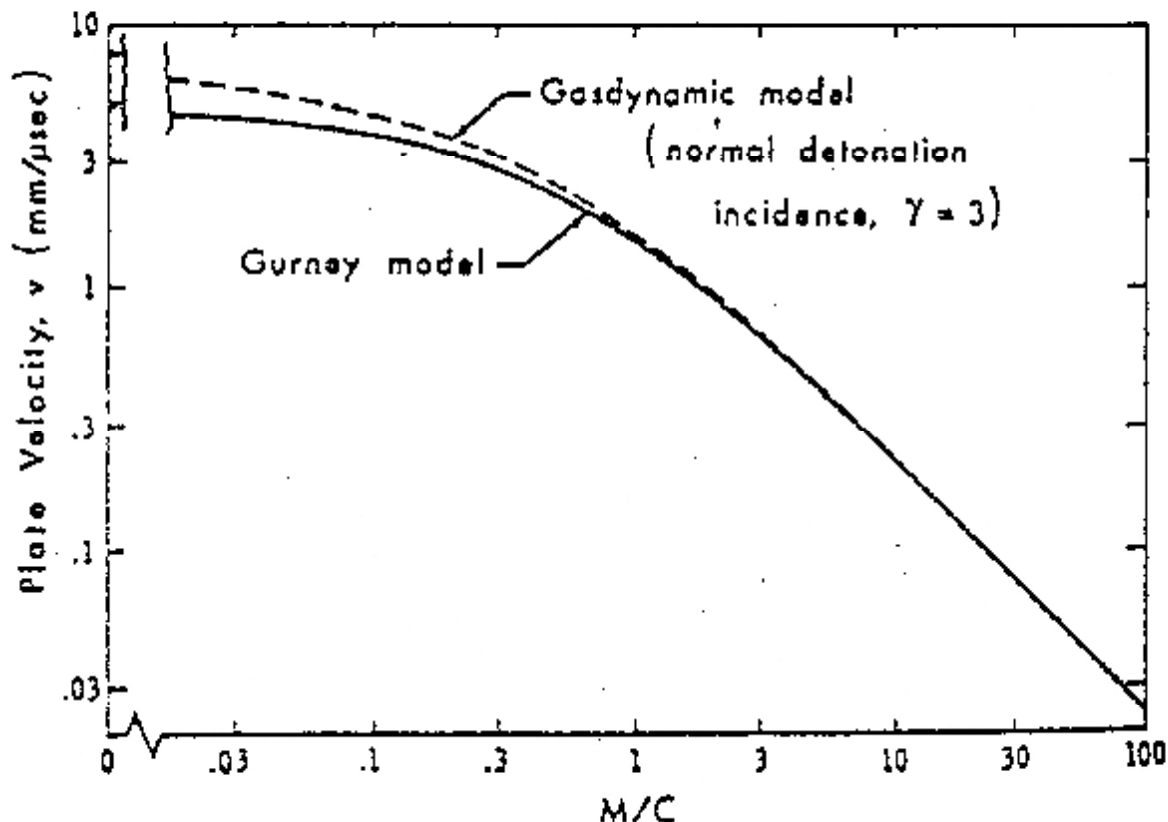


FIGURE 4: Comparison of gasdynamic and Gurney models for open-faced sandwich plate velocity  
Source: Kennedy (1972)

HOSKIN *et al* (1965) correlated their experimental results for tubular cylinders and flat-plates driven by Comp B very nicely by Gurney's equations. Their experimental results also agree well with 2-dimensional characteristic code calculations on these charge/metal configurations.

Terminal states calculated by this code are found to be very similar to those assumed in the Gurney model. Pressure (and hence density) decreases to an almost uniform distribution and the gas velocity is almost linear with distance measured along the direction of motion of the plate. They also calculate that the component of gas velocity normal to this direction is at most a fraction 0.06 of the detonation velocity. This value is considerably smaller than the average value of gas velocity according to the Gurney distribution. Furthermore, they confirmed that plate compressibility has very little influence on the pressure (and hence on plate velocity). Thus a very good estimate of plate velocity can be obtained by replacing it with an equivalent *rigid* mass-loading on the surface of the explosive, just as in the Gurney model.

Based on this work and that of KENNEDY, the Gurney model approximations of a one-directional gas flow with linear velocity distribution and constant density (and pressure) driving a rigid-plate is seen to fit the rigorously calculated solution quite well.

HOSKIN *et al* carried out a comparison between Gurney and 2-dimensional code predictions for plate velocity in the sandwich configuration under two extreme limiting conditions: one face of the explosive was rigidly confined or it was free. The comparison is shown in *Fig. 5* which plots the efficiency of energy transfer to the plate. It is seen that the Gurney model predicts this efficiency well.

HOSKIN *et al* also provide experimental data on plate velocities measured for open-faced sandwich geometries. The Gurney equation, written in the form of eq.[5], fits the pattern of velocity distribution very well. Gurney velocities are also within a few percent of the rigorously calculated values. These comparisons are presented in *Fig. 6*.

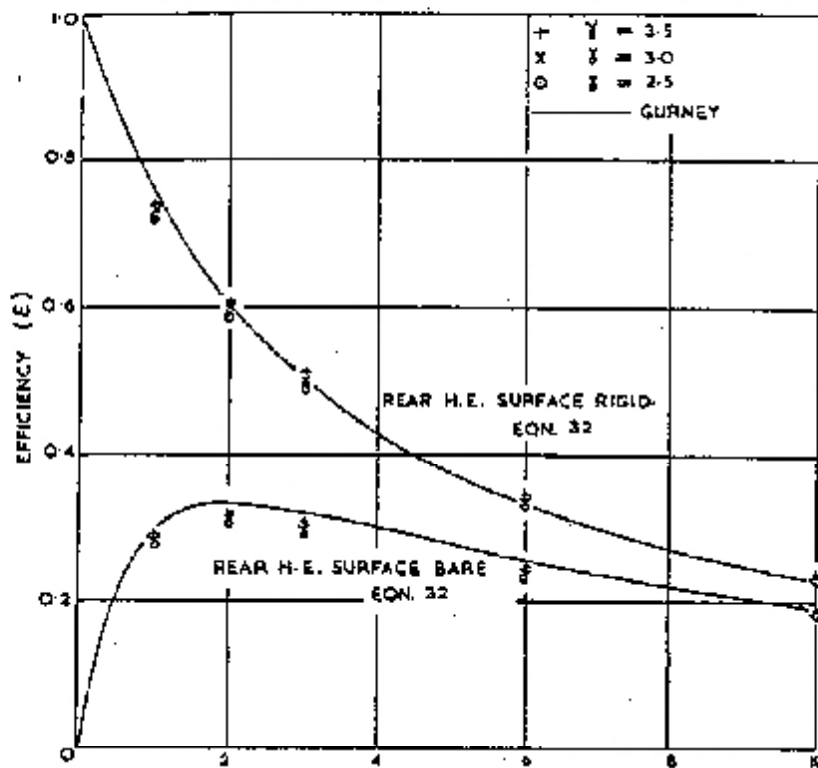


FIGURE 5: Efficiency of energy transfer to plate  
Source: Hoskin et al (1965)

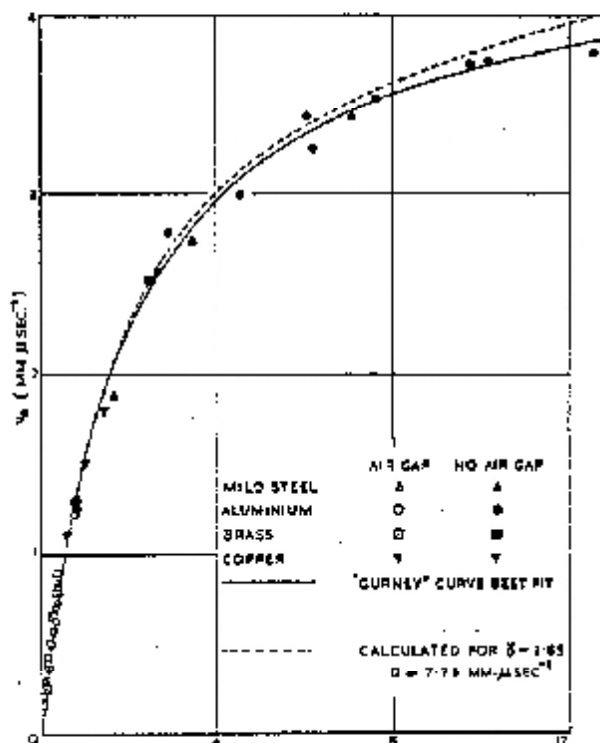


FIGURE 6: Comparison of Experimentally Determined and Predicted Plate Velocities  
Source: Hoskin et al (1965)

In conclusion, it seems that the Gurney model works well because the assumptions on which it is founded are reasonable simplifications of the actual conditions. The Gurney method allows metal velocities in a wide range of explosive/metal combinations to be predicted with a 10% accuracy, and often much better when calibrated for a particular configuration. The Gurney model is expected to be least accurate at very low metal-to-charge mass ratios. In these cases plate acceleration is so rapid that its terminal velocity becomes sensitive to details of gas flow, and to plate compressibility and shock phenomena.

### 3.2 Thermochemical Analysis of Gurney Energy

Let  $\epsilon$  denote the efficiency of energy transfer from the explosive to the metal plate. It is the ratio of the kinetic energy of the plate to the energy of the explosive, which is the product of its specific heat of detonation  $\delta H_d$  and its mass,  $C$ . By introducing the Gurney energy  $E$  and rearranging, the following definition of efficiency is obtained:

$$\epsilon = \frac{\frac{M V^2}{2 P}}{\frac{C \delta H_d}{E}} = \frac{\frac{V^2}{2 E}}{\frac{M}{C} \frac{E}{\delta H_d}}$$

Following KENNEDY, the above equation may be interpreted as follows.

The first term is the ratio of plate kinetic energy to the Gurney energy of the explosive. It is solely a function of  $M/C$  (or  $N/C$  where applicable) as may be seen from Fig. 2, and it can be evaluated explicitly for any given geometrical configuration, using the appropriate form for  $V/\sqrt{2E}$ .

The second term is the ratio of the Gurney energy (the specific energy converted to mechanical work) to the specific chemical energy of the explosive. The chemical energy may be identified with usual measures of explosive performance, such as heat of detonation and absolute strength. The question of great practical interest is, how is the ratio of Gurney energy to the chemical energy to be determined *a priori* for a given explosive?

KENNEDY has recommended that as a first estimate,  $E$  may be related to the heat of detonation as follows:

$$E = 0.7 \frac{\delta H}{d}$$

17

This appears to be appropriate mainly to high density explosives undergoing ideal detonation. A number of authors have demonstrated that the conversion efficiency of the heat of detonation to kinetic energy is only slightly dependent on the equation of state.

The work of HARDESTY & KENNEDY (1977) provides a rational basis for the formulation of a quantitative relationship between  $E$  and the heat of detonation.

HARDESTY & KENNEDY proposed that a specific *utilisable* energy (such as the Gurney-energy) is more appropriate for ballistic characterization of explosives than fundamental detonation properties. They argued that while  $\rho$  and  $D$  have traditionally been used as indicators of relative explosive 'effectiveness', the Gurney energy or velocity provide performance parameters of somewhat more practical importance to the explosive user.

Any measure of the energy output of a detonating explosive should be related to the internal energy states obtained during expansion of product gases from the Chapman-Jouguet conditions. Hardesty & Kennedy used the TIGER thermochemical code to calculate detonation states and product gas isentropes for a number of C-H-N-O explosives. The difference between the internal energy of the isentropically expanded products and that of the unreacted explosive defines, in the context of the Gurney model, the conversion of chemical energy to kinetic energy. When evaluated in this fashion, Gurney energies were shown to correlate well with code calculations provided internal energy changes were limited to a 3-fold expansion along the detonation isentrope.

Previous studies (eg. KURY (1965) have also indicated that the acceleration of metal in contact with explosive is essentially complete after product gases have expanded by a given (small) factor. Any internal energy remaining in the product gases after such a limited expansion does not contribute towards the kinetic energy of either the gases or the metal. Thus, it is not surprising that the experimentally determined value of the Gurney energy is significantly less than the available chemical energy of the explosive (eg. eq.[7]).

Following HARDESTY & KENNEDY, a functional definition of the Gurney energy in terms of gas internal energy is:

$$\sqrt{2 E_G} = \left[ \frac{2 E_o - E}{V} \right] \quad \text{at} \quad \frac{v}{v_o} = 3$$

Here V is volume; the subscript o denotes initial values, and the subscript G is used to distinguish the Gurney energy from other internal energy values. Hardesty & Kennedy explored a number of schemes for correlating the internal energy states with readily calculable or measurable explosive parameters. They proposed a correlation based on the so-called Kamlet parameter  $\Phi$ . However, in 1979, KAMLET & FINGER argued that a better correlation is afforded by another equation, namely

$$\sqrt{2 E_G} = 0.887 \Phi^{0.5} \rho_o^{0.4} \quad [8]$$

where  $\rho_o$  is the explosive density and  $\Phi$  is the Kamlet parameter defined by

$$\Phi = N M^{0.5} Q^{0.5}$$

Here N is the number of moles of gaseous detonation products per unit mass of explosive, M is the average molecular weight of these products, and Q is the heat of detonation. Data presented by these authors suggest that Gurney velocities derived by means of eq.[8] differ from measured values by an average of 1%.

### 3.3 Limitations of the Gurney Model

Simplifying assumptions made explicitly or implicitly in the Gurney model result in a restricted range of applicability. The effects of many of these limitations can be assessed on the basis of physical interpretations of the model in terms of gas dynamics and expansion isentropes of product gases as presented above.

When gas dynamics become important in the flow, the Gurney model underestimates metal velocities. This occurs typically when M/C is smaller than about 0.1. Under these conditions, shock pressures associated with the detonation front dominate acceleration behaviour, and the efficiency of the explosive is enhanced. A gasdynamic model or wave propagation computations should be used at low values of M/C. In this connection it may be noted that adding more and

more explosive to an open-faced sandwich configuration does not necessarily result in a proportionately increasing plate velocity. This may be viewed as a failure in 'communication'. The influence of additional explosive mass is propagated at the speed of sound, and may not be able to effect the acceleration behaviour of the plate before terminal velocity is reached for one reason or another. This is particularly true when plate velocity derives from only a limited expansion of the gases, because of two - dimensional effects, say.

The Gurney method ignores the shock characteristics of metals. Thus, a difference in plate velocity may be expected due to differences in the shock impedance of different metals even though the ratio  $M/C$  is held constant. Shock effects in the metal plate may also be expected to dominate acceleration behaviour at high  $M/C$  ratios, that is in thick plates backed by thin slabs of explosives. Various authors recommend that  $M/C$  should be limited to  $< 10$ . At larger ratios the metal velocities and the apparent efficiency of energy transfer will deviate from the Gurney values.

Substantial two-dimensional effects (eg. losses due to rarefaction waves from the sides of the charge) can cause the metal velocity to be somewhat lower than predicted. KENNEDY has discussed a method to discount the mass of the explosive rendered ineffective by side losses. Explosive material within  $30^\circ$  of the surface tangent along the sides cannot contribute to metal acceleration. In a columnar charge with a plate at one end, this method of discounting mass results in a cone of effective explosive mass backing the plate. There exists thus a finite charge length which will drive metal at a velocity which cannot be exceeded by further lengthening of the charge.

The Gurney method in its basic form cannot analyze the acceleration dynamics of metal. It is known that final plate velocity is attained when detonation product gases have expanded to between twice and seven times their original volume. JONES *et al* have adapted the Gurney method to yield time-dependent acceleration values for the plate. This method is somewhat contrived and gasdynamic models seem to present a better approach.

The Gurney method is basically a thermodynamic approach based on energy conservation. It cannot provide insight into details such as the influence of tapered plate thicknesses, the angle of incidence of the detonation wave, or the effects of material strengths and fracture or spallation behaviour.

## 4 Applications of Gurney Model

For the purposes of the *PrimerSlug* study, the most useful feature of the Gurney model is its ability to predict 'slug' or plate velocity in terms of practical explosive and design parameters. The appropriate equation for projection of a metal plate by an unconfined explosive is that for the asymmetric *open-faced sandwich*. This equation is, with  $z$  denoting  $M/C$ :

$$V_P = \sqrt{\frac{2 \cdot E}{G}} \sqrt{\frac{3}{4z^2 + 5z + 1}}$$

*Sub eqn.*

As discussed, some judgement must be exercised in the application of this equation regarding the appropriate values of the Gurney energy and  $M/C$ . This equation permits extensive parametric studies to be undertaken on the influence of various types of explosives (through the  $\sqrt{2E}$  term) and of the size and mass of the explosive and metal components (through  $M/C$ ). Design optimization need not be confined to considerations of plate velocity only. Given this velocity, the values of impulse and kinetic energy acquired by the plate follow immediately and reach optimal values at different combinations of design parameters.

The Gurney energy provides a more direct and practical indicator of the ability of an explosive to perform mechanical work in expansion than other more fundamental detonation and thermochemical properties (HARDESTY & KENNEDY). A special merit of the Gurney method is that it allows a quantitative comparison of the useful energy output of explosives rather than simply rank-ordering the explosives. The Gurney velocity may be predicted for a wide variety of loading conditions and geometries of interest and the efficiency of energy conversion derived.

A number of authors have cited the use of the Gurney model in applications as diverse as explosive-driven plates for initiation studies and for shock physics studies, the launching of a dielectric plate by electrical explosion of a metal foil, and the launching of fragments and other missiles by rapid combustion events. KENNEDY (1972) in particular has given an extensive discussion of applications including the following:

- impulse loading of structures by unconfined and lamped charges
- effects of confinement on explosive efficiency
- outflow velocity of gases from unconfined explosive surfaces
- division of gas flow (with or away from the plate)
- action of propellant charges on 'pistons'.



## **APPENDIX 4**

### **GAS DYNAMICS MODEL EQUATIONS**

# ACCELERATION OF METAL PLATES BY EXPLOSIVES

## I. Gasdynamic Models of Plate Motion

### Synopsis

*Equation of motion of an incompressible inert plate accelerated by a plane detonation wave is solved in terms of Taylor's solution for the flow of detonation product gases. Explicit formulae for plate motion are obtained analytically when the adiabatic exponent  $\gamma=3$ . The model is extended to include the case of a general value for  $\gamma$  and to describe plate motion explicitly in terms of time. Adjustments to the model necessitated by the lateral expansion of gases are also considered.*

Prepared by  
Dynamic Physics Consultants CC  
for  
Mr J.A. Cruise  
EXPLODE (Pty) Ltd

May 1993

ACCELERATION OF METAL PLATES BY EXPLOSIVES  
I. Gasdynamic Models of Plate Motion

TABLE OF CONTENTS

	<i>Page</i>
1. Gas Dynamics Models of Explosively-Driven Plates	1
2. The Aziz-Hurwitz-Sternberg Model	3
2.1 Governing Equations of Plate Motion	3
2.2 Solution for $\Gamma=3$	5
2.3 General Solution for $\Gamma = 3$	6
2.4 Time-Dependence of Plate Motion	8
3. 2-Dimensional Effects	10
4. Conclusions	14
Figures 1-5	

## Symbols

$C$	gas acoustic velocity
$D$	velocity of detonation
$L$	length of explosive column
$m_e$	explosive mass
$m_p$	plate mass
$P$	gas pressure
$t$	time
$U$	gas (particle) speed
$v$	specific volume
$V$	volume
$X$	general axial coordinate
$X$	coordinate at explosive/plate
$\rho$	density
$\Gamma$	adiabatic exponent
CJ	Chapman-Jouguet state

Subscript 1 denotes initial values at the CJ state

Barred parameters are scaled (dimensionless) values

## 1 Gas Dynamics Model of Explosively Driven Metal Plates

In many applications of explosive systems, it is often useful to have a simple method of estimating the velocity of explosively-driven plates of inert materials. Of particular interest would be the kinetics of plate acceleration and displacement, the amount of energy transmitted to the plate and the effects on the energy transmission process of such factors as the explosive-to-plate mass ratio, the explosives energy and the velocity of detonation. With certain reasonable assumptions, this problem can be solved exactly by formulating it as a problem in gas dynamics. This approach is based on the Taylor solution for the flow of detonation product gases.

The essential features of the gas dynamics problem are the following.

The initial physical configuration is shown in Fig.1. The flow after initiation at the surface O, and before the detonation front reaches the plate, is given by a simple wave centred at O: this is the Taylor wave. When the detonation front reaches the piston a shock is reflected. Being a weak shock, this is approximated by a compression wave. The piston is assumed to be rigid, so that it moves as a whole as soon as it is subjected to pressure. Thus its initial velocity increases smoothly from zero as it is accelerated.

The wave diagram that traces the gas/piston motion is given in Fig.2. Line OA traces the advance of the detonation front to its arrival at the plate at point A. Region I is the solid explosive. Region II delineates the simple wave (Taylor wave) region behind the detonation front. Region III represents the region of interaction between the Taylor wave and the wave reflected from the piston. The piston itself accelerates smoothly along path AB. Path OC traces the backward flow of gases. Whether this is into vacuum or air is unimportant for the model. Since the reflected wave does not reach the boundary OC, the conditions at the boundary cannot give rise to any signals influencing the behaviour of gases in region III.

*Figs.1 & 2* define the gas dynamic model of piston motion. Although it can be solved exactly and made to yield precise values of all parameters of interest, its basic validity must be assumed *a priori* and judged against the accuracy of its predictions. The model assumptions, though simple in concept, lead to certain implications of fundamental importance.

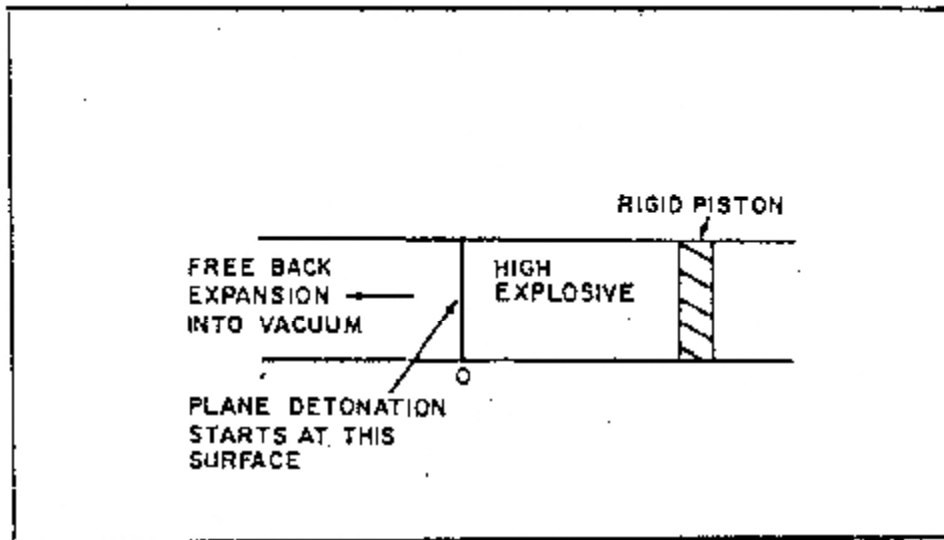


Figure 1: Initial Physical Configuration for Explosive Projection of Metal Plate

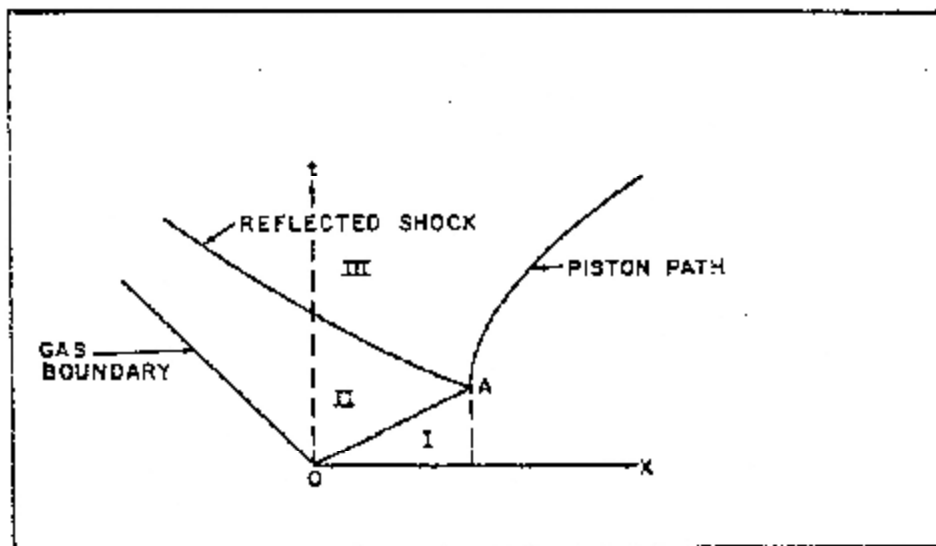


Figure 2: Space-Time Diagram for Metal Plate & Gas Motion

The wave assumption for the reflected shock in Region III gases implies that the linearity of the characteristic equation of Taylor's solution holds good even behind the front of the reflected wave, so that the equation

$$U + c = \frac{x}{t}$$

holds along the piston path. The assumption of a *rigid* piston obviates the necessity of considering wave phenomena in the piston itself. In an incompressible material sound velocity is infinite, and all parts of the piston start moving as a whole immediately after the application of pressure on its surface. The subsequent motion of the piston is then governed by Newton's laws of motion.

## 2 The Aziz-Hurwitz-Sternberg Model

### 2.1 Governing Equations for Plate Motion

The starting point for the Aziz model is the Taylor wave defined by:

$$U + c = \frac{x}{t} \quad [1]$$

$$U + c = U_1 + c_1 - \frac{\Gamma + 1}{2} \left[ \frac{U_1 - U}{1} \right] \quad [2]$$

Aziz introduces dimensionless variables and replaces initial values (denoted by the subscript 1) with their Chapman-Jouguet values, namely:

$$U_1 = \frac{D}{\Gamma + 1} \quad ; \quad c_1 = D \frac{\Gamma}{\Gamma + 1}$$

$$\rho_1 = \rho_0 \frac{\Gamma + 1}{\Gamma} \quad ; \quad P_1 = \frac{\rho_0 D^2}{\Gamma + 1}$$

The above values of gas speed, sound speed, density and pressure exist along the line OA in Fig.1. By introducing the following dimensionless variables:

$$\ddot{x} = \frac{x}{L} \quad \ddot{t} = \begin{bmatrix} D \\ L \end{bmatrix} t'' \quad \ddot{U} = \frac{U}{D}$$

$$\ddot{c} = \frac{c}{D} \quad \ddot{P} = \frac{P}{\rho_0 D^2}$$

Aziz writes eqs. [1,2] in the form:

$$\ddot{U} + \ddot{c} = \frac{\ddot{x}}{t} \quad [3]$$

$$\ddot{U} - \frac{2 \cdot \ddot{c}}{\Gamma + 1} = - \left[ \frac{1}{\Gamma - 1} \right] \ddot{x} \quad [4]$$

Eq. [4] follows from [2] after some algebraic manipulations when  $U_1$  and  $c_1$  are replaced by their C-J values and the parameters are normalized.

The assumption of the continuance of the Taylor solution in Region III permits the motion of the plate to be described by the following equations:

$$\ddot{U} + \ddot{c} = \frac{\ddot{X}}{t} \quad [5.1]$$

$$\ddot{P} = \frac{1}{\Gamma + 1} \left[ \frac{\Gamma + 1}{\Gamma - 1} \frac{2 \cdot \ddot{c}}{\Gamma - 1} \right] \ddot{x} \quad [5.2]$$

$$\frac{d}{dt} \ddot{U} = \frac{\ddot{c}}{P} \ddot{P} \quad [5.3]$$

$$\frac{d}{dt} \ddot{X} = \ddot{U} \ddot{x} \quad [5.4]$$



$\bar{P}$ ,  $\bar{U}$ ,  $\bar{c}$  are the pressure, gas velocity and gas sound velocity at the plate-explosive interface,  $\bar{X}$ . Because the plate is incompressible,  $\bar{U}$  is also the velocity of the plate. Eq.[5.2] for the pressure follows from the isentropic relation for polytropic gases:

$$P = P_1 \left[ \frac{c}{c_1} \right]^{\frac{2\Gamma}{\Gamma-1}}$$

Eq. [5.2] follows from the above equation when the C-J values are substituted for  $P_1$  and  $c_1$ .

### 2.2 Solution for $\Gamma = 3$

Eqs.[5] constitute a set of coupled, simultaneous differential and algebraic equation that must be solved together in order to derive a description of plate motion. Eqs. [5.1] and [5.2] describe the gases at the surface of the plate while it is being accelerated; eqs.[5.3] and [5.4] are the Newtonian equations of motion, defining the acceleration and velocity as smooth derivatives of time. The equations are solved with the following initial values:

$$\bar{U} = 0 \quad \bar{c} = 1 \quad \bar{P} = \frac{16}{27} \quad \bar{X} = 1 \quad \bar{t} = 1$$

The solution is much simplified when  $\Gamma = 3$  is chosen (as implicit in the initial value of  $P$  above). This is quite a good assumption since most condensed explosives seem to possess a polytropic coefficient in the range  $2.5 < \Gamma < 3$ : see Mader and references cited in Aziz.

The final plate velocity is then defined by a simple and elegant expression:

$$\frac{\bar{U}}{D} = \frac{z-1}{z+1} \quad \text{where} \quad z = 1 + \frac{32}{27} \frac{e}{p} \quad [5]$$

The following points should be noted about this solution:

- The solution is derived in the limit of infinite expansion, that is, as  $t \rightarrow \infty$ .
- The numerical value of  $32/27$  is specific to  $\Gamma=3$ .
- Since  $\Gamma$  can be expressed in a number of ways -- in terms of density, pressure, energy, particle velocity, sound velocity at the C-J state -- the effect of any detonation parameter is implicitly accounted for by eq.[6].
- It can be shown (see *Azis*) that the fraction of explosives energy transmitted to the plate is a maximum for a ratio of explosive-to-piston mass corresponding to  $81/32$ . This does not mean however that plate energy reaches a maximum: more explosive will always result in more plate energy. It is the efficiency of energy transfer that reaches a maximum.

#### General Solution for $\Gamma = 3$

The influence of  $\Gamma$  on plate velocity was derived by Azis on the basis of numerical calculation (that is, not within his analytical formulation). *Fig.3* is taken from his paper. The interesting fact is that low  $\Gamma$  explosives are more efficient than those with high  $\Gamma$  values. This is all the more interesting since  $\Gamma=3$  explosives are generally high density, high VOD 'military' types, whereas  $\Gamma < 3$  values are associated with more 'commercial'-type formulations. Physically, the improved efficiency of low  $\Gamma$  explosives can be understood on the basis that the pressure decreases more slowly with expansion when  $\Gamma$  is small.

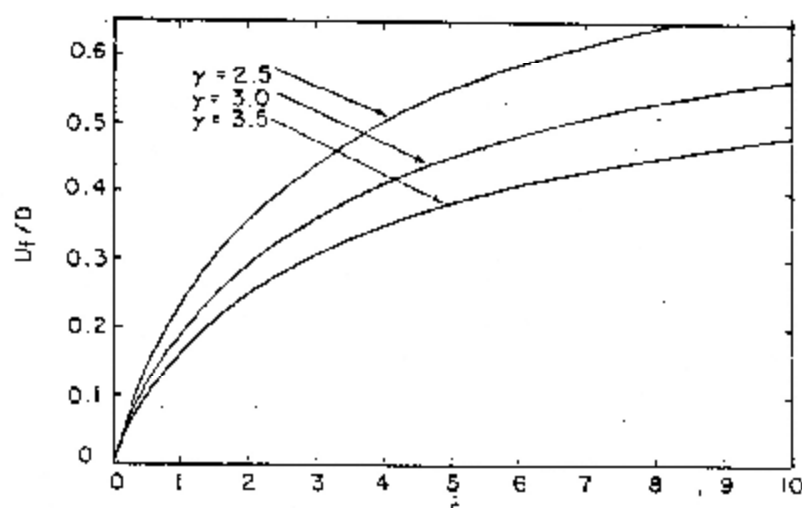


Figure 3: Effect of  $\Gamma$  on scaled piston velocity. Abscissa ( $r$ ) plot explosive-mass to piston-mass ratio. Source: Azis, Hurwitz, Sternberg (1961)

The experimental work of Deribas *et al* (1967) appears to confirm the improved efficiency of low- $\Gamma$  explosives. By using powdered and low density explosives with specific gravity of about 1, they found that experimental plate velocity values were about 20% higher than expected from the Azis equation. They attributed this to a decrease in the value of  $\Gamma$  below 3 for the explosive types they used.

In 1986 Yadav *et al* rederived the Azis velocity equation in a way that explicitly included a general value for  $\Gamma$ . His solution for the final plate velocity is extremely cumbersome and it is reproduced below from his paper:

$$\begin{aligned}
 U' = 1 - & \left( \frac{m+1}{z-1} \right) \left( \frac{z}{z-1} \right)^m \left[ \frac{z^{1-n} - 1}{1-n} \right. \\
 & - \frac{m}{1} \left( \frac{z^{1-n} - \frac{1}{z}}{2-n} \right) + \frac{m(m-1) \left( z^{1-n} - \frac{1}{z^2} \right)}{2!(3-n)} \\
 & - \frac{m(m-1)(m-2) \left( z^{1-n} - \frac{1}{z^3} \right)}{3!(4-n)} + \dots \\
 & \left. + (-1)^{N-1} \frac{m(m-1)(m-2) \dots (m-(N-2)) \left( z^{1-n} - \frac{1}{z^{N-1}} \right)}{(N-1)!(N-n)} \right]
 \end{aligned}
 \tag{7}$$

where

$$m = \frac{\Gamma - 3}{2}$$

$$n = \frac{\Gamma - 1}{\Gamma + 1}$$

$$z = 1 + \frac{\Gamma + 1}{2} \frac{e^{\frac{n}{p}}}{n} \frac{K}{1} \frac{K}{1} = \frac{1}{\Gamma + 1} \left[ \frac{\Gamma + 1}{\Gamma} \right]^{2 \frac{\Gamma}{\Gamma - 1}}$$

and  $N$  is the number of terms within the brackets in eq.[7]. (The general solution as given by eq.[7] converges to a limit, and the desired accuracy can be attained by terminating the number of terms at the proper level.) Yadav's Fig.1 suggests that decreasing values of  $\Gamma$  can change plate velocity by 10-20%, depending on the charge-to-metal mass ratio.

When  $\Gamma=3$  (and hence  $m=0$  and  $n=0.5$ ) the general solution, eq.[7], reduces to a much simpler form, namely:

$$\frac{U}{D} = 1 - \frac{1}{z-1} \left[ 2 \left[ \frac{1}{z} - 1 \right] \right] \quad [8]$$

where

$$z = \frac{32 \frac{m}{e}}{27 \frac{m}{P}}$$

as for Aziz. The Aziz formula eq.[6] and the Yadav formula eq.[8] appear to be equivalent and yield the same numerical values.

It can be argued that the use of the gamma-law for detonation gas expansions is simplistic. This law is equivalent to defining the specific gas energy as:

$$E = \frac{P v}{\Gamma - 1}$$

Strictly speaking, this equation of state is applicable only to ideal gases with a constant adiabatic exponent. In general,  $\Gamma$  is defined as

$$-\Gamma = \frac{d}{d(\ln V)} (\ln P)$$

the derivative being evaluated on the expansion adiabat (locus of constant entropy P-V states). It has been shown that in the vicinity of the C-J state  $\Gamma$  is approximately constant (see *Mader* for instance). The study by *Lee, Hornig & Kury* indicates that  $\Gamma$  is fairly constant to expansion ratios of 3 at least. Since it can be shown that the plate acquires most of its energy in this distance, the question of the precise value of  $\Gamma$  at large expansions is more of academic than practical importance.

#### 2.4 Time-Dependence of Plate Motion

Other than for the final plate velocity, Aziz formulated his solution in parametric form which is cumbersome to use and does not explicitly display the changes of plate velocity and displacement with time. In 1986 *W. Fickett* showed that the Aziz model can be adapted to give a simpler explicit solution for plate motion in terms of time.

The following formulas may be used for calculating the plate velocity ( $\bar{U}$ ) and displacement ( $\bar{X}$ ) as functions of time ( $\bar{t}$ ):

$$\bar{U} = (2\alpha + 1) - \alpha y - (\alpha + 1) y^{-1} \quad [9]$$

where  $y$  is a function of time, namely:

$$y(\bar{t}) = \sqrt{\left[ \frac{-1}{\alpha + 1} \right] - \frac{\alpha}{\bar{t}}} \quad [9]$$

and

$$\alpha = \frac{27}{32} \frac{m}{e} \frac{p}{e} \quad [9]$$

(The numerical factor derives again from the assumption of  $\Gamma=3$ .) Plate displacement is given by:

$$\bar{X} = \bar{U} \bar{t} + y^{-1} \quad [10]$$

The same scaled variables are used as defined by Aziz, so that the plate begins to move at scaled values of  $\bar{t} = 1$  and it is originally located at  $\bar{X} = 1$ .

In 1988 Yadav and Gupta, employing the same Aziz model, derived a different equation for the velocity of a flyer plate at any time. The model is based on the integration of the equation of motion of the plate, eq. [5.3]:

$$\frac{d}{dt} \bar{U} = \frac{c}{m} \bar{P} \quad [5.3]$$

once the pressure has been defined in terms of the time-dependent value of sound velocity. Using eq. [5.2] with  $\Gamma=3$ , the pressure is defined by

$$\bar{P} = \frac{16}{27} \left[ \frac{c}{c_0} \right]^3 \quad [5.4]$$

and according to Yadav and Gupta the sound velocity varies in time as

$$\overline{c(t)} = \frac{1}{t} \left[ 27 \frac{t}{m} + 32 \frac{(t-1)^2}{m} + 27 t \right] \quad [11]$$

The crucial element of this approach is eq.[11], and its validity and accuracy of derivation does need verification.

### 3 Two-Dimensional Effects

A strong assumption of the Aziz model is that gas flow is 1-dimensional -- and thus, implicitly, the lateral extent of plate and explosive is infinite and the detonation wave is planar. In practical configurations, neither of these requirements can be strictly satisfied. Thus the influence of the lateral expansion of gases needs to be considered.

The Aziz model was shown by *Lambourn & Hartley*, who used a code based on the method of characteristics, to give a very good representation of plate velocity provided it is associated with the centre-of-gravity of the plate. However, the model is expected to break down when rarefaction waves from the sides release the pressure behind the plate. The work of *Lambourn & Hartley* may be used to estimate the extent of deviation from the Aziz velocity when the acceleration is followed beyond some early stage where the one-dimensionality of gas flow is destroyed.

The early stage of plate motion, depicted in terms of wave propagation, is illustrated in Fig. 4. The flow is 1-dimensional but the compressibility of the plate is considered.

When the detonation wave meets the explosive-plate interface, a shock is transmitted into the plate and a rarefaction is reflected back into the detonation product gases. Following the detonation shock front is the Taylor wave that is transmitted into the plate as a rarefaction following the shock. When the shock reaches the free surface of the plate, this surface starts moving and a rarefaction is reflected back through the plate to the gas interface. It is reflected off the interface as a compression and the interface is accelerated to approximately the same velocity as the free surface. When the compression reaches the free surface, a second rarefaction is generated and this process of compression and rarefaction continues throughout the flight of the plate, though the magnitude of velocity changes at each reflection gradually diminishes.

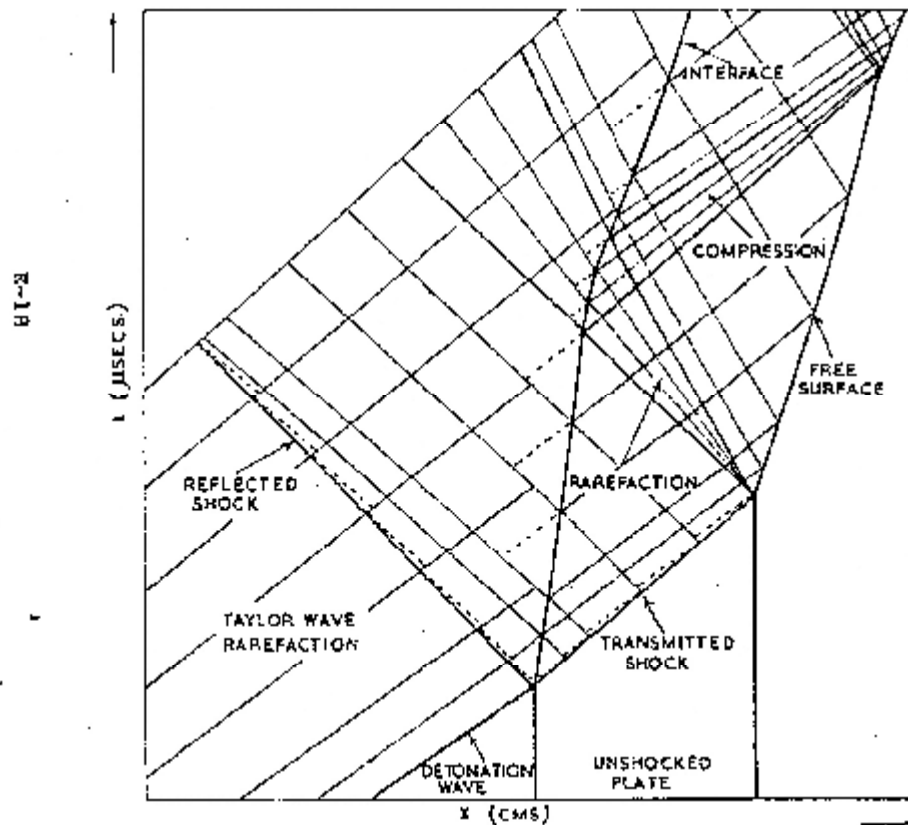


*Fig.4 Wave Phenomena During Plate Acceleration*  
*Source: Lambourn & Hartley (1965)*

The influence of the above reverberations of pressure pulses in the plate on plate velocity is illustrated in Fig.5. The full line is the velocity (calculated by the method of characteristics) at the explosive-metal interface. The velocity calculated according to the method of Aziz is indicated by the dotted line. The rigid-piston Aziz model is clearly a very good approximation to the average behaviour of the plate.

Lambourn & Hartley found that the plate acquires 40% of its final energy at the first reverberation, and 80% by the time of the third reverberation.

It follows that the Aziz model will tend to overestimate the final velocity (as this requires that the 1-dimensional gas flow persists as  $t \rightarrow \infty$ ). It is however expected to yield fairly accurate values of velocity (and displacement) in the early stages of acceleration provided the time interval considered corresponds to at least a few traverses of the plate by pressure waves.

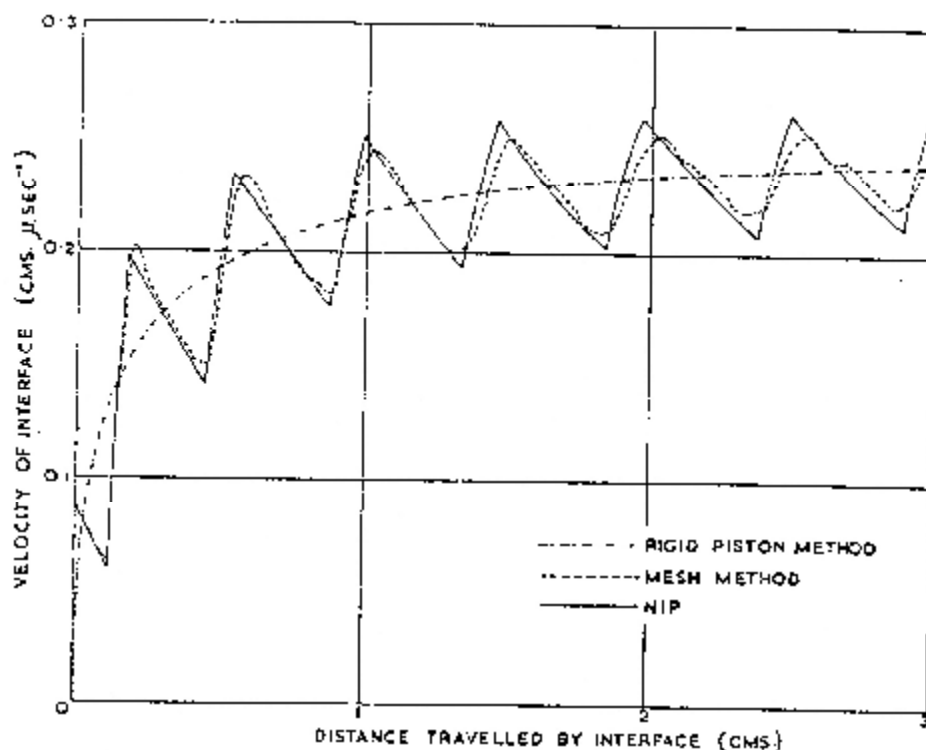


Figure 5: Calculated Velocity of Explosive-Plate Interface  
Source: Lambourn & Hartley (1965)

To compensate for the loss of accuracy over *late-times*, a number of schemes have been proposed for adjusting the Aziz velocity.

- (1) The acceleration of the plate is artificially terminated at an early stage. A common practice is to assume that plate acceleration is essentially complete when the gases have undergone a 3-fold expansion of volume. Put in terms of isentropic relations for polytropic gases, this statement is equivalent to:

$$\frac{P_f}{P_i} = \left( \frac{V_i}{V_f} \right)^\gamma = \left( \frac{1}{3} \right)^\gamma \quad (3)$$

where  $i, f$  denote initial and final values. The pressure ratio can also be written in terms of sound speed:



$$\frac{P_f}{P_1} = \left[ \frac{c_f}{c_1} \right]^{\frac{2\Gamma}{\Gamma-1}}$$

The ratio of sound speeds, equivalent to the scaled variable  $\bar{c}$ , enters into the Aziz model.

(2) Introduce an empirical factor that defines an 'effective' explosive mass, which is much less than the actual value. This in effect compensates for the fact that not all the explosive energy contributes towards the acceleration of the plate. In practice the Aziz equations are adjusted by replacing the charge-to-plate mass ratio with

$$C \frac{m_e}{m_p} = 1$$

where the factor  $C$  is of the order of 0.3 .

## 4 Conclusions

Metal acceleration driven by detonation waves in condensed explosives at normal incidence represents a one-dimensional unsteady hydrodynamic problem which has received considerable theoretical and experimental consideration.

The standard analytical solution to the problem due to AZIZ *et al* extends the Taylor solution of detonation gas flow behind the detonation front to describe the flow after reflection from the metal plate. The gas behind the plate is conceived as a simple-wave flow region in which certain (well-known) relations exist between the velocity of the gas, its sound velocity and pressure. The metal plate is considered to be incompressible and to undergo rigid-body acceleration which is describable in terms of Newtonian mechanics. More sophisticated (machine) calculations have shown this model to be a good approximation provided it is interpreted as representing the *average* behaviour of the whole plate.

The Aziz-model links the limiting plate velocity (at long expansion times) to the characteristics of the explosive (velocity of detonation and adiabatic exponent  $\Gamma$  of detonation product gases), and to the charge-to-metal mass ratio. In the simplest (analytical) formulation  $\Gamma=3$  is assumed. A solution was later derived (YADAV) that admits a general value of  $\Gamma$ . Model equations were also reformulated by FICKETT to reflect directly the dependence of plate motion on time.

In the later stages of plate motion edge effects perturb the one-dimensional flow pattern of many practical systems. This necessitates an adjustment to the calculated velocity of the plate in order to account for the rapid release of pressure by lateral expansion waves. At least two methods of an *ad hoc* nature exist for carrying out this adjustment. ■

## **APPENDIX 5**

### **SHOCK PHYSICS MODEL EQUATIONS AND CALCULATIONS**

# **A Shock Wave Model for Explosively Projected Metal Plate Velocity**

**Prepared for**

**Mr J.A.Cruise  
John Cruise Mining (Pty) Ltd  
Sandton**

**by**

**Thomas Szendrei**

***Dynamic Physics Consultants CC  
P.O.Box 90551 Bertsham 2013***

## **Abstract**

*A physical model is presented for calculating the velocity of a metal plate projected from the end of an explosive column. In this approach, plate velocity is calculated as its free-surface velocity, and it is twice the particle velocity that arises at the interface between the detonation wave front and the metal plate. The model is used to predict plate velocities for Composition B, TNT and Special Gelignite explosives. A consequence of the model is that the plate acquires its velocity in a time equal to two transits of the metal plate thickness by the shock wave.*

**January 1999**

## PLATE VELOCITY -- SHOCK MODEL

### Background

When a detonation wave strikes a metal plate at the end of an explosive column, a shock wave is transmitted into the plate (and a rarefaction is reflected into the detonation products). Following the detonation wave is the Taylor wave, a rarefaction centred on the back surface (plane of initiation) of the explosive. This is transmitted into the plate as a rarefaction following the shock. The problem is formally equivalent to the interaction of a nonuniform shock with a boundary between two media.

Drummond (J Appl Phys 28 (1) 75; 28 (12) 1437 (1957)) pointed out that if the shock wave is 'weak', that is, third order terms in particle velocity, density and sound speed changes are negligible, the entropy is unchanged and the flow is isentropic. In this approximation the locus of states which can be connected by a shock (the 'shock polar') is identical to the states that can be connected by adiabatic compression. In particular, this means that the flow behind a forward-facing shock front moving into a region with constant state is a forward-facing simple wave. Thus the flow behind both the incident (detonation) shock front in the explosive and the transmitted shock front in the metal is a simple wave.

The simple-wave model of explosive-plate interaction is valid to pressures of the order of tens of GPa (Drummond).

The state behind the transmitted shock is characterized by a particle velocity equivalent to the velocity of the interface between the explosive and the plate. The transmitted shock wave, on reflection from the free surface of the plate, creates a rarefaction wave that moves back towards the interface between the plate and the explosion products. The free surface of the plate is abruptly accelerated to twice the particle velocity (accurate to third order). The plate begins to move as a 'rigid' whole as soon as the rarefaction wave reaches the interface. Seen in terms of this phenomenological model, the so-called initial velocity of the plate is twice the velocity of the interface.

Since the detonation products are still at a high pressure, and the pressure in the metal has been released by rarefaction, a second shock wave of smaller amplitude is induced in the moving plate. This shock wave again reflects off the plate free face and thus increases its velocity. The reverberation of these shock and rarefaction waves within the plate continues until the pressure in the gas reaches a level where further release of pressure by the rarefaction wave does not cause the gas particles to move faster than the metal plate. (Yadiv & Gupta Int J Impact Engng 7(1) (1988) 71-81). However, the calculations of Lambourn & Hartley (4th Detonation Symposium) show that a thin steel plate is accelerated to about 80% of its final velocity after the first reflection off the interface (or after two transits of the plate by shock and rarefaction waves).

Consider an ideal one-dimensional detonation wave impinging upon a metal plate in a direction normal to its surface. Prior to contact, the HE behind the detonation front is at the C-J state. On impact, the detonation wave splits into two – one wave penetrates the metal, and the other reflects back into the HE reaction products. Continuity at the interface requires that the two waves have the same pressure and particle velocity at this time. These values are usually found on the intersection of the metal/gas Hugoniot. (Chou (1984) DE 89007303). Kinalovskii & Trishin (FGV 20(1) (1984) 126-133) provided an analytical approximation to the graphical solution.

### Mathematical Formulation

The following symbols apply:

- $\rho$  density ( subscript 'e' explosive; subscript 'p' metal plate)
- $P$  pressure
- $D$  detonation velocity
- $u$  particle velocity
- $c$  sound speed
- $J$  subscript: Chapman-Jouguet state parameter
- $I$  subscript metal/explosive interface condition
- $C_0$  velocity constant on linear shock adiabat
- $S$  linear shock adiabat constant

NOTE:  $C_0$  and  $S$  are defined by the linear adiabat

$$U_s = C_0 + S \cdot u_p$$

where  $U_s$  is the shock velocity and  $u_p$  the corresponding particle velocity.

We suppose that the gases satisfy an ideal gas EOS with constant polytropic exponent  $\Gamma=3$ . For such a gas

$$P = P_J \left( \frac{\rho}{\rho_J} \right)^\Gamma \quad \text{and} \quad c = c_J \left( \frac{P}{P_J} \right)^{\frac{\Gamma-1}{2\Gamma}}$$

[1]

The C-J values are the following:

$$\frac{P_J}{\rho_e D^2} = \frac{1}{\Gamma - 1} \quad \frac{\rho}{\rho_e} = \frac{\Gamma + 1}{\Gamma}$$

$$\frac{u}{D} = \frac{1}{\Gamma - 1} \quad \frac{c}{D} = \frac{\Gamma}{\Gamma + 1}$$

At the C-J plane

$$u_J + c_J = D_0$$

This value of the Riemann invariant is maintained along the characteristic which originates at the point of contact the metal and gas, so that after reflection from the plate, the gas is defined by a sound speed

$$u = D - c_0$$

Use dimensionless quantities as defined above for the C-J conditions. From (1), by rearrangement

$$P = \frac{P_J}{(c_J)^3} \cdot c_0^3$$

By substitution for C-J values, this equation transforms to:

$$\frac{P}{\rho_e \cdot D^2} = \frac{\Gamma + 1}{\Gamma^3} \cdot \left(\frac{c}{D}\right)^3 \quad \text{or} \quad \frac{P}{\rho_e \cdot D^2} = \frac{16}{27} \cdot \left(\frac{c}{D}\right)^3 \quad [2]$$

At the metal/gas interface, the pressure in the metal is

$$P_I = \rho_p \cdot U_S \cdot u_I^2$$

Introducing the linear shock adiabat

$$U_S = C_0 + S \cdot u_I$$

$$P_I = \rho_p \cdot C_0 \cdot u_I + \rho_p \cdot S \cdot u_I^2 \quad [3]$$

In the gas the pressure is

$$P_I = \frac{16}{27} \cdot c_I^3 \quad \text{or} \quad P_I = \frac{16}{27} \cdot \left[1 - \left(\frac{u_I}{D}\right)^3\right] \quad [4]$$

Equating the pressures on both sides of the interface leads to a quadratic equation (after neglecting terms in the third power since  $u/D$  is small)

$$3 \cdot \left(\frac{9}{16} \cdot m - 1\right) \cdot u_I^2 + 3 \cdot \left(1 + \frac{9}{16} \cdot R\right) \cdot u_I - 1 = 0$$

where  $m = \frac{S \cdot \rho_p}{\rho_e}$  and  $R = \frac{\rho_p \cdot C_0}{\rho_e \cdot D}$

Solving the quadratic equation, we obtain

$$u_I = \frac{\sqrt{\left(1 + \frac{9}{16} \cdot R\right)^2 + \left[\frac{4}{3} \left(\frac{9}{16} \cdot m - 1\right)\right]} - \left(1 + \frac{9}{16} \cdot R\right)}{2 \cdot \left(\frac{9}{16} \cdot m - 1\right)} \quad [5]$$

Given the interface velocity, the interface pressures in the plate and the gas are given by [3] and [4] respectively. Plate velocity resulting from shock-loading is (as outlined in the introduction) twice the interface velocity

### Running the Application

*Disk File .....*

Load MATHCAD applications package from the WINDOWS Programme Manager and open the file PLATESHK.MCD.

*Enter Data ....*

To run the application, first enter explosive and plate parameters on page 1. (The default values are simply edited – deleted and replaced – with your own values.) You must know at least the following:

**Explosive:** density; detonation velocity

**Plate:** density ; sound speed on the shock adiabat ( $C_0$ ); shock adiabat constant (S)

### Calculations

On page 2, the program evaluates constant groupings  $m$  and  $R$ , and evaluates eq. [5] for the interface velocity. As a check, the interface pressures in the metal and the detonation product gases are calculated – by continuity considerations, they must be the same.

The use of the program and the nature of physical deductions made from it are illustrated in:

T. Szendrei "Velocity of explosively-driven metal plate: Measurements and theoretical interpretations" Warheads 2000 Seminar, Somchem, Cape, 18-20 November 1996.



## PLATE VELOCITY - 1D SHOCK ACCELERATION:

Disk File PLATESHK.MCD

**ABSTRACT** This document calculates (initial) plate projection velocity from the end of an explosive column by deriving the particle velocity in the plate imparted to it by the detonation wavefront. The explosive is characterized by its CJ parameters and detonation product gases are described by a constant gamma law. Solution is obtained through continuity of pressures and particle velocities at the interface. Numerical solution is based on the approach of Kinelovskii & Trishin (FGV 20(1) (1984) 1126-133.) For definition of equations used in this file refer to file SHKPLATE.MCD.

### PREPARATION OF INPUT DATA ...

Enter charge and plate parameters ... Only a single explosive is considered.

#### 1. Explosive \*\*\*\*\*

Type : Comp. B

Density g/cc pe := 1.60

Detonation Velocity km/s VOD := 7.6

Polytropic Gamma Γ = 3

**NOTE:** Equations are specific to an assumed value of  $\Gamma=3$  which does not appear explicitly.

#### Library of constants

Type	Density	VOD
Comp B	1.60	7.6
TNT	1.55	6.7
Gelignite	1.49	5.6

#### 2. Plate \*\*\*\*\*

Type of Material Mild steel

Density g/cc pp := 7.8

Sound speed km/s (Us-up) Co := 3.6

Shock adiabat constant S := 1.68

**NOTE:** constant Co and S define the shock adiabat  $Us=Co+S*Up$

### 3. Constant groupings \*\*\*\*\*

$$R := \frac{\rho_p \cdot C_0}{\rho_e \cdot VOD} \quad m = \frac{S \cdot \rho_p}{\rho_e} \quad P_0 := \rho_e \cdot VOD^2$$

START CALCULATIONS.....

$$A := \left(1 + \frac{9}{16} \cdot R\right)^2 \quad B := \frac{4}{3} \cdot \left(\frac{9}{16} \cdot m - 1\right)$$

$$C := \left(1 + \frac{9}{16} \cdot R\right) \quad D := 2 \cdot \left(\frac{9}{16} \cdot m - 1\right)$$

Interface velocity is .....

$$u_I := \frac{\sqrt{A + B} - C}{D} \cdot VOD$$

$$u_I = 0.925 \quad \text{km/s}$$

Interface pressure is.....

In the plate.....  $P_p := \rho_p \cdot C_0 \cdot u_I + \rho_p \cdot S \cdot u_I^2$

$$P_p = 37.198 \quad \text{GPa}$$

In the gas .....

$$P_g = \frac{16}{27} \cdot \left(\frac{VOD - u_I}{VOD}\right)^3 \cdot P_0$$

$$P_g = 37.1 \quad \text{GPa}$$

Initial plate velocity:

$$V_{p0} := 2 \cdot u_I$$

$$V_{p0} = 1.85 \quad \text{km/s}$$

## PLATE VELOCITY - 1D SHOCK ACCELERATION:

Disk File PLATESHK.MCD

**ABSTRACT** This document calculates (initial) plate projection velocity from the end of an explosive column by deriving the particle velocity in the plate imparted to it by the detonation wavefront. The explosive is characterized by its CJ parameters and detonation product gases are described by a constant gamma law. Solution is obtained through continuity of pressures and particle velocities at the interface. Numerical solution is based on the approach of Kinelovskii & Trishin (FGV 20(1) (1984) 1126-133.) For definition of equations used in this file refer to file SHKPLATE.MCD.

### PREPARATION OF INPUT DATA ...

Enter charge and plate parameters ... Only a single explosive is considered.

#### 1. Explosive \*\*\*\*\*

Type: TNT

Density g/cc  $\rho_e = 1.55$

Detonation Velocity km/s **VOD = 6.7**

Polytropic Gamma  $\Gamma = 3$

**NOTE:** Equations are specific to an assumed value of  $\Gamma=3$  which does not appear explicitly.

#### Library of constants

Type	Density	VOD
Comp B	1.60	7.6
TNT	1.55	6.7
Gelignite	1.49	5.6

#### 2. Plate \*\*\*\*\*

Type of Material Mild steel

Density g/cc  $\rho_p = 7.8$

Sound speed km/s ( $U_s$ -up) **Co = 3.6**

Shock adiabat constant **S = 1.68**

**NOTE:** constant Co and S define the shock adiabat  $U_s = Co + S * U_p$

### 3. Constant groupings \*\*\*\*\*

$$R := \frac{\rho_p \cdot C_o}{\rho_e \cdot VOD} \quad m := \frac{S \cdot \rho_p}{\rho_e} \quad P_o := \rho_e \cdot VOD^2$$

START CALCULATIONS.....

$$A := \left(1 - \frac{9}{16} \cdot R\right)^2 \quad B := \frac{4}{3} \cdot \left(\frac{9}{16} \cdot m - 1\right)$$

$$C := \left(1 + \frac{9}{16} \cdot R\right) \quad D := 2 \cdot \left(\frac{9}{16} \cdot m - 1\right)$$

Interface velocity is .....

$$u_I = \frac{\sqrt{A + B - C}}{D} \cdot VOD$$

$$u_I = 0.758 \quad \text{km/s}$$

Interface pressure is.....

In the plate.....  $P_p := \rho_p \cdot C_o \cdot u_I + \rho_p \cdot S \cdot u_I^2$

$$P_p = 28.819 \quad \text{GPa}$$

In the gas .....

$$P_g := \frac{16}{27} \cdot \left(\frac{VOD \cdot u_I}{VOD}\right)^3 \cdot P_o$$

$$P_g = 28.76 \quad \text{GPa}$$

Initial plate velocity:

$$V_{po} := 2 \cdot u_I$$

$$V_{po} = 1.516 \quad \text{km/s}$$

## PLATE VELOCITY - 1D SHOCK ACCELERATION:

Disk File PLATESHK.MCD

**ABSTRACT** This document calculates (initial) plate projection velocity from the end of an explosive column by deriving the particle velocity in the plate imparted to it by the detonation wavefront. The explosive is characterized by its C.J parameters and detonation product gases are described by a constant gamma law. Solution is obtained through continuity of pressures and particle velocities at the interface. Numerical solution is based on the approach of Kinelovskii & Trishin (FGV 20(1) (1984) 1126-133.) For definition of equations used in this file refer to file SHKPLATE.MCD.

### PREPARATION OF INPUT DATA ...

Enter charge and plate parameters ... Only a single explosive is considered.

#### 1. Explosive \*\*\*\*\*

Type : Super Gelnite

Density g/cc  $\rho_e = 1.49$

Detonation Velocity km/s **VOD = 5.6**

Polytropic Gamma  $\Gamma = 3$

**NOTE:** Equations are specific to an assumed value of  $\Gamma=3$  which does not appear explicitly.

#### Library of constants

Type	Density	VOD
Comp B	1.60	7.6
TNT	1.55	6.7
Gelnite	1.49	5.6

#### 2. Plate \*\*\*\*\*

Type of Material Mild steel

Density g/cc  $\rho_p = 7.8$

Sound speed km/s (Us-up) **Co = 3.6**

Shock adiabat constant **S = 1.68**

**NOTE:** constant Co and S define the shock adiabat  $Us=Co+S*Up$

## 3. Constant groupings \*\*\*\*\*

$$R := \frac{\rho_p \cdot C_o}{\rho_e \cdot VOD} \quad m := \frac{S \cdot \rho_p}{\rho_e} \quad P_o := \rho_e \cdot VOD^2$$

START CALCULATIONS.....

$$A := \left(1 + \frac{9}{16} R\right)^2 \quad B := \frac{4}{3} \cdot \left(\frac{9}{16} m - 1\right)$$

$$C := \left(1 + \frac{9}{16} R\right) \quad D := 2 \cdot \left(\frac{9}{16} m - 1\right)$$

Interface velocity is .....

$$u_I := \frac{\sqrt{A + B - C}}{D} \cdot VOD$$

$$u_I = 0.567 \quad \text{km/s}$$

Interface pressure is.....

$$\text{In the plate.....} \quad P_p := \rho_p \cdot C_o \cdot u_I + \rho_p \cdot S \cdot u_I^2$$

$$P_p = 20.131 \quad \text{GPa}$$

In the gas .....

$$P_g = \frac{16}{27} \cdot \left(\frac{VOD \cdot u_I}{VOD}\right)^3 \cdot P_o$$

$$P_g = 20.103 \quad \text{GPa}$$

Initial plate velocity:

$$V_{po} := 2 \cdot u_I$$

$$V_{po} = 1.134 \quad \text{km/s}$$

## **APPENDIX 6**

### **ADVANCED DETONICS LABORATORY MEASUREMENTS**

## 6. ADVANCED DETONICS LABORATORY

Slug, velocity measurements were made at Naschem's Advanced Detonics Laboratory at Boskop in the North West Province.

### 6.1 First Set of Tests

The first set of tests were four tests of a directional primer charge comprising 65 g of Composition B explosive and a 6 g disc.

The charge details are presented in the Table below.

**TABLE A.6.1 DIRECTIONAL PRIMER CHARGE DETAILS**

Explosive Diameter (mm)	26
Explosive Length (mm)	60
Explosive Mass (g)	65
Explosive Type	Pour-cast Composition B
Velocity of Detonation ( $\text{ms}^{-1}$ )	7600
Disk Diameter (mm)	26
Disk Wall Thickness (mm)	1.6
Disk Mass (g)	6
Case Length (mm)	150
Case Material	PVC
Initiation	$\frac{1}{2}$ Powergel 813+no.6 IED

The measuring instrumentation comprised two 300 kV X-ray heads triggered by an ionization probe placed over the disc and a 1 mm printed circuit board placed on a steel witness plate as a timing screen, linked to the same external trigger.

The time-distance data required to calculate the slug velocity is presented in the Table below.



**TABLE A.6.2 SLUG TIME-DISTANCE MEASUREMENT CALCULATION**

<b>CHARGE#</b>	<b>DISTANCE (mm)</b>	<b>TIME (ms)</b>	<b>VELOCITY (ms<sup>-1</sup>)</b>
1	30 248	15.41 120.9	2070
2	50.4 201	25.41 100.5	2005
3	72.3 288.5	35.49 140.55	2060
4	26.9 175 636	10.96 80.49 315.5	2127

Four charges were fired. Only one usable signal was obtained from the witness plate shorting screen.

## **6.2 Second Set of Tests**

The second set of tests comprised measurements of nine cartridges of differing masses of Composition B ranging from 13,7 g to 48 g. The aim of the tests were to determine the slug velocity for various column charge lengths of nominally from 10 mm to 50 mm which have resulted in explosive masses ranging nominally from 12,5 mm to 44 mm. Actual explosive masses were determined by weighing the empty and filled assemblies.

Similar measurements to those undertaken in the first set of tests were taken and the charge details are presented in the Table below.

**TABLE A.6.3 DIRECTIONAL PRIMER CHARGE DETAILS**

Explosive Diameter (mm)	26
Explosive Length (mm)	12,5 to 44
Explosive Mass (g)	13,7 to 48
Explosive Type	Pour-cast Composition B
Velocity of Detonation	7600
Disk Diameter (mm)	26
Disk Wall Thickness (mm)	1.6
Disk Mass (g)	6
Case Length (mm)	150
Case Material	PVC
Initiation	½ Powergel 813 + no.6 IED

The instrumentation for the second set of tests was the same as for the first set of tests except that two timing screens were present – one on the witness plate (as before), and an additional screen placed between the charge and the witness plate. The measurements recorded are listed in Table A.6.4. The first two measurements are recorded by flash X-ray photography and the last two by shorting screens.

**TABLE A.6.4 SLUG TIME-DISTANCE MEASUREMENTS**

CHARGE NO.	EXPLOSIVE MASS (g)	TIME (ms)	DISTANCE (mm)
1	13.7	20 80 143.5	37 118 240
2	19.1	20 100 403.1 728.3	40 154 634 1010
3	26.2	20 100 465.1 662.5	44 171 740 1028
4	31.5	20 100 112.3 573.6	46 186 248 982
5	32.3	20 100 419.2 611.3	47 187 742 1040
6	35.5	20 100 403.9 568.9	47 193 741 1023
7	39.8	20 100 414.9 596.3	48 192 740 1028
8	41.4	20 100 392.8 549.7	48 200 742 1026
9	48	20 100 386.6 552.5	47.4 189.4 730 1020

The slug velocity as calculated from the flash X-ray measurements is presented in Table A.6.5.

**TABLE. A.6.5 SLUG VELOCITY FROM FLASH X-RAY DATA**

<b>CHARGE NO.</b>	<b>EXPLOSIVE MASS (g)</b>	<b>VELOCITY (ms<sup>-1</sup>)</b>
1	13.7	1350
2	19.1	1425
3	26.2	1588
4	31.5	1750
5	32.3	1750
6	35.5	1825
7	39.8	1800
8	41.4	1900
9	48.0	1900

### **6.3 Third Set of Tests**

The third set of tests comprised measurements of ten cartridges – eight cartridges containing 65 grams of Super Gelignite and two cartridges containing 93 grams Composition B explosives. The aim of the tests were to determine the slug velocity for Super Gelignite and Composition B using an 8 gram disc.

The charge details are presented in the Table below.

**TABLE A.6.6 DIRECTIONAL PRIMER CHARGE DETAILS**

Explosive Diameter (mm)	26
Explosive Column Length (mm)	Composition B : 85 Super Gelignite : 110
Explosive Mass (g)	Composition B : 93 Super Gelignite : 65
Explosive Type	Super Gelignite
Velocity of Detonation ( $\text{ms}^{-1}$ )	Composition B 7600 Super Gelignite 5600
Disk Diameter (mm)	26
Disk Thickness (mm)	2.0
Disk Mass (g)	8
Case Length (mm)	150
Case Material	PVC

The instrumentation for the third set of tests were the same as for the first set of tests, namely two flash X-ray heads and a timing screen on the witness plate.

The slug time-distance measurements and velocity calculations are presented in the Tables below.

**TABLE A.6.7 SLUG TIME-DISTANCE MEASUREMENTS AND VELOCITY**  
**CALCULATIONS FOR 80 GRAM SUPER GELIGNITE**

<b>CHARGE#</b>	<b>TIME (ms)</b>	<b>DISTANCE (mm)</b>	<b>VELOCITY (ms<sup>-1</sup>)</b>
1	10.5 35.7	214 247	1309
2	10.46 55.84 393.6	21 72 457	1126
3	20.49 65.57 404.8	29 80 447	1131
4	30.49 85.62 456.3	38 102 486	1161
5	40.66 108.02 301.0	49 129 436	1188
6	40.52 105.48 327.4	51 128 421	1185
7	40.58 105.81 255.15	43 113 420	1073
8	50 126 420	40/52 105.51 347.6	1169

Note only the recording for the shorting screen measurement for the first charge failed – the other seven were successful. Again the velocities have been calculated using the flash X-ray measurements only.

**TABLE A.6.8 SLUG TIME-DISTANCE MEASUREMENTS AND VELOCITY**  
**CALCULATIONS FOR 93 GRAM COMPOSITION B**

<b>CHARGE#</b>	<b>TIME (ms)</b>	<b>DISTANCE (mm)</b>	<b>VELOCITY (ms<sup>-1</sup>)</b>
3	25 113 451	20.56 65.54 249.8	1960
4	87 225 398	40.63 105.78 206.05	2118

Again, the velocities have been calculated using flash X-ray measurements only.

#### 6.4 Fourth Set of Tests

The fourth set of tests comprised measurements of eight cartridges of TNT explosive. Each cartridge contained 45 gram of TNT consisting of three pellets. The charge was initiated using a 30 mm long by 24 mm diameter booster of PETN, which represents 25 gram of additional high explosive charge similar to TNT. In order to compare results with Composition B and Super Gelignite in the third set of tests, an 8 gram disc was used.

The charge details are presented in the Table below.

**TABLE A.6.9 DIRECTIONAL PRIMER CHARGE DETAILS**

Explosive Diameter (mm)	25
Explosive Length (mm)	60
Explosive Mass (g)	45
Explosive Type	Pressed TNT pellets
Velocity of Detonation ( $\text{ms}^{-1}$ )	6700
Disk Diameter (mm)	26
Disk Mass (g)	8
Disk Thickness (mm)	2
Case Length (mm)	112
Case Material	1 mm Cardboard
Initiation	PETN Booster

The instrumentation for the fourth set of tests was the same as for the first and third sets of tests, namely two flash X-ray heads and a timing screen on the witness plate. The slug time-distance measurements and the velocity calculations are presented in the Table below.

**TABLE A.6.10 SLUG TIME-DISTANCE MEASUREMENTS AND VELOCITY  
CALCULATIONS 45 GRAM TNT WITH A 25 GRAM PETN BOOSTER**

CHARGE NO.	DISTANCE (mm)	TIME (ms)	VELOCITY (ms <sup>-1</sup> )
1	11.3 142.6 869	20.64 100.89 553.8	1636
2	14.3 130 865	20.73 100.85 582.56	1457
3	13.6 134.4 870	25.63 105.68 618.65	1509
4	38.6 166.0 770	30.66 110.69 560.75	1594
5	44.3 165.3 765	35.64 115.74 486.5	1511
6	48.8 181.3 821	40.68 120.59 577.6	1658
7	54.8 179.4 815	45.69 125.63 513.75	1559
8	192 325 890	150.69 230.77 592.25	1661

Although shorting screen measurements for all cartridges were recorded, to maintain consistency with the previous tests, the velocities have been calculated using the flash X-ray measurements only.



## **APPENDIX 7**

### **SHOCK EFFECTS GENERATED BY THE DIRECTIONAL PRIMER CHARGE**

# ANALYSIS OF SHOCK EFFECTS GENERATED BY HIGH-SPEED METAL SLUGS

## **Synopsis**

Two aspects of the terminal effects of a high-speed metal slug are examined. The first is the generation of an air shock by the supersonic motion of the slug. The characteristics of interest here are the velocity of the shock wave and the shock pressure. The second aspect relates to the nature of the pressure pulse created in rock by the impact of the slug. Various physical effects arising out of the impact are identified, and magnitudes and durations of the attendant pressure pulses are calculated.

Prepared by

Thomas Szendrei *Pr Sci Net*

Dynamic Physics Consultants

for

Mr J.A. Cruise

May 1999

## 1. Air Shock Ahead of Metal Slug

### 1.1 Equations of Shock Transition

The basic shock equations link the state of shocked material to its initial state. In the flow illustrated in Fig.1, the disturbance corresponding to the shock front is propagated from left to right with a velocity  $U_s$  into the undisturbed material.

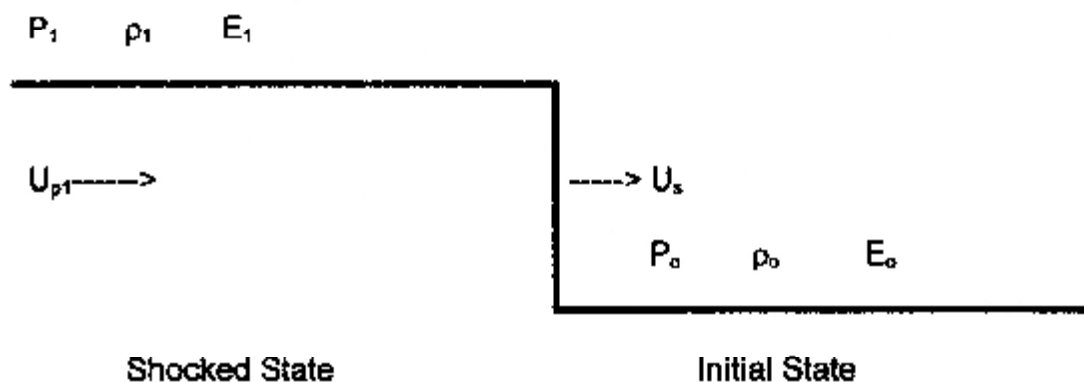


**FIGURE 1:** Schematic Representation of a Plane Shock Wave in Laboratory Coordinates (Initial state at rest)

The following notation is applicable:

- $U_s$  shock velocity
- $u_p$  particle- (or mass-) velocity
- $\rho$  density
- $E$  internal energy (per unit mass)
- $P$  pressure
- $0, 1$  subscripts denoting initial (0) and shocked (1) state respectively

In Fig.1 the initial state is characterised by values of pressure, density and energy denoted by  $P_0$ ,  $\rho_0$  and  $E_0$  respectively. The material is at rest ( $u_{p0}=0$ ). The shock front is assumed to consist of a time-independent (steady) pressure pulse. The initial material is accelerated to a particle speed of  $u_{p1}$  by

the passage of the shock front moving at velocity  $U_s$ , and is compressed to a density  $\rho_1 > \rho_0$ . The state of the shocked material is related to the initial state by a set of so-called jump conditions representing the conservation of mass, momentum and energy in the shock transition.

#### **Conservation of Mass**

$$\rho_0 \cdot U_s = \rho_1 \cdot (U_s - u_p) \quad [1]$$

#### **Conservation of Momentum**

$$P_1 - P_0 = \rho_0 \cdot U_s \cdot u_p \quad [2]$$

#### **Conservation of Energy**

$$P_1 \cdot u_p = \frac{1}{2} \cdot \rho_0 \cdot u_p^2 + \rho_0 \cdot U_s \cdot (E_1 - E_0) \quad [3]$$

the above equations can be rewritten in a form that directly displays the functional forms of the shocked state parameters, namely:

#### **Shock Velocity**

$$U_s = \frac{1}{\rho_0} \cdot \sqrt{\frac{P_1 - P_0}{\frac{1}{\rho_0} - \frac{1}{\rho_1}}} \quad [4]$$

#### **Particle Velocity**

$$u_p = \sqrt{(P_1 - P_0) \cdot \left( \frac{1}{\rho_0} - \frac{1}{\rho_1} \right)} \quad [5]$$

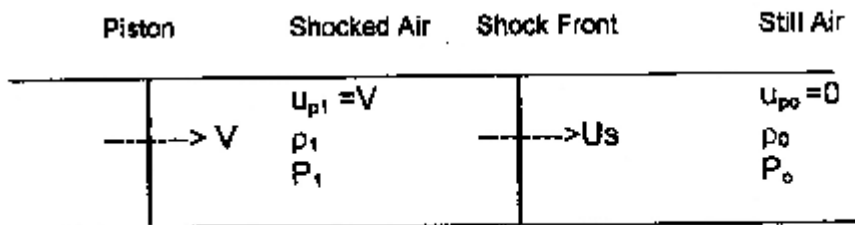
#### **Specific Energy**

$$E_1 - E_0 = \frac{1}{2} \cdot (P_1 + P_0) \cdot \left( \frac{1}{\rho_0} - \frac{1}{\rho_1} \right) \quad [6]$$

#### **'Piston' Model for Air Shock**

The above basic equations can be used to analyse the pressure pulse set up in a column of air by a rapidly-moving 'piston'. As long as the piston motion is steady, that is, velocity changes are slow enough for the column of air ahead of it to readjust itself to the changes in velocity, the following analysis is valid.

We expect the piston to be preceded by a strong compression wave when the piston velocity  $V$  is supersonic and much larger than the speed of sound in the air ahead of it. The resulting shock structure is sketched in Fig.2.



Because at the piston, the particle (or mass) velocity of air must of necessity be equal to the velocity of the piston ( $V$ ), the shock wave is such as to accelerate the initially still air across the front to a particle velocity that matches piston velocity (i.e.  $u_{p1} = V$ ).

As the air is effectively a perfect gas, and may be characterized by a constant value of the ratio of specific heats ( $\gamma$ ), the energy equation [6] can be rewritten as

$$E_1 - E_0 = \frac{R \cdot (T_1 - T_0)}{\Gamma - 1}$$

where  $R$  is the universal gas constant (287.06 J/kg-K) and  $T$  is the temperature. Furthermore

$$\frac{P}{\rho} = R \cdot T_0$$

and with the above substitutions the energy eq.[6] may be rewritten as follows, yielding the relative density of the shocked air:

$$\frac{\rho_1}{\rho_0} = \frac{(\Gamma + 1) \cdot P_1 + (\Gamma - 1) \cdot P_0}{(\Gamma - 1) \cdot P_0 + (\Gamma + 1) \cdot P_1} \quad [7]$$

By substitution for  $\rho_0$  and  $\rho_1$  in eq.[5] where  $u_{p1}$  in the present analysis is set equal to piston velocity ( $V$ ), and by a long process of algebraic manipulation, the following relationship is obtained between  $V$  and shock pressure  $P_1$ .

$$V^2 = \left[ \frac{2 \cdot R \cdot T_0 \cdot \left( \frac{P_1}{P_0} - 1 \right)}{(\Gamma + 1) \cdot \frac{P_1}{P_0} - \Gamma - 1} \right]^{\frac{1}{2}} \quad [8]$$

The above equation may be inverted to extract the shock pressure as a function of piston velocity, thus:

$$\frac{P_1}{P_0} = 1 + \left( \frac{\Gamma + 1}{4 \cdot R \cdot T_0} \right) \cdot V^2 + \frac{V}{\sqrt{R \cdot T_0}} \cdot \sqrt{\Gamma + \frac{(\Gamma + 1)^2}{16 \cdot R \cdot T_0} \cdot V^2} \quad [9]$$

Finally, the shock velocity is obtained by evaluating eq.[4]

$$U_s^2 = \frac{1}{2} \cdot R \cdot T_0 \cdot \left[ (\Gamma + 1) \cdot \frac{P_1}{P_0} + \Gamma - 1 \right]^{\frac{1}{2}} \quad [10]$$

The state of the air shock may thus be evaluated once the 'piston' velocity is known: For a given  $V$

- find the shock pressure  $P_1$  (eq.[9]).
- then derive shock velocity (eq.[10]), and
- density of shocked air (eq.[7]) in terms of the shock pressure  $P_1$ .

(These, essentially algebraic calculation are readily executed by means of MATHCAD.)

### Air Shock Calculations

Values of shock velocity, shocked air density and shock pressure are tabulated below for slug velocities from 1000 m/s to 2000 m/s.

**TABLE 1. Characteristics of Air Shock Created by Supersonic Metal Slug**

Slug Velocity (m/s)	Shock Velocity (m/s)	Shock Pressure (atm.)	Relative Air Density
1000	1293	16.1	4.42
1100	1405	19.1	4.60
1200	1519	22.3	4.76
1300	1633	25.8	4.90
1400	1748	29.6	5.02
1500	1864	33.7	5.12
1600	1980	38.0	5.21
1700	2097	42.7	5.28
1800	2213	47.6	5.35
1900	2331	52.8	5.41
2000	2449	58.2	5.45

It is seen that

1. the slug is preceded by a shock wave travelling about 25% faster than the slug
2. air is compressed to about 5 times its initial value
3. shock wave pressure is from 16 to 58 atmospheres

## 2. Impact Shock of Metal Slug

### 2.1 Physical Picture

When the initially freely translating slug strikes the bottom of the borehole, a shock impulse will arise in both slug and rock media. The material response zones immediately after impact are illustrated in Fig.2. All velocities indicated are relative to a set of coordinates fixed in the rock. (Since the rock is stationary, this set is equivalent to fixed, laboratory coordinates). Notation: as is customary,  $p$  denotes plate-and  $t$  denotes target-material;  $o$  indicates the initial state, and  $1$  the shocked state. Subscript ' $i$ ' refers to the interface or contact surface between the slug and rock.

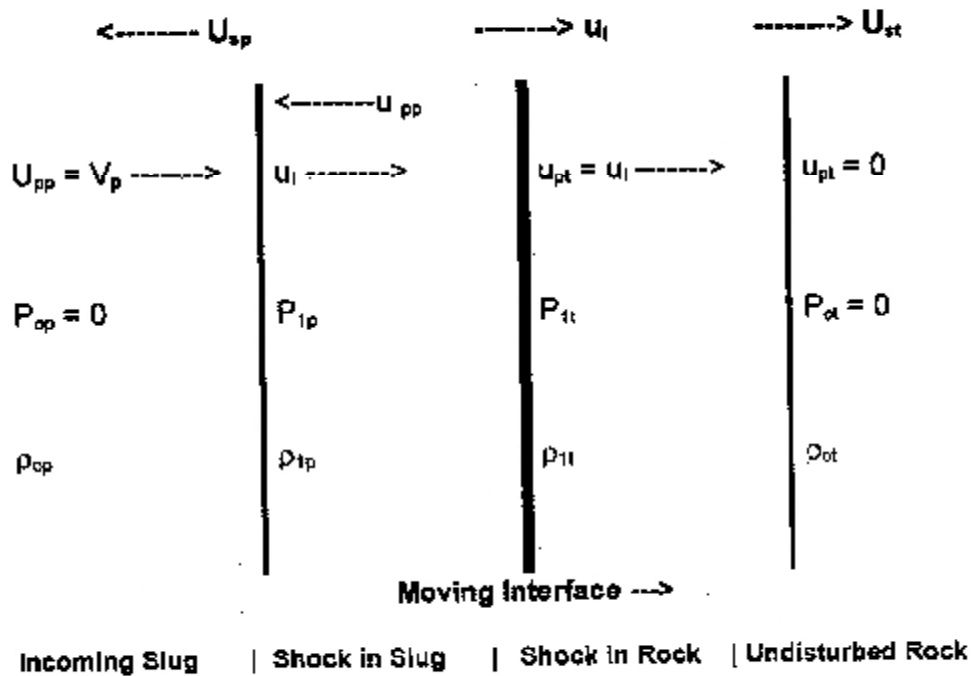


**FIGURE 2: Shock Structure for Impact of a Metal Plate on Rock**

On impact a region of compressed material is formed, bounded by the shock fronts moving away from the interface into the rock mass to the right, and back into the incoming slug from the left. The interface or contact surface itself moves at some constant velocity  $u_i$  to the right. Continuity and equilibrium considerations demand that on both sides of the interface the



mass velocities and shock pressures must be equal. Densities and shock front velocities may however be different in the two shocked regions.

The velocity of the contact surface  $u_i$  coincides with the mass (or particle-) velocity behind the shock wave in the rock. Thus

$$u_{pi} = u_i$$

In the plate, the particle velocity behind the left-moving shock front must be such to reduce the velocity of the incoming slug to the interface value, so that

$$V_p - u_{1p} = u_i$$

This ensures that material flow velocities on either side of the contact surface are the same as required by continuity.

## 2.2 Equations of Shock Transition

With the above physical definition of the impact shock structure, the jump conditions can be shown to be the following:

### ROCK (t)

#### Mass Conservation

$$\rho_{\alpha} U_{\alpha t} = \rho_{tt} [U_{\alpha t} - u_i]$$

#### Momentum Conservation:

$$P_{1t} = \rho_{\alpha} U_{\alpha t} u_i$$

### METAL SLUG (p)

#### Mass Conservation

$$\rho_{op} [U_{sp} + V_p] = \rho_{1p} [U_{sp} + u_i]$$

#### Momentum Conservation:

$$P_{1t} = \rho_{op} [U_{sp} + V_p] [V_p - u_i]$$

Making use of the linear shock-velocity/ particle velocity Hugoniot adiabat, namely that most materials may be characterised by two empirical constants  $C_0$  and  $S$  such that

$$U_s = C_0 + S u_p$$

the shock pressures in the rock and slug may be expressed as follows:

$$P_{1r} = \rho_{0r} [C_{0r} + S_r u_i] u_i$$

$$P_{1p} = \rho_{0p} [(C_{0p} + S_p [V_p - u_i]) [V_p - u_i]]$$

Equating the pressures leads to a non-linear equation in the interface velocity. This might be solved by a root-finding algebraic technique. They may also be solved by a graphical solution which consists of plotting the pressure equations in  $P$ - $u$  plane and locating the value of  $u_i$  as that value of particle velocity  $u$  at which the curves cross. This method is known as impedance matching.

The method is illustrated by evaluating the impact at 1600 m/s of a steel slug on quartzite rock. The Hugoniot constants used are:

	$C_0$	$S$
Quartzite	3.68	2.12
Steel	3.6	1.68

Fig.3 plots the pressure-particle velocity shock Hugoniots. From the intersection of the steel and rock curves, the impact conditions are located.

IMPACT SHOCK  
PRESSURE GPa

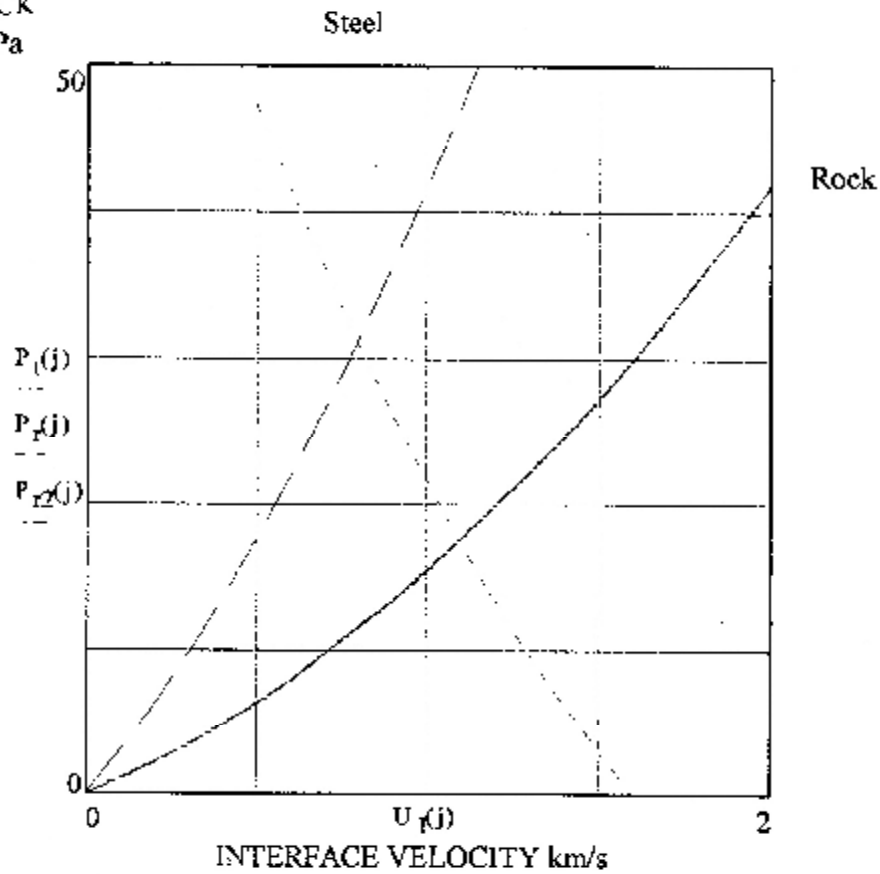


**FIGURE 3: Analysis of shock pressure and interface velocity for the impact of mild steel slug on quartzite at 1600 ms<sup>-1</sup>**

Impact conditions are:

Pressure	17.5 Gpa
Interface Velocity	1100 m/s
Shock velocity in rock	6000m/s

The full solution of steel on quartzite impact is summarised in Table 2.

**TABLE 2: Shock Impact Parameters of Steel Slug on Quartzite Rock**

<b>Slug Velocity (m/s)</b>	<b>Interface Velocity (m/s)</b>	<b>Shock Velocity in Rock (m/s)</b>	<b>Impact Pressure (GPa)</b>
1000	702	5.217	9.61
1100	769	5.31	10.81
1200	835	5.45	12.06
1300	901	5.59	13.36
1400	967	5.73	14.69
1500	1033	5.87	16.07
1600	1098	6.00	17.49
1700	1164	6.15	18.95
1800	1228	6.28	20.46
1900	1293	6.42	22.01
2000	1358	6.567	23.59

Results are displayed graphically in Figs. 4-5.

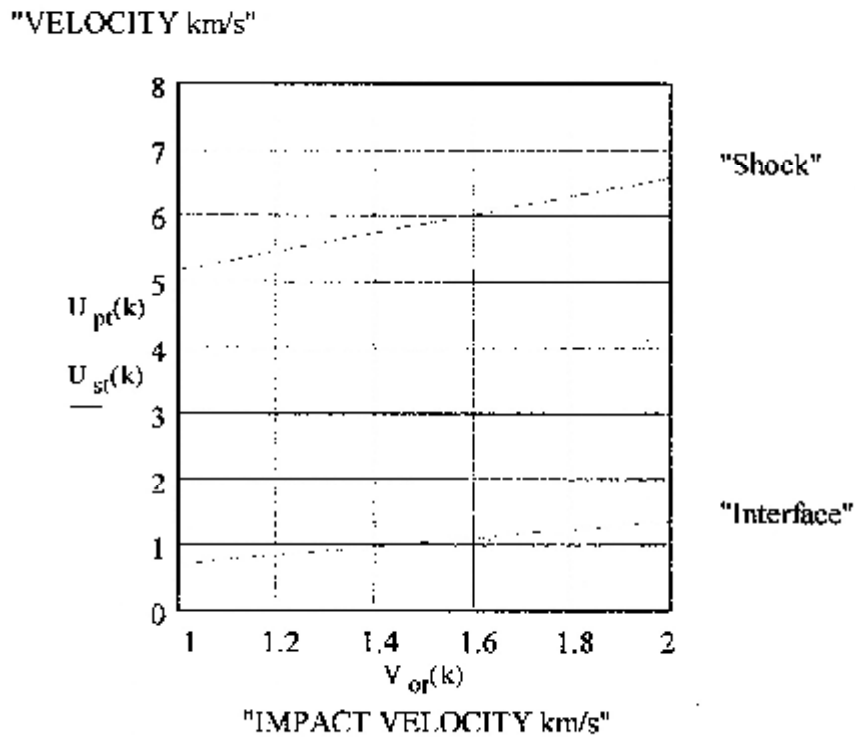


FIGURE 4: Shock velocity and interface velocity in quartzite for the Impact of a steel slug at 1000-2000  $ms^{-1}$ .

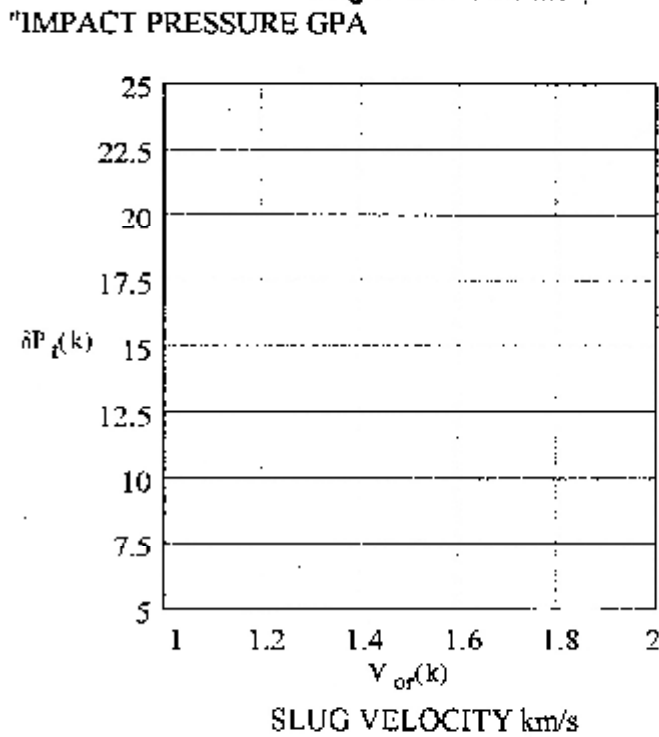


FIGURE 5: Shock pressure in quartzite for the impact of a steel slug at velocities 1000 -2000  $ms^{-1}$ .

---

### 3. Duration and Attenuation of Shock Waves

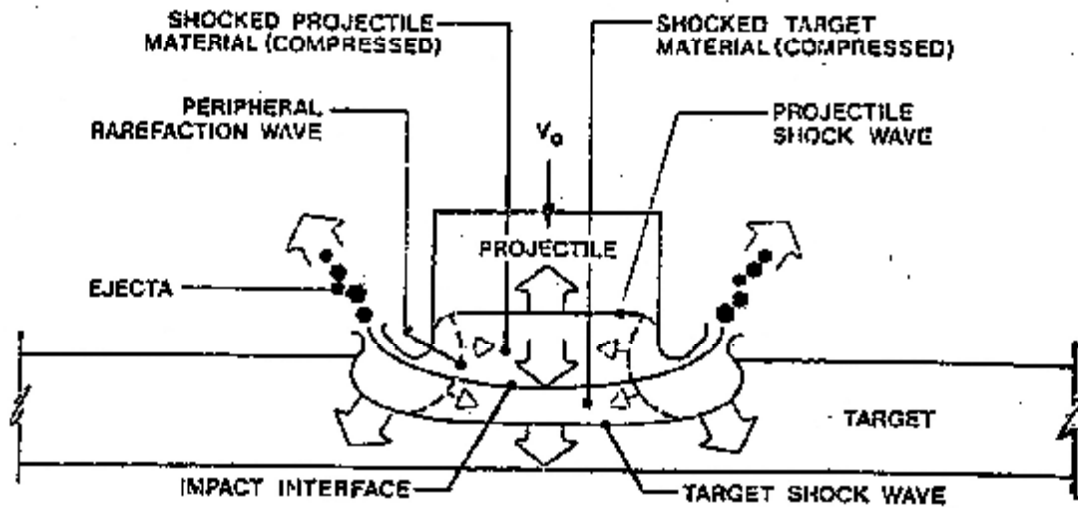
#### 3.1 Physical Picture

Given the impact pressures as calculated above, the immediate question of importance is how long does the pressure last? The attenuation of importance here is not that due to various dissipative effects such as energy losses by viscosity, heat conduction, etc. – but that due to geometrical considerations, the most important of which is the finite size of the metal slug. To illustrate the effects of finite size vis-à-vis impact shock structure, consider Fig. 6.

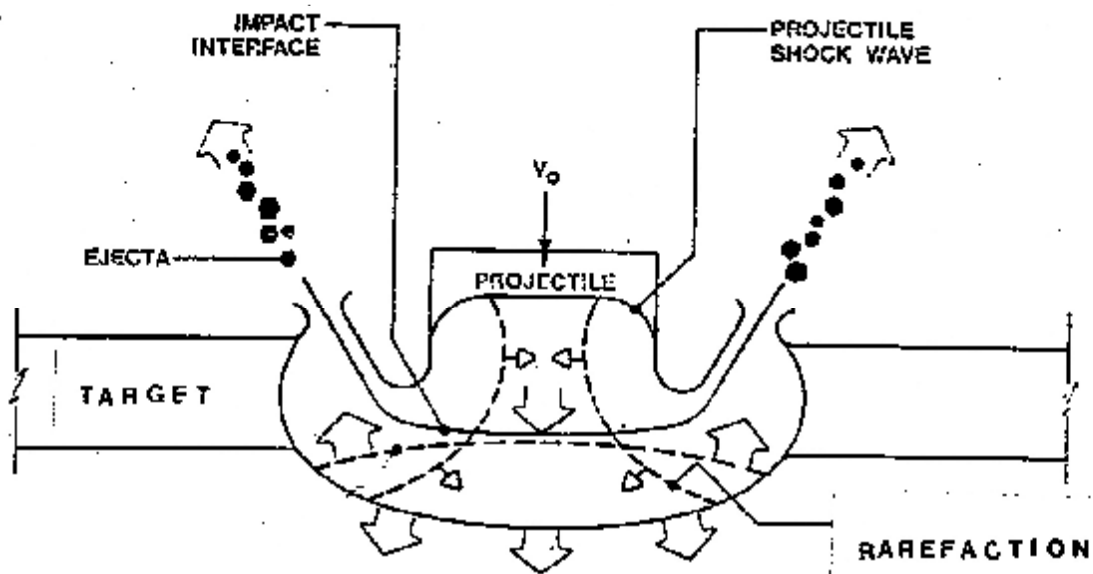
A right circular, and essentially flat-ended 'rod' impacts a target which is laterally unbounded (e.g. rock mass). At the moment of impact (on the scale of nano-seconds) shock waves are created which propagate away from the contact surface in both directions, as derived above. But because the rod is finite in lateral extent, the shock wave is reflected as rarefaction waves from the free boundaries around the periphery of the rod and propagate back towards the axis of symmetry of the rod. The rarefaction waves reduce the pressure in the shocked regions and allow material flow to take place. The expansion waves from the sides lead to zones of plastic flow radially in the frontal zones of the rod, the most prominent feature of this being the formation of a mushroomed rod tip. These effects are illustrated in Fig.9..

While the stress is being relieved at the contact surface by release waves from the sides, the shock wave propagates upstream in the rod. However, it does not outrun the release waves. On fundamental grounds, it can be shown that any disturbance (e.g. release wave) behind the shock will always propagate faster than the shock wave, and thus a rarefaction wave will always overtake the shock front in the rod. When this happens the high-pressure shock conditions in the rod are destroyed.

FIGURE 6: Wave structure in the high-velocity impact of a metal rod



(a) JUST AFTER IMPACT



(b) LATER TIME

FIGURE 13: Wave Structure in High-Velocity Rod Impact

From the above considerations, two approximations can be made for the duration of the high-pressure shock conditions:

- (1) the time required for the release of shock pressure along the contact surface by rarefaction waves from the side, and
- (2) the time required for the release waves to catch up with the shock wave propagated upstream in the rod.

### 3.2 Rarefaction Waves along the Contact Surface

For impact velocities below the elastic wave-speeds of the rod and target materials (approx. 4000 m/s for both steel and rock), the shock waves may be considered as being weak. In this case, we may consider velocities in the acoustic limit, and the speed of propagation of release waves from the sides is thus to a sufficient degree of accuracy given by the bulk sound speed. If the diameter of the rod is  $d$ , release waves will reach the centre of the rod in a time

$$\Delta t = \sqrt{(\rho / K)} \cdot d / 2$$

where  $K$  is the bulk modulus and  $\rho$  is the density. For steel,  $K = 160$  GPa; rod diameter at the leading tip is typically 10 mm, thus

$$\Delta t = 1.1 \text{ } [\mu\text{s}]$$

### 3.3 Rarefaction Waves behind the Shock Front in the Slug

Ravid *et al* has given a detailed analysis of wave propagation in the vicinity of the impact surface – refer to DPC Contract Report *Analysis of Shock Effects in High-Speed Impact* (July 1993).

The duration of the shock-dominated phase of impact is taken to be the time for rarefaction waves, generated at the periphery of the contact surface, to catch up with the shock wave traveling away from the contact surface. The Ravid analysis assumes that rarefaction waves travel at the adiabatic speed



of sound in the shocked material. Application of the Ravid model to the case of mild steel 'rod' striking quartzite rock at 1600 m/s yields the following results (as calculated by MATHCAD):

Interface Velocity	= 1098 m/s
Shock Velocity (rod)	= 4483 m/s
Shock Velocity (rock)	= 6009
Rarefaction Velocity (rod)	= 5020 m/s
Shock duration $t_s$	= 1.61 $\mu$ s
Rod deformation length in $t_s$	= 6.3 mm
Loss length (rod) in time $t_s$	= 0.8 mm
Advance of interface	= 1.8 mm

This analysis thus shows that rarefaction waves destroy the shock wave in the rod in time  $t_s = 1.61 \mu$ s and reduce the impact pressure to some lower value (which is to be defined in the following section). In this time the shock wave had progressed 6.3 mm up the rod, and the rod had undergone shortening by 0.8 mm due to flow of rod material laterally as the rarefaction waves arrived from the sides. The rock/metal interface had advanced 1.8 mm under the influence of shock pressure.

Analysis of transient impact conditions are summarised in Table 2 below for slug velocities from 1000 m/s to 2000 m/s.

**Table 3: Analysis of Impact Shock Attenuation for Slug Impact on Quartzite**

Slug Velocity (m/s)	Rarefaction Wave Speed (m/s)	Shock Duration $t_s$ ( $\mu$ s)	Advance of rock/metal interface (mm)
1100 <i>1600?</i>	4765	1.74	1.22
1100	4806	1.72	1.32
1200	4848	1.70	1.42
1300	4890	1.67	1.50
1400	4933	1.65	1.60
1500	4977	1.64	1.69

1600	5020	1.61	1.77
1700	5064	1.59	1.85
1800	5100	1.57	1.93
1900	5153	1.55	2.00
2000	5198	1.53	2.08

### 3.4 Penetration Pressure: Transient Phase

As described above, rarefaction waves release the high shock pressures at the contact surface between rod and rock, and also in the rod away from the contact surface. The time required for this is the time  $t_r$  defined in Table 3. The further evolution of contact pressure depends on the impact velocity in conjunction with the relative strengths of target and rod materials.

Tate (1969) has shown that for a given target/rod combination, there exists a minimum impact velocity below which the rod ceases to deform and proceeds to penetrate as a rigid body. This limit velocity is defined as:

$$V_{min} = \{2(Y_p - R_t) / \rho_t\}^{1/2}$$

where  $Y_p$  = plastic flow strength of penetrator = 0.9 GPa for mild steel  
 $R_t$  = resistance of target material to penetration = 0.3 GPa for strong rock  
 $\rho_t$  = target density = 2650 kg/m<sup>3</sup> for quartzite

The calculated limit velocity for mild steel impact on quartzite is 670 m/s. This is well below experimentally measured values. Thus we may expect that following impact shock and its attenuation, the rod will penetrate the rock in a non-rigid or deforming fashion. In fact, the rod will penetrate in the so-called hydrodynamic mode which is characterized by the erosion of the rod from its tip as it penetrates and the formation of a characteristic *mushroom-bulb*

The importance of this conclusion is twofold. It defines a transition period dominated by plastic flow, and identifies the final pressure obtained by the

readjustment of contact surface pressure as the to the quasi-steady state hydrodynamic penetration pressure.

Tate (1987) has argued that the transition from shock-dominated impact phase to the hydrodynamic mode of penetration involves the gross plastic distortion of the rod as it forms the tip mushroom. These distortion waves propagate at the shear plastic wave velocity. The details of this stage can be very complex, but as an approximation it may be assumed that the final steady-state penetration pressure is not realized until the plastic waves reach the axis of the rod.

In contrast to various speeds relevant to impact shock (such as interface velocity, and shock- and rarefaction wave velocities), plastic shear waves propagate at much lower speeds on the order of some hundreds of metres per second. The phase of plastic deformation and pressure reduction is at least as long as the initial transient shock phase, and probably significantly longer. In the context of the information given in Table 3, this phase is assigned a duration of 5  $\mu$ s.

The Ravid et al analysis described above shows that rarefaction waves reduce the shock pressure at the contact surface to 20% its peak value. This remaining pressure is then further reduced during the phase of plastic flow of the rod to a value corresponding to the steady-state penetration pressure.

### 3.5 Penetration Pressure— Steady Phase

The penetration pressure (often called the stagnation pressure) prevailing at the rod/rock interface during steady-state penetration is defined by

$$P_{hd} = 1/2 \rho_t U^2 + R_t$$

where U is the penetration velocity, that is, the rate of retreat of the crater bottom. R again denotes the strength of the rock (in units of GPa). Even for strong rocks, its value is relatively low compared to the magnitude of the first 'dynamic' pressure term. The penetration velocity is defined by

$$U = V / (1 + (\rho_r / \rho_a)^{0.5})$$

In the hydrodynamic penetration model, the rod enters the penetration zone at impact speed  $V$  while the penetration zone advances at speed  $U$ . The difference between these velocities is the rate of erosion of the rod. The duration of the penetration event is thus defined by the time it takes for a rod of length  $L$  to be consumed. Thus

$$\Delta t_{hd} = L / (V-U)$$

With  $L = 15 \text{ mm}$  (as measured by FX),  $V=1600 \text{ m/s}$  and  $U = 1012 \text{ m/s}$ , the duration is  $25 \mu\text{s}$ . *21,5  $\mu\text{s}$*

The analysis of hydrodynamic penetration pressure history is summarised in Table 3 for rod velocities from  $1000 \text{ m/s}$  to  $2000 \text{ m/s}$ .

**TABLE 4 Hydrodynamic Penetration Parameters for Steel Slug On Quartzite  
Rod Length 15mm**

Slug Velocity (m/s)	Penetration Velocity (m/s)	Penetration Pressure (GPa)	Duration ( $\mu\text{s}$ )	
1000	632	0.53	<del>24</del>	40,7
1100	696	0.64	<del>22</del>	37
1200	759	0.76	<del>20</del>	34
1300	822	0.89	<del>18</del>	31
1400	885	1.04	<del>17</del>	29
1500	949	1.193	<del>16</del>	27
1600	1012	1.35	<del>15</del>	25,5
1700	1075	1.53	<del>14</del>	24
1800	1139	1.72	<del>13</del>	23
1900	1202	1.91	<del>12</del>	21,5
2000	1265	2.12	<del>12</del>	20,4

### 3.6 Impact Pressure Pulse Profile

The general shape of the pressure pulse generated by the impact of a high-velocity metal slug on rock is defined in Table 5.

**TABLE 5: Pressure Pulse Time History for the Impact of Steel on Quartzite**  
Length of Slug = 15mm

Impact Phase	Pressure (GPa)	Duration ( $\mu$ s)
<b>Impact Velocity = 1000 m/s</b>		
Impact Shock	9.6	1.74
Plastic Flow	1.9	5
Hydrodynamic flow	0.53	23.7 40,7
<b>Pulse Duration (<math>\mu</math>s)</b>		
<b>Impact Velocity = 2000 m/s</b>		
Impact Shock	23.6	1.53
Plastic Flow	4.7	5
Hydrodynamic Flow	2.1	14 20,4
<b>Pulse Duration (<math>\mu</math>s)</b>		

The pressure profiles are plotted in Fig. 8 for impact velocities of 1000 m/s and 2000 m/s.

## **APPENDIX 8**

### **UNDERGROUND TEST MEASUREMENTS AND FREQUENCY DISTRIBUTION GRAPHS**

## Village Main Tests

Four series of tests were undertaken at Village main gold mine. The tests were of a comparative nature. Rounds would be blasted containing different explosive configurations of directional primer charges. These were interspersed with rounds containing no directional primer charges. These were termed standard rounds.

The first series of tests compared the results of directional primer charges containing 20 g, 35 g and 55 g of Composition B explosive.

The second series of tests were a continuation of the first but with 75 g and 95 g of Composition B explosive.

### 1. Summary of First and Second Series of Tests

The test number in the first column denotes the type of mass of explosive used.

The alphabetic letter denotes the explosive type i.e. b represents Composition B, STD represents a standard charge without the directional primer charge. The associated number is the mass of explosive in those charges using the directional primer i.e. B20 represents a charge containing 20 grams of Composition B. The last figure is the test blast number of that charge i.e. B20/3 is the third stopping face of 20 gram Composition B to be blasted.

TEST NO.	SAMPLE SIZE	MEAN SOCKET LENGTH	
		PER ROUND	PER SERIES
STD/1	26	208	
STD/2	18	94	
STD/3	21	73	
STD/4	12	103	120
STD/5	24	119	
STD/6	14	326	
STD/7	12	147	
STD/8	43	113	176
	170		148

Standard rounds nos. STD/1 TO std/4 were drilled 900 mm long and standard rounds nos. STD/5 TO std/8 were drilled 1200 mm long. As the majority of directional primer charge rounds were 1200 mm, standard rounds STD/5 TO STD/8 have been used for comparison.

TEST NO.	SAMPLE SIZE (NO. OS HOLES / BLAST)	MEAN SOCKET LENGTH (MM)	
		PER ROUND	PER SERIES
B20/1	22	121	
B20/2	18	66	
B20/3	13	125	104
<b>53</b>			

TEST NO.	SAMPLE SIZE (NO. OF HOLES / BLAST)	MEAN SOCKET LENGTH (MM)	
		PER ROUND	PER SERIES
B35/1	22	136	
B35/2	29	44	
B35/3	23	68	
B35/4	30	62	78
<b>104</b>			

TEST NO.	SAMPLE SIZE (NO. OS HOLES / BLAST)	MEAN SOCKET LENGTH (MM)	
		PER ROUND	PER SERIES
B55/1	<b>24</b>	120*	120



TEST NO.	SAMPLE SIZE (NO. OS HOLES / BLAST)	MEAN SOCKET LENGTH (MM)	
B75/1	15	97	
B75/2	12	65	
B75/3	26	96	86
<b>53</b>			

TEST NO.	SAMPLE SIZE (NO. OS HOLES / BLAST)	MEAN SOCKET LENGTH (MM)	
B95/1	32	78	
B95/2	12	53	
B95/3	22	85	
B95/4	22	68	71
<b>88</b>			

## 2. Summary of Third Series of Tests

TEST NO.	SAMPLE SIZE (NO. OF HOLES / BLAST)	MEAN SOCKET LENGTH
STD/9	22	252 mm
STD/10	42	122 mm
STD/11	28	131 mm
STD/12	17	50 mm
STD/13	16	94 mm
STD/14	23	126 mm
STD/15	20	73 mm

<b>TEST NO.</b>	<b>SAMPLE SIZE (NO. OF HOLES / BLAST)</b>	<b>MEAN SOCKET LENGTH</b>
B85/1	18	212 mm
B85/2	40	161 mm
B85/3	75	73 mm
B85/4	76	79 mm
B85/5	58	46 mm
B85/6	56	50 mm
B85/7	45	37 mm

### 3. Summary of Fourth Series of Tests

<b>TEST NO.</b>	<b>SAMPLE SIZE (NO. OF HOLES / BLAST)</b>	<b>MEAN SOCKET LENGTH</b>	<b>ZERO</b>
STD/16	23	229 mm	6
STD/17	50	170 mm	11
STD/18	63	155 mm	24
STD/19	52	147 mm	14

<b>TEST NO.</b>	<b>SAMPLE SIZE (NO. OF HOLES / BLAST)</b>	<b>MEAN SOCKET LENGTH</b>	<b>ZERO</b>
SG/1	38	101 mm	21
SG/2	28	68 mm	20
SG/3	27	32 mm	18

**Standard Primer**  
 From 30 September 1991 to 2 November 1991

#	Date	Pre-Blast Data					Post Blast Data				Charge
		Hole	Depth	Stoping	Burden	Spacing	Hole	Socket	Burden	Spacing	
1	07-Oct-91	T 1	1100		600		T 1	400	600		P+3
2		B 1	1150	1100	550	650	B 1	500	950	1100	
3		T 2	1100		550		T 2	70	700		
4		B 2	1300	1200	700	650	B 2	70	700	1100	
5		T 3	1200		600		T 3	0	700		
6		B 3	1150	1150	600	500	B 3	150	800	1050	
7		T 4	1100		550		T 4	0	700		
8		B 4	1100	1000	600	550	B 4	0	400	1100	
9		T 5	1100		650		T 5	0	600		
10		B 5	1100	1100	600	600	B 5	0	500	1050	
11		T 6	1200		500		T 6	150	500		
12		B 6	1200	1200	550	600	B 6	300	450	1100	
13		T 7	1200		550		T 7	250	600		
14		B 7	1200	1100	600	550	B 7	350	600	1000	
15		T 8	1200		600		T 8	400	1000		
16		B 8	1100	1050	600	500	B 8	150	500	950	
17		T 9	1100		650		T 9	50	750		
18		B 9	1100	1100	550	600	B 9	0	850	1000	
19		T 10	1100		600		T 10	0	700		
20		B 10	1100	1100	650	650	B 10	0	750	1050	
21		T 11	1100		600		T 11	0	750		
22		B 11	1200	1150	600	700	B 11	0	650	1100	
23		T 12	1200		700		T 12	0	900		
24	Gully	B 12	1200	1200	650	700	B 12	0	800	1100	
25	08-Oct-91	T 1	900		600		T 1	0	600		P+2
26		B 1	900	1100	700	800	B 1	0	750	1000	
27		T 2	900		650		T 2	350	700		
28		B 2	800	1000	550	700	B 2	250	600	1100	
29		T 3	800		600		T 3	400	650		
30		B 3	800	1000	550	700	B 3	400	600	900	
31		T 4	800		600		T 4	500	700		
32		B 4	800	1100	650	750	B 4	500	600	1100	
33		T 5	800		500		T 5	100	400		
34		B 5	800	1100	650	700	B 5	450	800	1000	
35		T 6	800		600		T 6	300	650		
36		B 6	800	850	500	700	B 6	200	600	1000	
37		T 7	800		600		T 7	400	700		
38		B 7	800	1000	600	700	B 7	0	650	1000	
39		T 8	800		450		T 8	300	400		
40		B 8	800	900	550	600	B 8	70	70	900	
41		T 9	800		600		T 9	300	450		
42		B 9	800	1000	650	700	B 9	50	350	900	
43		T 10	800		550		T 10	200	500		

44	B 10	800	900	600	700	B 10	400	800	770	
45	T 11	800		450		T 11	0			
46	B 11	800	1100	550	700	B 11	130		950	
47	T 12	800		550		T 12	0			
48	B 12	800	1200	650	700	B 12	0			
49	T 13	800		600		T 13	0			
50	Gully B 13	800	1100	550	700	B 13	0			
51	09-Oct-91 T 1	800		600		T 1	120	600		P+2
52	B 1	800	1050	650	700	B 1	150	450	650	
53	T 2	800		400		T 2	120	400		
54	B 2	900	1050	600	550	B 2	50	550	750	
55	T 3	800		550		T 3	100	400		
56	B 3	800	1000	450	550	B 3	50	600	750	
57	T 4	800		450		T 4	150			
58	B 4	800	1000	600	550	B 4	350		800	
59	T 5	900		450		T 5	10			
60	B 5	800	900	600	350	B 5	100			
61	T 6	900		450		T 6	0			
62	B 6	800	1000	550	550	B 6	0			
63	T 7	900		700		T 7	0			
64	B 7	800	1050	500	570	B 7	0			
65	T 8	800		450		T 8	0			
66	B 8	900	1100	600	550	B 8	50	650		
67	T 9	900		500		T 9	60	1000		
68	Gully B 9	900	1100	500	500	B 9	0	800	870	
69	10-Oct-91 T 1	900		550		T 1	330	950		P+2
70	B 1	800	1000	500	830	B 1	0	600	1100	
71	M 1	900		500		M 1				
72	T 2	900		150		T 2	0	850		
73	B 2	900	1000	470	630	B 2	50	900	1000	
74	M 2	900				M 2				
75	T 3	900		900		T 3	330	430		
76	B 3	900	1000	500	700	B 3	100	700	850	
77	T 4	900		450		T 4	600			
78	B 4	900	1000	500		B 4	0			
79	T 5	900		550		T 5	0			
80	B 5	900	1000	470	700	B 5	0			
81	T 6	850		550		T 6	0			
82	B 6	850	1000	550	750	B 6	0			
83	T 7	900		500		T 7	0			
84	B 7	900	1000	750	650	B 7	0			
85	T 8	900		970		T 8	120	400		
86	B 8	900	1050	450	700	B 8	0			
87	T 9	900		500		T 9	0			
88	B 9	900	900	600	700	B 9	0			
89	B 10	800	870		300	B 10	0			
90	11-Oct-91 T 1	900		850		T 1	170			P+2
91	B 1	900	1050	550	800	B 1	200			
92	M 1	900				T 2	520			
93	T 2	900		450		B 2	0			
94	B 2	800	1050	800	900	T 3	150			

95	T	3	900		670		B	3	0			
96	T	4	900		700		T	4	0			
97	B	4	900	900	800	550	B	4	0			
98	T	5	900		550		T	5	150			
99	B	5	800	300	600	700	B	5	0			
100	T	6	900		1100		T	6	160			
101	B	6	500	900	1300	800	B	6	0			
102	22-Oct-91	T	1	1200	1150	650	T	1	500	300		
103	Gully	B	1	1200	1200	600	B	1	0			
104	T	2	1200	1100	650		T	2	0	330		
105	B	2	1150	1200	700	650	B	2	270	540	760	
106	T	3	1200	1200	700		T	3	200	480		
107	B	3	1200	1150	500	700	B	3	300	850	1000	
108	T	4	1200	1100	350		T	4	400	460		
109	B	4	1200	1200	600	700	B	4	400	900	500	
110	T	5	1150	1200	450		T	5	500	500		
111	T11	B	5	1200	1200	550	700	B	5	100	650	800
112	T	6	1200	1200	700		T	6	300	700		
113	B	6	1200	1100	650	650	B	6	500	720	600	
114	T	7	1200	1150	650		T	7	400	380		
115	B	7	1200	1150	700	650	B	7	500	400	900	
116	23-Oct-91	T	1	1200	1150	650		T	1	180		
117	Gully	B	1	1200	1100	400	700	B	1	0		
118	T	2	1200	1200	500		T	2	0			
119	B	2	1200	1300	700	650	B	2	0	400		
120	T	3	1200	1150	400		T	3	0			
121	B	3	1200	1200	750	600	B	3	0			
122	T11	T	4	1200	1200	550		T	4	200	700	
123	B	4	1200	1200	650	720	B	4	0			
124	T	5	1200	1150	550		T	5	150	000		
125	B	5	1200	1100	700	560	B	5	700		900	
126	T	6	1200	1100	700		T	6	0	600		
127	B	6	1200	1150	450	640	B	6	530	660	1150	
128	02-Nov-91	T	1	1200				T	1	150		
129	B	1	1200				B	1	20			
130	T	2	1200				T	2	100			
131	B	2	1200				B	2	200			
132	T	3	1200				T	3	220			
133	B	3	1200				B	3	230			
134	T	4	1200				T	4	250			
135	B	4	1150				B	4	300			
136	T	5	1150				T	5	180			
137	B	5	1200				B	5	150			
138	T	6	1200				T	6	80			
139	B	6	1200				B	6	50			
140	T	7	1200				T	7	100			
141	B	7	1200				B	7	100			
142	T	8	1200				T	8	120			
143	B	8	1200				B	8	180			
144	T	9	1200				T	9	220			
145	B	9	1200				B	9	250			

P+3

P+3

P+3

146	T 10	1150
147	B 10	1200
148	T 11	1200
149	B 11	1200
150	T 12	1200
151	B 12	1200
152 TS	T 13	1200
153	B 13	1200
154	T 14	1200
155	B 14	1150
156	T 15	1200
157	B 15	1200
158	T 16	1200
159	B 16	1200
160	T 17	1200
161	B 17	1200
162	T 18	1200
163	B 18	1200
164	T 19	1200
165	B 19	1200
166	T 20	1200
167	B 20	1200
168	T 21	1200
169	B 21	1200
170 Free Face	T 22	1200

T 10	300
B 10	320
T 11	120
B 11	0
T 12	0
B 12	100
T 13	120
B 13	80
T 14	0
B 14	0
T 15	0
B 15	60
T 16	0
B 16	100
T 17	0
B 17	0
T 18	140
B 18	0
T 19	100
B 19	200
T 20	120
B 20	60
T 21	100
B 21	0
T 22	0

**Composition B Primer**  
 From 10 September 1991 to 2 November 1991

# Mines	Date	Pre-Blast Data				Post-Blast Data					
		Hole	Depth	Spacing	Burden	Hole	Socket	Burden	Spacing	Change (PM)	
1	30-Sep-91	T 1	1200	T8	330		T 1	180	450		
2		B 1	1200		500	800	B 1	200	650	1100	
3		T 2	1200		500		T 2	220	720		
4		B 2	1200		600	700	B 2	270	650	1100	
5		T 3	1200		600		T 3	300	700		
6		B 3	1200		600	800	B 3	420	750	1200	
7		T 4	1200		550		T 4	60	650		
8		B 4	1200		550	700	B 4	326	920	950	
9		T 5	1200		550		T 5	40	600		
10		B 5	1300		500	650	B 5	50	600	1000	
11		T 6	1200		550		T 6	210	600		
12		B 6	1200		600	650	B 6	0	650	980	
13		T 7	1200		600		T 7	123	450		
14		B 7	1200		500	550	B 7	70	520	1000	
15		T 8	1200		400		T 8	0	500		
16		B 8	1200		600	600	B 8	100	500	900	
17		T 9	1200		500		T 9	0	600		
18		B 9	1200		550	800	B 9	300	550	930	
19		T 10	1200		400		T 10	0	600		
20		B 10	1200		350	800	B 10	60	650	1100	
21		T 11	1200		500		T 11	60	400		
22		B 11	1200		500	800	B 11	0	500	1100	
23	20-Oct-91	T 1	900	T8	900		T 1	0	600		2
24		B 1	900		650	900	B 1	0	600	1100	2
25		T 2	900		650		T 2	0	500		2
26		B 2	900		700	750	B 2	0	600	900	2
27		T 3	900		500		T 3	0	600		2
28		B 3	900		500	700	B 3	0	700	1150	2
29		T 4	1000		700		T 4	0	800		2
30		B 4	900		600	800	B 4	0	500	1200	2
31		T 5	900		600		T 5	100	500		2
32		B 5	900		700	800	B 5	0	600	1100	2
33		T 6	900		600		T 6	0	300		2
34		B 6	900		800	830	B 6	150	450	1100	2
35		T 7	1100		600		T 7	0			2
36		B 7	1000		400	850	B 7	0		1200	3
37		T 8	1100		650		T 8	200	150		3
38		B 8	1000		550	800	B 8	420		1100	3
39		T 9	1100		500		T 9	270	750		3
40		B 9	1000		700	700	B 9	400	700	800	3
41		T 10	1100		400		T 10	300	700		3
42		B 10	1000		600	730	B 10	120	800	900	3
43		T 11	1000				T 11	720	650		3

44		B 11	900			1300		H 11	0	700	1100	2
45	55g02-Oct-91	T 1	1100			550		T 1	320	550		4
46		B 1	1100	1100		650	650	B 1	600	600	850	3
47		C 2	1100			600		T 2	520	800		2
48		E 2	1100	1000		450	800	B 2	600	850	750	3
49		T 3	1100			650		T 3	50			3
50		H 3	1100	1100		600	700	B 3	300		1000	3
51		T 4	1100			650		T 4	0			3
52		B 4	1100	1200		650	700	B 4	0			2
53		T 5	1100			500		T 5	150	650		2
54		B 5	1100	1200		700	750	B 5	150	700	1250	3
55		T 6	1100			550		T 6	150			3
56		B 6	1050	1300		450	850	B 6	0			3
57		T 7	900			500		T 7	0			2
58		B 7	900	1200		650	750	B 7	0			2
59		T 8	900			600		T 8	0			2
60		H 8	900	1200		450	750	B 8	50			2
61		T 9	900			500		T 9	0			1
62		B 9	900	1250		550	800	H 9	0			2
63		T 10	900			750		T 10	0			2
64		B 10	900	1250		700	650	B 10	0			2
65		T 11	900			600		T 11	0			2
66		B 11	900	1200		600	700	B 11	0			2
67		T 12	900			500		T 12	0			2
68		B 12	900	1150		650	700	B 12	0			2
69	35g03-Oct-91	T 1	1100			400		T 1	130	400		2
70		B 1	1100	1000		600	700	B 1	0	800	1350	2
71		M 1	1100			300	300	M 1	100	800	350	3
72		T 2	1100			600		T 2	270	1000		3
73		B 2	1100	1000		800	600	B 2	50	1050	1050	3
74		H 2	1100	1100		600	400	H 2	100	850	400	3
75		C 3	1100			600		T 3	0	700		3
76		F 3	1100	1200		700	700	E 3	0	1500	800	3
77		M 3	1100			650	350	M 3	0	600	350	3
78		T 4	1100			700		T 4	150	1100		3
79		B 4	900	1400		550	800	L 4	170		1100	3
80		M 4	1100	1350		550	450	M 4	270		450	2
81		T 5	1100			850		T 5	50	600		2
82		H 5	1100	1300		550	850	B 5	0			2
83		T 6	1100			600		T 6	0	750		2
84		B 6	1100	1100		700	800	B 6	0			2
85		T 7	1100			500		T 7	0	400		2
86		B 7	1100	1150		500	800	B 7	0			2
87		T 8	1100			600		T 8	0	300		2
88		B 8	1100	1200		650	700	H 8	0			2
89		T 9	1100			450		T 9	0	700		2
90		B 9	1000	1200		500	750	H 9	0			2
91		T 10	1100			600		T 10	0	550		2
92		B 10	1000	1250		600	750	B 10	0			2
93		T 11	1100			500		T 11	0	400		2
94		B 11	1100	1100		600	800	B 11	0			2



95		T 12	1100		700		T 12	0	600		3
96		B 12	1100	1050	650	850	B 12	0			3
97		T 13	1150	1050	500		T 13	0	300		3
98	35g 14-Oct-91	T 1	1100		550		T 1	600	500		
99		B 1	1100	1100	600	700	B 1	500	700	600	
100		M 1	1100		650	400	M 1	500	600	400	
101		T 2	1100		750		T 2	600	800		
102		B 2	1100	1150	800	650	B 2	700	700	650	
103		M 2	1100		700	350	M 2	200	700	300	
104		T 3	1100		700		T 3	250	600		
105		B 3	1100	1200	600	700	B 3	250	600	700	
106		M 3	1100		550	300	M 3	200	500		
107		T 4	1100		450		T 4	600	420		
108		B 4	1100	1300	700	900	B 4	100		750	
109		M 4	1100		600	350	M 4	200			
110		T 5	1100		450		T 5	0			
111		B 5	1100	1300	600	800	B 5	0			
112		T 6	1100		600		T 6	0			
113		B 6	1100	1300	650	850	B 6	0			
114		T 7	1100		700		T 7	0			
115		B 7	1100	1200	700	650	B 7	0			
116		T 8	1100		550		T 8	0			
117		B 8	1100	1200	600	600	B 8	0			
118		T 9	1100		550		T 9	0			
119		B 9	1100	1150	550	650	B 9	0			
120		T 10	1100		500		T 10	0			
121		B 10	1100	1100	600	700	B 10	0			
122		T 11	1100		600		T 11	150			
123		B 11	1200	1200	500	750	B 11	0			
124		T 12	1200		1000		T 12	0			
125		B 12	1200	1250	900	650	B 12	50			
126	20g 22-Oct-91	T 1	1200	1170	650		T 1	100	450		P+3
127		B 1	1200	1150	700	650	B 1	150	500	1150	
128		T 2	1200	1100	650		T 2	100	400		
129		B 2	1100	1200	700	700	B 2	300	800	1200	
130		T 3	1200	1200	550		T 3	250	800		
131		B 3	1200	1150	600	800	B 3	80	600	1200	
132		T 4	1200	1100	600		T 4	100	600		
133		B 4	1100	900	800	900	B 4	0	600	1200	
134	211	T 5	1100	1200	650		T 5	0	600		
135		B 5	1200	1200	700	650	B 5	0	620	1200	
136		T 6	1100	1150	700		T 6	0	590		
137		B 6	1200	1200	700	700	B 6	0	650	1150	
138		T 7	1100	1100	650		T 7	40	420		
139		B 7	1200	1200	650	900	B 7	0	300	1200	
140		T 8	1200	1200	500		T 8	80	500		
141		B 8	1100	1100	650	650	B 8	0	600	1200	
142		T 9	1200	1200	650		T 9	0	500		
143	Gully	B 9	1200	1200	700	600	B 9	0	550	150	
144	20g 23-Oct-91	T 1	1200		550		T 1	400	400		P+3
145		B 1	1200	1200	700	580	B 1	200	750	1150	

146		T	2	1200		450		T	2	130	550		
147		H	2	1200	1240	750	750	H	2	0	700	920	
148		T	3	1200		750		T	3	200	650		
149		B	3	1400	1250	720	860	B	3	250	450	1000	
150	RJ1	F	4	1200		700		T	4	50	650		
151		B	4	1200	1350	700	800	B	4	150	680	1100	
152		T	5	1200		470		T	5	0	700		
153		B	5	1200	1300	680	800	B	5	80	650	1000	
154		T	6	1200		750		T	6	120	700		
155		A	6	1200	1200	650	700	B	6	0	600	1150	
156	Gully	T	7	1200	1200	400		T	7	0	600		
157	23q28-Oct-91	T	1	1200	1300	650		T	1	0	450		P+1
158		R	1	1200	1350	700	680	B	1	450	1150	980	
159		T	2	1150	1200	300		T	2	250	650		B+1
160		B	2	1150	1250	550	550	B	2	370	500	840	B+1
161		T	3	1200	1200	700		T	3	230	1000		
162		B	3	1200	1200	550	650	B	3	400	750	900	
163		T	4	1200	1250	550		T	4	300	800		
164		B	4	1200	1200	650	600	B	4	0		750	
165		T	5	1200	1200	500		T	5	0			
166	35q29-Oct-91	T	1	1200		490		T	1	320	600		P+2
167		B	1	1200	1350	720	700	B	1	400	600	700	
168		T	2	1200		600		T	2	60	670		
169		B	2	1200	1450	720	670	B	2	300	720	600	
170	T11	T	3	1200		770		T	3	100	590		
171		B	3	1200	1400	550	730	B	3	220	630	650	
172		T	4	1300		1550		T	4	100	800		
173	Gully	B	4	1200	1150	1300	650	B	4	50	720	700	
174	35q30-Oct-91	T	1	1200		600		T	1	350	550		P+3
175		H	1	1150	1200	700	650	H	1	420	600	650	
176		T	2	1200		650		T	2	500	700		
177		H	2	1200	1300	650	700	B	2	620	600	700	
178	T11	T	3	1200		400		T	3	480	450		
179		B	3	1200	1250	500	720	B	3	240	500	720	
180		T	4	1150		600		T	4	320	500		
181	Gully	B	4	1200	1200	700	640	B	4	300	700	600	
182	35q30-Oct-91	T	1	1200		550		T	1	220	500		P+3
183		B	1	1200		750	720	B	1	200	500	700	
184		T	2	1200		600		T	2	100	700		
185		B	2	1150		700	760	B	2	160	600	700	
186	T8	T	3	1200		400		T	3	300	600		
187		B	3	1200		450	700	B	3	220	650	750	
188		T	4	1200		400		T	4	80	550		
189		B	4	1200		300	680	B	4	120	300	650	
190	35q31-Oct-91	T	1	1200		650		T	1	200	600		P+3
191		B	1	1200	1250	700	650	B	1	150	650	700	
192		T	2	1200		600		T	2	280	760		
193		B	2	1200	1300	750	700	B	2	300	650	700	
194	T11	T	3	1200		700		T	3	240	750		
195		B	3	1250	1150	500	700	B	3	260	600	650	
196		T	4	1200		700		T	4	150	650		

197		B 4	1200	1:50	600	650	B 4	120	700	500	
198	31-Oct-91	T 1	1200		700		T 1	100	650		F-3
199		B 1	1200		750	650	B 1	100	700	700	
200		T 2	1200		500		T 2	120	650		
201		B 2	1200		600	700	B 2	200	650	650	
202		T 3	1200		700		T 3	0	720		
203		B 3	1200		650	750	B 3	0	600	700	
204		T 4	1200		650		T 4	50	650		
205		B 4	1200		750	700	B 4	0	700	700	
206		T 5	1200		400		T 5	200	500		
207	T8	B 5	1250		550	650	B 5	0	600	600	
208		T 6	1200		600		T 6	0	620		
209		B 6	1200		500	500	B 6	0	600	600	
210		T 7	1200		600		T 7	0	600		
211		B 7	1200		700	500	B 7	0	750	550	
212		T 8	1250		650		T 8	120	650		
213		B 8	1200		650	700	B 8	80	650	730	
214		T 9	1200		700		T 9	100	700		
215		B 9	1200		600	650	B 9	150	600	650	
216		T 10	1200		600		T 10	0	650		
217		B 10	1200		600	700	B 10	0	650	720	
218		T 11	1200		650		T 11	0	600		
219		B 11	1250		700	650	B 11	160	700	650	
220		T 12	1200		400		T 12	0	550		
221	35g01-Nov-91	B 1	1200		650		B 1	200	400		P-3
222		T 1	1200		700	650	T 1	300	650	700	
223		B 2	1200		700		B 2	150	700		
224		T 2	1200		600	700	T 2	0	650	700	
225		B 3	1150		600		B 3	0	720		
226		T 3	1200		600	700	T 3	0	650	650	
227		B 4	1200		650		B 4	0	550		
228		T 4	1200		600	700	T 4	0	600	700	
229		B 5	1200		650		B 5	150	650		
230		T 5	1200		650	650	T 5	120	600	700	
231		B 6	1200		700		B 6	0	600		
232		T 6	1150		800	600	T 6	0	720	650	
233		B 7	1200		750		B 7	100	700		
234		T 7	1200		700	600	T 7	80	600	600	
235		B 8	1200		700		B 8	100	720		
236		T 8	1150		700	650	T 8	120	650	650	
237	T6	B 9	1200		600		B 9	0	600		
238		T 9	1200		500	700	T 9	160	550	650	
239		B 10	1200		400		B 10	0	400		
240		T 10	1200		550	650	T 10	0	600	700	
241		B 11	1150		500		B 11	100	500		
242		T 11	1200		610	600	T 11	50	600	650	
243		B 12	1200		650		B 12	0	700		
244		T 12	1200		650	700	T 12	50	650	650	
245		B 13	1250		600		B 13	100	600		
246		T 13	1150		650	650	T 13	0	650	650	
247		B 14	1200		650		B 14	0	650		

248	R 14	1200	600	650	H 14	0	600	700
249	T 15	1200	700		T 15	30	650	
250	B 15	1200	500	600	B 15	30	550	700

Standard Primer  
From 27 January 1992 to 19 February 1992

#	Date	Pre-Blast Data					Post-Blast Data				Charge
		Hole	Depth	Stoping	Burden	Spacing	Hole	Socket	Burden	Spacing	
1	14-Feb-92	T 1	1200		600		T 1	150	550		P-3
2		B 1	1200	1000	720	600	B 1	80	700	650	
3		T 2	1200		600		T 2	0	650		
4		B 2	1200	1150	650	700	B 2	100	650	700	
5		T 3	1200		500		T 3	120	500		
6		B 3	1200	1000	640	700	B 3	160	660	720	
7		T 4	1200		560		T 4	100	500		
8		B 4	1200	1150	700	800	B 4	0	700	750	
9		T 5	1200		700		T 5	140	600		
10		B 5	1200	1200	410	820	B 5	100	500	800	
11		T 6	1200		650		T 6	80	500		
12		B 6	1200	1200	600	700	B 6	50	650	650	
13		T 7	1200		600		T 7	100	620		
14		B 7	1200	1250	650	680	B 7	0	650	640	
15		T 8	1200		400		T 8	0	500		
16		B 8	1200	1200	550	720	B 8	0	570	680	
17		T 9	1200		600		T 9	100	550		
18		B 9	1200	1100	750	790	B 9	120	700	750	
19		T 10	1200		600		T 10	160	550		
20		B 10	1200	1200	400	600	B 10	200	450	820	
21		T 11	1200				T 11	0	500		

**Composition B Primer**  
 From 27 January 1992 to 19 February 1992

Pre-Blast Data							Post-Blast Data				Charge
# Mine	Date	Hole	Depth	Sloping	Burden	Spacing	Hole	Socket	Burden	Spacing	
1	75g27-Jan-92	T 1	1200		400		T 1	600	780		P+3
2		B 1	1200	1300	550	650	B 1	230	600	1100	
3		T 2	1200		500		T 2	780			
4		B 2	1300	1350	550	700	B 2	75			
5		T 3	1200		400		T 3	500			
6		B 3	1200	1150	500	700	B 3	0			
7		T 4	1200		620		T 4	60			
8		B 4	1200	1050	700	710	B 4	0	1000		
9		T 5	1200		500		T 5	0	850		
10		B 5	1200	1100	550	710	B 5	0			
11		T 6	1150		500		T 6	30	650		
12		B 6	1200	1080	310	750	B 6	0		850	
13		T 7	1200		500		T 7	0	1100		
14		B 7	1150	1130	580	920	B 7	15			
15		Face	T 8	1200	1000		T 8	250			
16	75g28-Jan-92	T 1	1200		550		T 1	220	580		P-3
17		B 1	1200	1100	400	600	B 1	140	500	550	
18		T 2	1200		600		T 2	60	550		
19		B 2	1200	1150	650	710	B 2	0	500	720	
20		T 3	1200		500		T 3	0	470		
21		B 3	1200	1100		730	B 3	0		700	
22	T 4	1200	1000			T 4	40				
23	75g30-Jan-92	T 1	1200		400		T 1	280	350		P+3
24		M 1	1200		600		M 1	220	600		
25		B 1	1190	1100	550	600	B 1	240	550	650	
26		T 2	1200		500		T 2	180	450		
27		M 2	1200		430		M 2	200	600		
28		B 2	1200	1200	400	630	B 2	150	500	600	
29		T 3	1200		430		T 3	50	500		
30		M 3	1200		600		M 3	60	400		
31		B 3	1200	1150	700	700	B 3	0	550	720	
32		T 4	1190		650		T 4	0	700		
33		M 4	1200		320		M 4	60	450		
34		B 4	1200	1200	550	650	B 4	0	600	600	
35	T 5	1200		600		T 5	0	700			
36	M 5	1200		700		M 5	0	650			
37	B 5	1200	1250	430	680	B 5	20	600	700		
38	75g31-Jan-92	T 1	1200		800		T 1	360	600		P+3
39		M 1	1200		700		M 1	840	3		
40		B 1	1200	1200	850	600	B 1	0	760	800	
41		T 2	1190		740		T 2	100	470		
42		M 2	1200		820		M 2	100			
43		Square	B 2	1200	1180	700	900	B 2	570	450	

44	Side	T 3	1200		650		T 3	400	420	
45		B 3	1200	1200	650	950	B 3	420	350	950
46		T 4	1200		740		T 4	340	300	
47		B 4	1200	1200	650	1000	B 4	230	420	350
48		T 5	1200		500		T 5	90	550	
49		B 5	1200	1300	550	1020	B 5	380	500	600
50		T 6	1200		500		T 6	350	600	
51		B 6	1200	1300	550	1100	B 6	280	600	1000
52	75g31-Jan-92	T 1	1200		750		T 1	100	800	
53		B 1	1200	1100	1000	1000	B 1	10	1020	890
54		T 2	1190		1250		T 2	90	1250	
55		B 2	1200	900	900	900	B 2	0	900	800
56		T 3	1200		700		T 3	180	750	
57		B 3	1210	980	800	700	B 3	230	750	770
58		T 4	1200		1000		T 4	60	900	
59	Stick-	B 4	1200	1500	1100	750	B 4	50	1070	780
60	wide	T 5	1200		1150		T 5	0		
61		B 5	1200	1030	1000	750	B 5	60		750
62		T 6	1200		900		T 6	0		
63		B 6	1200	1100	750	900	B 6	0		
64	75g10-Feb-92	T 1	1200		700		T 1	250	700	
65		B 1	1200		600	700	B 1	150		
66		T 2	1200	1100	600	700	T 2	130	620	700
67		B 2	1200		650		B 2	180	650	
68		T 3	1200	1100	600	750	T 3	0	600	750
69		B 3	1200	1250	720	600	B 3	90	650	
70		T 4	1200		750	600	T 4	120	750	650
71		B 4	1200		600		B 4	80	620	
72	Square-	T 5	1200	1150	550	680	T 5	60	500	700
73	side	B 5	1200	1250	650	700	B 5	100	700	
74		T 6	1200		700	700	T 6	120	680	650
75		B 6	1200		750		B 6	140	750	
76		T 7	1190	1300	600	550	T 7	260	600	600
77		B 7	1200		550		B 7	240	550	
78		T 8	1200	1250	600	650	T 8	180	640	650
79		B 8	1200		450		B 8	0	500	
80		T 9	1200	1300	500	700	T 9	180	500	700
81		B 9	1200		550		B 9	140	500	
82		T 10	1200	1300	600	720	T 10	0	500	700
83		B 10	1200		550		B 10	0	500	
84		T 11	1200	1350	650	960	T 11	80	600	800
85		B 11	1200		600		B 11	0	600	
86		T 12	1200	1300	500	740	T 12	60	540	780
87		B 12	1200		400		B 12	0	400	
88		T 13	1200	1350	550	700	T 13	0	500	750
89		B 13	1200		600		B 13	0	550	
90	95g11-Feb-92	T 1	1200		600		T 1	120	600	
91		B 1	1200	1150	700	600	B 1	80	720	600
92		T 2	1200		500		T 2	50	500	
93		B 2	1200	1000	600	550	B 2	100	650	600
94		T 3	1200		650		T 3	0	700	

95	B 3	1200	1250	760	650	B 3	0	650	650
96	T 4	1200		650		T 4	50	600	
97	B 4	1200	1000	610	650	B 4	100	600	700
98	T 5	1200		700		T 5	120	650	
99	B 5	1200	1100	650	700	B 5	50	650	720
100	T 6	1200		600		T 6	0	550	
101	B 6	1200	1250	650	720	B 6	0	680	680
102	T 7	1150		700		T 7	0	650	
103	B 7	1200	1300	700	700	B 7	0	700	650
104	T 8	1200		650		T 8	20	600	
105	B 8	1200	1300	550	750	B 8	50	550	750
106	T 9	1200		400		T 9	100	500	
107	B 9	1200	1320	450	750	B 9	80	500	720
108	T 10	1200		560		T 10	70	530	
109	B 10	1200	1330	500	700	B 10	130	500	740
110	T 11	1200		400		T 11	120	450	
111	B 11	1200	1350	600	720	B 11	80	600	720
112	T 12	1200		450		T 12	160	430	
113	B 12	1200	1360	400	700	B 12	220	450	740
114	T 13	1200		650		T 13	200	650	
115	B 13	1200	1400	700	740	B 13	180	700	740
116	T 14	1200		640		T 14	160	650	
117	B 14	1200	1480	600	760	B 14	100	650	700
118	T 15	1200		740		T 15	0	750	
119	B 15	1200	1450	650	700	B 15	0	600	700
120	T 16	1200		550		T 16	100	600	
121	B 16	1200	1400	600	720	B 16	80	620	700
122	Stope in reins T 1	1200		650		T 1	100	600	
123	B 1	1200	900	600	600	B 1	80	550	650
124	T 2	1200		540		T 2	0	600	
125	B 2	1200	950	400	750	B 2	0	450	700
126	T 3	1200		500		T 3	0	500	
127	B 3	1200	800	700	600	B 3	0	650	600
128	T 4	1200		650		T 4	0	650	
129	B 4	1200	1000	700	600	B 4	60	650	600
130	T 5	1200		400		T 5	120	420	
131	B 5	1200	1050	350	650	B 5	130	450	650
132	T 6	1200		600		T 6	60	600	
133	B 6	1200	1000	400	700	B 6	80	400	720
134	95g17-Feb-32 T 1					T 1	100	550	
135	B 1					B 1	120	650	700
136	T 2					T 2	0	650	
137	B 2					B 2	0	600	700
138	T 3					T 3	80	600	
139	B 3					B 3	60	500	760
140	T 4					T 4	100	600	
141	B 4					B 4	180	600	720
142	T 5					T 5	240	700	
143	B 5					B 5	100	700	750
144	T 6					T 6	120	600	
145	B 6					B 6	160	600	760



146	T 7							0	550	
147	B 7							0	550	700
148	T 8							0	600	
149	B 8							0	460	730
150	T 9							140	600	
151	B 9							00	600	780
152	T 10							60	670	
153	B 10							40	700	800
154	T 11							120	460	
155	B 11							180	650	700
156	95g15-Feb-52 T 1	1200		700				120	650	
157	B 1	1200	1100	650	800			100	650	750
158	T 2	1200		600				100	600	
159	B 2	1200	1150	600	720			80	600	700
160	T 3	1200		640				0	600	
161	B 3	1200	1000	700	100			0	600	800
162	T 4	1190		720				0	700	
163	B 4	1200	1180	640	700			70	650	700
164	T 5	1200		560				220	600	
165	B 5	1200	1150	600	950			200	600	900
166	T 6	1200		660				0	650	
167	B 6	1200	1200	420	950			140	460	950
168	T 7	1200		700				120	700	
169	B 7	1200	1100	650	800			80	650	900
170	T 8	1200		450				0	500	
171	B 8	1200	1000	600	720			0	600	750
172	T 9	1200		610				60	620	
173	B 9	1200	1000	730	740			50	700	750
174	T 10	1200		460				0	400	
175	B 10	1200	1150	700	800			20	700	800
176	T 11	1200		700				60	700	
177	B 11	1200	1100	620	860			80	650	900

**Standard Primer**  
 From 11 September 1992 to 2 October 1992

Pre-Blast Data						Post-Blast Data				
#	Date	Hole	Depth	Staging	Burden	Spacing	Hole	Socket	Burden	Spacing
1	11-Sep-92	T 1	1200		450		T 1	50	400	
2		B 1	1200	600	500	600	B 1	0		
3		T 2	1200		600		T 2	650	700	
4		B 2	1200	750	500	600	B 2	450	700	600
5		T 3	1200		550		T 3	250	800	
6		B 3	1200	700	500	500	B 3	200	800	700
7		T 4	1200		400		T 4	250	900	
8		B 4	1200	700	650	500	B 4	100	900	600
9		T 5	1190		700		T 5	0	350	
10		B 5	1200	650	650	600	B 5	0	400	700
11		T 6	1200		500		T 6	0	500	
12		B 6	1200	1000	400	800	B 6	400	600	650
13		T 7	1200		350		T 7	400	750	
14		B 7	1200	1100	600	850	B 7	450	750	600
15		T 8	1200		650		T 8	500	1000	
16		B 8	1200	1000	700	900	B 8	600	700	600
17		T 9	1200		600		T 9	0	250	
18		B 9	1200	1200	650	1000	B 9	100	400	750
19		T 10	1200		800		T 10	100	600	
20		B 10	1190	1000	600	850	B 10	100	400	800
21		T 11	1200		400		T 11	300	1000	
22		B 11	1200	950	650	700	B 11	150	600	800
23		T 12	1200		400		T 12	0		
24		B 12	1200	900	500	650	B 12	0		
25	16-Sep-92	T 13	1200		550		T 13	0	500	
26		B 13	1200	1100	600	700	B 13	0	700	600
27		T 14	1200		500		T 14	150	700	
28		B 14	1200	950	600	500	B 14	0		
29		T 15	1200		550		T 15	0	700	
30		B 15	1200	1000	600	650	B 15	0		
31		T 16	1200		600		T 16	0	350	
32		B 16	1200	900	500	650	B 16	0		
33		T 17	1200		500		T 17	0		
34		B 17	1200	900	650	650	B 17	0		
35	14-Sep-92	T 18	1200		500		T 18	0		
36		B 18	1200		500		B 18	0		
37		T 19	1200		500		T 19	0		
38		B 19	1200		500		B 19	0		
39		T 1	1200		400		T 1	400	550	
40		B 1	1200		450		B 1	450	700	500
41		T 2	1200		500		T 2	500	500	
42		B 2	1200		350		B 2	350	500	600
43		T 3	1200		300		T 3	300	500	
44		B 3	1200		250		B 3	250	600	500
45		T 4	1200		0		T 4	0	550	
46		B 4	1200		100		B 4	100	700	700
47		T 5	1200		150		T 5	150	600	

44	B 5	1200				B 5	100	400	700
45	T 6	1200				T 6	160	450	
46	B 6	1200				B 6	200	500	600
47	T 7	1200				T 7	300	500	
48	B 7	1200				B 7	350	600	500
49	T 8	1200				T 8	400	550	
50	B 8	1200				B 8	400	500	400
51	T 9	1200				T 9	400	600	
52	B 9	1200				B 9	350	600	500
53	T 10	1200				T 10	200	600	
54	B 10	1200				B 10	250	600	500
55	T 11	1200				T 11	500	600	
56	B 11	1200				B 11	100	550	500
57	T 12	1200				T 12	150	400	
58	B 12	1200				B 12	100	450	550
59	T 13	1200				T 13	120	550	
60	B 13	1200				B 13	160	500	600
61	T 14	1200				T 14	0		
62	B 14	1200				B 14	0		
63	T 15	1200				T 15	100	500	
64	B 15	1200				B 15	180	600	500
65	T 16	1200		400		T 16	100	400	
66	B 16	1200	500	450	300	B 16	0	400	350
67	T 17	1200		400		T 17	0	450	
68	B 17	1200	600	500	400	B 17	0	500	400
69	T 18	1200		450		T 18	120	400	
70	B 18	1200	600	450	400	B 18	80	450	450
71	T 19	1200		450		T 19	100	400	
72	B 19	1200	750	450	450	B 19	160	450	450
73	T 20	1200		450		T 20	200	450	
74	B 20	1200	650	450	500	B 20	250	600	500
75	T 21	1200		650		T 21	100	500	
76	B 21	1200	750	500	450	B 21	100	600	450
77	T 22	1200		600		T 22	50	550	
78	B 22	1200	550	600	400	B 22	0	650	500
79	T 23	1200		680		T 23	0	400	
80	B 23	1200	600	650	400	B 23	100	400	400
81	T 24	1200		450		T 24	100	500	
82	B 24	1200	500	450	400	B 24	0	600	500
83	T 25	1200		500		T 25	0	600	
84	B 25	1200	500	500	400	B 25	0	700	500
85	30-Sep-92 T 1	1200		400		T 1	600	400	
86	B 1	1200	600	500	400	B 1	500	500	500
87	T 2	1200		400		T 2	500	400	
88	B 2	1200	700	400	550	B 2	250	450	500
89	T 3	1200		400		T 3	600	500	
90	B 3	1200	600	450	500	B 3	200	500	500
91	T 4	1200		500		T 4	220	500	
92	B 4	1200	700	500	600	B 4	200	500	600
93	T 5	1200		500		T 5	0	400	
94	B 5	1200	700	400	600	B 5	100	400	700

501

95	T 6	1200		350		T 6	0	400	
96	B 6	1200	800	500	500	B 6	400	500	700
97	T 7	1200		600		T 7	400	500	
98	E 7	1200	500	500	450	E 7	400	500	500
99	T 8	1200		600		T 8	400	400	
100	B 8	1200	700	500	500	B 8	0	500	700
101	T 9	1200		400		T 9	100	350	
102	B 9	1200	500	500	300	B 9	0	500	300
103	T 10	1200		400		T 10	150	400	
104	B 10	1200	500	500	300	B 10	0	500	450
105	T 11	1200		600		T 11	0	550	
106	B 11	1200	700	450	400	B 11	0	500	400
107	T 12	1200		500		T 12	0	450	
108	B 12	1200	700	400	500	B 12	0	500	500
109	T 13	1200		500		T 13	0	500	
110	B 13	1200	700	600	500	B 13	100	700	500
111	T 14	1200		500		T 14	0	500	
112	B 14	1200	800	500	600	B 14	0	550	600
113	T 15	1200		400		T 15	100	400	
114	B 15	1200	700	500	500	B 15	100	300	500
115	T 16	1200		400		T 16	150	500	
116	B 16	1200	700	550	500	B 16	100	550	500
117	T 17	1200		500		T 17	100	500	
118	B 17	1200	800	600	600	B 17	0	550	600
119	T 18	1200		500		T 18	100	500	
120	B 18	1200	800	500	600	B 18	50	500	600
121	T 19	1200		500		T 19	150	600	
122	B 19	1200	700	450	550	B 19	0	500	500
123	T 20	1200		600		T 20	200	500	
124	B 20	1200	700	300	500	B 20	200	650	550
125	T 21	1200		500		T 21	300	500	
126	B 21	1200	600	400	450	B 21	500	550	500
127	T 22	1200		600		T 22	500	600	
128	B 22	1200	550	600	400	B 22	400	600	400
129	T 23	1200		500		T 23	350	500	
130	B 23	1200	700	500	500	B 23	400	400	500
131	T 24	1200		450		T 24	0	500	
132	B 24	1200	700	550	500	B 24	0	500	500
133	T 25	1200		300		T 25	0	450	
134	B 25	1200	600	500	400	B 25	0	500	500
135	T 26	1200		600		T 26	0	600	
136	B 26	1200	600	400	400	B 26	300	500	500
137	T 27	1200		500		T 27	0	600	
138	B 27	1200	800	500	600	B 27	0	500	600
139	T 28	1200		550		T 28	0	500	
140	B 28	1200	400	550	550	B 28	150	400	500
141	T 29	1200		500		T 29	200	500	
142	B 29	1200	600	500	550	B 29	0	450	500
143	T 30	1200		500		T 30	0	400	
144	B 30	1200	800	500	600	B 30	0	500	700
145	T 31	1200		500		T 31	100	600	

146	B 31	1200	800	500	600	B 31	120	500	800
147	T 32	1200				T 32	50		
148	12-Oct-92 T 1	1200		300		T 1	500	450	
149	B 1	1200	700	400	900	B 1	450	500	600
150	T 2	1200		600		T 2	300	500	
151	B 2	1200	700	550	550	B 2	300	400	500
152	T 3	1200		500		T 3	250	500	
153	B 3	1200	600	500	500	B 3	500	500	500
154	T 4	1200		600		T 4	400	550	
155	B 4	1200	700	400	500	B 4	400	400	500
156	T 5	1200		500		T 5	250	450	
157	B 5	1200	800	500	650	B 5	200	400	600
158	T 6	1200		350		T 6	200	600	
159	B 6	1200	900	500	600	B 6	150	600	700
160	T 7	1200		600		T 7	100	550	
161	B 7	1200	700	500	550	B 7	0	400	700
162	T 8	1200		550		T 8	0	500	
163	B 8	1200	600	500	500	B 8	0	400	500
164	T 9	1200		500		T 9	100	700	
165	B 9	1200	600	600	400	B 9	100	300	500
166	T 10	1200		400		T 10	80	350	
167	B 10	1200	600	400	400	B 10	50	500	400
168	T 11	1200		450		T 11	0	400	
169	B 11	1200	600	500	450	B 11	0	350	450
170	T 12	1200		500		T 12	0	400	
171	B 12	1200	700	450	500	B 12	0	500	500
172	T 13	1200		500		T 13	100	500	
173	B 13	1200	600	600	450	B 13	100	600	600
174	T 14	1200		500		T 14	100	700	
175	B 14	1200	800	500	650	B 14	150	500	500
176	T 15	1200		400		T 15	300	400	
177	B 15	1200	800	500	600	B 15	150	400	500
178	T 16	1200		500		T 16	0	500	
179	B 16	1200	700	500	500	B 16	0	550	600
180	T 17	1200		550		T 17	0	500	
181	B 17	1200	800	600	650	B 17	100	600	700
182	T 18	1200		300		T 18	200	550	
183	B 18	1200	800	500	600	B 18	250	500	600
184	T 19	1200		450		T 19	200	500	
185	B 19	1200	800	500	600	B 19	100	500	600
186	T 20	1200		500		T 20	150	600	
187	B 20	1200	700	350	500	B 20	300	400	700
188	T 21	1200		400		T 21	250	350	
189	B 21	1200	600	500	450	B 21	200	500	500
190	T 22	1200		550		T 22	0	500	
191	B 22	1200	550	600	500	B 22	100	450	500
192	T 23	1200		600		T 23	150	400	
193	B 23	1200	600	550	500	B 23	80	350	550
194	T 24	1200		600		T 24	100	500	
195	B 24	1200	500	400	350	B 24	100	600	400
196	T 25	1200		400		T 25	150	400	

197	B 25	1200	500	330	450	B 25	0	550	400
198	T 26	1200		330		T 26	0	500	
199	E 26	1200	500	400	400	E 26	0	530	500

Super-Galvanic Primer  
From 11 September 1992 to 2 October 1992

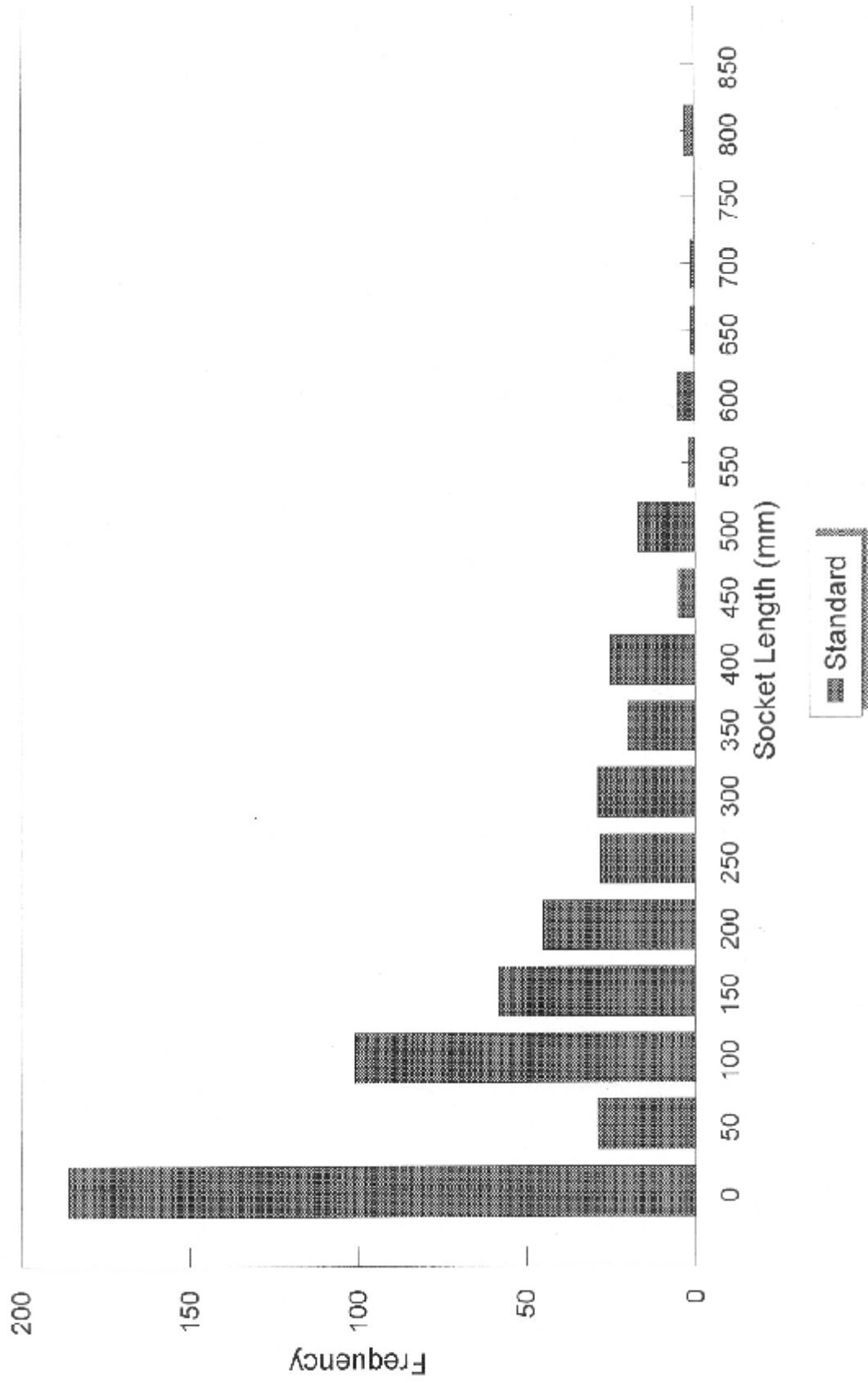
Pre-Blast Data				Post-Blast Data							
#	Date	Time	Depth	Spacing	Barren	Spacing	Notes	Socket	Barren	Spacing	Notes
1	15-Sep-92	2 1	1200		500	400	T 1	200	500	500	0
2		D 1	1200	700	700		B 1	300	650	500	10000
3		T 2	1200		600		T 2	450	600	600	0
4		D 2	1200	700	550	600	B 2	100	500	600	2500
5		T 3	1200		550		T 3	150	600	600	2500
6		D 3	1200	750	500	600	B 3	50	550	550	2500
7		T 4	1200		650		T 4	0	600	600	2500
8		B 4	1200	800	750	600	B 4	0	700	700	10000
9		T 5	1200		700		T 5	0	700	700	0
10		D 5	1200	800	700	650	B 5	0	700	650	0
11		T 6	1200		700		T 6	100	600	600	10000
12		B 6	1200	800	600	650	B 6	0	650	600	2500
13		T 7	1200		650		T 7	150	600	600	22500
14		B 7	1200	850	750	600	B 7	0	750	700	10000
15		T 8	1200		750		T 8	0	700	2500	0
16		B 8	1200	800	650	600	B 8	100	650	600	0
17		T 9	1200		600		T 9	50	600	600	0
18		B 9	1200	800	700	700	B 9	150	700	750	2500
19		T 10	1200		600		T 10	0	700	600	0
20		B 10	1200	650	600	550	B 10	100	600	600	2500
21		T 11	1200		700		T 11	0	550	600	0
22		B 11	1200	800	700	600	B 11	0	700	600	0
23		T 12	1200		800		T 12	0	650	22500	0
24		D 12	1200	850	900	700	B 12	100	900	700	0
25		T 13	1200		750		T 13	150	700	2500	0
26		B 13	1200	650	950	650	B 13	200	900	700	2500
27		T 14	1200		700		T 14	400	750	2500	0
28		D 14	1200	900	650	700	B 14	350	600	750	2500
29		T 15	1200		600		T 15	300	700	10000	0
30		B 15	1200	650	650	650	B 15	100	700	700	2500
31		T 16	1200		550		T 16	0	550	600	0
32		B 16	1200	900	600	650	B 16	100	600	600	2500
33		T 17	1200		650		T 17	150	600	2500	0
34		B 17	1200	600	600	650	B 17	50	650	700	2500
35		T 18	1200		600		T 18	100	600	600	0
36		B 18	1200	500	550	600	B 18	0	550	650	0
37		T 19	1200				T 19	0		700	0
38		B 19	1200	900	600	600	B 19	0	700	700	10000
39	16-Sep-92	T 1	1200		600		T 1	0	700	10000	57339
40		B 1	1200	950	500	600	B 1	350	500	800	48000
41		T 2	1200		600		T 2	600	700	10000	0
42		B 2	1200	700	750	550	B 2	500	800	700	22500
43		T 3	1200		450		T 3	0	400	2500	0

44	B 3	1200	700	650	350	B 3	0	550	500	10000	22500
45	T 4	1200	600	550	450	B 4	100	900	122500	0	0
46	T 5	1200	600	650	500	T 5	220	800	600	2500	22500
47	B 5	1200	700	500	500	B 5	120	600	700	0	40000
48	T 6	1200	900	500	700	T 6	300	1000	250000	0	0
49	M 1	1200	1050	800	700	M 1	250	900	750	10000	2500
50	B 1	1200	1000	1000	700	B 1	180	300	490000	0	0
51	T 2	1200	850	500	700	T 2	0	700	850	40000	22500
52	B 2	1200	1000	400	600	B 2	0	500	10000	0	0
53	T 3	1200	1000	750	600	T 3	120	450	900	90000	10000
54	B 3	1200	650	300	450	B 3	0	350	750	2500	0
55	T 4	1200	650	550	450	T 4	600	600	750	2500	90000
56	B 4	1200	750	500	500	B 4	290	650	950	90000	202500
57	T 5	1200	1000	400	600	T 5	50	900	250000	0	0
58	B 5	1200	1000	800	600	B 5	0	900	750	160000	22500
59	T 6	1200	1100	800	800	T 6	0	650	22500	0	0
60	B 6	1200	850	700	700	B 6	0	800	800	10000	0
61	T 7	1200	500	600	500	T 7	0	700	500	2500	40000
62	B 7	1200	800	600	500	B 7	0	750	22500	0	0
63	T 8	1200	800	600	500	T 8	0	550	2500	0	0
64	B 8	1200	800	600	500	B 8	0	600	62500	0	0
65	T 9	1200	800	600	500	T 9	0	450	700	2500	2500
66	B 9	1200	800	600	500	B 9	0	600	10000	0	0
67	T 10	1200	800	600	500	T 10	0	600	700	10000	62500
68	B 10	1200	800	600	500	B 10	0	400	62500	0	0
69	T 11	1200	900	600	450	T 11	0	600	700	2500	0
70	B 11	1200	900	650	450	B 11	0	700	500	2500	2500
71	T 12	1200	1000	650	550	T 12	0	350	40000	0	0
72	B 12	1200	1000	650	550	B 12	100	600	700	10000	62500
73	T 13	1200	1200	700	800	T 13	0	600	10000	0	0
74	B 13	1200	1200	700	800	B 13	0	450	62500	0	0
75	T 14	1200	1050	700	700	T 14	100	600	700	2500	0
76	B 14	1200	750	600	600	B 14	0	600	400	10000	40000
77	T 1	1200	750	600	600	T 1	0	500	10000	0	0
78	B 1	1200	1100	600	700	B 1	0	450	700	2500	0
79	T 2	1200	1100	600	700	T 2	0	600	10000	45109	0
80	B 2	1200	1100	600	700	B 2	0	600	400	0	40000
81	T 3	1200	1200	700	800	T 3	300	1000	700	2500	0
82	B 3	1200	1200	700	800	B 3	0	450	700	2500	0
83	T 4	1200	1000	800	700	T 4	180	1000	250	62500	22500
84	B 4	1200	1000	800	700	B 4	0	800	4000	0	0
85	T 5	1200	1200	800	700	T 5	0	900	40000	0	0
86	B 5	1200	1200	800	700	B 5	100	850	1100	160000	0
87	T 6	1200	1100	800	700	T 6	0	850	2500	0	0
88	B 6	1200	1100	800	700	B 6	0	950	122500	0	0
89	T 7	1200	1200	800	700	T 7	0	400	1150	40000	202500
90	B 7	1200	1300	800	600	B 7	0	850	62500	0	0
91	T 8	1200	1300	800	600	T 8	0	1150	1150	202500	302500
92	B 8	1200	1300	700	600	B 8	200	1150	1150	202500	302500
93	T 8	1200	1300	700	600	T 8	0	1150	1150	202500	302500
94	B 8	1200	1300	700	600	B 8	0	1150	1150	202500	302500

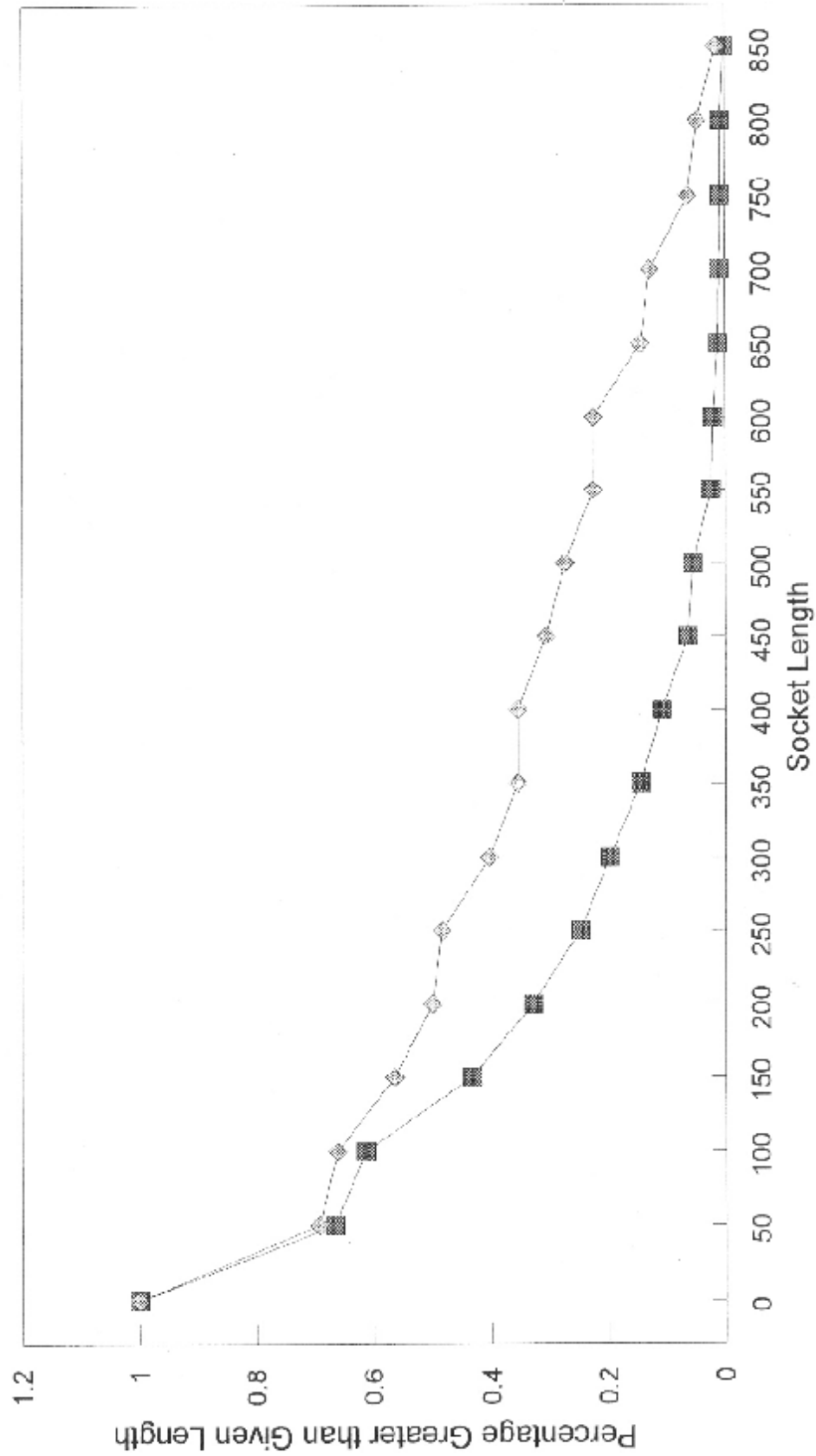


95	T 9	1200	700	600	T 9	0	600	10000	0
96	B 9	1200	500	700	B 9	0	700	40000	160000
97	T 10	1200	500	550	T 10	0	550	2500	0
98	B 10	1200	500	550	B 10	0	550	2500	160000
99	T 11	1200	550	850	T 11	0	850	90000	0
100	B 11	1200	600	500	B 11	30	750	22500	422500
101	T 12	1200	700	950	T 12	50	950	62500	0
102	B 12	1200	700	1200	B 12	80	1200	250000	62500
103	T 13	1200	600	650	T 13	0	650	2500	0
104	B 13	1200	600	900	B 13	0	900	90000	0
105	T 14	1200	600	0	T 14	0	0	0	0
106	T 1	1200	600	900	T 1	800	900	90000	66250
107	B 1	1200	500	800	B 1	700	800	90000	2500
108	T 2	1200	650	700	T 2	700	700	0	0
109	B 2	1200	500	600	B 2	600	500	0	10000
110	T 3	1200	550	500	T 3	400	500	2500	0
111	B 3	1200	500	700	B 3	300	900	160000	22500
112	T 4	1200	500	900	T 4	500	900	160000	0
113	B 4	1200	450	600	B 4	450	600	22500	2500
114	T 5	1200	500	600	T 5	0	600	10000	0
115	B 5	1200	500	750	B 5	300	750	62500	10000
116	T 6	1200	650	600	T 6	250	600	2500	0
117	B 6	1200	600	500	B 6	400	500	10000	90000
118	T 7	1200	450	800	T 7	500	800	122500	0
119	B 7	1200	500	600	B 7	650	600	10000	40000
120	T 8	1200	500	550	T 8	500	550	2500	0
121	B 8	1200	500	700	B 8	500	100	160000	2500
122	T 9	1200	500	650	T 9	550	650	22500	0
123	B 9	1200	500	550	B 9	300	400	10000	122500
124	T 10	1200	550	500	T 10	400	500	2500	0
125	B 10	1200	450	600	B 10	300	450	0	90000
126	T 11	1200	600	400	T 11	300	400	40000	0
127	B 11	1200	550	600	B 11	600	450	10000	10000
128	T 12	1200	500	950	T 12	600	950	202500	0
129	B 12	1200	500	600	B 12	200	600	10000	10000
130	T 13	1200	450	850	T 13	500	850	160000	0
131	B 13	1200	500	700	B 13	600	1100	360000	0

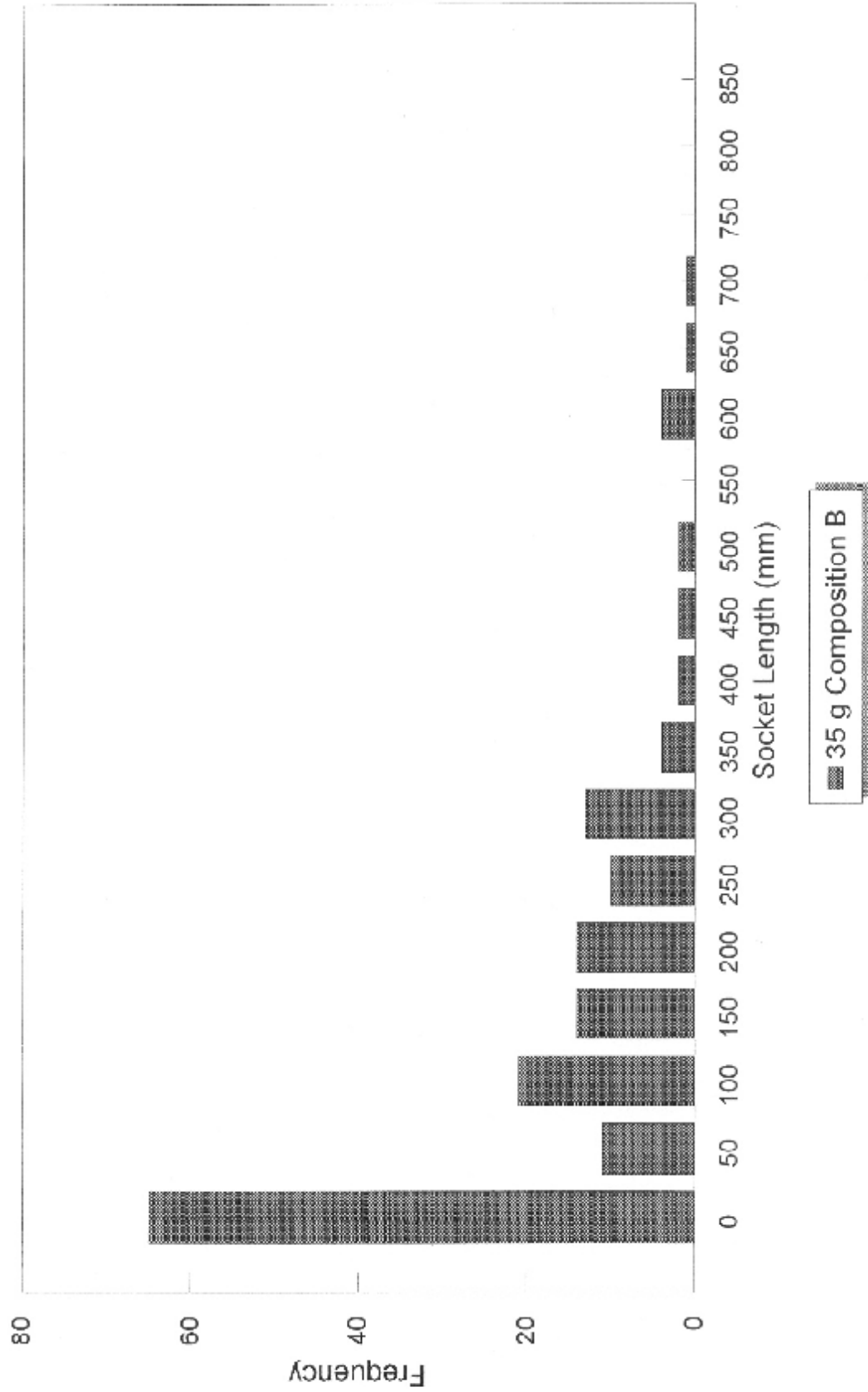
# Frequency Distribution



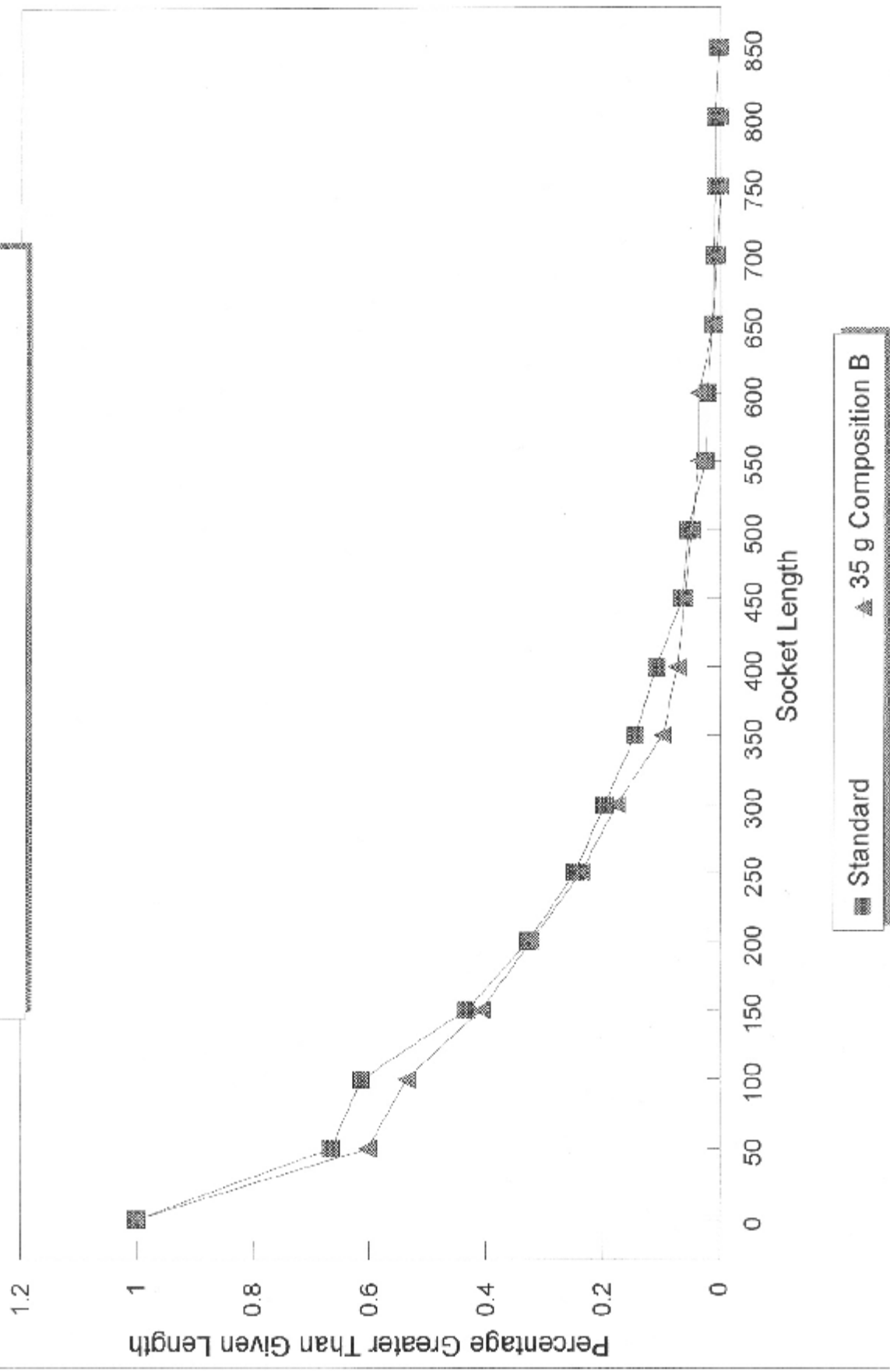
# Cumulative Distribution Frequency



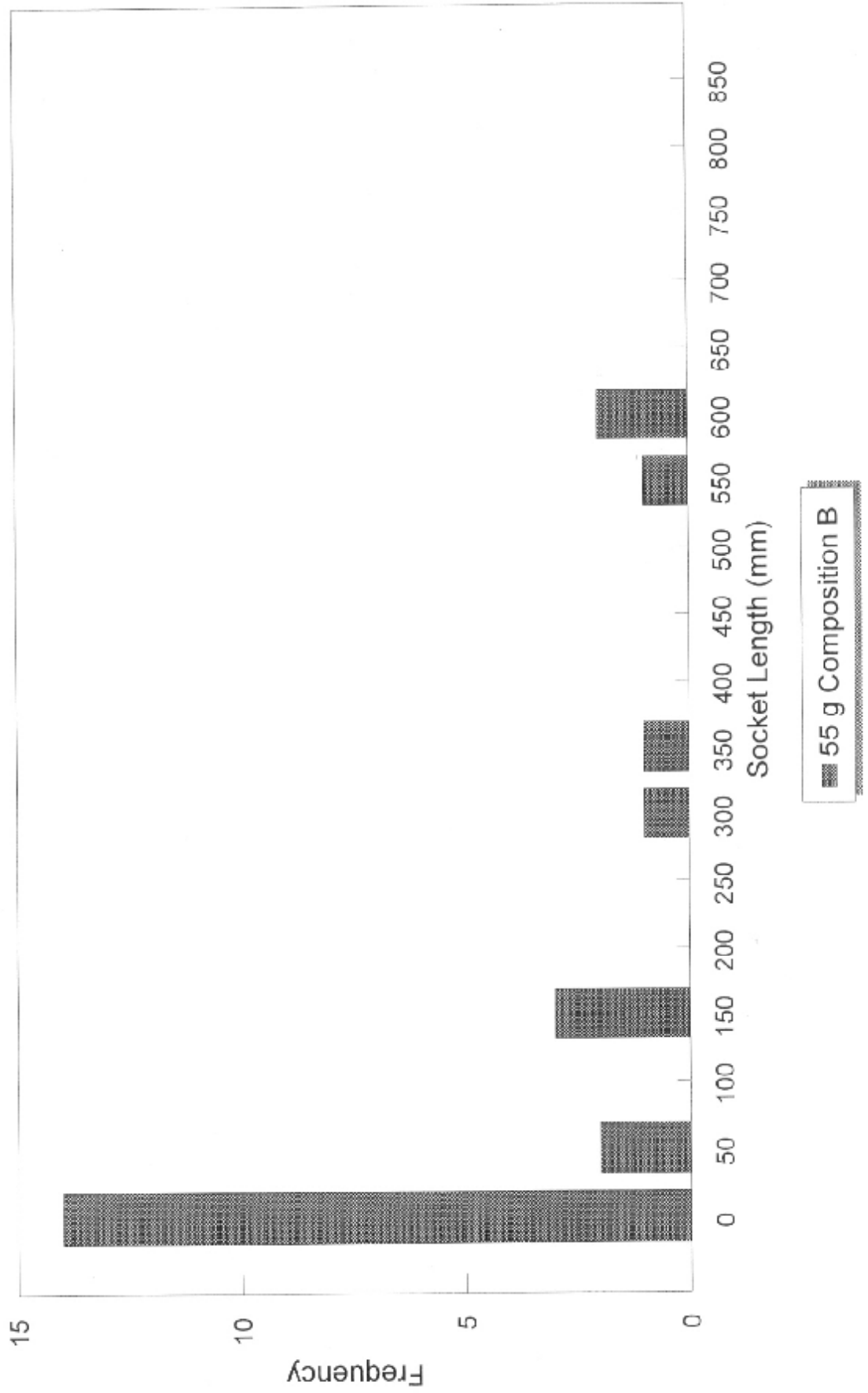
# Frequency Distribution



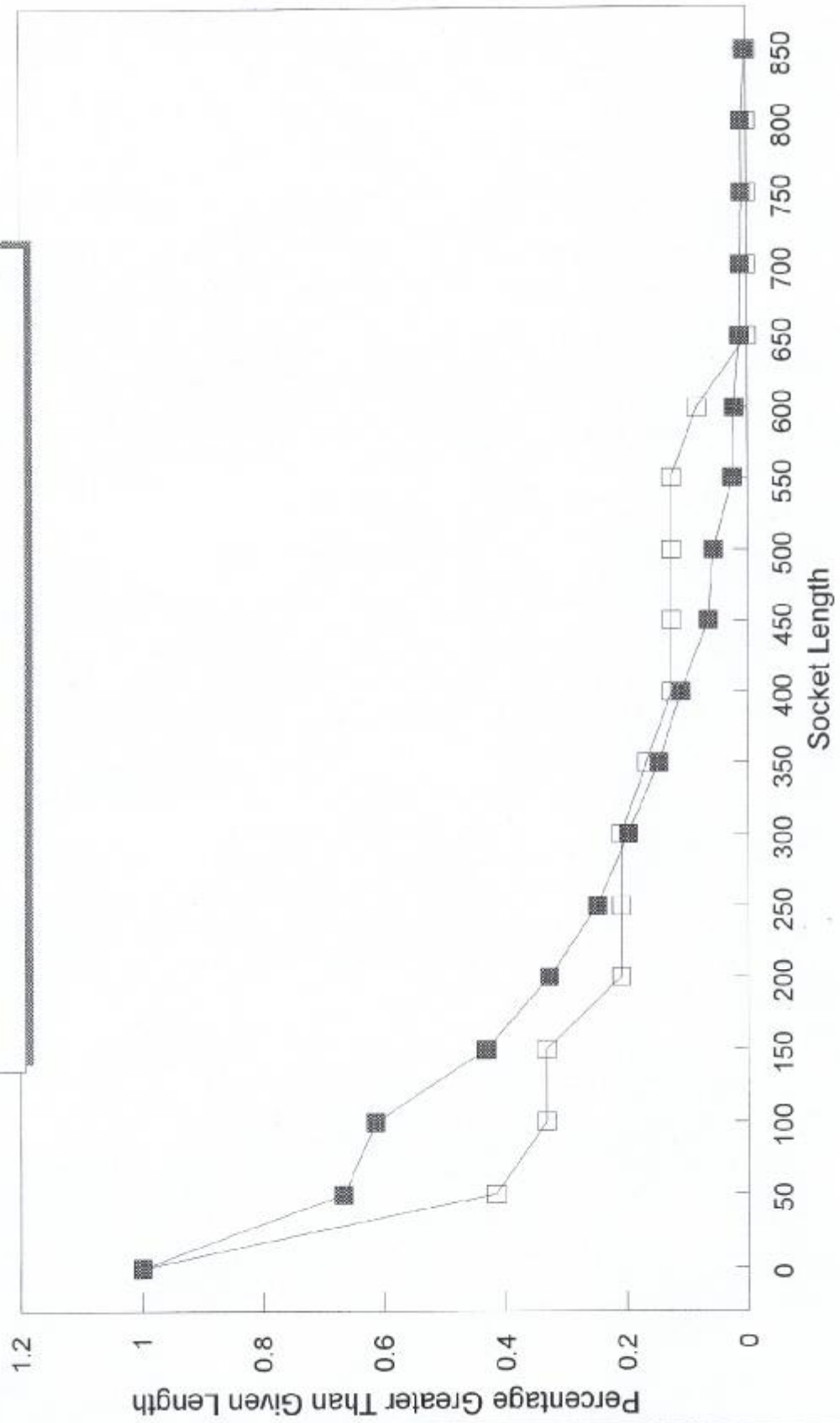
# Cumulative Distribution Frequency



# Frequency Distribution

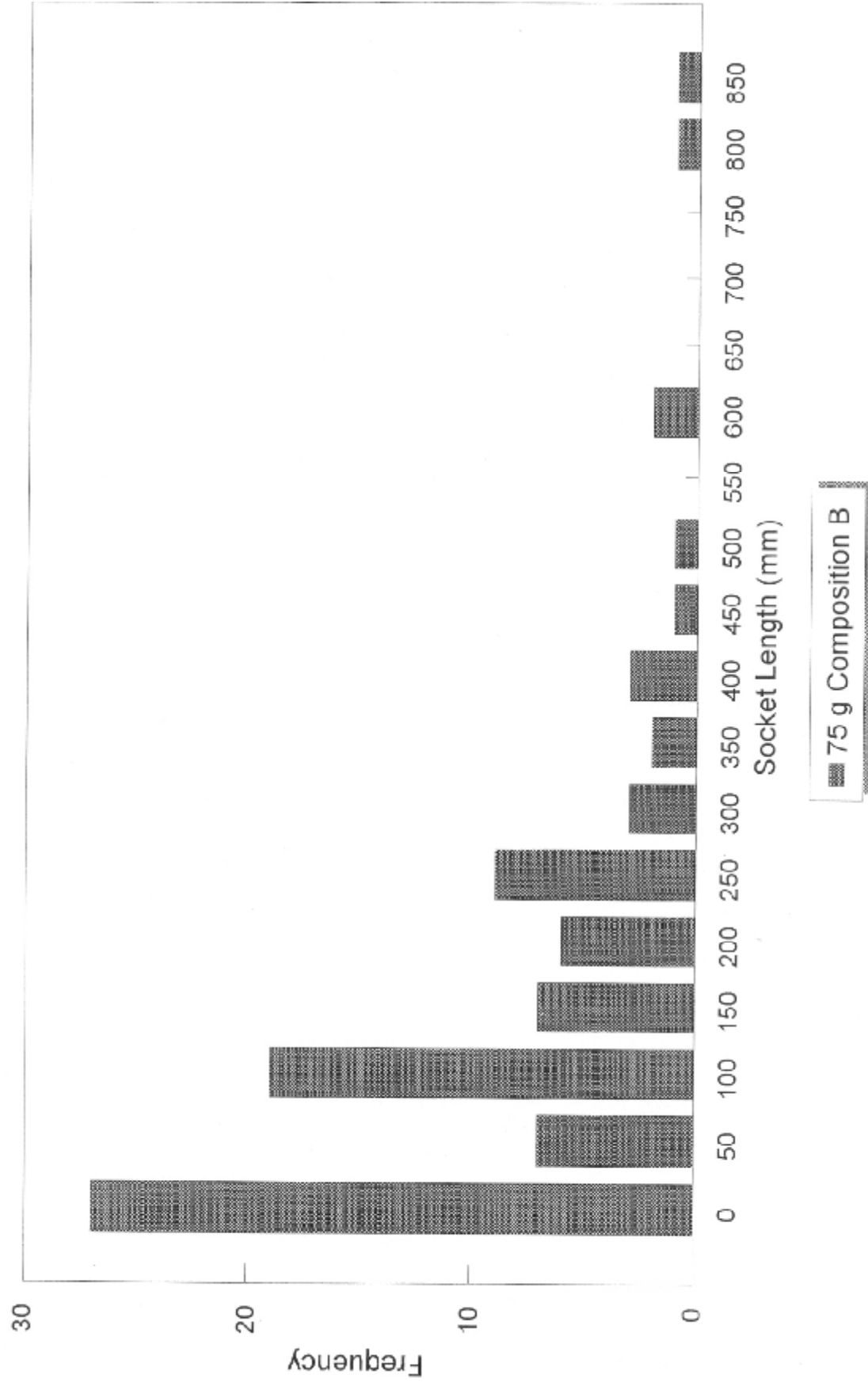


# Cumulative Distribution Frequency



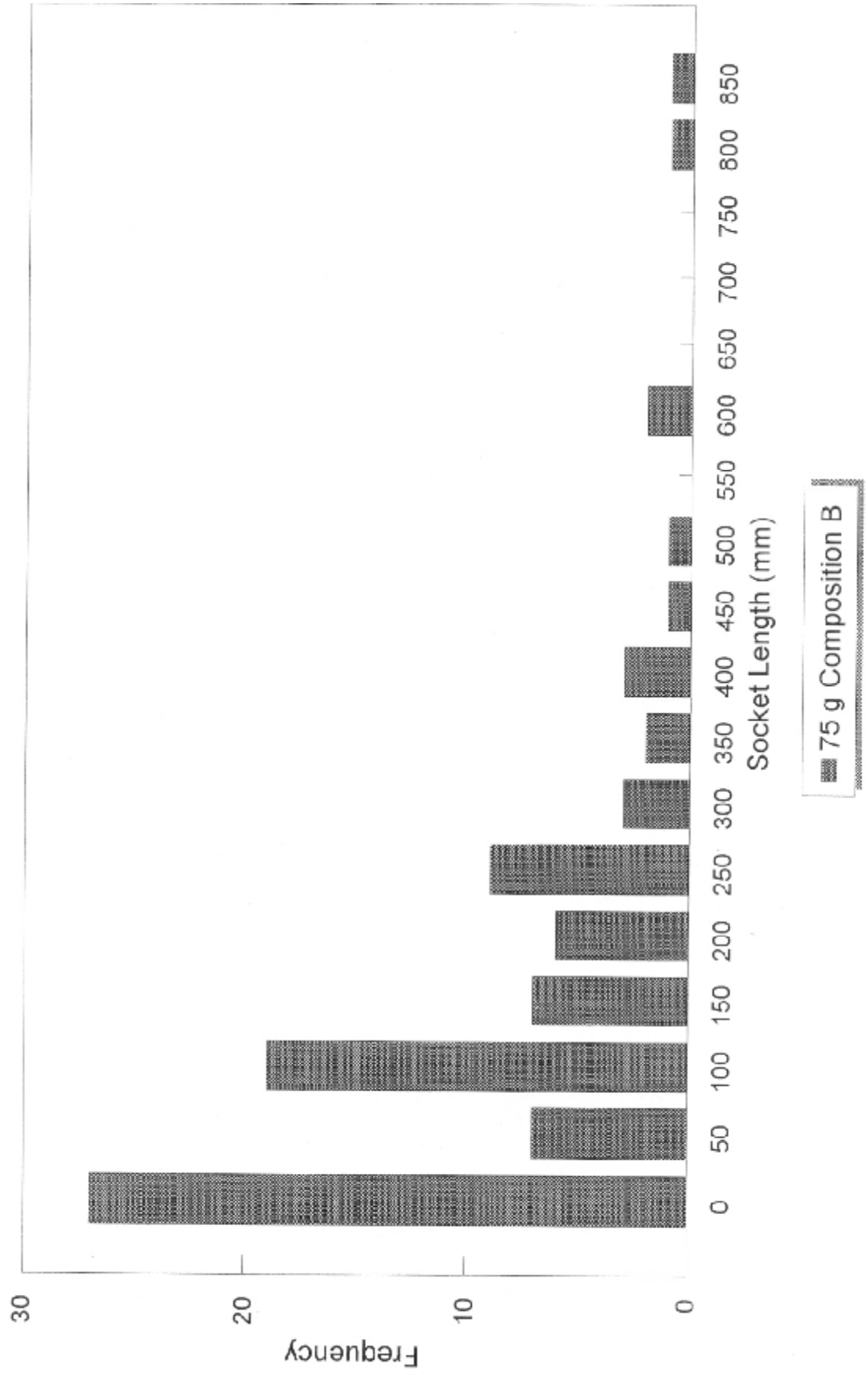
Standard
  55 g Composition B

# Frequency Distribution

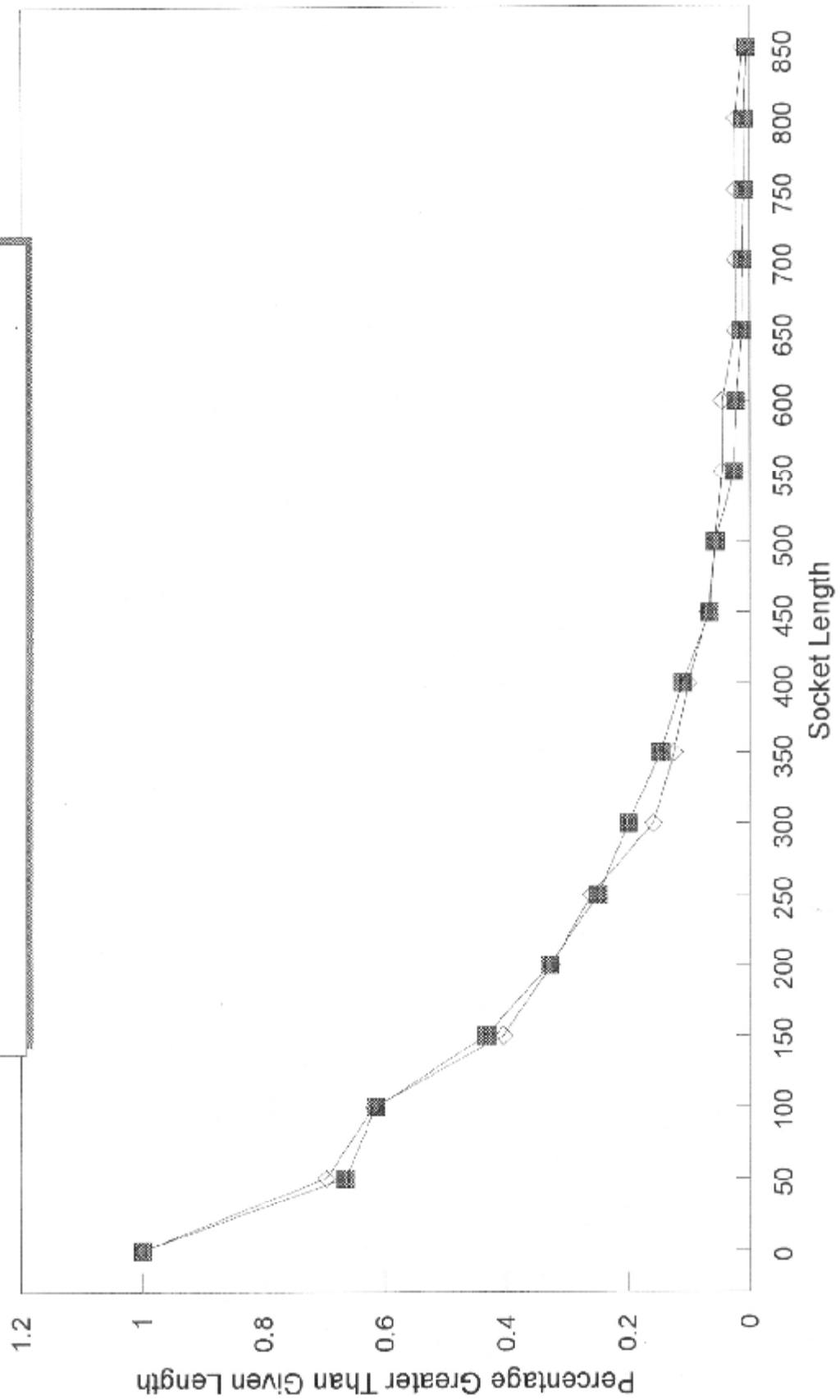




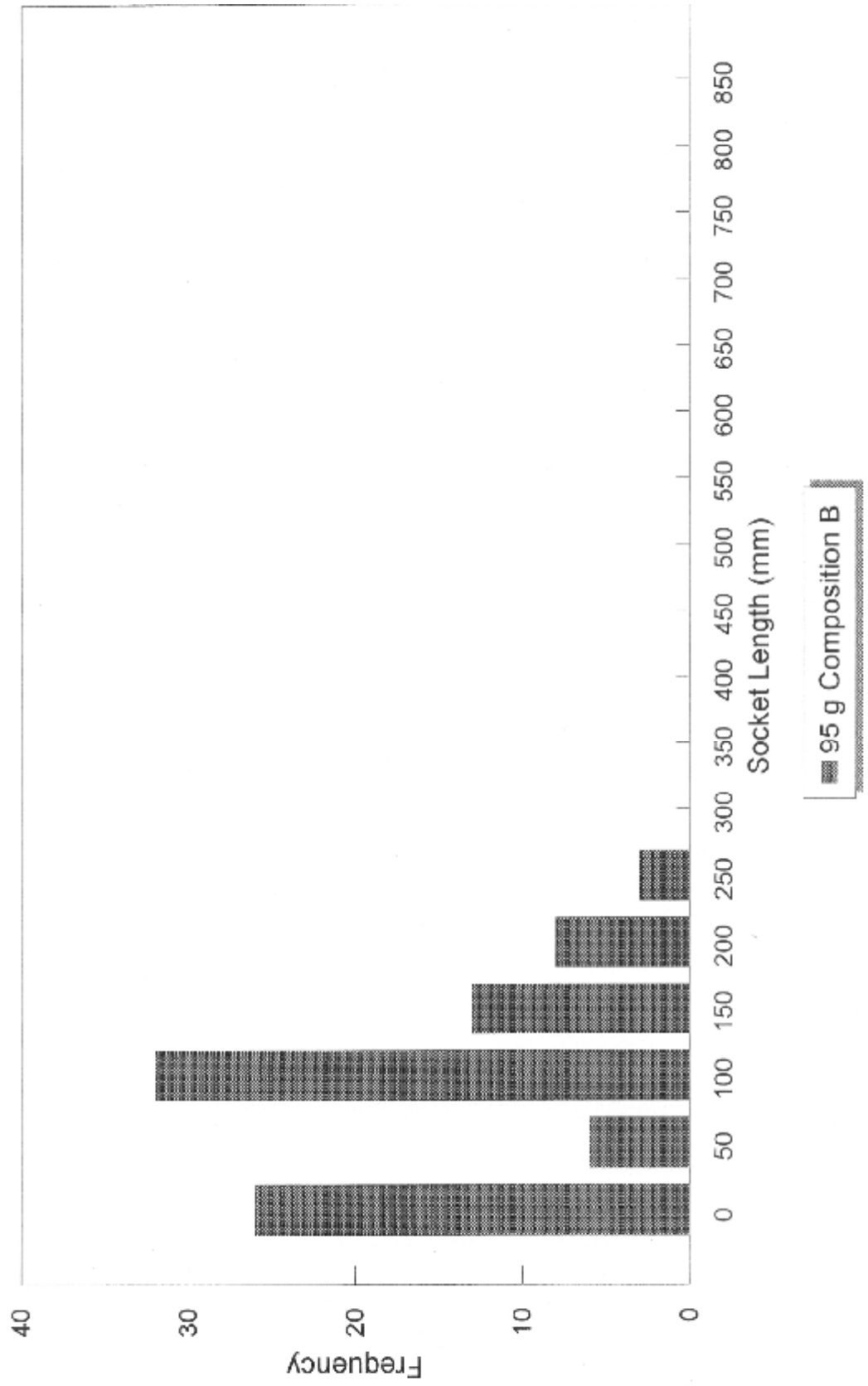
# Frequency Distribution



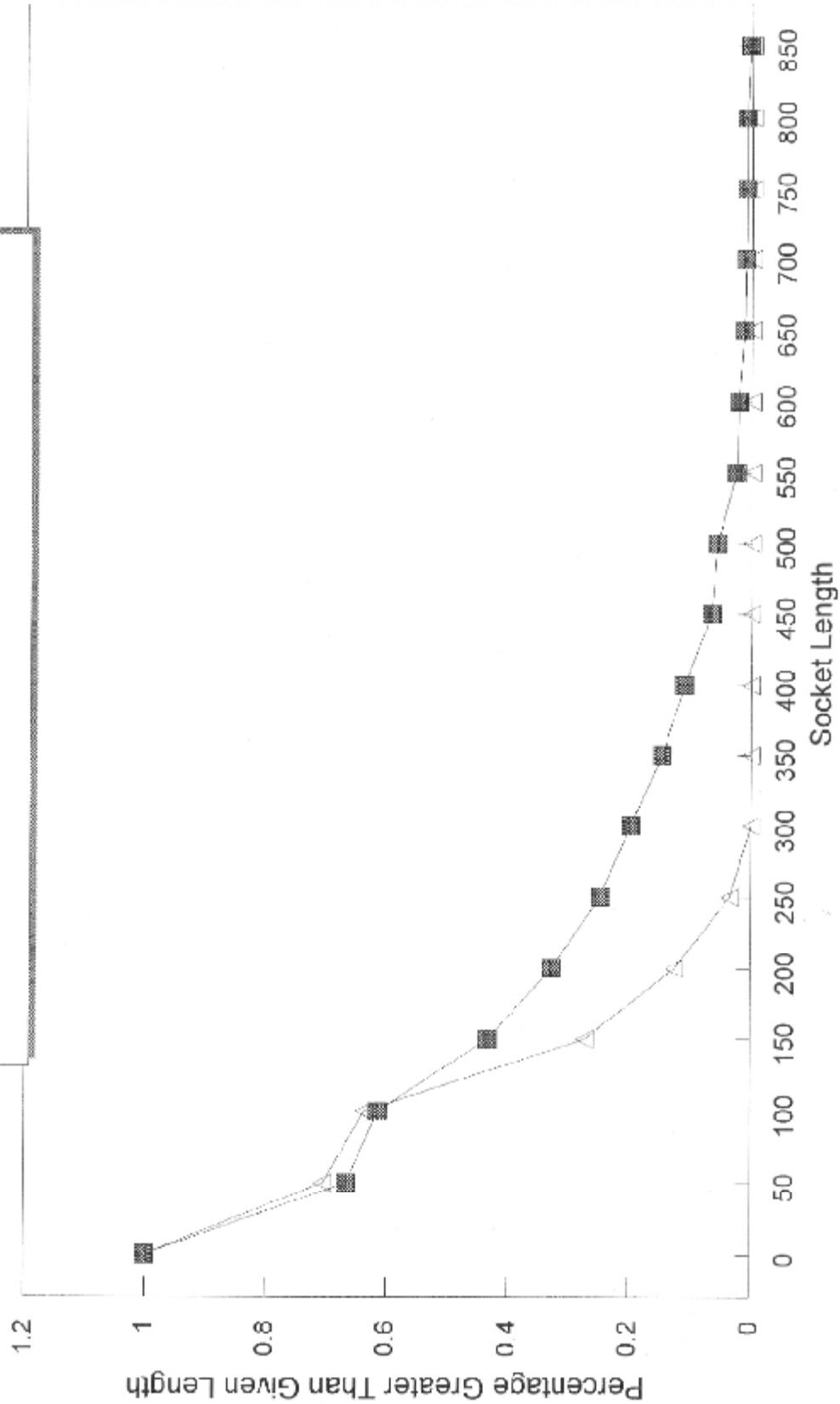
# Cumulative Distribution Frequency



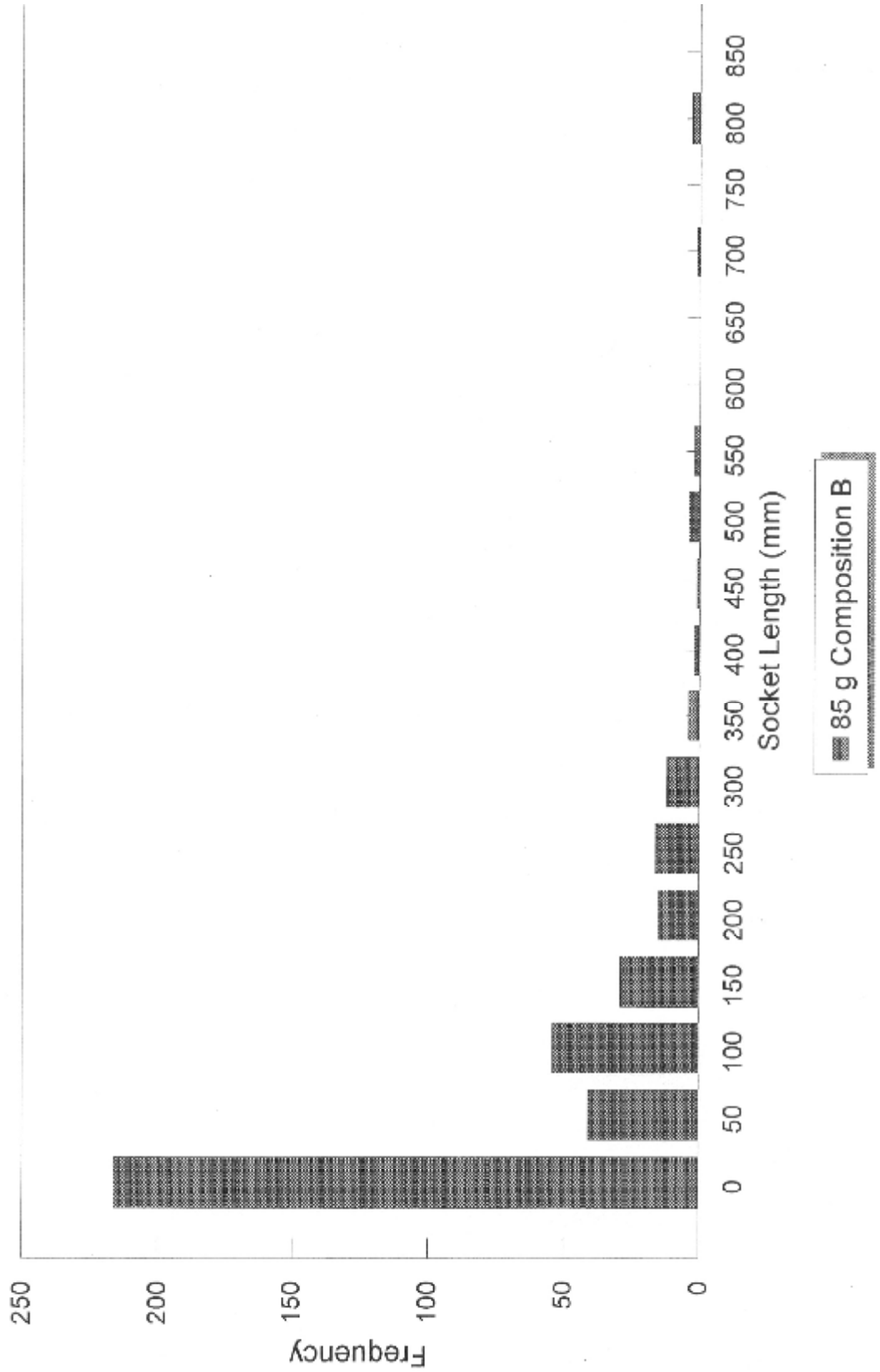
# Frequency Distribution



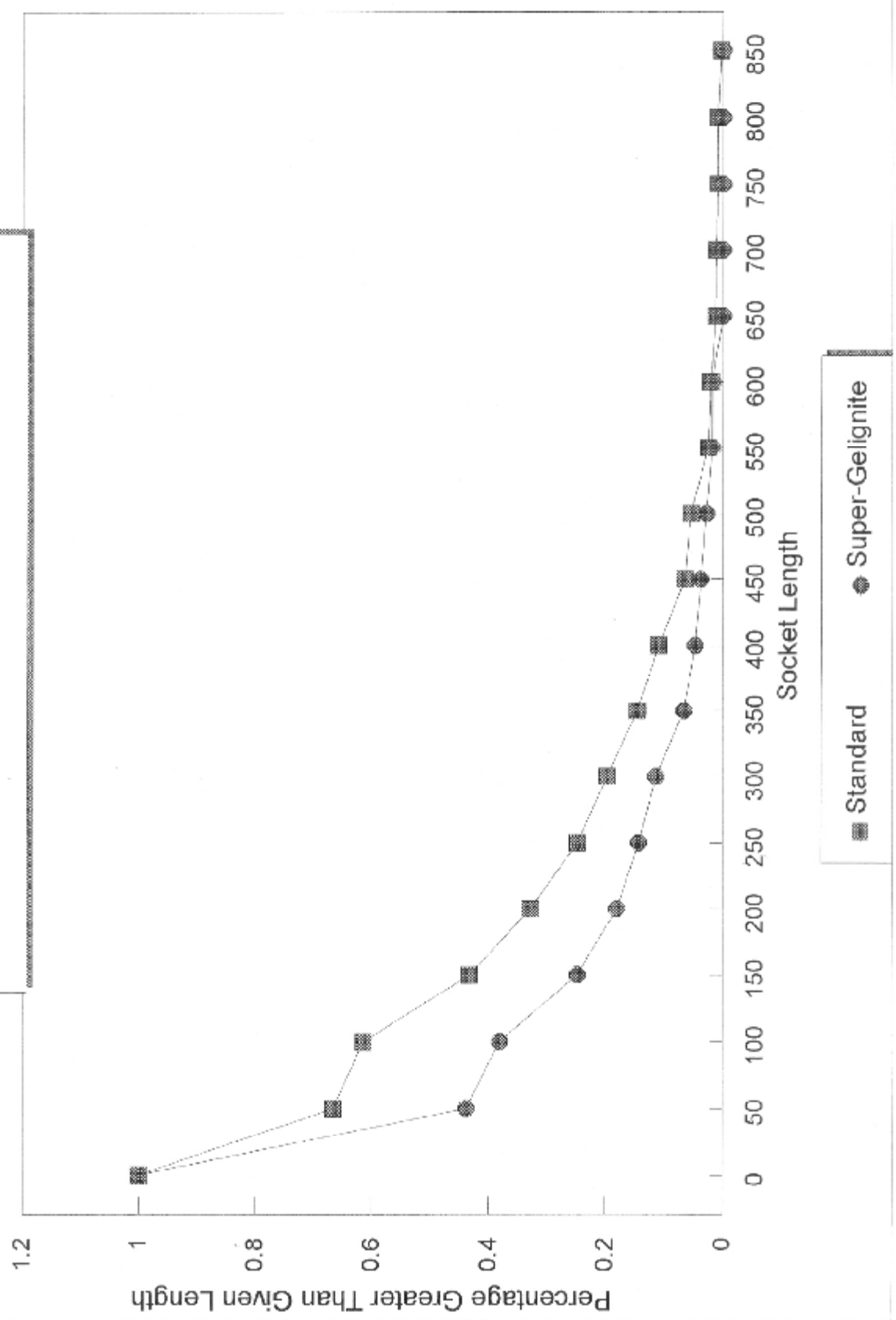
# Cumulative Distribution Frequency



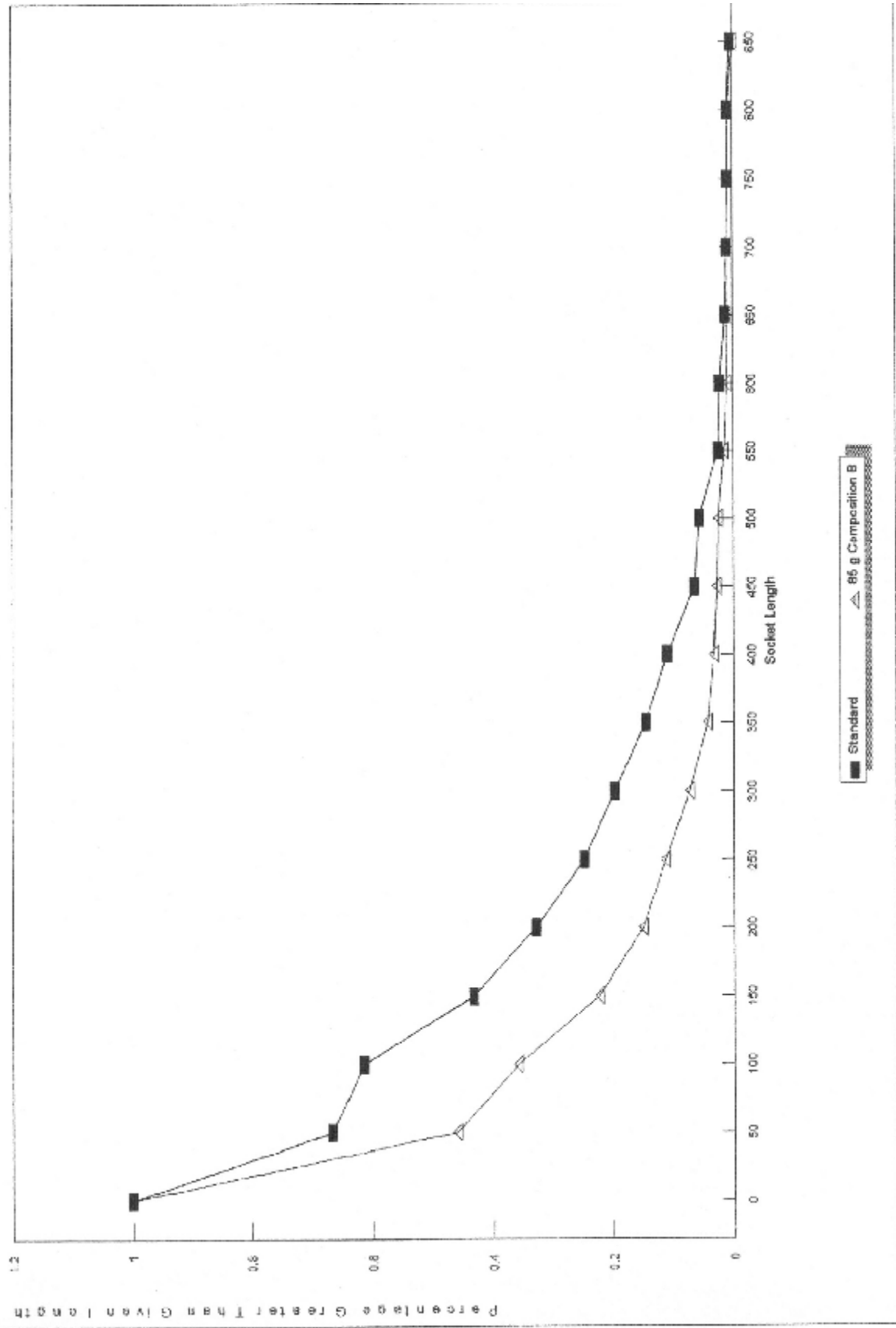
# Frequency Distribution



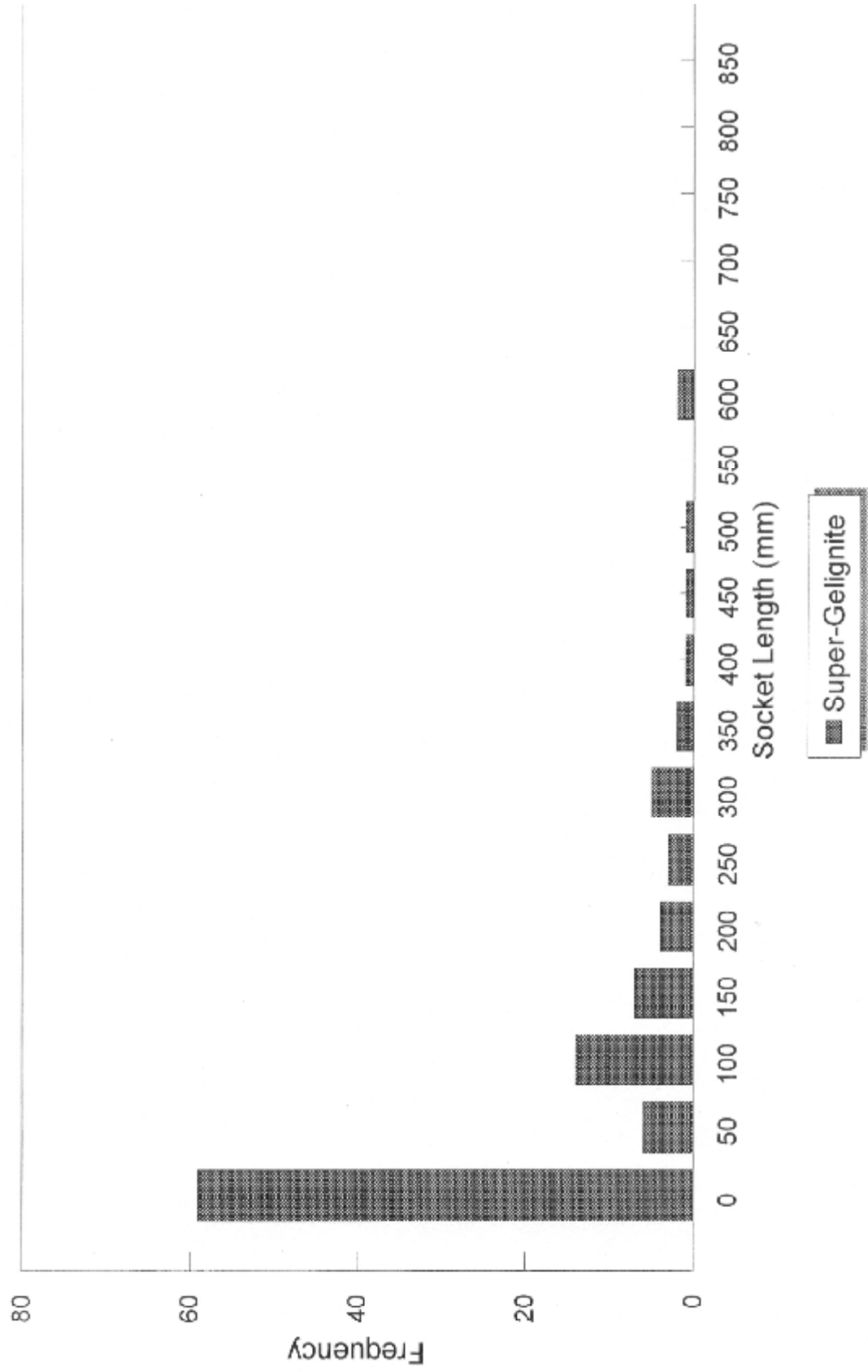
# Cumulative Distribution Frequency



**Cumulative Distribution Frequency**  
86 g Composition B & Standard

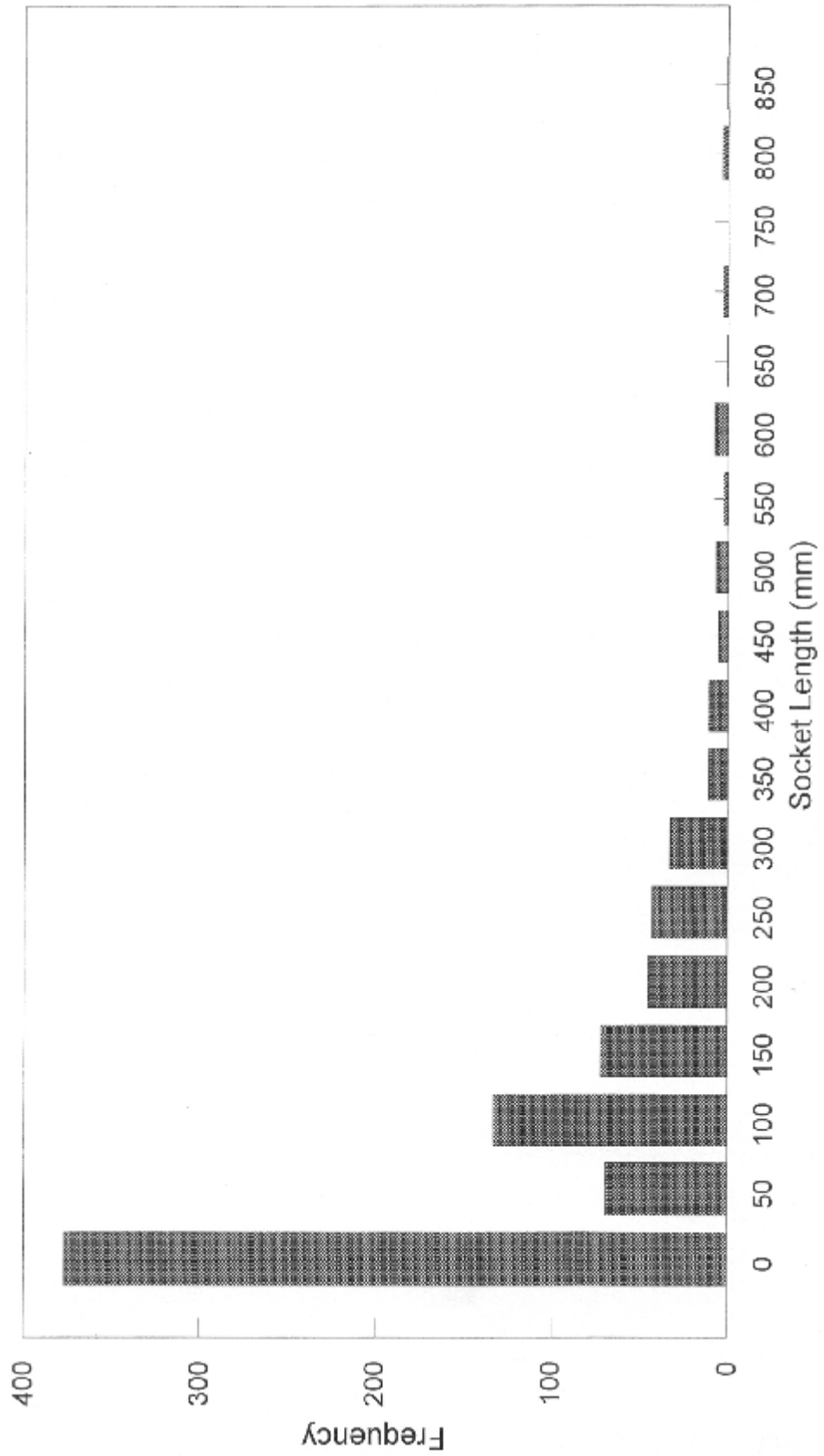


# Frequency Distribution



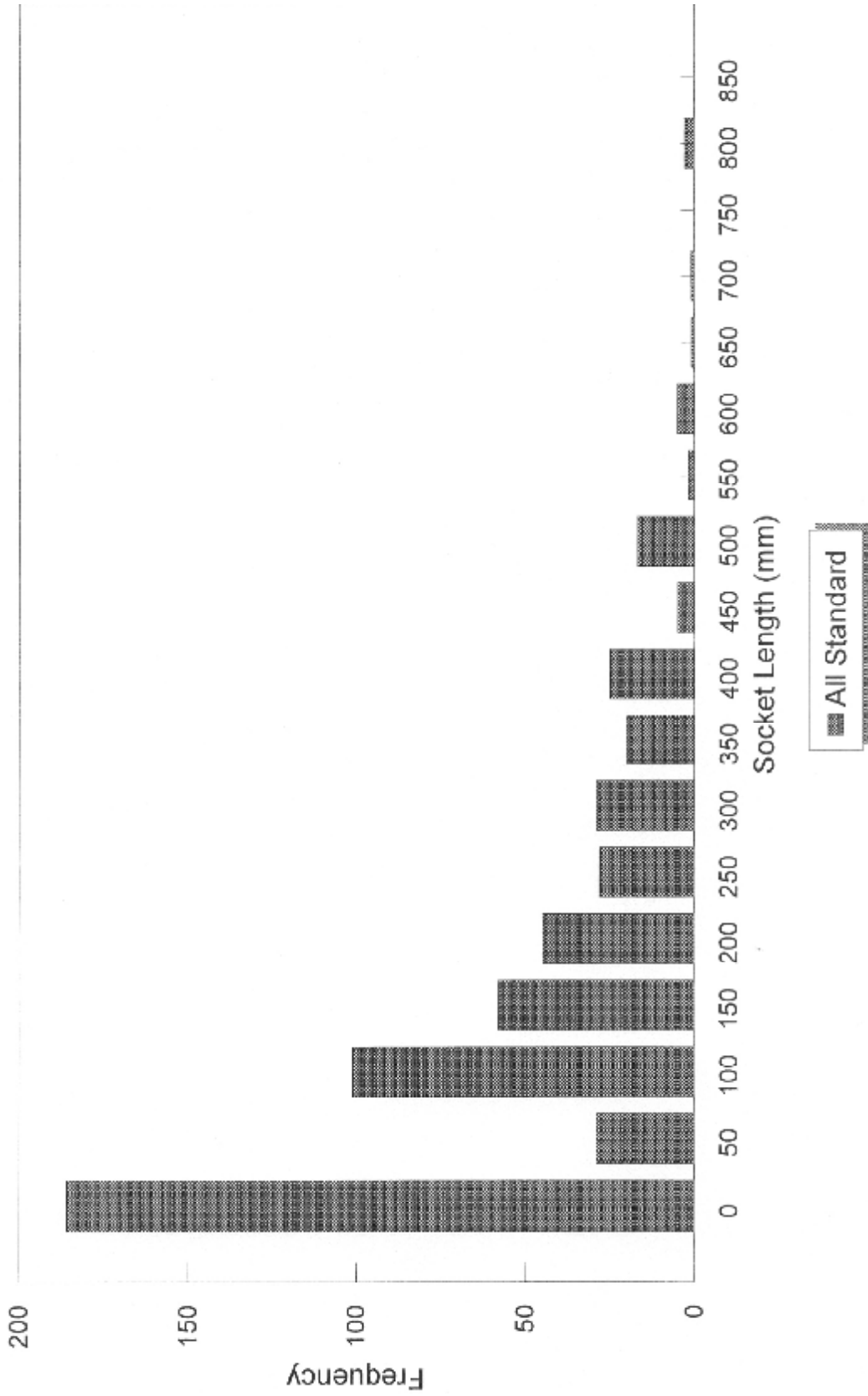


# Frequency Distribution

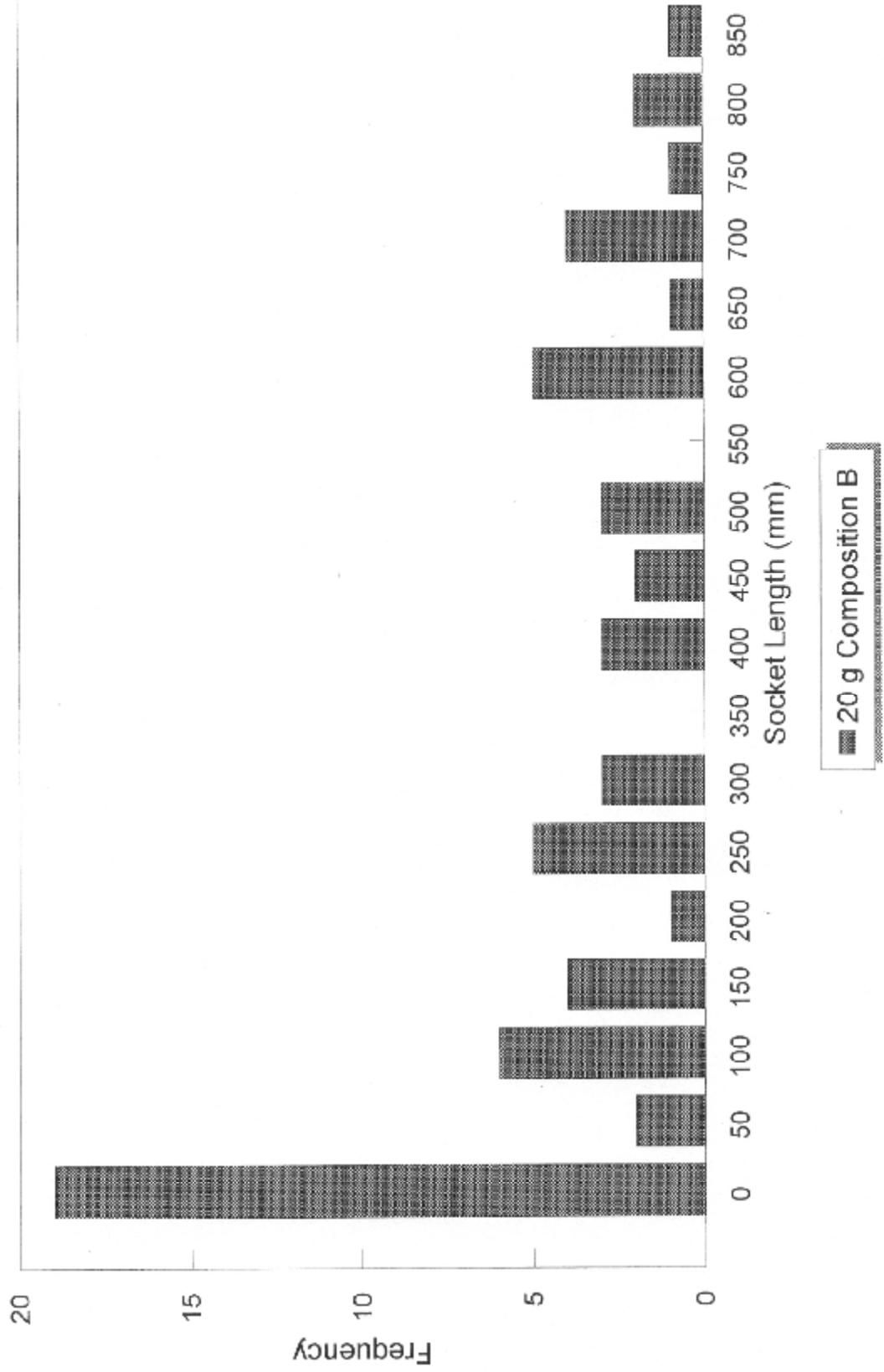


Composition B

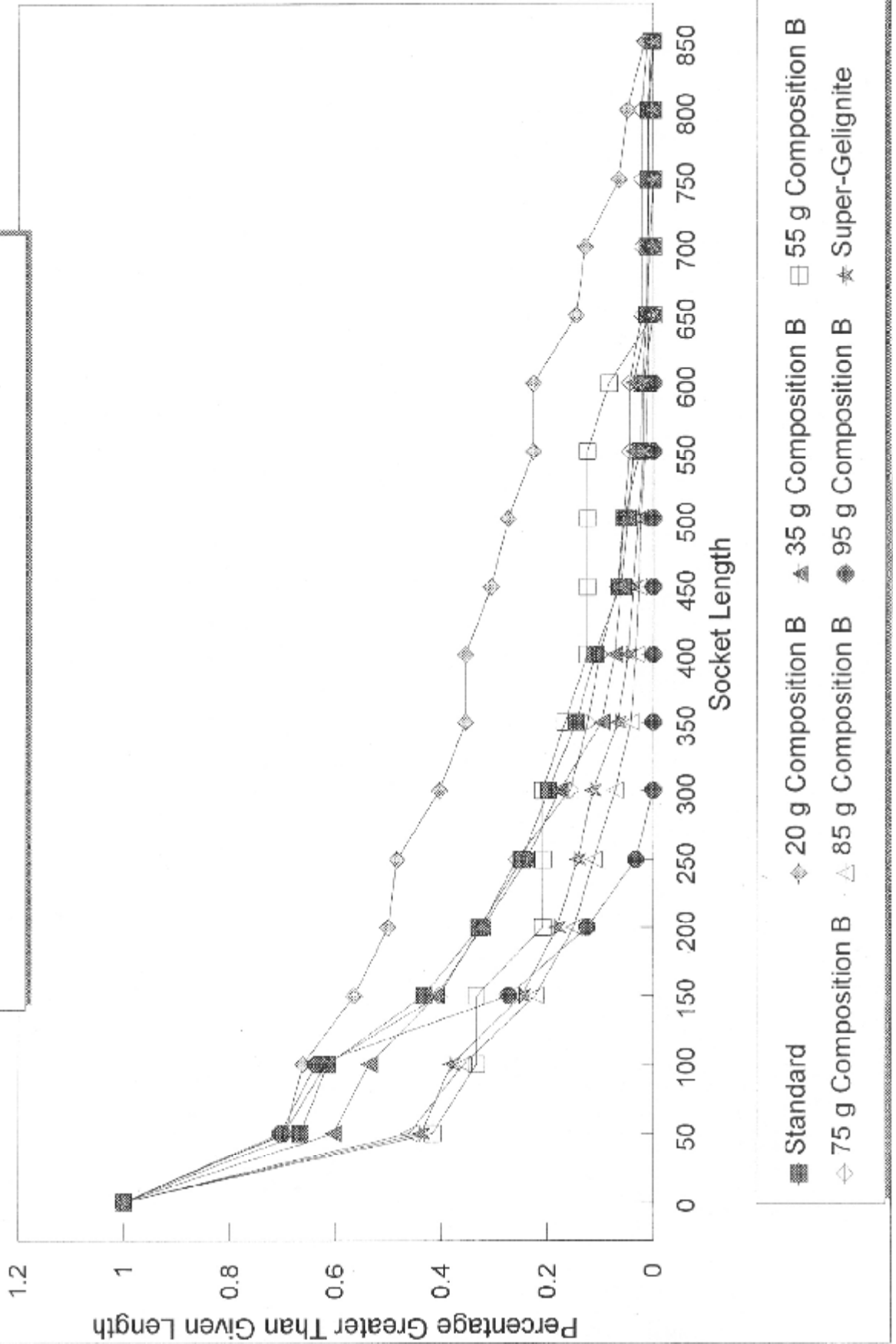
# Frequency Distribution



# Frequency Distribution



# Cumulative Distribution Frequency



## **APPENDIX 9**

### **SLUGSHOT PHOTOGRAPHS**

## APPENDIX 9    PHOTOGRAPHS

### PHOTOGRAPH 9.1

Photograph 9.1 shows the Slugshot Hang-up Clearance Charge with its accessories underground. The yellow bar is the support bar which is a modified Arrow prop with a universal support in which the 10 kg Slugshot is placed. A telescopic sight is placed on the Slugshot with the sight parallel to the axis of the Slugshot. The sight is removed after aiming and prior to firing.



## PHOTOGRAPH 9.2

Photograph 9.2 shows the Slugshot set up in an ore-pass with the detonator and fuse attached.



## **APPENDIX 10**

### **ADVANCED DETONICS LABORATORY PHOTOGRAPHS**



## APPENDIX 10 PHOTOGRAPHS

### PHOTOGRAPH 10.1

Photograph 10.1 shows the components of the directional primer charge. Four directional charges are shown – two lying on their side and two standing so that the contents can be viewed. The top standing charge shows the metal disc positioned inside at 35 mm stand-off. The bottom standing charge shows the contained Composition B explosive.

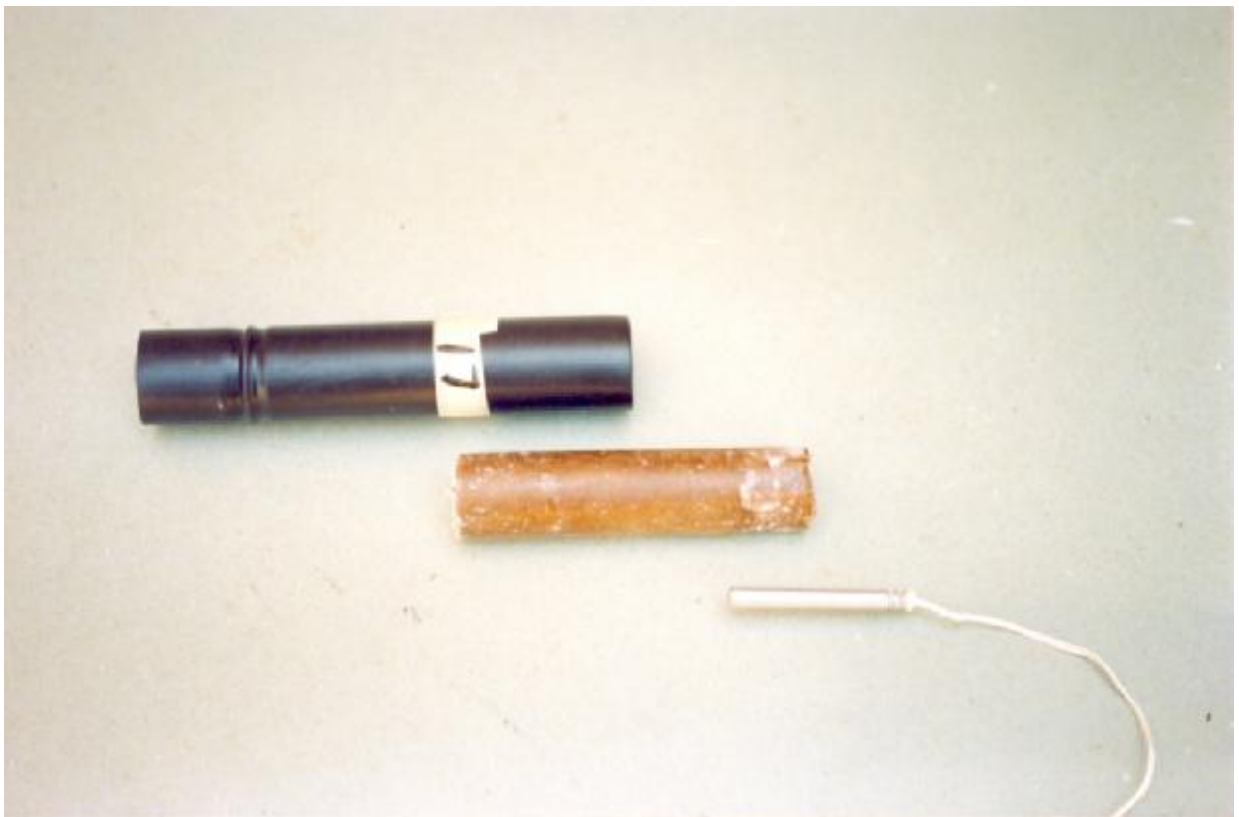
Also shown are three cartridges each of three different types of explosive, namely from left to right ammon dynamite, Powergel 813, ammon gelignite. These three were used in addition to dynagel and an emulsion explosive called EMEX as the booster for the high velocity of detonation charge Composition B.



## PHOTOGRAPH 10.2

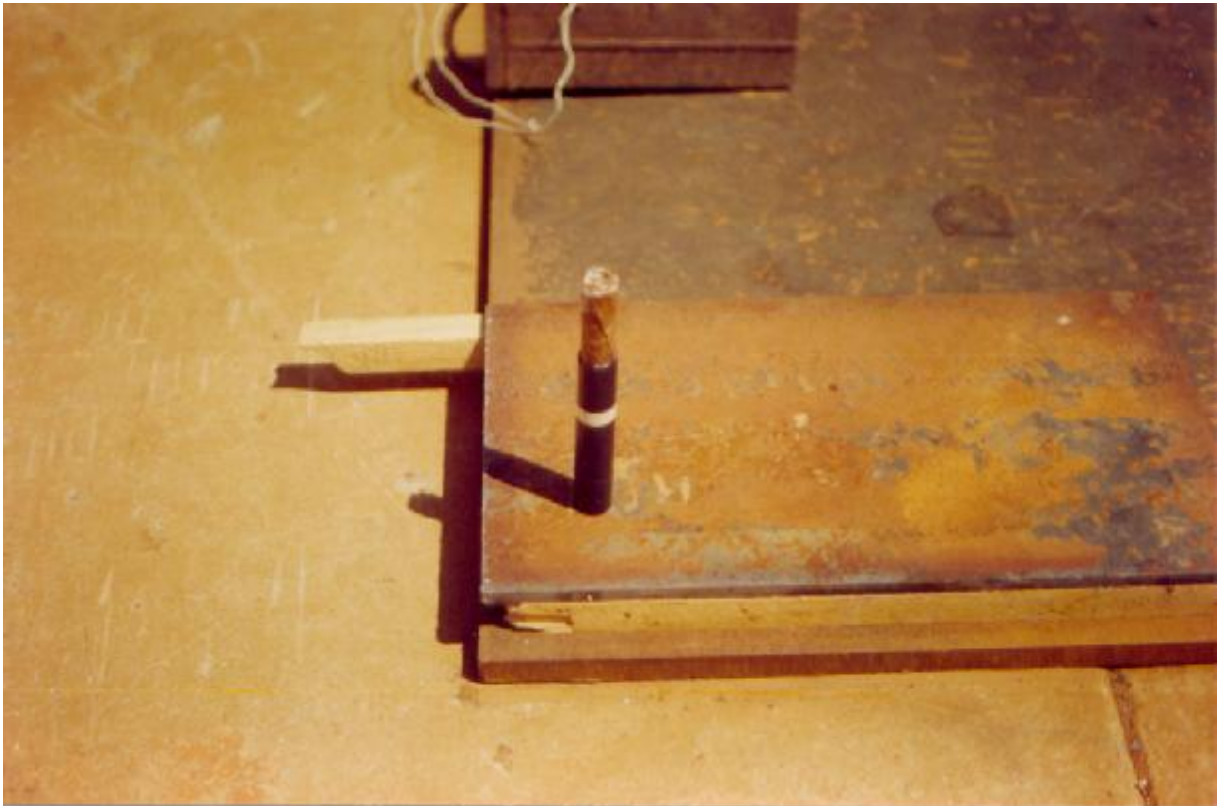
Photograph 10.2 shows the detonation chain. The directional primer charge is facing to the left i.e. the toe of the hole would be to the left of the charge. The charge is approximately 25 mm in diameter. The stand-off distance exists from the left end of the tube to where the metal disc is crimped into the tube at a position 35 mm from the left end. The high velocity of detonation explosive Composition B has been cast against the metal disc to approximately the position of the tape with the number 17 written on it. The charges came as a single unit to which were added the initiator of lower velocity of detonation and the detonator to the initiating explosive.

The detonation chain is thus from the detonator to the lower velocity of detonation explosive to the high velocity of detonation explosive. The high velocity of detonation explosive then drives the metal disc forward to the toe of the hole as a high velocity metal slug.



### PHOTOGRAPH 10.3

Photograph 10.3 shows the set-up of one of the experiments to determine the optimum stand-off distance using witness plates. The directional primer charge is mounted on the witness plate and is shown just prior to the insertion of the detonator into the lower velocity of detonation explosive, which in this case was ammon dynamite.



#### PHOTOGRAPH 10.4

Photograph 10.4 shows the partially exploded directional primer charge. The detonator initiated the lower velocity of detonation ammonium dynamite, which in turn did not initiate the high velocity of detonation Composition B. The unexploded explosive Composition B can be clearly seen in the partially destroyed housing.



## PHOTOGRAPH 10.5

Photograph 10.5 shows the deformed slug embedded in the witness plate. These two slugs are the result of directional primer charges containing no high velocity of detonation explosive. They are the result of ammon gelignite and Powergel 813 driven disc respectively.

Although they have forward punching power, it is not sufficient to penetrate the witness plate.



## PHOTOGRAPH 10.6

Photograph 10.6 shows the hole made through a 12 mm steel plate by a directional primer charge containing the high velocity of detonation explosive Composition B.



## PHOTOGRAPH 10.7

Photograph 10.7 shows the indentation made by the slug which passed through the 12 mm steel plate shown in Photograph 7.6 on the plate below the witness plate.

The hemispherical nature of the indentation can clearly be seen as can the remains of the slug which has been removed from the indentation and placed next to it.



## PHOTOGRAPH 10.8

Photograph 10.8 is the same as Photograph 10.7 except that the slug has been overturned to show its base.

Note that although the slug has passed through a 12 mm steel plate and has been embedded in the steel catch-plate, it appears to have maintained its mass in a single slug and has not broken up into a jet of smaller fragments.





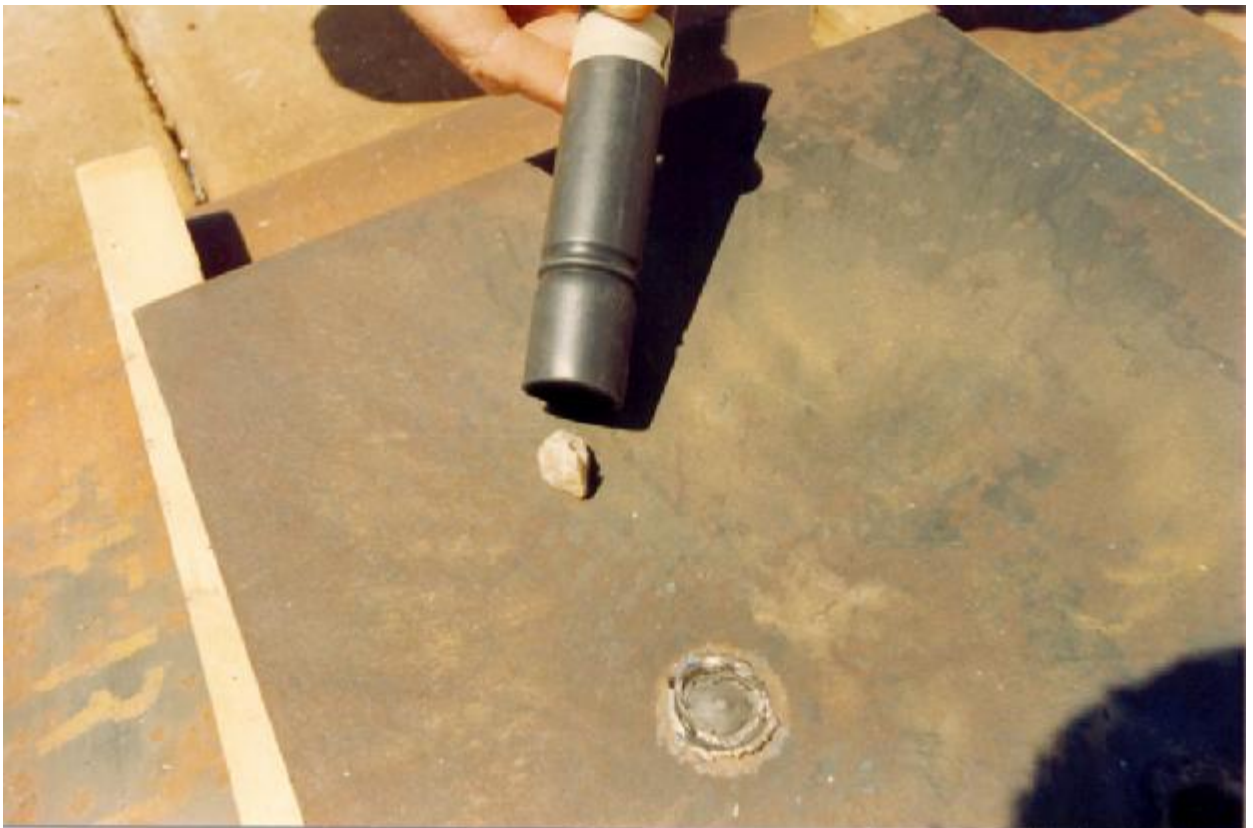
## PHOTOGRAPH 10.9

Photograph 10.9 shows an embedded slug next to a slug-made hole. The splaying out of metal on the circumference of the impact site can clearly be seen. Also the raised center of the impact zone can be seen in the case of the embedded slug.



## PHOTOGRAPH 10.10

Photograph 10.10 shows a foreign object, in this case a stone being placed in the stand-off void.



## PHOTOGRAPH 10.11

Photograph 10.11 shows the effect of the stone shown in Photograph 10.10. The penetrating effect into the plate is diminished. However, there is still considerable forward punching power.



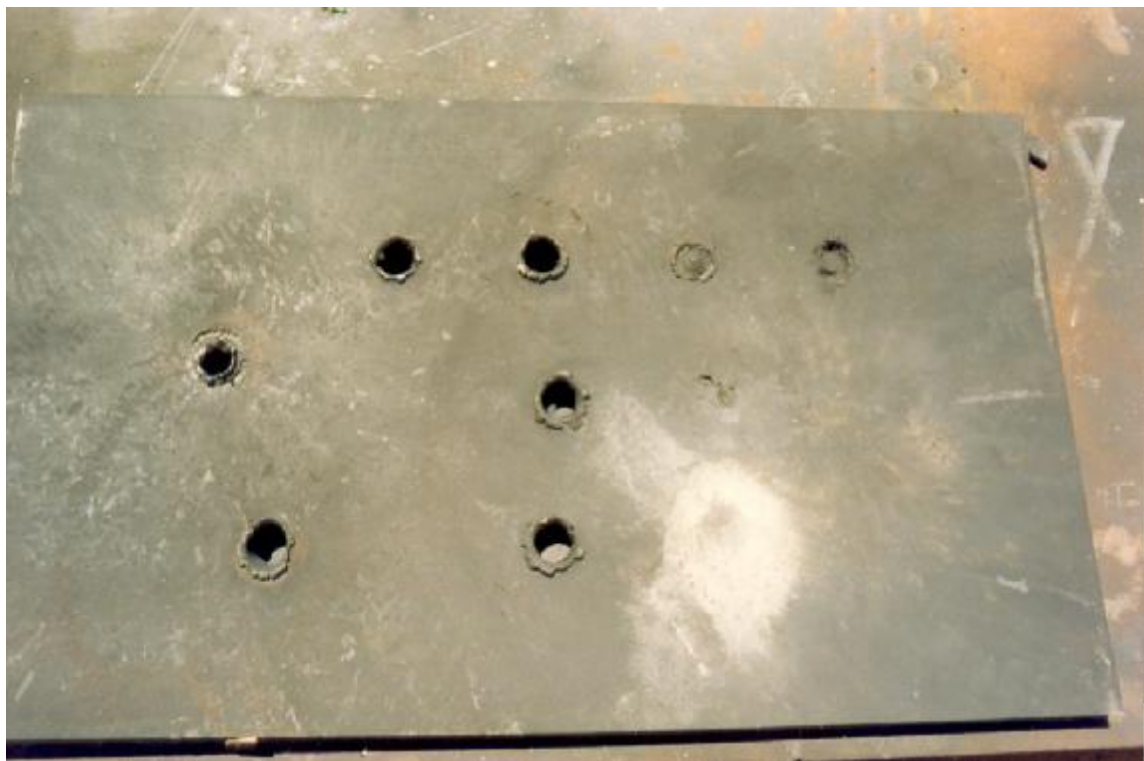
## PHOTOGRAPH 10.12

Photograph 10.12 shows another type of foreign matter, namely sand, being placed in the stand-off void.



### PHOTOGRAPH 10.13

Photograph 10.13 shows the result of many experiments of the stand-off distance on one plate. The top right indentation is that shown in Photograph 10.10 namely the stone in the stand-off void. The second from the right at the top is the indentation shown in Photograph 10.9. The result of the sand in void hardly shows in the position immediately below the top right indentation. The white area in the bottom row was made by a directional primer charge with no stand-off distance. All it has achieved is to remove the rust and scale from the plate.



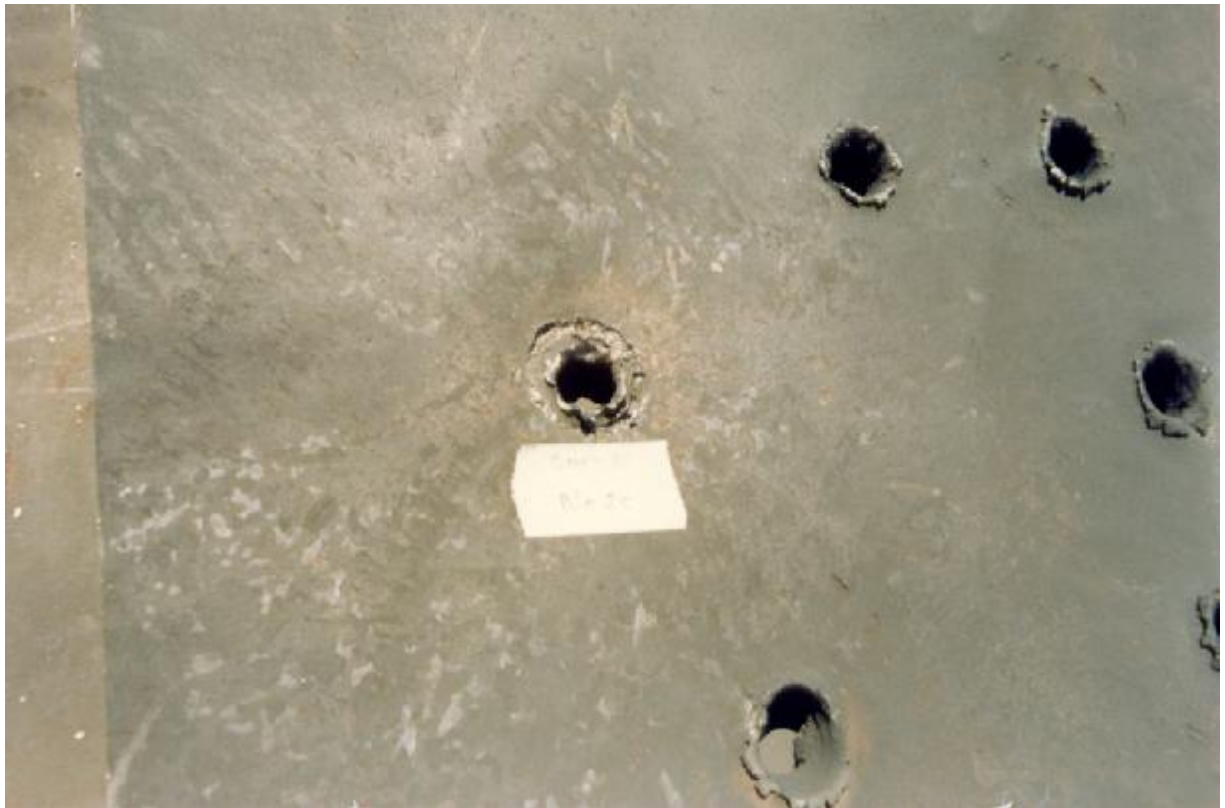
## PHOTOGRAPH 10.14

Photograph 10.14 shows the reverse side of the plate shown in Photograph 10.13. On the top left can be seen the bulging of the plate of the three indentations with embedded slugs.



## PHOTOGRAPH 10.15

Photograph 10.15 is a close-up of Photograph 10.13 showing the flow metal around the circumference of the holes.



## PHOTOGRAPH 10.16

Photograph 10.16 is the underside of the plate of Photograph 10.15. Again it shows the characteristic of metal flow at the circumference of the hole after the slug has passed clean through.

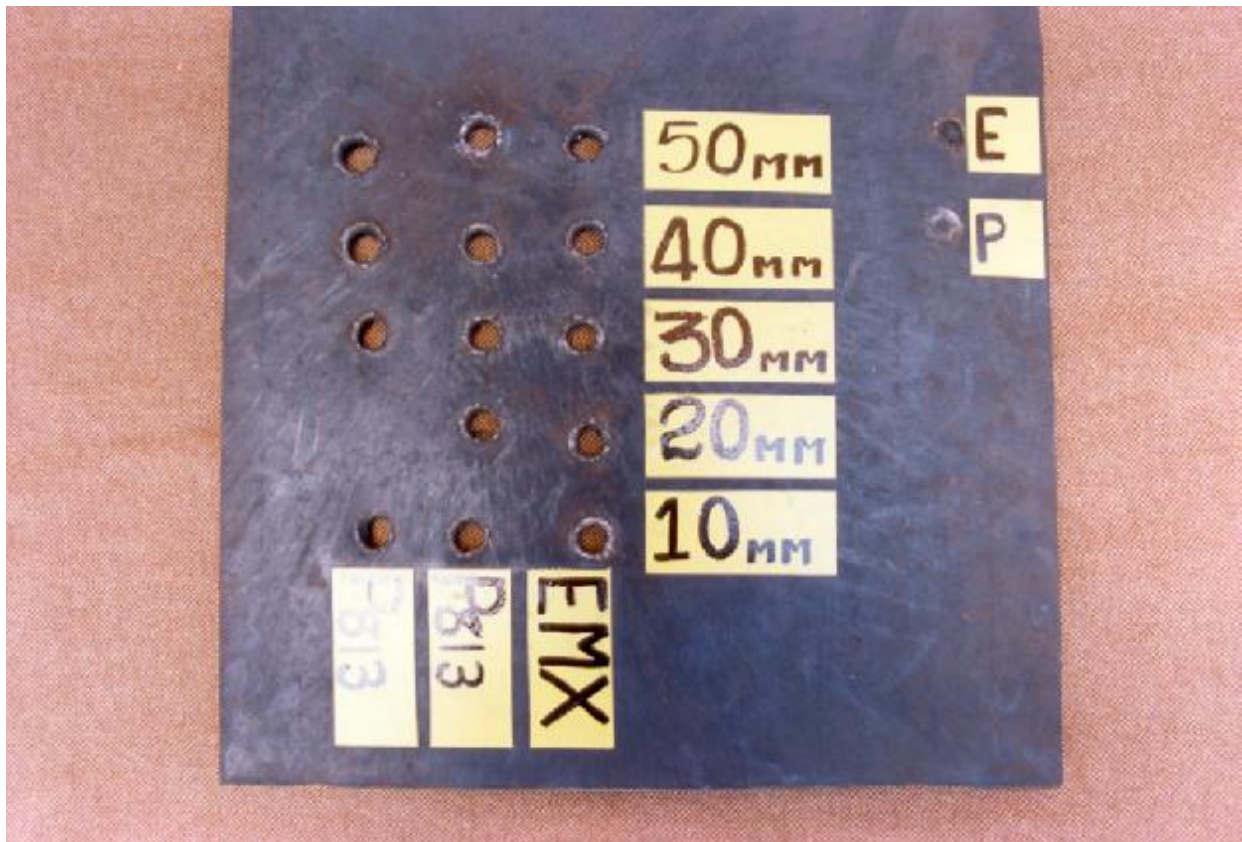




## PHOTOGRAPH 10.17

Photograph 10.17 shows a witness plate after a series of tests were undertaken using different column lengths of Composition B from 50 mm down to 10 mm in 10 mm steps, and using two different explosives for initiating the Composition B namely an emulsion EMEX and a watergel Powergel 813. All combinations punched clean through the plate (apart from one charge which misfired).

In addition, two charges which did not contain any Composition B, but were solely EMX or Powergel were fired (see top right hand corner). These did not penetrate the plate.



**PHOTOGRAPH 10.18**

Photograph 10.18 is the reverse-side to the plate shown in Photograph 10.17.



## PHOTOGRAPH 10.19

Photograph 10.19 shows a Powergel-initiated directional primer slug placed on a concrete floor.



## PHOTOGRAPH 10.20

Photograph 10.20 shows the crater formed by the charge in Photograph 10.19.



## PHOTOGRAPH 10.21

Photograph 10.21 shows a directional primer charge placed on a concrete block.



## PHOTOGRAPH 10.22

Photograph 10.22 shows the nature of the fracturing caused by the charge in Photograph 10.21. Clearly shown is the cattering effect at the surface of the block, the penetration of the slug for a certain distance into the block and then the formation of an umbrella-crack at the limit of the travel of the slug.



## PHOTOGRAPH 10.23 AND 10.24

Photograph 10.23 and 10.24 show the results of Photograph 10.22 from different angles.



## PHOTOGRAPH 10.25

Photograph 10.25 shows the Flash X-ray Radiography set-up. The board on the left is shielding the large sheet of X-ray film. The directional primer charge is secured in a horizontal position parallel to the X-ray film. As can be seen by the blue-wrapping, the initiating charge is Powergel. Also seen in the foreground are the conducting wires from the ionisation probes which are placed in the directional primer charge in order to trigger the timing mechanisms for the camera.

In front of the charge about a metre away is a large cylindrical steel catch plate in front of which is a graticule of wires which serve as a timing screen.





## PHOTOGRAPH 10.26

Photograph 10.26 is the same as Photograph 10.25 but taken from a slightly different angle. On the right is the bunker with the aperture for filming the formation and flight of the slug.



## PHOTOGRAPH 10.27 AND 10.28

Photographs 10.27 and 10.28 similar to Photograph 10.25 and 10.26 and show a different series of tests of the directional primer charge.



## PHOTOGRAPH 10.29

Photograph 10.29 shows the damage that the detonation of the directional primer charge does to the wooden board which protects the X-ray film (as shown in Photograph 10.25).

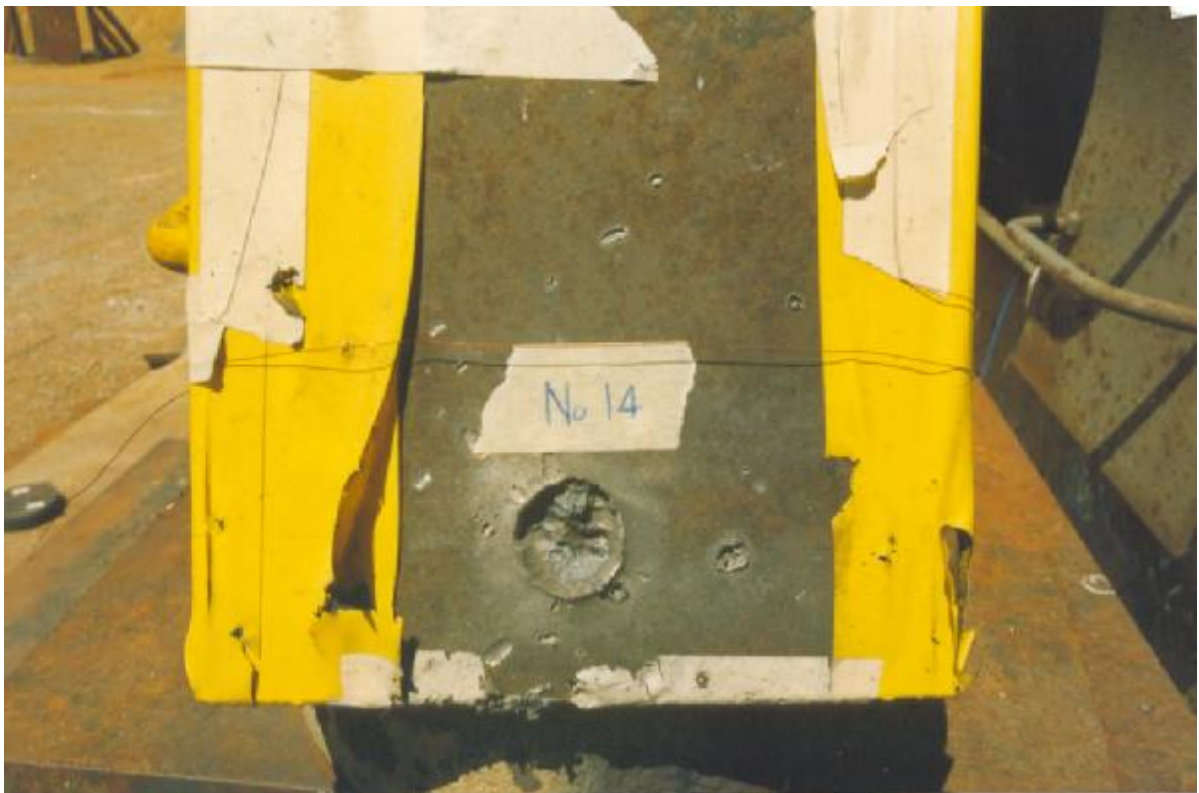
The ladder of reference lines can clearly be seen where the board has been blasted away.



### PHOTOGRAPH 10.30

Photograph 10.30 is the after photograph of Photograph 10.27 and 10.28. It shows the impact indentation of the slug in the catch-plate. The remnants of the shorting screen can be seen.

In addition, the effects of the shrapnel from the minor break-up of the slug in flight is shown as minor indentations in the catch-plate.



### PHOTOGRAPH 10.31, 10.32 AND 10.33

Photographs 10.31, 10.32 and 10.33 show the set-up of the testing of a similar device to the directional primer charge. These are shown to illustrate the multiple shorting screens can be used. Photograph 10.33 is a view taken from above which clearly shows the bunker with the photographing aperture and the extent of the explosive damage to the reinforced concrete wall.

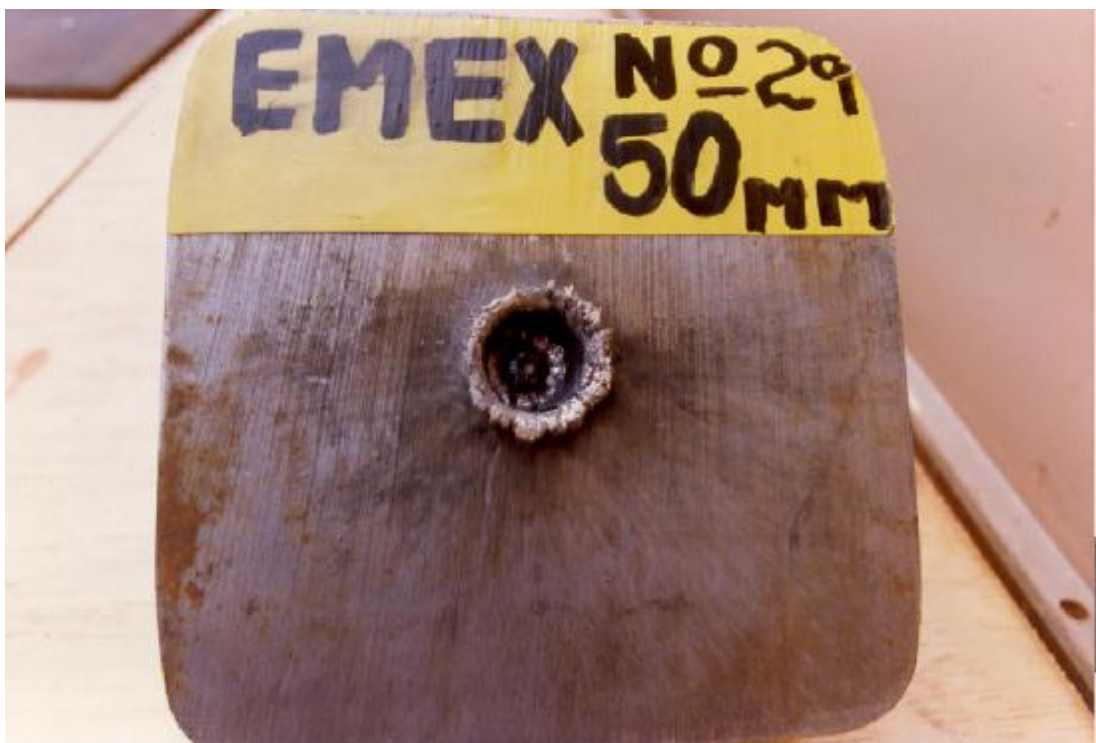




**PHOTOGRAPH 10.34, 10.35 AND 10.36**

Photograph 10.34, 10.35 and 10.36 show the slug indentations on the catch-plate for differing explosive configurations i.e. for EMEX and Powergel and 10 mm, 30 mm, 50 mm charge lengths of Composition B.

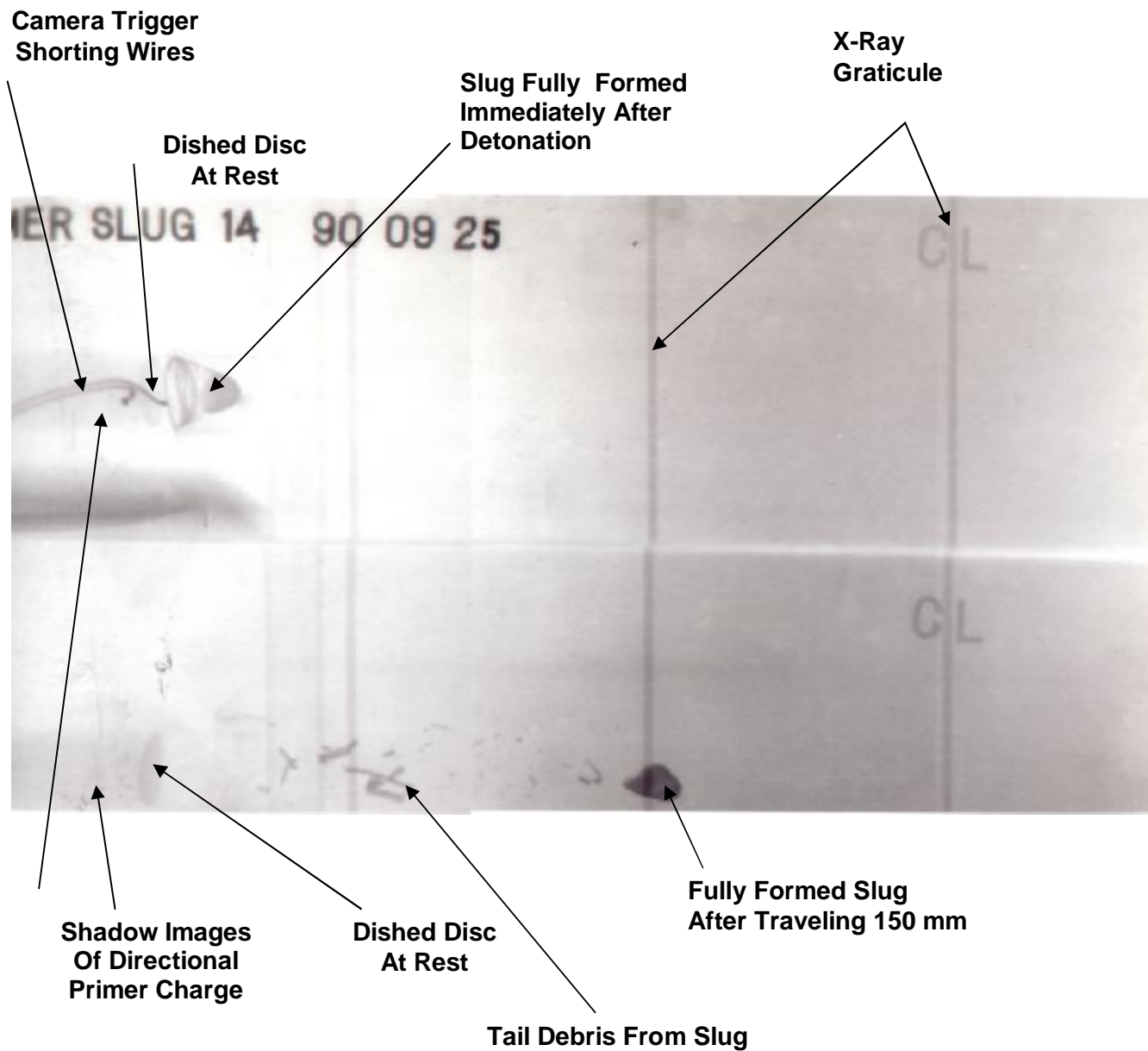




## **APPENDIX 11**

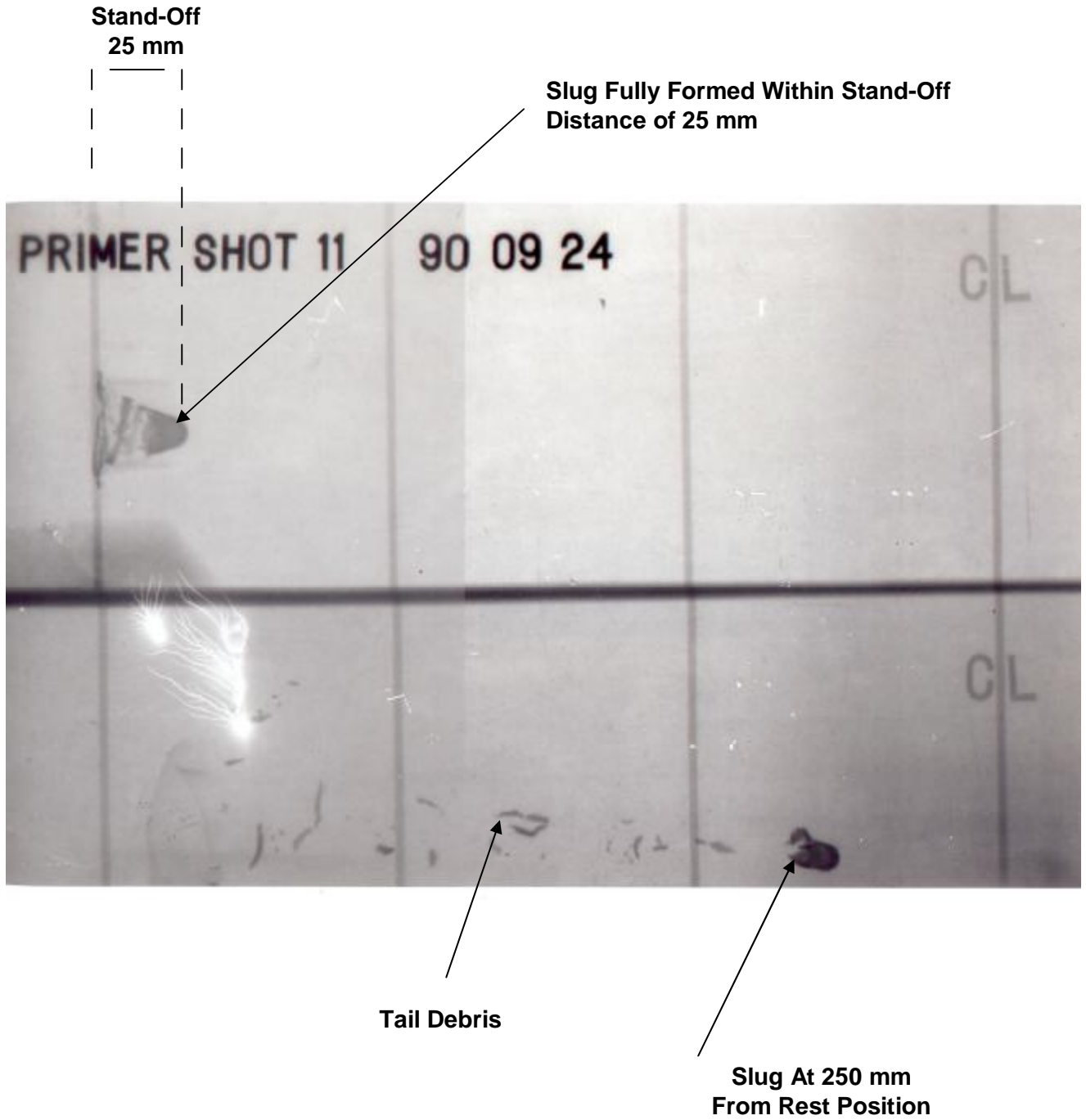
### **FLASH X-RAY PHOTOGRAPHS**





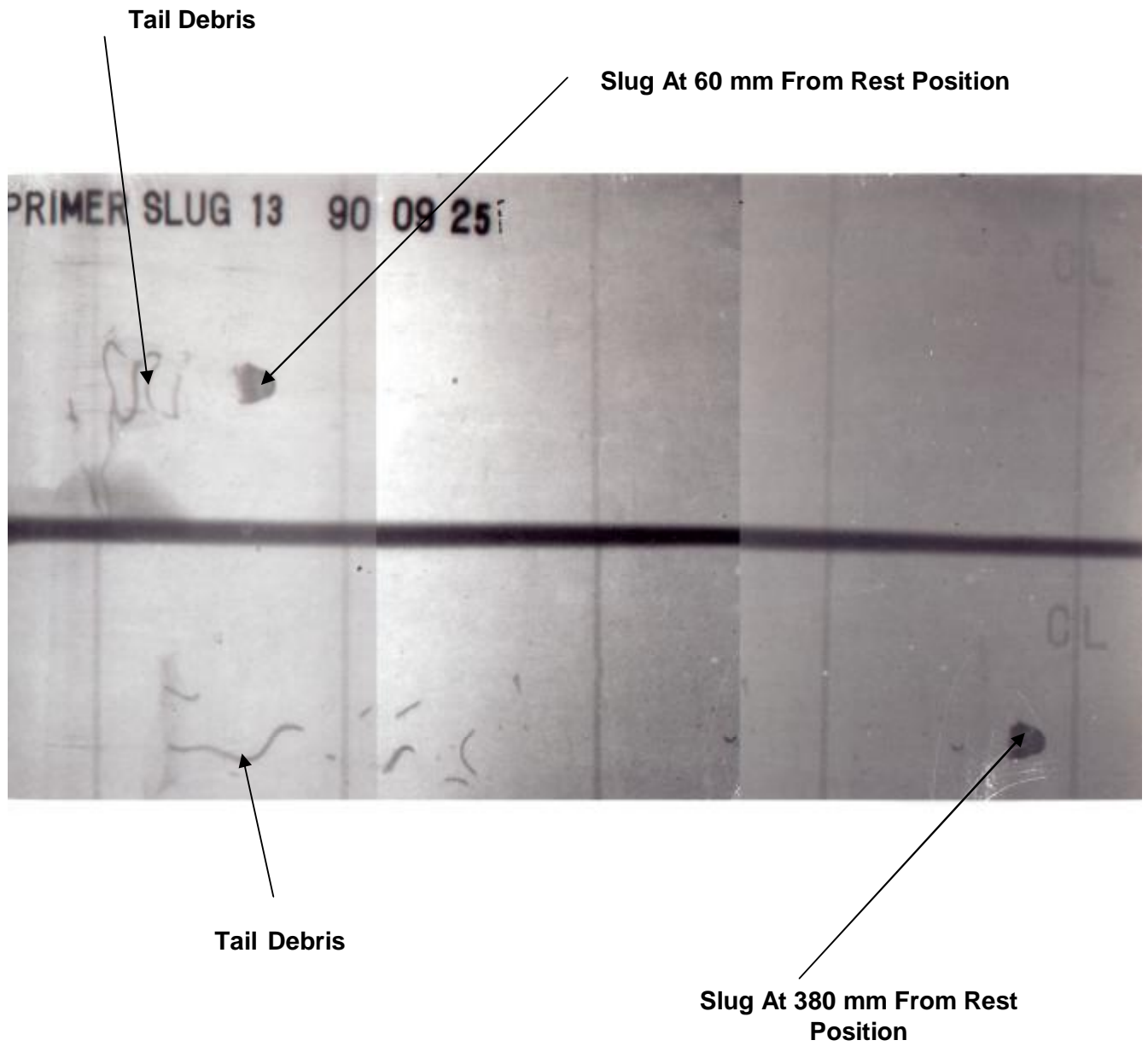
**FLASH X-RAY IMAGES NO.1**

**SHOWING DIRECTIONAL PRIMER CHARGE FORMATION AFTER 15 ms AND 75 ms**



**FLASH X-RAY IMAGES NO.2**

**SHOWING DIRECTIONAL PRIMER CHARGE SLUG FORMATION AT 15 ms AND  
125 ms AFTER DETONATION**



**FLASH X-RAY IMAGES NO.3**

**SHOWING DIRECTIONAL PRIMER CHARGE SLUG FORMATION AT 30 ms AND 190 ms AFTER DETONATION**

## **APPENDIX 12**

### **UNDERGROUND TESTS PHOTOGRAPHS**

## APPENDIX 12 PHOTOGRAPHS

### PHOTOGRAPH 12.1

Photograph 12.1 shows the standard explosives used underground on Village Main Gold Mine namely Stopecord 9 igniter cord, 8D detonator capped fire and Tovex 220 watergel explosive.



## PHOTOGRAPH 12.2

Photograph 12.2 shows a typical socket left after a blast. Note the radial cracks emanating from the hole which indicates that the hole has been blasted.



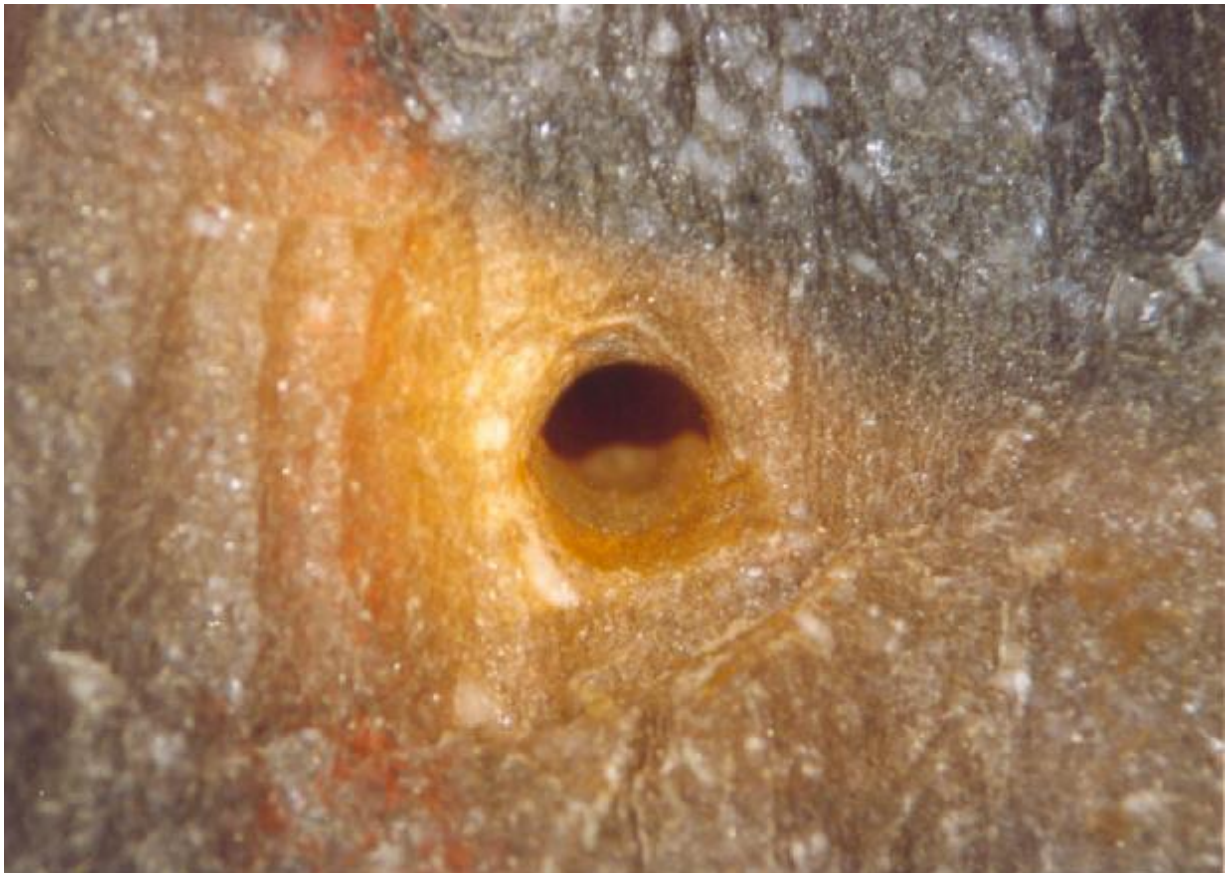
### PHOTOGRAPH 12.3

Photograph 12.3 shows a hole which has been blasted to its full length with the characteristic ‘wit koel’ at the toe of the hole. The wit koel is the “white shot” of the crushed rock at the toe of the hole. To have a face full of wit koels means that the round has broken out to its full length and will mean the minimum of face preparation for the next blast – minimum of fractured face rock to be barred down and removed and no pumping out of sockets.



#### PHOTOGRAPH 12.4

Photograph 12.4 shows a misfired hole. Note there is no crushed annulus or radial cracks emanating from the hole. This misfire was caused by detonator failure.





## PHOTOGRAPH 12.5

Photograph 12.5 shows a misfired hole which has only partially exploded. The primer is still evident in the hole and could have been caused by out-of-sequence firing with the following hole going off before this one, thus severing the charge column.



## PHOTOGRAPH 12.6

Photograph 12.6 shows the socket of a blasted hole of an apparently efficient blast. The socket length is the order of one caliber or 30 mm.



## PHOTOGRAPH 12.7

Photograph 12.7 shows an end hole broken out clearly to its full length. The end of the hole is clearly visible and the radial fracture at the toe of the hole, perpendicular to the axis of the hole is clearly in evidence.



## PHOTOGRAPH 12.8

Photograph 12.8 also shows good break out with a minimum socket.



## PHOTOGRAPH 12.9

Photograph 12.9 clearly shows the wit koel clean break and the perpendicular fracture at the toe of the hole.



## PHOTOGRAPH 12.10

Photograph 12.10 shows the clean break of a hole with the break-out of rock to the right of the hole in advance of the toe (negative socket effect).



## PHOTOGRAPH 12.11

Photograph 12.11 shows circumferential cracks around the hole indicating the effect of a high velocity of detonation explosive crushing the rock immediately adjacent to the hole.



## PHOTOGRAPH 12.12

Photograph 12.12 shows circumferential or concentric cracking close to the hole and radial cracking further away from the hole. Again minimal socket.

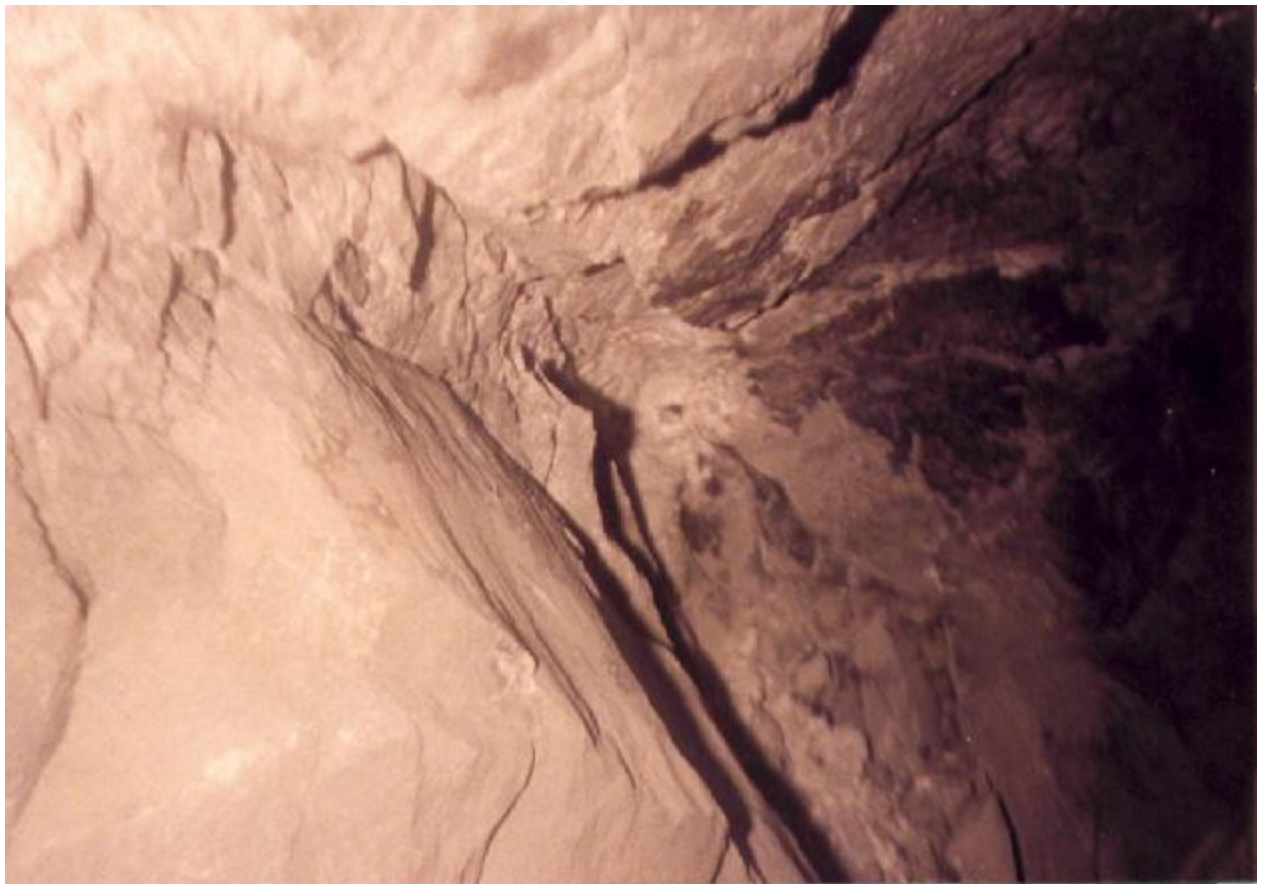




### PHOTOGRAPH 12.13

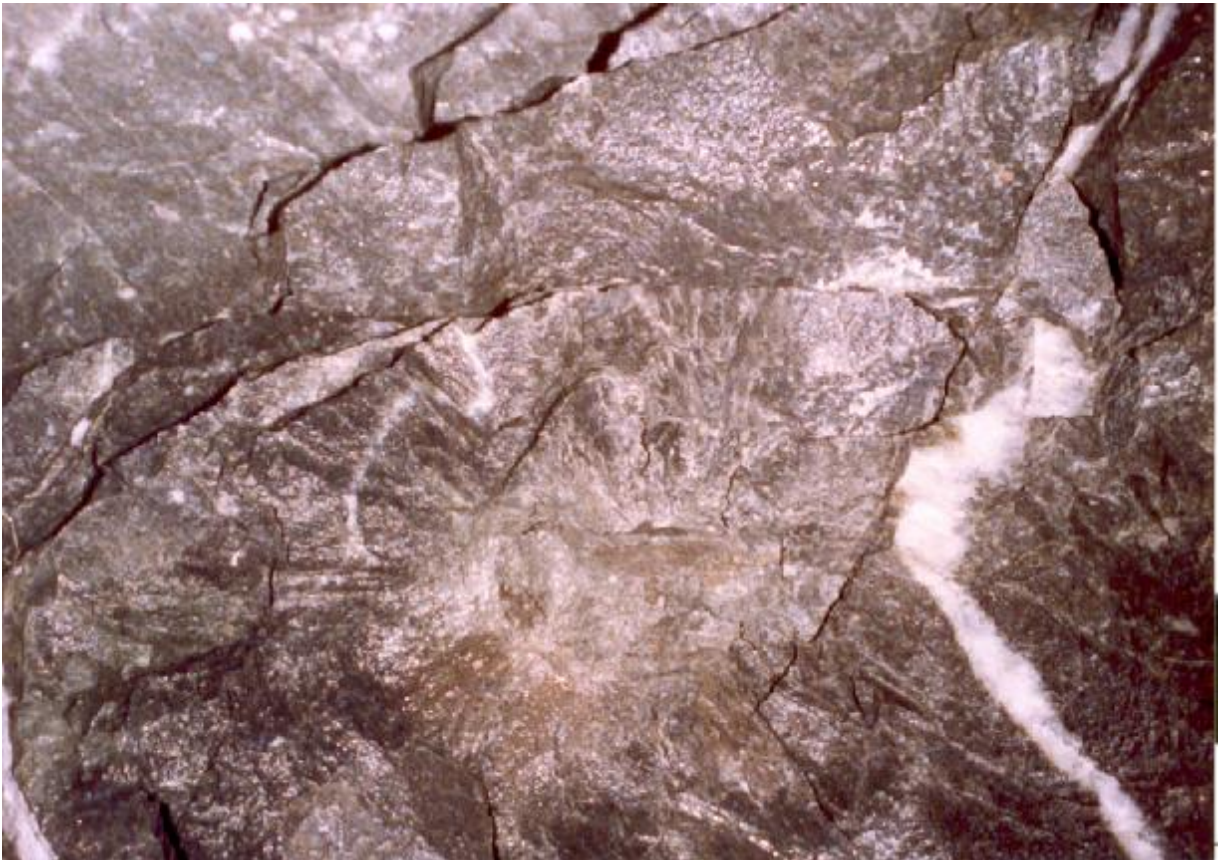
Photograph 12.13 shows the hole not only breaking out to its full length but also breaking away from the toe in a typical umbrella crack, giving a face advance greater than the hole length.

Of interest in this photograph is the presence of the remnants of the metal slug impacted into the toe of the hole.



## PHOTOGRAPHY 12.14

Photograph 12.14 shows the toe of the blasted hole with the typical umbrella fracture.



## PHOTOGRAPHY 12.15

Photograph 12.15 shows a hole which has broken out further than the toe of the hole. The half barrel of the blasthole can clearly be seen, as is the toe of the hole and the extent of the additional breakout to the right of the hole.



## PHOTOGRAPHY 12.16

Photograph 12.16 shows another hole which has broken out beyond the toe.



## PHOTOGRAPHY 12.17

Photograph 12.17 shows a blasthole broken out to its full length leaving no socket.



## PHOTOGRAPHY 12.18

Photograph 12.18 shows a top hole which has broken out to its full length. Note minimal blast damage to hanging wall.



## **APPENDIX 13**

### **COMPARISON OF THEORETICAL MODEL CALCULATIONS OF DISC VELOCITIES WITH MEASURED VELOCITIES FOR VARIOUS MASSES OF EXPLOSIVES AND DISCS**

### **A.13.1 A.D.L. TEST SERIES I**

**COMPOSITION B MASS = 65 grams**  
**DISC MASS = 6 grams**



## **A.13.1.1 GURNEY MODEL**

Explosive Type: Comp B

Test ID: #1 Series 1

VOD m/s:

$$D = 7600$$

Plate mass g:

$$m_p = 6$$

Charge Mass g:

$$C = 65$$

Measured Velocity

$$V_s = 2070$$

## DISPLAY RESULTS.....

Gurney constant

$$E_g = 2700$$

Reduced Gurney constant

$$E_{gr} = 1918.33$$

Particle speed in gas

$$U_p = 1900$$

C/M ratio

$$zI = 10.833$$

Velocity: standard Gurney

$$V_g = 3823.96$$

Velocity: reduced Gurney

$$V_{gr} = 2716.9$$

Velocity: momentum transfer

$$V_{pp} = 1603.9$$

Velocity: modified Gurney

$$V_{gm} = 3155$$

Measured Velocity

$$V_s = 2070 \quad \text{m/s}$$

Scroll to page 4 for derivation of efficiency factor f ...

Derive efficiency factor for effective explosive mass....standard Gurney model:.

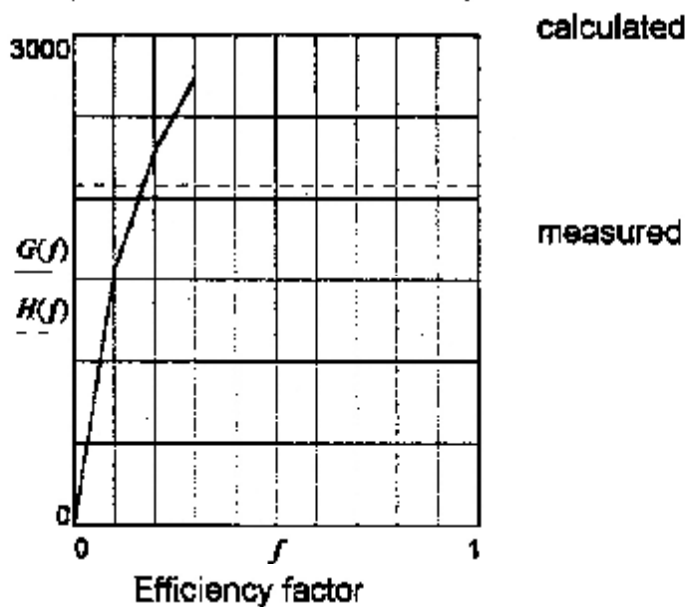
$$F(f) := E_g^2 \frac{3 \cdot z^2 \cdot f^2}{(f \cdot z + 1) \cdot (f \cdot z + 4)}$$

Check:  $\sqrt{F(f)} = 3824$       Should equal  $V_g = 3824$

Plot variation of calculated plate velocity with efficiency factor f:

$$G(f) = \sqrt{F(f)} \quad f = 0, 0.1 \dots 1 \quad H(f) = V_g$$

Variation of calculated velocity with factor f



Pick value of f close to the root of  $G(f) - H(f) = 0$

$$f := 0.1$$

Refine guess of f by iteration to locate root:

$$f = \text{root}((G(f) - H(f)), f) \quad f = 0.163$$

The efficiency factor is  $f = 0.163$

This is the fraction of explosive mass that contributes to the standard Gurney velocity of the plate.

Derive efficiency factor for effective explosive mass....modified Gurney model:

$$f = 1$$

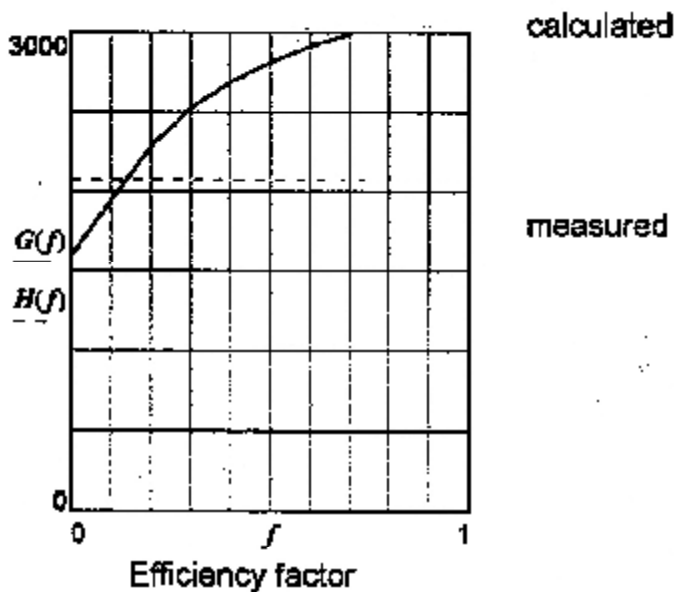
$$F(f) = E_{gr}^2 \frac{3z^2 f^2}{(fz+1)(fz+4)} + V_{pp}^2$$

Check:  $\sqrt{F(f)} = 3155$       Should equal  $V_{gm} = 3155$

Plot variation of calculated plate velocity with efficiency factor f:

$$G(f) = \sqrt{F(f)} \quad f = 0, 0.1 \dots 1 \quad H(f) = V_s$$

Variation of calculated velocity with factor f



Pick value of  $f$  close to the root of  $G(f) - H(f) = 0$

$$f = 0.1$$

Refine guess of  $f$  by iteration to locate root:

$$f = \text{root}((G(f) - H(f)), f) \quad f = 0.132$$

The efficiency factor is  $f = 0.132$

This is the fraction of explosive mass that contributes to the modified Gurney velocity of the plate.

Explosive Type: Comp B	
Test ID: #2 Series I	
VOD m/s:	$D = 7600$
Plate mass g:	$m_p = 6$
Charge Mass g:	$C = 65$
Measured Velocity	$V_s = 2005$

## DISPLAY RESULTS.....

Gurney constant	$E_g = 2700$	
Reduced Gurney constant	$E_{gr} = 1918.33$	
Particle speed in gas	$U_p = 1900$	
C/M ratio	$zI = 10.633$	
Velocity: standard Gurney	$V_g = 3824$	
Velocity: reduced Gurney	$V_{gr} = 2717$	
Velocity: momentum transfer	$V_{pp} = 1604$	
Velocity: modified Gurney	$V_{gm} = 3155$	
Measured Velocity	$V_s = 2005$	m/s

Scroll to page 4 for derivation of efficiency factor f ...

Derive efficiency factor for effective explosive mass...standard Gurney model:

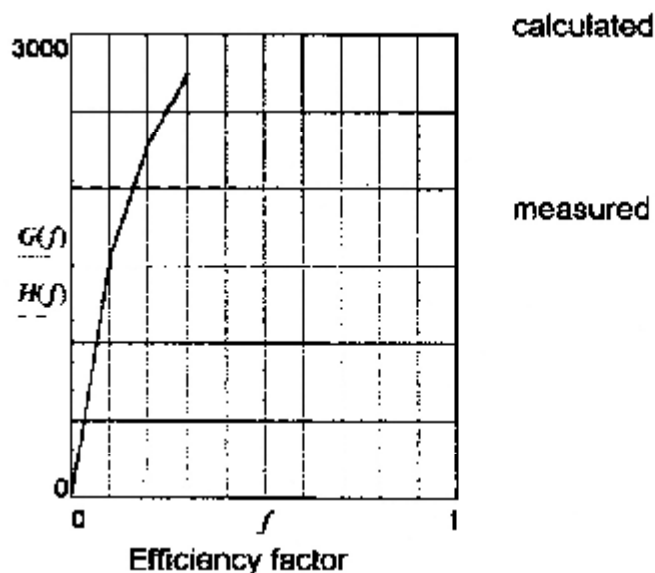
$$F(f) := E_g^2 \frac{3z^2 f^2}{(fz+1)(fz+4)}$$

Check:  $\sqrt{F(f)} = 3824$       Should equal  $V_g = 3824$

Plot variation of calculated plate velocity with efficiency factor f:

$$G(f) := \sqrt{F(f)} \quad f := 0, 0.1 \dots 1 \quad H(f) = V_g$$

Variation of calculated velocity with factor f



Pick value of  $f$  close to the root of  $G(f) - H(f) = 0$

$$f := 0.1$$

Refine guess of  $f$  by iteration to locate root:

$$f := \text{root}((G(f) - H(f)), f) \quad f = 0.154$$

The efficiency factor is  $f = 0.154$

This is the fraction of explosive mass that contributes to the standard Gurney velocity of the plate.

Derive efficiency factor for effective explosive mass...modified Gurney model..

$$f = 1$$

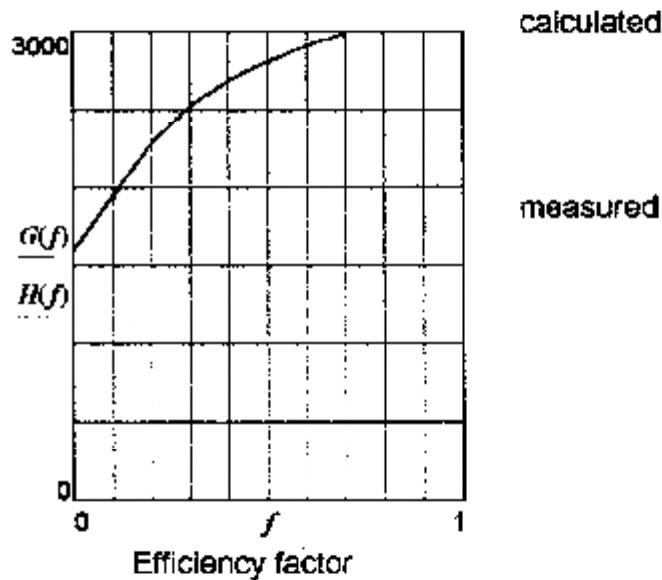
$$F(f) := E_{gr}^2 \frac{3z^2 f^2}{(fz+1)(fz+4)} + V_{pp}^2$$

Check:  $\sqrt{F(f)} = 3155$       Should equal  $V_{gm} = 3155$

Plot variation of calculated plate velocity with efficiency factor f:

$$G(f) := \sqrt{F(f)} \quad f := 0, 0.1..1 \quad H(f) := V_s$$

Variation of calculated velocity with factor f



Pick value of f close to the root of  $G(f)-H(f)=0$

$$f = 0.1$$

Refine guess of f by iteration to locate root:

$$f = \text{root}((G(f) - H(f)), f) \quad f = 0.115$$

The efficiency factor is  $f = 0.115$

This is the fraction of explosive mass that contributes to the modified Gurney velocity of the plate.

Explosive Type: Comp B	
Test ID: #3 Series I	
VOD m/s:	$D = 7600$
Plate mass g:	$m_p = 6$
Charge Mass g:	$C = 65$
Measured Velocity	$V_s = 2060$

## DISPLAY RESULTS.....

Gurney constant	$E_g = 2700$	
Reduced Gurney constant	$E_{gr} = 1918.33$	
Particle speed in gas	$U_p = 1900$	
C/M ratio	$zI = 10.833$	
Velocity: standard Gurney	$V_g = 3824$	
Velocity: reduced Gurney	$V_{gr} = 2717$	
Velocity: momentum transfer	$V_{pp} = 1604$	
Velocity: modified Gurney	$V_{gm} = 3155$	
Measured Velocity	$V_s = 2060$	m/s

Scroll to page 4 for derivation of efficiency factor f ...



Derive efficiency factor for effective explosive mass...standard Gurney model:

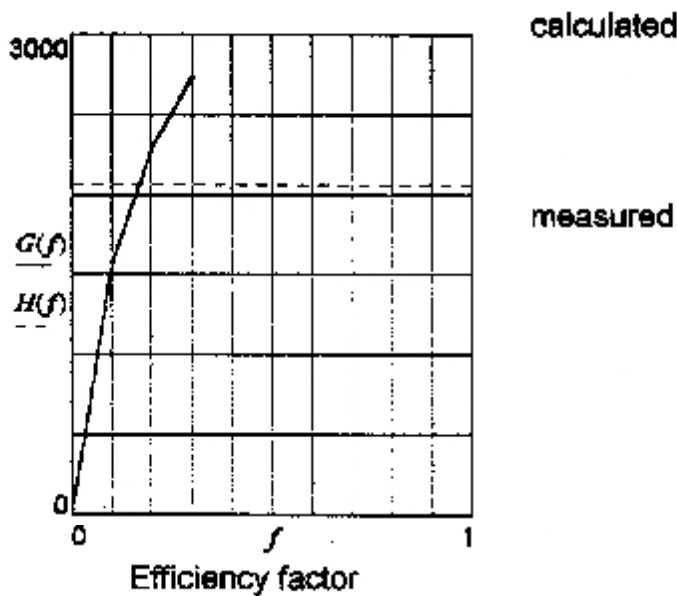
$$F(f) := E_g^2 \cdot \frac{3 \cdot z^2 \cdot f^2}{(fz - 1) \cdot (fz + 4)}$$

Check:  $\sqrt{F(f)} = 3824$       Should equal  $V_g = 3824$

Plot variation of calculated plate velocity with efficiency factor f:

$$G(f) = \sqrt{F(f)} \quad f = 0, 0.1, \dots, 1 \quad H(f) = V_g$$

Variation of calculated velocity with factor f



Pick value of  $f$  close to the root of  $G(f) - H(f) = 0$

$$f = 0.1$$

Refine guess of  $f$  by iteration to locate root:

$$f = \text{root}((G(f) - H(f)), f) \quad f = 0.162$$

The efficiency factor is  $f = 0.162$

This is the fraction of explosive mass that contributes to the standard Gurney velocity of the plate.

Derive efficiency factor for effective explosive mass....modified Gurney model:.

$$f = 1$$

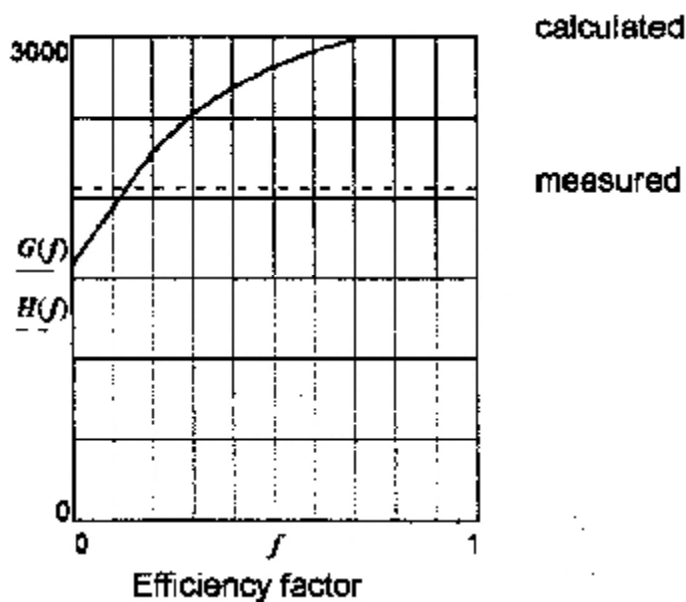
$$F(f) := E_{gr}^2 \cdot \frac{3 \cdot z^2 \cdot f^2}{(fz + 1) \cdot (fz + 4)} + V_{pp}^2$$

Check:  $\sqrt{F(f)} = 3155$       Should equal  $V_{gm} = 3155$

Plot variation of calculated plate velocity with efficiency factor f:

$$G(f) := \sqrt{F(f)} \quad f := 0, 0.1..1 \quad H(f) := V_s$$

Variation of calculated velocity with factor f



Pick value of f close to the root of  $G(f) - H(f) = 0$

$$f := 0.1$$

Refine guess of f by iteration to locate root:

$$f = \text{root}((G(f) - H(f)), f) \quad f = 0.129$$

The efficiency factor is  $f = 0.129$

This is the fraction of explosive mass that contributes to the modified Gurney velocity of the plate.

Explosive Type: Comp B	
Test ID: #4 Series I	
VOD m/s:	$D = 7600$
Plate mass g:	$m_p = 6$
Charge Mass g:	$C = 65$
Measured Velocity	$V_s = 2127$

## DISPLAY RESULTS.....

Gurney constant	$E_g = 2700$	
Reduced Gurney constant	$E_{gr} = 1918.33$	
Particle speed in gas	$U_p = 1900$	
C/M ratio	$z1 = 10.833$	
Velocity: standard Gurney	$V_g = 3824$	
Velocity: reduced Gurney	$V_{gr} = 2717$	
Velocity: momentum transfer	$V_{pp} = 1604$	
Velocity: modified Gurney	$V_{gm} = 3155$	
Measured Velocity	$V_s = 2127$	m/s

Scroll to page 4 for derivation of efficiency factor f ...

Derive efficiency factor for effective explosive mass....modified Gurney model:

$$f := 1$$

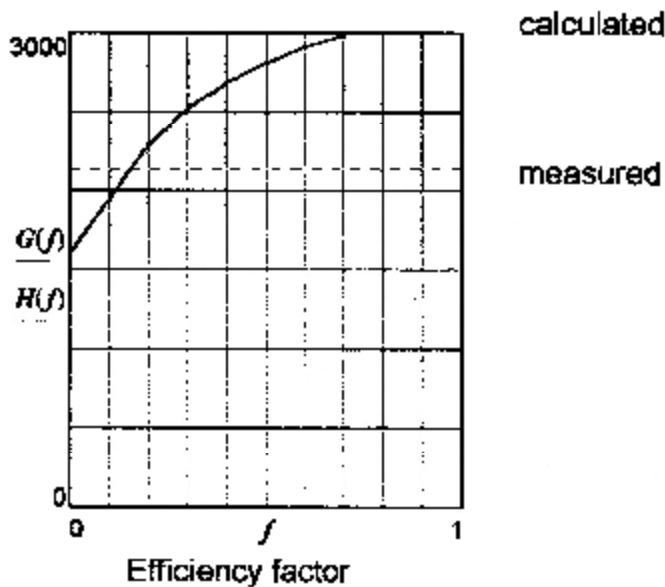
$$F(f) := E_{gr}^2 \cdot \frac{3 \cdot z^2 \cdot f^2}{(f \cdot z + 1) \cdot (f \cdot z + 4)} - V_{pp}^2$$

Check:  $\sqrt{F(f)} = 3155$       Should equal  $V_{gm} = 3155$

Plot variation of calculated plate velocity with efficiency factor f:

$$G(f) := \sqrt{F(f)} \quad f := 0, 0.1..1 \quad H(f) := V_s$$

Variation of calculated velocity with factor f



Pick value of f close to the root of  $G(f)-H(f)=0$ .

$$f := 0.1$$

Refine guess of f by iteration to locate root:

$$f := \text{root}((G(f) - H(f)), f) \quad f = 0.148$$

The efficiency factor is  $f = 0.148$

This is the fraction of explosive mass that contributes to the modified Gurney velocity of the plate.

Derive efficiency factor for effective explosive mass....standard Gurney model:

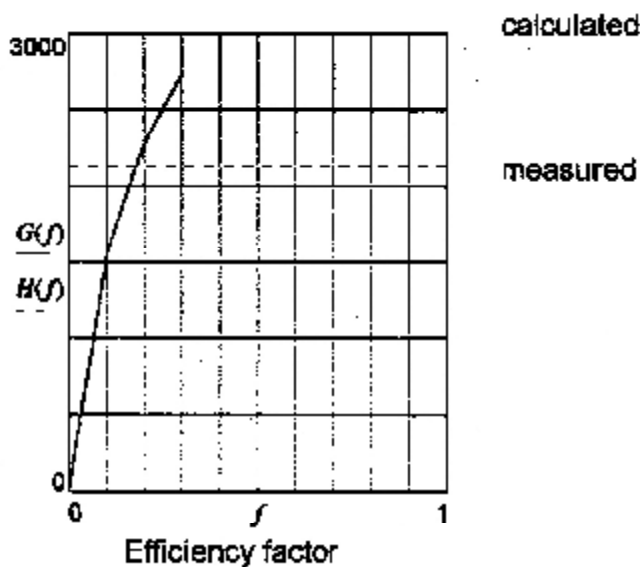
$$F(f) = E \frac{3z^2 f^2}{g^2 (fz+1)(fz+4)}$$

Check:  $\sqrt{F(f)} = 3824$       Should equal  $V_g = 3824$

Plot variation of calculated plate velocity with efficiency factor f:

$$G(f) = \sqrt{F(f)} \quad f = 0, 0.1, \dots, 1 \quad H(f) = V_g$$

Variation of calculated velocity with factor f



Pick value of  $f$  close to the root of  $G(f) - H(f) = 0$

$$f = 0.1$$

Refine guess of  $f$  by iteration to locate root:

$$f = \text{root}((G(f) - H(f)), f) \quad f = 0.172$$

The efficiency factor is  $f = 0.172$

This is the fraction of explosive mass that contributes to the standard Gurney velocity of the plate.

## **A.13.1.2      AZIZ MODEL**

## DISPLAY RESULTS ....Test : #1 Series I

Explosive = Comp B

Mass g	$C = 65$
VOD km/s	$D = 7.6$
Polytropic	$\Gamma = 3$
Plate mass g	$m_p = 6$
Measured velocity km/s	$V_s = 2.07$
Efficiency factor	$f = 1$
C/M ratio (actual)	$CM1 = 10.833$
C/M ratio (effective)	$CM2 = 10.833$
Detonation Velocity m/s	$D = 7.6$
Aziz velocity km/s (f=1)	$V_p = 4.38$
Aziz velocity (effective mass)	$V_{pf} = 4.38$
Measured Velocity m/s	$V_s = 2.07$
Plate Energy, calculated kJ	$E_p = 57.547$
Plate Energy, measured kJ	$E_{pm} = 12.855$
Explosive energy kJ	$E_o = 234.65$
Energy Efficiency, calculated	$E_f = 0.245$
Energy Efficiency, measured	$E_{fm} = 0.055$
Fraction Effective explosive mass	$f_e = 0.223$

Energy efficiency calculations suggest that only a fraction

$$f_e = 0.223$$

of the loaded explosive mass contributes to the Aziz-type one-dimensional gas expansion and plate acceleration.

Scroll to page 4 for determining efficiency factor f ....

## DERIVE CHARGE MASS EFFICIENCY FACTOR BASED ON VELOCITY.....

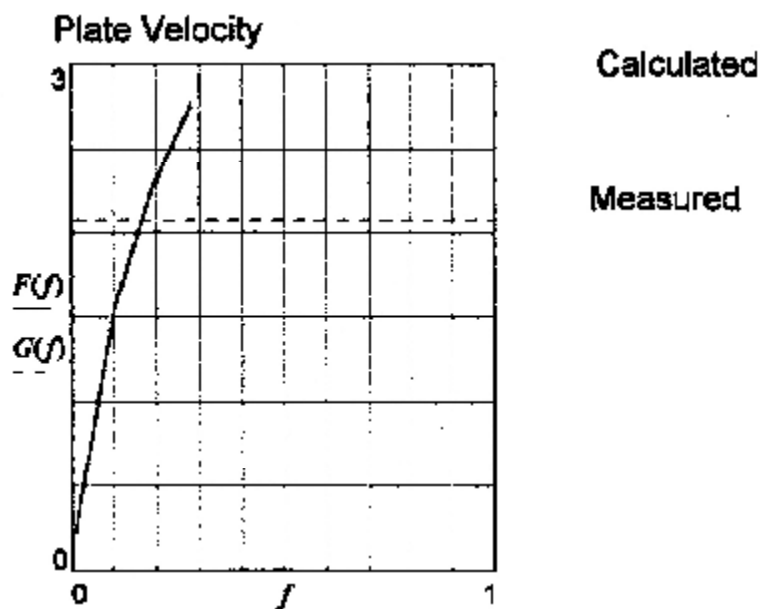
$$f := 0.01, 0.1 \dots 1$$

$$z(f) := \left[ \sqrt{\left( \frac{32}{27} \cdot CM2 \cdot f - 1 \right)} \right]$$

$$F(f) := D \cdot \frac{z(f) - 1}{z(f) + 1}$$

$$G(f) := V_s$$

Plot variation of calculated velocity with f ...



Pick a value of f close to the root of  $F(f) - G(f) = 0$

$f = 0.2$  ....first estimate of root

$f = \text{root}(|F(f) - G(f)|, f)$        $f = 0.16$       ...the root

The efficiency factor is       $f = 0.16$

This is the fraction of explosive mass that contributes to the one-dimensional gas expansion accelerating the plate to its final velocity.



## DISPLAY RESULTS ....Test : # Series I

Explosive = Comp B

Mass g	$C = 65$
VOD km/s	$D = 7.6$
Polytropic	$\Gamma = 3$
Plate mass g	$m_p = 6$
Measured velocity km/s	$V_s = 2.005$
Efficiency factor	$f = 1$
C/M ratio (actual)	$CM1 = 10.833$
C/M ratio (effective)	$CM2 = 10.833$
Detonation Velocity m/s	$D = 7.6$
Aziz velocity km/s (f=1)	$V_p = 4.38$
Aziz velocity (effective mass)	$V_{pf} = 4.38$
Measured Velocity m/s	$V_s = 2.005$
Plate Energy, calculated kJ	$E_p = 57.547$
Plate Energy, measured kJ	$E_{pm} = 12.06$
Explosive energy kJ	$E_o = 234.65$
Energy Efficiency, calculated	$E_f = 0.245$
Energy Efficiency, measured	$E_{fm} = 0.051$
Fraction Effective explosive mass	$f_e = 0.21$

Energy efficiency calculations suggest that only a fraction

$$f_e = 0.21$$

of the loaded explosive mass contributes to the Aziz-type one-dimensional gas expansion and plate acceleration.

Scroll to page 4 for determining efficiency factor f ....

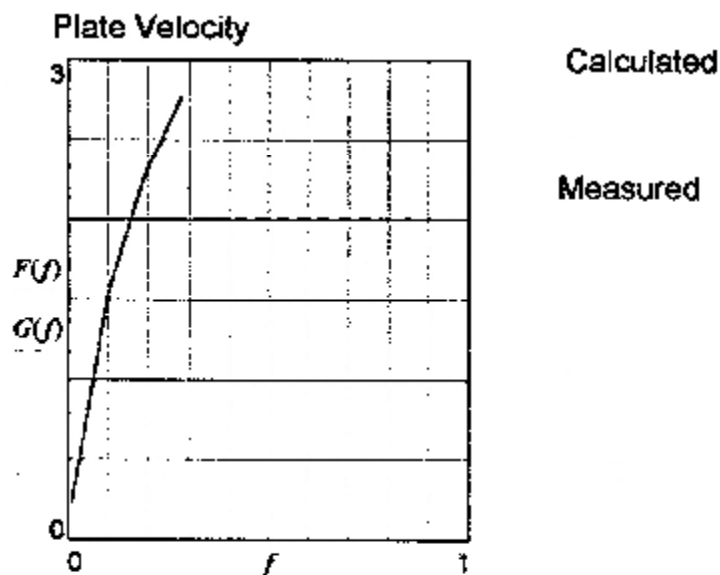
## DERIVE CHARGE MASS EFFICIENCY FACTOR BASED ON VELOCITY.....

$$f = 0.01, 0.1, 1$$

$$z(f) = \left[ \sqrt{\frac{32}{27} \cdot CM_2 f + 1} \right]$$

$$F(f) = D \cdot \frac{z(f) - 1}{z(f) + 1} \qquad G(f) = V_s$$

Plot variation of calculated velocity with f ...



Pick a value of  $f$  close to the root of  $F(f) - G(f) = 0$

$$f := 0.2 \qquad \dots \text{first estimate of root}$$

$$f := \text{root}(|F(f) - G(f)|, f) \qquad f = 0.152 \qquad \dots \text{the root}$$

$$\text{The efficiency factor is} \qquad f = 0.152$$

This is the fraction of explosive mass that contributes to the one-dimensional gas expansion accelerating the plate to its final velocity.

## DISPLAY RESULTS .... Test : #3 Series I

Explosive = Comp B

Mass g	$C = 65$
VOD km/s	$D = 7.6$
Polytropic	$\Gamma = 3$
Plate mass g	$m_p = 6$
Measured velocity km/s	$V_s = 2.06$
Efficiency factor	$f = 1$
C/M ratio (actual)	$CM1 = 10.833$
C/M ratio (effective)	$CM2 = 10.833$
Detonation Velocity m/s	$D = 7.6$
Aziz velocity km/s (f=1)	$V_p = 4.38$
Aziz velocity (effective mass)	$V_{pf} = 4.38$
Measured Velocity m/s	$V_s = 2.06$
Plate Energy, calculated kJ	$E_p = 57.547$
Plate Energy, measured kJ	$E_{pm} = 12.731$
Explosive energy kJ	$E_o = 234.65$
Energy Efficiency, calculated	$E_f = 0.245$
Energy Efficiency, measured	$E_{fm} = 0.054$
Fraction Effective explosive mass	$f_e = 0.221$

Energy efficiency calculations suggest that only a fraction

$$f_e = 0.221$$

of the loaded explosive mass contributes to the Aziz-type one-dimensional gas expansion and plate acceleration.

Scroll to page 4 for determining efficiency factor f ....

## DERIVE CHARGE MASS EFFICIENCY FACTOR BASED ON VELOCITY.....

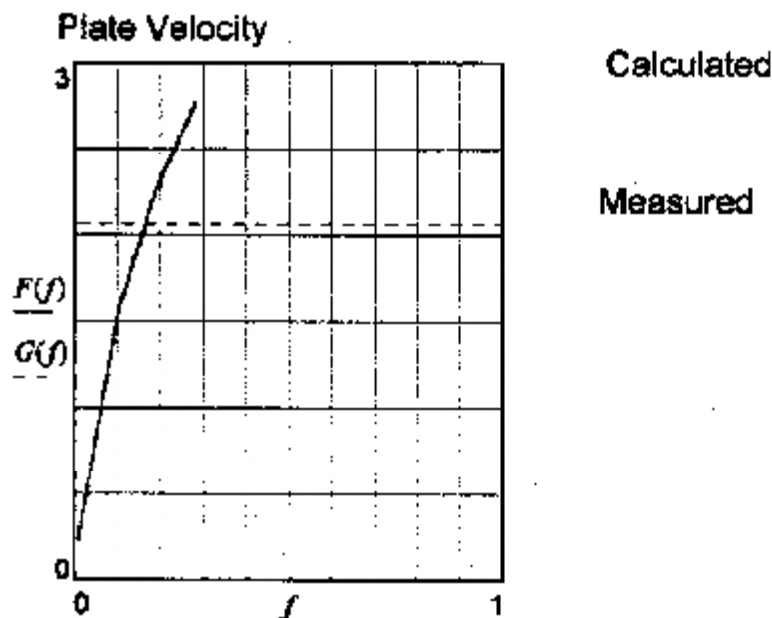
$$f := 0.01, 0.1, 1$$

$$z(f) := \sqrt{\left(\frac{32}{27} \cdot CM^2 \cdot f + 1\right)}$$

$$F(f) := D \cdot \frac{z(f) - 1}{z(f) + 1}$$

$$G(f) := V_s$$

Plot variation of calculated velocity with f ...



Pick a value of f close to the root of  $F(f) - G(f) = 0$

$$f = 0.2 \quad \dots \text{first estimate of root}$$

$$f := \text{root}(\cdot F(f) - G(f) | f) \quad f = 0.159 \quad \dots \text{the root}$$

$$\text{The efficiency factor is} \quad f = 0.159$$

This is the fraction of explosive mass that contributes to the one-dimensional gas expansion accelerating the plate to its final velocity.

## DISPLAY RESULTS .... Test : #4 Series I

Explosive = Comp B

Mass g	$C = 65$
VOD km/s	$D = 7.6$
Polytropic	$\Gamma = 3$
Plate mass g	$m_p = 6$
Measured velocity km/s	$V_s = 2.127$
Efficiency factor	$f = 1$
C/M ratio (actual)	$CM1 = 10.833$
C/M ratio (effective)	$CM2 = 10.833$
Detonation Velocity m/s	$D = 7.6$
Aziz velocity km/s (f=1)	$V_p = 4.38$
Aziz velocity (effective mass)	$V_{pf} = 4.38$
Measured Velocity m/s	$V_s = 2.127$
Plate Energy, calculated kJ	$E_p = 57.547$
Plate Energy, measured kJ	$E_{pm} = 13.572$
Explosive energy kJ	$E_o = 234.65$
Energy Efficiency, calculated	$E_f = 0.245$
Energy Efficiency, measured	$E_{fm} = 0.058$
Fraction Effective explosive mass	$f_e = 0.236$

Energy efficiency calculations suggest that only a fraction

$$f_e = 0.236$$

of the loaded explosive mass contributes to the Aziz-type one-dimensional gas expansion and plate acceleration.

Scroll to page 4 for determining efficiency factor f ....

## DERIVE CHARGE MASS EFFICIENCY FACTOR BASED ON VELOCITY.....

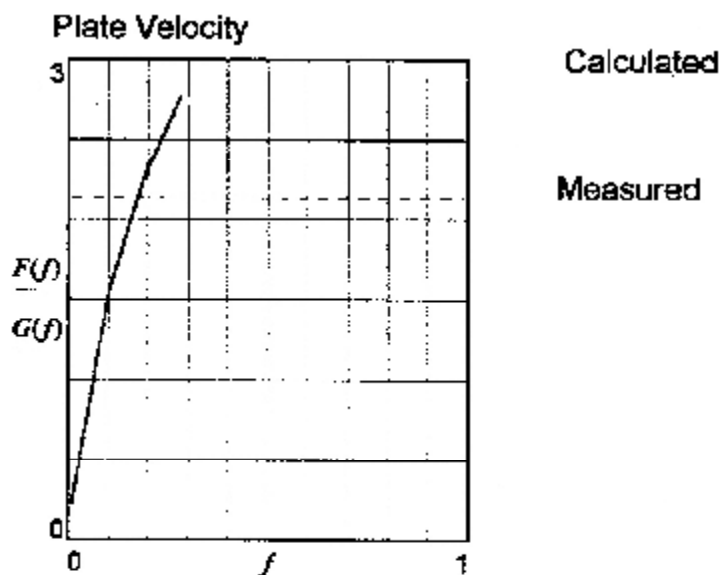
$$f = 0.01, 0.1, 1$$

$$z(f) = \sqrt{\left( \frac{32}{27} \cdot CM^2 \cdot f + 1 \right)^{1/3}}$$

$$F(f) = D \cdot \frac{z(f) - 1}{z(f) + 1}$$

$$G(f) = V_s$$

Plot variation of calculated velocity with f ...



Pick a value of  $f$  close to the root of  $F(f) - G(f) = 0$

$$f = 0.2 \quad \dots \text{first estimate of root}$$

$$f = \text{root}(|F(f) - G(f)|, f) \quad f = 0.168 \quad \dots \text{the root}$$

$$\text{The efficiency factor is} \quad f = 0.168$$

This is the fraction of explosive mass that contributes to the one-dimensional gas expansion accelerating the plate to its final velocity.

### **A.13.1.3 FICKETT MODEL**

Explosive Type: Composition B

Charge Length  $l = 60$   
 Charge mass g  $C = 65$   
 VOD km/s  $D = 7.6$   
 Polytropic  $\Gamma = 3$   
 Plate mass  $m = 6$  Sound speed km/s  $C_b = 3.6$   
 Measured Velocity m/s  $V_{exp} = 2070$

PRINT RESULTS OF CALCULATIONS (2) \*\*\*\*\*

	us	us	mm	m/s
	8.117	0.222	0.127	1049
	8.339	0.444	0.438	1704
	8.561	0.667	0.869	2154
	8.784	0.889	1.386	2484
	9.006	1.111	1.967	2736
$t =$	9.228	$t_{acc} = 1.333$	$X_{acc} = 2.598$	$V_p = 2936$
	9.45	1.556	3.269	3097
	9.673	1.778	3.973	3230
	9.895	2	4.703	3341
	10.117	2.222	5.456	3436
	10.339	2.444	6.229	3517
	10.561	2.667	7.019	3587
	10.784	2.889	7.823	3649
	11.006	3.111	8.64	3703
	11.228	3.333	9.468	3751
	11.45	3.556	10.306	3794
	11.673	3.778	11.154	3832
	11.895	4	12.009	3866
	12.117	4.222	12.872	3898
	12.339	4.444	13.741	3926

Time from  
detonation  
at start of  
explosive column

Time from  
start of  
plate  
acceleration

Plate  
displacement

Plate velocity



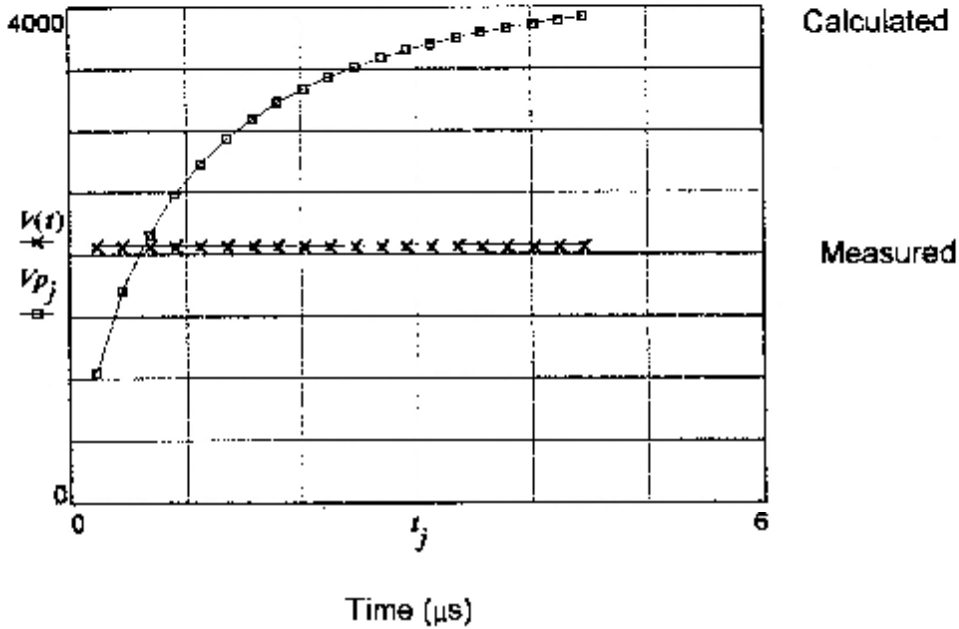
DISPLAY RESULTS OF CALCULATIONS\*\*\*\*\*

Define experimental value of plate velocity as a constant- value function of time...

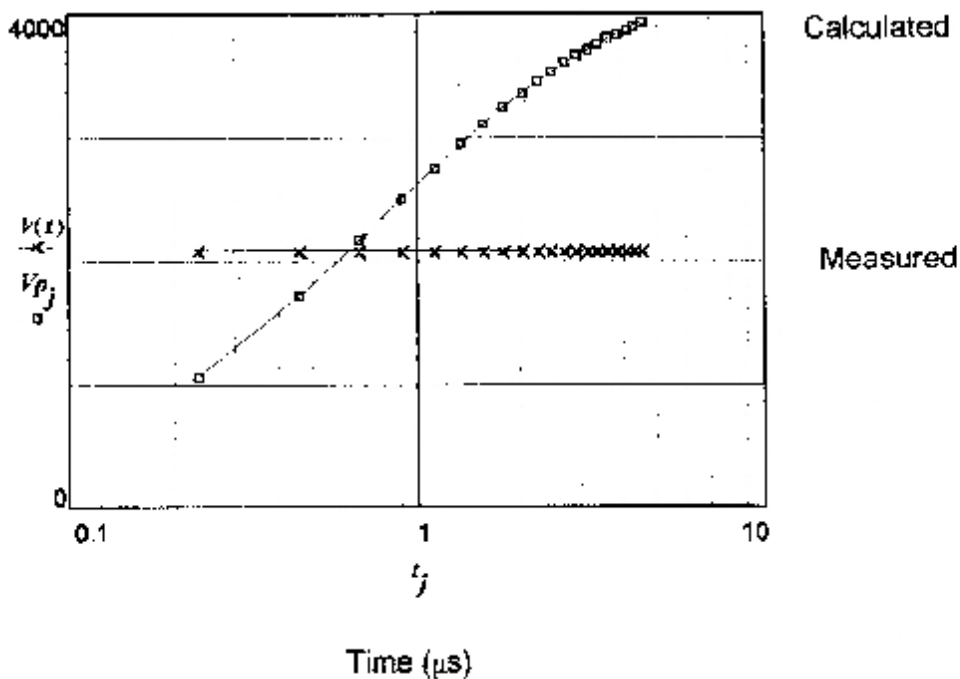
$$V(t) = V_{exp} \quad t := t_{acc} - 0.01 \quad > 0$$

TIME VARIATION OF PLATE VELOCITY

Velocity m/s



Plot time on logarithmic scale....



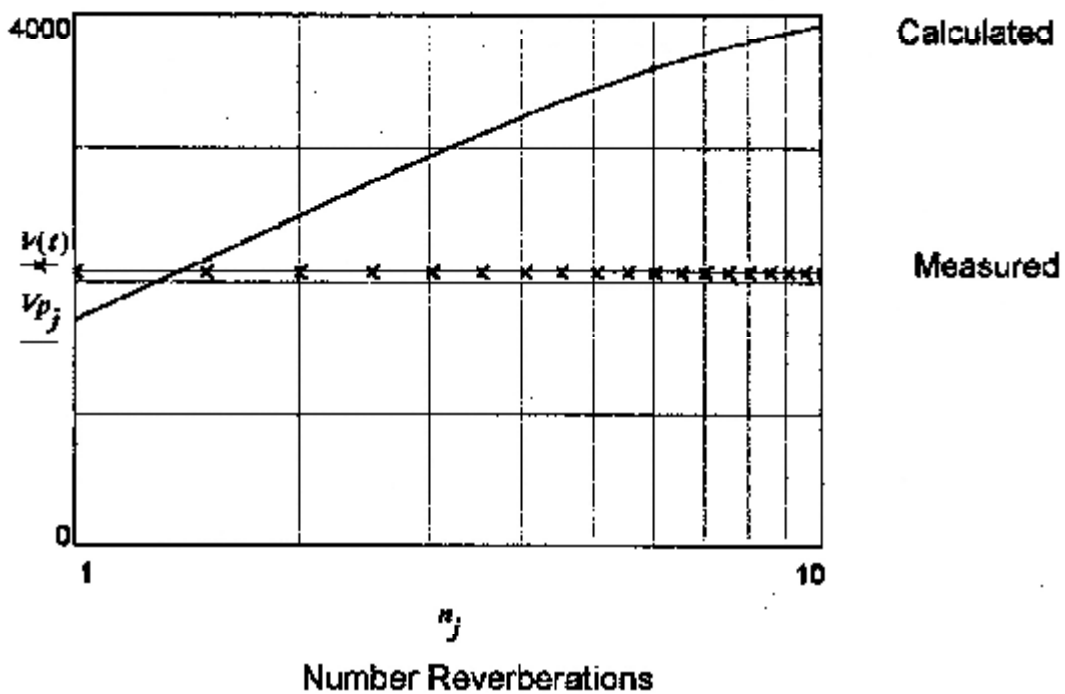
Plot velocity against number of pressure reverberations in plate....

$j := 1..N$  .... must be  $> 0$  for logarithmic axis

$n_j = \frac{j}{2}$  .... n is the number of transits ....

j denotes reverberation number, i.e. number of time increments as defined in section (1) under CALCULATIONS

Plate Velocity m/s



Plot indicates that measured plate velocity is attained shortly before the SECOND passage of the pressure pulse through plate thickness

Explosive Type: Composition B

Charge Length  $L = 60$   
 Charge mass g  $C = 65$   
 VOD km/s  $D = 7.6$   
 Polytropic  $\Gamma = 3$   
 Plate mass  $m = 6$  Sound speed km/s  $C_b = 3.6$   
 Measured Velocity m/s  $V_{exp} = 2005$

PRINT RESULTS OF CALCULATIONS (2) \*\*\*\*\*

	us	us	mm	m/s
	8.117	0.222	0.127	1049
	8.339	0.444	0.438	1704
	8.561	0.667	0.869	2154
	8.784	0.889	1.386	2484
	9.006	1.111	1.967	2736
$t =$	9.228	$t_{acc} =$ 1.333	$X_{acc} =$ 2.598	$V_p =$ 2936
	9.45	1.556	3.269	3097
	9.673	1.778	3.973	3230
	9.895	2	4.703	3341
	10.117	2.222	5.456	3436
	10.339	2.444	6.229	3517
	10.561	2.667	7.019	3587
	10.784	2.889	7.823	3649
	11.006	3.111	8.64	3703
	11.228	3.333	9.468	3751
	11.45	3.556	10.306	3794
	11.673	3.778	11.154	3832
	11.895	4	12.009	3866
	12.117	4.222	12.872	3898
	12.339	4.444	13.741	3926

Time from  
detonation  
at start of  
explosive column

Time from  
start of  
plate  
acceleration

Plate  
displacement

Plate velocity

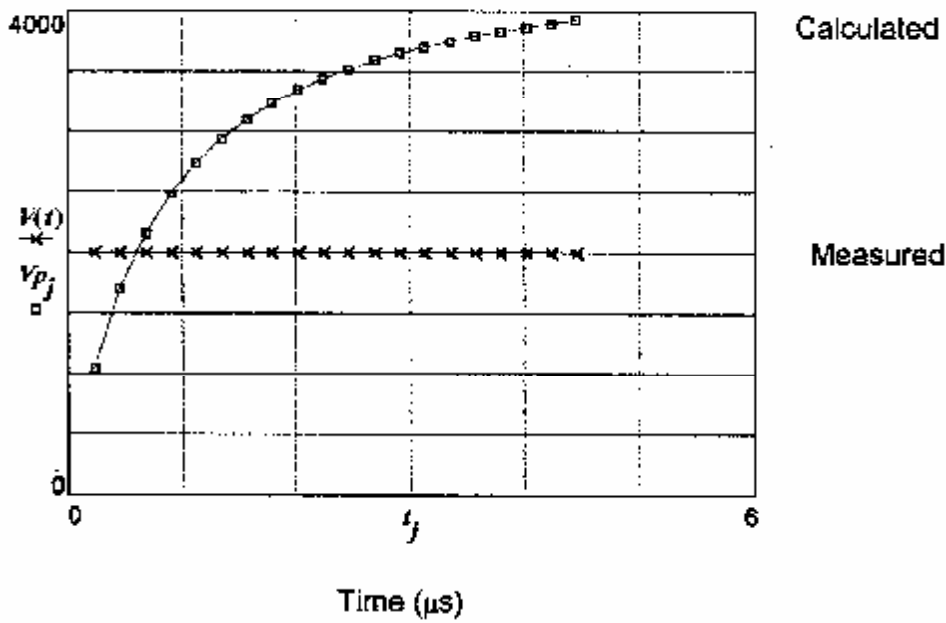
DISPLAY RESULTS OF CALCULATIONS\*\*\*\*\*

Define experimental value of plate velocity as a constant-value function of time...

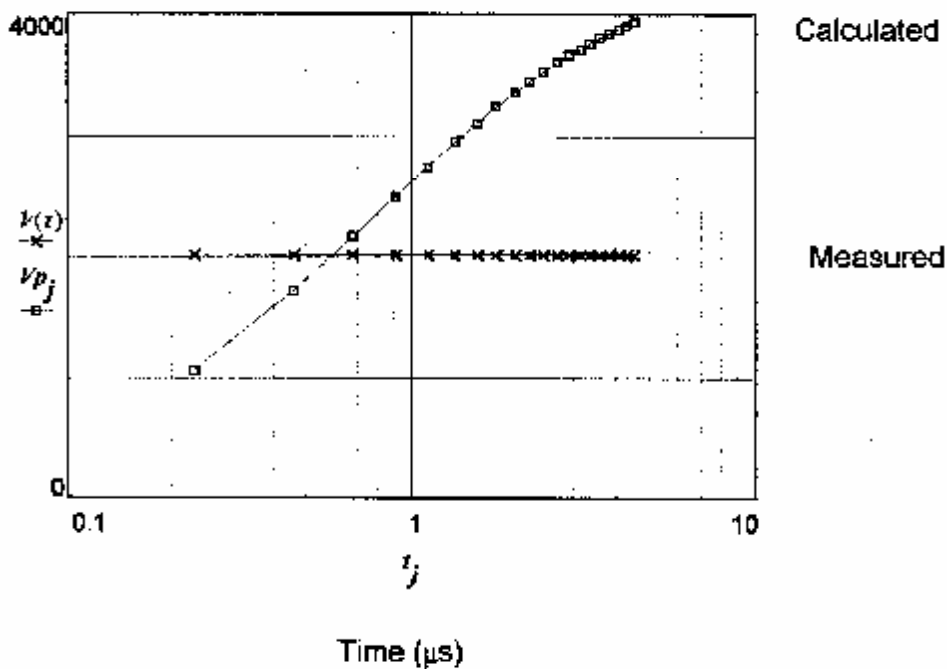
$$V(t) = V_{exp} \quad t := t_{acc} + 0.01 \quad >0$$

TIME VARIATION OF PLATE VELOCITY

Velocity m/s



Plot time on logarithmic scale....



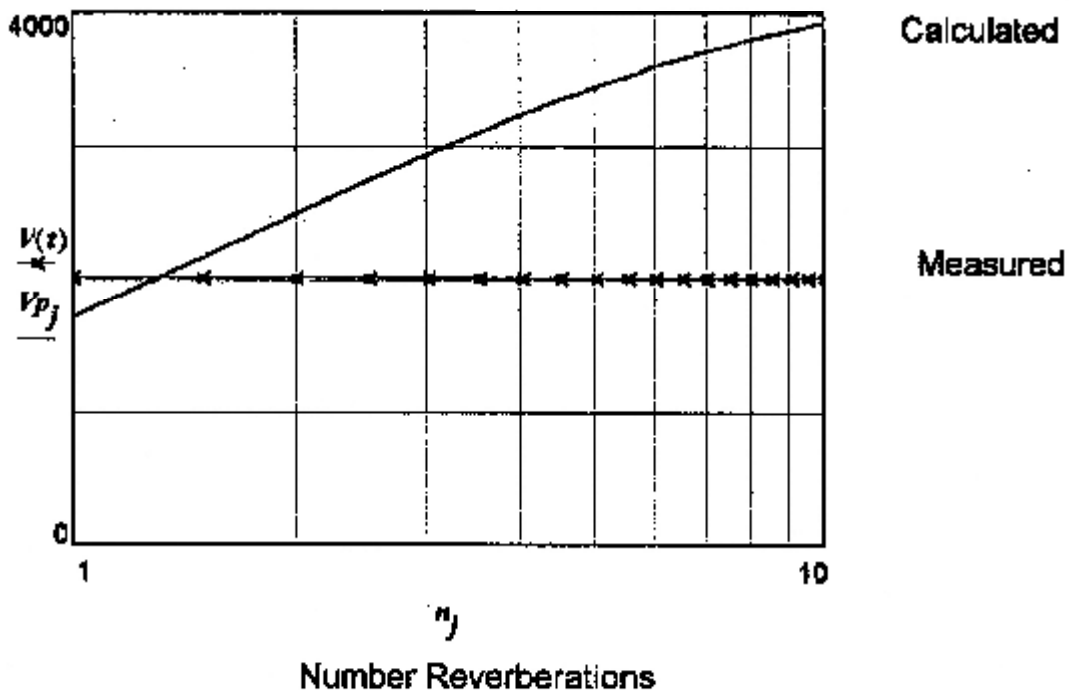
Plot velocity against number of pressure reverberations in plate....

$j := 1..N$  ....must be  $> 0$  for logarithmic axis

$n_j := \frac{j}{2}$  ....n is the number of transits ....

n denotes reverberation number, i.e. number of time increments as defined in section (1) under CALCULATIONS

Plate Velocity m/s



Plot indicates that measured plate velocity is attained shortly before the SECOND passage of the pressure pulse through plate thickness

Explosive Type: Composition B

Charge Length  $L = 60$   
 Charge mass g  $C = 65$   
 VOD km/s  $D = 7.6$   
 Polytropic  $\Gamma = 3$   
 Plate mass  $m = 6$       Sound speed km/s  $C_b = 3.6$   
 Measured Velocity m/s  $V_{exp} = 2060$

PRINT RESULTS OF CALCULATIONS (2) .....

	us	us	mm	m/s
	8.117	0.222	0.127	1049
	8.339	0.444	0.438	1704
	8.561	0.667	0.869	2154
	8.784	0.889	1.386	2484
	9.006	1.111	1.967	2736
$t =$	9.228	$t_{acc} = 1.333$	$X_{acc} = 2.598$	$V_p = 2936$
	9.45	1.556	3.269	3097
	9.673	1.778	3.973	3230
	9.895	2	4.703	3341
	10.117	2.222	5.456	3436
	10.339	2.444	6.229	3517
	10.561	2.667	7.019	3587
	10.784	2.889	7.823	3649
	11.006	3.111	8.64	3703
	11.228	3.333	9.468	3751
	11.45	3.556	10.306	3794
	11.673	3.778	11.154	3832
	11.895	4	12.009	3866
	12.117	4.222	12.872	3898
	12.339	4.444	13.741	3926

Time from  
detonation  
at start of  
explosive column

Time from  
start of  
plate  
acceleration

Plate  
displacement

Plate velocity

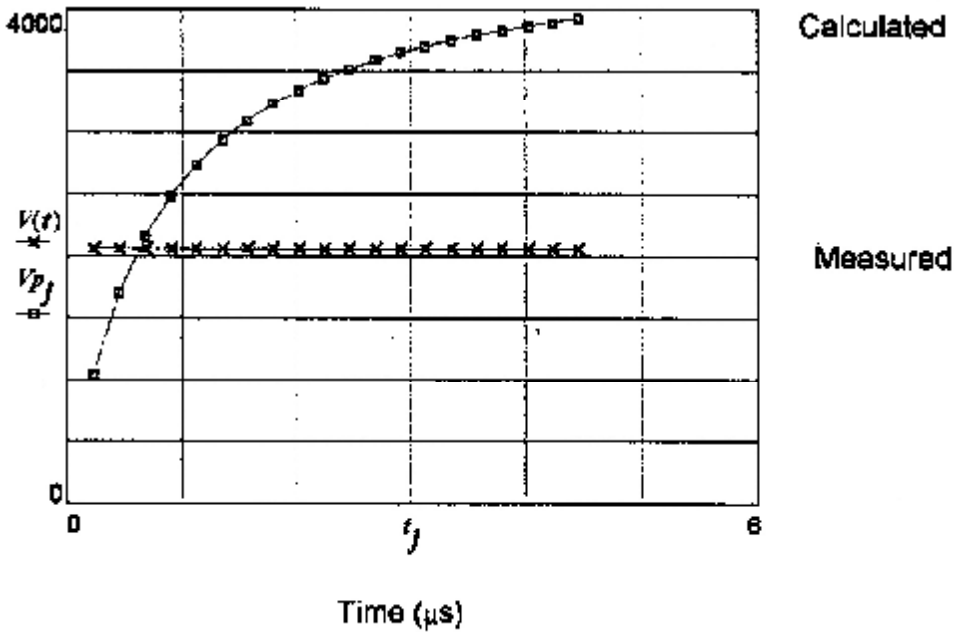
DISPLAY RESULTS OF CALCULATIONS\*\*\*\*\*

Define experimental value of plate velocity as a constant-value function of time...

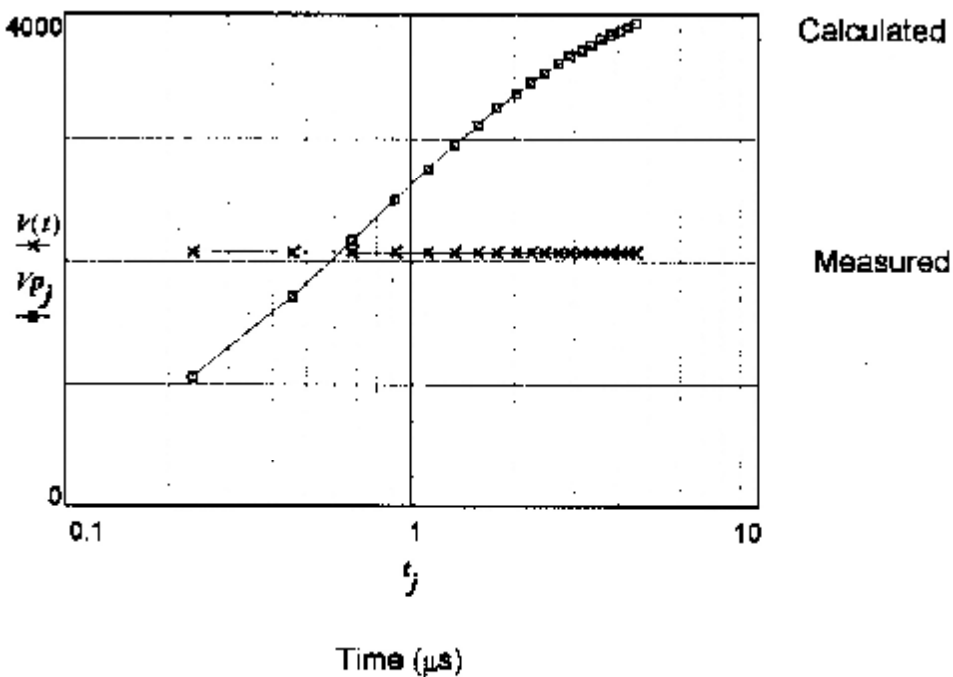
V(t) := V\_exp      t := t\_acc + 0.01      >0

TIME VARIATION OF PLATE VELOCITY

Velocity m/s



Plot time on logarithmic scale...



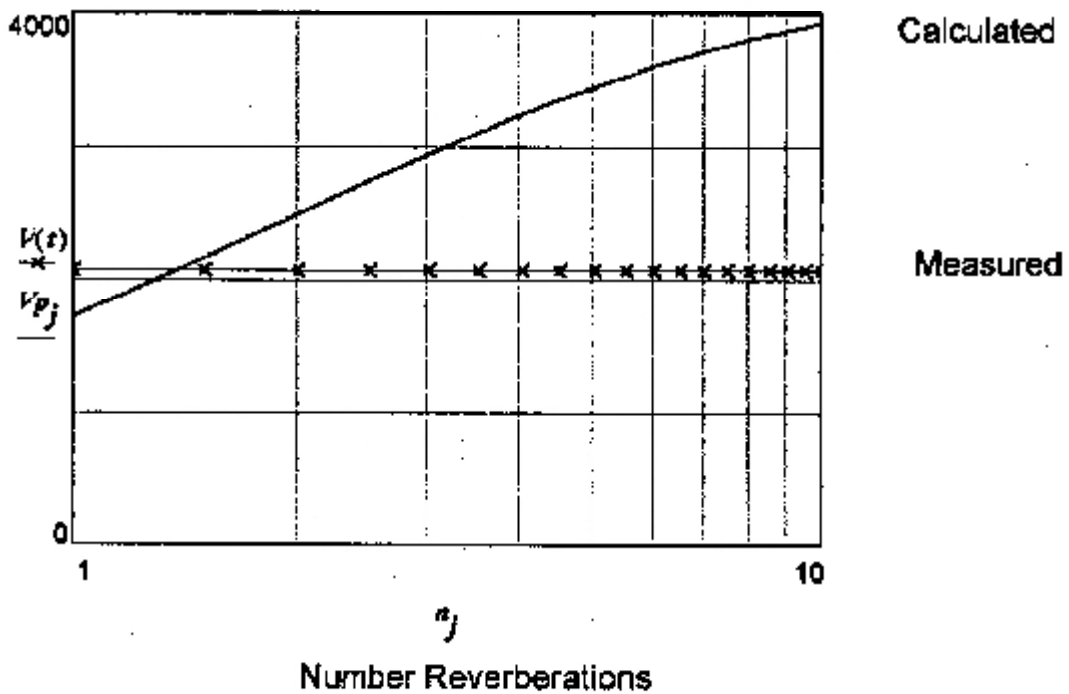
Plot velocity against number of pressure reverberations in plate....

$j = 1 \dots N$  ....must be  $> 0$  for logarithmic axis

$n_j = \frac{j}{2}$  ....n is the number of transits ....

n denotes reverberation number, i.e. number of time increments as defined in section (1) under CALCULATIONS.

Plate Velocity m/s



Plot indicates that measured plate velocity is attained shortly before the SECOND passage of the pressure pulse through plate thickness



Explosive Type: Composition B

Charge Length  $L = 60$   
 Charge mass g  $C = 65$   
 VOD km/s  $D = 7.6$   
 Polytropic  $\Gamma = 3$   
 Plate mass  $m = 6$       Sound speed km/s  $C_b = 3.6$   
 Measured Velocity m/s  $V_{exp} = 2127$

PRINT RESULTS OF CALCULATIONS (2) \*\*\*\*\*

	us	us	mm	m/s
	8.117	0.222	0.127	1049
	8.339	0.444	0.438	1704
	8.561	0.667	0.869	2154
	8.784	0.889	1.386	2484
	9.006	1.111	1.967	2736
$t =$	9.228	$t_{acc} =$ 1.333	$X_{acc} =$ 2.598	$V_p =$ 2936
	9.45	1.556	3.269	3097
	9.673	1.778	3.973	3230
	9.895	2	4.703	3341
	10.117	2.222	5.456	3436
	10.339	2.444	6.229	3517
	10.561	2.667	7.019	3587
	10.784	2.889	7.823	3649
	11.006	3.111	8.64	3703
	11.228	3.333	9.468	3751
	11.45	3.556	10.306	3794
	11.673	3.778	11.154	3832
	11.895	4	12.009	3866
	12.117	4.222	12.872	3898
	12.339	4.444	13.741	3926

Time from  
detonation  
at start of  
explosive column

Time from  
start of  
plate  
acceleration

Plate  
displacement

Plate velocity

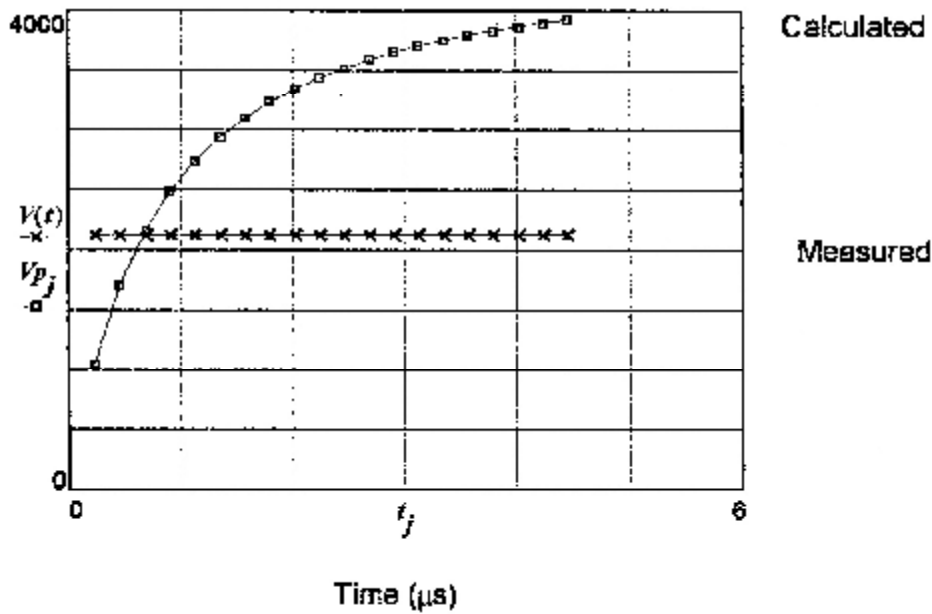
DISPLAY RESULTS OF CALCULATIONS\*\*\*\*\*

Define experimental value of plate velocity as a constant-value function of time...

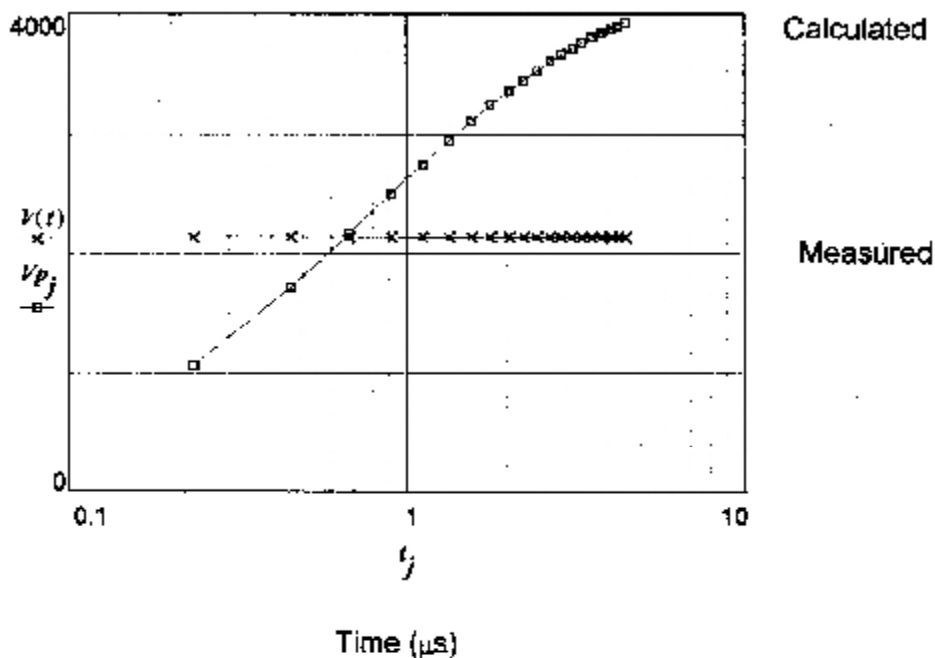
$$V(t) := V_{exp} \quad t := t_{acc} - 0.01 \quad > 0$$

TIME VARIATION OF PLATE VELOCITY

Velocity m/s



Plot time on logarithmic scale....



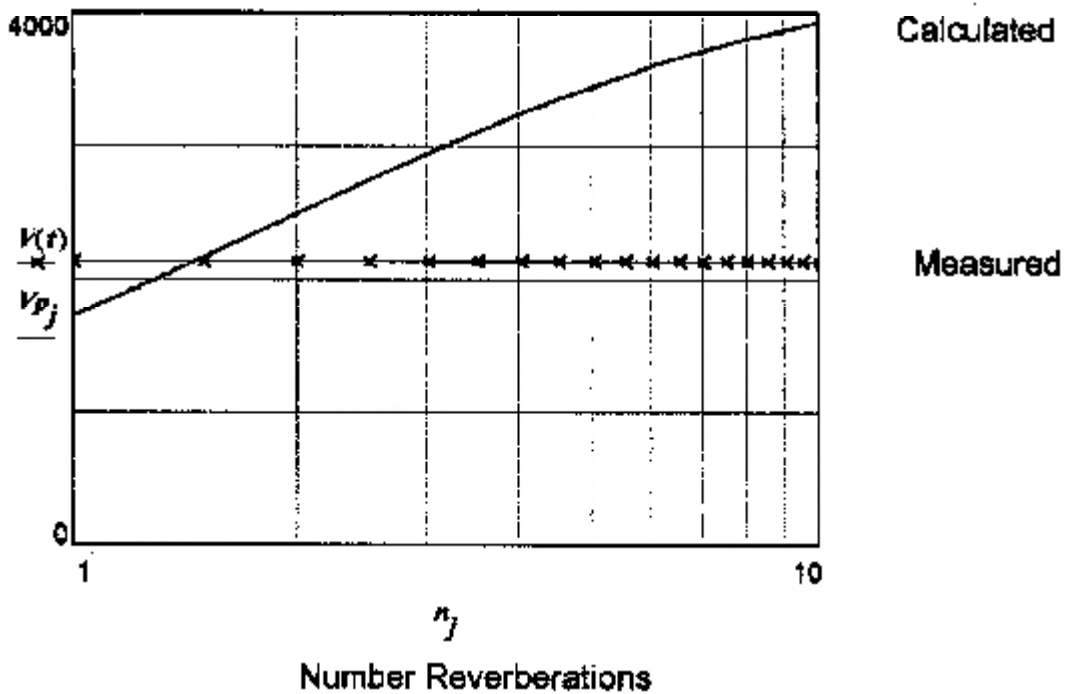
Plot velocity against number of pressure reverberations in plate....

$j := 1 \dots N$  ....must be  $> 0$  for logarithmic axis

$n_j = \frac{j}{2}$  ....n is the number of transits ....

n denotes reverberation number, i.e. number of time increments as defined in section (1) under CALCULATIONS

Plate Velocity m/s



Plot indicates that measured plate velocity is attained shortly before the SECOND passage of the pressure pulse through plate thickness

## **A.13.2 A.D.L. TEST SERIES II**

**COMPOSITION B MASS = 12,5 TO 44 grams**  
**DISC MASS = 6 grams**

## **A.13.2.1 GURNEY MODEL**

DISPLAY RESULTS.....

Gurney Constant  $E_g = 2700$  m/s

Reduced Gurney  $E_{gr} = 1814$  m/s

Particle speed  $U_p = 2000$  m/s

Plate mass  $m_p = 6$  g

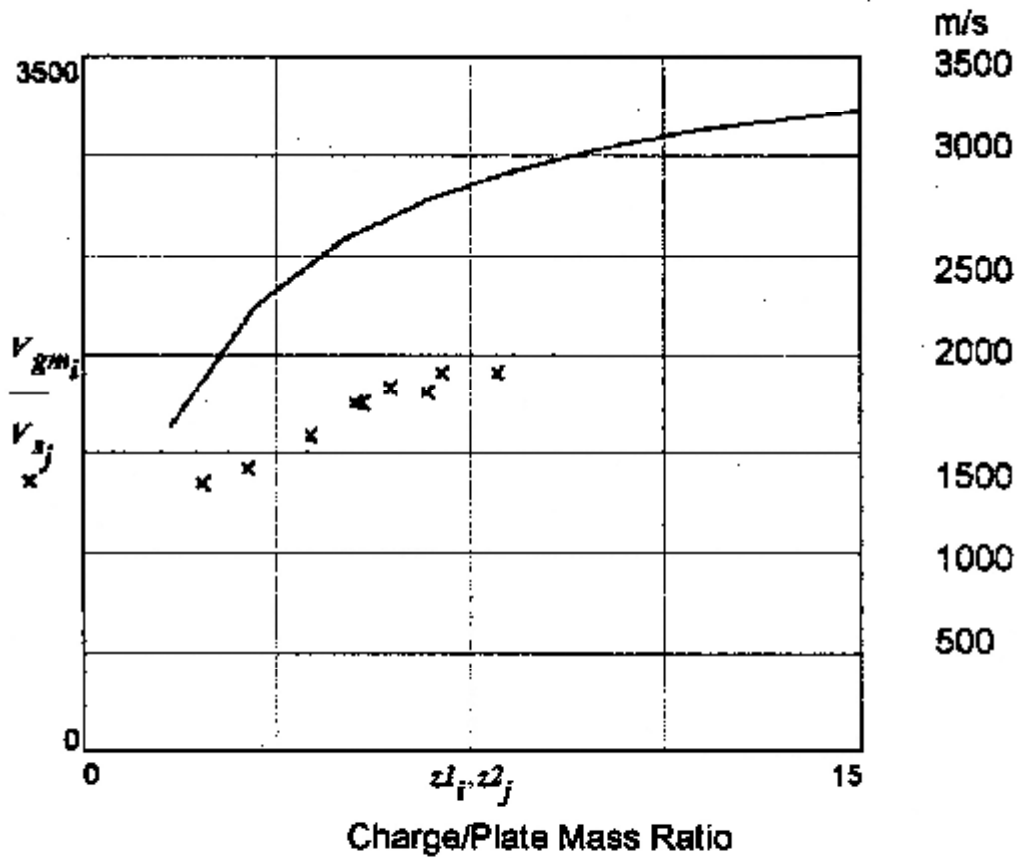
Charge Mass g	C/M	PLATE VELOCITY		
		Standard Gurney .....	Reduced Gurney	Momentum Transfer
10	1.667	2005	1347	909
20	3.333	2765	1858	1250
30	5	3182	2138	1429
40	6.667	3448	2316	1538
50	8.333	3632	2440	1613
60	10	3768	2532	1667
70	11.667	3873	2602	1707
80	13.333	3956	2658	1739
90	15	4023	2703	1765
100	16.667	4079	2740	1786

Modified Gurney plate velocity (Wickert et al model):

C/M Ratio	Velocity m/s	Effective C/M
1.667	1625	1.667
3.333	2239	3.333
5	2571	5
6.667	2780	6.667
8.333	2925	8.333
10	3031	10
11.667	3112	11.667
13.333	3176	13.333
15	3228	15
16.667	3271	16.667

Compare calculated Gurney velocities and measured values as a function of C/M mass ratio.

Plate velocity versus charge-to-plate mass ratio  
 \_\_\_\_\_ Calculated    xxxxxxxx -experimental



Compare calculated and measured plate velocities at the experimental values of C/M mass ratio.....

$$z = z \cdot f$$

$$V_{gr} = E_{gr} \sqrt{\frac{3 \cdot z^2}{(z+1) \cdot (z+4)}}$$

$$V_{pp} = U_p \left( \frac{z}{z+2} \right)$$

Modified Gurney .....

$$V_{gm} = \sqrt{V_{gr}^2 + V_{pp}^2}$$

...Standard Gurney

$$V_g = E_g \sqrt{\frac{3 \cdot z^2}{(z+1) \cdot (z+4)}}$$

$$R1 = \left( \frac{V_s}{V_g} \right)$$

$$R2 = \left( \frac{V_s}{V_{gm}} \right)$$

...velocity ratios

C/M ratio	Measured velocity	Modified Gurney velocity	Standard Gurney Vel.
2.283	1350	1906	2351
3.183	1425	2199	2716
4.367	1588	2464	3048
5.25	1750	2608	3229
5.383	1750	2627	3253
5.917	1825	2697	3341
6.633	1800	2777	3443
6.9	1900	2804	3477
8	1900	2900	3600

Velocity ratios ....

	0.708	0.574
	0.648	0.525
	0.644	0.521
	0.671	0.542
R2 =	0.666	R1 = 0.538
	0.677	0.546
	0.648	0.523
	0.678	0.546
	0.655	0.528



Derive EFFICIENCY FACTOR for effective explosive mass.....modified Gurney model

Number of velocity measurements:  $N = 9$

Pick a number (i) 0 to N-1:  $i = 0$   $TOL = 0.01$

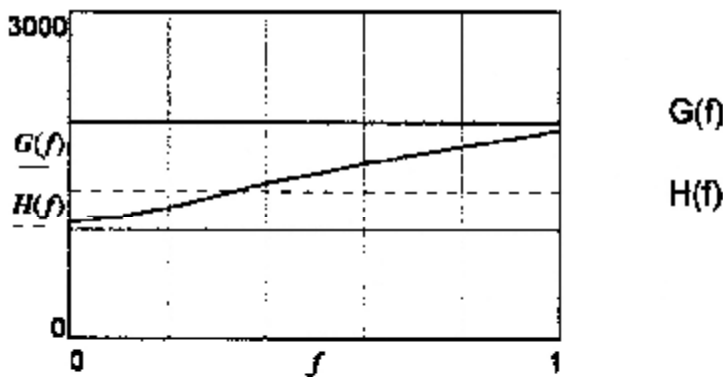
$z := z_i$   $V_{PP} := V_{PP_i}$   $V_s := V_{s_i}$

$$F(f) := E_{gr}^2 \frac{3z^2 f^2}{(fz+1)(fz-4)} + V_{PP}^2 \quad \sqrt{F(f)} = 1.906 \cdot 10^3$$

Plot variation of F(f) with  $0 < f < 1$ ....

$$G(f) := \sqrt{F(f)} \quad f = 0, 0.1, \dots, 1 \quad H(f) := V_s \quad V_s = 1350$$

Calculated velocity ..... measured velocity



Pick a value of f close to the root of  $G(f) - H(f) = 0$

$f = 0.2$  ..... estimate of root

$f = \text{root}(|G(f) - H(f)|, f)$   $f = 0.335$  ..... root

The efficiency factor is  $f = 0.335$

This is the fraction of explosive mass that contributes to the Gurney velocity of the plate (modified Gurney model).

Derive EFFICIENCY FACTOR for effective explosive mass... standard Gurney model

Number of velocity measurements:  $N = 9$

Pick a number (i) 0 to N-1:  $i := 0$   $TOL := 0.01$

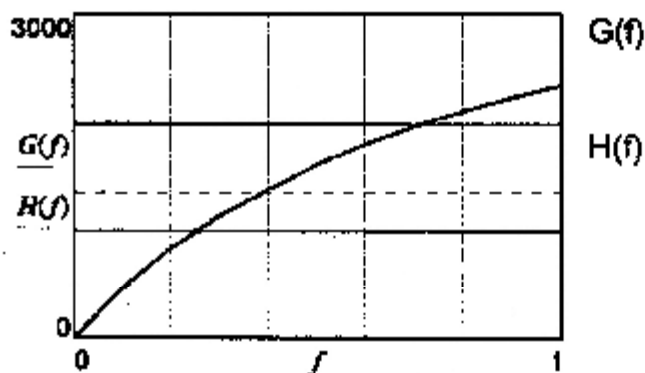
$z := Lz_i$   $f := 1$  .... default

$$F(f) := E \frac{3z^2 f^2}{(zf - 1)(zf + 4)} \quad \sqrt{F(f)} = 2.351 \cdot 10^3$$

Plot variation of F(f) with  $0 < f < 1$ ....

$$G(f) := \sqrt{F(f)} \quad f = 0, 0.1, \dots, 1 \quad H(f) := V_s \quad V_s = 1350$$

Calculated velocity ..... measured velocity



Pick a value of f close to the root of  $G(f) - H(f) = 0$

$f = 0.2$  ... estimate of root

$f = \text{root}(|G(f) - H(f)|, f)$   $f = 0.382$  ...root

The efficiency factor is  $f = 0.382$

This is the fraction of explosive mass that contributes to the standard Gurney velocity of the plate.

Derive EFFICIENCY FACTOR for effective explosive mass....modified Gurney model

Number of velocity measurements:  $N = 9$

Pick a number (i) 0 to N-1:  $i := 1$   $TOL := 0.01$

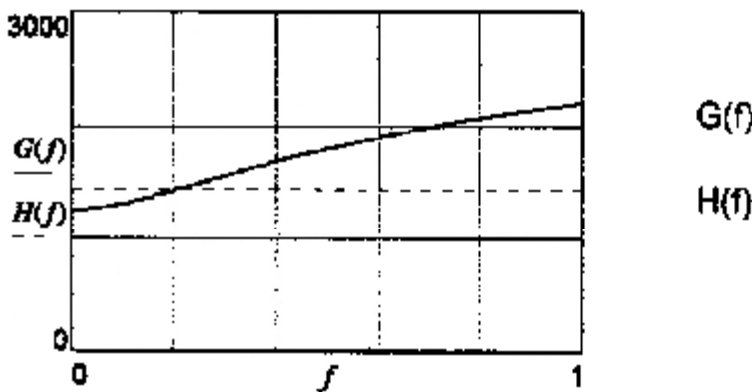
$$z := z_i \quad V_{pp} := V_{pp_i} \quad V_s := V_{s_i}$$

$$F(f) := E_{ST}^2 \cdot \frac{3 \cdot z^2 \cdot f^2}{(fz + 1) \cdot (fz - 4)} + V_{pp}^2 \quad \sqrt{F(f)} = 2.199 \cdot 10^3$$

Plot variation of F(f) with  $0 < f < 1$ ....

$$G(f) := \sqrt{F(f)} \quad f = 0, 0.1..1 \quad H(f) := V_s \quad V_s = 1425$$

Calculated velocity ..... measured velocity



Pick a value of f close to the root of  $G(f) - H(f) = 0$

$f = 0.2$  ..... estimate of root

$f = \text{root}(|G(f) - H(f)|, f)$   $f = 0.199$  ..... root

The efficiency factor is  $f = 0.199$

This is the fraction of explosive mass that contributes to the Gurney velocity of the plate (modified Gurney model).

Derive EFFICIENCY FACTOR for effective explosive mass... standard Gurney model

Number of velocity measurements:  $N = 9$

Pick a number (i) 0 to N-1:  $i := 1$   $TOL := 0.01$

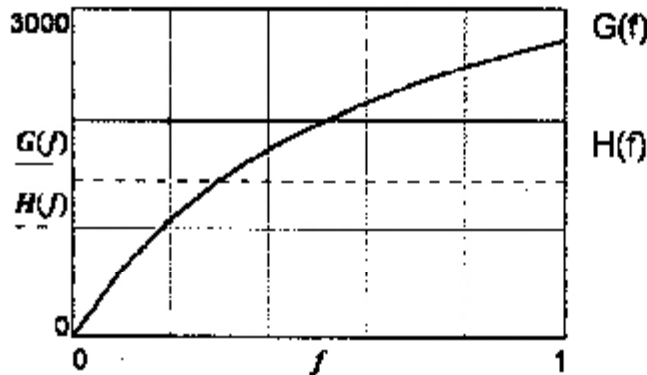
$z := z_2$   $f := 1$  ... default

$$F(f) = E_g^2 \cdot \frac{3 \cdot z^2 \cdot f^2}{(z \cdot f + 1) \cdot (z \cdot f + 4)} \quad \sqrt{F(f)} = 2.716 \cdot 10^3$$

Plot variation of F(f) with  $0 < f < 1$ ....

$$G(f) = \sqrt{F(f)} \quad f = 0, 0.1, \dots, 1 \quad H(f) := V_s \quad V_s = 1425$$

Calculated velocity ..... measured velocity



Pick a value of f close to the root of  $G(f) - H(f) = 0$

$f := 0.2$  ... estimate of root

$f := \text{root}(|G(f) - H(f)|, f)$   $f = 0.297$  ... root

The efficiency factor is  $f = 0.297$

This is the fraction of explosive mass that contributes to the standard Gurney velocity of the plate.

Derive EFFICIENCY FACTOR for effective explosive mass.....modified Gurney model

Number of velocity measurements:  $N = 9$

Pick a number (i) 0 to N-1:  $i := 2$   $TOL := 0.01$

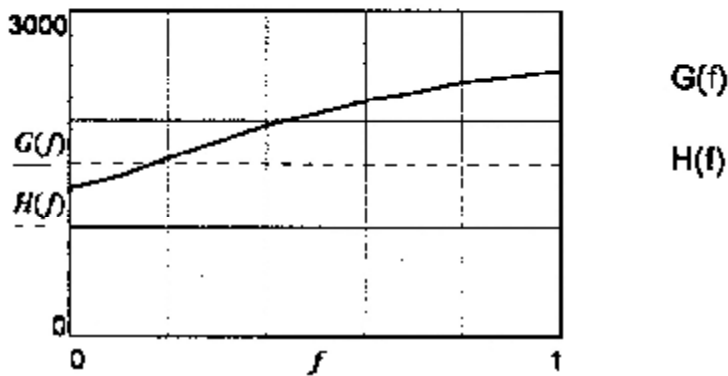
$z := z_i$   $V_{PP} := V_{PP_i}$   $V_s := V_{s_i}$

$$F(f) := E_{gr}^2 \frac{3z^2 f^2}{(fz+1)(fz-4)} + V_{PP}^2 \quad \sqrt{F(f)} = 2.464 \cdot 10^3$$

Plot variation of F(f) with  $0 < f < 1$ ....

$$G(f) := \sqrt{F(f)} \quad f := 0, 0.1 \dots 1 \quad H(f) := V_s \quad V_s = 1588$$

Calculated velocity ..... measured velocity



Pick a value of f close to the root of  $G(f)-H(f)=0$

$f := 0.2$  ...estimate of root

$f := \text{root}(G(f) - H(f) | f)$   $f = 0.167$  ...root

The efficiency factor is  $f = 0.167$

This is the fraction of explosive mass that contributes to the Gurney velocity of the plate (modified Gurney model).

Derive EFFICIENCY FACTOR for effective explosive mass... standard Gurney model

Number of velocity measurements:  $N = 9$

Pick a number (i) 0 to N-1:  $i = 2$   $TOL := 0.01$

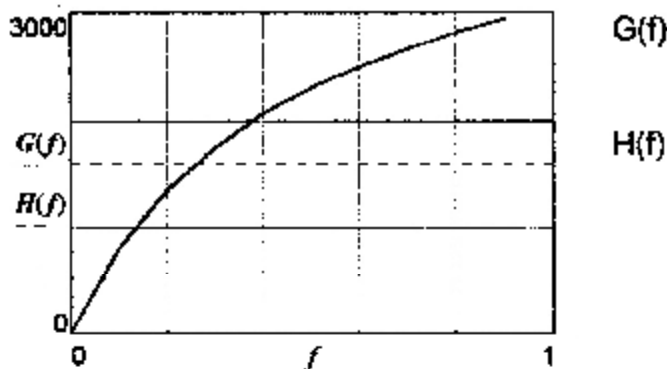
$z = z_i$   $f = 1$  ... default

$$F(f) := E \cdot g^2 \cdot \frac{3 \cdot z^2 \cdot f^2}{(z \cdot f + 1) \cdot (z \cdot f + 4)} \quad \sqrt{F(f)} = 3.048 \cdot 10^3$$

Plot variation of F(f) with  $0 < f < 1$ ...

$$G(f) := \sqrt{F(f)} \quad f = 0, 0.1, \dots, 1 \quad H(f) := V_s \quad V_s = 1588$$

Calculated velocity ..... measured velocity



Pick a value of f close to the root of  $G(f) - H(f) = 0$

$f = 0.2$  ... estimate of root

$f = \text{root}(|G(f) - H(f)|, f)$   $f = 0.256$  ...root

The efficiency factor is  $f = 0.256$

This is the fraction of explosive mass that contributes to the standard Gurney velocity of the plate.

Derive EFFICIENCY FACTOR for effective explosive mass....modified Gurney model

Number of velocity measurements:  $N = 9$

Pick a number (i) 0 to N-1:  $i := 3$   $TOL := 0.01$

$z := z_i$   $V_{PP} = V_{PP_i}$   $V_s := V_{s_i}$

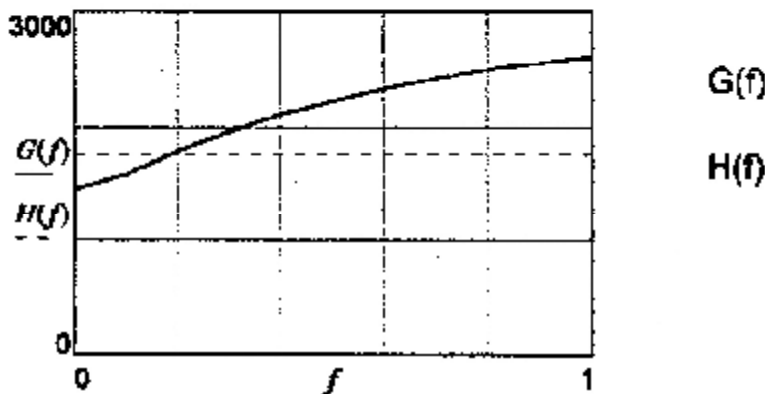
$$F(f) = E_{gr}^2 \frac{3 \cdot z^2 \cdot f^2}{(f \cdot z + 1) \cdot (f \cdot z + 4)} + V_{PP}^2 \quad \sqrt{F(f)} = 2.608 \cdot 10^3$$

Plot variation of F(f) with  $0 < f < 1$ ....

$$G(f) := \sqrt{F(f)} \quad f := 0, 0.1..1 \quad H(f) := V_s \quad V_s = 1750$$

Calculated velocity .....

measured velocity



Pick a value of f close to the root of  $G(f) - H(f) = 0$

$f := 0.2$  ...estimate of root

$f := \text{root}(\cdot G(f) - H(f); f)$   $f = 0.187$  ...root

The efficiency factor is  $f = 0.187$

This is the fraction of explosive mass that contributes to the Gurney velocity of the plate (modified Gurney model).

Derive EFFICIENCY FACTOR for effective explosive mass... standard Gurney model

Number of velocity measurements:  $N = 9$

Pick a number (i) 0 to N-1:  $i = 3$   $TOL = 0.01$

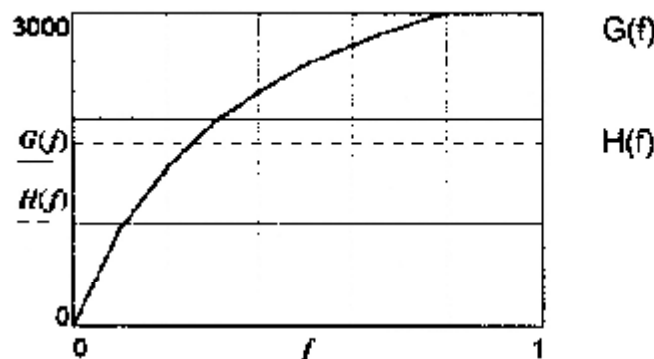
$z := z_i$   $f = 1$  ... default

$$F(f) := E \frac{3z^2 f^2}{8(zf+1)(zf+4)} \quad \sqrt{F(f)} = 3.229 \cdot 10^3$$

Plot variation of F(f) with  $0 < f < 1$ ...

$$G(f) := \sqrt{F(f)} \quad f := 0, 0.1..1 \quad H(f) = V_s \quad V_s = 1750$$

Calculated velocity ..... measured velocity



Pick a value of f close to the root of  $G(f) - H(f) = 0$

$f := 0.2$  ... estimate of root

$f := \text{root}(|G(f) - H(f)|, f)$   $f = 0.25$  ... root

The efficiency factor is  $f = 0.25$

This is the fraction of explosive mass that contributes to the standard Gurney velocity of the plate.



Derive EFFICIENCY FACTOR for effective explosive mass.....modified Gurney model

Number of velocity measurements:  $N = 9$

Pick a number (i) 0 to N-1:  $i := 4$   $TOL := 0.01$

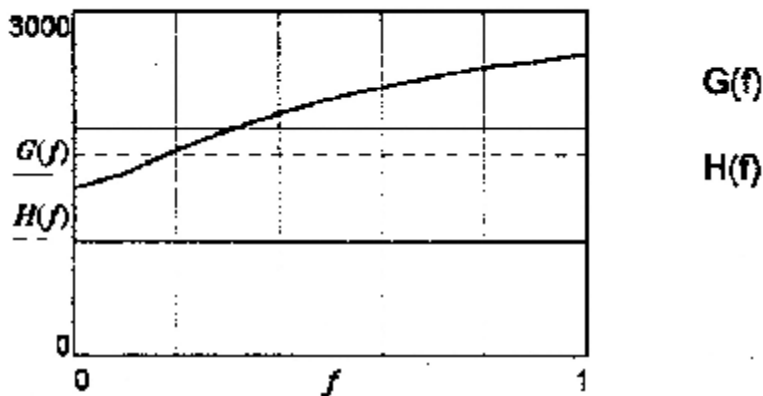
$z = z_i$   $V_{PP} := V_{PP_i}$   $V_s := V_{s_i}$

$$F(f) := E_{gr}^2 \cdot \frac{3 \cdot z^2 \cdot f^2}{(f \cdot z + 1) \cdot (f \cdot z + 4)} + V_{PP}^2 \quad \sqrt{F(f)} = 2.627 \cdot 10^3$$

Plot variation of F(f) with  $0 < f < 1$ ....

$$G(f) := \sqrt{F(f)} \quad f := 0, 0.1..1 \quad H(f) := V_s \quad V_s = 1750$$

Calculated velocity ..... measured velocity



Pick a value of f close to the root of  $G(f) - H(f) = 0$

$f := 0.2$  ...estimate of root

$f := \text{root}(|G(f) - H(f)|, f)$   $f = 0.178$  ...root

The efficiency factor is  $f = 0.178$

This is the fraction of explosive mass that contributes to the Gurney velocity of the plate (modified Gurney model).

Derive EFFICIENCY FACTOR for effective explosive mass... standard Gurney model

Number of velocity measurements:  $N = 9$

Pick a number (i) 0 to N-1:  $i = 4$   $TOL = 0.01$

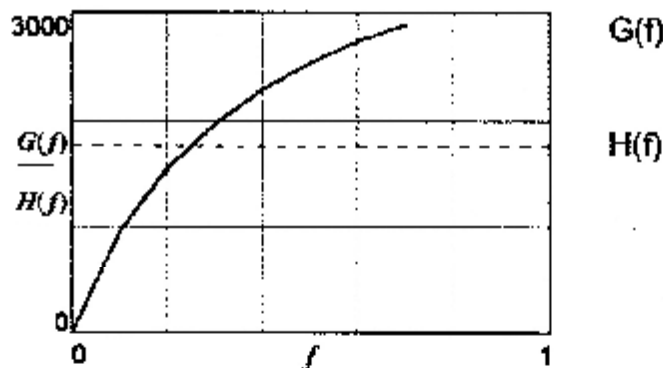
$z = z2_i$   $f = 1$  ... default

$$F(f) := E \frac{2}{g} \frac{3z^2 f^2}{(zf+1)(zf+4)} \quad \sqrt{F(f)} = 3.253 \cdot 10^3$$

Plot variation of F(f) with  $0 < f < 1$ ...

$$G(f) := \sqrt{F(f)} \quad f = 0, 0.1..1 \quad H(f) := V_s \quad V_s = 1750$$

Calculated velocity ..... measured velocity



Pick a value of f close to the root of  $G(f)-H(f)=0$

$f = 0.2$  ... estimate of root

$f := \text{root}(|G(f) - H(f)|, f)$   $f = 0.244$  ...root

The efficiency factor is  $f = 0.244$

This is the fraction of explosive mass that contributes to the standard Gurney velocity of the plate.

Derive EFFICIENCY FACTOR for effective explosive mass.....modified Gurney model

Number of velocity measurements:  $N = 9$

Pick a number (i) 0 to N-1:  $i := 5$   $TOL := 0.01$

$z := z_i$   $V_{pp} = V_{pp_i}$   $V_s := V_{s_i}$

$$F(f) = E \frac{2 \cdot 3 \cdot z^2 \cdot f^2}{g^2 \cdot (fz + 1) \cdot (fz + 4)} + V_{pp}^2 \quad \sqrt{F(f)} = 2.697 \cdot 10^3$$

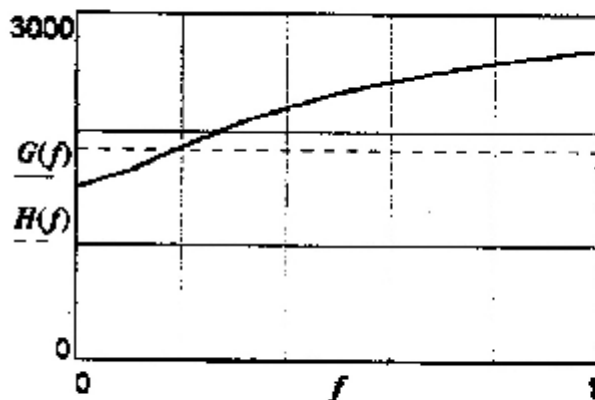
Plot variation of F(f) with  $0 < f < 1$ ....

$$G(f) := \sqrt{F(f)} \quad f := 0, 0.1..1$$

$$H(f) := V_s \quad V_s = 1825$$

Calculated velocity .....

measured velocity



G(f)

H(f)

Pick a value of f close to the root of  $G(f) - H(f) = 0$

$f = 0.2$  ...estimate of root

$f = \text{root}(|G(f) - H(f)|, f)$   $f = 0.183$  ...root

The efficiency factor is  $f = 0.183$

This is the fraction of explosive mass that contributes to the Gurney velocity of the plate (modified Gurney model).

Derive EFFICIENCY FACTOR for effective explosive mass... standard Gurney model

Number of velocity measurements:  $N = 9$

Pick a number (i) 0 to N-1:  $i = 5$   $TOL := 0.01$

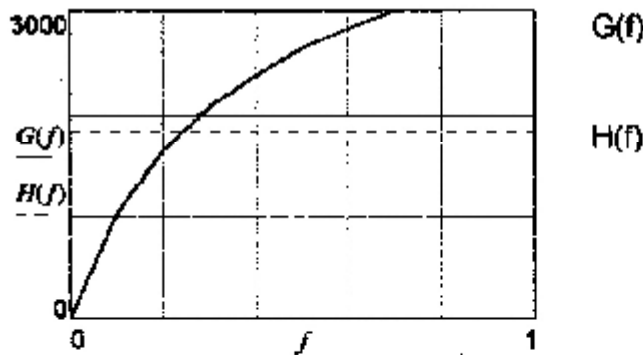
$z := z_i$   $f := 1$  .... default

$$F(f) := E_g^2 \cdot \frac{3 \cdot z^2 \cdot f^2}{(zf + 1) \cdot (zf + 4)} \quad \sqrt{F(f)} = 3.341 \cdot 10^3$$

Plot variation of F(f) with  $0 < f < 1$ ....

$$G(f) := \sqrt{F(f)} \quad f := 0, 0.1 \dots 1 \quad H(f) := V_s \quad V_s = 1825$$

Calculated velocity ..... measured velocity



Pick a value of f close to the root of  $G(f)-H(f)=0$

$f = 0.2$  ..... estimate of root

$f := \text{root}(G(f) - H(f) | f)$   $f = 0.238$  ....root

The efficiency factor is  $f = 0.238$

This is the fraction of explosive mass that contributes to the standard Gurney velocity of the plate.

Derive EFFICIENCY FACTOR for effective explosive mass.....modified Gurney model

Number of velocity measurements:  $N = 9$

Pick a number (i) 0 to N-1:  $i = 6$   $TOL := 0.01$

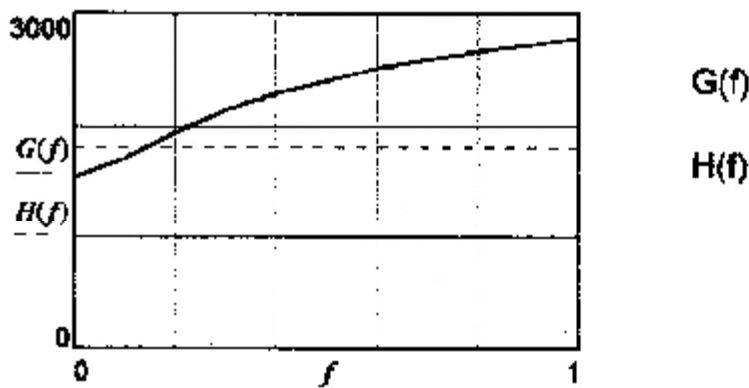
$z := z_i$   $V_{PP} := V_{PP_i}$   $V_s := V_{s_i}$

$$F(f) := E_{gr}^2 \cdot \frac{3 \cdot z^2 \cdot f^2}{(fz + 1) \cdot (fz + 4)} + V_{PP}^2 \quad \sqrt{F(f)} = 2.777 \cdot 10^3$$

Plot variation of F(f) with  $0 < f < 1$ ....

$$G(f) := \sqrt{F(f)} \quad f := 0, 0.1..1 \quad H(f) := V_s \quad V_s = 1800$$

Calculated velocity ..... measured velocity



Pick a value of f close to the root of  $G(f) - H(f) = 0$

$f = 0.2$  .....estimate of root

$f := \text{root}(|G(f) - H(f)|, f)$   $f = 0.138$  ...root

The efficiency factor is  $f = 0.138$

This is the fraction of explosive mass that contributes to the Gurney velocity of the plate (modified Gurney model).

Derive EFFICIENCY FACTOR for effective explosive mass... standard Gurney model

Number of velocity measurements:  $N = 9$

Pick a number (i) 0 to N-1:  $i := 6$   $TOL := 0.01$

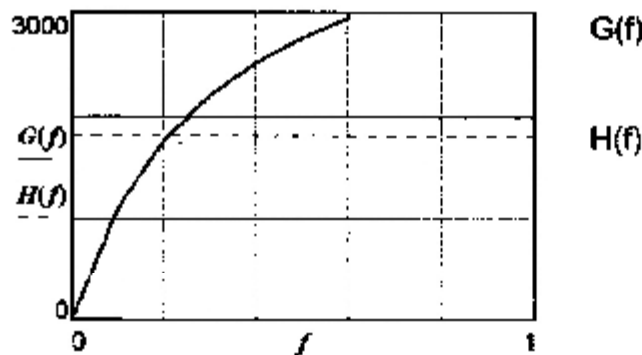
$z := z_i$   $f := 1$  .... default

$$F(f) := E \frac{2 \cdot 3 \cdot z^2 \cdot f^2}{(zf + 1) \cdot (zf + 4)} \quad \sqrt{F(f)} = 3.443 \cdot 10^3$$

Plot variation of F(f) with  $0 < f < 1$ ....

$$G(f) := \sqrt{F(f)} \quad f = 0, 0.1 \dots 1 \quad H(f) = V_g \quad V_g = 1800$$

Calculated velocity ..... measured velocity



Pick a value of f close to the root of  $G(f) - H(f) = 0$

$f := 0.2$  ... estimate of root

$f := \text{root}(|G(f) - H(f)|, f)$   $f = 0.207$  ...root

The efficiency factor is  $f = 0.207$

This is the fraction of explosive mass that contributes to the standard Gurney velocity of the plate.

Derive EFFICIENCY FACTOR for effective explosive mass ... modified Gurney model

Number of velocity measurements:  $N = 9$

Pick a number (i) 0 to N-1:  $i = 7$   $TOL := 0.01$

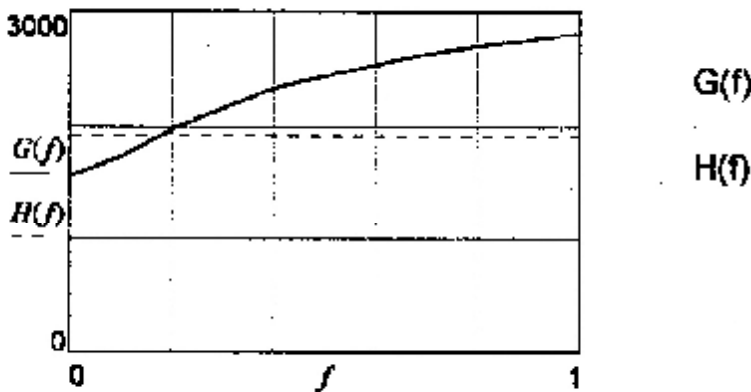
$z := z_i$   $V_{PP} := V_{PP_i}$   $V_s := V_{s_i}$

$$F(f) := E_{gr}^2 \frac{3 \cdot z^2 \cdot f^2}{(fz + 1) \cdot (fz + 4)} + V_{PP}^2 \quad \sqrt{F(f)} = 2.804 \cdot 10^3$$

Plot variation of F(f) with  $0 < f < 1$ ....

$$G(f) := \sqrt{F(f)} \quad f = 0, 0.1, \dots, 1 \quad H(f) := V_s \quad V_s = 1900$$

Calculated velocity ..... measured velocity



Pick a value of f close to the root of  $G(f) - H(f) = 0$

$f := 0.2$  ... estimate of root

$f := \text{root}(|G(f) - H(f)|, f)$   $f = 0.17$  ...root

The efficiency factor is  $f = 0.17$

This is the fraction of explosive mass that contributes to the Gurney velocity of the plate (modified Gurney model).

Derive EFFICIENCY FACTOR for effective explosive mass. ... standard Gurney model

Number of velocity measurements:  $N = 9$

Pick a number (i) 0 to N-1:  $i = 7$   $TOL = 0.01$

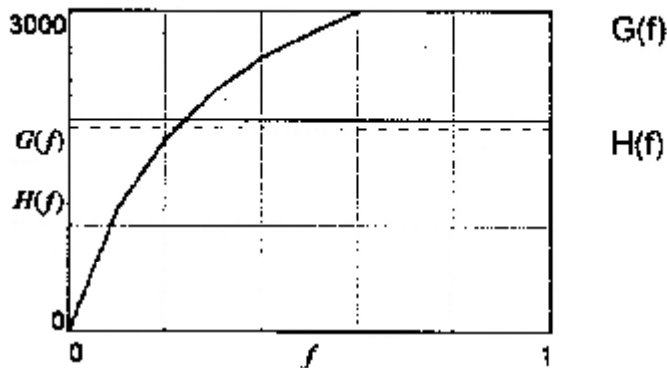
$z := z2;$   $f := 1$  ... default

$$F(f) := E \frac{2}{g} \frac{3z^2 f^2}{(zf+1)(zf+4)} \quad \sqrt{F(f)} = 3.477 \cdot 10^3$$

Plot variation of F(f) with  $0 < f < 1$ ....

$$G(f) := \sqrt{F(f)} \quad f := 0, 0.1..1 \quad H(f) := V_s \quad V_s = 1900$$

Calculated velocity ..... measured velocity



Pick a value of f close to the root of  $G(f) - H(f) = 0$

$f := 0.2$  ... estimate of root

$f := \text{root}(|G(f) - H(f)|, f)$   $f = 0.219$  ...root

The efficiency factor is  $f = 0.219$

This is the fraction of explosive mass that contributes to the standard Gurney velocity of the plate.



Derive EFFICIENCY FACTOR for effective explosive mass... modified Gurney model

Number of velocity measurements:  $N = 9$

Pick a number (i) 0 to N-1:  $i = 8$   $TOL = 0.01$

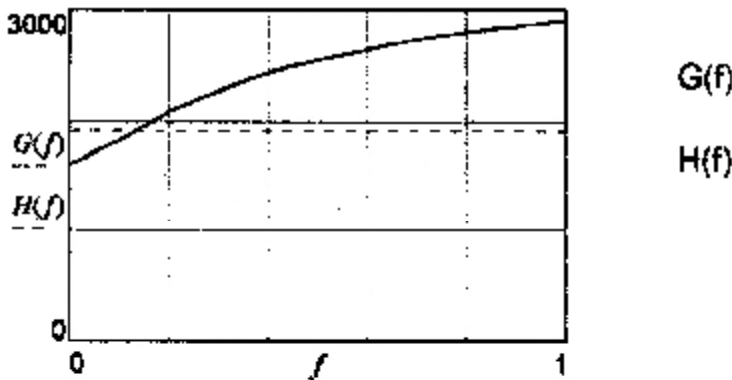
$z := z_i$   $V_{PP} := V_{PP_i}$   $V_s := V_{s_i}$

$$F(f) := E_{gr} \cdot \frac{3 \cdot z^2 \cdot f^2}{(fz + 1) \cdot (fz + 4)} + V_{PP}^2 \quad \sqrt{F(f)} = 2.9 \cdot 10^3$$

Plot variation of F(f) with  $0 < f < 1$ ....

$$G(f) := \sqrt{F(f)} \quad f := 0, 0.1 \dots 1 \quad H(f) := V_s \quad V_s = 1900$$

Calculated velocity ..... measured velocity



Pick a value of f close to the root of  $G(f) - H(f) = 0$

$f := 0.2$  ..... estimate of root

$f := \text{root}(|G(f) - H(f)|, f)$   $f = 0.131$  ..... root

The efficiency factor is  $f = 0.131$

This is the fraction of explosive mass that contributes to the Gurney velocity of the plate (modified Gurney model).

Derive EFFICIENCY FACTOR for effective explosive mass... standard Gurney model

Number of velocity measurements:  $N = 9$

Pick a number (i) 0 to N-1:  $i = 8$   $TOL = 0.01$

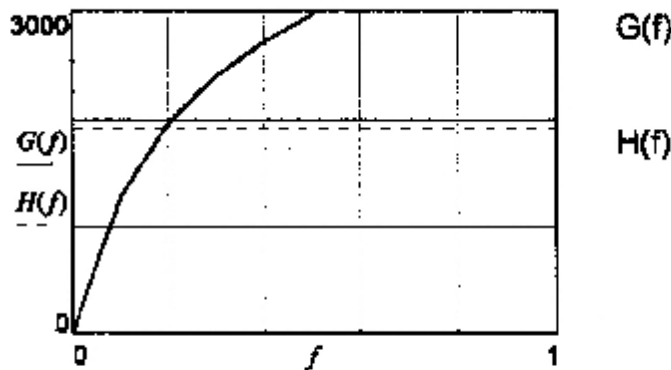
$z = z_i$   $f = 1$  ... default

$$F(f) = E_s^2 \cdot \frac{3 \cdot z^2 \cdot f^2}{(z \cdot f + 1) \cdot (z \cdot f + 4)} \quad \sqrt{F(f)} = 3.6 \cdot 10^3$$

Plot variation of F(f) with  $0 < f < 1$ ....

$$G(f) := \sqrt{F(f)} \quad f = 0, 0.1 \dots 1 \quad H(f) := V_s \quad V_s = 1900$$

Calculated velocity: ..... measured velocity



Pick a value of f close to the root of  $G(f) - H(f) = 0$

$f = 0.2$  ..... estimate of root

$f := \text{root}(|G(f) - H(f)|, f)$   $f = 0.189$  ...root

The efficiency factor is  $f = 0.189$

This is the fraction of explosive mass that contributes to the standard Gurney velocity of the plate.

## **A.13.2.2      AZIZ MODEL**

DISPLAY RESULTS ....

1 Velocity -----

Charge Mass (g)	Charge/Plate mass ratio:		Plate velocity calc. (m/s)
	loaded .....	effective	
10	1.667	1.667	2.022
15	2.5	2.5	2.518
20	3.333	3.333	2.887
25	4.167	4.167	3.177
30	5	5	3.415
35	5.833	5.833	3.614
40	6.667	6.667	3.784
45	7.5	7.5	3.933
50	8.333	8.333	4.063

$C =$        $CM1 =$        $CM2 =$        $V_p =$

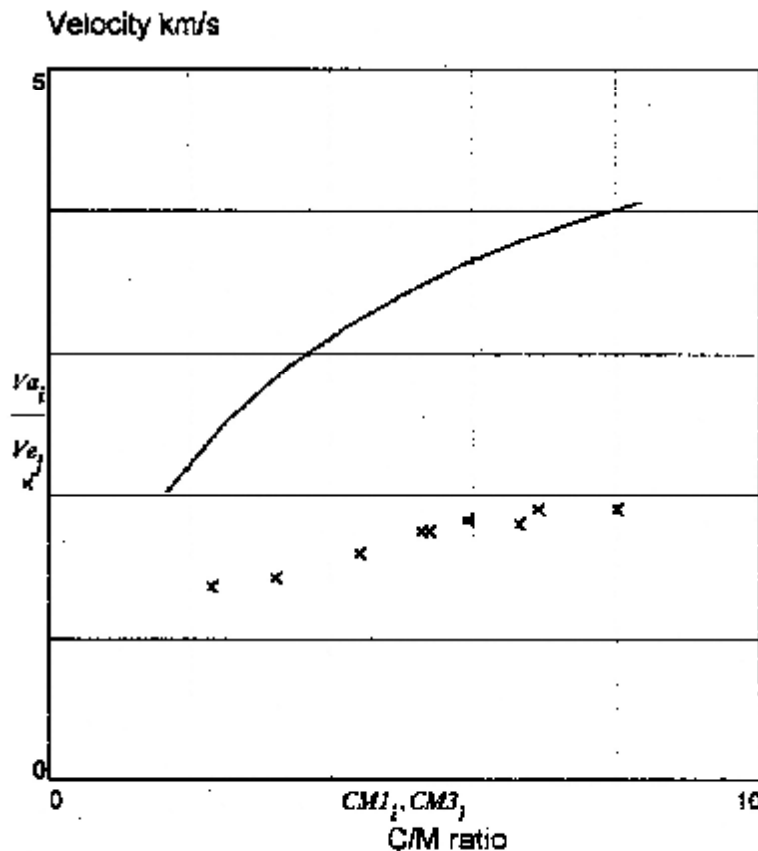
2 Compare measured and calculated velocities -----

$length(Vslug) = 9$        $N := length(Vslug)$        $j := 0..(N - 1)$

$Va := V_p$        $Ve := Vslug$       ... km/s

Plate velocity versus charge-to-plate mass ratio

\_\_\_\_\_ Aziz model    xxx measured



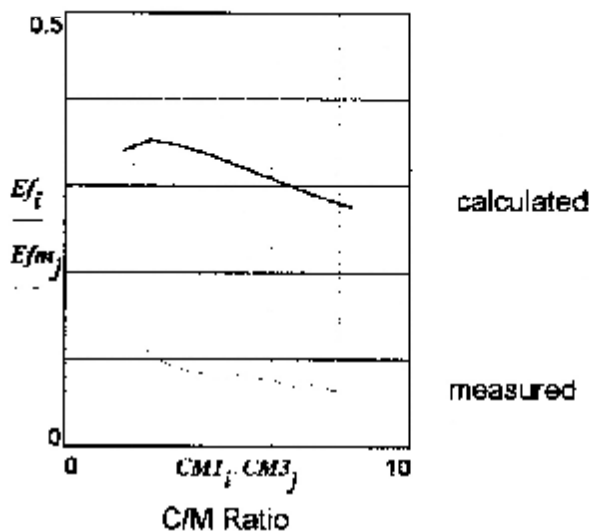
**3 Energy Efficiency**

		Calculated	
Velocity km/s		Energy kJ	Efficiency
$V_p =$	2.022	12.263	0.34
	2.518	19.015	0.351
	2.887	25.001	0.346
	3.177	30.287	0.336
	3.415	34.98	0.323
	3.614	39.178	0.31
	3.784	42.962	0.298
	3.933	46.397	0.286
	4.063	49.535	0.274

		Measured			
Velocity m/s		Energy kJ	Efficiency		
$V_{slag} =$	1.35	5.468	0.111	$R =$	0.325
	1.425	6.092	0.088		0.252
	1.588	7.565	0.08		0.231
	1.75	9.188	0.081		0.241
	1.75	9.188	0.079		0.244
	1.825	9.992	0.078		0.251
	1.8	9.72	0.068		0.227
	1.9	10.83	0.072		0.254
	1.9	10.83	0.063		0.228

$E_f = E_f$      $E_{fm} = E_{fm}$  ... variables for plotting

Efficiency of Energy Transfer to Plate



#### 4 Charge Mass Efficiency .....

Number of velocity measurements:  $N = 9$

Pick a number from 0 to N-1:  $i = 0$

Prepare variables for plotting:  $CM := CM3_i$   $V_s := Vslug_i$

Plot variation of calculated velocity with  $0 < f < 1$  .....

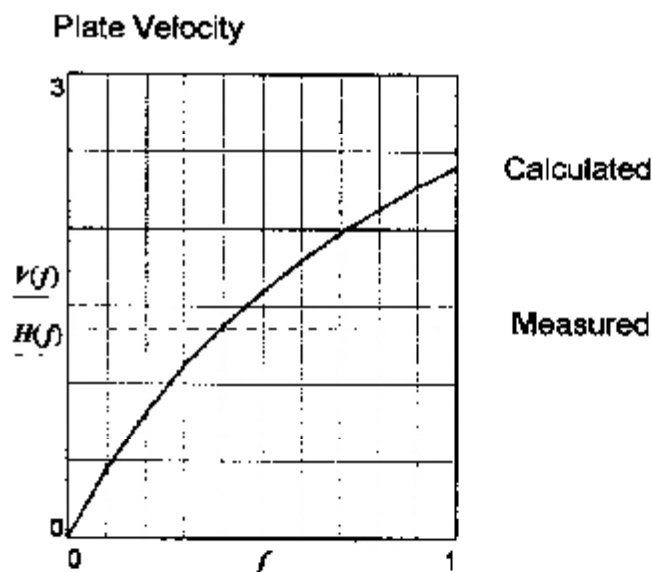
$$f := 0, 0.1 \dots 1$$

$$z(f) := \sqrt{\frac{32}{27} \cdot CM \cdot f + 1}$$

$$V(f) := D \cdot \frac{z(f) - 1}{z(f) + 1}$$

$$V_s = 1.35 \quad H(f) = V_s$$

Plot variation of calculated velocity with f ...



Pick a value of f close to the root of  $V(f) - H(f) = 0$

$f := 0.4$  ...first estimate of root

$f := \text{root}(|V(f) - H(f)|, f)$   $f = 0.388$  ...the root

The efficiency factor is  $f = 0.388$  at  $CM = 2.283$

This is the fraction of explosive mass that contributes to the one-dimensional gas expansion accelerating the plate to its final velocity.

**4 Charge Mass Efficiency .....**

Number of velocity measurements:  $N = 9$

Pick a number from 0 to N-1:  $i = 0$

Prepare variables for plotting:  $CM := CM_{B_i}$   $V_s := V_{slug_i}$

Plot variation of calculated velocity with  $0 < f < 1$  .....

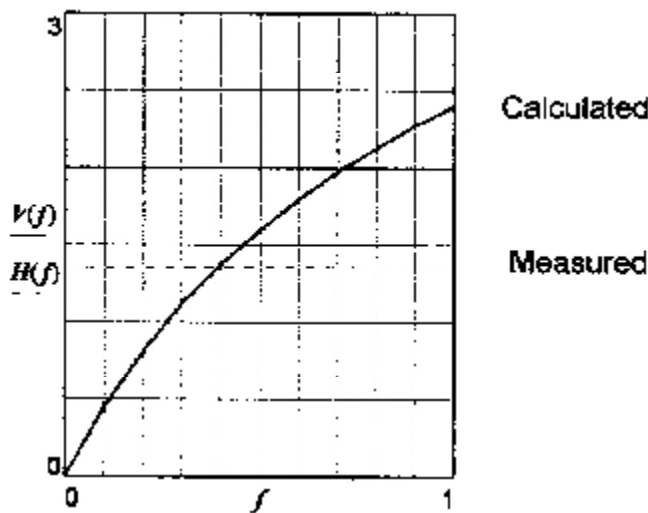
$$f := 0, 0.1 \dots 1$$

$$z(f) := \sqrt{\frac{32}{27} \cdot CM \cdot f + 1} \qquad V(f) := D \cdot \frac{z(f) - 1}{z(f) + 1}$$

$$V_s = 1.35 \qquad H(f) = V_s$$

Plot variation of calculated velocity with f ...

Plate Velocity



Pick a a value of f close to the root of  $V(f)-H(f)=0$

$f := 0.4$  ....first estimate of root

$f := \text{root}(|V(f) - H(f)|, f)$   $f = 0.388$  ...the root

The efficiency factor is  $f = 0.388$  at  $CM = 2.283$

This is the fraction of explosive mass that contributes to the one-dimensional gas expansion accelerating the plate to its final velocity.

**4 Charge Mass Efficiency .....**

Number of velocity measurements:  $N = 9$

Pick a number from 0 to N-1:  $i = 1$

Prepare variables for plotting:  $CM := CM3_i \quad V_s := Vslug_i$

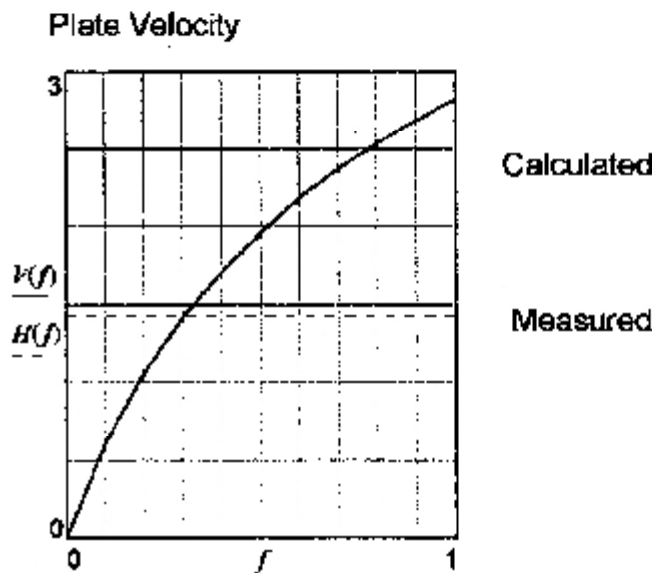
Plot variation of calculated velocity with  $0 < f < 1$  .....

$$f := 0, 0.1 \dots 1$$

$$z(f) = \sqrt{\frac{32}{27} CM f + 1} \quad V(f) := D \cdot \frac{z(f) - 1}{z(f) + 1}$$

$$V_s = 1.425 \quad H(f) := V_s$$

Plot variation of calculated velocity with f ...



Pick a a value of f close to the root of  $V(f)-H(f)=0$

$f := 0.4$  ....first estimate of root

$f := \text{root}(|V(f) - H(f)|, f)$   $f = 0.301$  ...the root

The efficiency factor is  $f = 0.301$  at  $CM = 3.183$

This is the fraction of explosive mass that contributes to the one-dimensional gas expansion accelerating the plate to its final velocity.



**4 Charge Mass Efficiency .....**

Number of velocity measurements:  $N = 9$

Pick a number from 0 to  $N-1$ :  $i := 2$

Prepare variables for plotting:  $CM := CM3_i$      $V_s := Vslug_i$

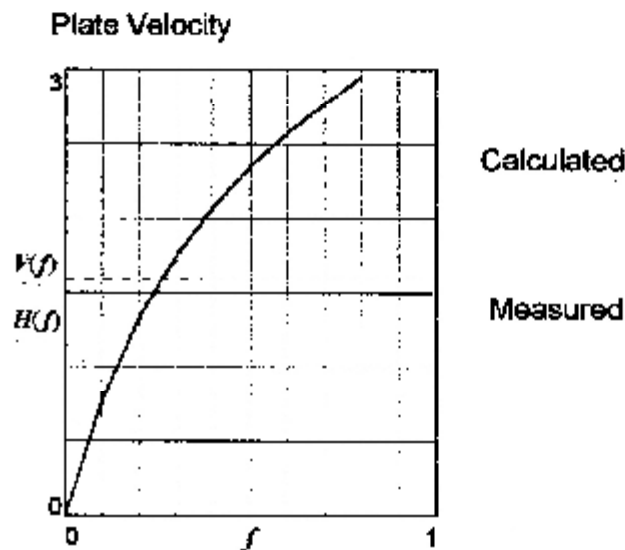
Plot variation of calculated velocity with  $0 < f < 1$  .....

$$f := 0, 0.1 \dots 1$$

$$z(f) := \sqrt{\frac{32}{27} \cdot CM \cdot f + 1} \qquad V(f) := D \cdot \frac{z(f) - 1}{z(f) + 1}$$

$$V_s = 1.588 \qquad H(f) = V_s$$

Plot variation of calculated velocity with f ...



Pick a a value of f close to the root of  $V(f)-H(f)=0$

$f := 0.4$     ...first estimate of root

$f := \text{root}(|V(f) - H(f)|, f)$      $f = 0.258$     ...the root

The efficiency factor is  $f = 0.258$  at  $CM = 4.367$

This is the fraction of explosive mass that contributes to the one-dimensional gas expansion accelerating the plate to its final velocity.

**4 Charge Mass Efficiency .....**

Number of velocity measurements:  $N = 9$

Pick a number from 0 to N-1:  $i = 3$

Prepare variables for plotting:  $CM = CM3_i \quad V_s = Vslag_i$

Plot variation of calculated velocity with  $0 < f < 1$  .....

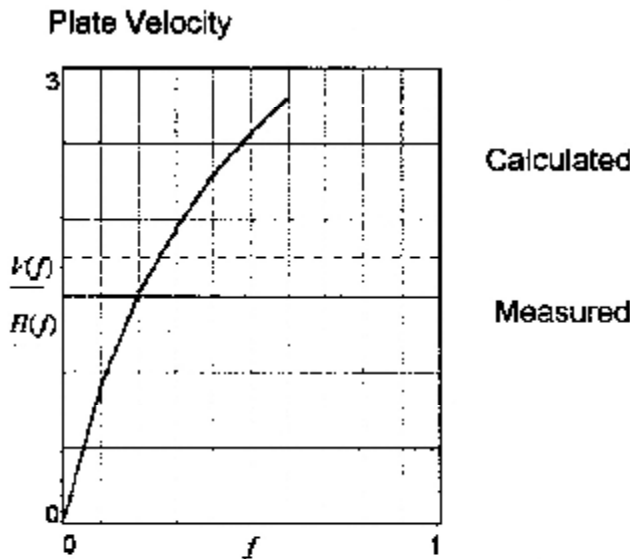
$$f := 0, 0.1 \dots 1$$

$$z(f) := \sqrt{\frac{32}{27} \cdot CM \cdot f + 1}$$

$$V(f) := D \cdot \frac{z(f) - 1}{z(f) + 1}$$

$$V_s = 1.75 \quad H(f) := V_s$$

Plot variation of calculated velocity with f ...



Pick a a value of f close to the root of  $V(f)-H(f)=0$

$f = 0.4$  ....first estimate of root

$f = \text{root}(|V(f) - H(f)|, f)$   $f = 0.25$  ...the root

The efficiency facor is  $f = 0.25$  at  $CM = 5.25$

This is the fraction of explosive mass that contributes to the one-dimensional gas expansion accelerating the plate to its final velocity.

**4. Charge Mass Efficiency .....**

Number of velocity measurements:  $N = 9$

Pick a number from 0 to N-1:  $i = 4$

Prepare variables for plotting:  $CM := CM3_i$      $V_s := Vslug_i$

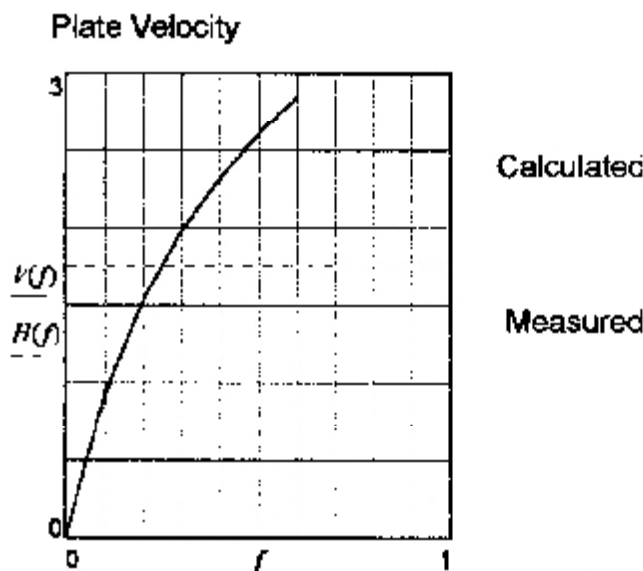
Plot variation of calculated velocity with  $0 < f < 1$  .....

$$f := 0, 0.1 \dots 1$$

$$z(f) := \sqrt{\frac{32}{27} CM f + 1} \qquad V(f) := D \cdot \frac{z(f) - 1}{z(f) - 1}$$

$$V_s = 1.75 \qquad H(f) := V_s$$

Plot variation of calculated velocity with f ...



Pick a a value of f close to the root of  $V(f)-H(f)=0$

$f := 0.4$     ....first estimate of root

$f := \text{root}(|V(f) - H(f)|, f)$      $f = 0.244$     ...the root

The efficiency factor is  $f = 0.244$     at  $CM = 5.383$

This is the fraction of explosive mass that contributes to the one-dimensional gas expansion accelerating the plate to its final velocity.

**4 Charge Mass Efficiency .....**

Number of velocity measurements:  $N = 9$

Pick a number from 0 to N-1:  $i = 5$

Prepare variables for plotting:  $CM_i = CM3_i$   $V_s = Vslug_i$

Plot variation of calculated velocity with  $0 < f < 1$  .....

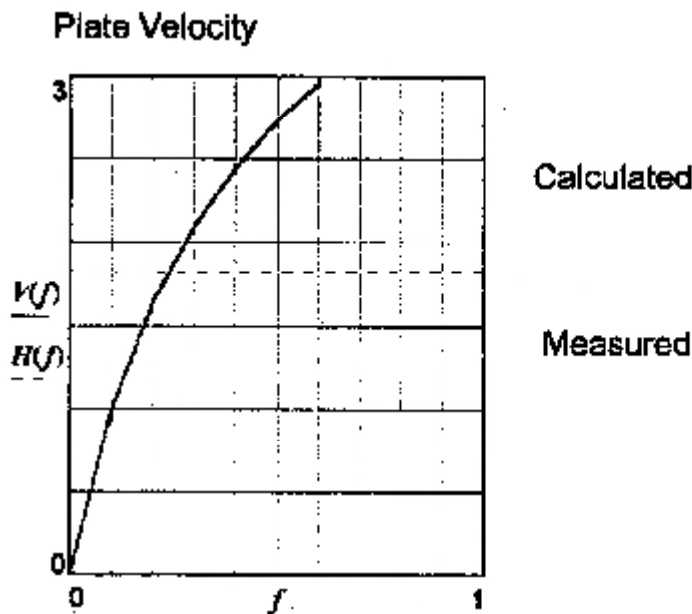
$f := 0, 0.1, \dots, 1$

$z(f) := \sqrt{\frac{32}{27} \cdot CM \cdot f} + 1$

$V(f) := D \cdot \frac{z(f) - 1}{z(f) + 1}$

$V_s = 1.825$   $H(f) := V_s$

Plot variation of calculated velocity with f ...



Pick a a value of f close to the root of  $V(f)-H(f)=0$

$f := 0.4$  ....first estimate of root

$f := \text{root}(|V(f) - H(f)|, f)$   $f = 0.237$  ...the root

The efficiency facor is  $f = 0.237$  at  $CM = 5.917$

This is the fraction of explosive mass that contributes to the one-dimensional gas expansion accelerating the plate to its final velocity.

**4 Charge Mass Efficiency .....**

Number of velocity measurements:  $N = 9$

Pick a number from 0 to N-1:  $i = 6$

Prepare variables for plotting:  $CM := CM3_i \quad V_s = Vslug_i$

Plot variation of calculated velocity with  $0 < f < 1$  .....

$$f := 0, 0.1 \dots 1$$

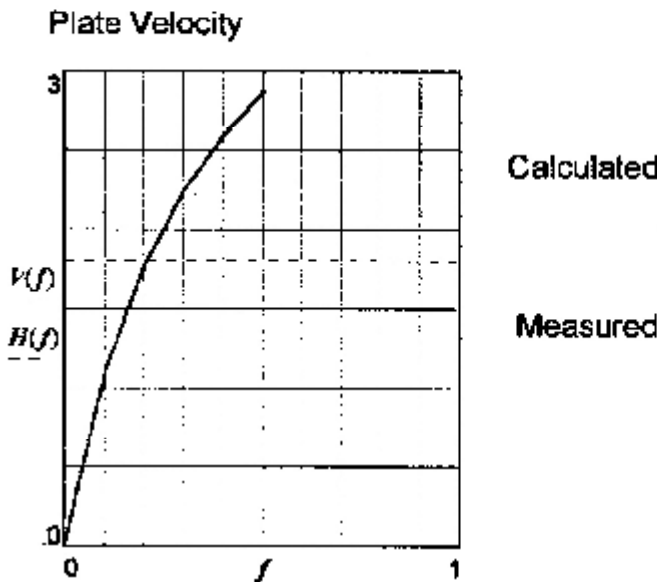
$$z(f) := \sqrt{\frac{32}{27} \cdot CM \cdot f + 1}$$

$$V(f) := D \cdot \frac{z(f) - 1}{z(f) + 1}$$

$$V_s = 1.8$$

$$H(f) := V_s$$

Plot variation of calculated velocity with f ...



Pick a value of f close to the root of  $V(f) - H(f) = 0$

$f := 0.4$  ....first estimate of root

$f = \text{root}( | V(f) - H(f) |, f ) \quad f = 0.207$  ...the root

The efficiency factor is  $f = 0.207$  at  $CM = 6.633$

This is the fraction of explosive mass that contributes to the one-dimensional gas expansion accelerating the plate to its final velocity.

**4 Charge Mass Efficiency .....**

Number of velocity measurements:  $N = 9$

Pick a number from 0 to N-1:  $i = 7$

Prepare variables for plotting:  $CM := CM3_i \quad V_s := Vslug_i$

Plot variation of calculated velocity with  $0 < f < 1$  .....

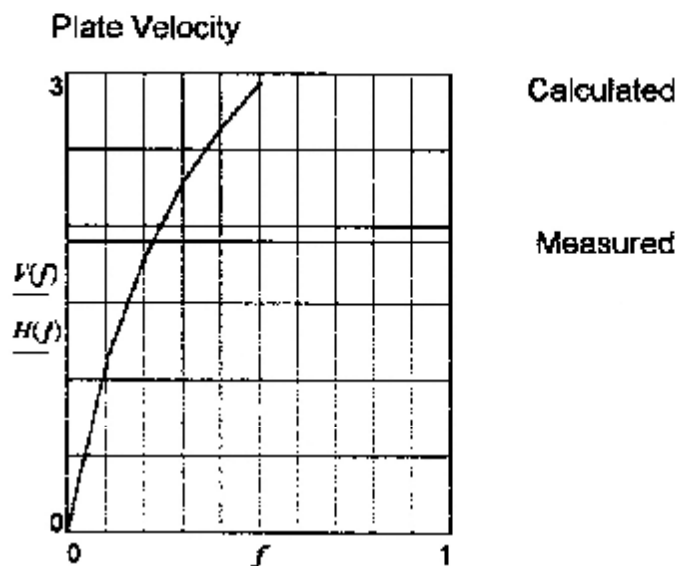
$$f := 0, 0.1 \dots 1$$

$$z(f) := \sqrt{\frac{32}{27} \cdot CM \cdot f + 1}$$

$$V(f) := D \cdot \frac{z(f) - 1}{z(f) + 1}$$

$$V_s = 1.9 \quad H(f) := V_s$$

Plot variation of calculated velocity with f ...



Pick a a value of f close to the root of  $V(f)-H(f)=0$

$f = 0.4$  ....first estimate of root

$f = \text{root}(|V(f) - H(f)|, f)$   $f = 0.217$  ...the root

The efficiency factor is  $f = 0.217$  at  $CM = 6.9$

This is the fraction of explosive mass that contributes to the one-dimensional gas expansion accelerating the plate to its final velocity.

**4 Charge Mass Efficiency .....**

Number of velocity measurements:  $N = 9$

Pick a number from 0 to N-1:  $i = 8$

Prepare variables for plotting:  $CM = CM_{i-1} \quad V_s = V_{slug_i}$

Plot variation of calculated velocity with  $0 < f < 1$  .....

$$f := 0, 0.1, \dots, 1$$

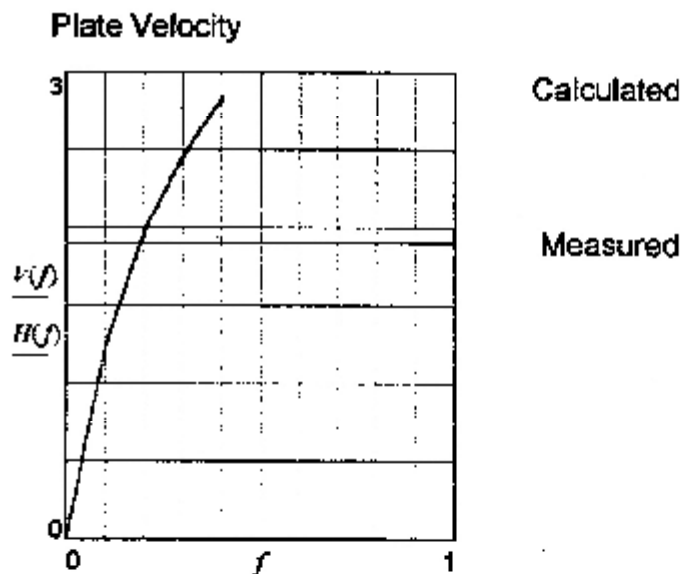
$$z(f) := \sqrt{\frac{32}{27} CM f + 1}$$

$$V(f) := D \frac{z(f)}{z(f) + 1}$$

$$V_s = 1.9$$

$$H(f) := V_s$$

Plot variation of calculated velocity with f ...



Pick a value of f close to the root of  $V(f)-H(f)=0$

$f = 0.4$  ....first estimate of root

$f := \text{root}( V(f) - H(f) | f)$   $f = 0.187$  ...the root

The efficiency factor is  $f = 0.187$  at  $CM = 8$

This is the fraction of explosive mass that contributes to the one-dimensional gas expansion accelerating the plate to its final velocity.

### **A.13.2.3 FICKETT MODEL**



Explosive Type: Composition B

Charge Length  $l = 12.5$   
 Charge mass g  $C = 13.7$   
 VOD km/s  $D = 7.6$   
 Polytropic  $\Gamma = 3$   
 Plate mass  $m = 6$       Sound speed km/s  $C_b = 3.6$   
 Measured Velocity m/s  $V_{exp} = 1350$

PRINT RESULTS OF CALCULATIONS (2) \*\*\*\*\*

	us	us	mm	m/s
	1.867	0.222	0.118	936
	2.089	0.444	0.382	1400
	2.311	0.667	0.726	1669
	2.534	0.889	1.117	1841
	2.756	1.111	1.54	1958
$t =$	2.978	$t_{acc} =$ 1.333	$X_{acc} =$ 1.985	$V_p =$ 2041
	3.2	1.556	2.446	2103
	3.423	1.778	2.918	2150
	3.645	2	3.401	2187
	3.867	2.222	3.89	2218
	4.089	2.444	4.385	2240
	4.311	2.667	4.885	2259
	4.534	2.889	5.389	2275
	4.756	3.111	5.896	2289
	4.978	3.333	6.406	2300
	5.2	3.556	6.918	2310
	5.423	3.778	7.433	2319
	5.645	4	7.949	2326
	5.867	4.222	8.467	2333
	6.089	4.444	8.986	2338

Time from detonation at start of explosive column	Time from start of plate acceleration	Plate displacement	Plate velocity
--	--	-----------------------	----------------

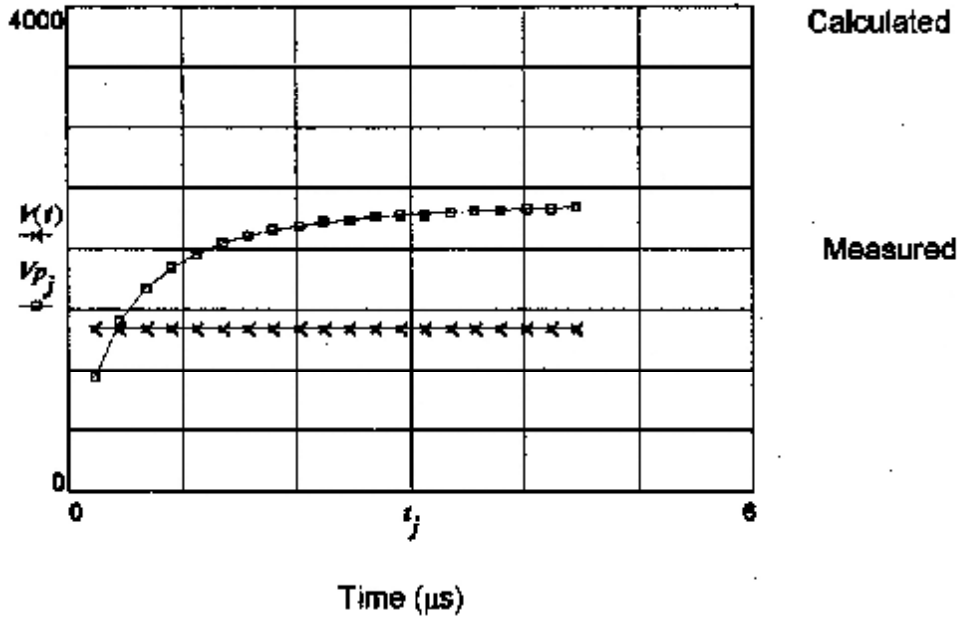
DISPLAY RESULTS OF CALCULATIONS\*\*\*\*\*

Define experimental value of plate velocity as a constant-value function of time...

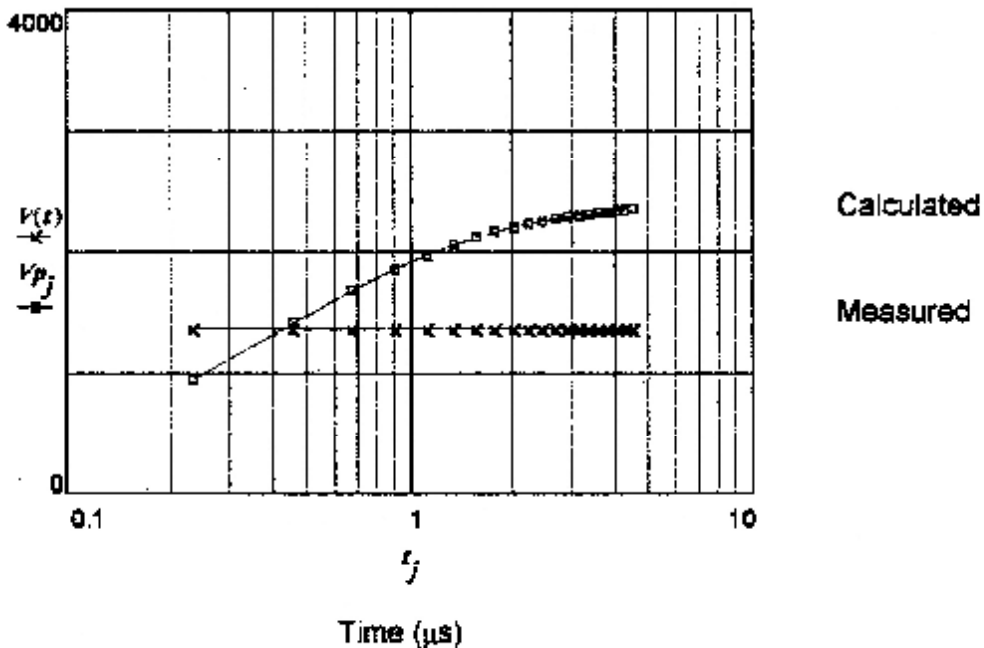
$$V(t) := V_{exp} \quad t := t_{acc} + 0.01 \quad >0$$

TIME VARIATION OF PLATE VELOCITY

Velocity m/s



Plot time on logarithmic scale....



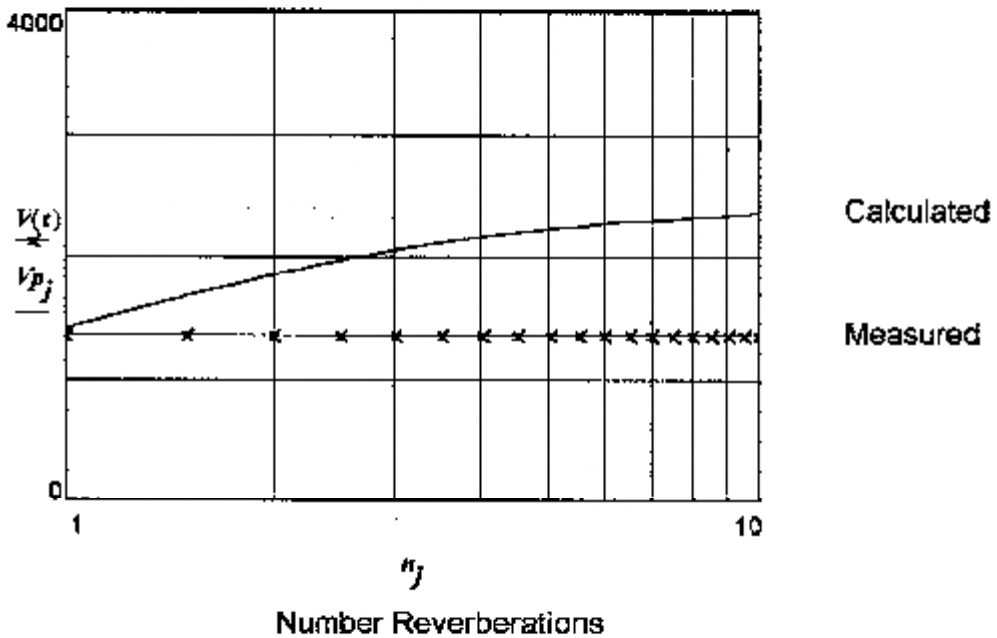
Plot velocity against number of pressure reverberations in plate....

$j = 1 \dots N$  .... must be  $> 0$  for logarithmic axis

$n_j = \frac{j}{2}$  .... n is the number of transits ....

n denotes reverberation number, i.e. number of time increments as defined in section (1) under CALCULATIONS

Plate Velocity m/s



Plot indicates that measured plate velocity is attained shortly before the FIRST passage of the pressure pulse through plate thickness

Explosive Type: Composition B

Charge Length  $L = 17.4$   
 Charge mass g  $C = 19.1$   
 VOD km/s  $D = 7.6$   
 Polytropic  $\Gamma = 3$   
 Plate mass  $m = 6$  Sound speed km/s  $C_p = 3.6$   
 Measured Velocity m/s  $V_{exp} = 1425$

PRINT RESULTS OF CALCULATIONS (2) \*\*\*\*\*

	us	us	mm	m/s
	2.512	0.222	0.121	978
	2.734	0.444	0.402	1501
	2.956	0.667	0.774	1821
	3.178	0.889	1.204	2034
	3.401	1.111	1.673	2184
$t =$	3.623	$t_{acc} = 1.333$	$X_{acc} = 2.172$	$V_p = 2295$
	3.845	1.556	2.691	2378
	4.067	1.778	3.227	2443
	4.289	2	3.776	2495
	4.512	2.222	4.335	2536
	4.734	2.444	4.903	2571
	4.956	2.667	5.477	2599
	5.178	2.889	6.057	2623
	5.401	3.111	6.643	2643
	5.623	3.333	7.232	2661
	5.845	3.556	7.825	2676
	6.067	3.778	8.421	2689
	6.289	4	9.02	2700
	6.512	4.222	9.621	2710
	6.734	4.444	10.224	2719

Time from  
detonation  
at start of  
explosive column

Time from  
start of  
plate  
acceleration

Plate  
displacement

Plate velocity

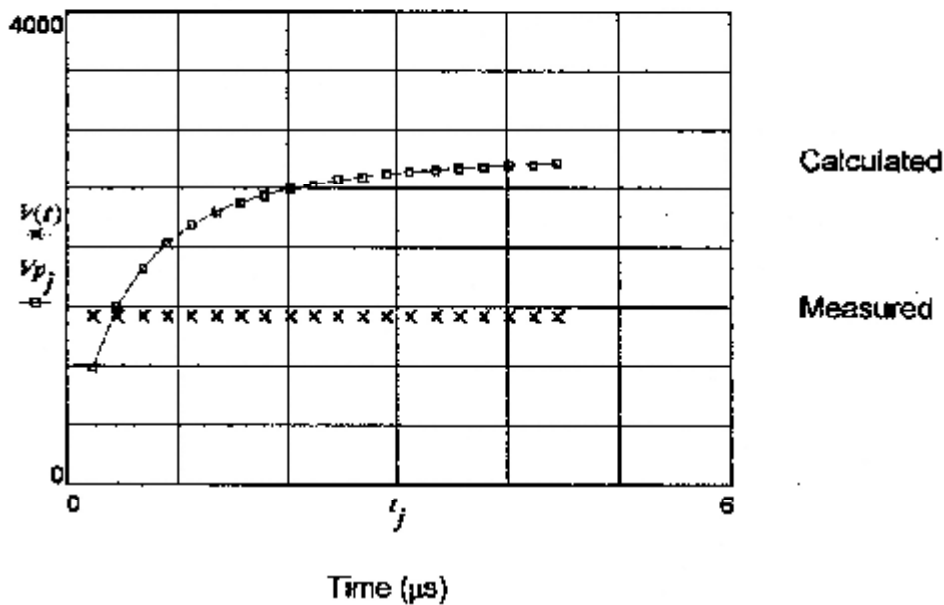
DISPLAY RESULTS OF CALCULATIONS\*\*\*\*\*

Define experimental value of plate velocity as a constant-value function of time...

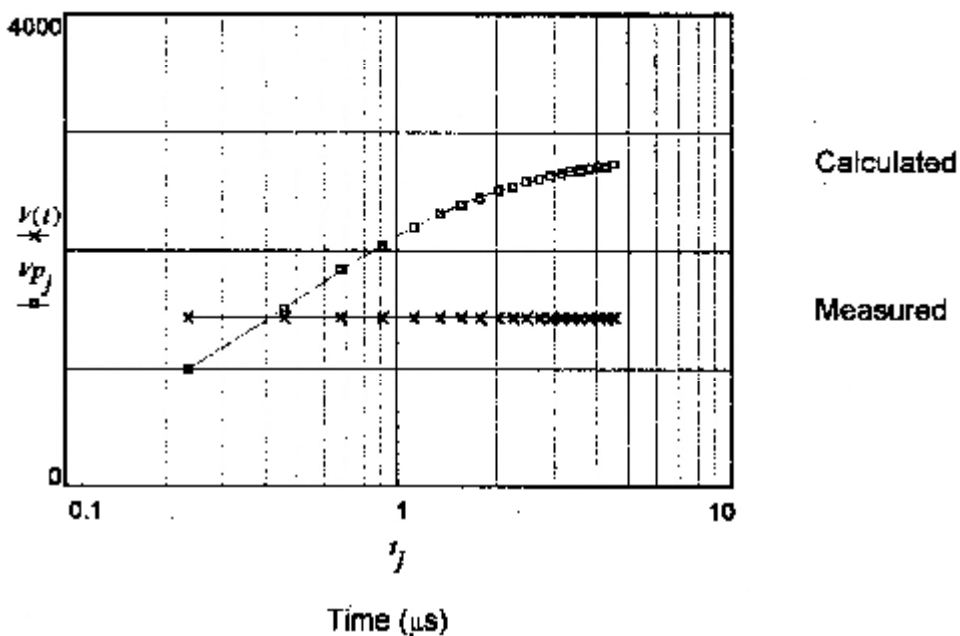
$$V(t) = V_{exp} \quad t := t_{acc} + 0.01 \quad >0$$

TIME VARIATION OF PLATE VELOCITY

Velocity m/s



Plot time on logarithmic scale....



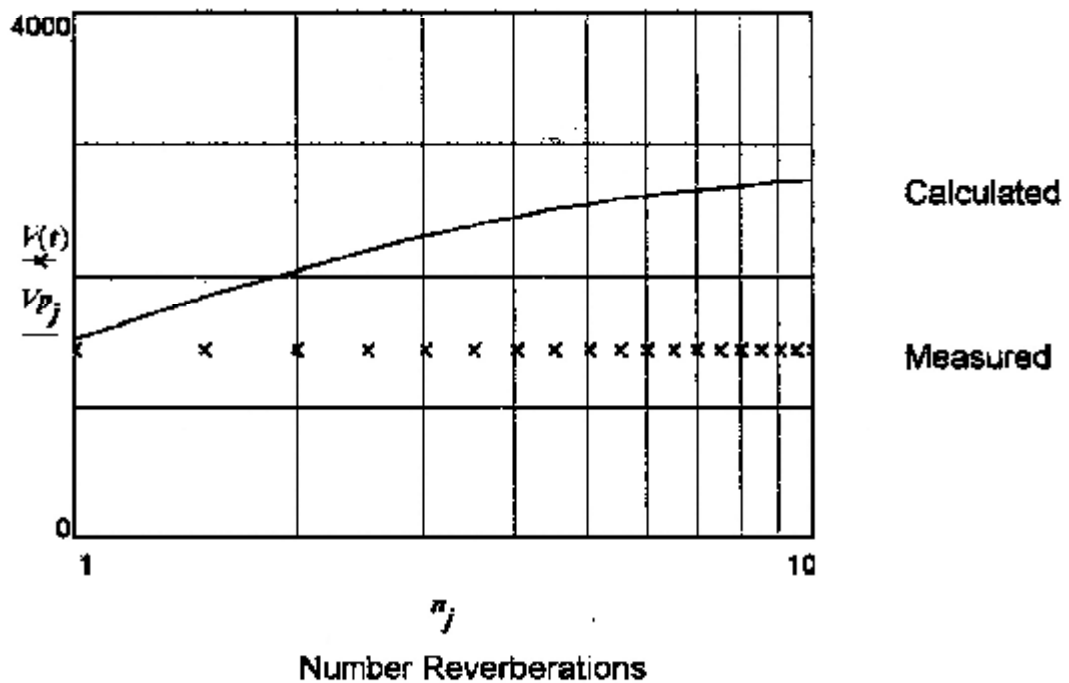
Plot velocity against number of pressure reverberations in plate....

$j = 1 \dots N$  ....must be  $> 0$  for logarithmic axis

$$n_j = \frac{j}{2} \quad \dots n \text{ is the number of transits } \dots$$

$n$  denotes reverberation number, i.e. number of time increments as defined in section (1) under CALCULATIONS

Plate Velocity m/s



Plot indicates that measured plate velocity is attained shortly before the FIRST passage of the pressure pulse through plate thickness

Explosive Type: Composition B

Charge Length  $l = 24$   
 Charge mass g  $C = 26.2$   
 VOD km/s  $D = 7.6$   
 Polytropic  $\Gamma = 3$   
 Plate mass  $m = 6$       Sound speed km/s  $C_b = 3.6$   
 Measured Velocity m/s  $V_{exp} = 1588$

PRINT RESULTS OF CALCULATIONS (2) \*\*\*\*\*

	us	us	mm	m/s
	3.38	0.222	0.123	1004
	3.602	0.444	0.415	1573
	3.825	0.667	0.807	1936
	4.047	0.889	1.267	2187
	4.269	1.111	1.774	2368
$t =$	4.491	$t_{acc} = 1.333$	$X_{acc} = 2.316$	$V_p = 2504$
	4.713	1.556	2.885	2610
	4.936	1.778	3.474	2693
	5.158	2	4.081	2761
	5.38	2.222	4.701	2816
	5.602	2.444	5.332	2862
	5.825	2.667	5.972	2901
	6.047	2.889	6.621	2934
	6.269	3.111	7.276	2962
	6.491	3.333	7.937	2987
	6.713	3.556	8.603	3008
	6.936	3.778	9.274	3027
	7.158	4	9.948	3043
	7.38	4.222	10.626	3058
	7.602	4.444	11.307	3071

Time from  
detonation  
at start of  
explosive column

Time from  
start of  
plate  
acceleration

Plate  
displacement

Plate velocity

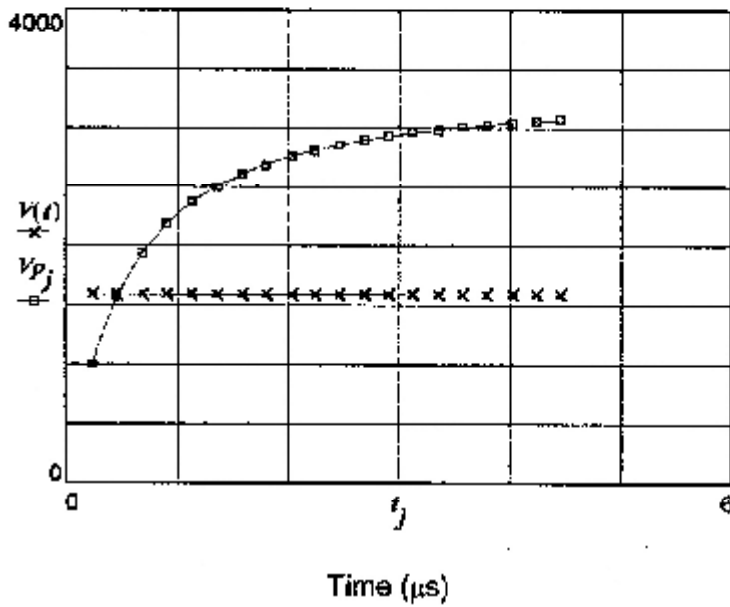
DISPLAY RESULTS OF CALCULATIONS\*\*\*\*\*

Define experimental value of plate velocity as a constant- value function of time...

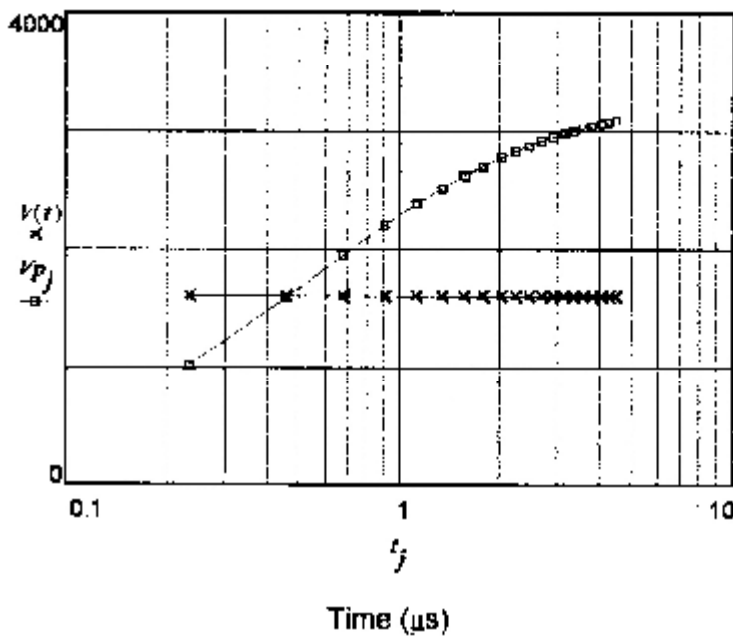
$$V(t) := V_{exp} \quad t := t_{acc} - 0.01 \quad > 0$$

TIME VARIATION OF PLATE VELOCITY

Velocity m/s



Plot time on logarithmic scale....





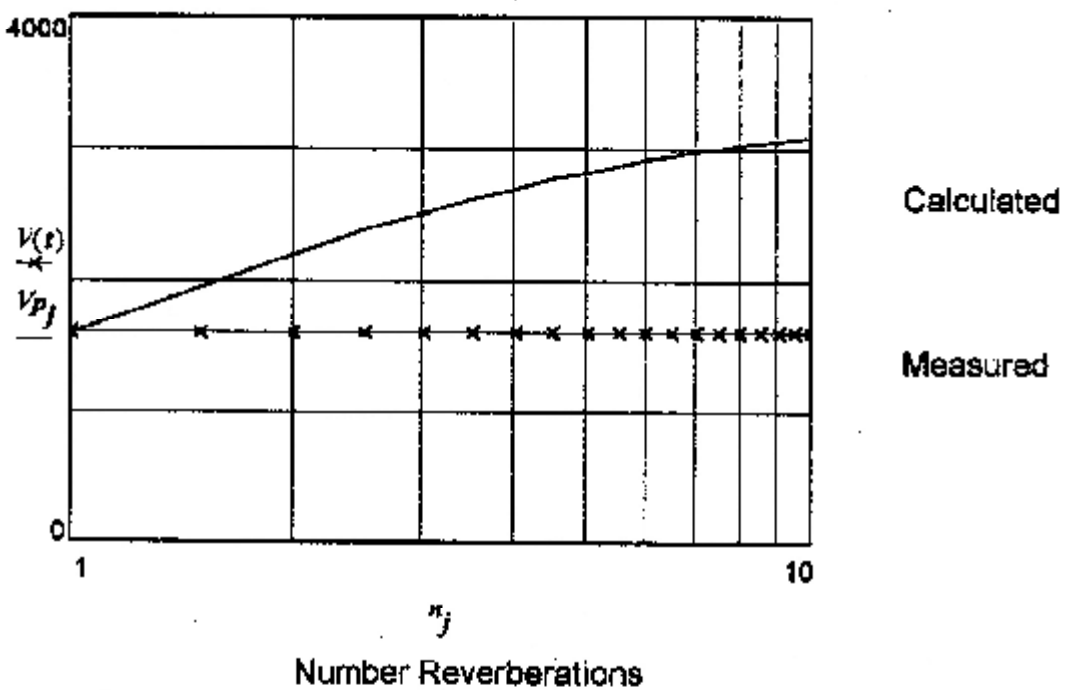
Plot velocity against number of pressure reverberations in plate....

$j := 1 \dots N$  ....must be  $> 0$  for logarithmic axis

$n_j := \frac{j}{2}$  ....n is the number of transits ....

n denotes reverberation number, i.e. number of time increments as defined in section (1) under CALCULATIONS

Plate Velocity m/s



Plot indicates that measured plate velocity is attained shortly before the FIRST passage of the pressure pulse through plate thickness

Explosive Type: Composition B

Charge Length  $L = 28.7$   
 Charge mass g  $C = 31.5$   
 VOD km/s  $D = 7.6$   
 Polytropic  $\Gamma = 3$   
 Plate mass  $m = 6$       Sound speed km/s  $C_b = 3.6$   
 Measured Velocity m/s  $V_{exp} = 1750$

PRINT RESULTS OF CALCULATIONS (2) \*\*\*\*\*

	us	us	mm	m/s
	3.999	0.222	0.125	1022
	4.221	0.444	0.423	1615
	4.443	0.667	0.828	2001
	4.665	0.889	1.304	2270
	4.887	1.111	1.831	2468
$t -$	5.11	$t_{acc} = 1.333$	$X_{acc} = 2.397$	$V_P = 2618$
	5.332	1.556	2.993	2736
	5.554	1.778	3.612	2830
	5.776	2	4.249	2907
	5.999	2.222	4.902	2970
	6.221	2.444	5.568	3023
	6.443	2.667	6.245	3068
	6.665	2.889	6.932	3106
	6.887	3.111	7.626	3140
	7.11	3.333	8.327	3168
	7.332	3.556	9.034	3194
	7.554	3.778	9.746	3216
	7.776	4	10.463	3235
	7.999	4.222	11.184	3253
	8.221	4.444	11.908	3269

Time from  
detonation  
at start of  
explosive column

Time from  
start of  
plate  
acceleration

Plate  
displacement

Plate velocity

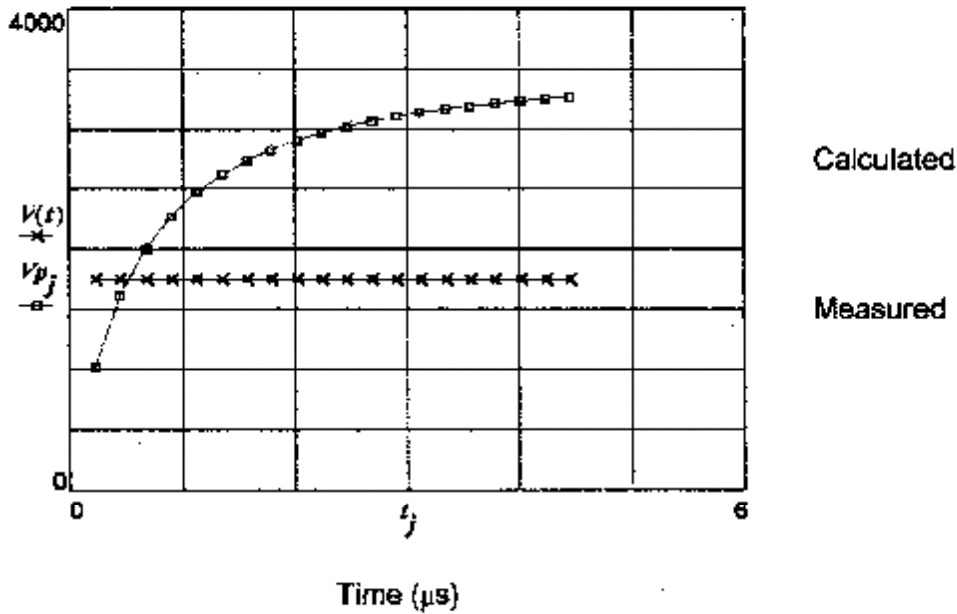
DISPLAY RESULTS OF CALCULATIONS\*\*\*\*\*

Define experimental value of plate velocity as a constant-value function of time...

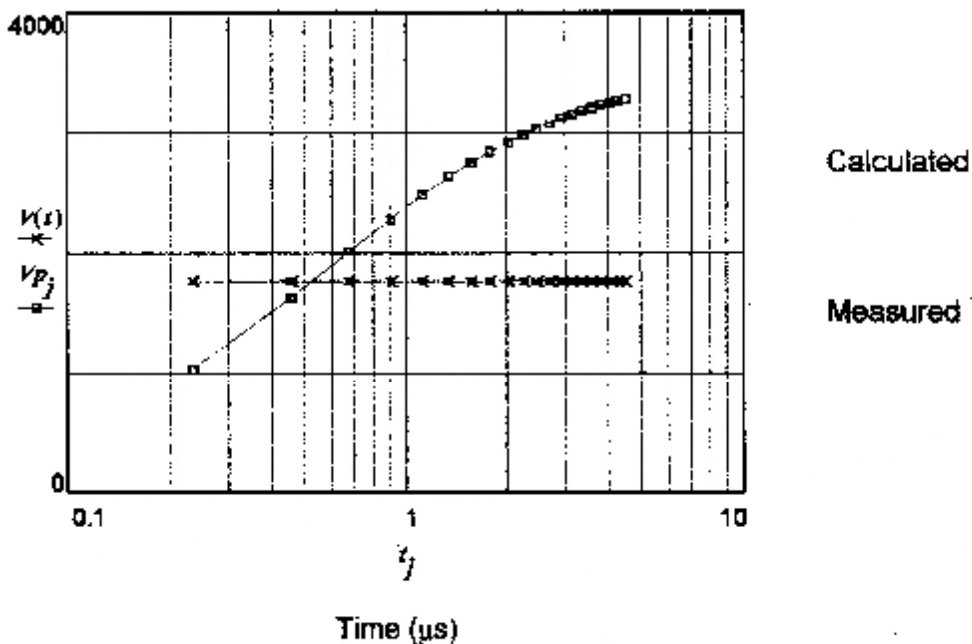
$$V(t) = V_{exp} \quad t := t_{acc} + 0.01 \quad >0$$

TIME VARIATION OF PLATE VELOCITY

Velocity m/s



Plot time on logarithmic scale....



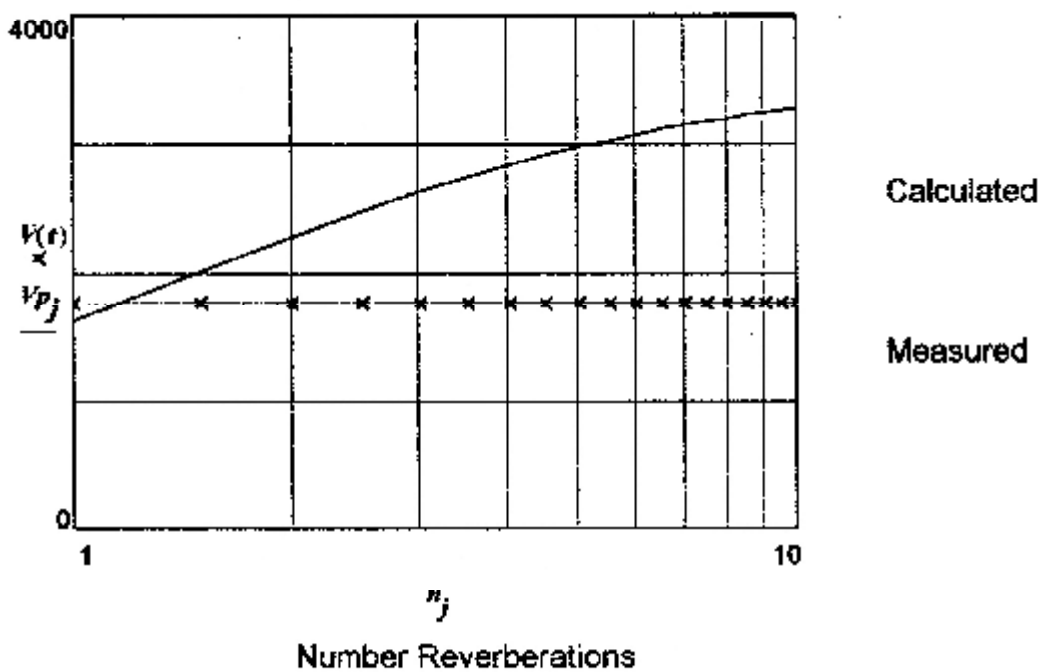
Plot velocity against number of pressure reverberations in plate....

$j = 1 \dots N$  ....must be  $> 0$  for logarithmic axis

$n_j = \frac{j}{2}$  ....n is the number of transits ....

n denotes reverberation number, i.e. number of time increments as defined in section (1) under CALCULATIONS

Plate Velocity m/s



Plot indicates that measured plate velocity is attained shortly before the FIRST passage of the pressure pulse through plate thickness

Explosive Type: Composition B

Charge Length  $L = 29.4$   
 Charge mass g  $C = 32.3$   
 VOD km/s  $D = 7.6$   
 Polytropic  $\Gamma = 3$   
 Plate mass  $m = 6$       Sound speed km/s  $C_b = 3.6$   
 Measured Velocity m/s  $V_{exp} = 1750$

PRINT RESULTS OF CALCULATIONS (2) \*\*\*\*\*

us	us	mm	m/s
4.091	0.222	0.125	1024
4.313	0.444	0.424	1620
4.535	0.667	0.83	2009
4.757	0.889	1.309	2261
4.98	1.111	1.839	2481
$t = 5.202$	$t_{acc} = 1.333$	$X_{acc} = 2.408$	$V_p = 2633$
5.424	1.556	3.007	2753
5.646	1.778	3.63	2848
5.868	2	4.271	2926
6.091	2.222	4.929	2990
6.313	2.444	5.6	3044
6.535	2.667	6.281	3090
6.757	2.889	6.973	3129
6.98	3.111	7.672	3163
7.202	3.333	8.378	3192
7.424	3.556	9.09	3218
7.646	3.778	9.808	3241
7.868	4	10.531	3261
8.091	4.222	11.257	3279
8.313	4.444	11.988	3295

Time from  
detonation  
at start of  
explosive column

Time from  
start of  
plate  
acceleration

Plate  
displacement

Plate velocity

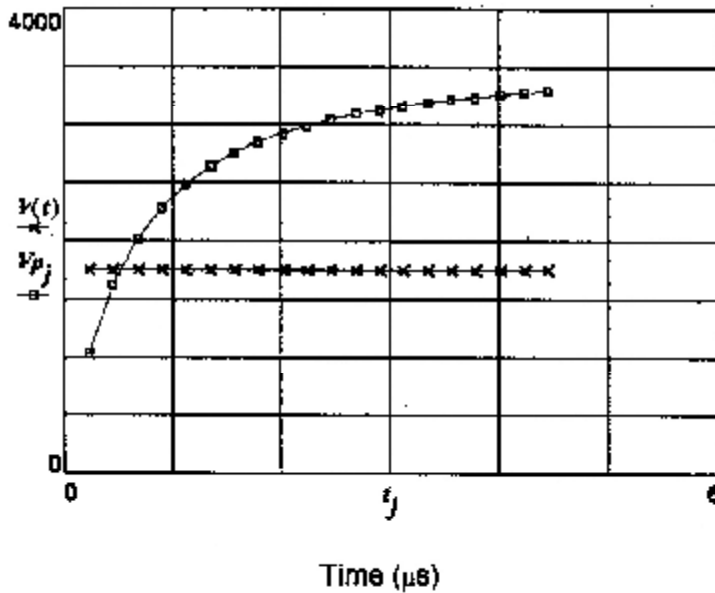
DISPLAY RESULTS OF CALCULATIONS\*\*\*\*\*

Define experimental value of plate velocity as a constant-value function of time...

$$V(t) = V_{exp} \quad t := t_{acc} = 0.01 \quad >0$$

TIME VARIATION OF PLATE VELOCITY

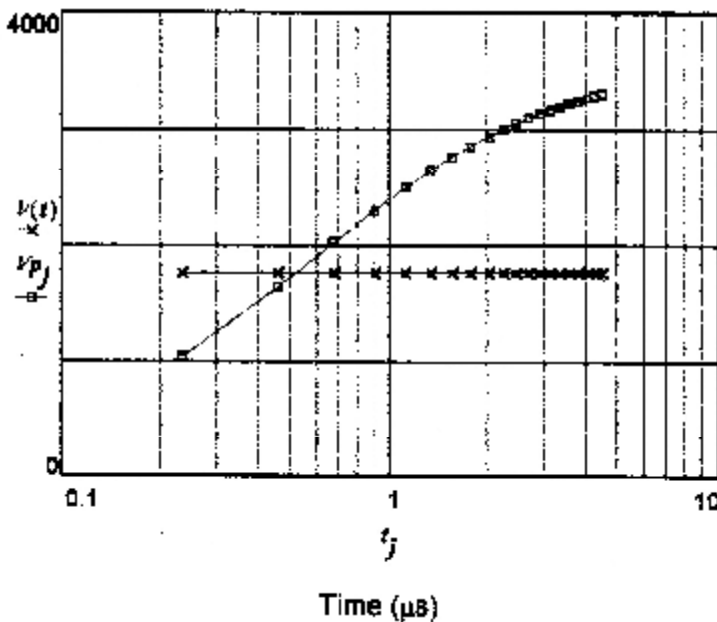
Velocity m/s



Calculated

Measured

Plot time on logarithmic scale....



Calculated

Measured

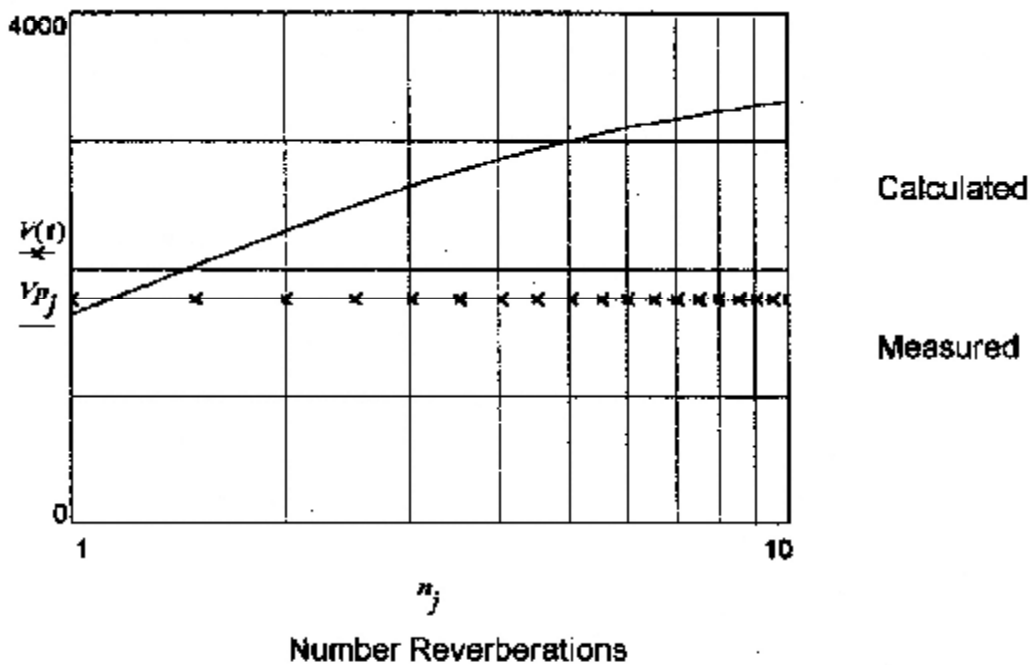
Plot velocity against number of pressure reverberations in plate....

$j = 1 \dots N$  ....must be  $> 0$  for logarithmic axis

$$n_j := \frac{j}{2} \quad \dots n \text{ is the number of transits } \dots$$

$n$  denotes reverberation number, i.e. number of time increments as defined in section (1) under CALCULATIONS

Plate Velocity m/s



Plot indicates that measured plate velocity is attained shortly before the FIRST passage of the pressure pulse through plate thickness

Explosive Type: Composition B

Charge Length  $L = 32.3$   
 Charge mass g  $C = 35.5$   
 VOD km/s  $D = 7.6$   
 Polytropic  $\Gamma = 3$   
 Plate mass  $m = 6$       Sound speed km/s  $C_b = 3.6$   
 Measured Velocity m/s  $V_{exp} = 1825$

PRINT RESULTS OF CALCULATIONS (2) \*\*\*\*\*

	us	us	mm	m/s
	4.472	0.222	0.126	1031
	4.694	0.444	0.428	1638
	4.917	0.667	0.839	2037
	5.139	0.889	1.324	2318
	5.361	1.111	1.863	2526
$t =$	5.583	$t_{acc} = 1.333$	$X_{acc} = 2.443$	$V_p = 2685$
	5.806	1.556	3.054	2811
	6.028	1.778	3.691	2912
	6.25	2	4.347	2994
	6.472	2.222	5.02	3063
	6.694	2.444	5.708	3120
	6.917	2.667	6.407	3170
	7.139	2.889	7.116	3212
	7.361	3.111	7.834	3248
	7.583	3.333	8.559	3280
	7.806	3.556	9.291	3308
	8.028	3.778	10.029	3332
	8.25	4	10.772	3354
	8.472	4.222	11.52	3374
	8.694	4.444	12.271	3391

Time from  
detonation  
at start of  
explosive column

Time from  
start of  
plate  
acceleration

Plate  
displacement

Plate velocity



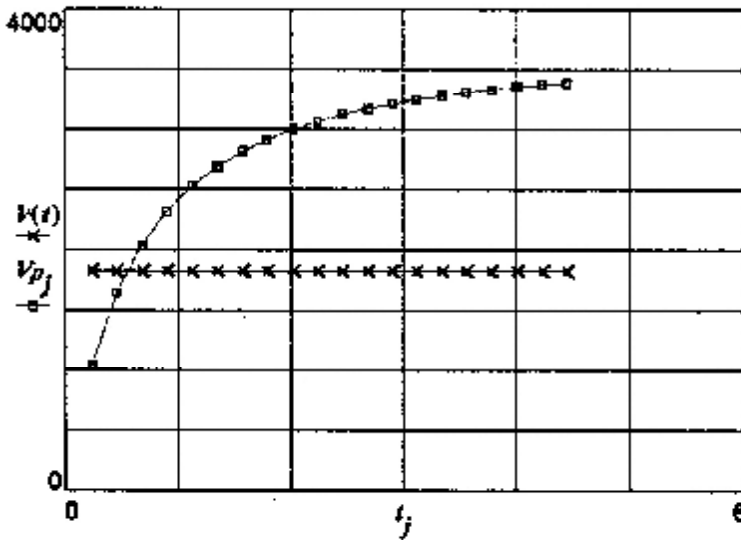
DISPLAY RESULTS OF CALCULATIONS\*\*\*\*\*

Define experimental value of plate velocity as a constant-value function of time...

$$V(t) = V_{exp} \quad t = t_{acc} + 0.01 \quad >0$$

TIME VARIATION OF PLATE VELOCITY

Velocity m/s

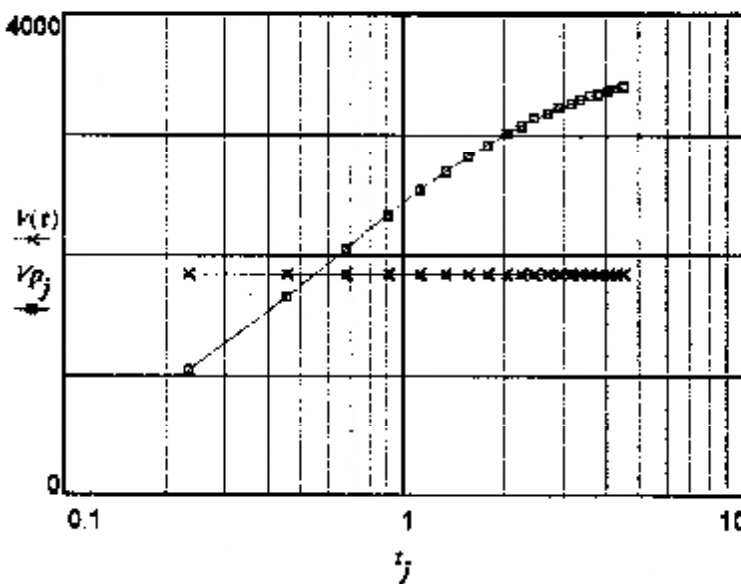


Calculated

Measured

Time ( $\mu$ s)

Plot time on logarithmic scale....



Calculated

Measured

Time ( $\mu$ s)

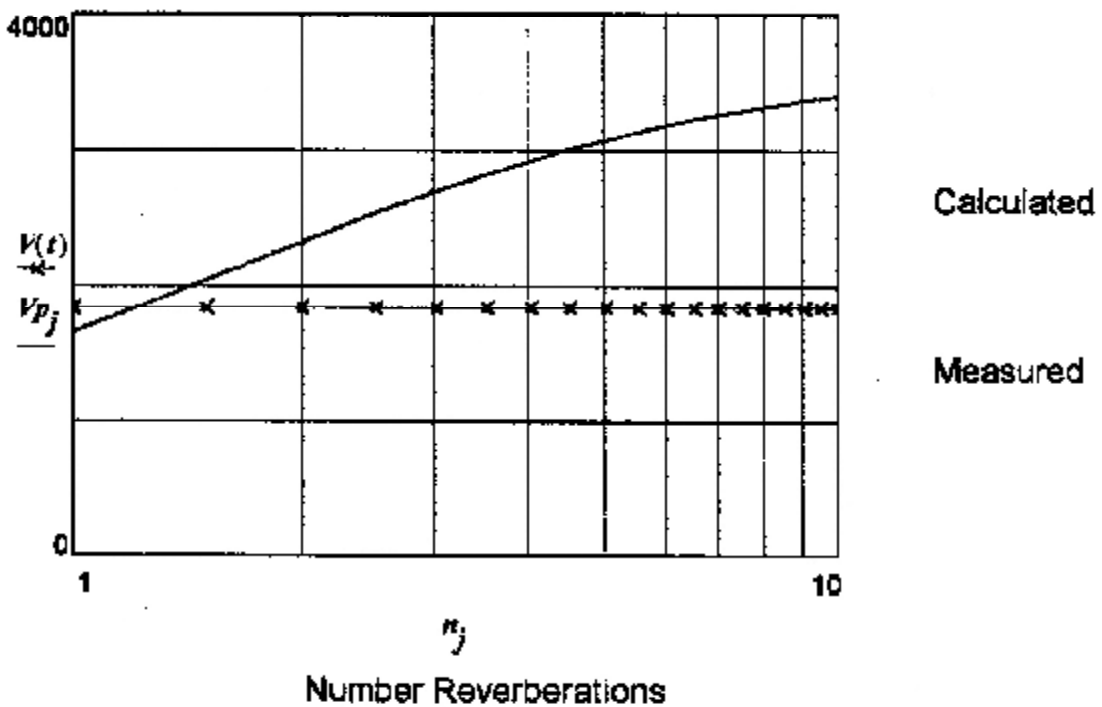
Plot velocity against number of pressure reverberations in plate...

$j = 1 \dots N$  ....must be  $> 0$  for logarithmic axis

$n_j := \frac{j}{2}$  ....n is the number of transits ....

n denotes reverberation number, i.e. number of time increments as defined in section (1) under CALCULATIONS

Plate Velocity m/s



Plot indicates that measured plate velocity is attained shortly before the FIRST passage of the pressure pulse through plate thickness

Explosive Type: Composition B

Charge Length  $L = 36.2$   
 Charge mass g  $C = 39.8$   
 VOD km/s  $D = 7.6$   
 Polytropic  $\Gamma = 3$   
 Plate mass  $m = 6$       Sound speed km/s  $C_b = 3.6$   
 Measured Velocity m/s  $V_{exp} = 1800$

PRINT RESULTS OF CALCULATIONS (2) -----

	us	us	mm	m/s
	4.985	0.222	0.127	1038
	5.208	0.444	0.431	1657
	5.43	0.667	0.848	2067
	5.652	0.889	1.341	2359
	5.874	1.111	1.891	2577
$t =$	6.096	$t_{acc} = 1.333$	$X_{acc} = 2.483$	$V_p = 2744$
	6.319	1.556	3.108	2877
	6.541	1.778	3.76	2984
	6.763	2	4.433	3073
	6.985	2.222	5.124	3148
	7.208	2.444	5.83	3208
	7.43	2.667	6.549	3261
	7.652	2.889	7.279	3307
	7.874	3.111	8.019	3347
	8.096	3.333	8.767	3382
	8.319	3.556	9.521	3412
	8.541	3.778	10.283	3439
	8.763	4	11.05	3463
	8.985	4.222	11.822	3485
	9.208	4.444	12.599	3504
Time from detonation at start of explosive column		Time from start of plate acceleration	Plate displacement	Plate velocity

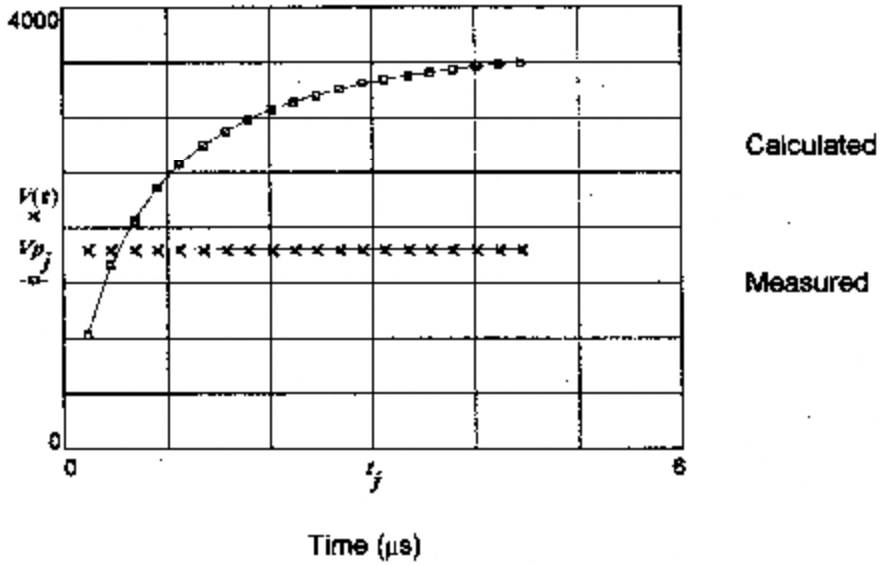
DISPLAY RESULTS OF CALCULATIONS.....

Define experimental value of plate velocity as a constant- value function of time...

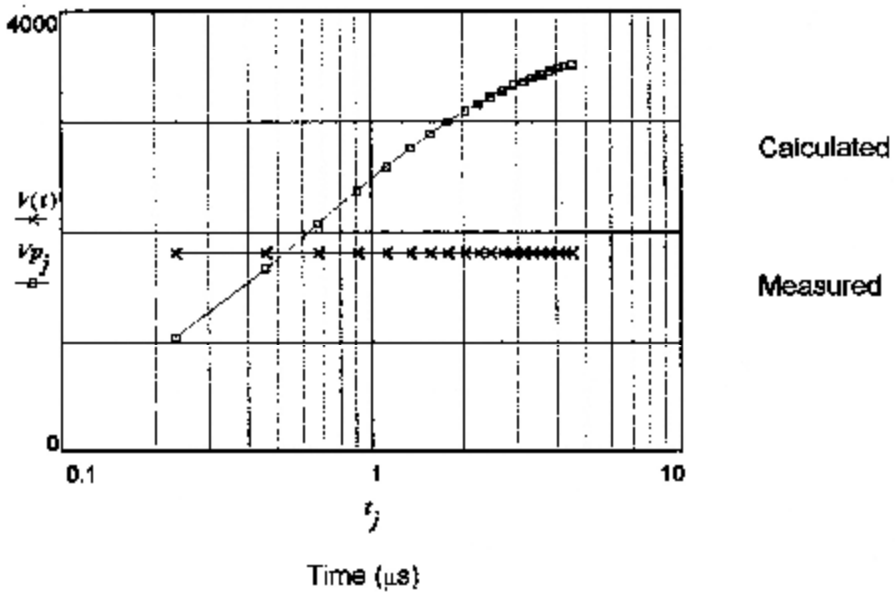
$$V(t) := V_{exp} \quad t := t_{acc} + 0.01 \quad >0$$

TIME VARIATION OF PLATE VELOCITY

Velocity m/s



Plot time on logarithmic scale....



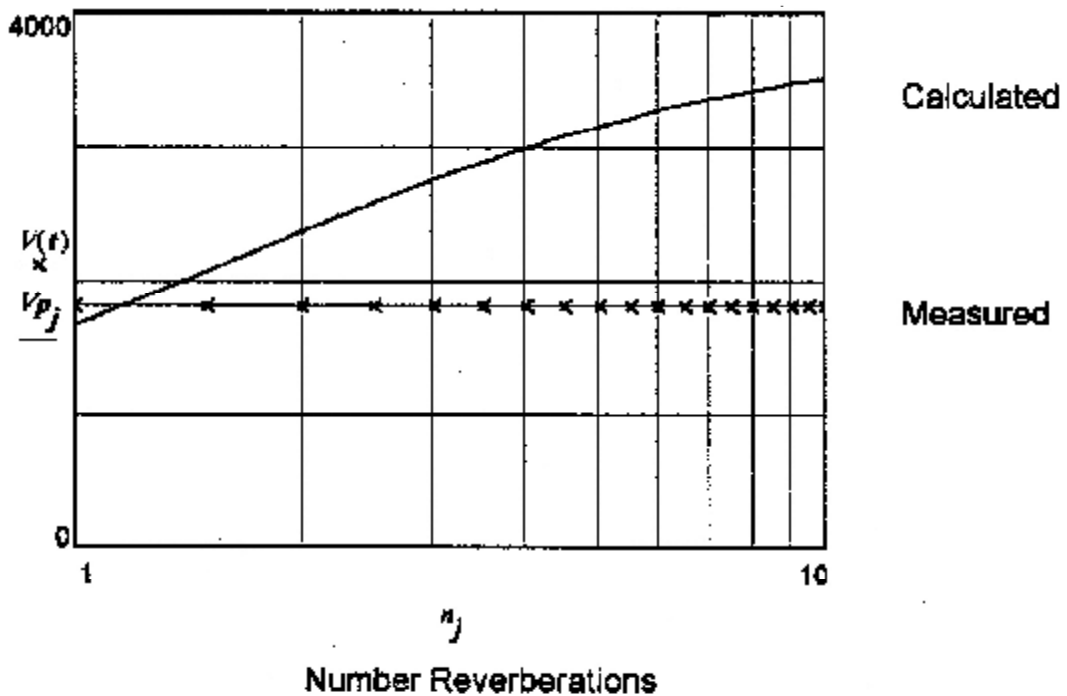
Plot velocity against number of pressure reverberations in plate....

$j = 1 \dots N$  .... must be  $> 0$  for logarithmic axis

$n_j = \frac{j}{2}$  .... n is the number of transits ....

n denotes reverberation number, i.e. number of time increments as defined in section (1) under CALCULATIONS

Plate Velocity m/s



Plot indicates that measured plate velocity is attained shortly after the FIRST passage of the pressure pulse through plate thickness

Explosive Type: Composition B

Charge Length  $L = 37.7$   
 Charge mass g  $C = 41.4$   
 VOD km/s  $D = 7.6$   
 Polytropic  $\Gamma = 3$   
 Plate mass  $m = 6$       Sound speed km/s  $C_b = 3.8$   
 Measured Velocity m/s  $V_{exp} = 1900$

PRINT RESULTS OF CALCULATIONS (2) \*\*\*\*\*

	us	us	mm	m/s
	5.183	0.222	0.127	1039
	5.405	0.444	0.432	1661
	5.627	0.667	0.85	2076
	5.849	0.889	1.346	2371
	6.072	1.111	1.898	2592
$t =$	6.294	$t_{acc} = 1.333$	$X_{acc} = 2.494$	$V_p = 2763$
	6.516	1.556	3.124	2898
	6.738	1.778	3.78	3007
	6.961	2	4.459	3098
	7.183	2.222	5.156	3173
	7.405	2.444	5.868	3237
	7.627	2.667	6.594	3291
	7.849	2.889	7.33	3338
	8.072	3.111	8.077	3379
	8.294	3.333	8.832	3415
	8.516	3.556	9.594	3447
	8.738	3.778	10.363	3474
	8.961	4	11.138	3499
	9.183	4.222	11.918	3522
	9.405	4.444	12.703	3542

Time from  
detonation  
at start of  
explosive column

Time from  
start of  
plate  
acceleration

Plate  
displacement

Plate velocity

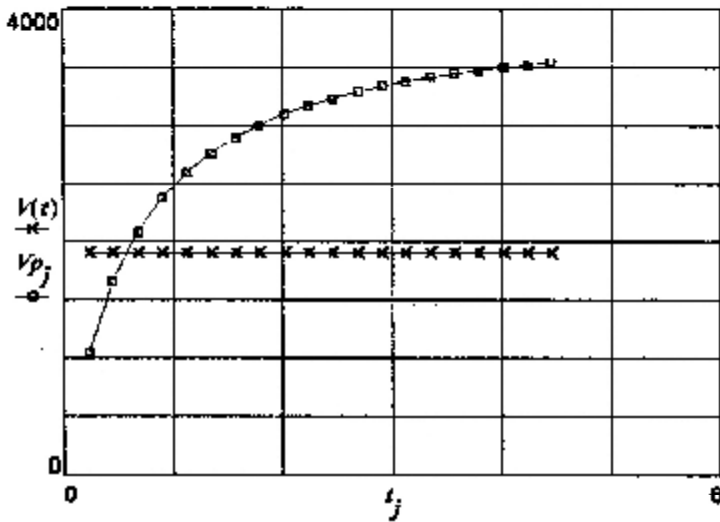
DISPLAY RESULTS OF CALCULATIONS\*\*\*\*\*

Define experimental value of plate velocity as a constant- value function of time...

$$V(t) = V_{exp} \quad t := t_{acc} + 0.01 \quad >0$$

TIME VARIATION OF PLATE VELOCITY

Velocity m/s

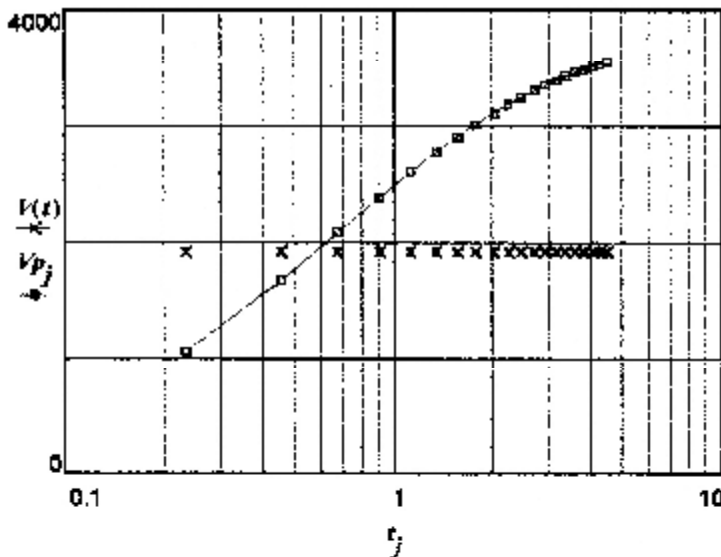


Calculated

Measured

Time (μs)

Plot time on logarithmic scale...



Calculated

Measured

Time (μs)

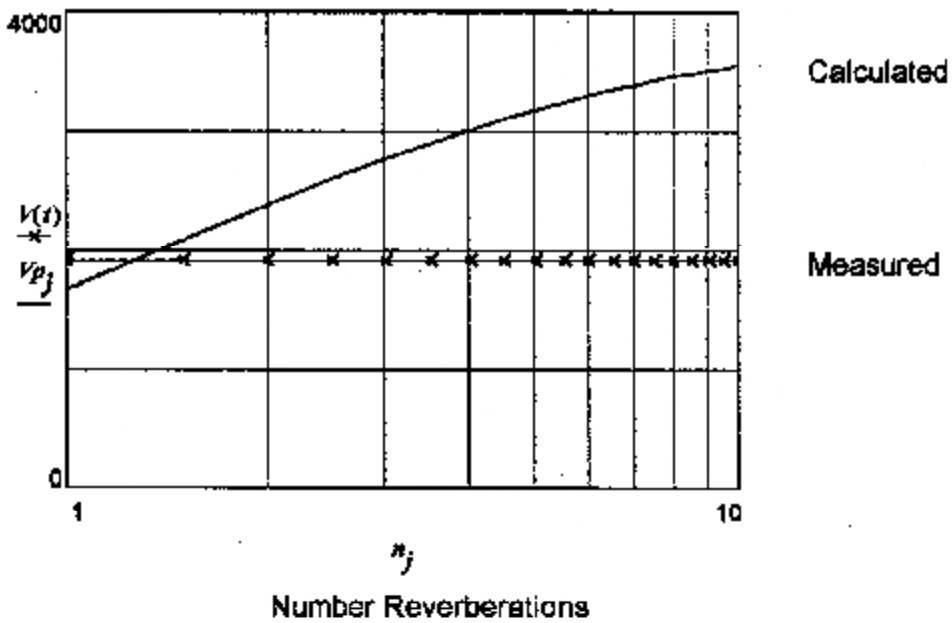
Plot velocity against number of pressure reverberations in plate....

$j := 1 \dots N$  ....must be  $> 0$  for logarithmic axis

$n_j := \frac{j}{2}$  ....n is the number of transits ....

n denotes reverberation number, i.e. number of time increments as defined in section (1) under CALCULATIONS

Plate Velocity m/s



Plot indicates that measured plate velocity is attained shortly after the FIRST passage of the pressure pulse through plate thickness



Explosive Type: Composition B

Charge Length  $L = 44$   
 Charge mass g  $C = 48$   
 VOD km/s  $D = 7.6$   
 Polytropic  $\Gamma = 3$   
 Plate mass  $m = 6$       Sound speed km/s  $C_b = 3.6$   
 Measured Velocity m/s  $V_{exp} = 1900$

PRINT RESULTS OF CALCULATIONS (2) \*\*\*\*\*

	us	us	mm	m/s
	6.012	0.222	0.127	1042
	6.234	0.444	0.434	1676
	6.456	0.667	0.856	2103
	6.678	0.889	1.36	2411
	6.901	1.111	1.923	2644
$t =$	7.123	$t_{acc} = 1.333$	$X_{acc} = 2.531$	$V_p = 2824$
	7.345	1.556	3.175	2969
	7.567	1.778	3.848	3087
	7.789	2	4.545	3184
	8.012	2.222	5.262	3266
	8.234	2.444	5.996	3336
	8.456	2.667	6.744	3396
	8.678	2.889	7.505	3448
	8.901	3.111	8.276	3493
	9.123	3.333	9.057	3533
	9.345	3.556	9.846	3568
	9.567	3.778	10.643	3600
	9.789	4	11.446	3628
	10.012	4.222	12.255	3653
	10.234	4.444	13.069	3676

Time from  
detonation  
at start of  
explosive column

Time from  
start of  
plate  
acceleration

Plate  
displacement

Plate velocity

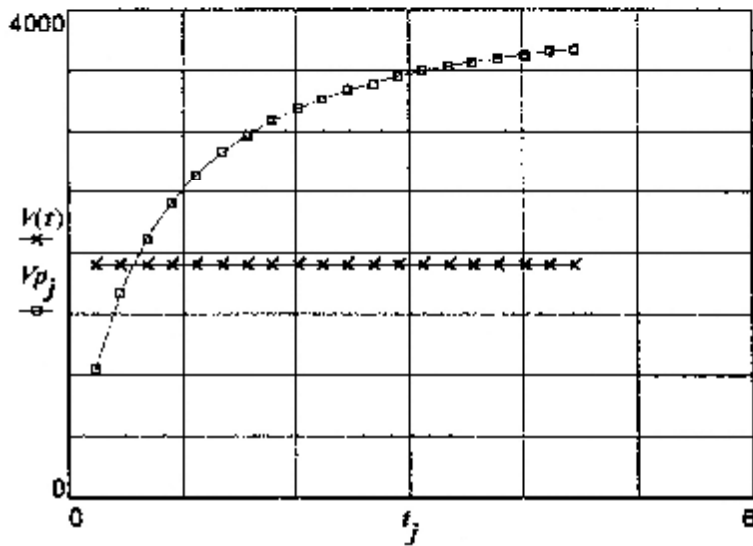
DISPLAY RESULTS OF CALCULATIONS\*\*\*\*\*

Define experimental value of plate velocity as a constant- value function of time...

$$V(t) := V_{exp} \quad t - t_{acc} + 0.01 > 0$$

TIME VARIATION OF PLATE VELOCITY

Velocity m/s

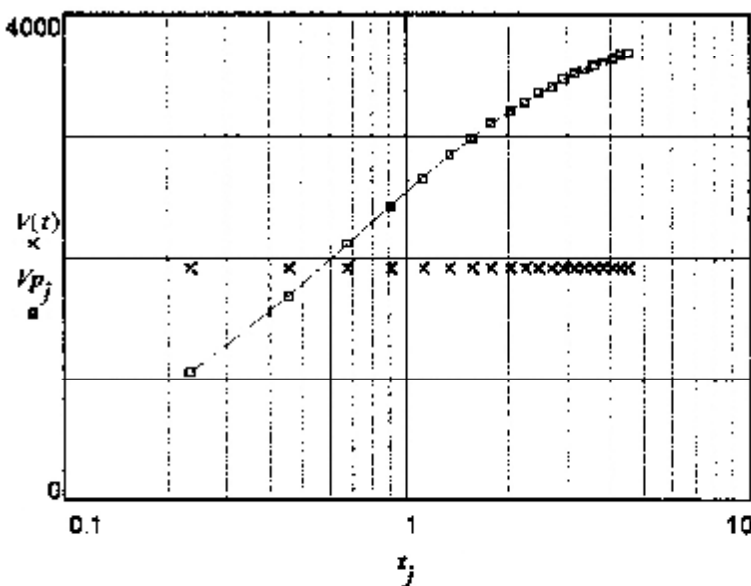


Calculated

Measured

Time (μs)

Plot time on logarithmic scale....



Calculated

Measured

Time (μs)

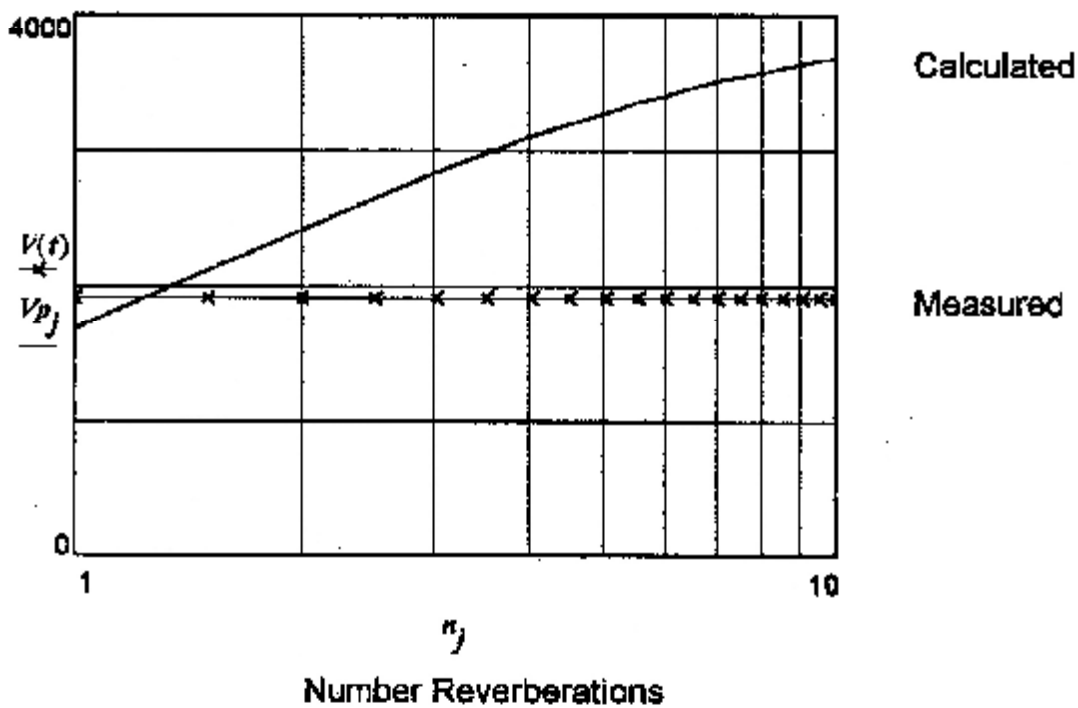
Plot velocity against number of pressure reverberations in plate....

$j := 1..N$  ....must be > 0 for logarithmic axis

$n_j := \frac{j}{2}$  ....n is the number of transits ....

n denotes reverberation number, i.e. number of time increments as defined in section (1) under CALCULATIONS

Plate Velocity m/s



Plot indicates that measured plate velocity is attained shortly after the FIRST passage of the pressure pulse through plate thickness

**A.13.3            A.D.L. TEST SERIES III(a)**

**COMPOSITION B MASS    =    93 grams**  
**DISC MASS                =    8 grams**

### **A.13.3.1 GURNEY MODEL**

Explosive Type: Composition B	
Test ID: RT #3 Series III	
VOD m/s:	$D = 7600$
Plate mass g:	$m_p = 8$
Charge Mass g:	$C = 93$
Measured Velocity	$V_s = 1960$

## DISPLAY RESULTS.....

Gurney constant	$E_g = 2700$	
Reduced Gurney constant	$E_{gr} = 1918.33$	
Particle speed in gas	$U_p = 1900$	
C/M ratio	$zI = 11.625$	
Velocity: standard Gurney	$V_g = 3871$	
Velocity: reduced Gurney	$V_{gr} = 2750$	
Velocity: momentum transfer	$V_{pp} = 1621$	
Velocity: modified Gurney	$V_{gm} = 3192.36$	
Measured Velocity	$V_s = 1960$	m/s

Scroll to page 4 for derivation of efficiency factor f ...

Derive efficiency factor for effective explosive mass... standard Gurney model:

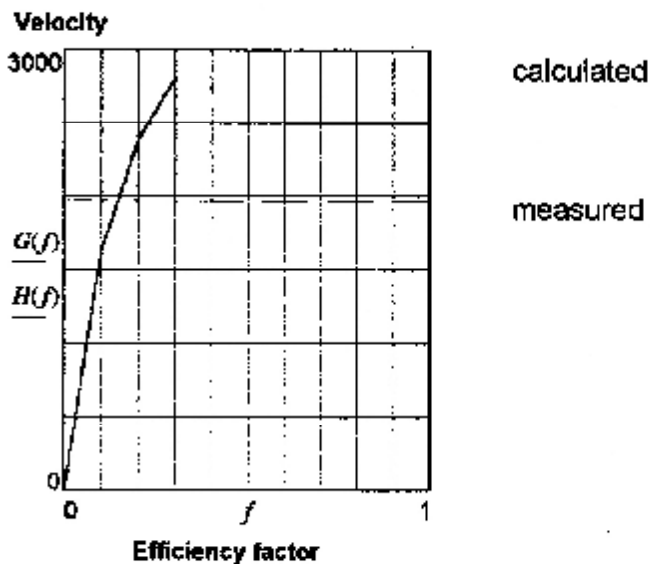
$$F(f) := E \frac{2}{g} \frac{3 \cdot z^2 \cdot f^2}{(f \cdot z + 1) \cdot (f \cdot z + 4)}$$

Check:  $\sqrt{F(f)} = 3871$       Should equal  $V_g = 3871$

Plot variation of calculated plate velocity with efficiency factor f:

$$G(f) := \sqrt{F(f)} \quad f = 0, 0.1 \dots 1 \quad H(f) := V_g$$

Variation of calculated velocity with factor f



Pick value of f close to the root of  $G(f) - H(f) = 0$

$$f := 0.1$$

Refine guess of f by iteration to locate root:

$$f := \text{root}((G(f) - H(f)), f) \quad f = 0.138$$

The efficiency factor is  $f = 0.138$

This is the fraction of explosive mass that contributes to the standard Gurney velocity of the plate.

Derive efficiency factor for effective explosive mass....modified Gurney model:

$$f = 1$$

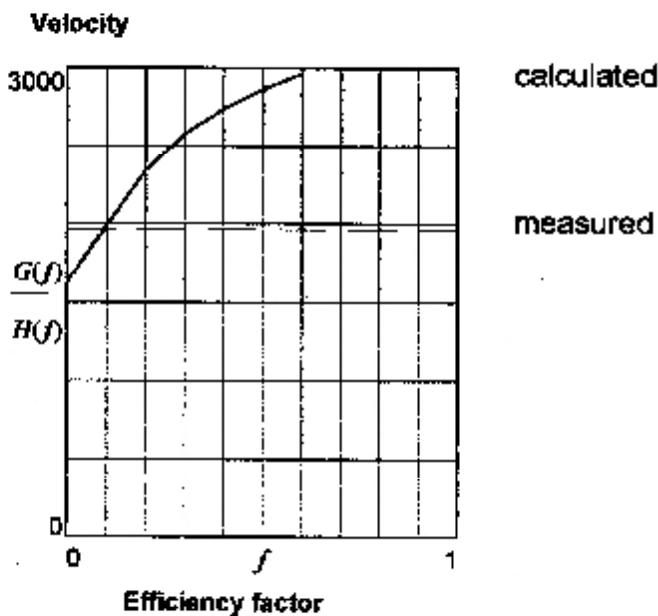
$$F(f) := R_{gr}^2 \frac{3z^2 f^2}{(fz+1)(fz+4)} - V_{pp}^2$$

Check:  $\sqrt{F(f)} = 3192.36$  Should equal  $V_{gm} = 3192.36$

Plot variation of calculated plate velocity with efficiency factor f:

$$G(f) := \sqrt{F(f)} \quad f := 0, 0.1 \dots 1 \quad H(f) := V_s$$

Variation of calculated velocity with factor f



Pick value of f close to the root of  $G(f) - H(f) = 0$

$$f := 0.1$$

Refine guess of f by iteration to locate root:

$$f := \text{root}((G(f) - H(f)), f) \quad f = 0.093$$

The efficiency factor is  $f = 0.093$

This is the fraction of explosive mass that contributes to the modified Gurney velocity of the plate.



Explosive Type: Composition B  
 Test ID: RT #4 Series III  
 VOD m/s:  $D = 7600$   
 Plate mass g:  $m_p = 8$   
 Charge Mass g:  $C = 93$   
 Measured Velocity  $V_s = 2118$

## DISPLAY RESULTS.....

Gurney constant  $E_g = 2700$   
 Reduced Gurney constant  $E_{gr} = 1918.33$   
 Particle speed in gas  $U_p = 1900$   
 C/M ratio  $zI = 11.625$   
 Velocity: standard Gurney  $V_g = 3871$   
 Velocity: reduced Gurney  $V_{gr} = 2750$   
 Velocity: momentum transfer  $V_{pp} = 1621$   
 Velocity: modified Gurney  $V_{gm} = 3192$   
 Measured Velocity  $V_s = 2118$  m/s

Scroll to page 4 for derivation of efficiency factor f ...

Derive efficiency factor for effective explosive mass....standard Gurney model:

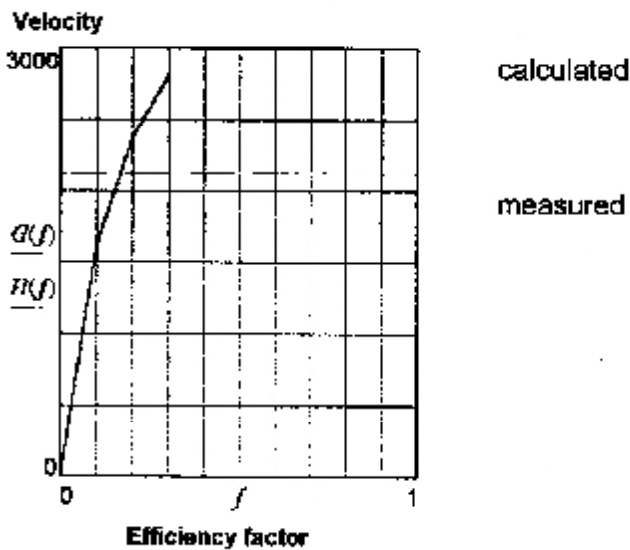
$$F(f) = E_R^2 \cdot \frac{3z^2 f^2}{(fz + 1)(fz + 4)}$$

Check:  $\sqrt{F(f)} = 3871$       Should equal  $V_g = 3871$

Plot variation of calculated plate velocity with efficiency factor f:

$$G(f) = \sqrt{F(f)} \quad f = 0, 0.1 \dots 1 \quad H(f) = V_g$$

Variation of calculated velocity with factor f



Pick value of f close to the root of  $G(f)-H(f)=0$

$$f = 0.1$$

Refine guess of f by iteration to locate root:

$$f = \text{root}((G(f) - H(f)), f) \quad f = 0.159$$

The efficiency factor is  $f = 0.159$

This is the fraction of explosive mass that contributes to the standard Gurney velocity of the plate.

Derive efficiency factor for effective explosive mass....modified Gurney model:

$$f := 1$$

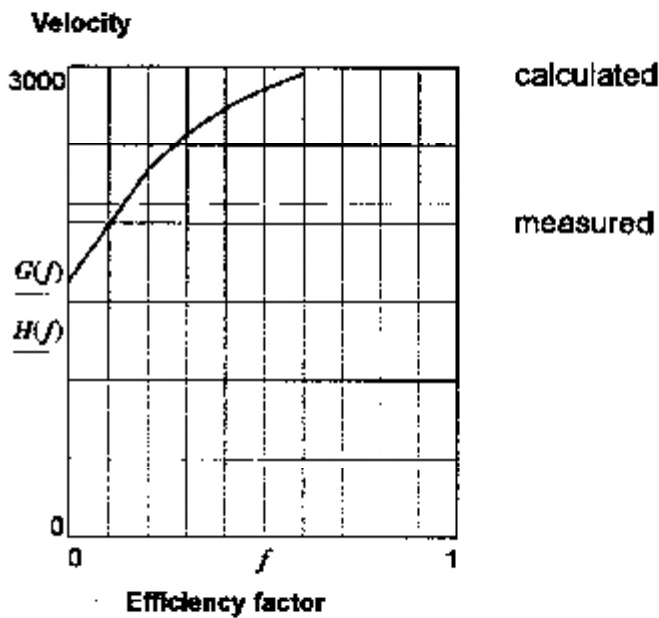
$$F(f) := E_{gr}^2 \frac{3z^2 f^2}{(fz+1)(fz+4)} + V_{pp}^2$$

Check:  $\sqrt{F(f)} = 3192$       Should equal  $V_{gm} = 3192$

Plot variation of calculated plate velocity with efficiency factor f:

$$G(f) := \sqrt{F(f)} \quad f := 0, 0.1..1 \quad H(f) := V_s$$

Variation of calculated velocity with factor f



Pick value of f close to the root of  $G(f) - H(f) = 0$

$$f := 0.1$$

Refine guess of f by iteration to locate root:

$$f := \text{root}((G(f) - H(f)), f) \quad f = 0.132$$

The efficiency factor is  $f = 0.132$

This is the fraction of explosive mass that contributes to the modified Gurney velocity of the plate.

## **A.13.3.2      AZIZ MODEL**

## DISPLAY RESULTS ...Test : RT#3 Series III

Explosive = Comp B

Mass g	$C = 93$
VOD km/s	$D = 7.6$
Polytropic	$\Gamma = 3$
Plate mass g	$m_p = 8$
Measured velocity km/s	$V_s = 1.96$
Efficiency factor	$f = 1$
C/M ratio (actual)	$CM1 = 11.625$
C/M ratio (effective)	$CM2 = 11.625$
Detonation Velocity m/s	$D = 7.6$
Aziz velocity km/s (f=1)	$V_p = 4.462$
Aziz velocity (effective mass)	$V_{pf} = 4.462$
Measured Velocity m/s	$V_s = 1.96$
Plate Energy, calculated kJ	$E_p = 79.646$
Plate Energy, measured kJ	$E_{pm} = 15.366$
Explosive energy kJ	$E_o = 335.73$
Energy Efficiency, calculated	$E_f = 0.237$
Energy Efficiency, measured	$E_{fm} = 0.046$
Fraction Effective explosive mass	$f_e = 0.193$

Energy efficiency calculations suggest that only a fraction

$$f_e = 0.193$$

of the loaded explosive mass contributes to the Aziz-type one-dimensional gas expansion and plate acceleration.

Scroll to page 4 for determining efficiency factor f ....

## DISPLAY RESULTS .... Test : RT#4 Series III

Explosive = Comp B

Mass g	$C = 93$
VOD km/s	$D = 7.6$
Polytropic	$\Gamma = 3$
Plate mass g	$m_p = 8$
Measured velocity km/s	$V_s = 2.118$
Efficiency factor	$f = 1$
C/M ratio (actual)	$CM1 = 11.625$
C/M ratio (effective)	$CM2 = 11.625$
Detonation Velocity m/s	$D = 7.6$
Aziz velocity km/s (f=1)	$V_p = 4.462$
Aziz velocity (effective mass)	$V_{pf} = 4.462$
Measured Velocity m/s	$V_s = 2.118$
Plate Energy, calculated kJ	$E_p = 79.646$
Plate Energy, measured kJ	$E_{pm} = 17.944$
Explosive energy kJ	$E_o = 335.73$
Energy Efficiency, calculated	$E_f = 0.237$
Energy Efficiency, measured	$E_{fm} = 0.053$
Fraction Effective explosive mass	$f_e = 0.225$

Energy efficiency calculations suggest that only a fraction

$$f_e = 0.225$$

of the loaded explosive mass contributes to the Aziz-type one-dimensional gas expansion and plate acceleration.

Scroll to page 4 for determining efficiency factor f ....

## DERIVE CHARGE MASS EFFICIENCY FACTOR BASED ON VELOCITY.....

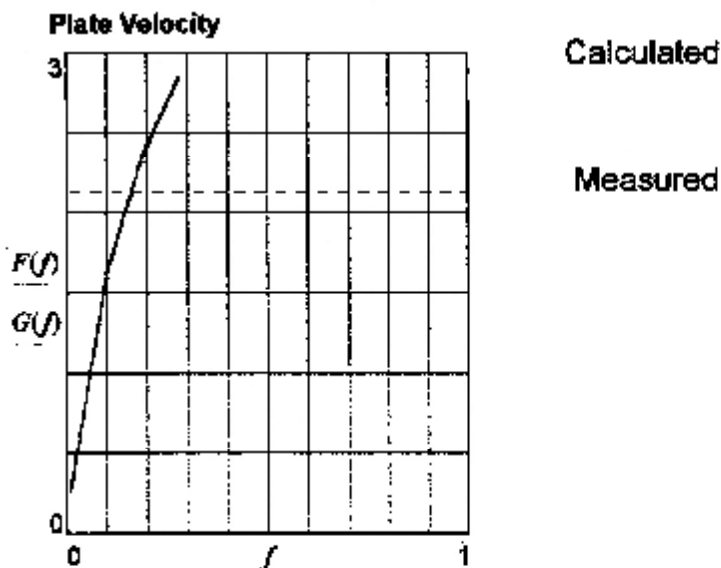
$$f := 0.01, 0.1 \dots 1$$

$$z(f) := \left[ \sqrt{\left( \frac{32}{27} CM^2 f + 1 \right)} \right]$$

$$F(f) := D \cdot \frac{z(f) - 1}{z(f) + 1}$$

$$G(f) := V_s$$

Plot variation of calculated velocity with f ...



Pick a value of f close to the root of  $F(f) - G(f) = 0$

$$f = 0.2 \quad \dots \text{first estimate of root}$$

$$f = \text{root}(|F(f) - G(f)|, f) \quad f = 0.156 \quad \dots \text{the root}$$

$$\text{The efficiency factor is } f = 0.156$$

This is the fraction of explosive mass that contributes to the one-dimensional gas expansion accelerating the plate to its final velocity.

### **A.13.3.3 FICKETT MODEL**



Explosive Type: Composition B

Charge Length  $L = 85$   
 Charge mass g  $C = 93$   
 VOD km/s  $D = 7.6$   
 Polytropic  $\Gamma = 3$   
 Plate mass  $m = 8$       Sound speed km/s  $C_h = 3.6$   
 Measured Velocity m/s  $V_{exp} = 1960$

PRINT RESULTS OF CALCULATIONS (2) \*\*\*\*\*

	us	us	mm	m/s
	11.462	0.278	0.152	1008
	11.74	0.556	0.527	1652
	12.018	0.833	1.052	2102
	12.295	1.111	1.684	2436
	12.573	1.389	2.398	2694
$t =$	12.851	$t_{acc} = 1.667$	$X_{acc} = 3.176$	$V_P = 2899$
	13.129	1.944	4.006	3057
	13.406	2.222	4.877	3205
	13.684	2.5	5.784	3322
	13.962	2.778	6.721	3422
	14.24	3.056	7.684	3508
	14.518	3.333	8.669	3583
	14.795	3.611	9.674	3648
	15.073	3.889	10.695	3706
	15.351	4.167	11.732	3758
	15.629	4.444	12.783	3804
	15.906	4.722	13.845	3845
	16.184	5	14.919	3883
	16.462	5.278	16.002	3917
	16.74	5.556	17.095	3948

Time from  
detonation  
at start of  
explosive column

Time from  
start of  
plate  
acceleration

Plate  
displacement

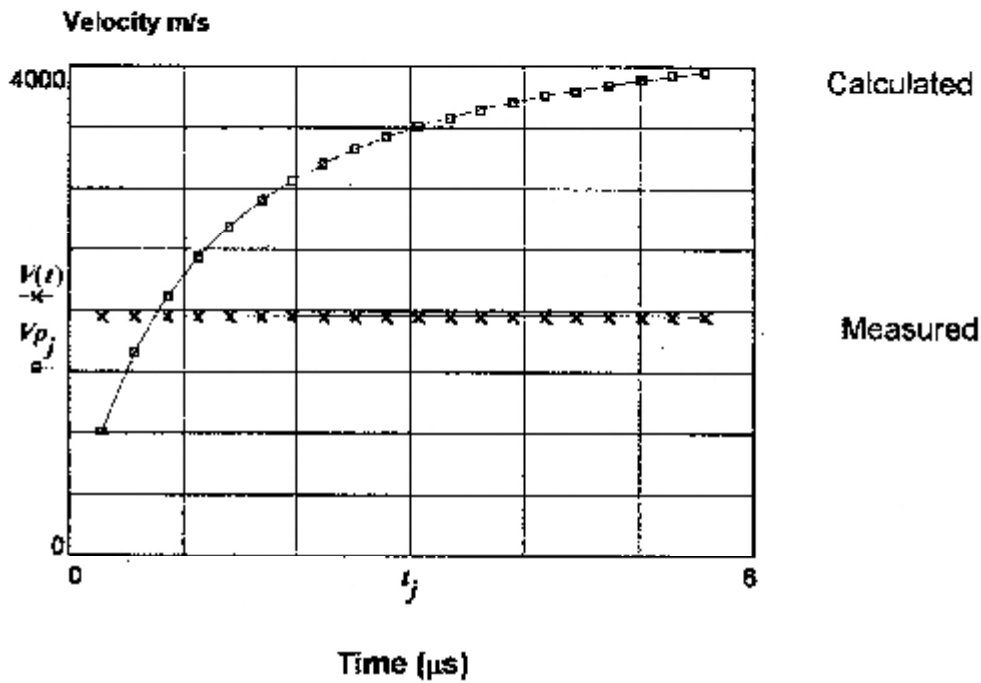
Plate velocity

DISPLAY RESULTS OF CALCULATIONS

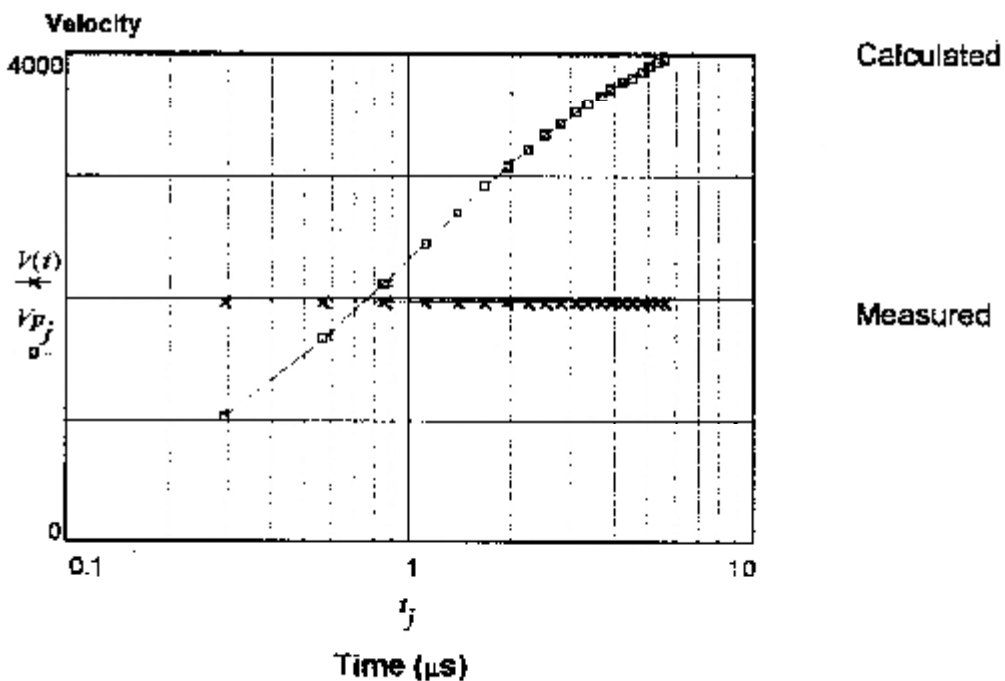
Define experimental value of plate velocity as a constant-value function of time...

$$V(t) = V_{exp} \quad t - t_{acc} + 0.01 > 0$$

TIME VARIATION OF PLATE VELOCITY



Plot time on logarithmic scale...



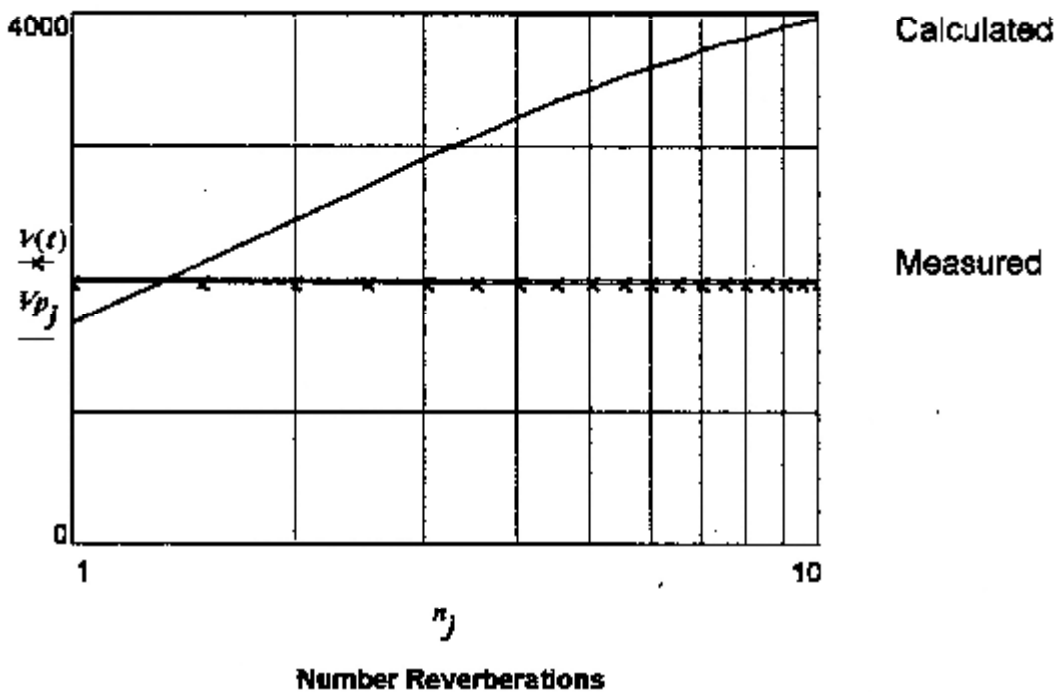
Plot velocity against number of pressure reverberations in plate....

$j = 1..N$  ....must be  $> 0$  for logarithmic axis

$n_j = \frac{j}{2}$  ....n is the number of transits ....

n denotes reverberation number, i.e. number of time increments as defined in section (1) under CALCULATIONS

Plate Velocity m/s



Plot indicates that measured plate velocity is attained shortly after the FIRST passage of the pressure pulse through plate thickness

Explosive Type: Composition B

Charge Length  $L = 85$   
 Charge mass g  $C = 93$   
 VOD km/s  $D = 7.6$   
 Polytropic  $\Gamma = 3$   
 Plate mass  $m = 8$       Sound speed km/s  $C_b = 3.6$   
 Measured Velocity m/s  $V_{exp} = 2118$

PRINT RESULTS OF CALCULATIONS (2) .....

	us	us	mm	m/s
	11.462	0.278	0.152	1008
	11.74	0.558	0.527	1652
	12.018	0.833	1.052	2102
	12.295	1.111	1.684	2436
	12.573	1.389	2.398	2694
$t =$	12.851	$t_{acc} =$ 1.667	$X_{acc} =$ 3.176	$V_p =$ 2899
	13.129	1.944	4.006	3067
	13.406	2.222	4.877	3205
	13.684	2.5	5.784	3322
	13.962	2.778	6.721	3422
	14.24	3.056	7.684	3508
	14.518	3.333	8.669	3583
	14.795	3.611	9.674	3648
	15.073	3.889	10.695	3706
	15.351	4.167	11.732	3758
	15.629	4.444	12.783	3804
	15.906	4.722	13.845	3846
	16.184	5	14.919	3883
	16.462	5.278	16.002	3917
	16.74	5.556	17.095	3948

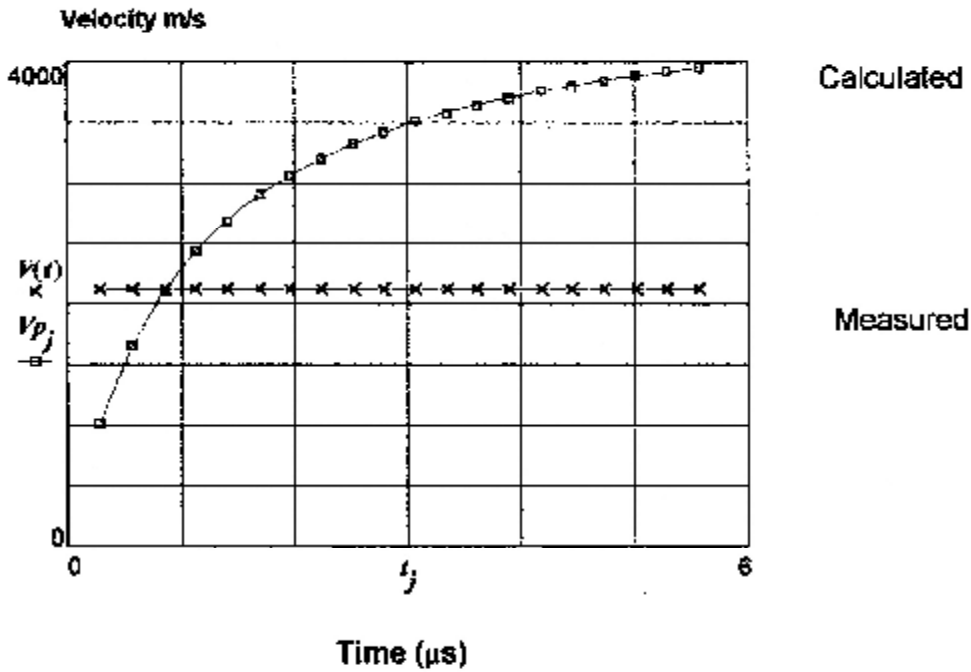
Time from detonation at start of explosive column      Time from start of plate acceleration      Plate displacement      Plate velocity

DISPLAY RESULTS OF CALCULATIONS

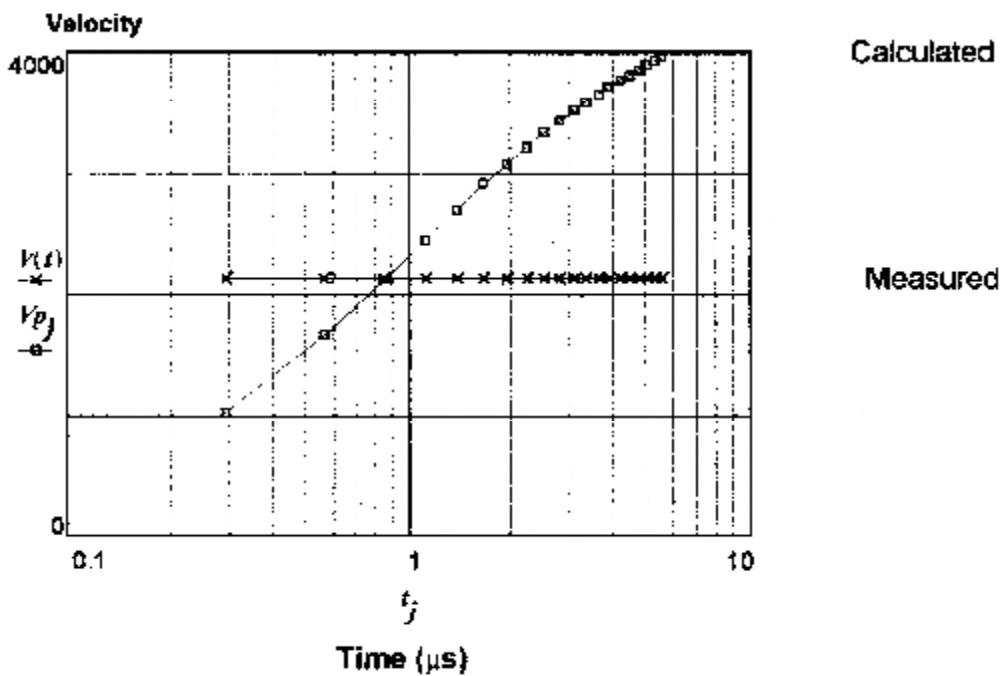
Define experimental value of plate velocity as a constant- value function of time ..

$$V(t) := V_{exp} \quad t := t_{acc} + 0.01 \quad >0$$

TIME VARIATION OF PLATE VELOCITY



Plot time on logarithmic scale....



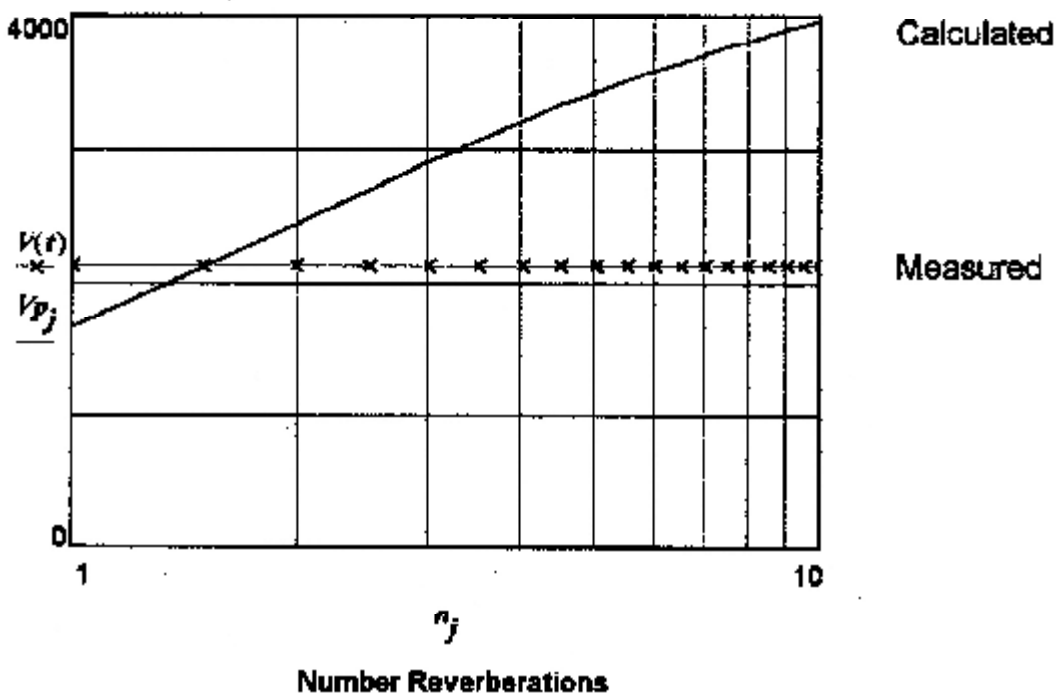
Plot velocity against number of pressure reverberations in plate....

$j = 1..N$  ....must be  $> 0$  for logarithmic axis

$n_j := \frac{j}{2}$  ....n is the number of transits ....

n denotes reverberation number, i.e. number of time increments as defined in section (1) under CALCULATIONS

Plate Velocity m/s



Plot indicates that measured plate velocity is attained between ONE and TWO passages of the pressure pulse through plate thickness

**A.13.4            A.D.L. TEST SERIES III(b)**

**SUPER GELIGNITE MASS            =    65 grams**  
**DISC MASS                                =    8 grams**

#### **A.13.4.1 GURNEY MODEL**



Explosive Type: Blasting Gelignite  
 Test ID: Average Series III  
 VOD m/s:  $D = 5600$   
 Plate mass g:  $m_p = 8$   
 Charge Mass g:  $C = 65$   
 Measured Velocity  $V_s = 1130$

## DISPLAY RESULTS.....

Gurney constant  $E_g = 2000$   
 Reduced Gurney constant  $E_{gr} = 1428$   
 Particle speed in gas  $U_p = 1400$   
 C/M ratio  $\lambda = 8.125$   
 Velocity: standard Gurney  $V_g = 2676$   
 Velocity: reduced Gurney  $V_{gr} = 1911$   
 Velocity: momentum transfer  $V_{pp} = 1123$   
 Velocity: modified Gurney  $V_{gm} = 2217$   
 Measured Velocity  $V_s = 1130$  m/s

Scroll to page 4 for derivation of efficiency factor f ...

Derive efficiency factor for effective explosive mass....standard Gurney model:

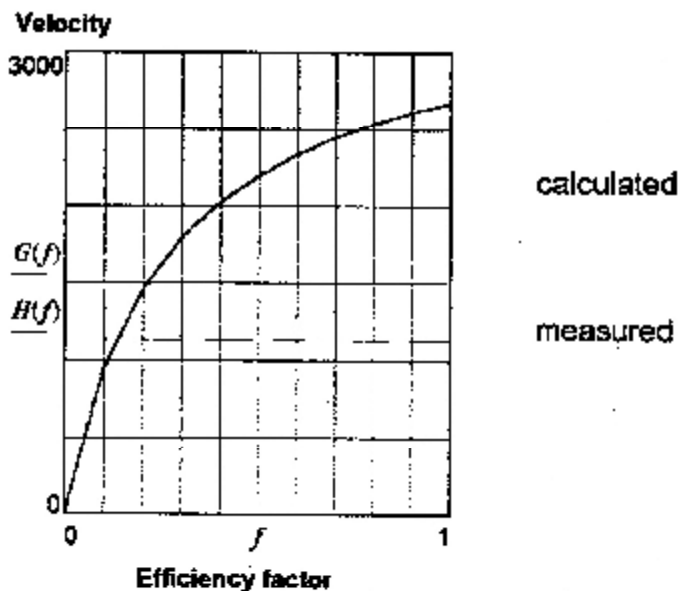
$$F(f) := E_g^2 \frac{3z^2 f^2}{(fz+1)(fz+4)}$$

Check:  $\sqrt{F(f)} = 2676$       Should equal  $V_g = 2676$

Plot variation of calculated plate velocity with efficiency factor f:

$$G(f) = \sqrt{F(f)} \quad f = 0, 0.1, \dots, 1 \quad H(f) := V_g$$

Variation of calculated velocity with factor f



Pick value of f close to the root of  $G(f)-H(f)=0$

$$f := 0.1$$

Refine guess of f by iteration to locate root:

$$f := \text{root}((G(f) - H(f)), f) \quad f = 0.129$$

The efficiency factor is  $f = 0.129$

This is the fraction of explosive mass that contributes to the standard Gurney velocity of the plate.

Derive efficiency factor for effective explosive mass....modified Gurney model:

$$f = 1$$

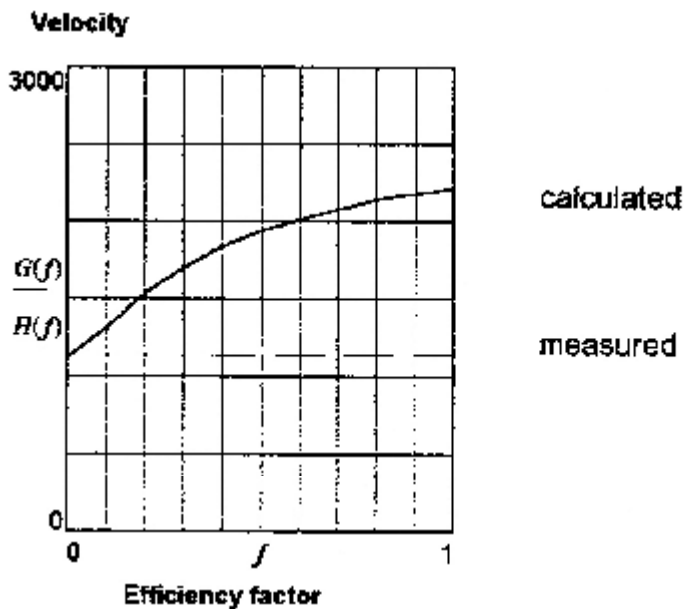
$$F(f) = E_{gr}^2 \frac{3z^2 f^2}{(fz+1)(fz+4)} + V_{pp}^2$$

Check:  $\sqrt{F(f)} = 2217$       Should equal  $V_{gm} = 2217$

Plot variation of calculated plate velocity with efficiency factor f:

$$G(f) = \sqrt{F(f)} \quad f = 0, 0.1, \dots, 1 \quad H(f) = V_s$$

Variation of calculated velocity with factor f



Pick value of f close to the root of  $G(f)-H(f)=0$

$$f = 0.1$$

Refine guess of f by iteration to locate root:

$$f = \text{root}((G(f) - H(f)), f) \quad f = 0.013$$

The efficiency factor is  $f = 0.013$

This is the fraction of explosive mass that contributes to the modified Gurney velocity of the plate.

## **A.13.4.2      AZIZ MODEL**

DISPLAY RESULTS .... Test : BG (average) Series IIII  
Explosive = Blasting Gelignite

Mass g	$C = 65$
VOD km/s	$D = 5.6$
Polytropic	$\Gamma = 3$
Plate mass g	$m_p = 8$
Measured velocity km/s	$V_s = 1.13$
Efficiency factor	$f = 1$
C/M ratio (actual)	$CM1 = 8.125$
C/M ratio (effective)	$CM2 = 8.125$
Detonation Velocity m/s	$D = 5.6$
Aziz velocity km/s (f=1)	$V_p = 2.971$
Aziz velocity (effective mass)	$V_{pf} = 2.971$
Measured Velocity m/s	$V_s = 1.13$
Plate Energy, calculated kJ	$E_p = 35.309$
Plate Energy, measured kJ	$E_{pm} = 5.108$
Explosive energy kJ	$E_o = 127.4$
Energy Efficiency, calculated	$E_f = 0.277$
Energy Efficiency, measured	$E_{fm} = 0.04$
Fraction Effective explosive mass	$f_e = 0.145$

Energy efficiency calculations suggest that only a fraction

$$f_e = 0.145$$

of the loaded explosive mass contributes to the Aziz-type one-dimensional gas expansion and plate acceleration.

Scroll to page 4 for determining efficiency factor f ....

## DERIVE CHARGE MASS EFFICIENCY FACTOR BASED ON VELOCITY.....

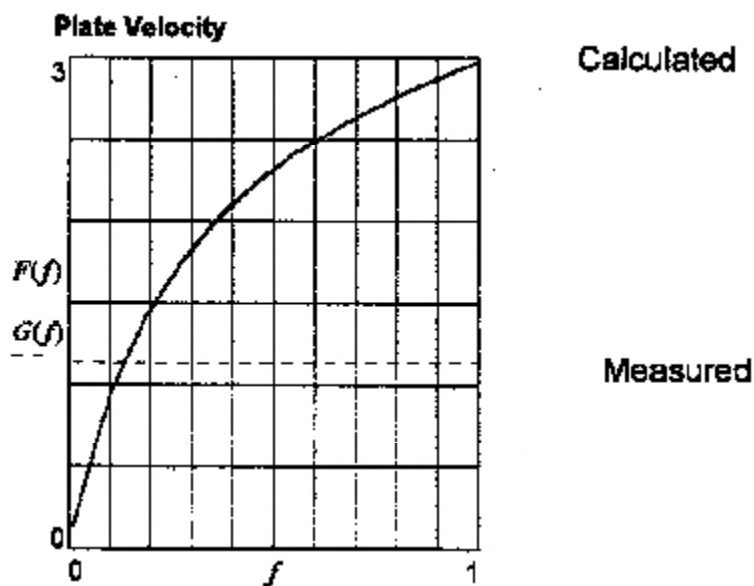
$$f := 0.01, 0.1, 1$$

$$z(f) := \sqrt{\left( \frac{32}{27} CM^2 f + 1 \right)}$$

$$F(f) := D \cdot \frac{z(f) - 1}{z(f) + 1}$$

$$G(f) := V_s$$

Plot variation of calculated velocity with f ...



Pick a value of f close to the root of  $F(f) - G(f) = 0$

$$f = 0.2 \quad \dots \text{first estimate of root}$$

$$f = \text{root}(|F(f) - G(f)|, f) \quad f = 0.132 \quad \dots \text{the root}$$

$$\text{The efficiency factor is} \quad f = 0.132$$

This is the fraction of explosive mass that contributes to the one-dimensional gas expansion accelerating the plate to its final velocity.

### **A.13.4.3 FICKETT MODEL**

Explosive Type: Special Blasting Gelignite

Charge Length  $L = 110$

Charge mass g  $C = 65$

VOD km/s  $D = 5.6$

Polytropic  $\Gamma = 3$

Plate mass  $m = 8$

Sound speed km/s  $C_b = 3.6$

Measured Velocity m/s  $V_{exp} = 1130$

PRINT RESULTS OF CALCULATIONS (2) \*\*\*\*\*

	us	us	mm	m/s
	19.921	0.278	0.049	340
	20.198	0.556	0.183	613
	20.476	0.833	0.385	837
	20.754	1.111	0.644	1026
	21.032	1.389	0.952	1186
$t =$	21.31	$t_{acc} =$ 1.667	$X_{acc} =$ 1.301	$V_p =$ 1324
	21.587	1.944	1.686	1445
	21.865	2.222	2.103	1551
	22.143	2.5	2.547	1644
	22.421	2.778	3.015	1728
	22.698	3.056	3.506	1803
	22.976	3.333	4.016	1870
	23.254	3.611	4.544	1931
	23.532	3.889	5.088	1987
	23.81	4.167	5.648	2038
	24.087	4.444	6.22	2084
	24.365	4.722	6.805	2127
	24.643	5	7.402	2167
	24.921	5.278	8.009	2204
	25.198	5.556	8.626	2237

Time from  
detonation  
at start of  
explosive column

Time from  
start of  
plate  
acceleration

Plate  
displacement

Plate velocity

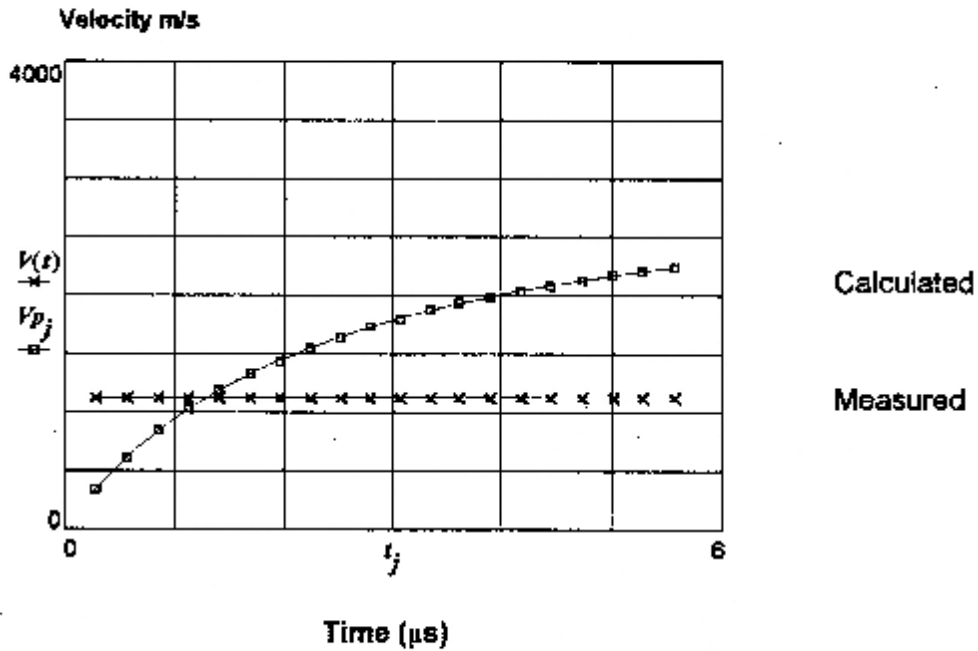


DISPLAY RESULTS OF CALCULATIONS\*\*\*\*\*

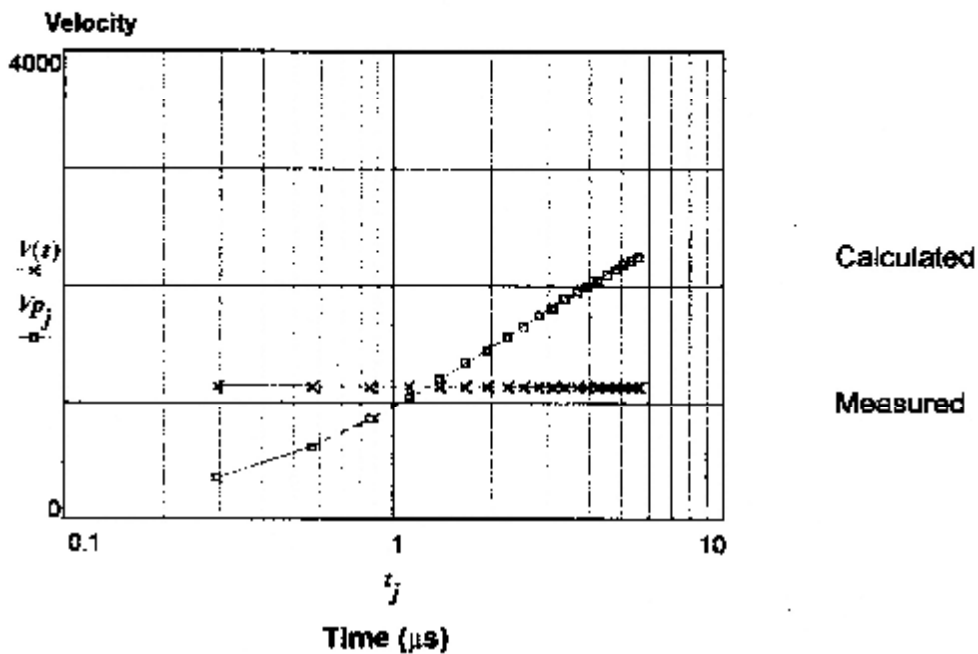
Define experimental value of plate velocity as a constant- value function of time...

$$V(t) = V_{exp} \quad t = t_{acc} = 0.01 \quad > 0$$

TIME VARIATION OF PLATE VELOCITY



Plot time on logarithmic scale...



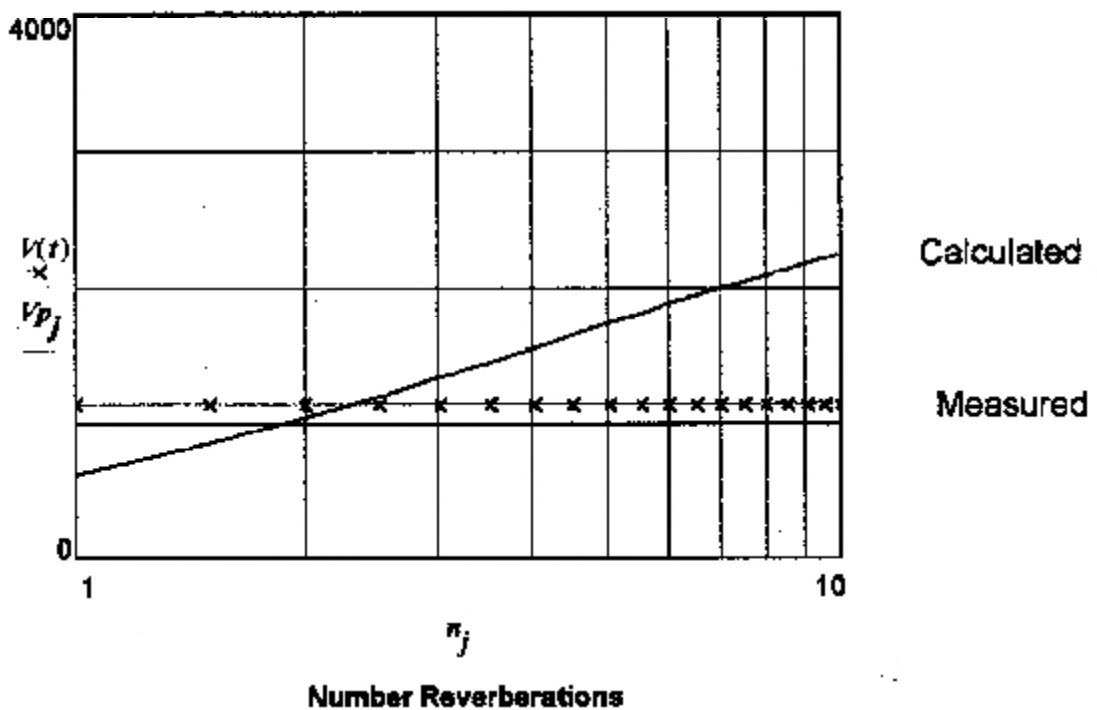
Plot velocity against number of pressure reverberations in plate....

$j := 1..N$  ....must be  $> 0$  for logarithmic axis

$n_j := \frac{j}{2}$  ....n is the number of transits ....

n denotes reverberation number, i.e. number of time increments as defined in section (1) under CALCULATIONS

Plate Velocity m/s



Plot indicates that measured plate velocity is attained shortly after TWO passages of the pressure pulse through plate thickness

**A.13.5            A.D.L. TEST SERIES IV**

**TNT MASS        =    45 grams**  
**DISC MASS      =    8 grams**

## **A.13.5.1 GURNEY MODEL**

Explosive Type: TNT	
Test ID: Average Series IV (8 tests)	
VOD m/s:	$D = 6600$
Plate mass g:	$m_p = 8$
Charge Mass g:	$C = 45$
Measured Velocity	$V_s = 1510$

## DISPLAY RESULTS.....

Gurney constant	$E_g = 2400$	
Reduced Gurney constant	$E_{gr} = 1743$	
Particle speed in gas	$U_p = 1650$	
C/M ratio	$zI = 5.625$	
Velocity: standard Gurney	$V_g = 2928$	
Velocity: reduced Gurney	$V_{gr} = 2126$	
Velocity: momentum transfer	$V_{pp} = 1217$	
Velocity: modified Gurney	$V_{gm} = 2450$	
Measured Velocity	$V_s = 1510$	m/s

Scroll to page 4 for derivation of efficiency factor f ...

Derive efficiency factor for effective explosive mass....standard Gurney model::

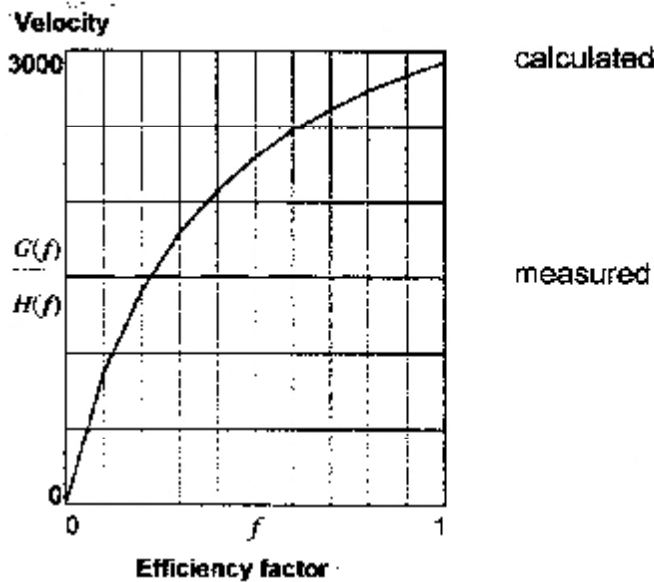
$$F(f) = E_s^2 \frac{3z^2 f^2}{(fz + 1)(fz - 4)}$$

Check:  $\sqrt{F(f)} = 2928$  Should equal  $V_g = 2928$

Plot variation of calculated plate velocity with efficiency factor f.

$$G(f) = \sqrt{F(f)} \quad f = 0, 0.1 \dots 1 \quad H(f) = V_s$$

Variation of calculated velocity with factor f



Pick value of f close to the root of  $G(f) - H(f) = 0$

$$f = 0.1$$

Refine guess of f by iteration to locate root:

$$f = \text{root}((G(f) - H(f)), f) \quad f = 0.222$$

The efficiency factor is  $f = 0.222$

This is the fraction of explosive mass that contributes to the standard Gurney velocity of the plate.

Derive efficiency factor for effective explosive mass....modified Gurney model:

$$f := 1$$

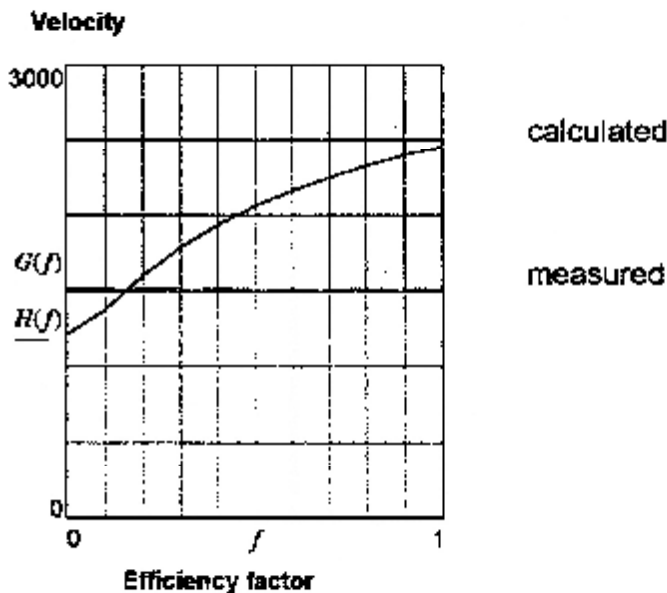
$$F(f) := E \frac{2}{8f} \frac{3-z^2 f^2}{(fz+1)(fz+4)} + V_{PP}^2$$

Check:  $\sqrt{F(f)} = 2450$  Should equal  $V_{gm} = 2450$

Plot variation of calculated plate velocity with efficiency factor f:

$$G(f) := \sqrt{F(f)} \quad f = 0, 0.1 \dots 1 \quad H(f) := V_s$$

Variation of calculated velocity with factor f



Pick value of f close to the root of  $G(f)-H(f)=0$

$$f := 0.1$$

Refine guess of f by iteration to locate root:

$$f := \text{root}((G(f) - H(f)), f) \quad f = 0.161$$

The efficiency factor is  $f = 0.161$

This is the fraction of explosive mass that contributes to the modified Gurney velocity of the plate.

## **A.13.5.2      AZIZ MODEL**



## DISPLAY RESULTS: ... Test : TNT (average)

Explosive = TNT pressed pellets

Mass g	$C = 45$
VOD km/s	$D = 6.6$
Polytropic	$\Gamma = 3$
Plate mass g	$m_p = 8$
Measured velocity km/s	$V_s = 1.51$
Efficiency factor	$f = 1$
C/M ratio (actual)	$CM1 = 5.625$
C/M ratio (effective)	$CM2 = 5.625$
Detonation Velocity m/s	$D = 6.6$
Aziz velocity km/s (f=1)	$V_p = 3.098$
Aziz velocity (effective mass)	$V_{pf} = 3.098$
Measured Velocity m/s	$V_s = 1.51$
Plate Energy, calculated kJ	$E_p = 38.381$
Plate Energy, measured kJ	$E_{pm} = 9.12$
Explosive energy kJ	$E_o = 122.512$
Energy Efficiency, calculated	$E_f = 0.313$
Energy Efficiency, measured	$E_{fm} = 0.074$
Fraction Effective explosive mass	$f_e = 0.238$

Energy efficiency calculations suggest that only a fraction

$$f_e = 0.238$$

of the loaded explosive mass contributes to the Aziz-type one-dimensional gas expansion and plate acceleration.

Scroll to page 4 for determining efficiency factor f .....

## DERIVE CHARGE MASS EFFICIENCY FACTOR BASED ON VELOCITY.....

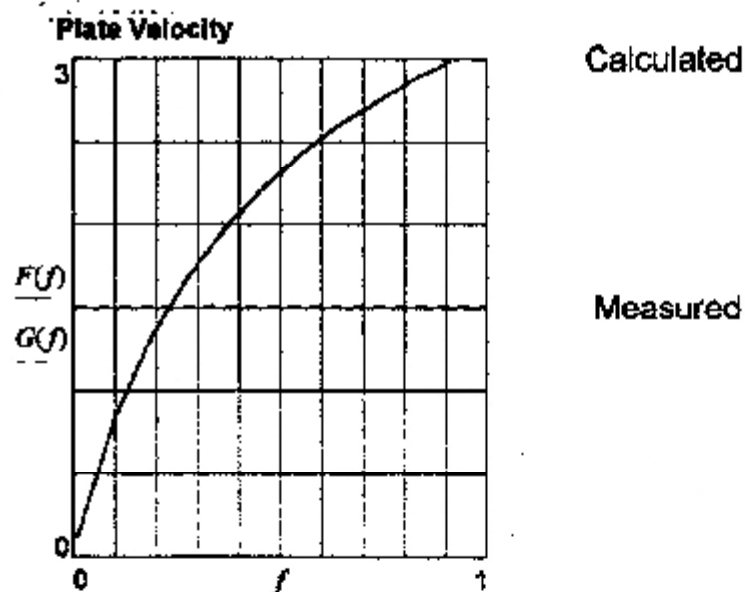
$$f := 0.01, 0.1, 1$$

$$z(f) := \sqrt{\left( \frac{32}{27} CM^2 f + 1 \right)}$$

$$F(f) = D \cdot \frac{z(f) - 1}{z(f) + 1}$$

$$G(f) := V_s$$

Plot variation of calculated velocity with f ...



Pick a value of  $f$  close to the root of  $F(f) - G(f) = 0$

$$f = 0.2 \quad \dots \text{first estimate of root}$$

$$f = \text{root}(|F(f) - G(f)|; f) \quad f = 0.231 \quad \dots \text{the root}$$

$$\text{The efficiency factor is } f = 0.231$$

This is the fraction of explosive mass that contributes to the one-dimensional gas expansion accelerating the plate to its final velocity.

### **A.13.5.3 FICKETT MODEL**

Explosive Type: Pressed TNT Pellets

Charge Length  $L = 60$   
 Charge mass g  $C = 45$   
 VOD km/s  $D = 6.6$   
 Polytropic  $\Gamma = 3$   
 Plate mass  $m = 8$  Sound speed km/s  $C_b = 3.6$   
 Measured Velocity m/s  $V_{exp} = 1510$

PRINT RESULTS OF CALCULATIONS (2) \*\*\*\*\*

	us	us	mm	m/s
$t =$	9.369	0.278	0.083	561
	9.646	0.556	0.297	964
	9.924	0.833	0.609	1266
	10.202	1.111	0.995	1502
	10.48	1.389	1.439	1691
	10.758	1.667	1.931	1845
	11.035	1.944	2.462	1973
	11.313	2.222	3.025	2081
	11.591	2.5	3.616	2173
	11.869	2.778	4.231	2252
	12.146	3.056	4.867	2321
	12.424	3.333	5.52	2382
	12.702	3.611	6.189	2435
	12.98	3.889	6.872	2482
	13.258	4.167	7.568	2524
	13.535	4.444	8.274	2562
	13.813	4.722	8.991	2596
	14.091	5	9.716	2627
	14.369	5.278	10.449	2654
	14.646	5.556	11.19	2680

Time from  
detonation  
at start of  
explosive column

Time from  
start of  
plate  
acceleration

Plate  
displacement

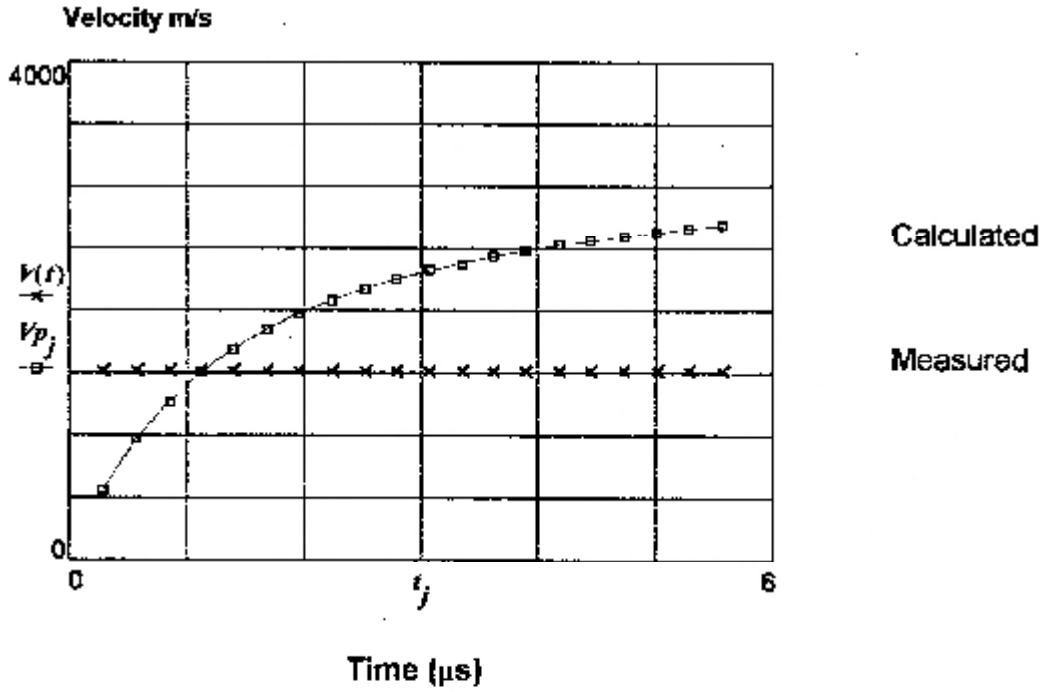
Plate velocity

DISPLAY RESULTS OF CALCULATIONS\*\*\*\*\*

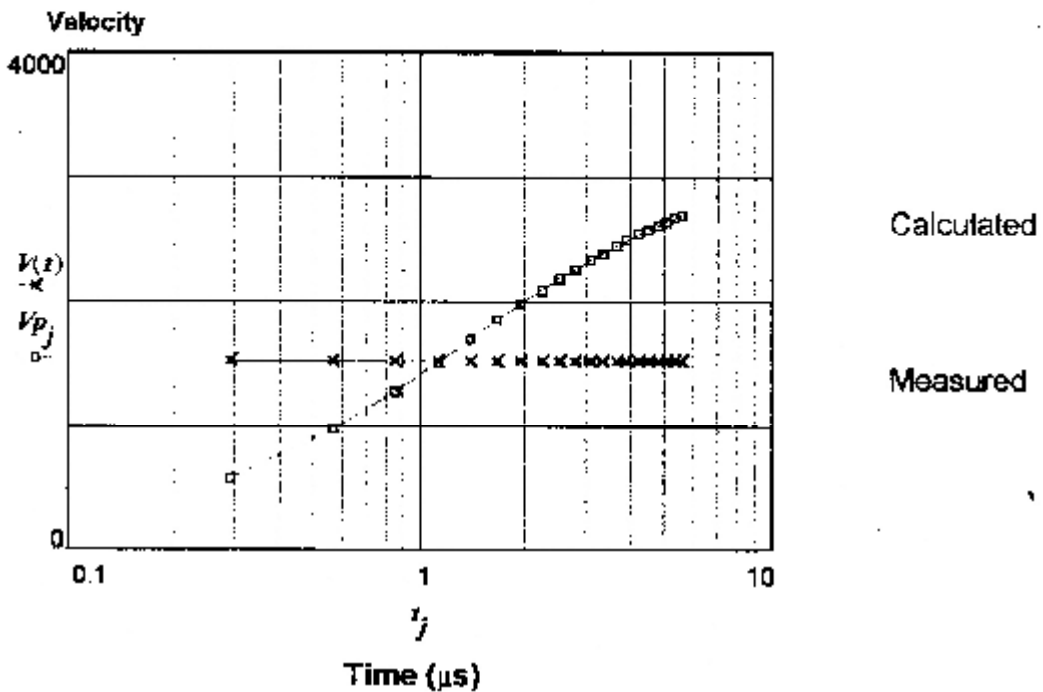
Define experimental value of plate velocity as a constant-value function of time...

$$V(t) : V_{exp} \quad t = t_{acc} + 0.01 \quad >0$$

TIME VARIATION OF PLATE VELOCITY



Plot time on logarithmic scale....



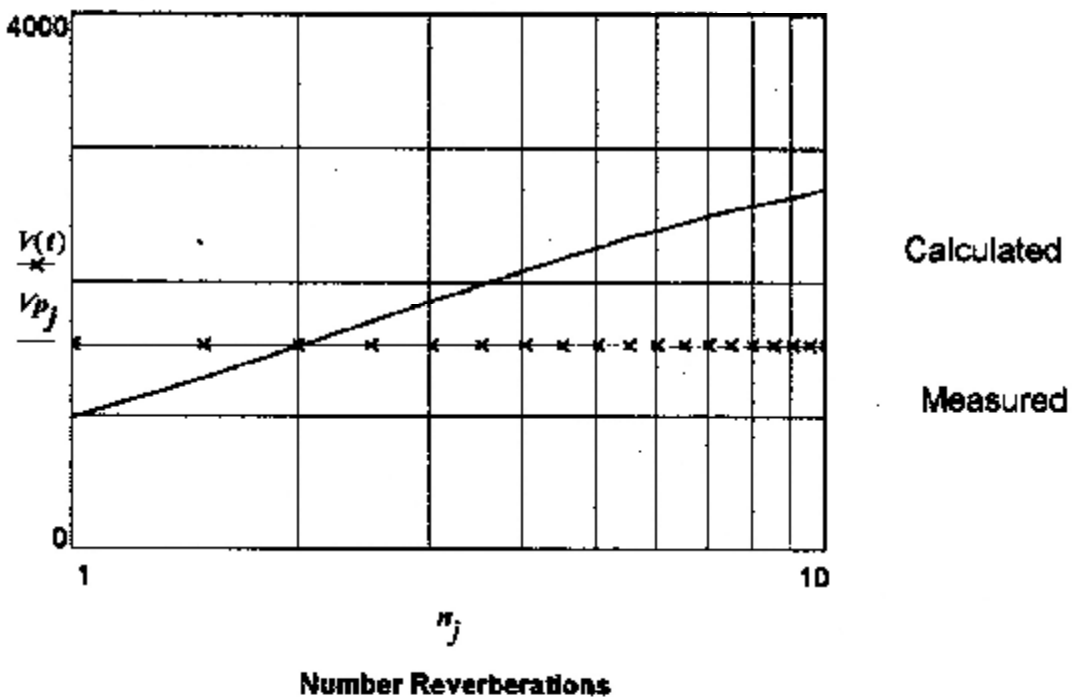
Plot velocity against number of pressure reverberations in plate....

$j = 1 \dots N$  ....must be  $> 0$  for logarithmic axis

$n_j = \frac{j}{2}$  ....n is the number of transits ....

n denotes reverberation number, i.e. number of time increments as defined in section (1) under CALCULATIONS

Plate Velocity m/s



Plot indicates that measured plate velocity is attained after TWO passages of the pressure pulse through plate thickness

## **REFERENCES:**

AEL (2004) Personal communication with African Explosives Limited 2004.

Austin, C.F. (1959) Lined-cavity shaped charges and their use in rock and earth materials, *State Bureau of Mines and Mineral Resources, New Mexico Institute of Mining and Technology, Bulletin no. 69*, 1959.

Austin, C.F. and Pringle, J.K. (1964) Conical shaped charges against brittle materials including rock and earth, *NAVWEPS report no. 8644*, U.S. Naval Ordnance Test Station, 1964.

Aziz, A.K. and Hurwitz, H. and Sternberg, H.M. (1961) Energy transfer to a rigid piston under detonation loading, *The Physics of Fluids*, March 1961.

Backofen, J.E. and Weikert, C.A. (1993) A Gurney formula for the forward projection from the end of an explosive charge, *Proceedings of the 14<sup>th</sup> International Symposium on Ballistics*, Quebec, September 1993.

Berkholtz, N.E. (1985) Evolution of the shaped charge, *Honeywell's Engineers Week Seminar*, February 1985.

Biccard Jeppe, C. (1946) *Gold Mining on the Witwatersrand*, Cape Times Ltd, 1946.

Birkhoff, G. and McDougall, D. and Pugh, E. and Taylor, G. (1948) Explosives with lined cavities, *Journal of Applied Physics*, vol. 19, 1948.

Brinkmann, J.R. (1994) Controlled blasting and its impact on profits. *South African Institute of Mining and Metallurgy School on Drilling and Blasting in Narrow Reefs and their Effects on the Profitability of Gold Mines*, 1994.

Chambers *Dictionary of Science & Technology* Ed. P.M.B. Walker, 2000.

Chanteret, P.Y. (1983) An analytical model for metal acceleration by grazing detonation. *Proceedings of 7<sup>th</sup> International Symposium on Ballistics, The Hague, Netherlands*, 1983.

Chapman, D.L. (1899) On the rate of explosion in gases, *Philosophical Magazine* no. 47, 1899.

Choe, P.C. and Carleone, J. (1977) The stability of shaped-charge jets, *Journal of Applied Physics*, vol. 48, no.10, 1977.

Clark, G.B. (1947) Studies of the design of shaped explosive charges and their effect in breaking concrete blocks. *American Institute of Mining and Metallurgical Engineering, Mining Technology*, vol. 11, *Technical Paper*, No. 2157, 1947.

Cruise, J.A. (1999) Blasting and explosives. *South African Institute of Mining and Metallurgy School on Narrow Tabular Orebody Mining*, 1999.

Cruise, J.A. and Fitzgerald, M.L.A. (1997) High speed tunneling in mining – three decades of experience. *TUNCON'97. South African National Council on Tunneling*, 1997.

Cruise, J.A. and Szendrei, T. (1987) A directional explosive device to bring down hangups *South African Institute of Mining & Metallurgy Colloquium*, 1987.

Davidson, S.H. and Westwater, R. (1949) The shaped or hollow charge, *Mine and Quarrying Engineering*, May 1949.

Davis, W.C. (1987) The detonation of explosives, *New Scientist*, May 1987.

DeCarli, P.E. and Meyer, M.A. *Shock Waves and High Strain-rate Phenomena in Metals* ed. Meyer and Muir, Plenum Press 1981.

Doering, W. (1943) On detonation processes in gases, *Applied Physics*, 1943.

Draper, H.C. and Hill, J.E. and Agnew, W.G. (1948) Shaped charges applied to mining, *U.S. Bureau of Mines, report RI 4371*, November 1948.

Du Pont (1977), *Blaster's Handbook 175<sup>th</sup> Anniversary Edition*, E.I. du Pont De Numours and Co., Wilmington 1977.

Duvall, G.E. and Erkman, J.O. and Ablow, C.M. (1969) Explosive acceleration of projectiles, *Israel Journal of Technology*, vol. 7, 1969.

Fickett, W (1987) Motion of a plate driven by an explosive, *Journal of Applied Physics*, December 1987.

Giltner, S.G. (1992) The penetration and fracturing mechanisms generated in brittle rock by the impingement of a high velocity jet. PhD Thesis, University of the Witwatersrand, 1992.

Green et al, (1955) United States Army in World War II. The Technical Services, The Ordnance Department, *Planning Munitions for War*, 1955.



Gurney, R.W. (1943) The initial velocities of fragments from bombs, shells and grenades *US Army Ballistic, Research Laboratory Report no. 405*, 1943.

Gurney, R.W. (1947) Fragmentation of bombs, shells and grenades, *BRL report 635*, 1947.

Held, M. (1993) *Flash Radiography, Tactical Missile Warheads* Joseph Corleone (ed.), vol. 155, Progress in Astronautics and Aeronautics A1AA, 1993.

Hermann, J.W. and Randers-Pehrson, G. AND Berus, E.R. (1977) Experimental and analytical Investigations of self-forging fragments for the defeat of armor at extremely long standoff, *Proceedings of 3<sup>rd</sup> International Symposium on Ballistics*, Karlsruhe, 1977.  
Hill, R. and Mott, N. and Pack, D. (1944) ARD, *Theoretical Research Report no. 2/44, and 13/44*, 1944.

Hornemann, U. and Schroder, G.A. and Weimann, K. (1987) Explosively-formed projectile warheads, *Military Technology 4/87*, 1987.

Huttl, J.B. (1946) The shaped charge for cheaper mine blasting, *Engineering and Mining Journal*, vol. 147, 1946.

Jamet, and Thomer, (1976) *Flash Radiography*, Elsevier New York, 1976.

Jouguet, E. (1905) On the propagation of chemical reaction in gases, *Journal de Mathematique Pures et Appliquees*, 1905.

Lambourn, B.D. and Hartley, J.E. (1965) The calculation of the hydrodynamic behaviour of plane one dimensional explosive / metal system. *U.S. Naval Ordnance Laboratory – Fourth Symposium on Detonation*, 1965.

Lewis, R.S. and Clark, G.B. (1946) Applications of shaped explosive charges to mining operations, *University of Utah Bulletin*, 1946.

Lindroth, D.P. and Anderson, S.J. (1982) Safe, effective hangup clearance for underground mines, *U.S. Bureau of Mines report RRRRI 8651*, 1982.

Lindroth, D.P. and Anderson, S.J. (1983) Effective hangup clearance, *S.A.Mining and Engineering Journal*, 1983.

Minerals Act, Act no. 50 of 1991.

Munroe, C. (1888a) Wave-like effects produced by the detonation of guncotton, *American Journal of Science*, Silliman, 1888.

Munroe, C. (1888b) Modern explosives, *Scribner's Magazine*, 1888.

Munroe, C.E. (1900) The application of explosives, *Popular Science Monthly*, 1900.

Neumann, E. (1914) Hohlkoerper aus brisanzstoffen *Zeitschrift fuer das Gesomte Schiess – und Springstoffwesen*, May 1914.

Neumann, M. (1911) Einiges ueber brisante sprengstoffe, *Zeitschrift Fuer Angewandte chemie*, November 1911.

Ordnance Board Minute 8220, (1913).

Ordnance Board Minute 8847, (1913).

Pack, D.C. and Evans, W.M. (1951) Penetrations by high-velocity (Munroe) jets, *Proceedings of the Physical Society vol. 64*, 1951.

Persson, P.A. and Holmberg, R. and Lee J. (1994) *Rock Blasting & Explosives Engineering*, CRC Press, 1994.

Pugh, E.M. and Eichelberger, R.J. and Rostoker, N. (1952) Theory of jet formation by charges with lined conical cavities, *Journal of Applied Physics*, vol. 23, 1952.

Ravid, M, Bodner, S.R. and Holoman, I. *International Journal of Engineering Science*, vol. 25(4) 1987.

SA Patent, (1989). South African patent no. 89/3235.

Schardin, H. (1954) Ueber die entwicklung der ausgekleideten hohlladung, *Wehrtechnische Hefte* 1954.

Sukharevskii, M. (1925) *Tekhnika i Snabzhenie Krasnoi Armii*, 1925.

Sukharevskii, M. (1926) *Voina i Tekhnika*, 1926.

Szendrei, T. (1996) Velocity of explosively-driven metal plate, measurements and theoretical interpretations, *Warheads 2000 Seminar*, November 1996.

Taylor, G.I. (1941) Analysis of the explosion of a long cylindrical bomb detonated at one end, *The scientific papers of Sir Geoffrey Ingram Taylor vol. III*, G.K. Batchelor (ed.) Cambridge University Press, 1963.

Taylor, G.I. (1950) The dynamics of the combustion products behind plane and spherical detonation fronts in explosives, *Proceedings of the Royal Society*, 1950.

Tate, A. (1967) A theory for the deceleration of long rods after impact, *Journal of the Mechanics and Physics of Solids* vol. 15, 1967.

Tate, A. (1969) Further results in the theory of long rod penetrations, *Journal of the Mechanics and Physics of Solids* vol. 17, 1969.

Thomanek, F.R. (1960) Die entwicklung der ausgekleideten hohlladung explosivstoffe, August 1960.

Tuck, J.L. (1943) Note on the theory of the Munroe Effect, *U.K. report*, A.C. 3596, 1943.

Von Baader, F. (1792) Versuch liner theorie der spregarbeit bergmannisches, *Journal von Koehler & Hoffman*, March 1792.

Von Foerster, (1883) Versuche mit comprimierter schiessbaumwolle *Mittler & Sohn*, Berlin, 1883.

Von Neumann, J. (1942) Theory of detonation waves, *Office of Scientific Research and Development Report No.549*, 1942.

Walters, W.P. and Zukas, J.A. (1989) *Fundamentals of Shaped Charges*, Wiley, 1989.

WASAG, (1911). German patent no. 249630, Verfahren zur herstellung von springkoerpern, *British patent no. 28030*, filed December 1911.

Watermeyer, G.A. and Hoffenberg, S.N. (1932) *Witwatersrand Mining Practice*, Horton, 1932.

Weickert, C.A. and Gallagher, P.J. and Backofen, J.E. (1995) The effect of explosive properties, confinement and detonation wave geometry on the forward projection from the end of a charge, *Proceedings of the 15<sup>th</sup> International Symposium on Ballistics*, Jerusalem, May 1995.

Wood, R.W. (1936) Optical and physical effects of High Explosives *Proceedings of the Royal Society*, London, 1936.

Yadav, H.S. and Gupta, N.K. (1988) Flyer plate motion and its deformation during flight, *International Journal of Impact Engineering* vol.7, 1988.

Zeldovich, Y.B. (1940) On the theory of the propagation of detonation in gaseous systems  
*Journal of Experimental Theory (Russians)*, 1940.